DEVELOPMENT OF SUBMARINE CANYON SYSTEMS ON ACTIVE MARGINS: HIKURANGI MARGIN, NEW ZEALAND

A thesis submitted in partial fulfilment of the requirements for the

Degree of

Doctor of Philosophy in Geology

in the University of Canterbury

by

Joshu J Mountjoy

University of Canterbury

2009

The Hikurangi Subduction Margin

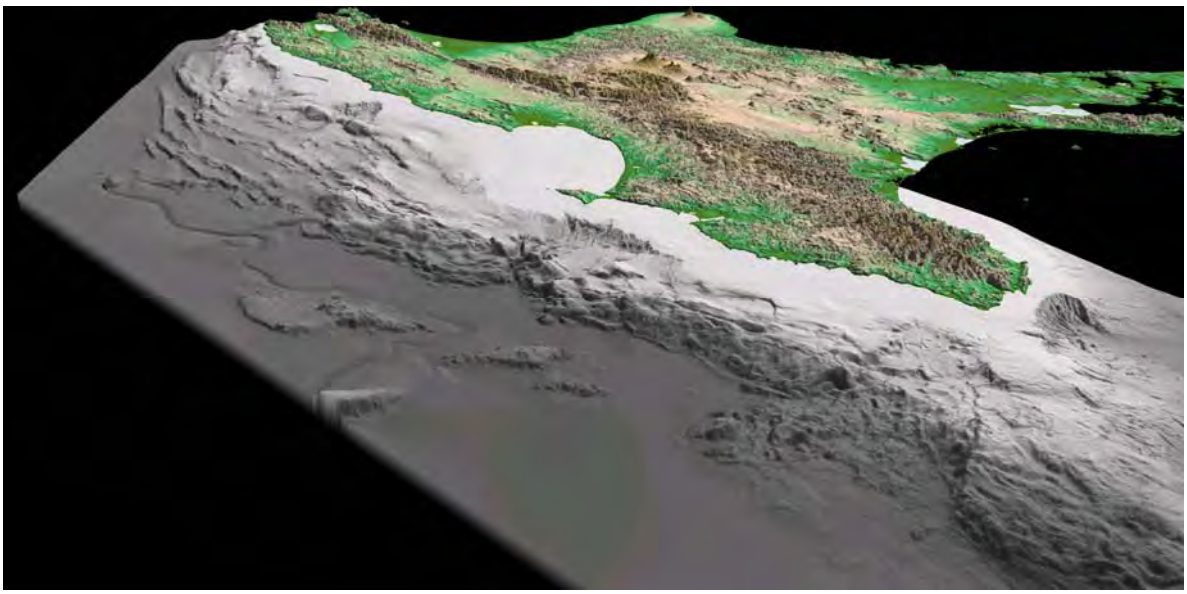

Aerial oblique view of the Hikurangi Margin from the north-east. This image is based on 100m digital elevation models. The offshore component incorporates over 50 years of accumulated bathymetric data from NZOI and NIWA

Table of contents

List of Figures

List of Tables

Appendices

Acknowledgments

First of all the unwavering love and support of my partner Aliki and our children Gabriel and Josef, as well as extensive support from our extended families, has really enabled me to complete this doctorate amongst the ongoing distractions of a busy family life.
Encouragement by Jarg Pettinga stimulated me to pursue doctoral study, and in terms of project setup people at both the University of Canterbury (UoC) and New Zealand's National Institute of Water & Atmospheric Research (NIWA) put significant effort into making it happen.
The support of my supervisory team of Professor Jarg R Pettinga and Dr Philip M Barnes has been first rate. Special thanks are due to Phil who has been at hand to provide top-notch guidance, assistance and feedback throughout the entire project. Personal financial assistance, travel monies and university fees have been provided by a Tertiary Education Commission of New Zealand Top Achiever Doctoral Scholarship. The reality of the project has, however, been made possible through the support of NIWA by providing project data, logistical support and additional financial support via capability funding (thank you Charlotte Severne). Valuable technical support and scientific input has been readily forthcoming from NIWA staff, including Claire Castellazzi, Miles Dunkin, Geoffroy Lamarche, Kevin Mackay, John Mitchell, Scott Nodder, Alan Orpin, Arne Pallentin, and Anne-Laure Verdier. Geoffroy Lamarche and John Mitchell are especially thanked for collecting additional data during voyage transits. John Mitchell also led the Cook Strait multibeam voyages that much of the work in Cook Strait is based on. Keith Lewis led the Tan0106 survey in Poverty Bay, collecting both multibeam and MCS data that are critical to this study. Additionally, Keith's insights into Hikurangi Margin processes have helped to shape this project. The MED Crown Minerals Group provided access to the 05CM MCS survey along the central and northern Hikurangi Margin. The support of UoC Department of Geological Sciences staff Anekant Wandres and Pat Roberts is appreciated. Input and advice from Jim McKean on matters of morphometric analysis and earthflow mechanics has been very valuable, and Josh Roering provided some useful computer code. JP Walsh and other NSF-Margins team members have happily provided data and useful discussion. Jane Connor and Richard Mclachlan have proof read chapters of the thesis for me. Jane especially reviewed several chapters and has made this thesis a significantly more concise, consistent and readable document and I am very grateful to her.
Thanks to my biking buddies for not giving up on me and dragging me out for rides in rain and shine to keep me fit and motivated.

Abstract

The development and activity of submarine canyons on continental margins is strongly influenced by temporal and spatial changes in sediment distribution associated with orbitally-forced sea-level cyclicity. On active margins, canyons are also strongly influenced by tectonic processes such as faulting, uplift and earthquakes. Within this framework the role of mass-wasting processes, including sediment failures, bedrock landslides and sediment gravity flows, are to: 1) transport material across the slope; 2) act as intra-slope sediment sources; and 3) shape seafloor morphology. In this project the seafloor-landscape signatures of tectonic and geomorphic processes are analysed to interpret the development of submarine canyon morphology on active margins. Datasets include high-resolution bathymetry data (Simrad EM300), multichannel seismic reflection data (MCS), high-resolution 3.5 kHz seismic reflection data, sediment cores, and dated seafloor samples. High-resolution bathymetric grids are analysed using techniques developed for terrain-roughness analysis in terrestrial landscapes to objectively map and interpret features related to seafloor mass-wasting processes.

The Hikurangi subduction margin of New Zealand provides world-class examples of the control of tectonic and sedimentary processes on margin development, hosting multiple examples of deeply-incised canyon systems across a range of scales. Two main study sites, in Poverty Bay and Cook Strait, provide examples of canyon formation. From these examples conceptual and representative models are developed for the spatial and temporal relationships between active tectonic structures, geology, sediment supply, slope- and shelf-incised canyons, slope gully systems, and bedrock mass failures.

The Poverty Bay site occurs on the subduction-dominated northern Hikurangi Margin, where the ~3000 km^2 Poverty re-entrant hosts the large Poverty Canyon system, the only shelf-break-to-subduction-trough canyon on the northern margin. The geomorphic development of the re-entrant is affected by gully development on the upper slope, and multi-cubic-kilometre-scale submarine landslides. From this site the study focuses on the initiation and development of upper-slope gullies and the role of deep-seated slope failure in upper-slope evolution. The Cook Strait site occurs on the southern Hikurangi Margin in the subduction-to-strike-slip transition zone. The 1800 km^2 Cook Strait Canyon incises almost 50 km into the continental shelf, with a multi-branching canyon head converging to

a deeply slope-incised meandering main channel fed by multiple contributing slope canyons. Other medium-sized canyons are incised into the adjacent continental slope. Fluvial sediment supply to the coast is relatively low on the southern margin, but Cook Strait is subject to large diurnal tidal currents that mobilise sediment through the main strait area.

Prior to the morphostructural analysis of the Cook Strait and Poverty study sites a revision of the tectonic structure was undertaken. In Cook Strait a revision of the available fault maps was undertaken as part of a wider, related tectonic study of the central New Zealand region. In Poverty Bay very limited prior information was available, and as part of this study the structure and stratigraphy of the entire shelf and upper slope has been interpreted.

On active tectonic margins submarine canyons respond to tectonics at: 1) margin-setting scales relating to their ability to become shelf incised; 2) regional scales relating to canyon-incision response to base-level perturbations; and 3) local scales relating to propagating structures affecting canyon location and geometry.

Interpretation of the spatial distribution of fluid vent sites, gully development and landslide scars leads to the conclusion that seepage-driven failure is not a primary control on the widespread instances of gully formation and landslide erosion affecting structurally-generated relief across the margin. Rather, the erosion of tectonic ridges is dominated by tectonics by: slope oversteepening; weakening of the rockmass in fault-damage zones; and triggering of slope failure by earthquake-generated cyclic loading.

Deep-seated mass failures affect numerous aspects of submarine landscapes and play a major role in the enlargement of canyon systems. They enable the development of slope gully systems and represent a major intra-slope sediment source. Quantitative morphometric analysis together with MCS data indicate that landslides may evolve to be active complexes where landslide debris is remobilized repeatedly, analogous to terrestrial-earthflow processes. This process has not previously been documented on submarine slopes.

A model is presented for the evolution of active margin canyons that contrasts highstand and lowstand canyon activity in terms of channel incision, sedimentary processes and slope-erosion processes. During sea-level highstand intervals, canyons become decoupled from their terrestrial/coastal sediment-supply source areas, while during sea-level lowstand intervals, canyons are coupled to fluvial and littoral sediment-supply sources, and top-down

(i.e. shelf-to-lower-slope) sediment transport and channel incision is active. Canyon-head areas are incision dominated during the lowstand while mid to lower canyon reaches experience both a transient increase in sediment in storage and canyon-fill degradation and incision into bedrock. Tectonics influences the canyon landscape through both uplift-controlled perturbations to canyon base-levels and earthquake-triggering of mass movement. Following sea-level rise the sediment supply to canyon heads will be switched off at a certain threshold sea level. From this point canyon heads become aggradational. Mid to lower canyon reaches continue to incise due to continuing tectonic uplift and earthquake-triggered slope instability. Knickpoints are propagated up channel and excavate canyon and sub-canyon channels from the bottom up. Thus, while top-down infilling of non-coupled canyons occurs during sea-level highstands, the lower reaches of active margin canyons continue to incise due the influence of tectonic processes.

Preamble: Project objectives and structure

This doctoral project focuses on the use of high-resolution bathymetric data, in combination with multichannel and high-resolution seismic data, to elucidate the principal controls on the development of submarine canyon systems on active tectonic margins. Focus sites on the Hikurangi subduction margin of New Zealand are used as case studies in this project.

This work has been carried out under a co-supervision arrangement between the Department of Geological Sciences at the University of Canterbury and the Ocean Geology Group at the National Institute of Water and Atmospheric Research (NIWA). I received a Top Achiever Doctoral Scholarship from the Tertiary Education Commission of New Zealand, with additional funding from NIWA to support the project. The majority of the data used has been collected during previous ocean cruises by NIWA and other organisations, with a minor component of data collected during the period of study. The project has been primarily office based, although I have had the opportunity to participate in seagoing voyages on two occasions to gain some hands-on understanding of the data acquisition process.

This preamble sets out the chapter structure of the thesis and defines how journal publications to which I have contributed fit into this structure.

Thesis structure

The thesis is divided into seven chapters, not including this preamble (Figure 0.1). It includes four journal manuscripts to which I have contributed, two as lead author (Mountjoy et al., 2009a; Mountjoy et al., 2009b). These two manuscripts are included as sections within the body of the thesis. They are my work unless stated otherwise. The figures within the manuscripts retain their own numbering system and will be referred to as, for example (Mountjoy et al., 2009a - Figure 1).

For the remaining two manuscripts included in the thesis, I am third author (Law et al., 2009) and eighth author (Barnes et al., 2009). These two manuscripts are included in appendices in their entirety, and the areas to which I have contributed are drawn out within the relevant thesis chapters.

The graphics in this thesis have been prepared in scientific journal format to streamline future publication of the unpublished portion of the thesis work. All of the original files and interpretations, both electronic and hard copy, are held by NIWA Wellington.

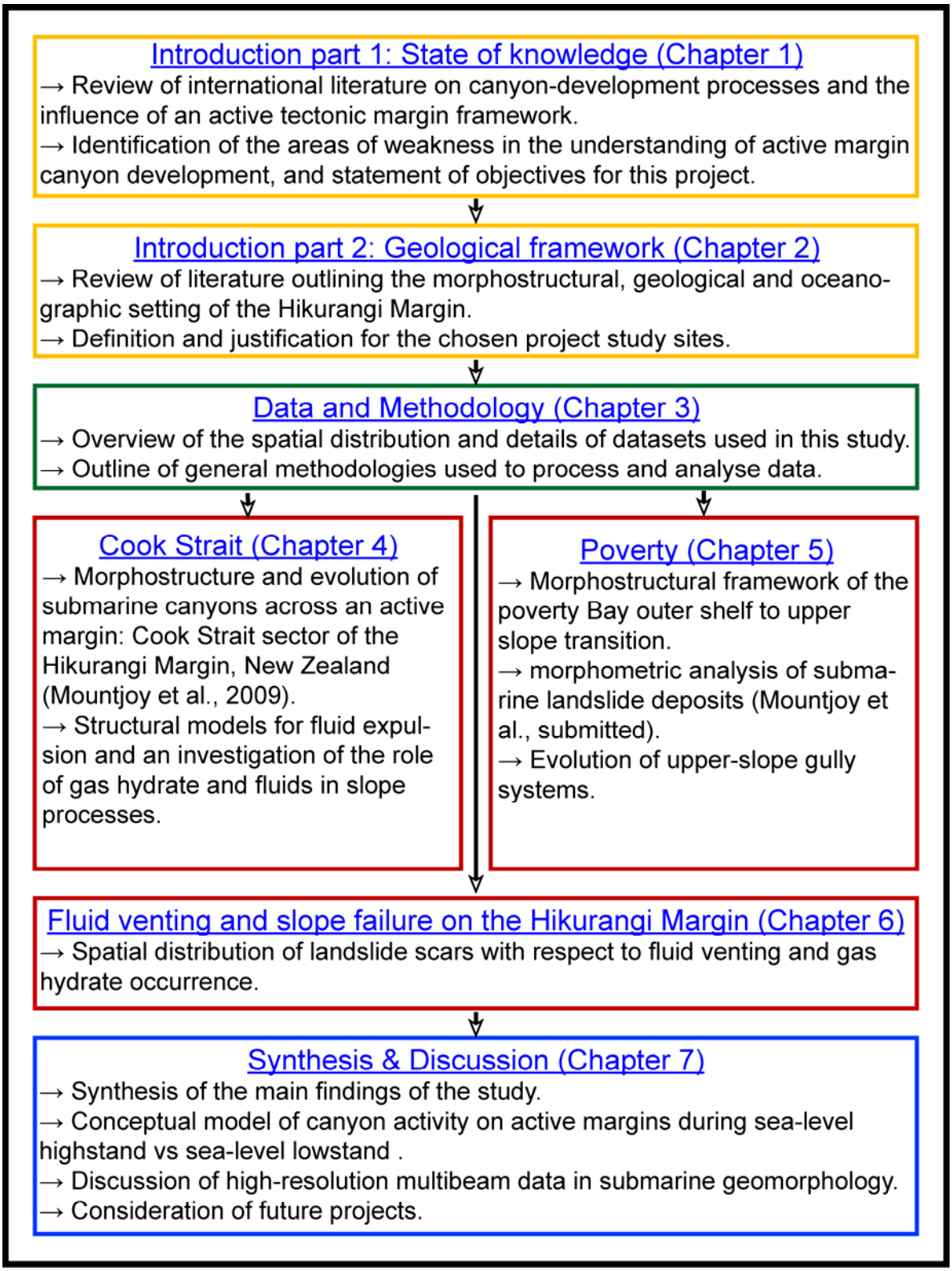

Figure 0.1: Flow chart defining the structure of this thesis.

Introductory material: Chapters 1 and 2.

An introduction to the project has been divided into two sections.

Chapter 1 provides background to the current thinking on submarine canyon development, identifying the niche where this thesis sits. Canyon development is considered in terms of both regional environmental "forcing factors" and local processes shaping the seafloor. Emphasis is given to submarine landslides as these are: 1) ubiquitous on active tectonic margins, particularly within submarine canyons; and 2) they are a process that has received little detailed attention with respect to their role in canyon and slope development.

Chapter 2 provides a thorough background to Hikurangi Margin geology, tectonics, geomorphology and oceanography. This is important in understanding the context within which the two main study sites fit and providing a framework for applying the wider implications of the study to the whole margin. The background in this chapter is relatively broad in geographical extent, giving a context for the specific study sites. Further more detailed scene-setting information is provided within the relevant chapters.

Project data and methodology: Chapter 3

Chapter 3 outlines the data available for the project. The datasets are shown in the context of the whole Hikurangi Margin. Where data is used for specific components of the study the location of data is presented in that chapter. Simple methodologies are also presented here, such as the computer programmes used, which data required post-processing, and details of generic analyses.

Results: Chapters 4, 5 & 6

These three chapters form the results section of the thesis. Chapters 4 and 5 cover the two main study sites. Chapter 6 covers results from the additional minor sites across the margin, drawing on the work included in Barnes et al. (2009).

The main results chapters (Chapters 4 & 5) build on the background material provided in Chapter 2 and develop the analysis and interpretation of the data within that chapter. Discussion within these chapters considers the results in the context of the specific study sites. Further discussion on the implication of these results for active margin canyon development in general is deferred to Chapter 7.

The inclusion of manuscripts in their published/submitted form in Chapters 4 & 5 results in some repetition of introductory material. However, this is considered to have limited detrimental impact on the overall flow of the thesis.

Synthesis and discussion: Chapter 7

The discussion chapter brings together the main findings of the thesis and places them into the context of international understanding of active margin canyon evolution.

The main findings of the thesis are summarised, in terms of the primary drivers of canyon development, with specific examples drawn from the study sites. These findings are used to develop a conceptual model of canyon activity during sea-level lowstand vs sea-level highstand, with reference to the primary drivers already outlined. The role of high-resolution multibeam bathymetric data in the emerging and evolving field of submarine geomorphology is considered, including the application of quantitative morphometric techniques to such data to gain insight into seafloor processes. A future work section looks at what might be done in future to build on this work and to extend our understanding of submarine landscape development.

Chapter 1: Introduction to topic

Incised bedrock canyons are primary features of submarine continental margins. Like major river valleys in subaerial landscapes they are the principal sediment-transfer conduits, moving material from coastal environments to deep-ocean basins. They are not only fundamental to the sediment transfer from terrestrial and intra-slope sources to the deep ocean, but also play an integral role in many aspects of continental margin development. While fluctuating sea level and sediment supply are first-order controls for passive margin development (e.g. Vail et al., 1977; Posamentier et al., 1988), active margins are strongly influenced by tectonic controls such as faulting, folding and large-magnitude earthquakes. Sea-level fluctuations on millennial timescales contrast with perturbations by large-magnitude earthquakes occurring on centurial timescales. Subduction margins experience multiple Mw 7, 8 and even 9 events over a sea-level cycle. Much of what we know about submarine canyons has been learned from sediment cores, marine seismic reflection data, side-scan sonar and coarse-resolution bathymetric data. It is only in the last ~10 years that high-resolution bathymetric data has become available. This data enables examination and quantification of the details of geomorphic processes taking place within canyons. Interpretation of these processes can provide insight into the external forces that guide why, where and how canyons evolve to a particular form.

In this thesis, state-of-the-art middle-depth multibeam bathymetric data, multichannel seismic reflection, high-resolution seismic reflection, and sediment cores from the Hikurangi subduction margin are used to decipher the relative roles of climatic and tectonic forcing in canyon evolution. Special attention is given to the spatial and temporal relationships between active tectonic structures, slope gully systems and canyon development, and to the bedrock mass failures that occur widely on active tectonic margins.

1.1 Brief history of submarine canyon research

The occurrence of submarine canyons was first noted in the late 19th century and followed up with several pioneering works into the early 1900s (Dana, 1863; Spencer, 1903; Shepard, 1932; Daly, 1936; Veatch and Smith, 1939; Bucher, 1940a; b). These early workers had the great challenge of deciphering what might cause such large-scale features

to develop on the seafloor based on minimal data. They lacked knowledge of the submarine landscape-shaping processes comparable to those observed to shape subaerial landscapes. Several hypotheses were proposed during these early days, including suggestions that the features resulted from drowned river-cut canyons (Spencer, 1903), erosion by tsunami waves (Bucher, 1940b), and extreme fluctuations in relative sea level (Veatch and Smith, 1939). Many of these ideas have been shown to be erroneous, being either misguided speculation or based on local effects not applicable on a regional scale. Clearly, submarine canyons are being influenced by terrestrial processes (input from rivers, etc.) but are also subject to a raft of processes that primarily occur only in the submarine environment.

One of the most important discoveries of the early 20th century was the recognition of turbidity currents as a fundamental agent of canyon erosion (Daly, 1936). It is now acknowledged that there is a broad spectrum of processes that contribute to the development of submarine canyons (Shepard, 1981). While some of these may be universal in their role, for the most part the oceanographic, tectonic and sedimentary setting of the continental slope system within which the canyon occurs dictates the processes of primary importance to a particular canyon's development.

Two models are widely cited to explain the process of canyon initiation: upslope vs downslope erosion. From observations of canyons on the Atlantic seaboard of North America a model was proposed that fundamentally involves the upslope development of a canyon channel from the continued retrogressive failure of a landslide complex initiated on the continental slope (Twichell and Roberts, 1982; Farre et al., 1983). This model distinguishes between "youthful" submarine canyons that are slope-confined and resulted purely from this landslide retrogression; and more "mature" canyon systems that have breached the shelf break and receive sediment from shelf sources that contributed to canyon erosion. In response to observations that canyons were utilising older buried canyon courses that extended upslope of the surface channel, a model was proposed, integrating the ideas of Daly (1936), that canyons are initiated by downslope eroding sediment flows (Pratson et al., 1994; Pratson and Coakley, 1996). A further variation of the upslope model has been used to explain the occurrence of non-shelf-connected slope canyons on accretionary margin ridges with little upslope "catchment" area. This proposes that canyon systems are developed by retrogressive slope failures initiated by seepage forces induced by the expulsion of fluids from accretionary wedges (Orange and Breen, 1992; Orange et al., 1997).

Once canyons have been initiated, and are developed as sediment conduits within the shelf, slope [should this be shelf-slope?] and deep-ocean system, they will continue to evolve under the influence of numerous specific erosive and depositional processes. They are also influenced by a framework of regional environmental controls operating over longer time scales. It is these “environmental framework” factors that provide the first-order differences in canyon development on contrasting continental margin settings. Submarine canyons occur on passive continental margins (e.g. Pratson et al., 1994; Exon et al., 2005a) and active tectonic margins (e.g. Lewis and Barnes, 1999; Kukowski et al., 2001; Greene et al., 2002; Laursen and Normark, 2002; Chiang and Yu, 2006; Lastras et al., 2008; Noda et al., 2008). These include a variety of more specific settings such as: high-latitude glacio-marine margins (Carlson and Karl, 1984; Laberg et al., 2007); major fluvially connected channel fan systems (Damuth and Flood, 1984 ; Droz et al., 1996; Michels et al., 2003); and volcanic island arcs (Coulbourn et al., 1974; Krastel et al., 2001). The majority of published studies on canyon inception and development, however, are based on passive margin systems, where canyons are predominantly linear single-channel features of limited areal extent that generally do not incise a great distance into the continental shelf (e.g. Pratson et al., 1994; Exon et al., 2005b; Mitchell, 2005; Green et al., 2007). In contrast, canyons on active tectonic margins can have a very large areal extent, be multi-branching and highly meandering systems, and can become deeply incised into the continental shelf (e.g. Greene et al., 1991). Active tectonic margins comprise a significant proportion of global continental margins. While many of the key processes and environmental factors are the same as, or similar to, those acting on passive margins, the influence of active tectonics provides a distinctive context for canyon evolution that has not been fully explored.

The environmental factors and processes that influence the occurrence, initiation and evolution of canyons across active margins are summarised in Figure 1.1. These “forcing factors” can be considered as both: 1) regional, i.e. affecting regional landscapes and the development of the environment within which canyons occur; and 2) local, i.e. directly shaping the submarine landscape through erosion and deposition.

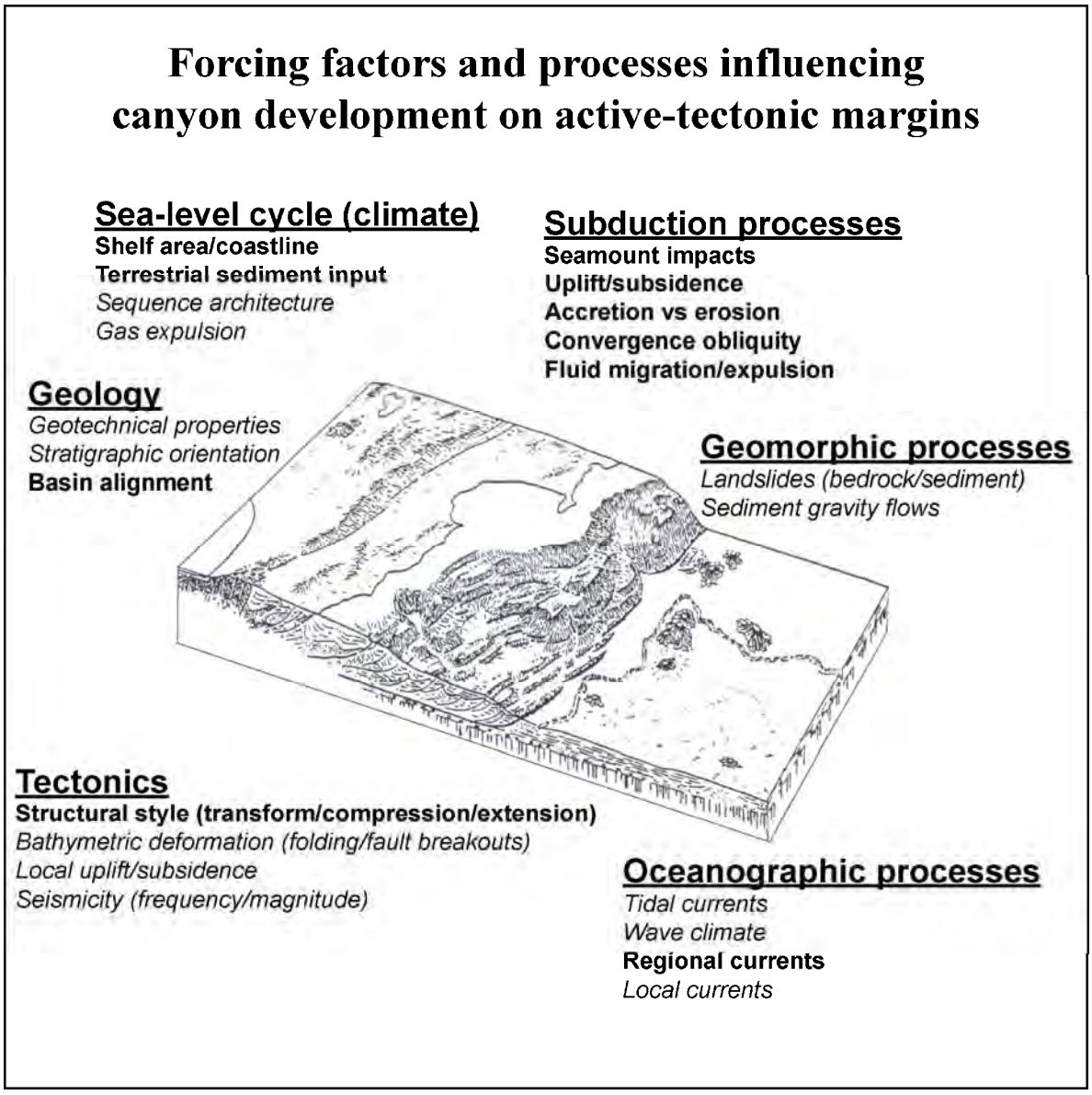

Figure 1.1: Forcing factors and processes influencing canyon development on active tectonic margins. The six main headings incorporate the principal groups of processes that shape active continental margins. Forcing factors and processes listed under these are both regional (bold) and local (italic). The centrepiece is an interpretive block diagram of the central Hikurangi Margin, illustrating the relationship between tectonic structure, bathymetry and margin morphology. Modified from Lewis and Pettinga (1993).

1.2 Regional forcing factors affecting canyon development

Regional forcing factors that define the longer-term framework within which submarine canyons evolve can be divided into climatic forcing, in terms of sea-level variation, and tectonic forcing, in terms of the tectonic contribution to the morphological evolution of active margins.

1.2.1 Orbitally-forced sea-level variation

A fundamental and often-cited time-variable control on canyon system activity is large-scale fluctuation in sea level. This occurs on a cyclic basis in response to varying global ice volumes, which reflect semi-cyclic climatic change forced by variations in the earth's orbital parameters (eccentricity, obliquity and precession) (e.g. Imbrie and Imbrie, 1979). Global sea levels are well documented to fluctuate on regular time frames and be subject to minor fluctuations within this cycle (Figure 1.2) (Pillans et al., 1998). Over the last ~900 kyrs the cycle has been about 100 kyr with up to 120 m range in sea level, while in the early part of the Pleistocene the cycle was closer to 40 kyr with sea-level variability typically 60–90 m (Crundwell et al., 2008). Inter-glacial periods such as the present day are referred to as sea-level "highstand" periods, while glacial periods when sea level is lowered are referred to as "lowstand" periods. The transition between high and low sea levels is highly asymmetric, with the sea level lowering very gradually (and erratically) over several tens of thousands of years, but rising from lowstand to highstand more rapidly and with less intermediate fluctuation (Figure 1.2).

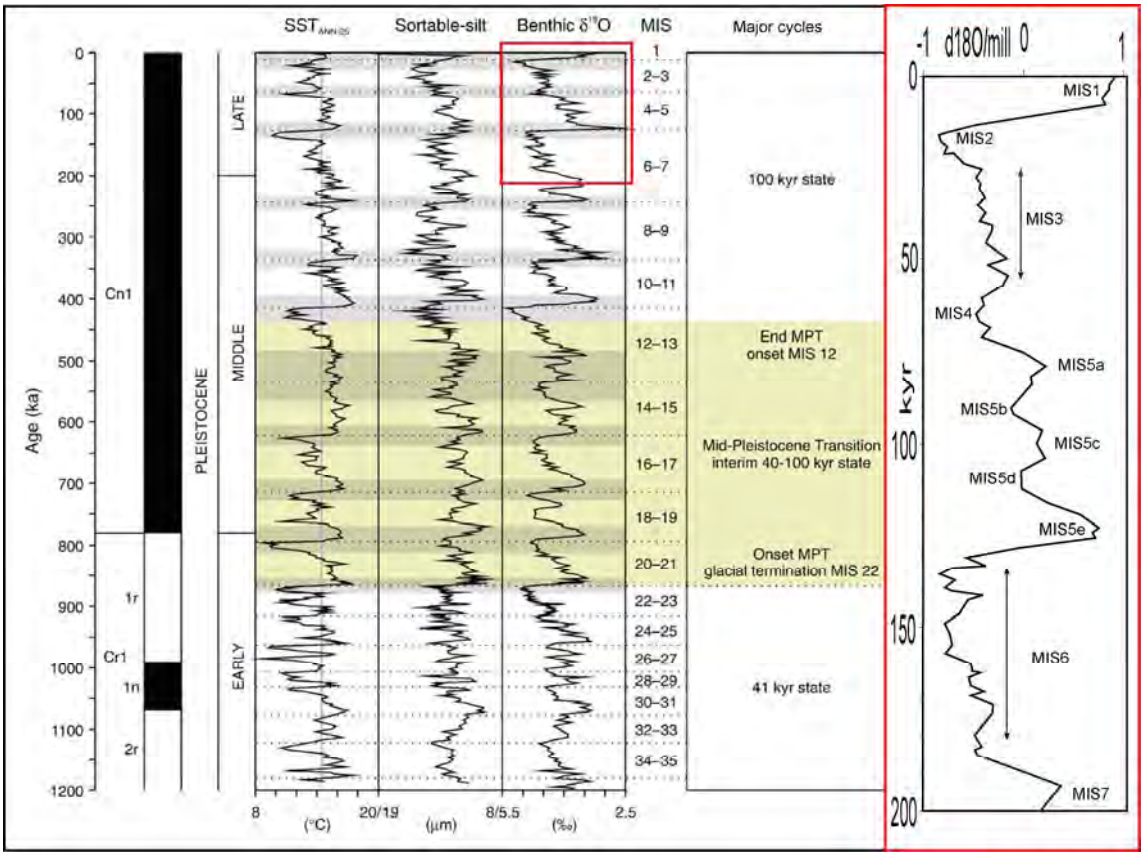

Figure 1.2: Major sea-level cyclicity. Main image shows plotted sea-level proxies from ODP site 1123 to the east of New Zealand, illustrating the mid-Pleistocene transition.

The enlargement of the last glacial cycle from MIS7 to the present day is shown outlined in red (Martinson et al., 1987; Crundwell et al., 2008).

A first-order result of lowered sea level is that subaerial landmasses become substantially greater in extent. Figure 1.3 shows an approximation of the New Zealand landmass during the last glacial maximum (LGM) at c. 20 kyrs BP (c.f. Alloway et al., 2007). With falling sea level, the shoreline migrates outward across the continental shelf, leaving much of the shelf exposed to become a coastal plain. Commonly, this puts the shoreline at the outer shelf and near or at the continental slope edge and the heads of slope canyon systems. Major rivers will cross the shelf and may become connected to canyon systems, though it is often hard to find decisive evidence of this in the geological record. This lack of evidence of lowstand river systems is partly due to erosional processes that occur during sea-level rise. Typically the landward-migrating coastline and wave-abrasion zone erodes the continental shelf surface, removing a component of the lowstand shelf deposits and developing an unconformity referred to as a transgressive ravinement or transgressive surface of erosion (e.g. Posamentier and Vail, 1988).

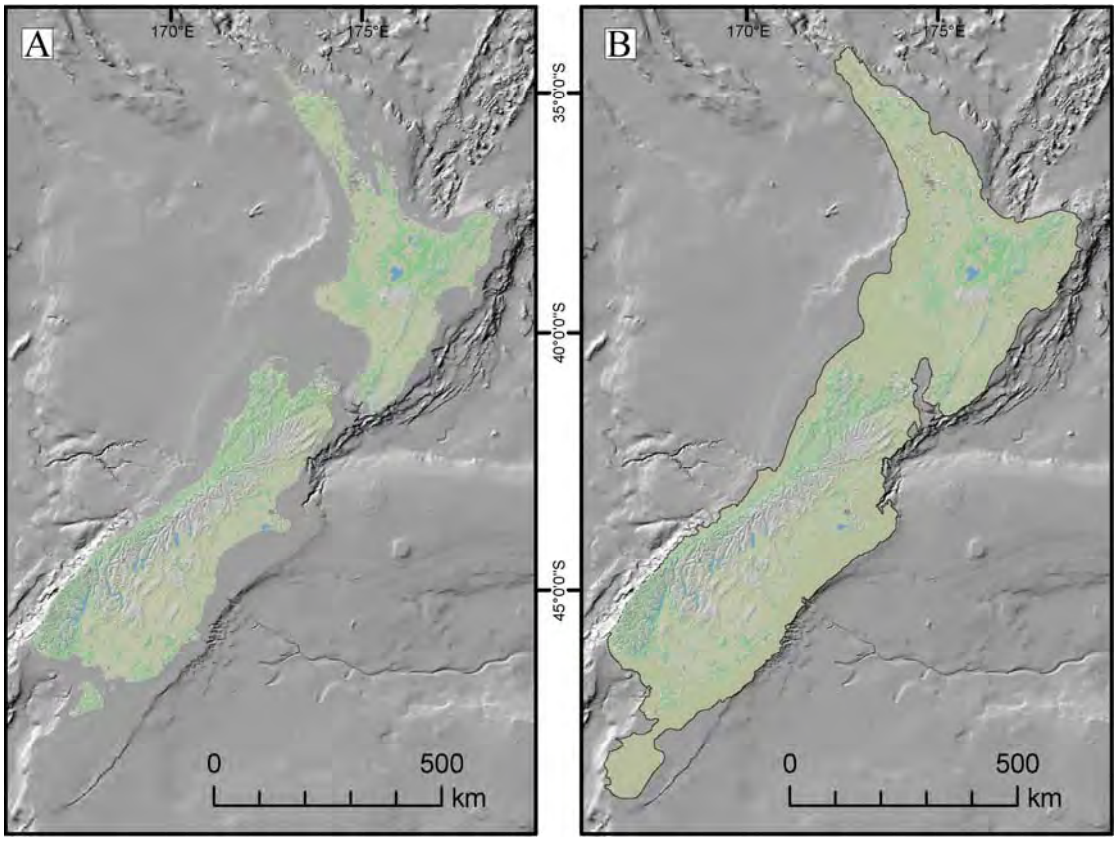

Figure 1.3: New Zealand landmass at sea-level highstand vs lowstand. A) New Zealand under today's sea-level highstand conditions showing the extent of the

landmass and offshore bathymetry. B) New Zealand under sea-level lowstand conditions in the Last Glacial Maximum (LGM), assuming a 120 m drop in sea level. This is an approximation, as the modern -120 m bathymetric contour has been used and so does not account for the last 20 kyrs of tectonic deformation.

It is widely recognised that lowstands are periods of enhanced sediment supply, and evidence of this is well recorded in increased terrigenous sediment fluxes in the deep ocean (Haq, 1991; Carter et al., 2000; Carter et al., 2002). The increased sediment supply reflects increased erosion in glaciated catchments (e.g. Molnar and England, 1990; Hallet et al., 1996; Montgomery, 2002), as well as the change to a colder and wetter climate in non-glaciated areas, likely to enhance slope erosion rates (e.g. Zhu et al., 2008).

There are significant differences in the activity and dominant processes of sea-level cyclicity within submarine canyons. Some canyons remain connected to active coastal littoral systems during highstand periods, typically due to a narrow continental shelf or deep incision of the canyon system into the continental shelf, and can remain perpetually active (e.g. Lewis and Barnes, 1999; Greene et al., 2002; Paull et al., 2003; Smith et al., 2005; Chiang and Yu, 2006; Smith et al., 2007; Lastras et al., 2008). In contrast, many canyons are either confined to the continental slope or are only partially shelf-indenting and therefore do not receive the direct input of littoral material during sea-level highstand periods (Laursen and Normark, 2002; Baztan et al., 2005; Exon et al., 2005b; Noda et al., 2008). While it has generally been accepted that canyons that are removed from highstand littoral systems are primarily active only during sea-level lowstand (Farre et al., 1983; Posamentier et al., 1991), recent studies have shown that this is not always the case and that slope-incised canyons can also remain active during sea-level highstand (e.g. Ogston et al., 2008).

Orbitally forced sea-level cyclicity plays a significant role in the development of continental margins. On passive margins it is widely accepted that this has a first-order role in margin building, with off-shelf erosion and deposition being enhanced during sea-level lowstand (e.g. Vail et al., 1977; Posamentier et al., 1988). On active tectonic margins, such as the Hikurangi Margin of New Zealand, sea-level cyclicity plays a significant role in many aspects of margin development. Furthermore, high-order geomorphic processes including bedrock landslides and gully erosion are subject to the influences of tectonic forcing such as structural deformation and earthquake-generated strong ground motion, which continue regardless of the sea-level cycle.

1.2.2 Regional tectonic forcing

The long-term role of tectonics, through continental margin deformation and the development of structurally generated topography, is a key factor in differentiating canyons on active margins from those on passive margins. The structurally controlled morphology of convergent margins has been well studied, demonstrating the response of bathymetric relief to upper-plate structural deformation (e.g. McAdoo et al., 1996; Liu et al., 2004; McAdoo et al., 2004; Kukowski et al., 2008); the latter may vary in response to variation in the local character of the subducting plate (Dominguez et al., 1998; Kukowski et al., 2008; Morgan et al., 2008). The strong deformational response of the upper plate to asperities on the subducting plate (e.g. seamounts) may control where canyons occur (e.g. Laursen and Normark, 2002). The influence of regional and local structure on canyon alignment and geometry has been investigated on a number of active margins, demonstrating controls such as: the influence of local uplift on channel gradient (Huyghe et al., 2004); the alignment and displacement of canyon axes along faults (Greene et al., 1991); and the deflection of canyon paths around structural ridges (Kukowski et al., 2001; Chiang and Yu, 2006).

In terms of bathymetric data sets, the majority of studies to date concerning geomorphic processes on active margins have been limited to coarse-resolution bathymetric (100+ m) grids, which provide information solely on macro-scale morphology. It is only recently that it has been possible to image details of the effects of tectonic processes in canyon systems using high-resolution (<30 m) continuous-coverage multibeam bathymetry. This allows detailed examination of the relationships between structural deformation, seafloor processes and canyon development (e.g. Greene et al., 2002; Rahiman and Pettinga, 2006), information that cannot be readily gained from coarser-resolution bathymetry.

1.3 Local forcing factors and processes in canyon development

While regional forcing factors define the environment within which canyons evolve, local processes work to directly shape canyon bathymetry. A wide range of processes affect submarine slope development. Some of these might be considered minor, such as biogenic erosion (e.g. Paull et al., 2005), or specific to certain environments (e.g. carbonate dissolution), but some are applicable to a wide range of settings. In the following sections a preferential focus is given to material transport processes. While other processes, such as earthquake-generated strong ground motion, contribute to the development of canyons they do this indirectly through their influence on material transport processes, and this influence is discussed where appropriate.

1.3.1 Current-driven and intermittent fluidised material transport processes

Down-canyon erosional, depositional and sediment-transport fluid-dominated processes have been shown to be fundamental to canyon development and can be divided into: 1) regularly occurring (cyclic) diurnal or seasonal current-flow processes; and 2) intermittent or event-driven grain-flow processes.

Cyclic current flow processes

In addition to processes transporting material across the continental shelf, such as flood events (Palanques et al., 2005), storm events (Puig et al., 2004; Palanques et al., 2008a), and tides (Puig et al., 2003), there are regularly occurring flow processes that have been shown to contribute to both the transport of sediment down and the erosion of submarine canyon systems.

Internal waves and internal tides are an oceanographic process of gravity-influenced waves generated by interactions of tidal currents and bathymetric variability in stratified water bodies (e.g. Garett and Kunze, 2007). Internal tides can be significantly amplified in submarine canyons, by up to an order of magnitude in comparison to open-ocean currents, with enhanced flow occurring in a several-hundred-metre-thick boundary layer in canyon bottoms (Kunze et al., 2002; Lee et al., 2009a). The energy generated by these has been postulated to play a role in material transport within canyon systems, being shown to be capable of inhibiting the deposition of fine-grained material, with bottom current speeds up to 40 cm/s and possible erosion of existing substrate (Cacchione et al., 2002; Xu et al., 2008; Lee et al., 2009b).

Recent work on Mediterranean canyon systems has shown that large bodies of cold, dense water developing on the continental shelf sink and “cascade” down through canyons, predominantly during winter months (Canals et al., 2006; Palanques et al., 2006). This dense water cascading has been shown to be fundamental in both transporting sediment through, and eroding the base of, submarine canyons affected by this process (Lastras et al., 2007; Ogston et al., 2008; Palanques et al., 2008b; Puig et al., 2008).

These bathymetrically affected large-scale current-flow processes are specific to particular locations and require detailed oceanographic studies to provide evidence of their occurrence. While these processes may have a role in many slope canyon systems, without specific knowledge of the in-canyon oceanography, they cannot necessarily be invoked as a contributing process.

Event-driven sediment gravity-flow processes

In contrast to the current processes discussed above, sediment gravity flows (including turbidity currents) have long been accepted as being a dominant mechanism in the erosion of submarine canyons across the range of margin settings and in the cross-margin transport of sediment to the deep ocean (e.g. Daly, 1936). Subsequent to this early work, a significant number of studies have demonstrated their importance to many sub-disciplines, from active seabed processes through to ancient rock records (e.g. review of Mutti et al., 2009).

In recent years some important aspects of the role of sediment gravity flows have been deciphered in the context of submarine canyons, including the direct recording of events (Paull et al., 2003). Sediment gravity-flow events have been shown to be important in a number of aspects of canyon development, including lateral slope erosion and undercutting that may lead to further slope failure (Smith et al., 2005); axial incision in canyon channels (Baztan et al., 2005); in-canyon terrace development (Gaudin et al., 2006); and channel bypass that may lead to canyon avulsion due to canyon wall overtopping by sediment gravity flows (Lamb et al., 2008).

Sediment gravity flows can have a wide range of forms, depending on the concentration of sediment within the flow and the constituent grain size, which determine the formation of end members such as debris flows and turbidity currents (Figure 1.4A). The composition of the sediment significantly affects factors such as velocity, travel distance and erosive capability. Fluidised flows can be initiated by events such as the resuspension of sediment by waves and currents (Wright et al., 2001), but they predominantly develop following mass failure of sediment or bedrock (e.g. Figure 1.4B) (Piper et al., 1999; Hutton and Syvitski, 2004; Talling et al., 2007a; Talling et al., 2007b). Mass failure thus has a significant role in slope development, both through the generation of secondary flow events and through the direct effect of material excavation, transport and deposition.

1.3.2 Bedrock mass failures

Submarine landslide research essentially forms a discipline of its own, with application to the hydrocarbon industry (e.g. Welbon et al., 2007); engineering hazard assessment (e.g. Kvalstad et al., 2005); tsunami hazard assessment (e.g. McAdoo and Watts, 2004); and continental margin evolution studies (e.g. Greene et al., 2002). It is apparent that whenever the morphology of canyons on active margins is described from high-resolution bathymetric data, bedrock landslide scars are ubiquitous features (e.g. Greene et al., 2002;

Rahiman and Pettinga, 2006; Lastras et al., 2008). Findings related to the effect of landslides on submarine canyon development include the significant contribution of bedrock landslides to canyon widening and canyon-head enlargement (Sultan et al., 2004a), and the periodic disturbance to sedimentary systems as landslide dams block canyon axes (Greene et al., 2002).

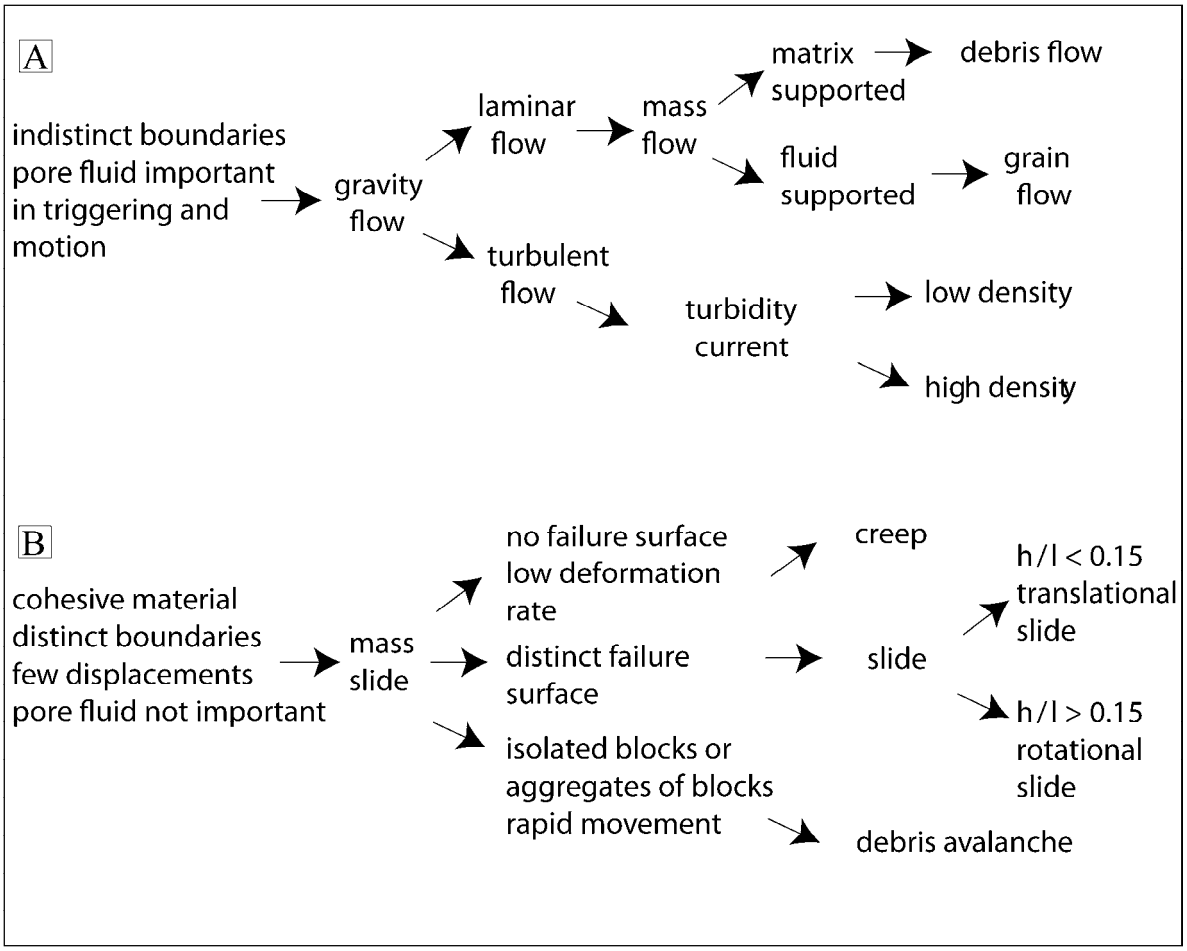

Figure 1.4: Types of submarine landslides. A) End member types of sediment gravity flows, dependent on turbulence, sediment concentration and sediment type. B) Broad classification of cohesive slope failures. Modified from Masson et al. (2006).

Submarine landslides occur on a huge range of scales, from cubic-metre-scale to thousands-of-cubic-kilometre-scale "mega-failures" (Bugge et al., 1988; Moore et al., 1994; Collot et al., 2001). While these mega-failures are uncommon and occur very irregularly across the world's continental margins, landslides at intermediate to smaller scales can be very common and usually cluster in submarine canyon areas (Lee, 2005). Middle-water-depth, higher-resolution multibeam bathymetry (e.g. <30m from Simrad EM300) is able to resolve the geomorphic evidence for slope failures down to scales of tens-of-metres, but it is still

likely to be missing a component of the landslide size spectrum below ~10 m-scales. Nevertheless, the widespread evidence for moderate size landslides within canyons show these are an important process in canyon slope evolution and worthy of further research focus.

Classification of submarine landslides

The first-order classification of submarine mass failures is shown in Figure 1.5, including only broad categories for landslides (vs flows). More detailed classification schemes for submarine landslides have been developed fundamentally as modifications of terrestrial landslide classification schemes (Figure 1.5B). In the classification shown in Figure 1.5A, submarine landslides are divided into five categories related to the initial movement, then into derivative types related to kinematics or subsequent transformation (runout mechanism). This classification is defined in isolation from material type, in comparison to the subaerial classification scheme shown in Figure 1.5B, where each movement category is based on its composition of rock vs engineering soil. This distinction is important, and in the submarine environment it appears that more emphasis has been given to sediment gravity-flow processes and smaller-scale unconsolidated sediment failures than to deeper-seated bedrock mass failures. A further significant point to note is that, while submarine landslides are often mapped as landslide complexes made up of repeated failures resulting in overlapping or adjacent deposits (e.g. Haflidason et al., 2004; Greene et al., 2006), these are interpreted as resulting from multiple events that are mobilising fresh material with each failure event. Submarine landslides termed “active” are typically repeated mass failure at the same location (e.g. Walsh et al., 2006). This differs significantly from subaerial settings, where landslides can be active on daily to seasonal timescales, progressively transporting material downslope. While subsurface strata have been interpreted as resulting from submarine creep or retrogressive landsliding, these have commonly been shown to more than likely be sediment wave deposits (Lee et al., 2002; Berndt et al., 2006). Despite extensive literature searches undertaken as part of this thesis, no accounts have been found of submarine landslide complexes interpreted as active in the sense that landslide material is repeatedly mobile. It is noted that movement within active subaerial landslide complexes is predominantly controlled by precipitation-generated piezometric pressure, whereas submarine landslides are not subject to precipitation as a triggering mechanism.

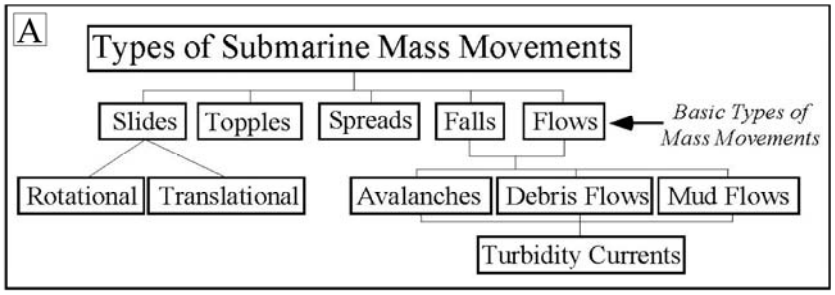

B Types of Subaerial Mass Movement

TYPE OF MOVEMENT		TYPE OF MATERIAL		
		BEDROCK	ENGINEERING SOILS	
			Predominantly coarse	Predominantly fine
FALLS		Rock fall	Debris fall	Earth fall
TOPPLES		Rock topple	Debris topple	Earth topple
SLIDES	ROTATIONAL	Rock slide	Debris slide	Earth slide
	TRANSLATIONAL			
LATERAL SPREADS		Rock spread	Debris spread	Earth spread
FLOWS		Rock flow (deep creep)	Debris flow (soil creep)	Earth flow
COMPLEX		Combination of two or more principal types of movement		

Figure 1.5: Published submarine landslide classification schemes. A) Submarine mass-movement classification, after Locat and Lee (2002). B) Subaerial mass-movement classification, after Varnes (1978).

Triggering mechanism and controls on submarine mass movements

Submarine landslides may be triggered by a range of mechanisms that occur across many environments. The stability of a slope can be described by the Factor of Safety, being the ratio of forces resisting failure to those driving failure (e.g. Morgenstern, 1967). Fundamentally, a slope is brought to the point of failure by forces that reduce the strength of slope materials and/or increase stresses within the slope (Figure 1.6). The majority of slopes into which canyons are incised occur in water depths beyond the shelf break (typically >100m) and so are below storm wave base and the direct influence of tides. Of the processes shown in Figure 1.6, those relevant to slope instability in submarine canyons (depending on the setting) are earthquakes, gas expulsion, diapirism and sedimentation, as well as other processes that may degrade slope materials (e.g. weathering). Additionally, in submarine canyons the effect of slope destabilisation due to channel incision must be considered (e.g. Sultan et al., 2007) as incision "oversteepens" lower slopes of canyon walls. The term "oversteepened slope" is used to describe slopes that exceed the average

continental margin slope. This may come about through canyon axis incision, and also through surface deformation related to propagating tectonic structures. The primary control on the stability of slopes is the development of excess pore-water pressure reducing the shear resistance to failure (Masson et al., 2006). Though excess pore-water pressure is cyclically generated by processes such as earthquakes and rapid sedimentation, and so its occurrence is highly temporally variable, it can be resident in marine sediments for long periods of time (e.g. Leynaud et al., 2007). Specific analysis of landslides in submarine canyons has shown that, while larger failures are sensitive to factors such as earthquake-generated strong ground motion and sediment loading, smaller-scale failures may be initiated in response to canyon channel processes such as sediment gravity-flow erosion of the canyon channel and lower slope (Sansoucy et al., 2007; Sultan et al., 2007).

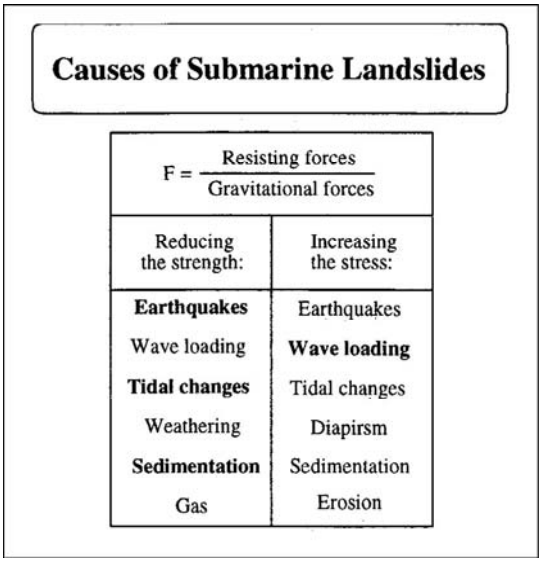

Figure 1.6: Triggering mechanisms in submarine slope instability. Modified from Hampton et al (1996).

Earthquakes are the most widely cited triggering mechanism for submarine slope failure, by inference and by direct correlation (e.g. Piper et al., 1999). While many factors contribute to the instability of slopes, numerical modelling of large mass failures regularly demonstrates that earthquake-generated strong ground motion is required to initiate failure (e.g. Leynaud et al., 2007; Locat et al., 2009). Medium to large bedrock slope failures that occur widely on active tectonic margins, where high levels of earthquake ground shaking are regularly experienced, should significantly contribute to the development of submarine canyons and slope geomorphology. With the increasing resolution of continuous-coverage

multibeam bathymetry data, we are now in a position to determine the relationship between landslides and canyon systems on a regional scale.

1.4 Geomorphic processes from high-resolution multibeam bathymetric data

Since the initial discovery of submarine canyons in the 19th century from point soundings (Dana, 1863), the quality of ocean-floor bathymetry has progressively improved. The advent of swath bathymetry systems has enabled the acquisition of large areas of continuous-coverage bathymetric data from the shelf to the deep ocean in a relatively short period of time. Although this was initially at relatively low resolution, with grids in the order of 100-200 m derived from 12 kHz systems (e.g. Collot et al., 1996; McAdoo et al., 1997b), technological developments (e.g. Simrad EM300) now enable 10–25 m grid resolution in ~50–4000 m water depth. The resulting data from these systems is providing unprecedented detail and quantitative information on the processes that shape the seafloor (e.g. Greene et al., 2002; Laberg et al., 2007; Lastras et al., 2007). A small selection of studies have applied terrestrial quantitative morphometric analysis techniques to bathymetric data as a means of objectively mapping the signature of seafloor shaping processes (e.g. McAdoo et al., 2004; Micallef et al., 2007a; 2008), and quantitative morphometric analysis is expected to become a prominent tool in the emerging field of submarine geomorphology.

1.5 Perceived knowledge gaps and the contribution of this study

High-resolution bathymetry is available for limited areas of a small selection of the global active margins. Since 2001 the National Institute of Water and Atmospheric Research of New Zealand (NIWA) has been mapping significant areas offshore of New Zealand, including large canyon systems on our active margins, using a hull-mounted Simrad EM300 multibeam sonar device on the 70 m Research Vessel RV *Tangaroa*. This thesis project is focused around the use of EM300 multibeam data, together with a variety of seismic reflection data, to elucidate the processes contributing to the evolution of submarine canyons and continental slopes on active tectonic margins, using examples on the Hikurangi subduction margin.

While a huge body of work exists on the development of submarine canyons and submarine slopes, the following knowledge gaps are perceived: 1) the control of actively propagating tectonic structure on shelf-to-trench sediment transfer; 2) the role of bedrock landslides in canyon initiation and enlargement; 3) the processes of sediment redistribution on slopes

during sea-level highstand; and 4) kinematics of submarine slope failures, particularly the development of landslide complexes.

This thesis addresses the following questions:

1. What are the conceptual models of tectonic forcing of canyon systems and submarine slope processes?
2. Can we isolate critical drivers of highstand vs lowstand morphological development of canyon systems and continental slopes?
3. What characterises the role of large bedrock landslides in canyon initiation, canyon enlargement and the long-term evolution of the upper continental slope?
4. Can techniques for the quantitative morphometric interpretation of slope failure processes define activity in landslide complexes?

These questions are addressed by drawing on examples from two primary study sites on the Hikurangi Margin of New Zealand. The two sites offer complimentary insights into processes contributing to canyon system development on active margins. In addition, other minor study sites are drawn on along the central Hikurangi Margin.

The first study site is the Cook Strait sector on the southern Hikurangi Margin, which includes the 1800 km^2 shelf indenting Cook Strait canyon system. From this site the study primarily focuses on tectonic and climatic forcing of large scale submarine canyon systems that cross the continental slope.

The second site is offshore of Poverty Bay on the northern Hikurangi Margin. Here the study looks specifically at processes shaping slopes in the wider submarine canyon system "catchment". While the Poverty Bay study site also contains a large, cross continental slope canyon system; this study does not focus on this canyon.

The two sites have a number of distinct differences; having contrasting tectonic, oceanographic and sedimentary controls. Together the two areas provide comprehensive examples of active convergent-margin processes that can be used to understand holistic controls on submarine canyon system development on tectonically active margins globally.

Chapter 2: Setting of the Hikurangi subduction margin

The Hikurangi Margin has been an active subduction margin for ~24 Ma, having developed through the progressive anticlockwise rotation of the south-eastern part of the New Zealand continent (Walcott, 1978; Lewis and Pettinga, 1993; Nicol et al., 2007) (Figure 2.1A-C). The continent now straddles the boundary of the Pacific and Australian tectonic plates, with opposing subduction zones off the eastern North Island (Hikurangi Margin) and south-western South Island (Fiordland Margin). These subduction zones are linked by transverse and transpressional structures through the western and northern South Island (Figure 2.1D). The Fiordland subduction margin to the south-west of the South Island has a steep continental slope of relatively limited extent, dominated by dextral strike-slip tectonics (e.g. Barnes et al., 2005). In contrast, the Hikurangi Margin is an extensive accretionary margin approximately 600 km long off the eastern North Island. It exhibits world-class examples of active subduction margin features including a well-formed accretionary wedge, structurally generated bathymetry, mega-landslides and numerous submarine canyons (Figure 2.2) (Lewis and Pettinga, 1993; Collot et al., 1996; Lewis et al., 2004; Barnes et al., 2009).

2.1 Morphostructure of the Hikurangi Margin

The offshore Hikurangi Margin is characterised by a variable-width (25-125 km) shelf in the north that narrows to just a few kilometres off Wairarapa (Figure 2.2). The shelf widens again through Cook Strait and then narrows to nothing near Kaikoura at the head of the Hikurangi Trough. Beyond the shelf edge at 120–150 m water depth, the continental slope projects down at a few degrees to the relatively deep (~3000 m) Hikurangi Trough. To the south and east the seafloor ascends to the Chatham Rise and Hikurangi Plateau respectively, defining the depression of the Hikurangi Trough. The Hikurangi Trough widens to the north, hosting the meandering Hikurangi Channel in its axis (Lewis et al., 1998).

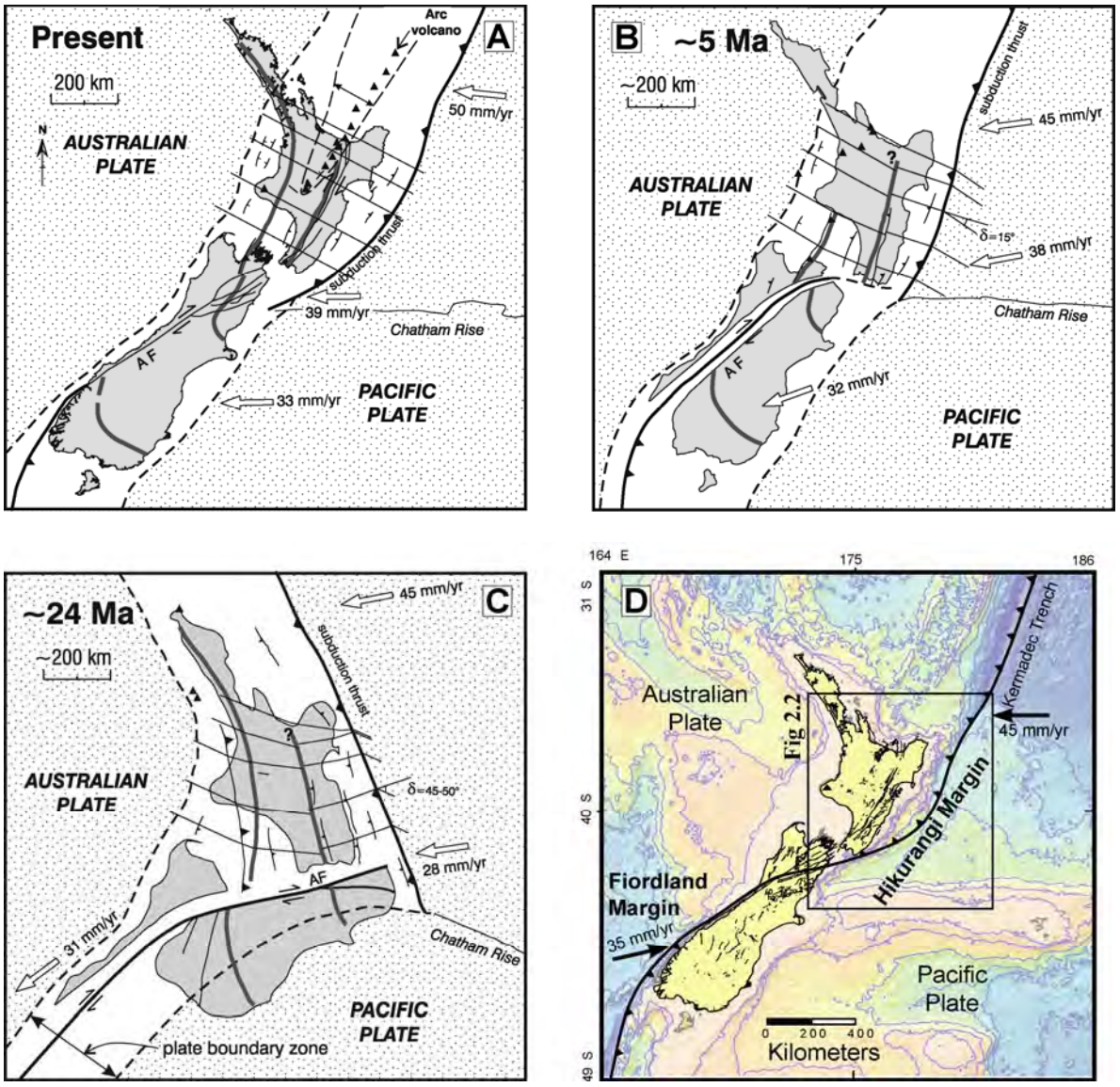

Figure 2.1: Geodynamic evolution of the Hikurangi Margin and the current plate-boundary setting of the New Zealand continent. A-C) Evolution of the Hikurangi Margin subduction zone from its inception at ~24 Ma (panel C) to the present day (panel A). At ~5Ma the landmass has achieved an approximation of the current configuration. Modified from Nicol et al. (2007). B) Current tectonic setting and bathymetric relief of the New Zealand continent sitting astride the Pacific-Australian plate boundary. The distribution of onshore active fault traces are shown as fine black linework. Modified from Barnes et al. (2009).

In cross-section the margin contains the characteristic features of a transpressional subduction arc: 1) a forearc with trough, slope and sedimentary basins; 2) a transverse axial range; and 3) a backarc domain dominated by tectonic extension and volcanism (Figure 2.2 inset). The structure of the forearc domain is primarily characterised by seaward-verging margin-parallel imbricated thrust faults. In more detail, the Hikurangi Margin can be

laterally segmented into the four primary morphostructural domains (shown in Figure 2.2), which are described in the following sections.

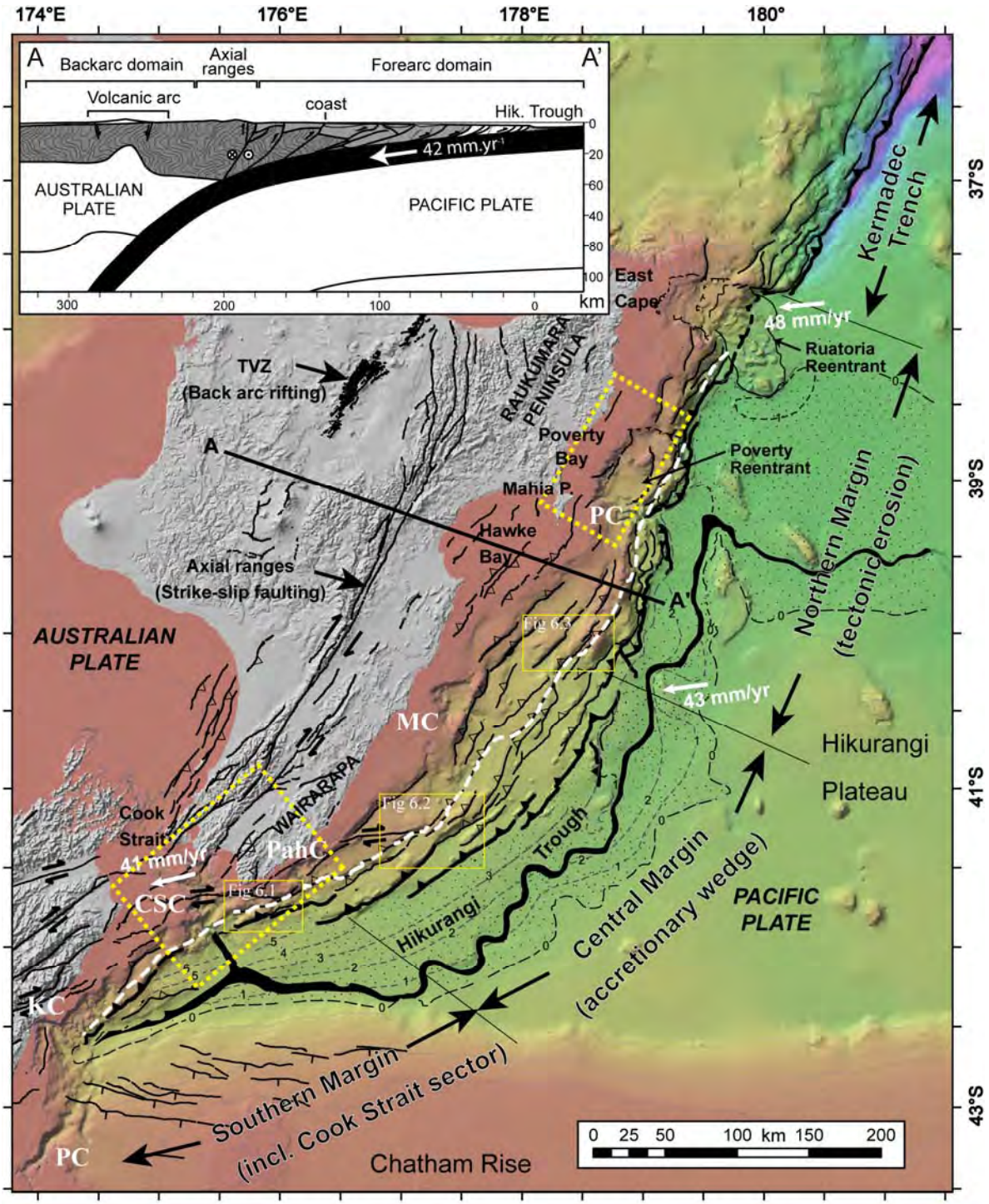

Figure 2.2: The Hikurangi Margin showing onshore and offshore structure and the main structural domains. Abbreviations in white text indicate the major submarine canyon systems: PC Pegasus Canyon; KC Kaikoura Canyon; CSC Cook Strait Canyon; PahC Pahaua Canyon; MC Madden Canyon; and PC Poverty Canyon. The Hikurangi Channel is mapped in black through the Hikurangi Trough, with contours indicating turbidite fill depth in km (Lewis et al., 1998). The dashed white line

running up much of the length of the margin separates the modern accretionary wedge from the deforming pre-subduction backstop. The inset schematic cross-section illustrates the major plate-boundary features. The two main study areas for this project are shown outlined in yellow, and are informally referred to as the Cook Strait sector (in the south) and Poverty sector (in the north). Modified from Barnes et al. (2009).

Southern Kermadec Margin: Sediment starved

To the north-east of the New Zealand landmass, the Hikurangi Trough merges into the Kermadec Trench, where it deepens to over 10 km. This segment of the margin is dominated by the principal plate-boundary thrust, which daylights at the deformation front with minor upper-plate structures mapped on the continental slope (Collot et al., 1996). No canyon systems have been documented on the southern Kermadec Margin segment.

Northern Hikurangi Margin: Seamounts and tectonic erosion

The northern Hikurangi Margin, which encompasses the area from East Cape to the southern end of Hawke's Bay, includes numerous seamounts on the incoming Pacific Plate and exhibits a combination of tectonic erosion in the north and limited accretionary wedge development. Seamounts are exposed at the seafloor in the Hikurangi Trough, encroaching on the deformation front and subducting under the Australian Plate (Lewis and Pettinga, 1993; Collot et al., 1996; Pecher et al., 2005; Barnes et al., 2009). These have a significant effect on the morphostructure of the upper plate, inhibiting the development of a critical taper accretionary wedge, affecting the distribution and mode of structures within the upper plate, and possibly leading to mass collapse. The impact of seamounts on the upper-plate morphostructure is recognised in several other subduction zones (e.g. Masson et al., 1990; Okino and Kato, 1995; Huhnerbach et al., 2005). A range of upper-plate deformation end members reflect factors such as the geometry of the subducting asperity (Dominguez et al., 1998). On the Hikurangi Margin two large-scale seamount-related upper-plate deformations are recognised: the Ruatoria re-entrant and giant debris avalanche (Collot et al., 2001; Lewis et al., 2004); and the Poverty re-entrant (Lewis and Pettinga, 1993; Collot et al., 1996; Lewis et al., 1998).

Offshore upper-plate structure is well constrained from Mahia Peninsula south to southern Hawke's Bay (Barnes et al., 2002; Barnes and Nicol, 2004) and is characterised by compressional faulting between the deformation front and the coast. North from Mahia Peninsula to East Cape, upper-plate structure is poorly constrained and what is know has

been mapped from coarse-resolution bathymetry and poor-quality older vintage MCS (Collot et al., 1996; Field et al., 1997; Lewis et al., 1997). The structure across the Poverty shelf has been reinterpreted as part of this study and is presented in Chapter 5.

Central Hikurangi Margin: Accretion

A well-defined accretionary wedge has developed along approximately 200 km of the central Hikurangi Margin (Lewis, 1980; Pettinga, 1980; Davey et al., 1986a; Davey et al., 1986b; Lewis and Pettinga, 1993). Through the central margin to the south, tectonic deformation is expressed as asymmetric right-stepping margin-parallel thrust-fault-bounded fold ridges (Lewis and Pettinga, 1993; Barnes and Mercier de Lepinay, 1997). The local steepness of these ridges (commonly over 20º) contrasts with the overall gentle slopes of the accretionary wedge, characteristically 2.5º–5º in the upper wedge and 0.4º–1.0º in the lower wedge.

Tectonic structure is well constrained through parts of the central Hikurangi Margin, particularly in the south (Barnes and Mercier de Lepinay, 1997; Barnes et al., 1998a), though significant gaps occur through the shelf area and parts of the northern accretionary wedge. Structure is dominated by compressional faulting, striking margin parallel, but also includes the strike-slip Palliser-Kaiwhata Fault that strikes oblique to the margin and sub-parallel to the nouvel-1A plate-motion vector (Barnes et al., 1998a). As the accretionary wedge tapers to the south, thrust-fault-propagated ridges increase in size.

Southern Hikurangi Margin: Transition to collision

The Southern Hikurangi Margin domain, including the Cook Strait Canyon through to Kaikoura Canyon and Pegasus Canyon at the head of the Hikurangi Trough, defines the southern termination of the Hikurangi Margin. From Wairarapa south, the strike of the margin alters from approximately SSW-NNE (30°) to WSW-ENE (65°), accompanied by an inward (NW) stepping of the deformation front and accommodating the increasing obliquity of plate convergence (Figure 2.2), and then realigns SSW-NNE south of Cook Strait. Structure through this strike change is characterised by both thrust and strike-slip deformation. Thrust faults driving seafloor deformation on the continental slope continue through to Kaikoura Canyon (Barnes et al., 1998a), while the high obliquity of plate convergence is reflected in strike-slip faulting across the continental shelf and into the South Island (Barnes and Audru, 1999b). Modelling suggests that the plate interface is currently locked under the southern North Island (Wallace et al., 2004), with subduction

potentially terminating at Cook Strait. Significant recent work focused on the active structure of central Cook Strait has demonstrated that, while several highly active structures are present, there is no connection between the fault systems of the North and South Islands (Pondard et al., in prep). This work is unpublished and therefore not able to be presented here. Further east on the outer shelf near Cook Strait Canyon and onto the upper slope, structure is relatively well constrained (Barnes et al., 1998a; Barnes and Audru, 1999a), however the detail of mapped structures requires updating in light of data collected subsequent to these studies.

A reinterpretation of the structure in this area is presented in Chapter 4 of this thesis (Mountjoy et al., 2009a).

2.2 Regional geology of the Hikurangi Margin

The stratigraphy of the Hikurangi Margin is clearly complex and reflects both the 25 Ma evolution of the subduction system and pre-subduction geological processes. At the first order, the geology comprises an imbricated accretionary wedge, deforming against a backstop of greywacke basement rocks (e.g. Lewis and Pettinga, 1993). The thick turbidite sequence on the incoming Pacific Plate is being accreted onto the overlying Australian Plate, forming the modern accretionary wedge (Figure 2.2). Inboard of this is a deforming backstop of pre-accretion material. Overlying the offshore accretionary wedge and parts of the emergent wedge are Miocene to recent slope basin and cover sequences (Pettinga, 1982; Lewis and Pettinga, 1993; Barnes et al., 2009). In parts of the continental shelf older Paleogene rocks are exposed at the seafloor as a result of structural exhumation processes (Barnes et al., 2002; Barnes and Nicol, 2004). Quaternary sea-level cycle controlled sedimentary systems tracts occur widely along the length of the margin mantling the shelf and upper slope (e.g. Lewis et al., 2004; Paquet et al., 2009).

Further detail of the geology and stratigraphy of the specific study areas is provided in the relevant chapters.

2.3 Hikurangi Margin oceanography

The ocean currents off the east coast of New Zealand are dominated by the southward-flowing East Cape Current (Figure 2.3A). Between this and the coast, however, flow is northward in the Southland Current (off the South Island) and the Wairarapa Coastal Current (off the North Island).

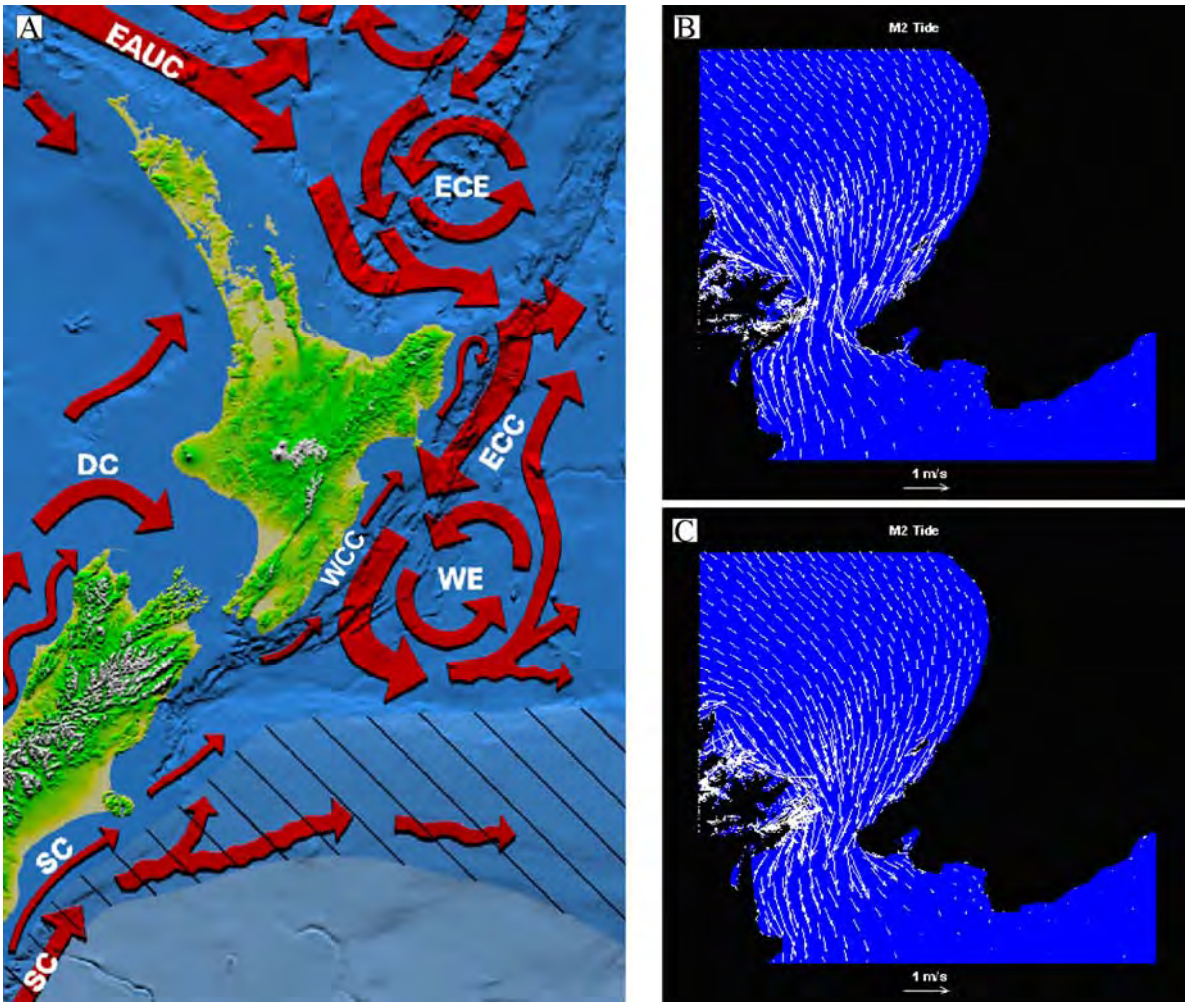

Figure 2.3: Ocean currents in the New Zealand region. A) Major ocean circulation currents of New Zealand including the East Auckland Current (EAUC), East Cape Current (ECC), D'Urville Current (DC), Southland Current (SC), East Cape Eddy (ECE) and the Wairarapa Eddy (WE). Source Carter et al. (1998). B) M2 peak tidal flow in Cook Strait to the north, and C) to the south. Image courtesy of NIWA.

New Zealand is recognised as generally having relatively strong tidal currents (Goring and Walters, 2002). Tidal flows are particularly amplified between the two islands in the Cook Strait seaway, and the strong semi-diurnal M2 tide through Cook Strait is capable of producing currents up to 2 ms (Figure 2.3B&C) (Vennell, 1994). New Zealand also experiences a strong wave climate, reflecting its position in the southern latitudes (e.g. Gorman et al., 2003). The east coast of New Zealand predominantly experiences wave energy from the south and south-southwest, with mean swells of around 1.2 m but with event waves ranging from 14 to >19 m in exposed areas (Stephens and Gorman, 2006).

While little work has focussed specifically on the effects of currents on canyon development in the New Zealand region, studies show that tidal currents strongly affect

surficial seafloor stability in Cook Strait (Carter et al., 1991). Coastal littoral zone processes (wave and current affected) also transport large amounts of sediment north up the coast and into the Kaikoura Canyon head (Lewis and Barnes, 1999).

2.4 Modern sediment-dispersal systems

Sediment input at the coast of eastern New Zealand is dominated by the large river systems in the north-eastern North Island, particularly the Waipaoa and Waiapu rivers (Hicks and Shankar, 2003; Addington et al., 2007; Marden et al., 2008). The modern sediment input from these rivers is 50 Mt/yr, over half the approximately 90 Mt/yr that is introduced to the coast by river systems along the entire length of the Hikurangi Margin (Hicks and Shankar, 2003). The Raukumara Peninsula region thus receives an order of magnitude more sediment than any other east coast region, compared with a total of 1 Mt/yr on the south coast of the North Island. From its arrival at the coast, sediment is either trapped on the continental shelf or transported to the continental slope (Lewis, 1973; Carter, 1992; Foster and Carter, 1997; Orpin, 2004; Addington et al., 2007; Ma et al., 2008; Alexander et al., submitted). The only canyon on the Hikurangi Margin known to receive direct sediment input from coastal sources under the present sea-level regime is the Kaikoura Canyon (Lewis and Barnes, 1999). At the base of the slope the ~2000 km long Hikurangi Channel transports material northward from the southern end of the Hikurangi Margin (Lewis et al., 1998).

2.4.1 Canyon systems

There are three “large” canyon systems on the Hikurangi Margin which cross the continental slope from the shelf edge to the Hikurangi Trough unimpeded: the Poverty Canyon system (Lewis et al., 1998; Orpin et al., 2006); the Cook Strait Canyon (Mitchell and Lewis, 1996; Lewis et al., 1998); and the Kaikoura Canyon (Lewis and Barnes, 1999; Lewis and Pantin, 2002). Several mid-sized canyons occur as upper-slope-to-trough features (Lewis et al., 1998). In addition there are many smaller canyon systems that either head into the upper slope and do not reach the slope base, being baffled by slope basins (Lewis and Kohn, 1973), or head into the mid to lower continental slope.

There has been a modest amount of research focused on Hikurangi Margin canyon systems. The following is a brief summary of available information; canyons are located in Figure 2.2:

- **Pegasus Canyon:** Documented to be mud-draped, suggesting inactivity since the LGM (Herzer, 1979).
- **Kaikoura Canyon:** The primary source of modern sediment input to the Hikurangi Trough and Channel system (Lewis et al., 1998). It receives gravel, sand and mud from the littoral zone and has an estimated input of 1.5 x 10^6 m^3/yr, which accumulates in the canyon head and is likely to fail co-seismically, flushing through the canyon system (Lewis and Barnes, 1999). Turbidites in cores from overbank deposits in the proximal Hikurangi Channel suggest that turbidity currents occur every 300–400 yrs.
- **Cook Strait Canyon:** Little is known about active sedimentary processes within the canyon. The mobility of sand and gravel material through the western Cook Strait shelf area has received the most attention (Carter et al., 1991; Carter, 1992; Lewis et al., 1994; Carter and Lewis, 1995). It has been suggested that upper parts of the Cook Strait Canyon are blocked by large landslides (Carter, 1992), and based on this, the canyon has not been considered to be a significant sediment contributor to the Hikurangi Trough during sea-level highstand (Lewis, 1994; Lewis and Pantin, 2002). There is no age control on turbidity current activity through the Cook Strait Canyon, though cores from the lower canyon do show turbidites in the upper substrate (Lewis and Pantin, 2002).
- **Pahaua Canyon:** Crosses the continental slope from the shelf break to the Hikurangi Trough (Mitchell, 1988). No information is available on the morphology or activity of sedimentary processes in this canyon.
- **Madden Canyon:** A large canyon head that is well incised into the continental shelf (Garlick and Mitchell, 2002). Very little published information is available on this canyon. It is readily apparent from bathymetric maps that the canyon exits to basins on the middle continental slope. The course of the canyon is baffled by thrust-fault-propagated anticlines (Barnes et al., 2009).
- **Poverty Canyons/Poverty Sea Valleys:** The Poverty Canyons and Poverty Sea Valleys (Arron and Lewis, 1992) refer respectively to the upper-slope canyons and main cross-slope canyons that occur within the Poverty re-entrant. These have jointly been referred to as the Poverty Canyon system (Orpin, 2004; Orpin et al., 2006), and this more suitable terminology will be used here. The Poverty Canyon

system is the only direct cross-continental-slope sediment conduit on the central and northern domains of the Hikurangi Margin (Lewis et al., 1998). The large canyon system is incised deeply into the Poverty re-entrant and is partly incised into the continental shelf (Orpin, 2004). Some work has been published on the continental shelf sediment-dispersal system in Poverty Bay (Foster and Carter, 1997; Orpin et al., 2006) and the sedimentation on the continental slope in the Poverty re-entrant (Orpin, 2004; Alexander et al., submitted). There is also a large body of work that has been ongoing for the last few years as part of the NSF funded Margins Source-to-Sink programme (Kuehl et al., 2006). It is apparent that the heads of the Poverty Canyon system are inactive and are experiencing highstand infilling (Walsh et al., 2007).

Canyon systems of the Hikurangi Margin can be summarised in the context of their links to the Hikurangi Trough and Channel (Lewis, 1994; Lewis et al., 1998). At the head of the Hikurangi Trough the Pegasus and Kaikoura Canyon both traverse the continental slope. The Pegasus Canyon is inactive while the Kaikoura Canyon is coupled to the littoral sediment-transport system. Minor canyons here include the Kowhai Sea Valleys. The Cook Strait Canyon is the next canyon north; nothing is known about the amount of sediment fed through this major canyon during sea-level highstand. The Pahaua Canyon crosses the entire continental slope, but likewise, next to nothing is known about this canyon. Between Pahaua Canyon and the Poverty Canyon system, slope canyons exist but are baffled by continental slope basins, and Poverty Canyon is the northernmost canyon on the Hikurangi Margin.

Despite the occurrence of exceptional examples of active margin canyons, only the study of Lewis and Barnes (1999) has specifically dealt with aspects of the sedimentary activity and development of a canyon system on the Hikurangi Margin. A significant amount of data now exists in this region to address questions related to canyon evolution across active margins. For this study, two main sites have been chosen to develop concepts, models and understanding of active margin canyon evolution.

2.5 Chosen study sites for this project

Two primary study sites are chosen to develop models for the development of submarine canyons on active margins: the Cook Strait Canyon and canyons on the adjacent continental slope; and the Poverty Canyon system and gully systems in the Poverty re-entrant. These two sites exhibit contrasting: structural settings; local sedimentary processes; extent of

canyon shelf-indentation; and oceanographic setting. These contrasts provide a comprehensive range of formative controls relevant to canyon development across a wide range of active margin settings. Additional information is drawn from other study sites along the Hikurangi Margin.

The two main areas are imaged with high-resolution bathymetric data from the continental shelf to the Hikurangi Trough, and have varied multi-channel seismic, high-resolution seismic and seafloor sample data. In Chapter 3 details of the data sets are provided.

Chapter 3: Project dataset and general methodology

The dataset for this project draws on data collected by NIWA and the New Zealand Oceanographic Institute (NZOI) over the last ~50 years. In addition, data is been available from other sources including petroleum industry surveys, government-funded petroleum surveys and internationally funded science surveys. I have had the good fortune to contribute to planning additional data acquisition during the course of this doctoral project. The following sections outline available data (most but not all of which will be presented or discussed in this thesis), details of the processing carried out prior to my receiving the data, and, where applicable, details of subsequent data processing required.

This chapter also includes a section on methodology which outlines software used and general methods of data analysis. Specific methodologies are covered in the appropriate chapters.

3.1 Regional bathymetry

Regional bathymetry for the Hikurangi Margin draws on NIWA's coastal and regional bathymetry database, which has been an evolving data-compilation project from the inception of NZOI, with areas being upgraded as new data is acquired. The database is in the form of bathymetric contours, available for most of the offshore Hikurangi Margin shelf, slope and trough in increments of 10 m to 200 m depth and 50 m thereafter to approximately 3500 m for the coastal bathymetry. The regional bathymetry dataset has 50 m contour intervals to 200 m and 250 m contour intervals thereafter, which continue to 9250 m depth in the Kermadec Trench. Data sources for the coastal bathymetry include single-beam echo soundings and multibeam swath soundings.

A continuous regional bathymetric grid has been constructed at 100 m cell size covering the Hikurangi Margin shelf and slope from north of East Cape to the south-eastern tip of the North Island (Figure 3.1). This was formed from contours extracted from the coastal bathymetry database, with additional contours from the regional bathymetry database in

deeper water using the "topo to raster" command in Esri ArcMAP®. An additional 100 m resolution grid is available for the southern Hikurangi Margin (Barnes et al., 1998b).

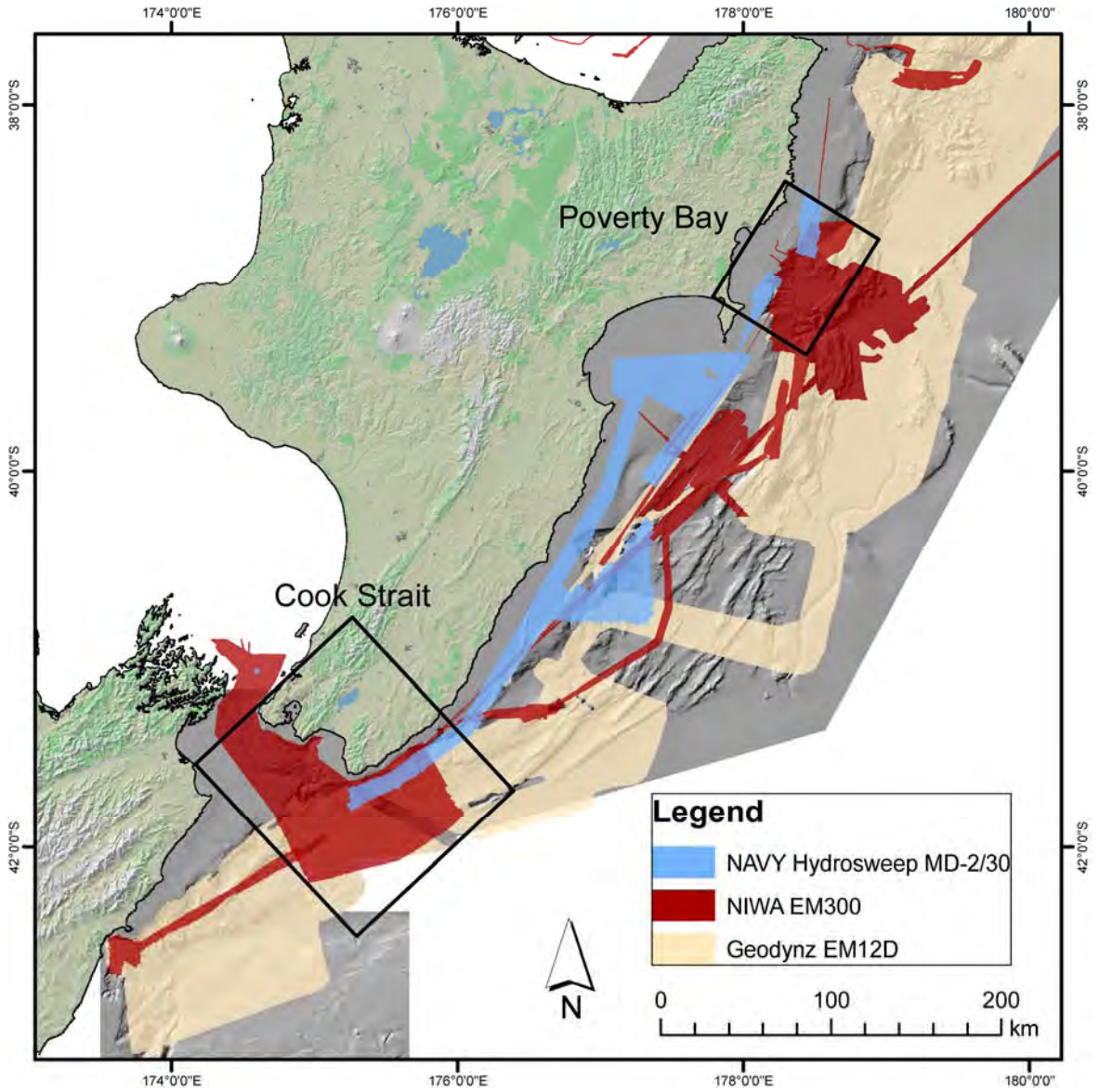

Figure 3.1: Distribution of bathymetry grids on the Hikurangi Margin. The underlying greyshade shaded-relief map is based on a 100 m grid constructed from the NIWA coastal and regional bathymetry contour databases. The specific surveys shown are the regional 12 kHz GeodyNZ multibeam survey (yellow); selected NIWA 30 kHz surveys (red); and Royal Navy 30 kHz surveys (blue). The location of the two study sites at Cook Strait and Poverty Bay are shown.

3.2 High-resolution bathymetry

As the primary focus areas of this study are Cook Strait and Poverty Bay, a detailed description of the multibeam dataset for these two areas is given. The multibeam extent and

instrument type covering additional areas addressed within the thesis are shown in Figure 3.1.

Most multibeam data has been collected using NIWA's 30 kHz system. The RV *Tangaroa* has a hull-mounted Simrad EM300 multibeam system, operating 135 beams at 30 kHz frequency, with approximately 1° beam width. Surveys are undertaken to International Hydrographic Organisation (IHO) standards. Shipboard navigation comprises a POS/MV system with differential GPS. Navigational accuracy is ± 5 m and vertical accuracy in 1000 m water depth is ± 2 m.

Additionally, multibeam data has been collected by the Royal New Zealand Navy for hydrographic purposes (to IHO standards), using an Atlas Hydrosweep MD-2/30 system and processed in Caris HIPs to 10 x 10 m bin size. This system has a manufacturer-stated accuracy of ± 0.15 m + 0.2% water depth.

3.2.1 Cook Strait

Details of the Cook Strait multibeam dataset are also provided in Chapter 4. Five EM300 surveys were carried out in Cook Strait between 2002 and 2005, covering an area of approximately 8400 km^2 (TAN0204, TAN0211, TAN0215, TAN0309 and TAN0510). Data from four of these surveys was stitched into a seamless grid at 10 m resolution. The fourth survey grid (TAN0510) was also processed at 10 m resolution. This fine grid scale revealed several NODATA holes. The two grids were combined in ESRI ArcGIS using "mosaic to new raster" and then the NODATA gaps were removed. For this a focal mean command (e.g. "focalmean ([ELEVGRID], rectangle, x, x, data") was employed in "single output map algebra". This was run three times using a 5 x 5 cell focal mean, which means the NODATA gaps were progressively filled from the data edges inward using a mean interpolation. The result of this was a seamless 10 m resolution grid across the entire canyon system, upon which subsequent analysis was based.

Atlas Hydrosweep MD-2/30 multibeam data from the Royal New Zealand Navy is also used (Figure 3.1), as provided in 10 m grids processed in Fledermaus®.

3.2.2 Poverty Bay

The primary multibeam dataset in Poverty Bay comes from a 2001 EM300 survey (TAN0106). This was gridded during acquisition to 25 m in HydroMap®. Subsequently, selected lines covering the upper slope were reprocessed to 10 m resolution in HydroMap®. Two additional EM300 surveys collected in 2006 and 2008 (TAN0613 and TAN0810) are

available, as well as two small amounts of data collected on voyage transits (TAN0803 and TAN0805).

Simrad EM1000 data made available online by the NSF Margins programme (http://www.marine-geo.org/tools/search/entry.php?id=KM0503) was reprocessed to 10 m resolution using HydroMap® (limited distribution not shown in Figure 3.1).

Atlas Hydrosweep MD-2/30 multibeam data from the Royal New Zealand Navy is also available for this area (Figure 3.1), as provided in 10 m grids processed in Fledermaus®.

3.2.3 Other areas

Additional Simrad EM300 and Atlas Hydrosweep MD-2/30 multibeam datasets are available from across the Hikurangi Margin (Figure 3.1). Where used, this data is in its as-provided grid form. Data presented in Chapter 6 has been developed for Barnes et al. (2009); for details on this multibeam dataset, refer to that manuscript (Appendix II).

3.3 Multichannel seismic

A large amount of multichannel seismic (MCS) data is available along the length of the Hikurangi Margin, ranging from 1960s era single-channel data of marginal quality to contemporary high-quality multichannel data. The distribution of this is not always systematic and coverage is limited in some areas. Figure 3.2 shows the MCS surveys that have been used in this study, in the context of the wider margin. Where specific lines are reproduced, these will be accompanied by more detailed location maps.

3.3.1 Cook Strait

MCS datasets available in Cook Strait include:

1. Petroleum industry surveys: Magellan Petroleum NZ Ltd, 1969; Mobil Oil, 1972; and Gulf Oil, 1973. 3-12 fold multichannel seismic profiles (Uruski, 1992; Barnes and Mercier de Lepinay, 1997; Barnes et al., 1998a; Barnes and Audru, 1999a; b).
2. RV *l'Atalante,* 1992 (GEODYNZ-SUD). 6 channel seismic profiles using twin 75 cubic inch GI guns. Data was collected at underway speeds (~10 knots) (Collot et al., 1994; Collot et al., 1996; Barnes and Mercier de Lepinay, 1997; Barnes et al., 1998a).
3. RV *Sonne,* 2007 (SO191 New Vents). 32 channel seismic profiles using a GI gun source in 250/105 mode (Bialas et al., 2007; Barnes et al., 2009).

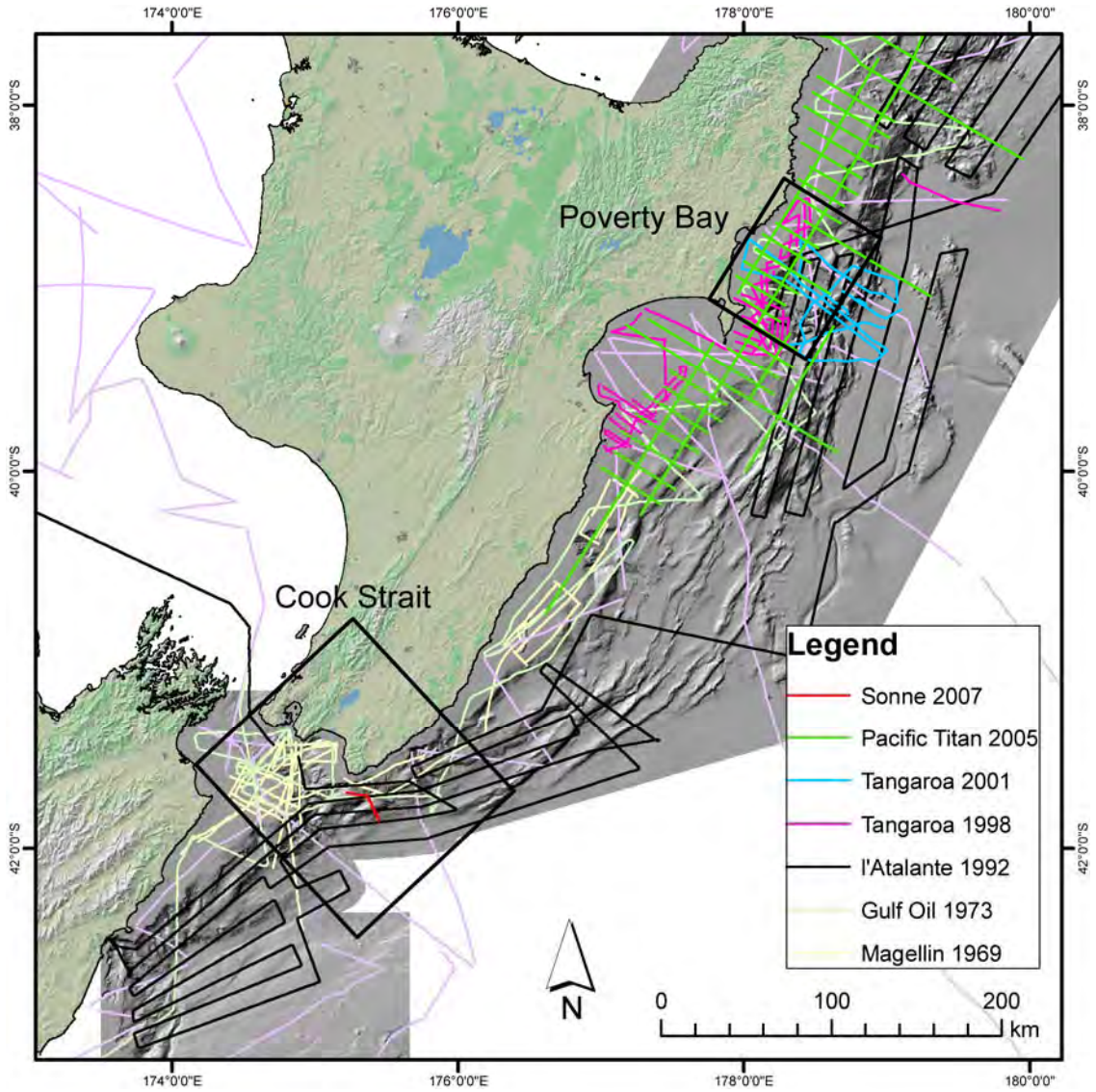

Figure 3.2: Distribution of multichannel seismic surveys used in the study, shown in the context of the wider Hikurangi Margin. The location of the two study sites at Cook Strait and Poverty Bay are shown.

3.3.2 Poverty Bay

MCS datasets available in Poverty Bay include:

1. RV *l'Atalante*, 1992 (GEODYNZ-SUD). 6 channel seismic profiles using twin 75 cubic inch GI guns. Data was collected at underway speeds (~10 knots) (Collot et al., 1994; Collot et al., 1996; Barnes and Mercier de Lepinay, 1997; Barnes et al., 1998a).

2. RV *Tangaroa*, 1998 (CR3044). 6 fold, 24-channel seismic profiles using a GI gun source in 45/105 mode (unpublished).

3. RV *Tangaroa*, 2001 (TAN0106). 6 fold, 24-channel seismic profiles using a GI gun source in 45/105 mode (unpublished).
4. MV *Pacific Titan*, 2005 (CM05). 960-channel high fold 2D seismic reflection data recorded to 12 seconds TWT (Multiwave, 2005).

3.4 High-resolution seismic

High-resolution seismic reflection data used in this study is 3.5 kHz data collected while underway on a variety of multibeam voyages and held in NIWA's archives. Data is held as hard copy records of variable quality and, more recently, as digital records only. Figure 3.3 shows a plot of 3.5 kHz lines available for this study in the context of the wider margin. Where specific lines are reproduced, these will be accompanied by more detailed location maps.

3.5 Seafloor samples

A large collection of seafloor sample data is held in the NIWA archives, including rock dredges, short cores and grab samples. Analysis of these archived samples ranges from none to detailed stratigraphic and physical properties logging, and dating of material (Carter, 1992; Foster and Carter, 1997; Barnes et al., 1998a; Barnes and Audru, 1999a; b; Lewis and Pantin, 2002; Orpin, 2004; Orpin et al., 2006). The distribution of seafloor samples is not presented in this chapter, but where specific samples are referred to these are accompanied by location maps.

3.6 Methodology

The datasets dealt with in this project are inherently spatial datasets and therefore most suitable for analysis in a GIS framework. Numerous tools have been used to analyse the various data types to develop derivative datasets. In this section, tools and methodologies that have been widely used for multiple datasets are covered.

3.6.1 Spatial data manipulation and mapping

The primary software used for this project has been the proprietary GIS software, ESRI's ArcGIS®. Initially this was version 9.1 and subsequently version 9.2 as this upgrade was rolled out halfway through the project. Three software packages within the ArcGIS® suite have been utilised: ArcCatalogue®, ArcView® and ArcScene®.

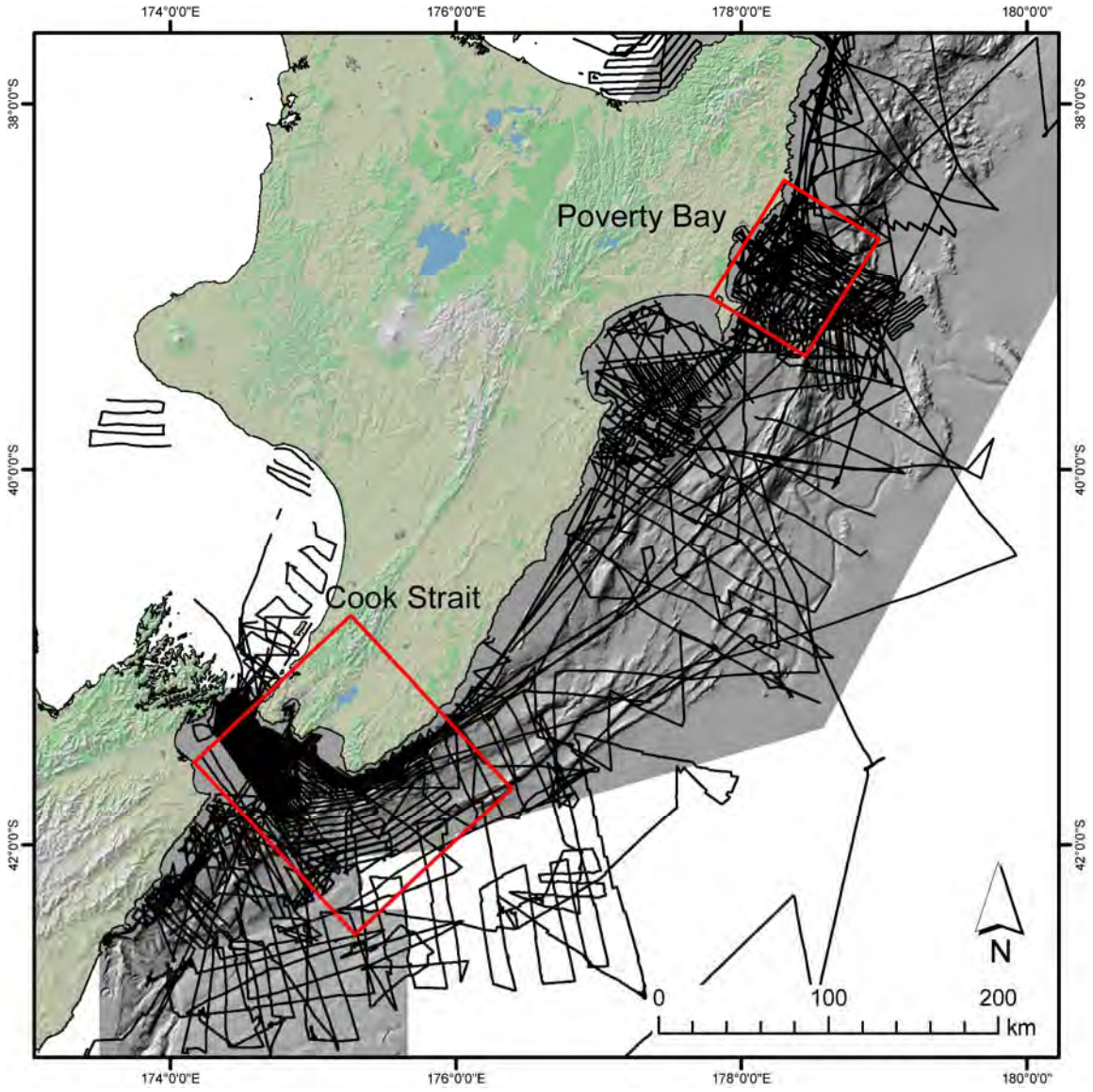

Figure 3.3: Distribution of high resolution seismic surveys examined in the study, shown in the context of the wider Hikurangi Margin. The location of the two study sites at Cook Strait and Poverty Bay are shown.

The majority of geomorphic mapping has been undertaken directly on screen within the ArcView® environment, using DTM derivatives including shaded-relief maps, slope-gradient maps and aspect maps. During the mapping process, perspective views of the bathymetry in ArcScene® have been used to assist interpretation.

In addition to the standard Spatial Analyst toolbox tool suite, several freeware add-in programmes have been utilised. These include: X-Tools, ET-Geowizards, TauDEM and, Hawths Tools, all of which have proved invaluable for streamlining many processes and tasks. A significant amount of help has been gained from the ESRI Knowledge Web.

All spatially referenced figures have been developed in the ArcGIS® environment and exported for manipulation in graphics software.

3.6.2 Seismic interpretation

Seismic interpretation has been carried out using a combination of digital and analogue data.

Geographix Seisvision®

The majority of MCS data held by NIWA is stored in the proprietary oil industry seismic data interpretation software Geographix Seisvision®. This software has been exceptionally useful for detailed wavelet-scale interpretation, particularly relating to landslide deposits and tracing stratigraphic horizons. The software also enables data interpolation (e.g. kriging) to construct three dimensional surfaces. Seisvision® has also proved useful for exporting digital-format postscript images of seismic profiles with user-defined vertical exaggeration for presentation purposes, and in some instances interpretations made within Seisvision® have also been exported.

Hard copy bench plots

The majority of structural interpretation of MCS data has been carried out on hard copy bench plots, generally plotted on 600 mm roll paper at 2.5 times vertical exaggeration. The perspective gained from a plotted seismic section is difficult to replicate in the digital environment, and this technique is considered invaluable in making robust seismic interpretations.

Structure maps have been developed from MCS interpretations by using A0 sized base maps with ship navigation, bathymetry, sample data and relevant existing mapping plotted. Tectonic structures mapped as active in MCS have been cross-checked against high-resolution seismic reflection data to confirm Holocene activity. 3.5 kHz and Boomer datasets are predominantly available as shipboard plots, though more recent 3.5 kHz data is available in digital format. Any direct interpretation onto high-resolution datasets has required photocopying of the relevant sections. 3.5 kHz shipboard plots typically have very high vertical exaggeration (50–100 times), which needs to be accounted for. Once hard copy base maps are finalised, these have been scanned, spatially referenced and digitised into ArcGIS®.

3.6.3 Graphics production

The majority of graphics have been developed in Adobe Illustrator®. Graphics exported from ArcGIS® have been created as .eps files that retain the separate layering structure. Likewise tiffs from Seisvision® and other sources are imported into Illustrator® for subsequent manipulation.

3.6.4 Additional software

Other software used during this project includes: Fledermaus, HydroMap, Matlab, AutoCad, Grapher and the ubiquitous Microsoft Office suite.

Chapter 4: The Cook Strait sector

The Cook Strait sector of the Hikurangi Margin is an unofficial term coined by Mountjoy et al (2009a) referring to the southern part of the Hikurangi Margin in the Wairarapa–Cook Strait region (Mountjoy et al., 2009a - Figure 1). The sector includes the Pahaua Canyon on the thrust-ridge-dominated Wairarapa slope, some smaller unnamed canyons, and the largest canyon on the Hikurangi Margin, the Cook Strait canyon system. The contrast between the very large multi-branching and shelf-indenting Cook Strait Canyon and the smaller slope-confined canyons on the Wairarapa slope provides an excellent opportunity to study canyon evolution, and to gain insights into what the dominant controls on canyon form, location and geometry are. It is also recognised that landslide scarring is widespread in the Cook Strait Canyon (Barnes, 2005; Berryman, 2005), though very little work has been undertaken to understand these features, either on an individual case study basis (as is often the case with submarine landslides) or holistically to assess their role in canyon development. The Cook Strait sector of the Hikurangi Margin, including the shelf area through Cook Strait to the north, is imaged with Simrad EM300 multibeam data at 10 m grid size (see Figure 3.1). This provides an excellent dataset upon which to analyse the morphological "signature" of processes shaping the seafloor.

Concurrently with this project, several other studies have been undertaken, or are in progress, that broadly relate to this work:

- "Its Our Fault" is a multi-disciplinary project funded by the NZ Earthquake Commission (EQC) to better understand the likelihood and size of large earthquakes in the Wellington region to increase the city's resilience to earthquake hazard (Van Dissen et al., 2009). As part of "Its Our Fault" NIWA was subcontracted by project leaders GNS Science to compile slip-rate data on offshore structures (Barnes et al., 2008). Primarily the NIWA component of "Its Our Fault" has been undertaken by NIWA staff Dr N. Pondard and Dr P. Barnes, focussing primarily on obtaining paleo-earthquake data from Boomer seismic records (Pondard et al., in prep). This thesis project has contributed to "Its Our Fault" in terms of a reinterpretation of the major tectonic structures in the outer-shelf canyon area and on the Wairarapa slope

(Mountjoy et al., 2009a). This work has been incorporated into the regional structure map used for derivative modelling work in the "Its Our Fault" project.

- Ongoing work by NIWA researchers Dr S. Nodder and Dr C. Law on the time-varying expulsion of methane from vent sites on the Wairarapa slope has linked into this thesis project from the perspective of contributing to the understanding of the structural model of venting sites (Law et al., 2009).
- Related to this, the Wairarapa vent site was chosen as a case study for the 2006 "New Vents" project involving a survey by the German research vessel RV *Sonne* (Bialas et al., 2007). Significant work has now been undertake to characterise this active methane vent site and the data and interpretations from this thesis project have contributed to a regional characterisation of vent sites along the Hikurangi Margin and landslide mapping in several locations (Barnes et al., 2009).

Structure of this chapter

This chapter of the thesis brings together the body of work undertaken in the Cook Strait sector of the Hikurangi Margin. In Section 4.1 the main study of the canyon systems is presented as a now published manuscript (Mountjoy et al., 2009a). This manuscript forms the bulk of the chapter and covers the background information for the study area, building on that presented in Chapter 2. In the second part of the chapter (Section 4.2) results and discussion of the fluid-venting systems on the Wairarapa slope are presented. Where figures are referred to from the Mountjoy et al. (2009a) manuscript these are referred to as e.g. (Mountjoy et al. (2009a) - Figure 4).

4.1 Morphostructure and evolution of submarine canyons across an active margin: Cook Strait sector of the Hikurangi Margin, New Zealand (Mountjoy et al., 2009a)

This section comprises a manuscript presented in its published form.

Mountjoy, J.J., Barnes, P.M. and Pettinga, J.R., 2009. Morphostructure and evolution of submarine canyons across an active margin: Cook Strait sector of the Hikurangi Margin, New Zealand. *Marine Geology*, 260(1-4): 45-68.

Marine Geology 260 (2009) 45–68

Contents lists available at ScienceDirect

Marine Geology

journal homepage: www.elsevier.com/locate/margeo

Morphostructure and evolution of submarine canyons across an active margin: Cook Strait sector of the Hikurangi Margin, New Zealand

Joshu J. Mountjoy [a,b,*], Philip M. Barnes [b], Jarg R. Pettinga [a]

[a] Dept. Geological Sciences, University of Canterbury, Private Bag 4800, Christchurch, New Zealand
[b] National Institute of Water and Atmospheric Research Ltd, Private Bag 14901, Wellington, New Zealand

ARTICLE INFO

Article history:
Received 23 June 2008
Received in revised form 19 January 2009
Accepted 30 January 2009

Keywords:
submarine landslide
submarine canyon evolution
morphostructure
submarine base-level
active margin
high stand activity

ABSTRACT

The Cook Strait sector of the Hikurangi Margin contains several canyons including New Zealand's largest canyon, the multi-branched shelf-indenting Cook Strait Canyon. The morphology of the canyons reflects the transition from subduction related thrust faulting to oblique collision and strike–slip faulting. High resolution EM300 multibeam and multichannel seismic reflection data reveal: i) widespread, deep-seated bedrock landsliding as a principal control on canyon enlargement; ii) a retrogressive entrenchment of tributary submarine catchments in response to a base-level perturbation which has rejuvenated canyons inferred to have been inactive as top to bottom sediment conduits since the last glaciation; and iii) the control of structurally generated bathymetric relief on both the routing of sediment pathways and the erosion of inter-canyon slopes. The models of canyon evolution demonstrated here have widespread implications for canyon development and evolution on other tectonically actively continental margins.

1. Introduction

Large submarine canyon systems occur on active tectonic margins around the world and act as principal sediment conduits from the shelf to deep ocean basins (Lewis and Barnes, 1999; Milia, 2000; Laursen and Normark, 2002; Chiang and Yu, 2006). Studies of submarine canyons date from their first documentation well over a century ago (e.g. Dana, 1880) and cover many aspects such as: i) their initiation and development in both an upslope and downslope fashion (Shepard, 1981; Pratson et al., 1994; Pratson and Coakley, 1996); ii) their erosion by turbidity currents (e.g. Daly, 1936; Shepard, 1963; Shepard and Dill, 1966; Mulder et al., 1997; Mitchell, 2006); and iii) the regional and local structural influence on canyon alignment and geometry (Nagel et al., 1986; Mascle et al., 1990; Greene et al., 1991; Kukowski et al., 2001; Greene et al., 2002; Huyghe et al., 2004; Chiang and Yu, 2006; Rahiman and Pettinga, 2006).

Many previous studies have been limited by the lack of detailed bathymetric data over large areas since up until c. 10 yrs ago the spatial resolution of bathymetric grids has been limited to 100 m or more. This relatively low-resolution bathymetry has limited the ability to resolve geomorphic features at the level required to "fingerprint" smaller scale, high recurrence erosional processes. For example, on tectonically active margins, mass wasting on a variety of spatial scales, often triggered by frequent seismic ground-shaking, can be a significant process in the evolution of canyon landscapes (e.g. Hampton et al., 1996; McAdoo et al., 2004). Furthermore, moderate sized failures (e.g. volumes in the order of 10^8–10^9 m^3) have higher recurrence times than easily defined "mega-failures" (>10^{10} m^3) (e.g. Collot et al., 2001). These smaller scale failures may only be fully evident in high resolution bathymetry and such features may pose a significant tsunami hazard (e.g. McAdoo and Watts, 2004; Rahiman et al., 2007). With the advent of high resolution multibeam swath mapping technology over the last decade, large areas of submarine canyon geomorphology can now be mapped in detail from continental shelf to deep ocean depths (e.g. Greene et al., 2002; Baztan et al., 2005; Gaudin et al., 2006; Lastras et al., 2007; Smith et al., 2007; Xu et al., 2008).

In this study we use high resolution Simrad EM300 multibeam data, combined with high resolution and multichannel seismic reflection profiles, to examine the morphostructural submarine landscape evolution of major shelf-incising canyons on the active tectonic eastern margin of central New Zealand. We characterise the dominant erosive processes as a function of active tectonic forcing at a variety of spatial and temporal scales and discuss the influence of active tectonic structures on the morpho-evolution of the 1800 km^2 Cook Strait canyon system. Comparison with canyons incised into the adjacent continental forearc slope allows us to develop models of morphostructural forcing for multiple contrasting situations. Because these systems are major sediment conduits, associated with high rates of sedimentation, sealevel cyclicity, subduction related thrust and

* Corresponding author. National Institute of Water and Atmospheric Research Ltd, Private Bag 14901, Wellington, New Zealand. Tel.: +64 4 3860336.
E-mail address: J.Mountjoy@niwa.co.nz (J.J. Mountjoy).

0025-3227/$ – see front matter © 2009 Elsevier B.V. All rights reserved.
doi:10.1016/j.margeo.2009.01.006

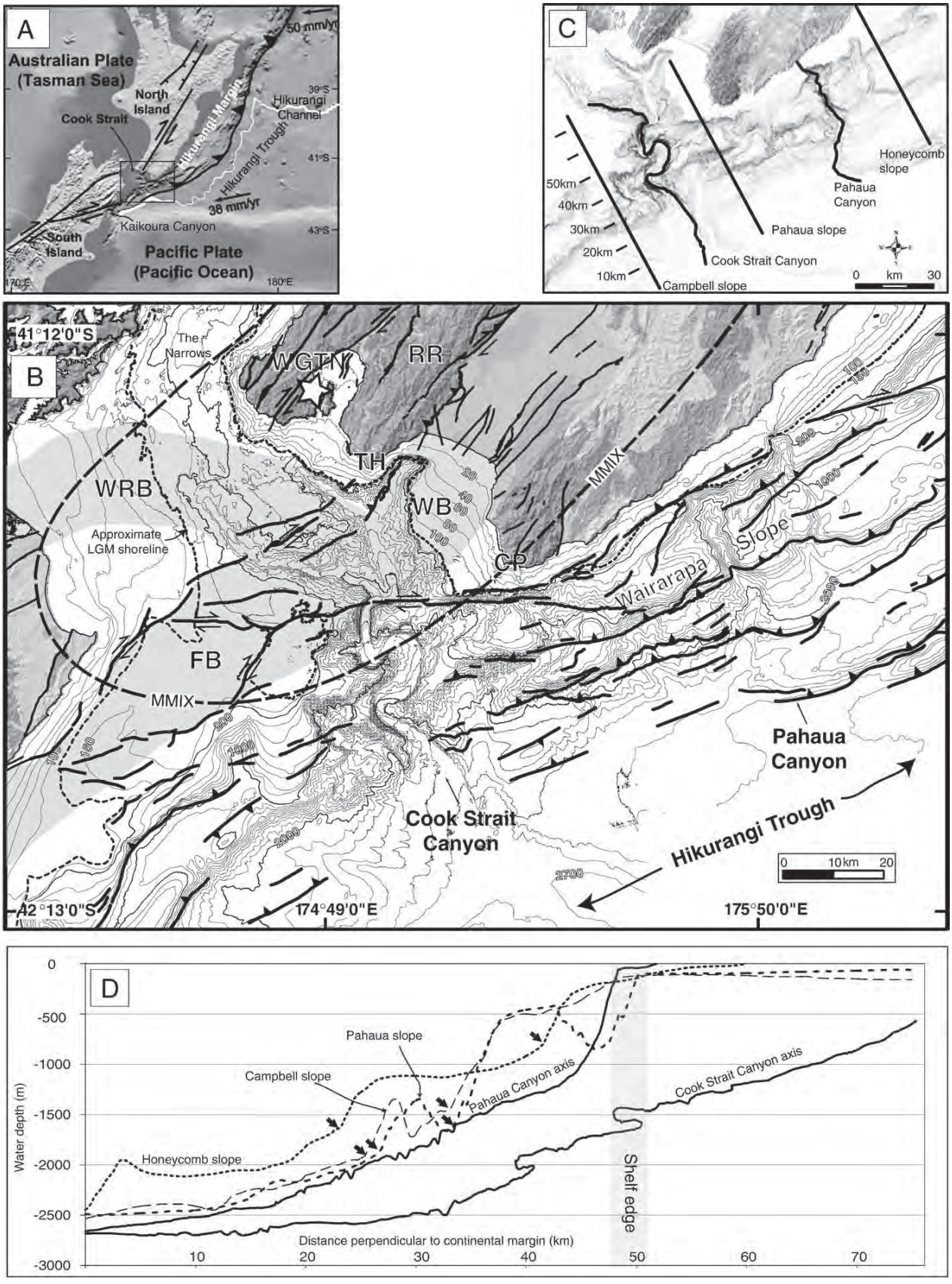
A
Australian Plate
(Tasman Sea)
North
Island
Cook Strait
Hikurangi Margin
Hikurangi Channel
Hikurangi Trough
50 mm/yr
38 mm/yr
39°S
41°S
43°S
Kaikoura Canyon
South
Island
Pacific Plate
(Pacific Ocean)
170°E
180°E
C
Honeycomb
slope
Pahaua
Canyon
Pahaua slope
50km
40km
30km
20km
10km
Cook Strait Canyon
Campbell slope
0 km 30
B
41°12'0"S
The
Narrows
WGTN
RR
TH
WRB
WB
MMIX
Approximate
LGM shoreline
CP
Wairarapa
Slope
FB
MMIX
Pahaua
Canyon
Cook Strait
Canyon
Hikurangi Trough
0 10km 20
42°13'0"S
174°49'0"E
175°50'0"E
D
Water depth (m)
0
-500
-1000
-1500
-2000
-2500
-3000
Pahaua slope
Campbell slope
Pahaua Canyon axis
Cook Strait Canyon axis
Honeycomb slope
Shelf edge
Distance perpendicular to continental margin (km)
10
20
30
40
50
60
70

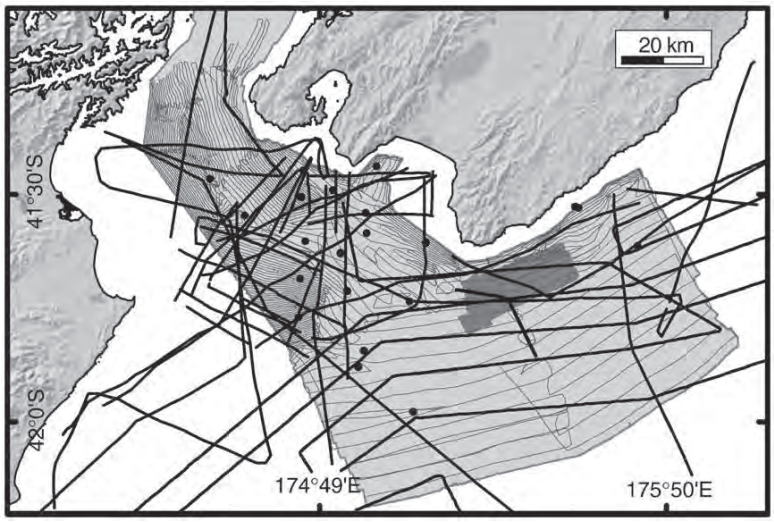

Fig. 2. Data set used in this study. Main NIWA multibeam coverage indicated by the grey polygon with associated 3.5 kHz tracks as fine weight lines. Additional Royal NZ Navy multibeam data coverage indicated by darker grey polygon. Multichannel seismic tracks from multiple scientific and industry surveys shown as heavy weight lines. Dots show locations of selected seabed samples.

strike–slip faulting and high recurrence earthquake generated ground shaking; they offer an excellent opportunity to decipher the fundamental drivers of canyon geomorphology on active margins.

2. Regional setting

2.1. Tectonics

The eastern margin of New Zealand's North Island is characterised by an active subduction zone referred to as the Hikurangi Margin (Fig.1A). Subduction of the Pacific Plate under the Australian Plate becomes increasingly oblique from north to south, until the relative Plate motion is ~38 mm/yr at 050° oblique to the plate margin at the "Cook Strait sector" of the Hikurangi Margin (Lewis and Pettinga, 1993; DeMets et al., 1994; Collot et al., 1996; Barnes et al., 1998). Oblique subduction has formed a tapered and highly deformed subduction wedge terminating at Cook Strait, with a frontal accretionary wedge narrowing from approximately 80 km at 41° S to approximately 13 km some 100 km to the south west. The rate of convergence of the eastern margin relative to the subducting Pacific Plate is about 20–25 mm/yr (Wallace et al., 2004). Reflecting its location at the transition from oblique subduction to continental collision, Cook Strait is traversed by a combination of active thrust and strike–slip faults (Collot et al., 1996; Barnes et al., 1998; Barnes and Audru, 1999a,b).

2.2. Physiography, oceanography and sediment supply

Cook Strait links the Tasman Sea with the Pacific Ocean through central New Zealand, pinching to just 22 km in width at "the Narrows" and widening to over 80 km in the south (Fig. 1). Much of the seabed is at water depths of less than 150 m except through The Narrows where depths reach >300 m, and to the south east in the Cook Strait canyon system. The Cook Strait canyon system is incised some 40 km into the shelf with a three-branched canyon head comprising the Nicholson, Wairarapa and Cook Strait canyon arms (Mitchell and Lewis, 1996). The shelf incised canyons converge near the shelf edge and cross the continental slope to meet the Hikurangi Channel, a northward flowing turbidite channel located within the Hikurangi Trough (Lewis, 1994; Lewis and Pantin, 2002).

The main Cook Strait canyon has several tributary canyons joining it on the continental slope, including the Palliser Canyon (Mitchell, 1988). Other continental slope canyons in the Cook Strait sector of the Hikurangi Margin include Pahaua Canyon and Opouawe Canyon (Mitchell, 1988; Barnes and Mercier de Lepinay, 1997; Lewis and Pantin, 2002).

The Cook Strait seaway experiences strong tidal flows dominated by the lunar semi-diurnal (M_2) component. Cook Strait acts as an amphidromic node, meaning that the difference between tides either side of Cook Strait is either 140° out of phase or roughly 5 h leading to near high tide on one side and low tide on the other (Bowman et al., 1980). Additionally, the area is prone to regular rough sea states as it is exposed to both large swells from Southern Ocean and locally intensified storms, and to strong westerly winds through the axial range gap between the North and South Islands producing a wind tunnelling effect (Harris, 1990). Tidal currents up to 1.2 m s^{-1} induce high bottom stresses in the Narrows (up to 26 N m^{-2}) which ease toward the south (Bowman et al., 1980). These currents develop prominent erosional and depositional bed-forms, including large scour holes and that extend from west of the Narrows, through the central strait and into the heads of the canyons (Carter et al., 1991; Carter, 1992; Lewis et al., 1994; Vennell, 1994).

During glacial periods of lowered sea level a land-bridge formed to the west of the Narrows, joining the North and South islands and creating a large embayment and maintaining strong tidal currents through southern Cook Strait (Proctor and Carter, 1989).

Fig. 1. Geological and structural setting of the Cook Strait sector of the Hikurangi Margin. (A) Plate margin setting shows direction and magnitude of Nuvel-1A plate motion vectors. (B) Cook Strait canyon system bathymetry with main structural elements, the approximate location of the Last Glacial Maximum shoreline and the MM IX isoseismal from the 1855 Wairarapa Earthquake (Downes, 2005). Dark shaded areas onshore indicate undifferentiated basement rocks (Begg and Johnston, 2000; Lee and Begg, 2002), light shaded areas offshore indicate approximate extents of Cenozoic sedimentary basins. Abbreviations are WGTN = Wellington City, TH = Turakirae Head, CP = Cape Palliser, RR = Rimutaka Ranges, WB = Wairarapa Basin, FB = Flaxbourne Basin, WRB = Wairau Basin. (C) Location of bathymetric profiles presented in D. (D) Bathymetric profiles across the Cook Strait sector of the Hikurangi Margin. Canyon axis profiles have been projected onto a margin normal line so profile lines are plotted as depth vs distance perpendicular to the margin.

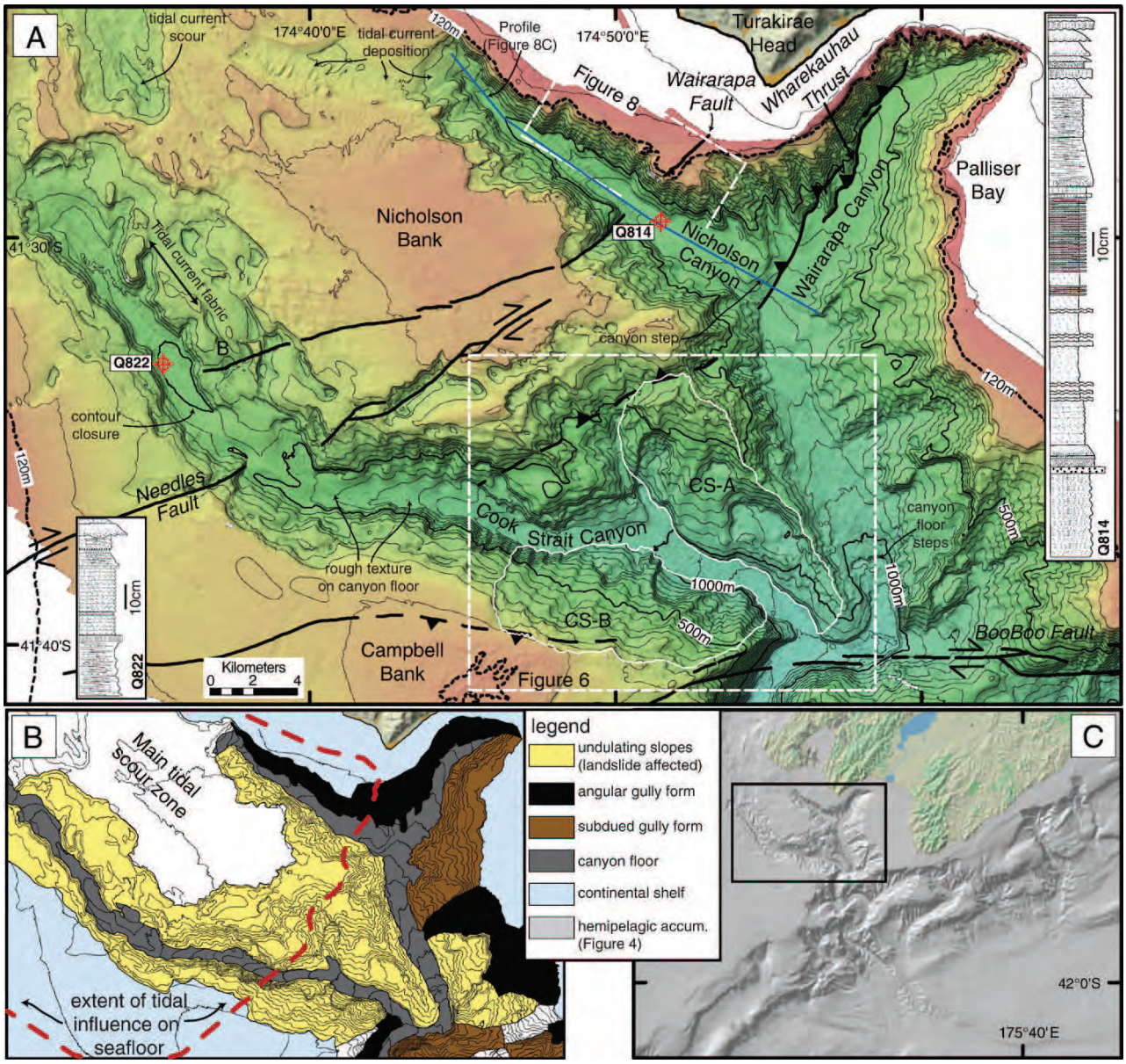

Fig. 3. Shelf-indenting part of the Cook Strait canyon system. (A) Shaded relief map illustrating canyon morphology. Shaded relief map has 5 times vertical exaggeration. Contour interval is 50 m. Dashed white key boxes refer to location of subsequent Figs. 6 and 8. Core logs are located with red targets in Nicholson and Cook Strait canyon arms. Horizontal scale of logs is grainsize increasing to the right, up to fine gravel. Contacts are sharp (straight line) of irregular (wavy line) (B) interpreted geomorphic domains. The dashed red line is the interpreted extent of tidal current scour. (C) Location of the shelf-indenting part of the Cook Strait canyon system.

The ~120 m lowering of sea level at the Last Glacial Maximum (LGM, ~20 ka BP) (e.g. Pillans et al., 1999) means that parts of the current continental shelf would have been a coastal plain, with segments of the coastline at or near to the rim of the upper canyon system. Modern sediment input to the Cook Strait south of the Narrows predominantly comes from three fluvial sources: the Wairau and Awatere rivers in the NE South Island (~1.05 million tonnes per year suspended sediment and bedload), and the Ruamahunga River in the southern North Island (~0.60 million tonnes per year suspended sediment and bedload) (Hicks and Shankar, 2003). A small component of additional net sediment transport occurs from the north, through the Narrows (Carter, 1992; Lewis et al., 1994; Carter and Lewis, 1995). During the LGM the Awatere and Wairau River catchments were glaciated (Eden, 1989; McCalpin, 1992) and likely had significantly increased the sediment load available for transport to the canyon system. It is not clear precisely if or where the South Island rivers traversed the shelf under low stand conditions, but it is possible they would have deposited sediment directly into the canyon system during this time.

2.3. Geology

Onshore geology is dominated by Mesozoic basement rocks, principally indurated sandstone and argillites of the Torlesse Supergroup, which form the major ranges of the southern North Island and NE South Island (Begg and Johnston, 2000; Rattenbury et al., 2007)

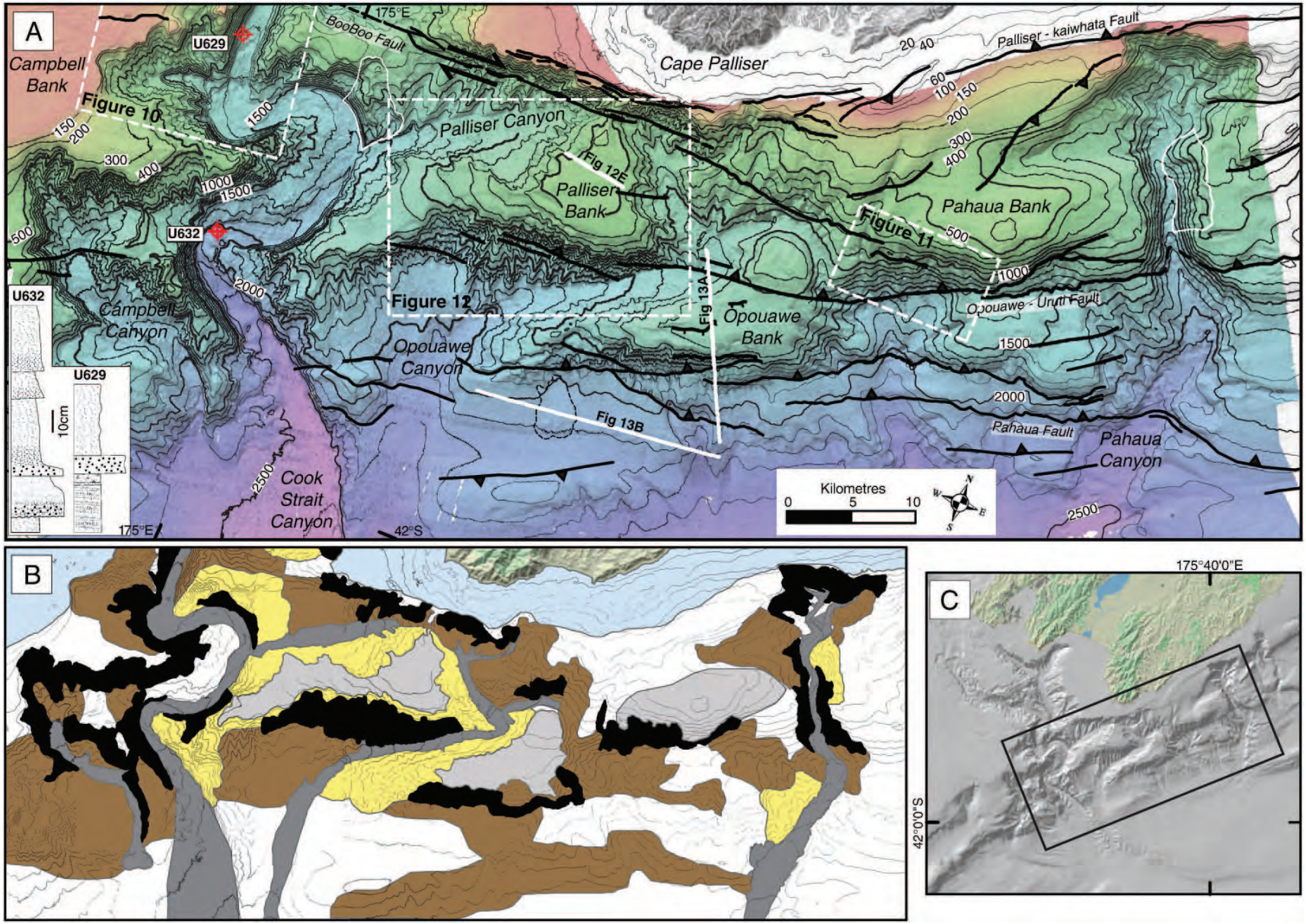

Fig. 4. Slope-confined canyons on the Cook Strait sector of the Hikurangi Margin. (A) Shaded relief map illustrating continental slope morphology. Shaded relief map has 5 times vertical exaggeration. Contour interval is 100 m on the slope. Dashed white key boxes refer to subsequent Figs. 10–12, and solid white lines) and seismic lines (solid white lines). Fine dashed black line crossing Fig. 12B location indicates landslide debris evident in multibeam data. Shaded relief map has 5 times vertical exaggeration, and contour interval is 100 m below 200 m water depth. Core logs are located with red targets in main Cook Strait Canyon. Horizontal scale of logs is grainsize increasing to the right, up to fine gravel. Contacts are sharp (straight line) of irregular (wavy line) (B) interpreted geomorphic domains. Refer Fig. 3 for legend. (C) Extent of slope canyon study area.

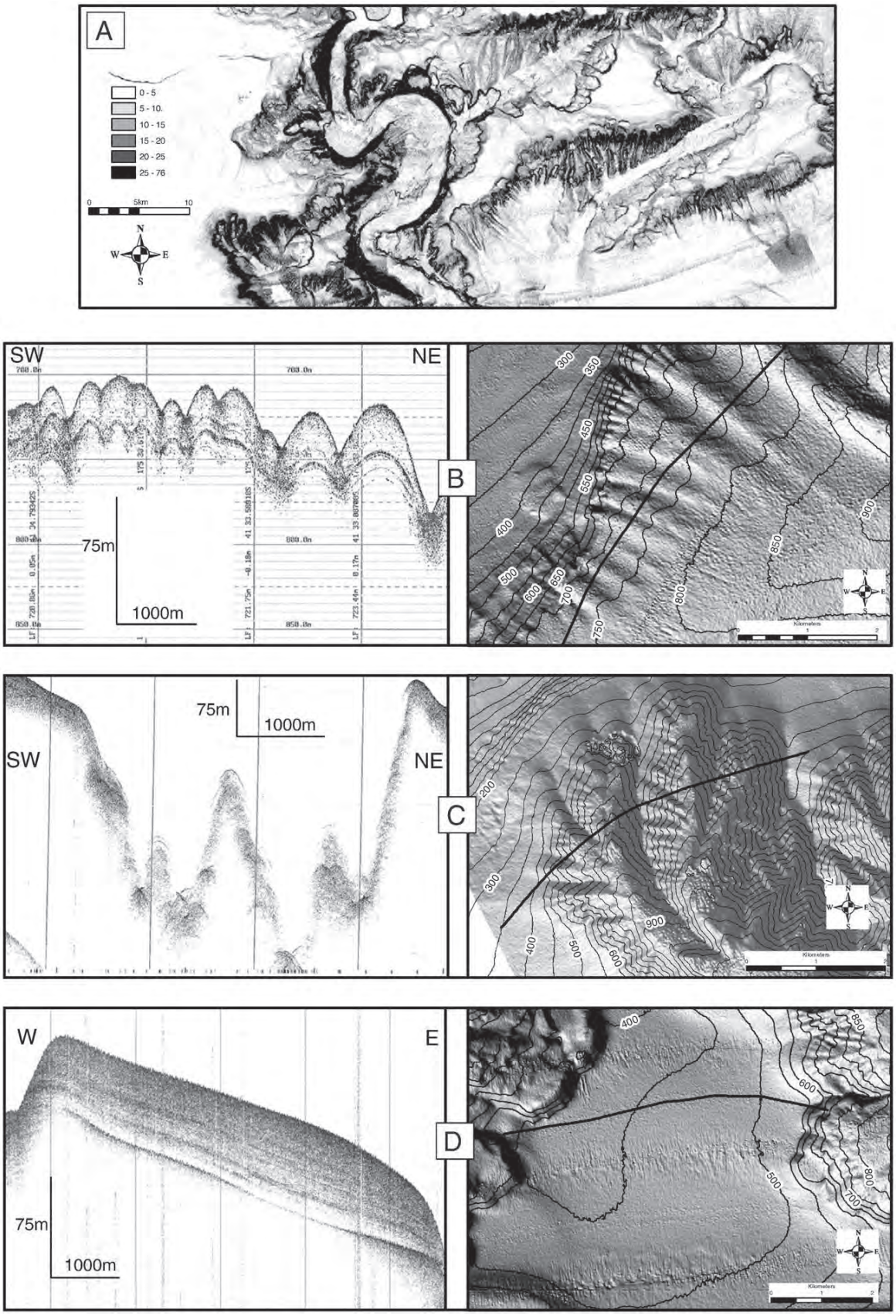
A
0 - 5
5 - 10.
10 - 15
15 - 20
20 - 25
25 - 76
0
5km
10
N
W
E
S
SW
NE
B
75m
1000m
300
350
450
550
400
900
650
600
700
800
750
850
Kilometers
75m
1000m
SW
NE
C
200
300
900
400
500
600
W
E
D
75m
1000m
400
850
600
500
800
700
Kilometers

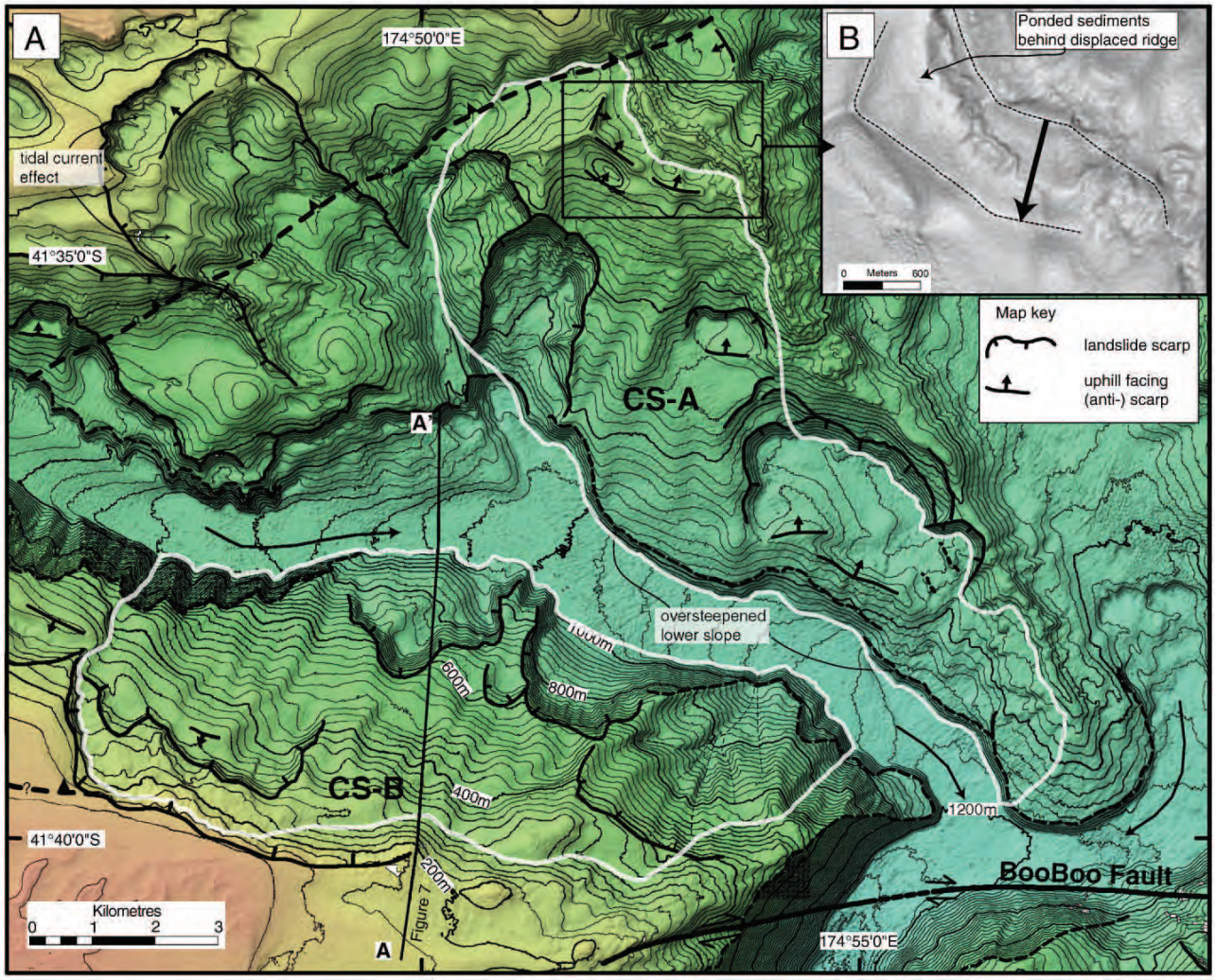

Fig. 6. (A) Shaded relief map showing deep-seated failures CS-A and CS-B on opposing walls of the Cook Strait Canyon (location on Fig. 3). Shaded relief map has 5 times vertical exaggeration. Contour interval is 20 m. Sections A–A′ refers to multichannel seismic profile presented in Fig. 7. (B) Enlarged area of the displaced ridge crest in CS-A, with displacement vector shown by black arrow. Bathymetric image is a slope map with a 32 bin classified greyshade pallet, darker colours are steeper slopes.

(Fig. 1). The continental shelf in Cook Strait is principally underlain by three major sedimentary basins: the onshore–offshore Wairarapa Basin; the Flaxbourne Basin in southern and central Cook Strait; and the Wairau Basin to the east. These Tertiary basins are variably overlain by a post last-glacial sedimentary sequence and Recent sedimentary cover. The Wairarapa Basin underlies the upper reaches of the canyon system, is about 15–20 km wide, and contains about 3 km of gently dipping Miocene to Pliocene mudstone and siltstone (Carter et al., 1988; Uruski, 1992; Barnes and Audru, 1999a). The Flaxbourne Basin underlies the southern shelf, is about 15–20 km wide, and is infilled with >4.5 km of sedimentary sequence at the Cook Strait Canyons (Uruski, 1992; Barnes and Audru, 1999a). Flaxbourne Basin sedimentary sequences are correlated to Motunau and Awatere groups comprising sandstone, siltstone and mudstone units (Audru, 1996). The upper continental slope is underlain by deformed slope basins forming a structural backstop to the accreted trench fill of the lower slope (Collot et al., 1996). Beyond the continental slope to the south east, the Hikurangi Trough has accumulated a >5 km thickness of hemipelagites and turbidite deposits with a minor component of volcanic tephra (Field et al., 1997; Lewis et al., 1998).

3. Data set

Multibeam bathymetric data were collected by the NIWA vessel RV *Tangaroa* during five surveys between 2002 and 2005, covering an area of approximately 8400 km^2 (Fig. 2). The RV *Tangaroa* has a hull-mounted Simrad EM300 multibeam system, operating 135 beams at 30 kHz frequency, with approximately 1° beam width. Surveys are undertaken to International Hydrographic Organisation (IHO) standards. Shipboard navigation comprises a POS/MV system with differential GPS. Navigational accuracy is ±5 m and vertical accuracy in 1000 m water depth is ±2 m. Data were processed using C&C Technologies HydroMap software, and gridded to a 10 m×10 m bin

Fig. 5. Examples of geomorphic domain mapping classes. (A) Slope map indicating the distribution of steep (>25°) slopes. (B) Subdued gully form example showing 3.5 kHz profile (left) and shaded relief map (right). (C) Angular gully form example showing 3.5 kHz profile (left) and shaded relief map (right). (D) Hemipelagic accumulation example showing 3.5 kHz profile (left) and shaded relief map (right).

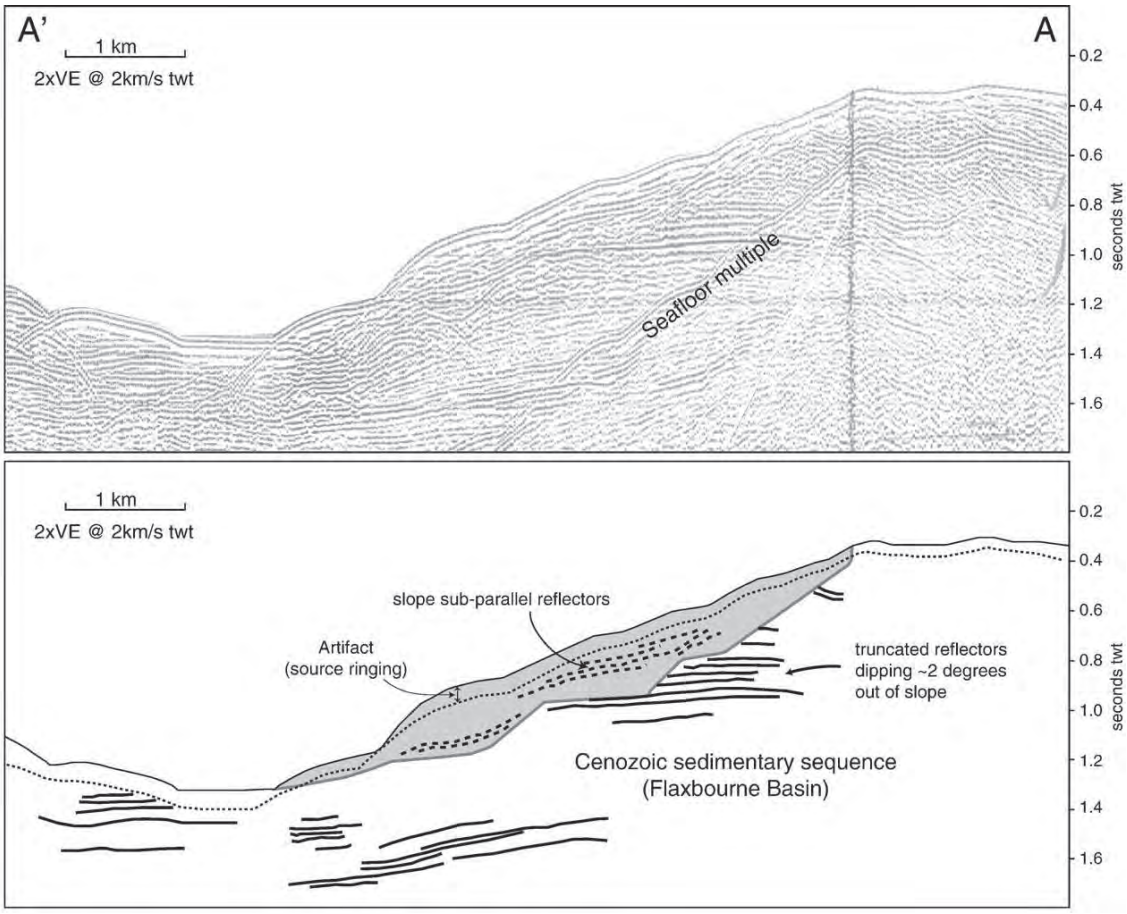

Fig. 7. Multichannel seismic reflection profile (Magellan Petroleum NZ Ltd, 1969) across deep seated landslide CS-B, profile location in Fig. 6. Both uninterpreted and interpreted profiles are shown.

size, providing virtually continuous coverage of the entire 8400 km^2 survey area. Additional multibeam data were collected by the Royal New Zealand Navy for hydrographic purposes (IHO standards), using an Atlas Hydrosweep MD-2/30 system and processed in Caris HIPs to 10 × 10 m bin size. This system has a manufacturer stated accuracy of ±0.15 m + 0.2% water depth. These bathymetry data are augmented by singlebeam Royal New Zealand Navy data and sounding data from the adjacent continental shelf (Mitchell and Lewis, 1996) and Simrad EM12D multibeam bathymetric data on the slope (Collot et al., 1995).

Multibeam tracks have high resolution 3.5 kHz seismic reflection profiles collected concurrently, providing subsurface penetration of up to several tens of metres (Fig. 2). Sediment cores referred to in this study are from NIWA archives. Multichannel seismic reflection data have been collected across the Cook Strait area since the late 1960's by oil industry surveys and scientific cruises. Profiles used for this study were collected during the following surveys: Magellan Petroleum NZ Ltd, 1969; Gulf Oil, 1973; RV *l'Atalante* GEODYNZ-SUD, 1992; and, RV *Sonne* SO191 New Vents, 2007 (Barnes et al., 1998; Barnes and Audru, 1999a,b; Bialas et al., 2007) (Fig. 2).

4. Morphostructure of the Cook Strait sector of the Hikurangi margin in light of new multibeam data

The location of Cook Strait canyon system within a major tectonic transition zone characterised by numerous active faults is expected to have a strong influence on canyon evolution in terms of regional seafloor physiography and erosional and sediment transport processes. To provide a suitable level of tectonic framework for this study we have reinterpreted the morphostructure of Cook Strait sector of the Hikurangi Margin in the light of the newly available dataset.

4.1. Morphological character of the canyons

The Cook Strait sector of the Hikurangi Margin comprises a large area of continental shelf that varies in width from as little as 1.3 km to over 30 km, a c. 40 km wide continental slope, and the broad turbidite plain of the Hikurangi Trough (Fig. 1). Canyons on the Cook Strait sector of the Hikurangi Margin can be subdivided into two principal components; the 910 km^2 shelf indenting portion of the Cook Strait canyon system (Fig. 3), and the ~5000 km^2 area of incised continental slope which includes the ~890 km^2 lower part of the Cook Strait canyon system (Fig. 4). Margin normal profiles across the continental slope, and in canyon axes illustrate the deep incision of the Cook Strait Canyon, both in comparison to the regional form of the margin (Honeycomb, Campbell and Pahaua slope) and inboard of the shelf break (Fig. 1C and D).

The upper part of the Cook Strait canyon system represents by far the largest shelf-incised canyon system on the Hikurangi Margin. The largest arm of the upper canyon system is the 45 km long Cook Strait Canyon which lies approximately in the centre of Cook Strait with a canyon rim at 150–180 m water depth and canyon floor at 300–1200 m water depth (Fig. 3). Cook Strait Canyon widens from ~7 km at the head to ~12 km above the confluence with the other two canyon arms, and has a relatively symmetrical cross sectional form with

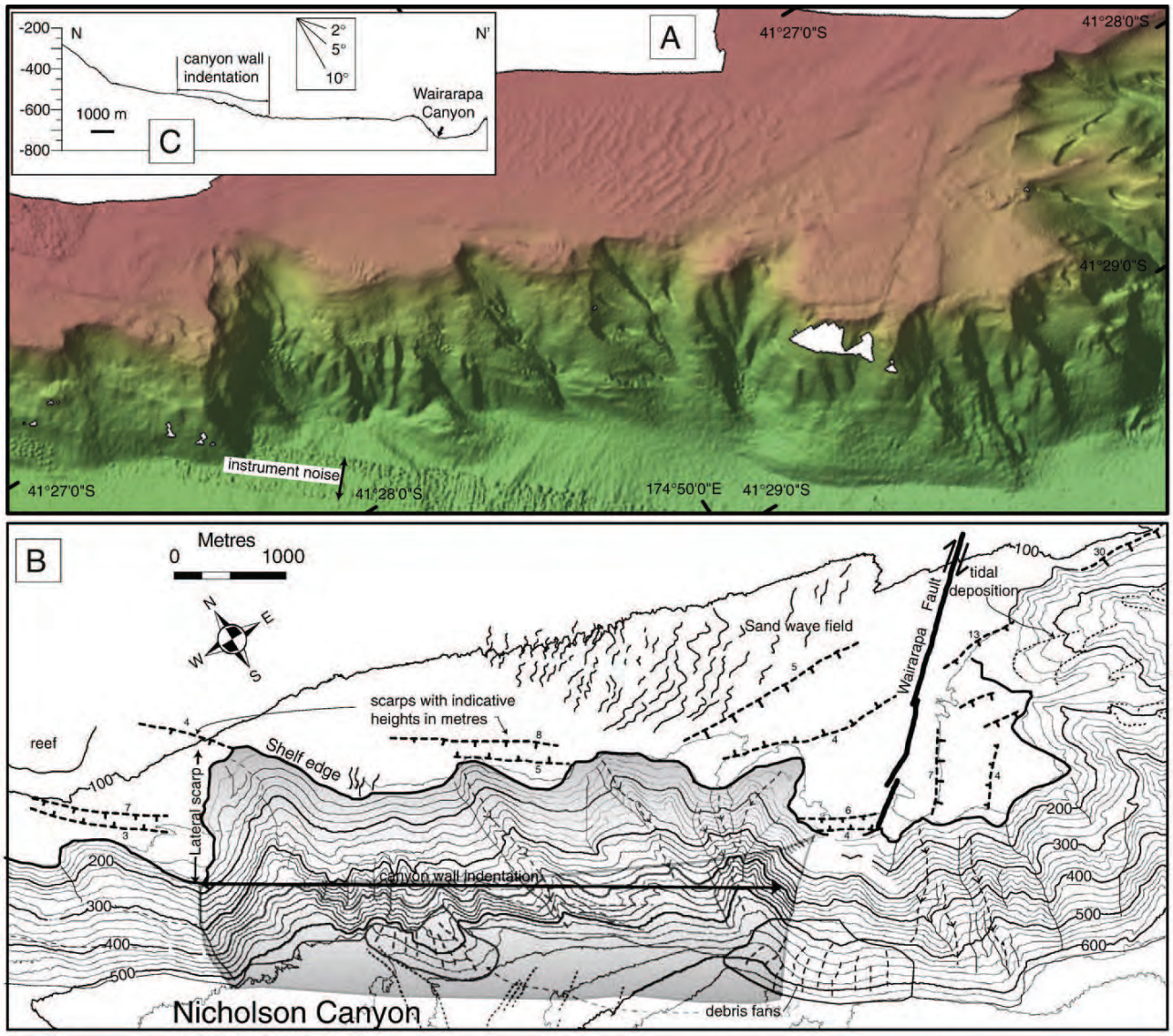

Fig. 8. Canyon enlargement into Mesozoic bedrock. (A) Shaded relief map with 5 times vertical exaggeration (note image is rotated so north is at approximately 330°). (B) Geomorphic interpretation map. Contour interval is 20 m. Key features include grabens with scarp heights annotated, a large canyon wall indentation (slope failure scar indicated by grey shading), and debris aprons at slope base. (C) Long profile down Nicholson Canyon (location Fig. 3). The high vertical exaggeration (10×, refer true dip lines inset) is used to illustrate the convex anomaly coincident with the canyon wall indentation.

overall slope angles in the order of 3–10° with the lower value reflecting widening to the north east in the canyon head. To the north east of Cook Strait Canyon are the Nicholson Canyon and Wairarapa Canyon (Fig. 3). These two canyon arms are ~18 km and ~14 km long respectively but merge together for 20 km before joining Cook Strait Canyon in the vicinity of the shelf edge. The lower part of this Nicholson/Wairarapa canyon arm is ~12 km wide, 600–1000 m deep, and has a south western wall defined by the tapering ridge between it and the Cook Strait Canyon and a north eastern wall characterised by scallop shaped indentations into the shelf break. The Nicholson and Wairarapa canyons encroach closest to the coast, with Wairarapa Canyon coming within 1.2 km. These two canyon arms both show quite a distinctive asymmetric cross sectional form with overall slope angles on the landward side of the canyons (Turakirae Head Fig. 3) in the order of 11–20°, while the opposing walls are in the order of 7–10°, a similar range to the majority of Cook Strait Canyon. Generally the canyon walls of the upper canyon system have a broadly undulating form, with occasional gully affected slopes. An exception to this is the two landward walls of Wairarapa and Nicholson Canyon which, as well as showing steeper overall slopes, exhibit comparatively angular form with regular gully systems from canyon rim to canyon floor. The majority of canyon floors in the upper canyon system are smooth and flat or broadly undulating, however some notable features are indicated in Fig. 3 and include: a contour closure in Cook Strait Canyon indicating a depression in the upper part of this canyon; an area of "lumpy" irregular texture down canyon of this; an area of ripple features in the head of Nicholson Canyon; a 110 m smooth step down where Nicholson Canyon joins Wairarapa Canyon; and, a series of irregular steps at the lower end of the merged Nicholson/Wairarapa canyon.

From the convergence of the upper canyon arms the Cook Strait Canyon crosses the slope in a series of sweeping meander bends to join the Hikurangi Channel (Figs. 1 and 4). This main canyon of the slope confined Cook Strait canyon system is ~70 km long, 6–12 km

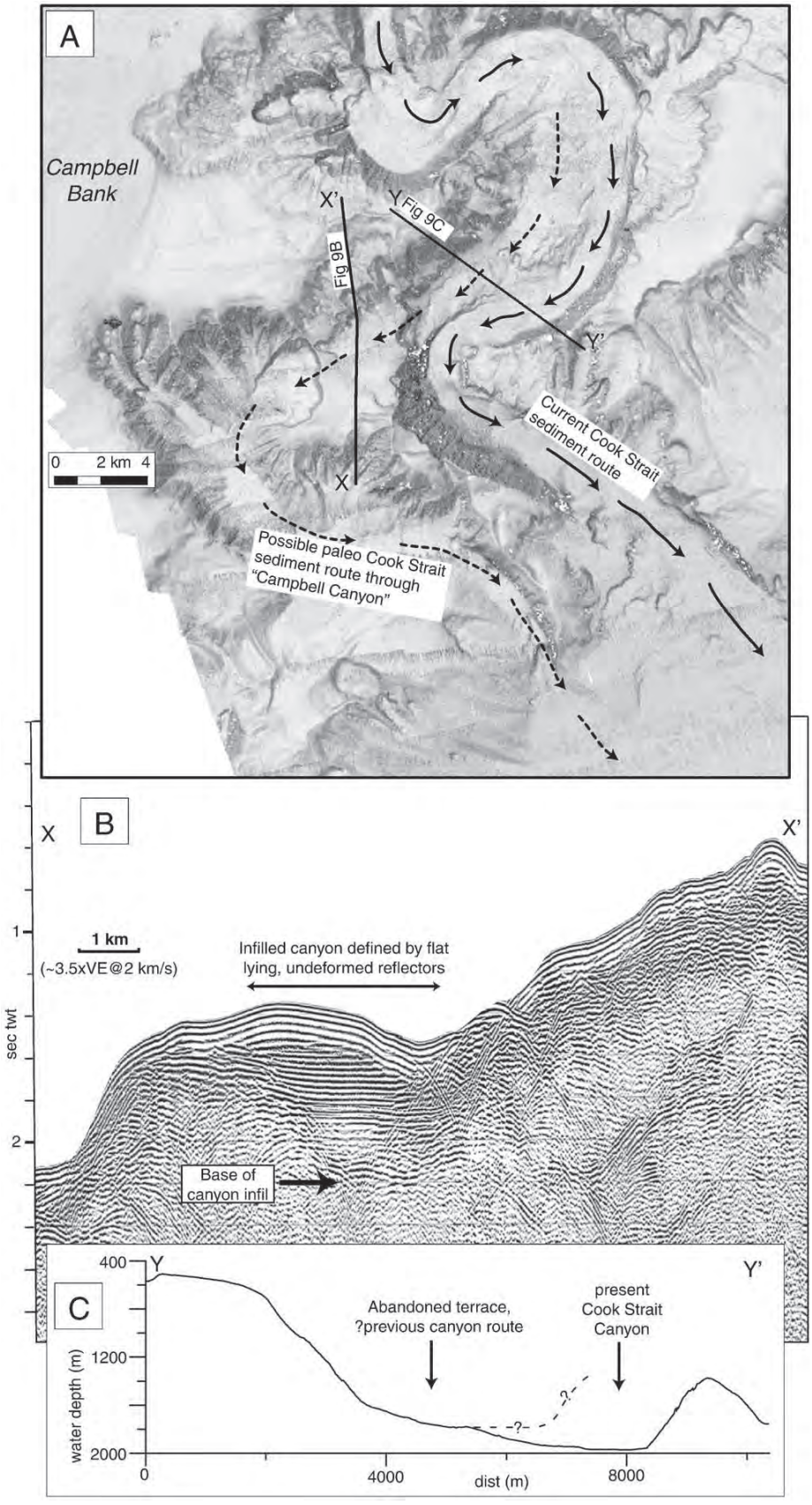
A
Campbell Bank
X'
Y
Fig 9C
Fig 9B
Y'
X
0 2 km 4
Current Cook Strait sediment route
Possible paleo Cook Strait sediment route through "Campbell Canyon"
B
X
X'
1 km
(~3.5xVE@2 km/s)
Infilled canyon defined by flat lying, undeformed reflectors
sec twt
1
2
Base of canyon infil
C
400
Y
Y'
Abandoned terrace, ?previous canyon route
present Cook Strait Canyon
water depth (m)
1200
2000
0
4000
dist (m)
8000

wide and has canyon floor depths from 1200–2700 m. The canyon exhibits steep walls on the outer curve of meander bends with walls up to 1100 m high with 28–30° overall slope angles. The canyon floor is irregular, with 100 m high steps, 100 m deep holes, broad irregular undulations and large wavelength (1500–2500 m) bedforms (Lewis and Pantin, 2002) towards the lower canyon. Two large canyons contribute to the lower Cook Strait canyon, the Palliser Canyon and an unnamed canyon bordering Campbell Bank (Fig. 4).

In addition to the Cook Strait canyon system, three other canyons are incised into the continental slope within the study area, the informally named Campbell Canyon, the Opouawe Canyon and the Pahaua Canyon (Fig. 4). The Campbell Canyon is a 45 km long canyon that heads into Campbell Bank to water depths of ~200 m and exits to the lower end of the Cook Strait canyon system in 2400 m water depth. Opouawe Canyon, to the east of the Cook Strait canyon system, has a complex multi-branched canyon head which traverses the slope over ~60 km, from the narrow continental shelf south of Cape Palliser in water depths as shallow as 80 m, in dog-leg fashion to meet the Hikurangi Channel at 2600 m water depth. Pahaua Canyon has a broad head incised into the outer shelf to ~55 m water depth. The canyon head has well developed gully forms that extend laterally either side of the main canyon head. The canyon takes the most direct route of all the main slope canyons, making just one turn in its 45 km length to exit to the lower slope at ~2550 m water depth. Much of the continental slope in the Cook Strait sector of the Hikurangi Margin is affected by closely spaced gully features across local slopes and canyon heads.

The other main physiographic features of the continental slope are elongate margin parallel ridges, one previously named Opouawe Bank (Mitchell, 1988), and two referred to in this study as the Palliser and Pahaua banks (Fig. 4). Such physiographic features occur widely along the Hikurangi Margin (e.g. Lewis and Pettinga, 1993; Barnes and Mercier de Lepinay, 1997) and on other accretionary margins elsewhere (e.g. Liu et al., 1997; Kukowski et al., 2001; Huyghe et al., 2004; McAdoo et al., 2004; Chiang and Yu, 2006), as the seafloor expression of convergent structural deformation.

4.2. Structure

The principal structural elements of the Cook Strait sector of the Hikurangi margin have been documented in previous studies (Barnes et al., 1998; Barnes and Audru, 1999a). In this study we have reinterpreted the slope and shelf structure in light of high resolution multibeam bathymetry and new seismic data.

Structure on the continental slope is dominated by discontinuous westward-dipping thrust faults striking ~065° (margin parallel) that have formed the well developed ridge and basin relief through active anticlinal folding and associated passive syncline formation (Figs. 1 and 4). The two principal mid-slope thrust faults are the Opouawe–Uruti Fault and the Pahaua Fault, which are northwest dipping thrusts likely to project to seismogenic depth (Barnes et al., 1998). Pahaua Fault is a discontinuous right stepping fault trace that can be traced across Pahaua Canyon and is deforming Opouawe Bank and an unnamed bank immediately west of Pahaua Canyon. Opouawe–Uruti Fault is also a discontinuous trace that is deforming Pahaua Bank and Palliser Bank as well as cutting across the landward part of Opouawe Bank. Both thrust faults continue to the north, beyond the extent of Figs. 1 and 4. Two major shelf-edge faults traverse the upper slope: the northwest dipping Palliser–Kaiwhata reverse fault and the dextral strike–slip BooBoo Fault, which continues across the Cook Strait Canyon and onto Campbell Bank (Figs. 1, 3 and 4). A number of other minor landward and seaward vergent reverse faults have also been mapped in the area. Although there is a discontinuity of slope structures across Cook Strait Canyon (Fig. 1), we believe this is more of an artefact of the lack of data than a true structural boundary. Future collection of multichannel seismic data in this area is needed to resolve this issue.

Strike–slip faults striking ~070–090° dominate shelf structure (Figs. 1 and 3). This orientation (sub-parallel to the nuvel-1A plate motion vector) reflects the transition from the increasingly oblique convergent margin along New Zealand's east coast to transpressive continental collision onshore into the South Island. The main active tectonic features of the shelf around Cook Strait Canyon are the strike slip Wairarapa Fault which crosses Nicholson Canyon into Nicholson Bank, the Wharekauhau Thrust at the base of the northwest wall of Wairarapa canyon, and the BooBoo Fault (Fig. 3).

The concentration of significant active structures in this study site combined with the onshore structures means that the area is subject to relatively frequent, high magnitude earthquakes. The 1855 M8.2 Wairarapa earthquake was associated with rupture of one or both of the Wairarapa Fault and the Wharekauhau Thrust, with the rupture trace well defined onshore and causing up to 6 m of co-seismic uplift at Turakirae Head as well as the very large (13–17 m) dextral movement (Begg and Johnston, 2000; Little and Rodgers, 2005; McSaveney et al., 2006), and induced Modified Mercalli intensities of MMIX+ in Cook Strait (Grapes and Downes, 1997) (Fig. 1B). Beach ridges also suggest repetitive, similar magnitude uplift events (average 7.3 m) with a return time of approximately 2000 yrs (McSaveney et al., 2006). Additionally, the 1848 M7.5 Marlborough earthquake on the Awatere Fault in northern South Island induced Modified Mercalli intensities of MMVIII in Cook Strait (Grapes et al., 1998). Probabilistic seismic hazard modelling suggests peak ground accelerations in the area are likely to be in the order of 0.5 g at the 475 yr return time (Stirling et al., 2002b).

5. Morpho-domains from multibeam and 3.5 kHz seismic

The study area has been mapped into morpho-domains based on both surface and near surface character, using 10×10 m DEM derivatives in ArcGIS© (i.e. shaded relief, slope gradient, slope aspect) and 3.5 kHz seismic data (Figs. 3B and 4B). The intention of the domaining exercise is particularly to use the high resolution bathymetry to assess the relative distribution of different surface morphologies that might be related to processes influencing erosion and deposition in the canyon system. Firstly we have delimited the continental shelf and canyon floors, principally defined by the slope-break in slope gradient maps. The canyon slope morpho-domains shown in Figs. 3B and 4B are: angular gully morphology (black); subdued gully morphology (brown); broadly undulating slopes interpreted as affected by bedrock slope failure (yellow). We also recognise sites of long term hemipelagic accumulation on the continental slope (light blue), and leave areas affected by undifferentiated depositional processes as white.

Smoothed gully morphology is primarily interpreted from shaded relief maps, and is correlated to 3.5 kHz showing sediment drape over buried gully morphology (Fig. 5B).Angular gully morphology is defined in slope gradient maps by extensive areas of where slopes exceed ~25°, and with local slopes reaching 60° (Fig. 5A). The sculpted

Fig. 9. Possible ancestral lower Cook Strait Canyon. (A) Shaded relief map of the lower end of Cook Strait Canyon, indicating current sediment transport route (solid arrows) and inferred past canyon location through "Campbell Canyon" (dashed arrows). Shaded relief map has 5 times vertical exaggeration. (B) Multichannel seismic reflection profile across the inferred paleo-canyon shows flat lying undeformed reflectors confined to a v-shaped area, consistent with canyon infilling (Magellan Petroleum NZ Ltd (1969) line F2). (C) Relief cross section through lower Cook Strait Canyon with an interpretation of canyon topography, pre-lateral migration. This illustrates how the abandoned "terrace" on the inside of the meander bend could have developed. Current canyon floor is approximately 200 m below abandoned terrace.

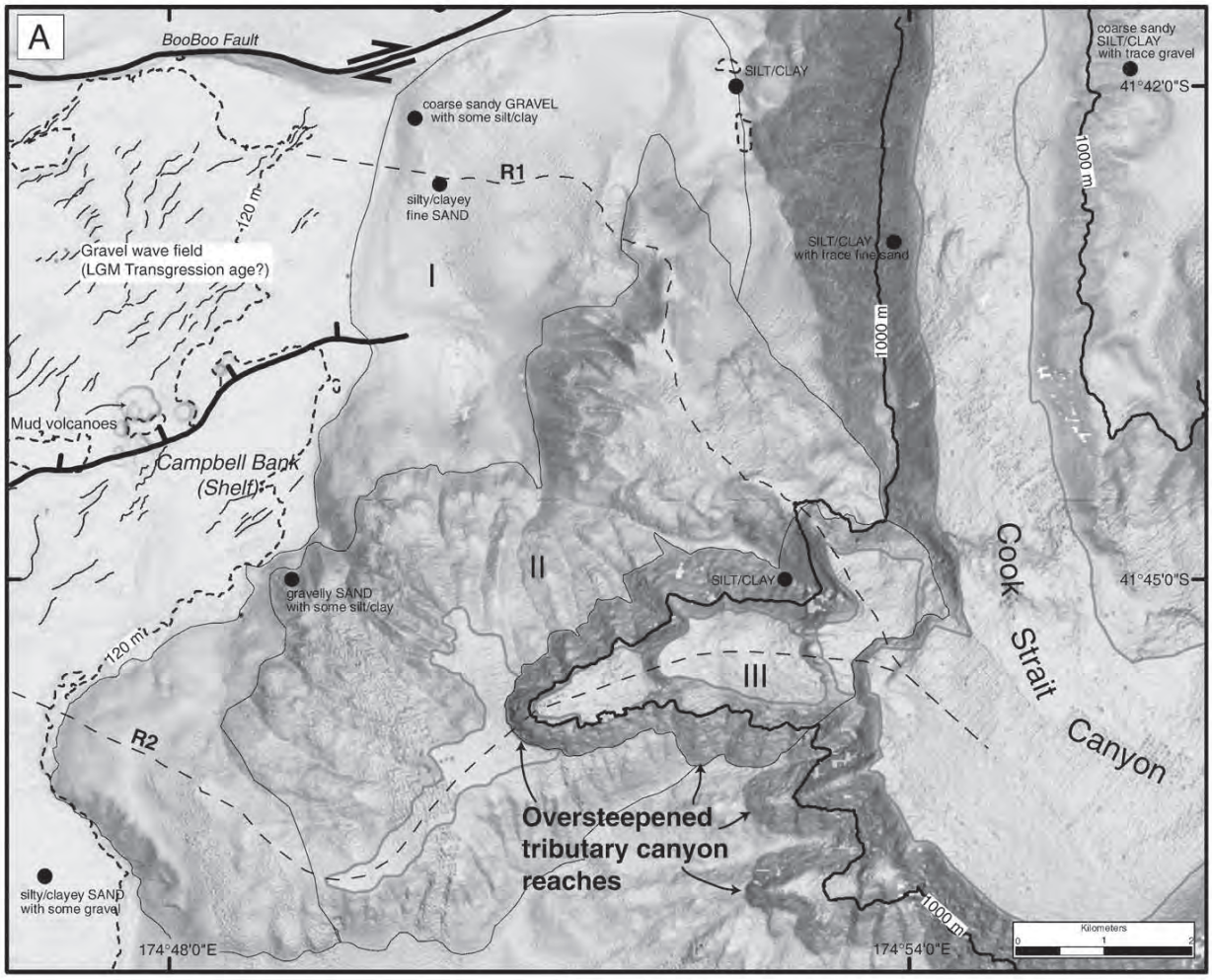
A
BooBoo Fault
coarse sandy GRAVEL with some silt/clay
SILT/CLAY
coarse sandy SILT/CLAY with trace gravel
41°42'0"S
R1
silty/clayey fine SAND
120 m
1000 m
Gravel wave field (LGM Transgression age?)
SILT/CLAY with trace fine sand
I
Mud volcanoes
Campbell Bank (Shelf)
II
SILT/CLAY
41°45'0"S
Cook Strait Canyon
gravelly SAND with some silt/clay
III
R2
Oversteepened tributary canyon reaches
silty/clayey SAND with some gravel
174°48'0"E
174°54'0"E
Kilometers
B
frequency (percentage)
slope angle (degrees)
C
Water depth (m)
R1
R2
distance from Cook Strait Canyon (m)
D
Terrestrial sed input
Longshore sed input
Glacial sea-level
general canyon wall
incised channel base
Transient aggradation in main canyon due to high sed load. Channel incision into bedrock unlikely or limited
Subcanyon incises due to high sed throughput. Sed bypasses slope to main canyon
Ongoing tectonic uplift
E
Interglacial sea-level (+120m)
residual shell/ gravel lag
Sub-canyon re-entrenched from bottom in response to local base-level fall
top-down partial filling of sub-canyon with sea-level rise
Main canyon incises into bedrock reflecting lower sed supply and tect uplift
Ongoing tectonic uplift

for of these gullies is readily apparent in shaded relief maps and is typically characterised in 3.5 kHz seismic by multiple diffractions (Fig. 5C). Sites of long term hemipelagic accumulation are recognised from 3.5 kHz character and generally flat lying topography (Fig. 5D). Slopes interpreted as affected by bedrock slope failure are related to MCS and shaded relief map interpretation of deep-seated slope failure extrapolated to slopes exhibiting similar undulating morphology (e.g. interpretations in Figs. 6 and 7).

5.1. Indicators of down-canyon sediment transport process

No studies have yet clearly shown which processes are driving sediment through the Cook Strait Canyon. The following section presents core and bathymetric interpretations to provide some information on sediment transport processes and canyon activity. It has been suggested Cook Strait Canyon and adjacent slope canyons would not have been abundant sediment suppliers to the Hikurangi Trough, following the post-glacial sea level rise (Lewis et al., 1998; Lewis and Pantin, 2002). This inference is based on both the lack of near shore littoral or fluvial input to the upper Cook Strait Canyon and the slope confined canyon systems, and the interpretation by Carter (1992) that the Cook Strait and Nicholson arm of the upper canyon have landslide debris in the canyon axis. The Carter (1992) 3.5 kHz echocharacter interpretation is based on seismic profiles spaced at ~5 km, some of which show hyperbolic character indicative of blocky landslide deposits. However, while the hyperbolic character may indeed relate to landslide deposits at the base of canyon walls there is no indication in multibeam bathymetry that blocky landslide deposits are distributed across the canyon floor of any of the main arms of the upper Cook Strait Canyon (Fig. 3). We do note that the ~40 m high in the Cook Strait Canyon arm, immediately down canyon of the contour closure indicated in Fig. 3, indicates a disruption of the "equilibrium profile" of the canyon.

A strong NW–SE trending fabric characterises the surficial morphology of the upper reaches of the Nicholson and Cook Strait arms of the upper Cook Strait canyon system and the surrounding shelf (Fig. 3B). Sand and fine grained material is shown to be transported into Nicholson and Cook Strait canyon heads by diurnal tidal currents (Carter, 1992), and this is supported by sediment waves and ripples aligned normal to the canyon axis at Nicholson Canyon head (Fig. 3). While the floors of the Nicholson, Cook Strait and Wairarapa canyon arms are generally smooth with only minor undulations, the lower Wairarapa/Nicholson canyon, and the length of the lower Cook Strait Canyon, show an irregular, stepped morphology. Many parts of the upper canyon walls exhibit a steep (30°+) slope at the toe of the canyon wall (Fig. 3).

Logs for four cores are presented from Nicholson and upper Cook Strait canyon (Fig. 3) and lower Cook Strait canyon (Fig. 4). Both the cores in the upper canyons clearly show repeated graded beds from silty clay to sand with erosional basal contacts, and the first of these initiate at the most 20 mm from the core top. In the lower canyon, core U632 (Lewis and Pantin, 2002) shows repeated graded gravel to silty clay beds with sharp and sometimes erosional basal contacts. In contrast, Core U629 shows no graded beds but contains laminated silty beds with organics, as well as gravel beds comprising poorly indurated sub-angular to sub-rounded mudstone clasts. Unfortunately no material has been dated from any of these archived cores, but they clearly show a lack of any large accumulation of hemipelagic sequence in the floor of the canyon system.

6. Enlargement of shelf-indenting canyons

The upper shelf-indenting portion of the Cook Strait canyon system is excavating into the Late Cenozoic sedimentary sequences of the Flaxbourne, Wairau and Wairarapa Basin (Fig. 1). Bedrock landsliding is considered to have an important control on the morphological evolution of the upper canyon walls, based on the interpreted widespread distribution of landslides (~55% of canyon in Fig. 3B) and the "geomorphic fingerprint" of deep-seated landslides on the large-scale morphology of canyon walls. Along the north eastern and north western walls of Nicholson and Wairarapa Canyon respectively, canyons are outside the extent of sedimentary basins and likely to be formed in the Mesozoic basement rock of the adjacent Turakirae Head. Deep-seated slope failures are interpreted on canyon walls in both of these geological materials, but show a contrasting kinematic style.

6.1. Canyon enlargement into Late Cenozoic sedimentary sequences

Numerous slope failure scars are evident in the bathymetry in the upper canyon area from steep arcuate headscarps (Fig. 6). In addition to these smaller scale failures we interpret two global slope failures, each ~50 km^2, extending from canyon floor to slope crest (CS-A and CS-B in Figs. 3 and 6).

A multichannel seismic profile through CS-B shows apparent dips on reflectors at ~2° towards Cook Strait Canyon (Fig. 7). Reflectors are truncated within the upper 300 ms, and above this truncation reflectors are oriented parallel to slope. Reflector truncation occurs in a series of steps down the slope, alternating between conformable and unconformable with overlying material. The volume of material above the unconformity is calculated to be in the order of 10 km^3. While an artefact in the MCS data affects the upper 100 ms, it does not obscure the unconformable reflector relationship (Fig. 7). An over-steepened slope is evident along the upper boundary of the interpreted global failure CS-B, interpreted as a head scarp in Fig. 6A.

MCS adjacent to CS-A (not presented here) also indicates a low apparent dip towards Cook Strait Canyon. A basin-like feature near the ridge crest within CS-A suggests displacement in the order of 800 m (Fig. 6B). The main ridge crest from which this has detached has a very rubbly appearance both at this point and down its length. Multiple uphill facing scarps are recognised in landslide complex CS-A. We note that the inferred north west dipping thrust fault occurs at the head/lateral boundary of CS-A, and may have a role in slope deformation.

The majority of the disrupted material within these large slope failure complexes remains "in-storage" on the slope, in terms of its potential to be more readily removed by future mass movement than adjacent unfailed slope material. The morphology of these complexes is considered representative of much of the bedrock mass movement domain, although the size of slope failures varies and these are at the upper end of the observed range within this study area.

6.2. Canyon enlargement into Mesozoic bedrock

The northern walls of the Wairarapa and Nicholson canyons are forming in Mesozoic basement rock of the Torlesse Supergroup, projected and correlated from the onshore geological mapping in southern North Island (Begg and Mazengarb, 1996) and corroborated by multichannel seismic data (Barnes and Audru, 1999a). Torlesse Supergroup greywacke comprises very well indurated and slightly metamorphosed, interbedded mudstones and silty sandstones that

Fig. 10. Tributary of Cook Strait Canyon incising into Campbell Bank. (A) Bathymetric image is a slope gradient plot with a 32 bin classified greyshade pallet, darker colours are steeper slopes. The 120 m and 1000 m contours are shown as well as the locations of surface sediment samples from NIWA archives with a brief description. (B) Plot of local slope gradient vs frequency of occurrence, defined by the local slope gradient within domains I–III as a percentage of the population of local slope gradient values for the entire tributary catchment area. (C) Along section plot of the two sediments routes, determined using DEM based flow accumulation techniques in ArcGIS©. (D) Schematic of glacial maximum situation. (E) Schematic of interglacial situation.

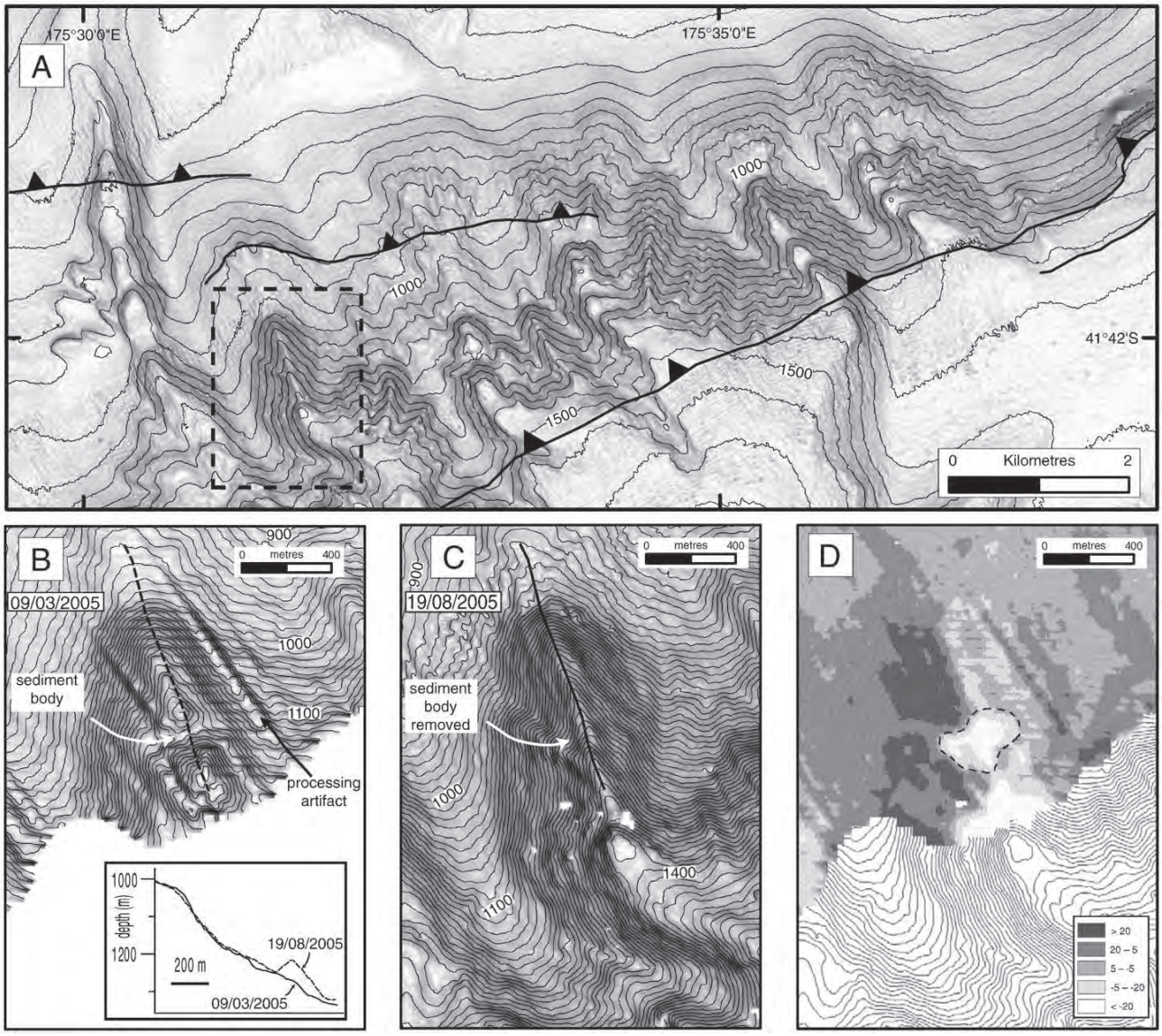

Fig. 11. Re-entrenchment of antecedent flow paths on the seaward flank of Pahaua Bank. (A) Bathymetric image is a slope gradient plot with a 32 bin classified greyshade pallet, darker colours are steeper slopes. Contours interval is 50 m. Simrad EM300 data collected by NIWA 19/08/2005. (B) Hydrosweep bathymetry data gridded to 10 m and shown with 10 m contours, courtesy of Royal NZ Navy. Inset is a comparison of canyon axis long profiles from two surveys. (C) NIWA Simrad EM300 data gridded to 10 m and shown with 10 m contours. (D) Difference of the two grids in metres. White colours show loss of material from B to C. Dark colours show addition of material from B to C. Refer to the text for discussion of apparent addition of material on the left side of the canyon.

are characterised by very high unweathered rock material strengths (unconfined strength up to 350 MPa) but, due to being characterised onshore by very closely spaced defect and regular crush zones, have comparatively low overall rock-mass strength (e.g. from Rock Mass Rating and Q-System ratings) (Read et al., 2001). As indicated by the morpho-domain interpretation (Fig. 3B) these walls are characterised by steep, canyon-normal gully systems that initiate sharply at the shelf-edge and end at the canyon floor some 400–500 m below, with average overall slope angles of 15–18°, but with local slope angles commonly over 30°. The north eastern wall of Nicholson Canyon and adjacent shelf exhibits geomorphic features suggestive of both past and incipient large scale slope deformation (Fig. 8).

The Wairarapa Fault is expressed on the shelf as a 2–3 m high discontinuous scarp striking NE–SW, sub-perpendicular to the Nicholson canyon axis. Adjacent to this, several subtle scarps occur, aligned sub-parallel to the canyon axis. These scarps occur in opposing pairs, with vertical heights between 3 and 8 m, and are located between 100 and 1000 m from the canyon rim edge. From north west to south east (down-canyon) the general trend of the canyon wall is disrupted by a 90°, 1000 m long, lateral step into the shelf (shown as a "lateral scarp" in Fig. 8B). The canyon wall then continues on a similar trend as before for ~4.5 km before stepping back to the original canyon wall trajectory. Reconstruction of the canyon wall to calculate the volume of this indentation suggests approximately 1 km^3 of material is missing (shaded area in Fig. 8B), though post-removal modification of the canyon wall means the error of this calculation is likely to be large, possibly ± 20%. Debris fans at the base of the slope are indicative of small-scale failure of the slope in this area. A bathymetric profile down Nicholson Canyon floor shows broad-scale undulations (Fig. 8C). The canyon starts relatively steep (~5°) then levels out before steepening again to ~2.5°. The canyon then flattens until just prior to joining Wairarapa Canyon, where it actually slopes slightly

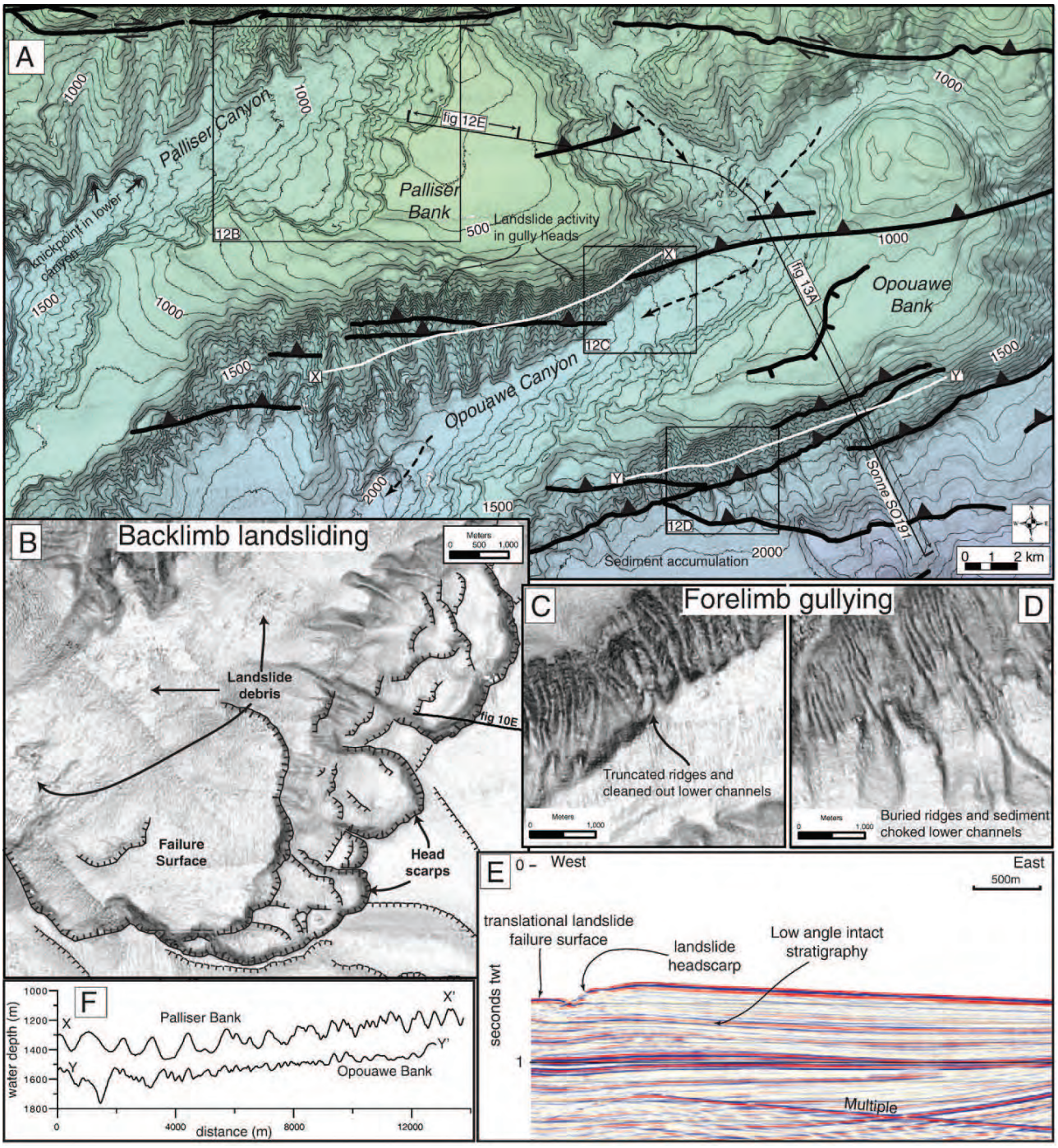

Fig. 12. Palliser and Opouawe bank morphology. (A) Shaded relief image with mapped tectonic structure and sediment transport routes. Location of B–E and Fig. 13A is shown. Shaded relief map has 5 times vertical exaggeration. Contour interval is 50 m. (B) Enlargement of the Palliser Bank landslide complex. Bathymetric image is a slope gradient plot with a 15 bin classified greyshade pallet, darker colours are steeper slopes. (C and D) Comparison of the lower boundary condition of the gully systems on Palliser and Opouawe banks. Image is a slope gradient plot as for 12B. (E) Seismic reflection profile across Palliser Bank illustrating low stratigraphic dips in relationship to bedding plane landslide head scarp (shown at 1.5×VE, 2 km/s twt), location in A and B (RV *Sonne* SO191 (2007) line 9–10). (F) Relief profiles across the gully systems on Palliser and Opouawe banks, location in A. Plots have 5 times vertical exaggeration.

uphill before dropping sharply at ~10° to Wairarapa Canyon. The base of this ~10° slope is coincident with the mapped trace of the Wharekauhau Thrust (Fig. 3). The central (~2.5°) steepening occurs directly adjacent to the indentation into the north eastern wall of Nicholson Canyon.

7. Development of canyons on the continental slope

Canyons on the continental slope include the lower part of the Cook Strait canyon system, Pahaua canyon, Opouawe Canyon, Campbell Canyon and other minor unnamed sediment pathways

(Figs. 1 and 4). The main axis of the Cook Strait Canyon is deeply incised into the slope in comparison to the other canyons (Fig. 1D), and additionally has numerous slope confined tributaries. Selected observations in the main Cook Strait Canyon axis, from a tributary canyon to the Cook Strait Canyon, and from inter-canyon slopes are presented in this section.

7.1. Main Cook Strait Canyon axis

Despite the deep entrenchment of the main Cook Strait Canyon axis into the slope, there is some indication that the lower reach of the canyon has potentially followed a different course at some time in the past. The canyon may have routed through a smaller canyon to the west, informally referred to here as the Campbell Canyon (Fig. 9). The seismic reflection profile in Fig. 9B images a possible buried channel, with a "v-shaped" ~700 ms thick stack of undeformed, horizontal and parallel reflectors, reconcilable with infilling of an abandoned channel section of a large canyon. The depth of infill in the seismic profile (650–750 m, assuming 2000 ms^{-1} two way travel time) agrees with the projection of the canyon axis down this adjacent canyon. Bathymetric cross-sections of the main Cook Strait Canyon illustrate a terrace on the inside of the meander bend, which suggests a vertical entrenchment of the canyon by approximately 200 m (Fig. 9C).

7.2. Cook Strait Canyon tributary

A ~60 km^2 tributary canyon to Cook Strait Canyon illustrates the development of the smaller scale contributing slope canyon systems (Fig. 10). This is selected from the "angular gully form" morphodomain in Fig. 4. The tributary system has a depth range of over 1200 m, from the shelf-edge at ~120 m water depth to the canyon floor at ~1340 m water depth. Interpretation of shaded relief maps and slope angle distribution maps defines three distinct geomorphic zones within the tributary catchment, characterised by the distribution of local slope angles (Fig. 10B). From the shelf-break and deeper we see: i) smooth slopes with low slope angles and a mode of 5° and a broad ridge-valley morphology, indicative of smothering by a thick sediment drape; ii) well defined but smooth gully morphology with

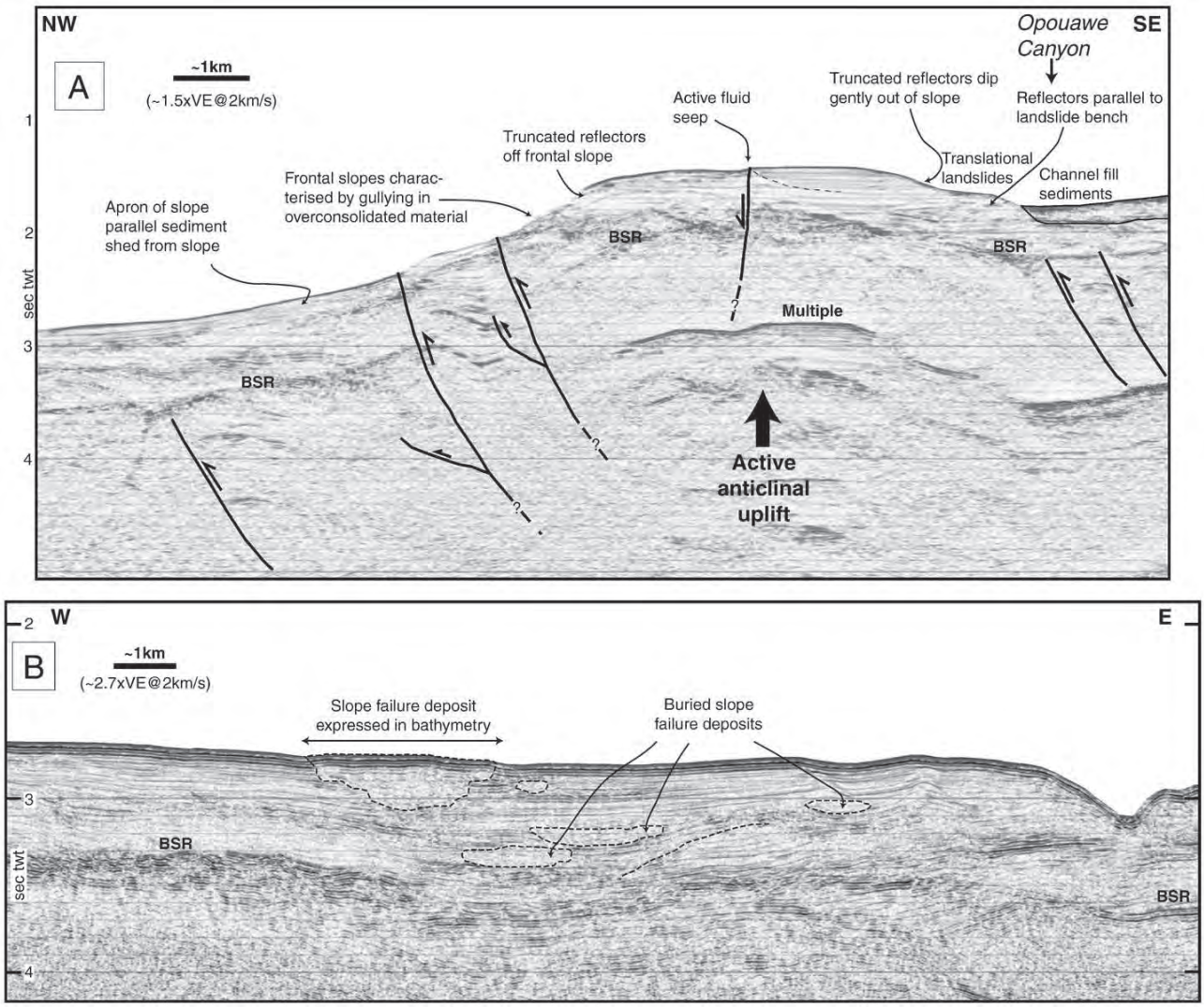

Fig. 13. (A) Seismic reflection profile *X*–*X*′ across Opouawe Bank illustrating the structural style of the thrust fault uplifted anticline ((RV *Sonne* SO191 (2007) line 9–10)). Location in Fig. 12A. (B) Seismic reflection profile *Y*–*Y*′ across sediments down slope of Opouawe Bank (RV *l'Atalante* GEODYNZ-SUD (1992) line P51). Location in Fig. 4A.

a normal distribution of slope angles around a mode of 15° is interpreted as gully formation with some sediment drape, as per Fig. 5B; and, iii) the lower end of the catchment showing a bi-modal distribution of slopes with strong peaks at 33° reflecting a steep step in the canyon axis that continues around the adjacent slopes, and 9° reflecting the flat canyon floor. Canyon axis longitudinal profiles show that the step in the canyon floor reaches a maximum height in channel "R2" (Fig. 10A and C), with an approximately 240 m high wall sloping between 15° and 40°+ and including over 100 m at 40°+ (Fig. 10C). Laterally, this oversteepened slope has developed small scale gullies that align with gully forms on the slopes above. A similar oversteepened canyon slope also occurs in two smaller canyons to the south (Fig. 10A).

7.2.1. Subcanyon modification

In another small canyon, within the "angular gully form" morphodomain (Fig. 4) repeated multibeam surveys capture some bathymetric change (Fig. 11A). Multibeam surveys are available for March 2005 and August 2005, and between these survey dates an anomalous area of seafloor in the canyon axis has been removed (Fig. 11B and C). The anomalous area is distinctly apparent in Fig. 11B as a contour closure in the gully axis (cf. Fig. 11C), and is well illustrated by the long profile comparison from the two surveys (inset Fig. 11B). The anomalous material in the March 2005 data is recorded on multiple soundings from two separate survey passes and the ship turn is not in the vicinity of the anomaly. Data artefacts noted in Fig. 11B are aligned perpendicular to the anomalous material and are a function of the fan sweep system. We are confident that this anomaly is not a data artefact, but acknowledge that the possibility cannot be completely discounted. The geometric form of the anomaly is consistent with a canyon blockage, and is not something observed in any other canyons within the multibeam extent. A difference of the two survey grids returns a volume for the anomalous area of 1.3×10^6 m^3 (Fig. 11D), however there is likely to be a high error associated with this figure. Fig. 11D shows a significant difference (~25 m) on the western gully wall, a pattern repeated in other adjacent gullies and thought to be related to the surveying direction. This regional style of data artefact is widely recognised in our grid differencing and has a distinctive and intuitively explainable form compared to the anomaly observed in Fig. 11B. The error on the volume estimate may therefore be as much as 65%. The difference in the canyon axes is typically null, however, and gives confidence in the ~60 m thick anomaly in the canyon long profiles (inset Fig. 11B).

The important piece of information here is not the precise volume of material but the observation that a bathymetric anomaly with the form of a canyon blockage has been removed from this gully within the six month inter-survey period.

7.3. Development of inter-canyon slopes

The majority of slope processes are taking place on inter-canyon slopes, contributing to the enlargement of canyons as well as responding to signals from the canyon as a local base level. Much of the relief between slope-confined canyons on the Cook Strait sector of the Hikurangi Margin is forming in response to active anticlinal folding. The Palliser, Opouawe and Pahaua banks are mature examples of folding and bathymetric uplift in the hanging wall of northwest-dipping thrust faults that intersect the sea-floor on the steeper seaward relief of the forelimb (Figs. 4A, 12A and 13A). The long-term structural deformation results in a distinctive asymmetric form to sea-floor ridges, in terms of both the relief generated and the erosional processes acting on the slopes. Fig. 13A illustrates the structural form of Opouawe Bank, showing the imbricate thrust fault system at the frontal edge of the anticlinal bank, and the gentle dipping reflectors on the back limb. A strong Bottom Simulating Reflector (BSR) occurs ~500 ms below the sea floor, and active fluid venting has been documented at the surface (Bialas et al., 2007), in the vicinity of the extensional structure near the crest of the bank. It is likely that many more small scale fault splays and deformation zones occur in the imbricate thrust zone and associated to the observed extension that are beyond the resolution of this data.

Forelimb (seaward) slopes are generally about twice as high as the backlimb slope, and forelimbs are generally steeper with overall gradients from ridge crest to channel of around 15–20° as opposed to less than 10° on the backlimb. Forelimb morphology is dominated by linear, generally parallel and evenly spaced ridge and gully systems, while backlimb morphology is dominated by sub-horizontal benches separated by steeply sloping, arcuate landslide headscarps (Fig. 12).

7.3.1. Forelimb gullying

Well established forelimb slope gully systems show a distinctive regularity in terms of channel spacing, incision depth and channel steepness; however, there are distinctive differences between the gully systems on Palliser and Opouawe banks. The Palliser Bank gully systems have a lower boundary defined by the Opouawe Canyon, the floor of which has a scoured and sculptured form. Gully systems on Opouawe Bank do not have such a well defined lower boundary, as they exit to the smoothly undulating lower continental slope (Fig. 12A–C). Landslides scars are widespread in the head-zones of gullies on both banks, contrasting with adjacent abandoned or relict gully head-zones (showing faint gully morphology) that still have steep and angular gully forms downslope of them. Additionally, there is evidence for larger scale landslide activity off the frontal slopes of Opouawe Bank, with several chaotic deposits visible in MCS (Fig. 13B) and an area of irregular seafloor in multibeam bathymetry in agreement with the MCS interpretation (Fig. 4A). Work on the Cascadia Margin has documented the occurrence of fluid seep sites within small scale canyons on similar anticline ridges (McAdoo et al., 1997; Orange et al., 1997), and seepage forces are suggested to be the principal driving mechanism for slope failure and the formation of these non-shelf connected ("headless") canyons. Recently this area of the Wairarapa Slope has received a lot of attention as a significant cold vent site (Bialas et al., 2007), however none of the work we are aware of has documented vents within the frontal gully systems.

7.3.2. Backlimb translational landslides

The backlimb (northern flank) of Palliser Bank shows widespread evidence of deep-seated landsliding and we interpret that ~30 km^2 of the slope has failed in this manner (Fig. 12B). MCS shows that the very low angle of the exposed failure surfaces (~2°) is coincident with the apparent stratigraphic dip (Fig. 12E). High-frequency acoustic profiles indicate that failure material is likely composed of sequences of Pleistocene hemipelagic sediments, as documented elsewhere on the Hikurangi Margin (e.g. Carter and Manighetti, 2006), and characteristic of what is mapped as "long term hemipelagic accumulation" (Figs. 4B and 5D). Failure areas are separated by head and lateral scarps that range from 50–160 m in height, reflecting the thickness of landslide failure blocks. The large accumulation of blocky landslide debris in the Palliser canyon (Fig. 12B) suggests that landslides do not completely disintegrate upon failure. Given these factors, the most likely failure mode is that of translational block slides along the ~2° bedding plane surfaces. In terrestrial settings, it is relatively common for the failure surface of translational landslides in upper Cenozoic marine sequences to be controlled by thin, laterally extensive layers with shear strength properties much lower than the dominant rock material (Stout, 1977; Bell and Pettinga, 1988; Mountjoy and Pettinga, 2006), and similar controls have been documented in marine slope instability studies (Bryn et al., 2005a; Leynaud et al., in press). While we cannot unequivocally document this here, it is likely the failure surfaces utilise elastically weak material in the sedimentary pile and the mechanism is similar to that documented onshore. An additional controlling influence recognised in failures occurring in subaerial

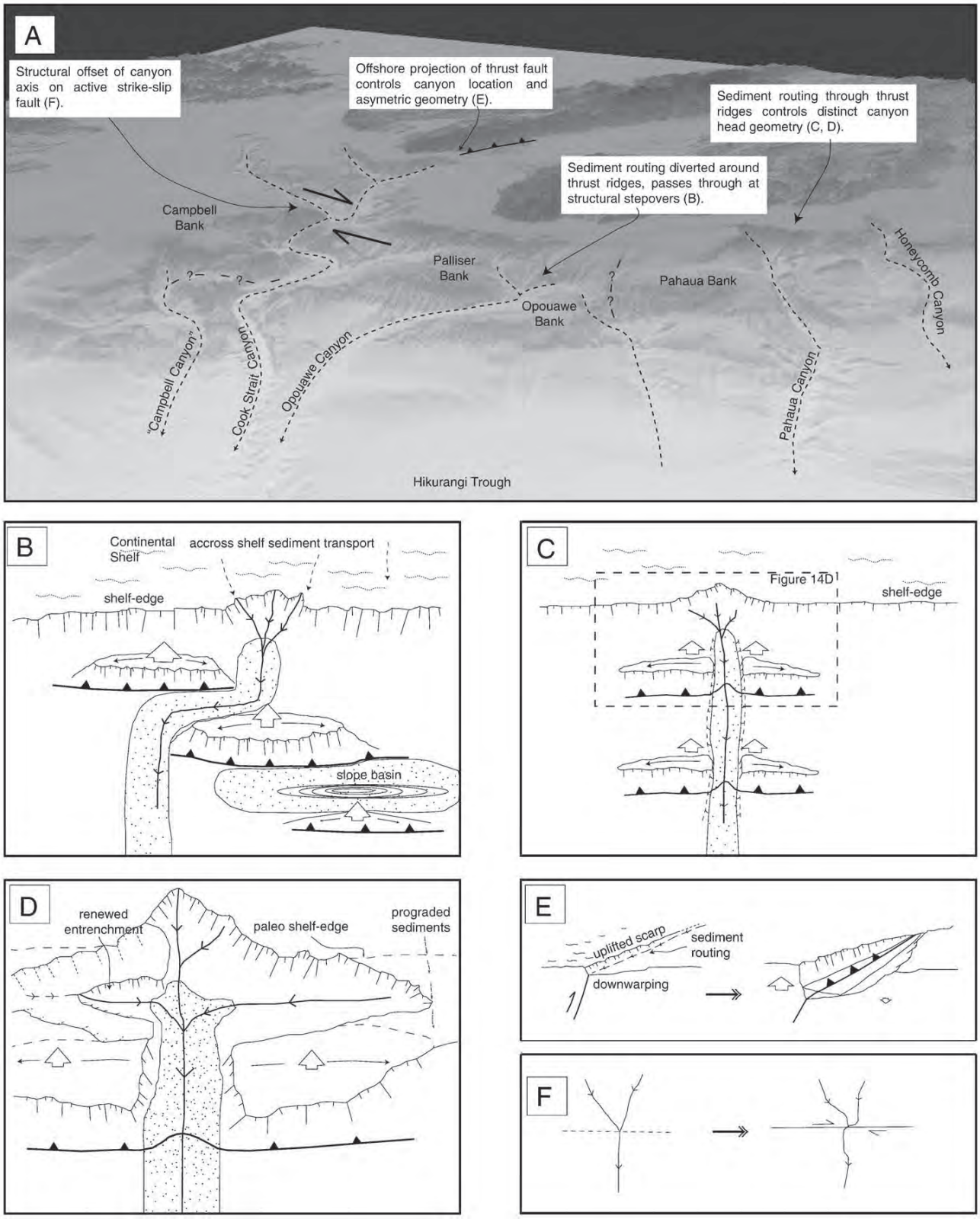

Fig. 14. Structural influence on canyon location, geometry and evolution. (A) Oblique image of Cook Strait/Wairarapa margin (3 × VE) illustrating sediment routes as dashed lines, and showing illustrative examples of canyon controls, as discussed in text, and with reference to schematic drawings in B–F. (B) Simple deflection of sediment routing around structurally controlled relief. (C) Dissection of tectonically growing relief by sediment routing across thrust ridges. (D) Distinctive mushroom-shaped morphologic development of canyon head zone resulting from situation illustrated in C. (E) Development of a canyon along the trace of an active thrust fault. (F) Influence of lateral fault slip on canyon path.

marine sequences is the control of rock-mass defects (i.e. faults, joints and bedding planes) which define lateral and headward release surfaces.

8. Discussion

Cook Strait marks the discontinuity between the major axial ranges of the North and South Island, and their respective upper plate fault systems (Carter et al., 1988; Barnes et al., 1998). It is suggested that Cook Strait evolved through the rotation and alignment of several sedimentary basins in the mid-Pleistocene and has subsequently experienced opening and closing in line with major glacial cycles, with a land bridge developing to the west of the narrows (Proctor and Carter, 1988; Lewis et al., 1994). Although likely to be related to the mid-Pleistocene opening of the Cook Strait seaway, the timing of the initial inception of the Cook Strait canyon system remains unconstrained. Modelling by Proctor and Carter (1988) suggests that during low stands, tidal currents resonating in the embayment west of the Narrows are amplified compared with the present day. With the breach of the land bridge due to rising sea-levels (last at c. 15 ka B.P.) it is likely that the Cook Strait canyon system receives a large and rapid influx or pulse of sediment in a relatively short period of time and this would be a time of significantly enhanced activity in the canyon system. In addition, periodically glaciated terrestrial catchments would provide enhanced material loads through fluvial systems during and immediately following glaciations. The apparent maturity of the canyon system suggests a relatively long period of evolution, possibly through several major (100 ka type) glacial cycles.

With Cook Strait being the only open seaway through the New Zealand landmass, it is intuitive that related oceanographic currents must be a major factor in the development of the largest submarine canyon system on the Hikurangi Margin. Whereas in the north of the margin submarine canyon development is proposed to be facilitated by upper plate deformation in response to subducting seamounts (Lewis et al., 1998; Collot et al., 2001), there is no indication that this process played any role in the formation of submarine canyons in the south. We speculate that the Cook Strait canyon system started as a slope canyon system heading into the shelf break, much like the Pahaua Canyon, which at some point during its evolution incised its way across the shelf until c. 50% of the canyon systems areal extent is shelf-incising.

Initial shelf encroachment may have been along the traces of major faults following structurally generated seafloor relief, and local structural alignment of Cook Strait Canyon is still evident in the Wairarapa Canyon arm which is aligned along a major thrust fault (Barnes and Audru, 1999a) (Fig. 3). It is likely that fault generated relief led to the inception of this canyon, with uplift in the hanging wall (NW side) and subsidence in the footwall creating a bathymetric depression that has subsequently become a major conduit for sediment transport to the deep ocean with subsequent canyon enlargement (Fig. 14E). Additionally, the strike–slip BooBoo Fault traverses the Cook Strait Canyon where the three canyons merge (Fig. 3), and appears to offset the alignment of these upper canyons from the lower principal canyon by some 3 km (Fig. 14F).

Another factor we recognise as likely to be important in the extensive shelf extent of this canyon system, in comparison to others on Hikurangi margin, is the occurrence and geometry of the three major Cenozoic sedimentary basins (Fig. 1). In contrast to much of the Hikurangi Margin, where sedimentary basins are aligned parallel to the margin and occur against a backstop of similarly aligned and less easily eroded greywacke basement, sedimentary basins occur through the axis of Cook Strait allowing shelf ward incision of the canyon system.

Regardless of its origin, the Cook Strait Canyon is located in a highly active tectonic area, and is strongly affected by glacio-eustatic sealevel cyclicity. Thus the activity of the canyon both in the present day and over geomorphic time must be considered within the framework of these two major forcing factors.

8.1. Climatic and tectonic base-level controls on canyon activity and entrenchment

Since the LGM at ~20 ka B.P., climatically controlled sea-level rise of ~120 m has shifted the shoreline from near or at the rim of the Cook Strait Canyon to its present location at the very least 1.2 km away from the canyon edge. During the glacial low-stand, terrestrially derived sediment may cross the shelf, transported by the major fluvial systems, and feed directly into the canyon system. This is immediately apparent for the Wairarapa Canyon arm (Fig. 3) where the canyon head comes within close proximity of the coast and present day river systems, but is much less certain for the western canyon (e.g. Cook Strait Canyon arm) which are well removed from the coast. Sea level low stands are widely recognised as a time of much higher sediment flux offshore (e.g. Carter and Manighetti, 2006). While the continental shelf between canyons typically progrades seaward during lowstand times, in the canyons themselves much of the sediment input into the system will bypass the slope system in down-canyon transport and will scour out the connected branches of the canyon system. Following sea-level rise these sediment conduits will be closed off to direct terrestrial sediment input from fluvial and/or littoral transport, in all but those cases where canyons are incised across the shelf to remain connected to these systems, e.g. Kaikoura Canyon (Lewis and Barnes, 1999), Monterey Canyon (Greene et al., 2002; Smith et al., 2005), and Kaoping Canyon (Chiang and Yu, 2006) among others.

It is apparent that despite not being connected to either fluvial and/or littoral processes a certain amount of erosion and active sedimentary transport has continued to occur during the Holocene. Cores from both the upper and lower parts of Cook Strait Canyon show repeated sandy turbidite deposits. Though we have no age constraint on the emplacement of these deposits, there is no significant thickness of laminated mud in the upper part of the cores, which would have accumulated if down-canyon processes were not active. Similarly, high frequency acoustic profiles do not show laminated sediments but typically have a sharp non-penetrative echo characteristic of coarse grained sediment (e.g. Carter, 1992). Likewise we see numerous instances of canyon wall mass failure at a variety of scales, as expected in a region of high tectonic activity, but very little debris accumulating in the canyon axes. While this is far from being conclusive evidence of an active canyon system, these observations do support a model of some high stand activity. The most likely source of regular sediment input is tidally transported material from the west, into the Cook Strait and Nicholson Canyon arms.

In the slope canyons and tributaries of the Cook Strait Canyon there are also morphological indications that high stand activity is occurring. A simple model of canyon behaviour during sea-level low-stand and high-stand periods (glacial–interglacial) is that tributary canyons experience top-down vertical channel entrenchment during the low-stand as coarse clastics are fed directly into tributary canyon heads, while principal canyons (e.g. lower Cook Strait Canyon) may become overwhelmed with sediment and experience transient aggradation (Fig. 10D). Following the marine transgression at the termination of the LGM, and the abandonment of the direct coarse clastic sediment supply, canyon head infilling can occur (cf. Walsh et al., 2007) and the upper portion of the catchment may be blanketed with fine sediment (Fig. 10E). It is apparent that rather than remaining inactive during high-stand interglacial periods, the canyon "rejuvenates" through a bottom-up process of channel coupled incision or entrenchment, which will induce instability on adjacent slopes as a 'knickpoint' migrates up canyon. This process is believed to be occurring through repeated small scale collapses of the entrenchment headwall, as oppose to hydrodynamic processes, given the limited extent and apparent lack of activity of the upper catchments

where this process is observed (e.g. Figs. 10 and 11). We have documented failure activity likely to be related to a similar style of entrenchment headwall in repeated multibeam surveys (Fig. 11), and believe this mechanism is widely applicable to high stand submarine drainage rejuvenation. The initiation of channel entrenchment in Fig. 11 almost certainly relates to hanging wall uplift on the large lower slope thrust fault inducing a lowering of channel base level. It is probable that headwall failure is triggered by ground shaking events, but also possibly by other means such as fluid expulsion.

In the situation illustrated in Fig. 10 there is no lower slope fault to provide a local base level fall, yet there is clearly a wave of channel incision passing up several adjacent "catchments". This is believed to be related to a more regional base level control.

8.1.1. Tectonic base level on the continental slope

Sediment sourced from both shelf and intra-slope sources is channelled through canyons to the Hikurangi Trough and, in the same sense that the ocean acts as the base-level for onland fluvial systems, this may be considered as the regional base-level for the continental shelf and slope sediment transport system. The combination of sea-level rise and fall altering the sediment transport path lengths, and regional and local tectonic uplift modifying slope bathymetry, is a driver for canyon base level perturbations that may influence the rates and mechanisms of erosional processes shaping canyon systems.

In tributaries of the main Cook Strait Canyon the local base-level is defined by the main channel floor. Accelerated incision of the Cook Strait Canyon axis provides a simple mechanism for lowering local base level, which could in turn migrate up the tributary canyons thereby initiating a renewed phase of incision and channel coupled slope instability as the entrenchment knick-point migrates up channel. Furthermore, regional uplift of the upper margin could provide a relative lowering of the regional base level (the Hikurangi Trough) providing a sufficient perturbation to initiate a period of canyon down-cutting to maintain grade. Lower in the main Cook Strait Canyon we see evidence suggesting a lateral channel shift (as well as total course change) and entrenchment of the active channel in the order of 200 m (Fig. 10). This canyon modification may be in response to a regional, tectonically forced base-level lowering event, the effect of which is still being actively propagated up through tributary canyons of the main canyon system. However, regardless of the forcing mechanism, we observe a systematic re-excavation, or retrogressive erosion, of older (inferred lowstand) antecedent canyon systems that have most likely been inactive as top to bottom sediment conduits at least since sea-level reached its present height at ~6.5 ka B.P. (Gibb, 1986).

8.2. Localised structural controls on canyon geometry

In addition to regional tectonic forcing and glacial-cycles providing a relatively regular long-term control on canyon processes; tectonic forcing in terms of structural uplift, folding, fault breakouts and high level co-seismic ground shaking at differing time scales have a profound influence on the evolution of canyon morphology. The Hikurangi Margin accretionary wedge tapers to the south accommodated by the progressive landward stepping of upper plate deformation front structures (Fig. 1). By Cook Strait, the mid-slope of the margin is characterised by comparatively short (~20 km long) thrust fault bound anticlinal ridges that are offset in response to fault segmentation and step-over relationships. Margin-normal bathymetry profiles illustrate how canyons have incised deeply through structurally generated relief (Fig. 1C). The Honeycomb slope profile shows a "classical" active margin slope configuration of regular steps up to the continental shelf, whereas the Campbell and Pahaua slopes show much more variation in relief as these cross well incised margin-parallel canyons and structurally propagated bathymetric ridges.

Sediment must bypass this structurally generated relief to reach the Hikurangi Trough, such that canyons will incise in a specific location on the continental slope dependant on the interplay of numerous factors, including: structure location, segmentation boundaries and differential uplift rates; sedimentation rates; sea-level cycles; and, current-driven and other sediment transport processes. The well developed accretionary margin physiography, combined with examples of intermediate-scale canyon systems on the southern Hikurangi Margin, provides an excellent opportunity to assess the first-order controls on canyon location across an active margin.

8.2.1. Channel deflection around thrust fault discontinuities

Sediment transport processes (e.g. turbidity currents) will generally divert around areas of high bathymetric relief, with mass-flow mobility controlled by the combined effects of local slope gradient, flow turbulence, channel width and sediment load. Offshore ridges on the Wairarapa margin are developing by long-term localised structural uplift, overprinted on regional margin uplift. Thrust faults of limited length are facilitating the development of elongated ridges that taper to their ends reflecting the plunge of thrust fault propagated fold structures and a reduction in fold amplitude toward fault tips. It follows then that where canyons pass between thrust ridges, they will do so at structural step-overs, as illustrated in Fig. 14A and B. Once flow pathways have developed between structures continued uplift, both increasing relative relief and driving channel erosion, contributes to channels becoming further entrenched and maintaining their position across the continental slope. An excellent example of this process is where the Opouawe Canyon is strongly deflected between Opouawe Bank and Palliser Bank (Fig. 14A).

8.2.2. Channel incision through structures

In the situation where structurally generated bathymetric relief directly blocks the path of a sediment route, a canyon may need to dissect the structure to pass through to the lower slopes (Fig. 14C). An example of this situation is where the Pahaua Canyon entrenches across the Opouawe–Uruti and Pahaua faults (Fig. 4A). The concept of antecedent drainage paths across propagating structures (e.g. Burbank et al., 1996) provides one explanation for this phenomenon, whereby folds develop across an existing flow path that is able to maintain its position through the structure. Basins formed behind structural relief may also outpace uplift rates and fill to the extent whereby sediment flows can cross a structural saddle on the top of structures and subsequently erode into them. This style of incision initiation is likely when thrust ridges occur near the shelf-break and low-stand progradation of the shelf may inundate basins with very high sediment loads, filling them to the level of ridge crests and allowing channels to develop over the crest. The depression behind Pahaua Bank reveals a situation where this process may have occurred, with indications of sedimentary fill in the order of 300 m thick filling part of the canyon head and onlapping onto apparently relict gully systems (see example Fig. 5B), but that fill is now being excavated from the bottom up (Fig. 14D).

Once a channel is established across a (basin-bounding) anticline ridge it may quickly incise into the structure to obtain grade with the base-level at the foot of the continental slope. The lateral excavation of weaker slope basin sediments from behind anticlinal ridges forms depressions that we observe to have a distinctive "mushroom" geometry (Fig. 14D). An excellent example of this process is the shelf-incised portion of the Pahaua Canyon head where lateral erosion of sediments accumulated behind the Pahaua Bank anticlinal ridge appears to be occurring. It is most likely that the long-term evolution of these features is punctuated by periods of infilling and periods of re-entrenchment of drainage systems. Where Pahaua Canyon cuts through Pahaua Bank large-scale gravitational failure is occurring, contributing to the retrogression of canyon walls and the maintenance of the canyon's location through the active anticline (Fig. 4).

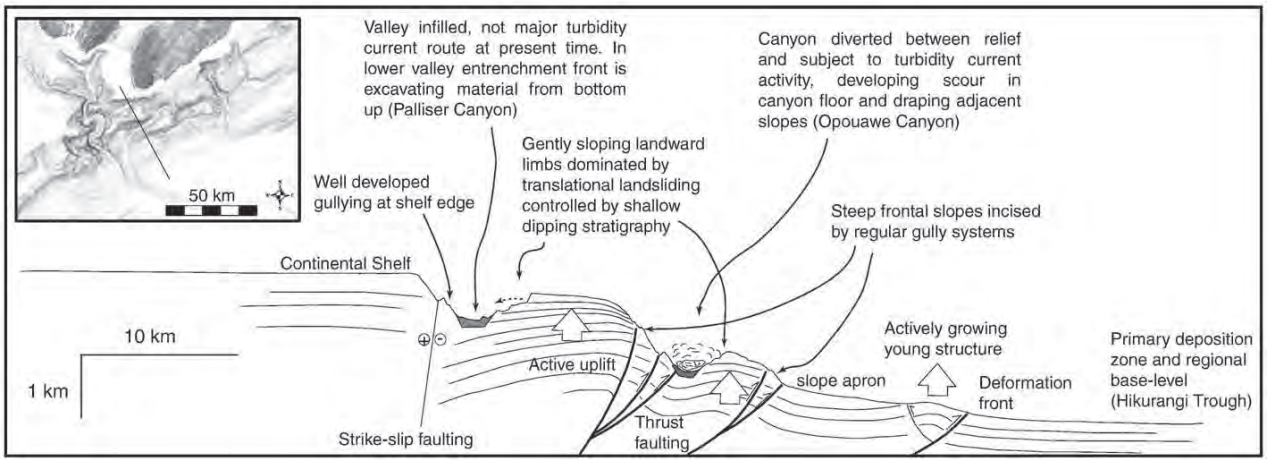

Fig. 15. Annotated schematic section through the Cook Strait margin from shelf to trough. Bathymetric profile is derived from multibeam data on a 10 m DTM (location inset).

8.3. Structurally generated relief and erosion of the continental slope

In this study, we show that erosion and the development and modification of relief is occurring on the continental slope is partly occurring in response to thrust fault driven, asymmetric folding as reflected in the observed sea-floor relief. The schematic section in Fig. 15 illustrates the progression from a young fold on the lower slope just developing seafloor expression to the structurally evolved Opouawe and Palliser banks on the upper-mid slope. The processes dominating the erosion of both Palliser and Opouawe banks contrast between the forelimb (seaward) and backlimb (landward) flanks of the structures. Stratigraphically controlled, translational slope failure dominates backlimb flanks, whereas regular, linear gully systems dominate forelimb flanks. The contrast in mass-movement process principally reflects the uplift and asymmetric folding of progressively more overconsolidated sequences in the hanging wall section of thrust faults. This mechanism controls the development of steepened bedding dips and the localised concentration of thrust-faulted sequence disruption and material degradation on the forelimb, compared to gently dipping, undisturbed bedded sequences on the backlimb. Although the same asymmetric structural morphology and distinctive mass movement processes are occurring on both Palliser and Opouawe banks, the scale and detail of geomorphic expression of the processes differs: for example gullying on the eastern flank of Palliser Bank exhibits dominant principal ridges and a crest spacing generally over 1000 m, while Opouawe Bank has a more uniform, cross-gully profile with regular sized ridge spacing of just a few hundred metres. The primary control on the difference between these gully systems is inferred to be the lower boundary condition of the slopes. The lower boundary of Palliser Bank gully systems is Opouawe Canyon, which exhibits a scoured canyon floor possibly indicating regular erosive activity which would removing any material eroding from gullies frontal gully systems. In this way, the system is channel-coupled and the incision rate of individual gullies is detachment-limited. On Opouawe Bank, the lower boundary of the gully systems is a mid-slope depositional zone and subsequently any material eroded from the upper reaches of gullies will accumulate at the foot of the gully and limit erosion. In this case, therefore, gullies are non-coupled and the rate of incision is considered to be transport-limited. Gullies are eroding through a combination of both bottom up failure with periodic perturbation stimulating a new phase of headward channel entrenchment, and by down-canyon scour by failed material from head-zone landslides travelling down the existing channel.

Similarly, differences in the appearance of translational landslide complexes on the landward side of the two banks are considered to be strongly influenced by the lower boundary condition. On the north western flank of Palliser Bank, landslide scarps and evacuated scars are clearly defined, with blocky landslide debris accumulating in the canyon below where limited down-canyon sediment transport is occurring. Conversely, on the north western flank of Opouawe Bank landslide scarps are more diffuse and the canyon below shows no evidence of landslide debris accumulation. We infer that landslide complexes may be similarly active on both structures, but that in the Opouawe case turbidity current transported sediment in Opouawe Canyon will overtop the channel and spill onto the adjacent slopes, draping these complexes with fine sediment. Despite the differences outlined, both ridges are being eroded in a very similar manner and this reflects clear structural controls on the bathymetric development of the ridge and canyon system.

The occurrence of deep-seated mass movement and slope deformation on frontal ridge slopes in the early phases of topographic-structural development of the banks may pre-position the ridge for the more widespread gullying they subsequently experience through the creation of initial relief and the exposure of older, overconsolidated material. We observe large landslide scars and deposits related to mass failure of the frontal slopes of these ridges (Figs. 4 and 13B). Focused fluid-flow on active margin thrust ridges is one mechanism proposed for slope failure and gully system initiation (McAdoo et al., 1997; Orange et al., 1997; Lewis et al., 1998). Cold fluid seepage has been documented on Opouawe Bank (Bialas et al., 2007), although no evidence for fluid seepage has been found on Palliser Bank. Given that the slopes we are talking about are up to 1 km in height sloping at 15–20°; it seems likely that erosive processes would develop independently of a requirement for a direct local driver. We suggest that while fluid flow may well be playing a role, the influence of local, regularly occurring, high magnitude co-seismic ground motion on oversteepened slopes will be an important (if not dominant) force in the destabilisation of forelimb slopes.

8.4. Bedrock removal processes

Sediment routing across the continental slope through established canyon systems leads to the inevitable requirement of excavating bedrock material if canyons are to enlarge and evolve in a tectonic and climatic framework. In this study, we have documented the widespread occurrence of bedrock slope failures, occurring in varied lithological and morphostructural settings with multiple failure modes. Bedrock landslides dominate slopes in the upper canyon area (Fig. 3B), and are also widespread on the continental slope (Fig. 4B). The largest landslides mapped, developed from canyon floor

to upper slope crest and involving volumes up to 10 km^3, occur on the walls of the principal canyons (Figs. 3 and 4). Additionally most of these occur adjacent to major tectonic structures, and it is apparent that the large failures are structurally influenced gravitational collapses, as well as being affected by high levels of co-seismic ground shaking.

The M8.2 1855 Wairarapa Earthquake is a good example of the level of effect of a local earthquake. It is possible that both the Wairarapa fault and Wharekauhau Thrust ruptured during the event, and the Nicholson and Wairarapa canyons were most likely encompassed entirely by the MM10 isoseismal (Downes, 1995). Canyon slopes would have experienced extraordinarily high co-seismic peak ground accelerations, ≥0.5 g (Dowrick, 2005). Onshore, co-seismic landslides in the Rimutaka Ranges (Fig. 1) were widespread (Hancox, 2005), and the landscape is still removing the generated sediment. On the outer shelf-edge in Nicholson Canyon a combination of structurally influenced rock mass disturbance during fault rupture, and localised very high ground shaking levels, provide the most likely triggers for major canyon wall failure. Slopes will be pre-conditioned for further failure through bedrock mass weakening by deep-seated gravitational collapse processes, and rock mass dilation evident from extensional grabens on the outer shelf supports this model (Fig. 8).

Seismic reflection data show that deep-seated slope failures in late Cenozoic sequences (Figs. 4 and 6), and on the back limb of anticlines within the slope confined part of the Cook Strait canyon system (Fig. 12), have stratigraphically controlled geometries. It is speculated that failure surfaces of the majority of the large bedrock landslides in the Cook Strait canyon system are facilitated by weak layers within the bedded marine sequences, providing control on the depth of the failure surface and critical strength parameters. One possibility for the origin of such mechanically weak layers is thin, discrete volcanic ash layers altered to smectite clay, as is documented to control deep seated failure of bedded marine sequences onland (Mountjoy and Pettinga, 2006). Sedimentary sequences forming on the southern Hikurangi Margin (such as those subject to deep-seated instability in the Cook Strait canyon system) are punctuated by volcanic (typically rhyolitic) tephra, documented back to the mid Miocene (Carter et al., 2004a). Additionally, Miocene–Pliocene marine sedimentary rocks exposed onshore in the adjacent lower North Island contain rhyolitic tephra horizons (Lee and Begg, 2002). Alteration of rhyolitic tephra to smectite clays may occur in shallow marine, deep marine and terrestrial environments alike (e.g. Naish et al., 1993; Bakker et al., 1996; Carter et al., 2004a). The most well documented instance of weak layer control on landslides is from the Storegga slide offshore Norway (Bryn et al., 2005a; Kvalstad et al., 2005). In this situation weak layers are clay rich, sensitive and brittle contourites, within comparatively coarse glacio-marine and glacial sediments leading them to have a controlling influence on landslide failure plane location (Bryn et al., 2005b). While extensive contourites or drifts have been documented elsewhere on New Zealand's continental margin (e.g. Carter et al., 2004b) we know of none documented in sedimentary sequences in the Cook Strait sector of the Hikurangi Margin.

Excess pore pressures developing in comparatively high permeability (e.g. sand-rich) horizons has been recognised as another key parameter for deep-seated submarine slope instability (e.g. Sultan et al., 2004). Modelling of the residence time of elevated pore pressures developed during rapid sedimentation shows these may persist for very long periods (10^3 yrs) in certain materials (Leynaud et al., 2007). While basin sedimentation rates are not well constrained, the Cook Strait study area lies in a zone of high seismicity with numerous active faults. Cyclic loading during earthquake generated strong ground motion is also a mechanism by which excess pore pressure may be generated in permeable horizons (Sultan et al., 2004). Given the high concentration of active faults in Cook Strait (Figs. 1, 3 and 4), the historical occurrence of two M7.5+ earthquakes (Downes, 1995) and the modelled frequent occurrence of relatively high earthquake generated strong ground motion (Stirling et al., 2002a), it is very likely that earthquake generated strong ground motion plays a pivotal role in slope destabilisation within the Cook Strait canyon system. Specifically, the entire upper Cook Strait canyon system is enclosed by the MMIX felt intensity isoseismal of the M8.2 Wairarapa Earthquake (Fig. 1B), and the three large landslides documented in the upper canyon area all occur adjacent to major faults acting as significant earthquake sources (Figs. 3, 6 and 8). We infer that failures occur as either co-seismic events or that slopes are partially deformed during ground shaking and fail post-seismically in subsequent earthquakes or by other mechanisms, having been conditioned for failure by earthquake generated strong ground motion through rock mass disturbance and/or the generation of excess pore pressure that remains in residence through to the next large earthquake.

The ubiquitous occurrence of deep-seated failures on canyon walls suggests that the undercutting and lateral stress relief of the sedimentary sequence is also an integral factor in the destabilisation of the rock mass. Large scale bedrock failures on canyon walls result in large volumes of disturbed and weakened material, which facilitates numerous smaller magnitude failures that excavate the remaining failed slide mass and encroach into slopes through headwall and lateral scarp failure as toe support is progressively removed. Subsequently, once failure complexes are initiated they remain a locus of ongoing slope failure, contributing to both the enlargement of the canyon, and providing punctuated but ongoing sediment supply. The canyon in turn conveys this material to the major subduction axis, in this case the Hikurangi Trough where material is either deposited or transported north in the Hikurangi Channel.

9. Summary and conclusions

Canyons on the Cook Strait sector of the Hikurangi Margin are evolving in response to both tectonic and climatic forcing factors. The Cook Strait Canyon is a deeply incised, shelf-indenting canyon occurring at the transition from thrust fault dominated, oblique subduction to oblique strike–slip dominated collision at the active Pacific–Australian plate boundary. The development of this canyon into the largest Hikurangi Margin canyon system is inferred to be strongly affected by the presence of both ocean currents related to the open Cook Strait seaway and the large, elongate and margin normal sedimentary basins within which it is incised. The well entrenched meandering geometry of Cook Strait Canyon observed today results from the combined effects of structurally controlled bathymetry and active sediment transport processes. The key role of structural deformation is clearly seen when comparing Cook Strait Canyon to the less evolved examples of canyons on adjacent slopes to the north east.

The main findings of this study are:

- The location and geometry of canyons on this tectonically active continental slope is controlled by structural elements both deflecting and obstructing sediment routing, thereby developing distinctive end member configurations.
- Submarine “catchment” systems that have likely been inactive post sea-level rise (since ~15 ka) are being rejuvenated by a bottom up process of entrenchment migration affecting multiple catchments simultaneously. The mechanism of erosion is via relatively small-scale headwall failure and sediment removal.
- The simultaneous rejuvenation of adjacent relict “catchments” indicates that the submarine landscape is responding to a perturbation of the local base-level, and possibly the regional base-level.
- Bedrock landslides affect large areas of the canyon slopes and are strongly influenced by lithology, existing rockmass defects and slope undercutting by canyon entrenchment. The geomorphic fingerprint

of bedrock failures contrasts strongly between those occurring in Mesozoic greywacke, and those in Cenozoic marine strata.
- Cyclic loading associated with high levels of co-seismic ground shaking is inferred to be an important trigger for slope failures. However, documentation of active small-scale failure activity on the mid-slope shows that canyon excavation continues during inter-seismic periods. This may reflect the "pre-conditioning" influence of large magnitude earthquakes on slopes, facilitating ongoing failure throughout the seismic cycle, and also may be related to active fluid sapping.
- Large landslide complexes host multiple, smaller scale failures that strongly influence the development of canyon slopes and provide a significant intra-slope sediment source.
- Thrust propagated anticline ridges on the southern Wairarapa region of the subduction zone are eroding in a distinctive asymmetric fashion controlled by local stratigraphic dips and slope gradients. Frontal leading-edge slopes are dominated by intensive gullying, while trailing limb slopes are dominated by extensive translational failure of 100 m+ thick bedrock slabs.
- The maturity, geomorphic expression and relative incision rate of both gullying and translational landslide processes on anticline ridges is controlled by the lower boundary condition, which varies significantly between active sediment routing and depositional slopes.

The advent of instruments capable of collecting high-resolution bathymetric data covering large areas of the ocean floor, from shelf to trench depths, may provide unprecedented insight into morphostructural processes controlling the evolution of active margins. The insights gained from New Zealand's active convergent margin at Cook Strait are almost certainly applicable to many other active margins around the world. Further acquisition of targeted seismic reflection data and sediment coring to provide age constraints will facilitate further development of these models, allowing them to be widely applied to other regions, and thereby increasing our understanding of process rates involved in the initiation and evolution of submarine canyons on active margins.

Acknowledgments

The multibeam data that this work is primarily based on was collected under the Foundation of Research Science and Technology contracts. We particularly thank John Mitchell of NIWA for leading several of the multibeam surveys. Joshu J Mountjoy received a Top Achiever Doctoral Scholarship (2006–2009) from the New Zealand Tertiary Education Commission to undertake this research. NIWA technicians Claire Castellazzi, Kevin Mackay, Arne Pallentin and Miles Dunkin are thanked for their contributions. Early versions of this manuscript benefited from reviews by Dr S. Nodder, Dr L. Carter and Dr G. Lastras.

References

Audru, J.-C., 1996. From the Hikurangi subduction zone to the Alpine Fault, Marlborough, New Zealand. Unpublished PhD Thesis, University of Nice, France, 268 pp.

Bakker, L., Lowe, D.J., Jongmans, A.G., 1996. A micromorphological study of pedogenic processes in an evolutionary soil sequence formed on Late Quaternary rhyolitic tephra deposits, North Island, New Zealand. Quat. Int. 34–36, 249–261.

Barnes, P.M., Audru, J.-C., 1999a. Quaternary faulting in the offshore Flaxbourne and Wairarapa Basins, southern Cook Strait, New Zealand. N.Z. J. Geol. Geophys. 42, 349–367.

Barnes, P.M., Audru, J.-C., 1999b. Recognition of active strike–slip faulting from high-resolution marine seismic reflection profiles: Eastern Marlborough fault system, New Zealand. Geol. Soc. Amer. Bull. 111 (4), 538–559.

Barnes, P.M., Mercier de Lepinay, B., 1997. Rates and mechanics of rapid frontal accretion along the very obliquely convergent southern Hikurangi margin, New Zealand. J. Geophys. Res. 102 (B11), 24931–24952.

Barnes, P.M., Mercier de Lepinay, B., Collot, J.-Y., Delteil, J., Audru, J.-C., 1998. Strain partitioning in the transition area between oblique subduction and continental collision, Hikurangi Margin, New Zealand. Tectonics 17 (4), 534–557.

Baztan, J., Berne, S., Olivet, J.-L., Rabineau, M., Aslanian, D., Gaudin, M., Rehault, J.-P., Canals, M., 2005. Axial incision: the key to understand submarine canyon evolution (in the western Gulf of Lion). Mar. Pet. Geol. 22 (6–7), 805–826.

Begg, J.G., Johnston, M.R., 2000. Geology of the Wellington area. Institute of Geological and Nuclear Sciences 1:250 000 geological map 10. Institute of Geological and Nuclear Sciences Ltd, Lower Hutt, New Zealand.

Begg, J.G., Mazengarb, C., 1996. Geology of the Wellington area, scale 1:50,000,. Geological map, 22. Institute of Geological and Nuclear Sciences (IGNS).

Bell, D.H., Pettinga, J.R., 1988. Bedding-controlled landslides in New Zealand soft rock terrain. Proceedings of the International Symposium on Landslides: Comptes Rendus du Symposium International sur les Glissements de Terrain, vol. 5, pp. 77–83.

Bialas, J., Greinert, J., Linke, P. and Pfannkuche, O., 2007. FS Sonne Fahrtericht/Cruise Report SO 191 — New Vents "Puaretanga Hou", Wellington-Napier-Auckland, 11.01–23.03.2007, IFM-GEOMAR Berichte aus dem Leibniz-Institut für Meereswissenschaften an der Christian-Albrechts-Universität zu Kiel.

Bowman, M.J., Kibblewhite, A.C., Ash, D.E., 1980. M2 tidal effects in greater Cook Strait, New Zealand. J. Geophys. Res. 85, 2728–2742.

Bryn, P., Berg, K., Forsberg, C.F., Solheim, A., Kvalstad, T.J., 2005a. Explaining the Storegga Slide. Mar. Pet. Geol. 22 (1-2 SPEC. ISS.), 11–19.

Bryn, P., Berg, K., Stoker, M.S., Haflidason, H., Solheim, A., 2005b. Contourites and their relevance for mass wasting along the Mid-Norwegian Margin. Mar. Pet. Geol. 22 (1-2 SPEC. ISS.), 85–96.

Burbank, D., Meigs, A., Brozovic, N., 1996. Interactions of growing folds and coeval depositional systems. Basin Res. 8 (3), 199–223.

Carter, L., 1992. Acoustical characterisation of seafloor sediments and its relationship to active sedimentary processes in Cook Strait, New Zealand. N.Z. J. Geol. Geophys. 35, 289–300.

Carter, L., Lewis, K.B., 1995. Variability of the modern sand cover on a tide and storm driven inner shelf, south Wellington, New Zealand. N.Z. J. Geol. Geophys. 38, 451–470.

Carter, L., Manighetti, B., 2006. Glacial/interglacial control of terrigenous and biogenic fluxes in the deep ocean off a high input, collisional margin: a 139 kyr-record from New Zealand. Mar. Geol. 226, 307–322.

Carter, L., Lewis, K.B., Davey, F.J., 1988. Faults in Cook Strait and their bearing on the structure of central New Zealand. N.Z. J. Geol. Geophys. 31, 431–446.

Carter, L., Wright, I.C., Collins, N., Mitchell, J.S., Win, G., 1991. Seafloor stability along the Cook Strait power cable corridor. 10th Australasian Conference on coastal and ocean Engineering, pp. 565–570.

Carter, L., Alloway, B., Shane, P., Westgate, J., 2004a. Deep-ocean record of major late Cenozoic rhyolitic eruptions from New Zealand. N.Z. J. Geol. Geophys. 47 (3), 481–500.

Carter, L., Carter, R.M., McCave, I.N., 2004b. Evolution of the sedimentary system beneath the deep Pacific inflow off eastern New Zealand. Mar. Geol. 205 (1–4), 9–27.

Chiang, C.-S., Yu, H.-S., 2006. Morphotectonics and incision of the Kaoping submarine canyon, SW Taiwan orogenic wedge. Geomorphology 80, 199–213.

Collot, J.Y., Delteil, J., Lewis, K., Audru, J.C., Barnes, P., Chanier, F., Chaumillon, E., Davy, B., Lallemand, S., Lamarche, G., Mercier de Lepinay, B., Orpin, A., Pelletier, B., Sosson, M., Toussaint, B., Uruski, C., 1995. From the Kermadec Trench to the southern termination of the Hikurangi Trough: results of the GEODYNZ-SUD, Leg 1 swath-mapping survey. C. R. Acad. Sci., Sér. 2, Paris 320 (4 Part 2), 295–302.

Collot, J.-Y., Delteil, J., Lewis, K.B., Davy, B., Lamarche, G., Audru, J.-C., Barnes, P., Chanier, F., Chaumillon, E., Lallemand, S.E., Mercier de Lepinay, B., Orpin, A., Pelletier, B., Sosson, M., Toussaint, B., Uruski, C., 1996. From oblique subduction to intra-continental transpression; structures of the southern Kermadec–Hikurangi margin from multibeam bathymetry, side-scan sonar and seismic reflection. Mar. Geophys. Res. 18 (2–4), 357–381.

Collot, J.-Y., Lewis, K.B., Lamarche, G., Lallemand, S.E., 2001. The giant Ruatoria debris avalanche on the northern Hikurangi Margin, New Zealand: result of oblique seamount subduction. J. Geophys. Res. 106 (B9), 19,271–19,297.

Daly, R.A., 1936. Origin of submarine "canyons". Am. J. Sci. 401–420.

Dana, J.D., 1880. Manual of Geology, Treating of the Principles of the Science with Special Reference to American Geological History.

DeMets, C., Gordon, R.G., Argus, D.F., Stein, S., 1994. Effect of recent revisions to the geomagnetic reversal time scale on estimates of current plate motions. Geophys. Res. Lett. 21 (20), 2191–2194.

Downes, G., 1995. Atlas of Isoseismal Maps of New Zealand Earthquakes. Monograph, vol. 11. Institute of Geological and Nuclear Sciences, Lower Hutt.

Downes, G., 2005. The 1855 January 23 M8+ Wairarapa earthquake — what contemporary accounts tell us about it. In: Townend, J., Langridge, R., Jones, A. (Eds.), The 1855 Wairarapa Earthquake symposium, Wellington.

Dowrick, D.A., 2005. Strong ground shaking in the 1855 Wairarapa Earthquake. In: Townend, J., Langridge, R., Jones, A. (Eds.), The 1855 Wairarapa Earthquake symposium, Wellington.

Eden, D.N., 1989. River terraces and their loessial cover beds, Awatere River valley, South Island, New Zealand. N.Z. J. Geol. Geophys. 32 (4), 487–497.

Field, B.D., Uruski, C.I., et al., 1997. Cretaceous–Cenozoic Geology and Petroleum Systems of the East Coast region, New Zealand. Institute of Geological and Nuclear Sciences Monograph, vol. 19. GNS. 301 pp.

Gaudin, M., Mulder, T., Cirac, P., Berne, S., Imbert, P., 2006. Past and present sedimentary activity in the Capbreton Canyon, southern Bay of Biscay. Geo-Mar. Lett. 26 (6), 331–345.

Gibb, J.G., 1986. A New Zealand regional Holocene eustatic sea-level curve and its application to determination of vertical tectonic movements. A contribution to IGCP-Project 200. R. Soc. N.Z. Bull. 24, 377–395.

Grapes, R.H., Downes, G., 1997. The 1855 Wairarapa, New Zealand, earthquake — analysis of historical data. Bull. N.Z. Soc. Earthqu. Eng. 30 (4), 271–369.

Grapes, R.H., Little, T.A., Downes, G., 1998. Rupturing on the Awatere Fault during the 1848 October Marlborough earthquake, New Zealand: historical and present day evidence. N.Z. J. Geol. Geophys. 41, 387–399.
Greene, H.G., Clarke Jr., S.H., Kennedy, M.P., 1991. Tectonic evolution of submarine canyons along the California continental margin. In: Osbourne, R.H. (Ed.), From shoreline to abyss: contributions in marine geology in honor of Francis Parker Shepard. Soc. of Econ. Paleontologists and Mineralogists, pp. 231–248.
Greene, H.G., Maher, N.M., Paull, C.K., 2002. Physiography of the Monterey Bay National Marine Sanctuary and implications about continental margin development. Mar. Geol. 181 (1–3), 55–82.
Hampton, M.A., Lee, H.J., Locat, J., 1996. Submarine landslides. Rev. Geophys. 34, 33–59.
Hancox, G.T., 2005. Landslides and liquefaction effects caused by the 1855 Wairarapa Earthquake: then and now. In: Townend, J., Langridge, R., Jones, A. (Eds.), The 1855 Wairarapa Earthquake symposium, Wellington.
Harris, T.E.W., 1990. Greater Cook Strait: Form and Flow. DSIR Marine and Freshwater, Wellington, N.Z. 212 pp.
Hicks, D.M. and Shankar, U., 2003. Sediment from New Zealand rivers, NIWA Chart, Miscellaneous Series No. 79.
Huyghe, P., Foata, M., Deville, E., Mascale, G., Group, C.W., 2004. Channel profiles through the active front of the Barbados prism. Geology 32 (5), 429–432.
Kukowski, N., Schillhorn, T., Huhn, K., von Rad, U., Husen, S., Flueh, E.R., 2001. Morphotectonics and mechanics of the central Makran accretionary wedge off Pakistan. Mar. Geol. 173 (1–4), 1–19.
Kvalstad, T.J., Andresen, L., Forsberg, C.F., Berg, K., Bryn, P., Wangen, M., 2005. The Storegga slide: evaluation of triggering sources and slide mechanics. Mar. Pet. Geol. 22 (1–2 SPEC. ISS.), 245–256.
Lastras, G., Canals, M., Urgeles, R., Amblas, D., Ivanov, M., Droz, L., Dennielou, B., Fabrés, J., Schoolmeester, T., Akhmetzhanov, A., Orange, D., García-García, A., 2007. A walk down the Cap de Creus canyon, Northwestern Mediterranean Sea: recent processes inferred from morphology and sediment bedforms. Mar. Geol. 246 (2–4), 176–192.
Laursen, J., Normark, W.R., 2002. Late Quaternary evolution of the San Antonio Submarine Canyon in the central Chile forearc (~33°S). Mar. Geol. 188 (3–4), 365–390.
Lee, J.M., Begg, J.G., 2002. Geology of the Wairarapa area. Institute of Geological and Nuclear Sciences 1:250,000 geological map 11. 1 sheet + 66 pages. Institute of Geological and Nuclear Sciences Ltd, Lower Hutt, New Zealand.
Lewis, K.B., 1994. The 1500-km-long Hikurangi Channel: trench-axis channel that escapes its trench, crosses a plateau, and feeds a fan drift. Geo-Mar. Lett. 14, 19–28.
Lewis, K.B., Barnes, P.M., 1999. Kaikoura Canyon, New Zealand: active conduit from near-shore sediment zones to trench-axis channel. Mar. Geol. 162 (1), 39–69.
Lewis, K.B., Pantin, H.M., 2002. Channel-axis, overbank and drift sediment waves in the southern Hikurangi Trough, New Zealand. Mar. Geol. 192 (1–3), 123–151.
Lewis, K.B., Pettinga, J.R., 1993. The emerging, imbricate frontal wedge of the Hikurangi margin. In: Ballance, P.F. (Ed.), South Pacific sedimentary basin. Sedimentary Basins of the World, vol. 2. Elsevier Sciences publishers, Amsterdam, pp. 225–250.
Lewis, K.B., Carter, L., Davey, F.J., 1994. The opening of Cook Strait: interglacial tidal scour and aligning basins at a subduction to transform plate edge. Mar. Geol. 116 (3–4), 293–312.
Lewis, K., Collot, J.-Y., Lallemand, S., 1998. The dammed Hikurangi Trough: a channel-fed trench blocked by subducting seamounts and their wake avalanches (New Zealand–France GeodyNZ Project). Basin Res. 10 (4), 441–468.
Leynaud, D., Sultan, N., Mienert, J., 2007. The role of sedimentation rate and permeability in the slope stability of the formerly glaciated Norwegian continental margin: the Storegga slide model. Landslides 4 (4), 297–309.
Leynaud, Mienert, J., Vanneste, M., in press. Submarine mass movements on glaciated and non-glaciated European continental margins: a review of triggering mechanisms and preconditions to failure. Mar. Pet. Geol.
Little, T.A., Rodgers, D.W., 2005. Co-seismic slip during the 1855 Earthquake, Southern Wairarapa Fault, New Zealand. In: Townend, J., Langridge, R., Jones, A. (Eds.), The 1855 Wairarapa Earthquake symposium, Wellington.
Liu, C.-S., Huang, I.L., Teng, L.S., 1997. Structural features off southwestern Taiwan. Mar. Geol. 137 (3–4), 305–319.
Mascle, A., Endignoux, L., Chennouf, T., 1990. Frontal accretion and piggyback basin development at the southern edge of the Barbados Ridge accretionary complex. Proc., scientific results, ODP, Leg 110, Barbados Ridge, pp. 17–28.
McAdoo, B.G., Watts, P., 2004. Tsunami hazard from submarine landslides on the Oregon continental slope. Mar. Geol. 203 (3–4), 235–245.
McAdoo, B.G., Orange, D.L., Screaton, E., Lee, H., Kayen, R., 1997. Slope basins, headless canyons, and submarine palaeoseismology of the Cascadia accretionary complex. Basin Res. 9 (4), 313–324.
McAdoo, B.G., Capone, M.K., Minder, J., 2004. Seafloor geomorphology of convergent margins: implications for Cascadia seismic hazard. Tectonics 23 (6).
McCalpin, J.P., 1992. Glacial geology of the upper Wairau valley, Marlborough, South Island. N.Z. J. Geol. Geophys. 35, 213–224.
McSaveney, M.J., Graham, I.J., Begg, J.G., Beu, A.G., Hull, A.G., Kim, K., Zondervan, A., 2006. Late Holocene uplift of beach ridges at Turakirae Head, south Wellington coast, New Zealand. N.Z. J. Geol. Geophys. 49 (3), 337–358.
Milia, A., 2000. The Dohrn canyon: a response to the eustatic fall and tectonic uplift of the outer shelf along the eastern Tyrrhenian Sea margin, Italy. Geo-Mar. Lett. 20 (2), 101–108.
Mitchell, J.S., 1988. Palliser Bathymetry, 2nd Edition. N.Z. Oceanographic Institute Chart, Coastal Series. 1:200 000.
Mitchell, N.C., 2006. Morphologies of knickpoints in submarine canyons. Bull. Geol. Soc. Am. 118 (5–6), 589–605.
Mitchell, J.S., Lewis, K.B., 1996. Cook Strait Bathymetry, 3rd edition. N.Z. Oceanographic Institute Chart, Coastal Series.
Mountjoy, J., Pettinga, J.R., 2006. Controls on large deep-seated landslides in soft rock terrain: rock mass defects and seismic triggering. Proceedings of The New Zealand Geotechnical Society Symposium on Earthquakes and Urban Development. NZGS, Nelson.
Mulder, T., Savoye, B., Syvitski, J.P.M., 1997. Numerical modelling of a mid-sized gravity flow: the 1979 Nice turbidity current (dynamics, processes, sediment budget and seafloor impact). Sedimentology 44 (2), 305–326.
Nagel, D.K., Mullins, H.T., Greene, H.G., 1986. Ascension Submarine Canyon, California—evolution of a multi-head canyon system along a strike–slip continental margin (USA). Mar. Geol. 73 (3–4), 285–310.
Naish, T.R., Nelson, C.S., Hodder, A.P.W., 1993. Evolution of Holocene sedimentary bentonite in a shallow-marine embayment, Firth of Thames, New Zealand. Mar. Geol. 109 (3–4), 267–278.
Orange, D.L., McAdoo, B.G., Moore, J.C., 1997. Headless submarine canyons and fluid flow on the toe of the Cascadia accretionary complex. Basin Res. 9, 303–312.
Pillans, B., Chappell, J., Naish, T., 1999. A review of the Milankovitch climatic beat: template for Plio-Pleistocene sea-level changes and sequence stratigraphy. Sediment. Geol. 122, 5–21.
Pratson, L.F., Coakley, B.J., 1996. A model for the headward erosion of submarine canyons induced by downslope-eroding sediment flows. Geol. Soc. Amer. Bull. 108 (2), 225–234.
Pratson, L.F., Ryan, W.B.F., Mountain, G.S., Twichell, D.C., 1994. Submarine canyon initiation by downslope-eroding sediment flows; evidence in late Cenozoic strata on the New Jersey continental slope. Geol. Soc. Amer. Bull. 106 (3), 395–412.
Proctor, R., Carter, L., 1988. Tidal and sedimentary response to the late Quaternary closure and opening of Cook Strait, New Zealand: results from numerical modelling. Paleoceanography 4 (2) 167:180.
Proctor, R., Carter, L., 1989. Tidal and sedimentary response to the late Quaternary closure and opening of Cook Strait, New Zealand: results from numerical modelling. Paleoceanography 4 (2) 167:180.
Rahiman, T.I.H., Pettinga, J.R., 2006. The offshore morpho-structure and tsunami sources of the Viti Levu Seismic Zone, southeast Viti Levu, Fiji. Mar. Geol. 232 (3–4), 203–225.
Rahiman, T.I.H., Pettinga, J.R., Watts, P., 2007. The source mechanism and numerical modelling of the 1953 Suva tsunami, Fiji. Mar. Geol. 237 (1–2), 55–70.
Rattenbury, M.S., Townshend, D.B. and Johnston, M.R., 2007. Geology of the Kaikoura Area QM13. GNS Science, pp. 70 p., 1 map.
Read, S.A.L., Richards, L., Perrin, N.D., 2001. Assessment of New Zealand greywacke rock masses with the Hoek Brown failure criterion. In: Sarkka, Eloranta (Eds.), Rock Mechanics — A challenge for society. Eurorock 2001 Swets and Zeitlinger Lisse.
Shepard, F.P., 1963. Importance of submarine valleys in funneling sediments to the deep sea. Prog. Oceanogr. 3 (C), 321–332.
Shepard, F.P., 1981. Submarine canyons: multiple causes and long-time persistence. Am. Assoc. Pet. Geol. Bull. 65, 1062–1077.
Shepard, F.P., Dill, R.F., 1966. Submarine Canyons and Other Sea Valleys. Rand McNally, Chicago, p. 381.
Smith, D.P., Ruiz, G., Kvitek, R., Iampietro, P.J., 2005. Semiannual patterns of erosion and deposition in upper Monterey Canyon from serial multibeam bathymetry. Bull. Geol. Soc. Am. 117 (9–10), 1123–1133.
Smith, D.P., Kvitek, R., Iampietro, P.J., Wong, K., 2007. Twenty-nine months of geomorphic change in upper Monterey Canyon (2002–2005). Mar. Geol. 236 (1–2), 79–94.
Stirling, M.W., McVerry, G.H., Berryman, K.R., 2002a. A new seismic hazard model for New Zealand. Bull. Seismol. Soc. Am. 92 (5), 1878–1903.
Stirling, M.W., Rhoades, D., Berryman, K.R., 2002b. Comparison of earthquake scaling relations derived from data of the instrumental and pre-instrumental eras. Bull. Seismol. Soc. Am. 92, 812–830.
Stout, M.L., 1977. Utiku Landslide, North Island, New Zealand. Rev. Eng. Geol. 3, 171–184 Landslides.
Sultan, N., Cochonat, P., Canals, M., Cattaneo, A., Dennielou, B., Haflidason, H., Laberg, J.S., Long, D., Mienert, J., Trincardi, F., Urgeles, R., Vorren, T.O., Wilson, C., 2004. Triggering mechanisms of slope instability processes and sediment failures on continental margins: a geotechnical approach. Mar. Geol. 213 (1–4), 291–321.
Uruski, C.I., 1992. Sedimentary Basins and Structure of Cook Strait. 92/3, Institute of Geological and Nuclear Sciences, Lower Hutt, New Zealand.
Vennell, R., 1994. Doppler current profiler measurements of tidal phase and amplitude in Cook Strait, New Zealand. Cont. Shelf Res. 14 (4), 353–364.
Wallace, L.M., Beavan, J., McCaffrey, R., Darby, D., 2004. Subduction zone coupling and tectonic block rotations in the North Island, New Zealand. J. Geophys. Res. 109 (B12406).
Walsh, J.P., Alexander, C.R., Gerber, T., Orpin, A.R., Summers, B.W., 2007. The demise of a submarine canyon? Evidence for highstand infilling on the Waipaoa River continental margin, New Zealand. Geophys. Res. Lett. 34 (L20606).
Xu, J.P., Wong, F.L., Kvitek, R., Smith, D.P., Paull, C.K., 2008. Sandwave migration in Monterey Submarine Canyon, Central California. Mar. Geol. 248 (3–4), 193–212.

4.2 Fluid Venting on the Wairarapa Slope: Structural controls and slope gully development

Fluid venting was first recognised on the Wairarapa slope in 1996 as a seafloor "flare" in echo-sounder data (L. Carter pers. Comm., NIWA unpublished data). Following up on these observations NIWA scientists have been monitoring the site for several years to characterise water column and sediment geochemistry, and to determine the temporal variability of methane emissions (Law et al., 2009). The Wairarapa vent sites occur in the area dominated by margin-parallel, thrust-propagated ridges (Mountjoy et al., 2009a - Figure 4); shown to be characteristic of methane vent sites along the Hikurangi Margin (Lewis and Marshall, 1996; Faure et al., 2006; Barnes et al., 2009). While Barnes et al. (2009) provide a generalised model for fluid expulsion from the Hikurangi Margin accretionary wedge, a specific model has not been proposed for the Wairarapa site. Here a specific structural model is developed for fluid venting on the Wairarapa slope and integrated with other published information.

This work represents an expansion of that contributed to the paper by Law et al. (2009) which is included in its entirety in Appendix I.

4.2.1 Structural model for fluid venting on the Wairarapa margin

Vent distribution on the Wairarapa slope can be directly related to upper-plate structures mapped in this study (Mountjoy et al., 2009a - Figure 1B). It is widely recognised that fluid expulsion is associated with structure on active tectonic margins (e.g. Henry et al., 2002) and in the majority of cases this is based on the relationship between surface observations of vent structure, subsurface interpretations in MCS, and models of local structural behaviour. The development of specific models for the vent sites on the Wairarapa slope provides insight into local controls on fluid expulsion, with model constraints provided by the high-resolution imaging of vent-related features in parallel studies stemming from the RV *Sonne* voyage (Bialas et al., 2007; Klaucke et al., 2009; Netzeband et al., 2009). Particularly from the point of view of this project, it is important to look for any relationship that can be shown between fluid venting, mass movement and canyon development, as fluid expulsion has been proposed to be a significant contributing factor to gully development on submarine slopes (Orange and Breen, 1992). The presence of gas hydrate is inferred across much of the Hikurangi Margin based on the widespread interpretation of a bottom simulating reflector (BSR) in MCS profiles (e.g. Katz, 1981; Henrys et al., 2003).

Four major sites of fluid expulsion are recognised on the Cook Strait sector of the Hikurangi Margin (Figure 4.1). Two of these sites occur on Opouawe Bank, at the northern-eastern and south-western ends, which were the focus of the New Vents surveys in 2007. Two further sites are documented by Law et al. (2009) away from Opouawe Bank; the "Pahaua Seep" and "Campbell Bank mud volcano". The combination of the excellent study site and the comprehensive MCS dataset available (Figure 4.2A) provide a good opportunity to establish a type example of structurally-controlled fluid venting.

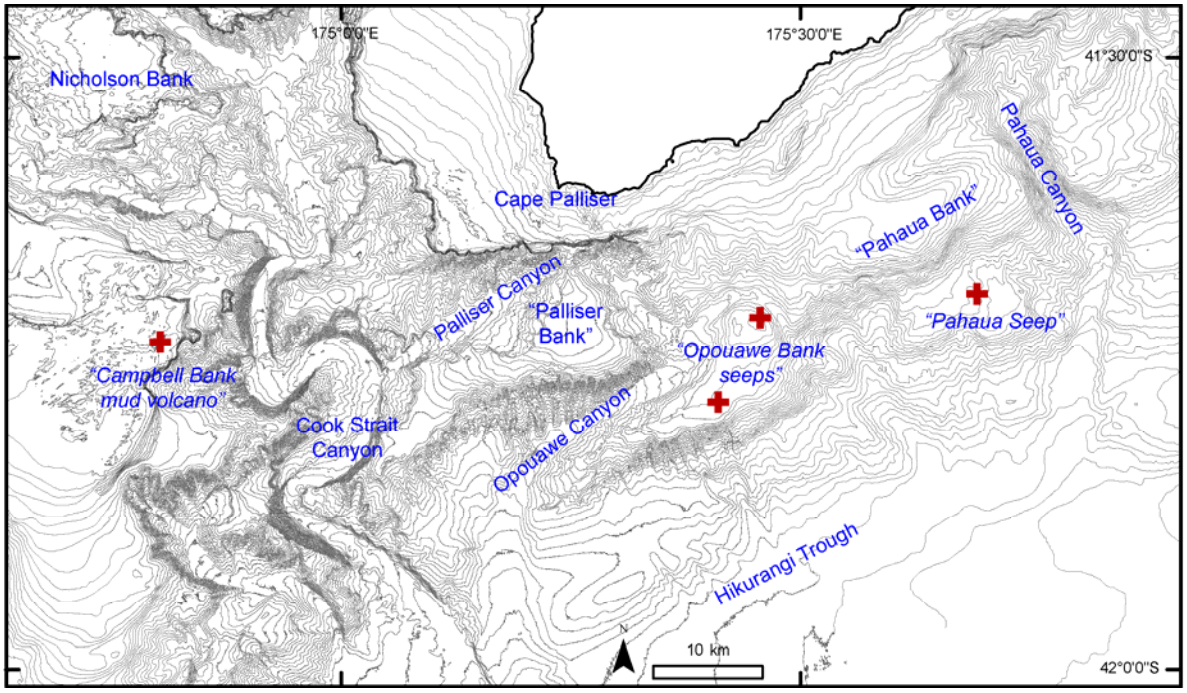

Figure 4.1: Location of identified vent sites on the Cook Strait sector of the Hikurangi Margin. Crosses indicate general location of vent sites with informal names shown. Several vent sites occur across Opouawe Bank.

Opouawe Bank: The "Wairarapa Seep" site as a type example

Multiple vent sites have been identified across Opouawe Bank based on geo-acoustic imaging (Barnes et al., 2009; Klaucke et al., 2009; Law et al., 2009). Using MCS reflection data, Netzeband et al. (2009) interpret 28 vents in total and suggest this is among the most active vent sites in the world. The characterisation of the subsurface "plumbing system" of these vent sites in MCS profiles reveals numerous chimneys and "faults" interpreted as fluid pathways. While a strong BSR is interpreted at several locations in MCS profiles (Barnes et al., 2009; Netzeband et al., 2009), it is apparent that in locations where the fluid plumbing systems are present the BSR is disrupted. Netzeband et al (2009) infer that fluids

migrate through a network of faults (or fractures) to accumulation areas (delineated by "bright spots" of high reflectivity) and then are expelled to the seafloor via discrete "chimney" pathways. These details are imaged in the upper ~1 second of MCS profiles and provide no information in terms of upper-crustal structural control on fluid vent locations.

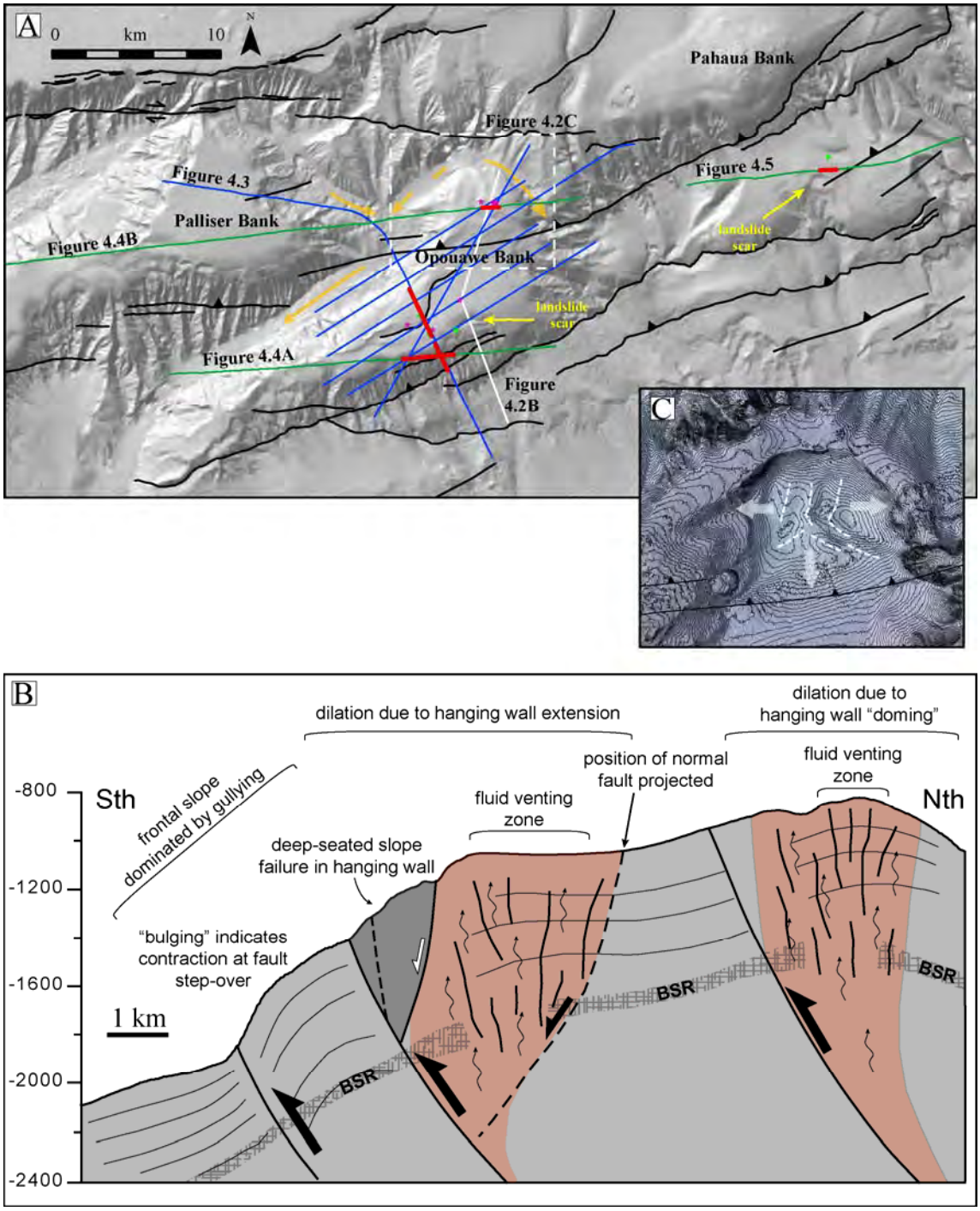

Figure 4.2: Morphostructure of the "Wairarapa Seep Site". A) Location of MCS profiles collected during the RV *Sonne* New Vents expedition (blue), and additional MCS profiles presented in this study (green). Tectonic structure after Mountjoy et al. (2009a) is shown. Vent site locations shown are from New Vents (blue stars) and

NIWA surveys (red stars). Thick red lines indicate areas of BSR disturbance identified in MCS profiles referred to in text. Yellow arrows indicate canyon flow paths. B) Schematic profile across Opouawe Bank (location in A). Bathymetric profile uses true-scale topography and the interpretation is based on MCS data presented by Mountjoy et al. (2009a); Netzeband et al. (2009); and in subsequent figures in this chapter.

The general structural style of deformation of Opouawe Bank is illustrated in MCS profiles as being dominated by imbricated frontal-thrust faults with uplift and deformation in the hanging wall along the crest of the main bank (Mountjoy et al., 2009a - Figure 13) (Figure 4.3). At the north-eastern end of the bank an elevated area is interpreted as being related to the through-going Opouawe-Uruti Fault (Mountjoy et al., 2009a - Figure 4). Along the crest of the south-western bank a fault scarp is interpreted as reflecting hanging-wall extension, with subsidence into the frontal thrusts (Figure 4.2). The relationship between the geometry of these structures and their control on brittle deformation in the hanging wall is proposed to facilitate the high rates of fluid expulsion at this location. Effectively the fracture mesh and localised dilation of the rock-mass is providing a plumbing system along which fluids can migrate upwards and escape to the seafloor. Figure 4.2B shows an interpretive cross section based on actual topography through Opouawe Bank, aligned to cross both the general fluid seepage area and frontal gravitational collapse. Fluid vent sites are preferentially located in the hanging wall at the fold crest, and the same relationship is shown for the other vent sites documented on the Hikurangi Margin (Barnes et al., 2009). Given the structural variation controlling contractional ridges along the Hikurangi Margin, location specific (but non-unique) structural controls are likely to influence fluid expulsion at specific sites. The Opouawe Bank example provides a case study for such a site and will be considered in detail.

Figure 4.3: Sonne MCS profile SO191-9/10 crossing Opouawe and Palliser Banks (following page). This line is also partly presented in two journal papers included in this thesis (Barnes et al., 2009; Mountjoy et al., 2009a). The profile is located in Figure 4.2. A) Uninterpreted MCS profile. B) Linework interpretation of structure and features relating to the presence of gas hydrates. The large area of high amplitude reflectivity is coincident with the main vent locations, and the disruption of the BSR.

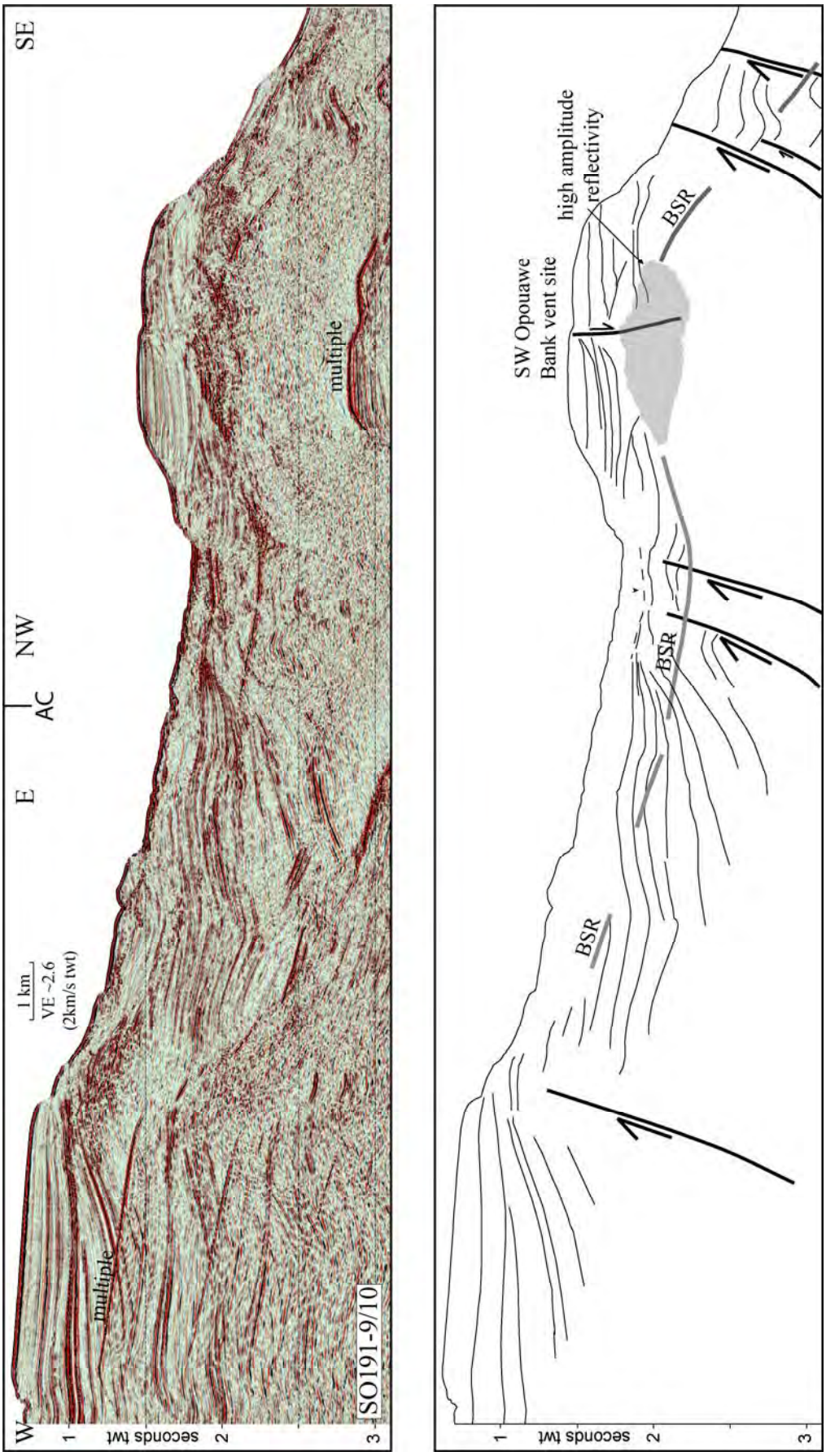

Figure 4.3 (caption on previous page).

South-western Opouawe Bank

The south-western Opouawe Bank vent site has a normal fault scarp along the bank axis around which the majority of vent sites are clustered (Figure 4.2). Netzeband et al. (2009) show that below this area numerous faults are closely associated with fluid conduits. The extension in the hanging wall that allows this fracturing and rock mass dilation to occur is inferred to be related to the structural step-over on the ridge-bounding frontal thrust. Differential movement at the step-over is inducing contractional deformation of the rock between the overlapping faults (Figure 4.2B), but could conversely be inducing extension in the hanging wall. The occurrence of a large mass failure in the frontal slope at this location supports a model of localised extension, and this step-over-related extension is also inferred to be the mechanism controlling the development of the normal fault at the ridge crest.

North-eastern Opouawe Bank

The north-eastern Opouawe Bank vent site actually occurs on a separate structure which may be considered to be more of a southern, now isolated, "remnant" of Pahaua Bank rather than part of Opouawe Bank (Figure 4.2). Canyon erosion has isolated this dome feature, and the removal of lateral support may have destabilised the still uplifting dome, leading to structural/gravitational-induced relaxation and rock-mass dilation. Bathymetric lineaments on the dome are inferred to reflect gravitational/structural collapse (Figure 4.2C), though there is no clear support for localised dislocation associated with these lineaments in MCS profiles other than the fracture networks at depth (Figure 4.4). Barnes et al. (2009) interpret rockmass dilation at the Rock Garden site from clear surface lineaments, interpreted as being related to a subducting seamount. Similarly to the north-eastern Opouawe Bank vent site, data at the Rockgarden site shows no evidence of subsurface displacement related to surface lineaments. It is noted that Netzeband et al. (2009) infer a very low-angle fault in the north Opouawe Bank area, which may be associated with dome collapse.

Distribution of venting

While Netzeband et al. (2009) identify 28 vents on Opouawe Bank, they do not show a map of vent locations. The main vents identified from water column and seafloor data cluster in localised areas (Figure 4.2), however, it is clear from the interpreted MCS profiles of Netzeband et al. (2009) that vent chimneys occur in several locations across Opouawe

Bank. MCS profiles across Opouawe Bank (Figure 4.3 and 4.4), and to the north adjacent to Pahaua Seep (Figure 4.5), show clear disturbance of the BSR localised in the shallow subsurface beneath the fluid seepage areas. The distribution of these zones across Opouawe Bank (Figure 4.2A) agrees with the model that seepage is not uniformly distributed across the bank but occurs in localised areas. BSR disturbance mapped in Figure 4.2A occurs across the upper frontal-slope of Opouawe Bank, though no vent sites have been identified there. The characteristic disturbance to acoustic reflectivity is also observed near the "Pahaua Seep" site of Law et al. (2009) (Figure 4.2 and 4.5). At the Pahaua Seep, not only is the BSR significantly disturbed, but a clear acoustic "bright spot" occurs between the BSR and the seafloor in the area of disturbed acoustic reflectivity. This bright spot occurrence has been attributed to free-gas accumulation (Holbrook et al., 2002). The structural setting of the "Pahaua Seep" is directly analogous to that of the Opouawe Bank vent sites in that is occurs at the crest of a thrust-fault-bounded anticlinal structure, although dip-aligned MCS profiles are lacking to clarify if extensional deformation is occurring in this ridge. It is noted that a kilometre-scale mass-failure scars occur adjacent to the area of mapped acoustic disturbance (Figure 4.2).

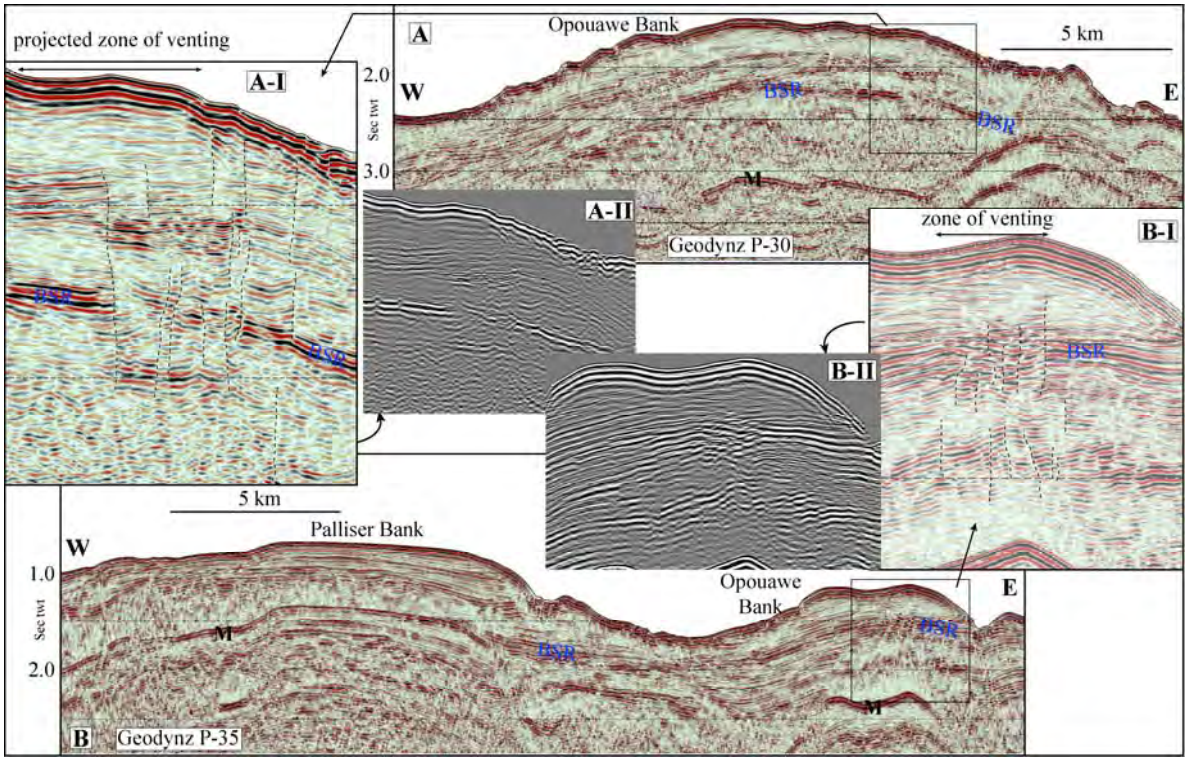

Figure 4.4: GeodyNZ MCS profiles P-30 and P-35 aligned approximately along the strike of the Palliser and Opouawe banks. Location in Figure 4.2. A) Profile along Opouawe Bank showing significant disturbance to the BSR in the area of the south-western Opouawe Bank vent sites (Figure 4.2). A-I shows detail of BSR disruption and

interpreted fault/fracture systems. A-II is a greyscale "amplitude" image of A-I to highlight BSR disturbance. B) Profile along Palliser Bank and Opouawe Bank illustrating the lack of disturbance to the BSR on Palliser Bank, and showing disturbance to the BSR adjacent to the north-eastern Opouawe Bank vent sites (Figure 4.2). B-I shows detail of BSR disruption and interpreted fault/fracture systems on Opouawe Bank. A-II is a greyscale "amplitude" image of B-I to highlight BSR disturbance.

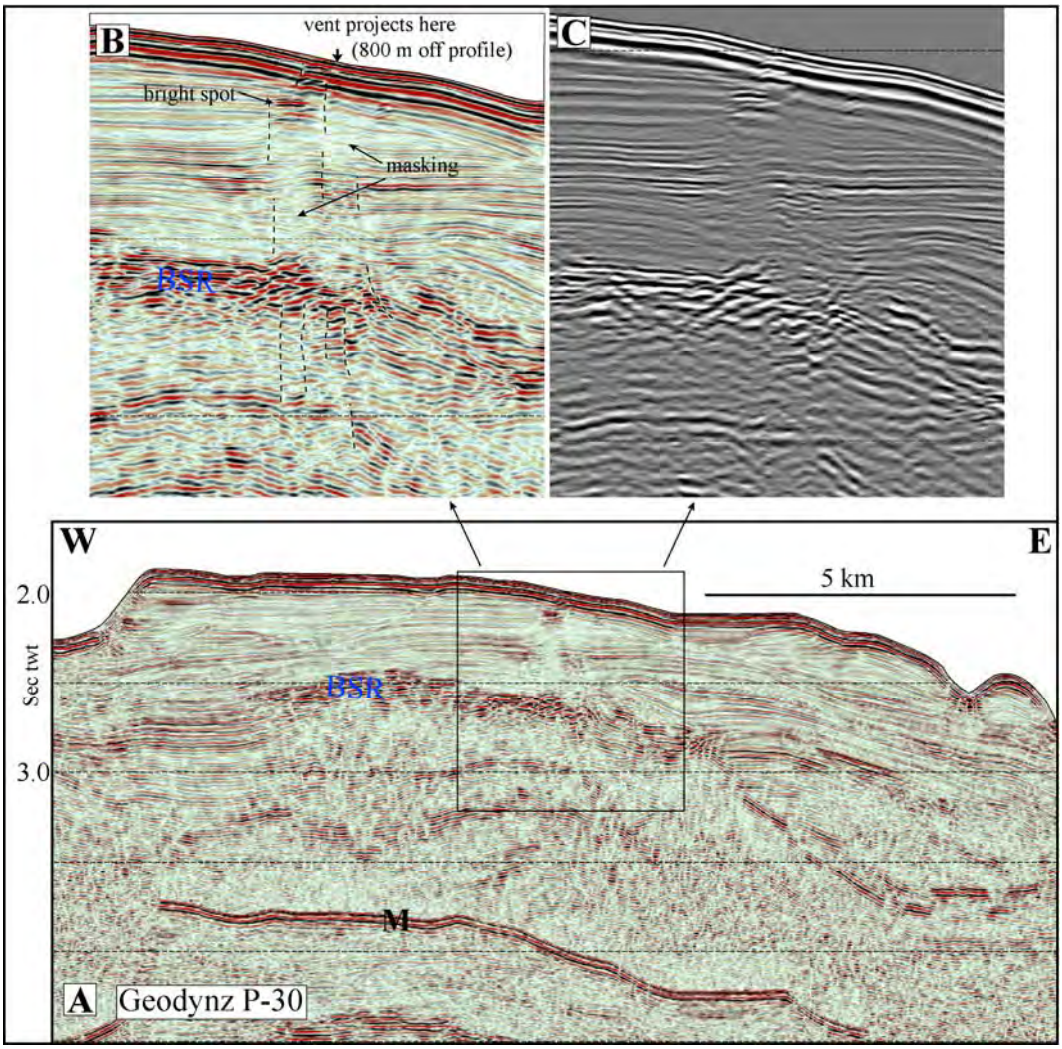

Figure 4.5: GeodyNZ MCS profile P-30 aligned along the strike of the unnamed bank hosting the "Pahaua Seep", location in Figure 4.2. A) MCS profile showing disturbance to the BSR in the area of the "Pahaua Seep" site (Figure 4.2). B) Detail of BSR disruption and acoustic "blanking zones". Note also the bright spot above the acoustic "blanking zones" C) Greyscale "amplitude" image of B to highlight acoustic disturbance of the BSR.

Barnes et al. (2009) show that fluid venting on the Hikurangi Margin is associated with the boundary between the modern accretionary wedge and the deforming Cretaceous and

Paleogene backstop. Opouawe Bank, the Pahaua Seep, and Palliser Bank are located adjacent to this boundary (Figure 4.2). In contrast to the multiple vent sites observed on Opouawe Bank, no fluid vent sites have been identified across the main part of Palliser Bank despite extensive echo-sounder surveys in the area. While a BSR is clearly imaged in several MCS profiles across Opouawe Bank, immediately outside of vent areas (e.g. Figures 4.3 and 4.4), there is no indication of a BSR underlying Palliser Bank. Palliser Bank shows no indication of carbonate development at the surface or in high-frequency sub-surface data, this is in contrast to Opouawe Bank where carbonate development is widespread and indicative of vent occurrence (c.f. Klaucke et al., 2009). Palliser Bank shows no evidence for extensional deformation in swath bathymetry or MCS profiles, and this may be a factor inhibiting fluid expulsion – assuming Palliser Bank is a gas hydrate host (note apparent lack of BSR).

Despite the stark contrast between the fluid expulsion activity on these two ridges, both exhibit well developed frontal-slope gully formation (Mountjoy et al., 2009a). The comparison poses interesting questions regarding the role of fluid seepage in slope destabilisation and gully development.

4.2.2 Role of fluids in slope destabilisation and gully development

Fluid venting through contractional structures on accretionary margins has been proposed to be a primary driver for the development of so-called “Headless Canyons” or slope-confined gully systems on the Cascadia accretionary margin (Orange and Breen, 1992; Orange et al., 1994), and has subsequently been inferred to be responsible for gully development on the Hikurangi Margin (Lewis et al., 1998). Subsequent work making use of direct measurements of in-situ pore pressure, however, indicates that seepage head-gradients on the Cascadia Margin are an order of magnitude too low to solely induce sediment failures in thrust-ridge gully systems (McAdoo et al., 1997a). Recent work on terrestrial and extra-terrestrial seepage-induced canyon development concludes that the development of canyons by seepage-driven failure of rock material (vs unconsolidated sediment) is unlikely (Lamb et al., 2006). Opouawe and Palliser banks are directly analogous to the studied Cascadia Margin ridges, hosting sculptured, parallel linear gullies incised into the frontal slopes (Mountjoy et al., 2009a). The clear question is: What might be said about the role of fluid expulsion in the development of these gullies in light of the increased knowledge of structurally-controlled fluid seepage?

The first obvious observation relating fluid venting and gully development is that all the known vents occur on the crests of ridges and are entirely lacking on side slopes. Critically, there is no evidence for vent occurrence across either the top or frontal slope of Palliser Bank, with the sole vent site located at the north-western edge (Barnes et al., 2009). Mountjoy et al. (2009a) (this chapter) propose that: 1) gullies are initiated early on in the development of ridge structures in the scars of mass failures; 2) they evolve with the progressive development of increasing bathymetric relief; and 3) triggering of failures is inferred to be dominated by earthquake-induced strong ground motions. Numerous landslide scars occur in the head-zones of gully systems indicating that these control the release of sediment that is likely to shape these features. Additionally the lower boundary of the gully systems appears to play a significant role in their development, with contrasting gully morphology observed between gully complexes that terminate at apparently active canyons and those that exit to depositional slopes (Mountjoy et al., 2009a).

While it is not possible to establish or refute any causal linkage between fluid venting and frontal-slope gully development, it is apparent that the most well developed gullies occur on Palliser bank (Mountjoy et al., 2009a), while Opouawe Bank experiences significantly more widespread fluid expulsion. The seep–gully relationship developed on the Cascadia Margin (Orange and Breen, 1992; McAdoo et al., 1997a) used direct observation from manned submersibles to map vent sites from faunal assemblages. It is likely that with this level of detailed observation similar assemblages might be observed in the Palliser and Opouawe gully systems. It is concluded here, however, that the occurrence of these is mostly coincidental and fluid seepage is not an instrumental process in gully development.

Observations on the Wairarapa continental slope show that fluid vent sites populate the crests of thrust-fault-propagated ridges. This is in agreement with observations along the greater Hikurangi Margin (Barnes et al., 2009). No vent sites have been observed on the flanks of ridges, suggesting that if they occur they are secondary to the primary vents at the ridge-crest. These have been detected with echo-sounder images of water-column gas-bubble plumes (Jones et al., 2009), and significant vent-related plumes from ridge flanks would also be likely to be detected if they were active at the time of surveys. While geomechanical and in-situ pore pressure data are lacking from the Wairarapa field area, precluding any critically useful modelling effort, the distribution of fluid venting in the area supports a model of gully development that is not dependant on seepage-driven failure. Instead it is inferred that the combination of regular high levels of strong ground motion,

high (500–1000 m) and steep (~20°) overall slopes, and large-scale mass failures in the early stages of ridge development are sufficient to enable gully development to occur.

4.3 Chapter summary

The Cook Strait sector of the Hikurangi Margin has proved to be an insightful area to consider the dominant forcing factors controlling canyon development and shaping the Hikurangi Margin continental slope. The role of tectonics in canyon location and geometry has been demonstrated with "type examples" of the structural forcing of canyons on the Wairarapa slope. The main Cook Strait canyon system is responding to perturbations of tectonic base level at a variety of scales – from the displacement of the seafloor by local tectonic structures – to local and margin-wide uplift across the continental slope. Canyons are shown to be actively eroding and are behaving similarly to terrestrial catchments experiencing knickpoint propagation. Deep-seated landslides occur widely throughout the canyons and are shown to play a significant role in the development of the upper canyon system. Active fluid venting on the Wairarapa Slope is shown to be strongly structurally controlled and occurs in localised areas on thrust-fault-propagated ridge crests. It is unlikely that fluid venting is the primary driver of the development of slope gully systems.

Despite the host of high-quality and high-resolution bathymetric data in the Cook Strait study area, the MCS coverage is limited. While it is clear that landslide scars are a dominant feature of canyon walls and intervening slopes, the lack of landslide debris retained in the canyon system complicates detailed landslide case study analysis, and inhibits the development of linkages between landslides and slope evolution. The concentration of landslide scarring but lack of debris does indicate, however, that this is a very active environment that is regularly removing any mass-failure deposits produced, and suggests that more studies are necessary to elucidate on this as an example of an active, non- coast-coupled highstand canyon.

Chapter 5: The Poverty sector

The Poverty sector of the Hikurangi Margin lies offshore of Poverty Bay and includes a wide continental shelf and the Poverty re-entrant, a significant geometrical anomaly into the continental slope and outer shelf (see Figure 2.2). The majority of slopes in the Poverty re-entrant feed into the Poverty Canyon system in the re-entrant axis. The re-entrant is thus considered as part of the Poverty Canyon system in the sense of the definition of a terrestrial river catchment. This project does not, however, focus on understanding the evolution of the Poverty re-entrant beyond providing background from previous studies. Nor does it focus specifically on the Poverty Canyon system, but is rather concerned with the development of the upper slope.

The Poverty re-entrant is inferred to result from one or more impacts by asperities (seamounts) on the down-going Pacific Plate (Lewis and Pettinga, 1993; Collot et al., 1996; Lewis et al., 1998). Figure 5.1 shows an interpretation of the deformational evolution of the margin since the Pliocene in terms of seamount impacts. This model suggests that the Poverty re-entrant results from margin-scale mass failure, as has occurred in the Ruatoria re-entrant (Collot et al., 2001; Lewis et al., 2004). Recent work suggests that the Poverty re-entrant has predominantly formed due to significant structural deformation (including tectonic erosion, subsidence, and local fault and ridge growth) and localised slope erosion (Bodger et al., 2006). It is likely, given the plate-convergence rate, and the high concentration of seamounts on the Pacific Plate, that the re-entrant has developed through the influence of more than one seamount impact. The establishment of the Poverty Canyon system as a cross-margin feature with large contributing slope areas (e.g. the upper slope gully systems) is inferred to be dependant on the presence of negative relief in the Poverty re-entrant. In terms of broad-scale controls it can be hypothesised that the margin is accommodating the perturbation of seamounts in the subduction system with a combination of structural deformation, erosion and sedimentation; all occurring within the temporal framework of orbitally-forced sea-level cyclicity.

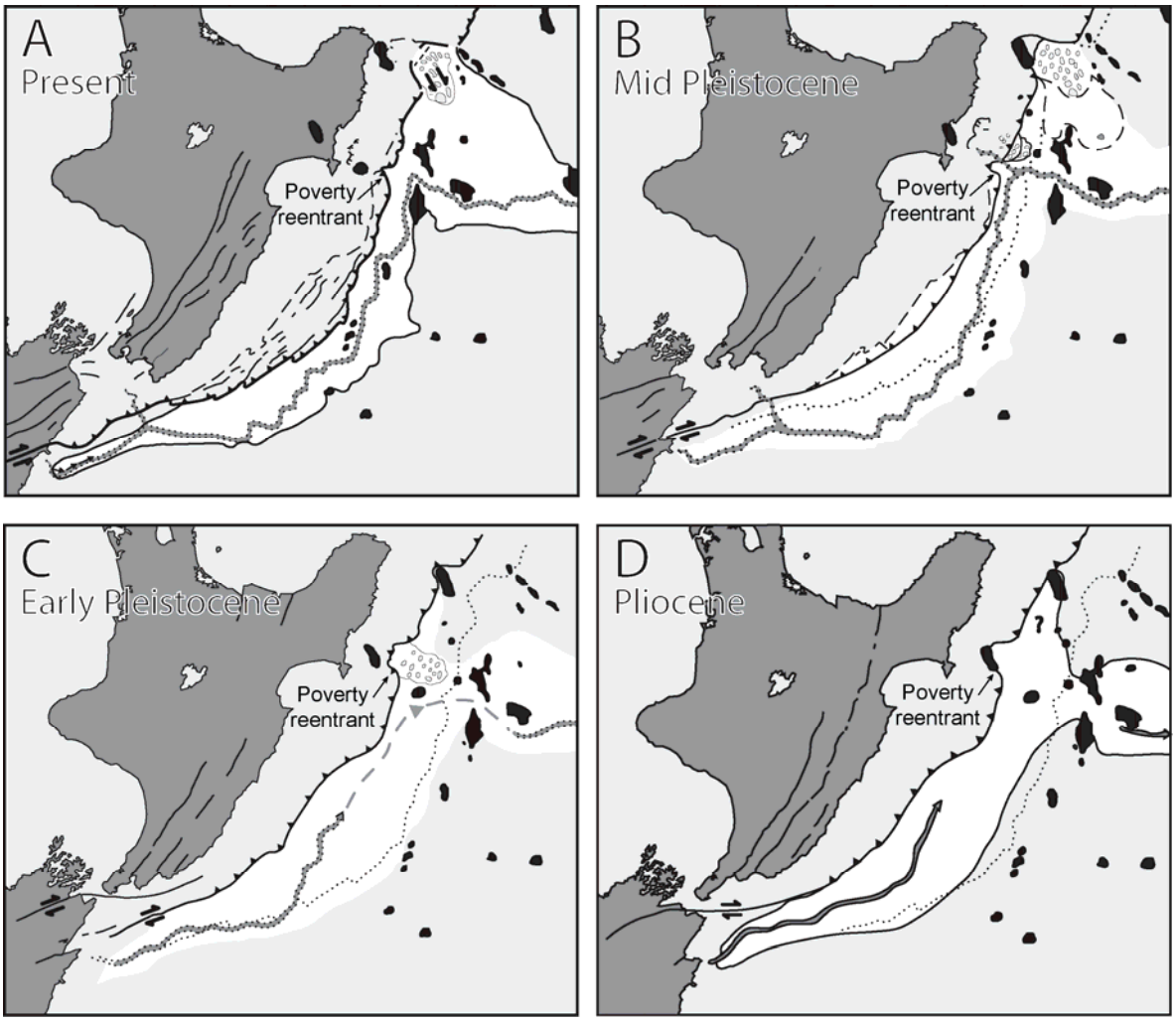

Figure 5.1: Evolution of the Hikurangi Trough since the Pliocene. The four panels, A–D, show the response of the margin to the impact of large seamounts. The letters P and R stand for Poverty re-entrant and Ruatoria re-entrant respectively. Note the dashed line on panels B–D showing the location of the modern deformation front. After Lewis et al (1998).

The primary advantages of the Poverty Bay site and dataset to this study are:

1. Coverage of the upper slope of the Poverty re-entrant with high-resolution multibeam data;
2. A high-quality grid of MCS data, providing subsurface information to augment bathymetry;
3. The existence of large landslide deposits that may be related to source scars;
4. The presence of a well-formed erosional morphology on the upper slope; and,

5. A background of other studies focused on surface processes and margin evolution.

The focus of the study meshes well with other research being undertaken in this geographic area. The high sediment supply from the Waipaoa River and the well-imaged shelf-capture system (Foster and Carter, 1997; Orpin, 2004; Orpin et al., 2006) has led to this area being widely studied as part of the NSF-funded Margins Source-to-Sink initiative (Kuehl et al., 2006) with a particular focus on Holocene and Recent sediment-dispersal patterns and processes (e.g. Walsh et al., 2007; Gerber et al., 2009; Alexander et al., submitted; Brackley et al., submitted). Additionally the doctoral project of Kate Pedley (nee Bodger) currently underway is focused on the morphostructural evolution of the re-entrant as a whole, in terms of its response to seamount impact (Bodger et al., 2006; Pedley et al., 2009).

The approach taken to understanding upper-slope gully development in the Poverty re-entrant is to:

1. Address the gap in the knowledge of outer shelf and upper slope stratigraphy and tectonic structure, as these are expected to be relatively high-order controls on gulley formation;
2. Develop models for the development of the large-scale mass failures that have occurred in the upper and mid slope area;
3. Analyse the morphology of the existing gully systems; and,
4. Bring this information together to develop a model for the spatial and temporal evolution of upper-slope gully systems, and elucidate the primary forcing factors and processes affecting them.

To set the framework for this analysis, a summary description is provided of the morphostructure of the Poverty re-entrant as a sediment transfer system.

5.1 Broad-scale morphostructure and sedimentary systems of the Poverty re-entrant.

The Poverty sector study site encompasses an approximately 85 km length of the Hikurangi Margin shelf and slope system from Mahia Peninsula north past Gable End Foreland (Figure 5.2A). The setting of the Poverty re-entrant above the Pacific–Australian Plate interface megathrust is reflected in the macro-scale structure. This structure predominantly comprises forward-thrust faults splaying off the intra-plate thrust, controlling the development of bathymetric ridges that retain sedimentary basins and deposits on the mid

and upper slope (Figure 5.2B). On the lower slope, margin-parallel ridges result from deformation on these imbricated forward-thrust systems (Pedley et al., 2009). There is currently little tectonic deformation occurring on the mid to upper slope, and it is not until the outer shelf that significant active structure is again present. The structure of the shelf and upper slope area will be elaborated on in significantly more detail in Section 5.2.

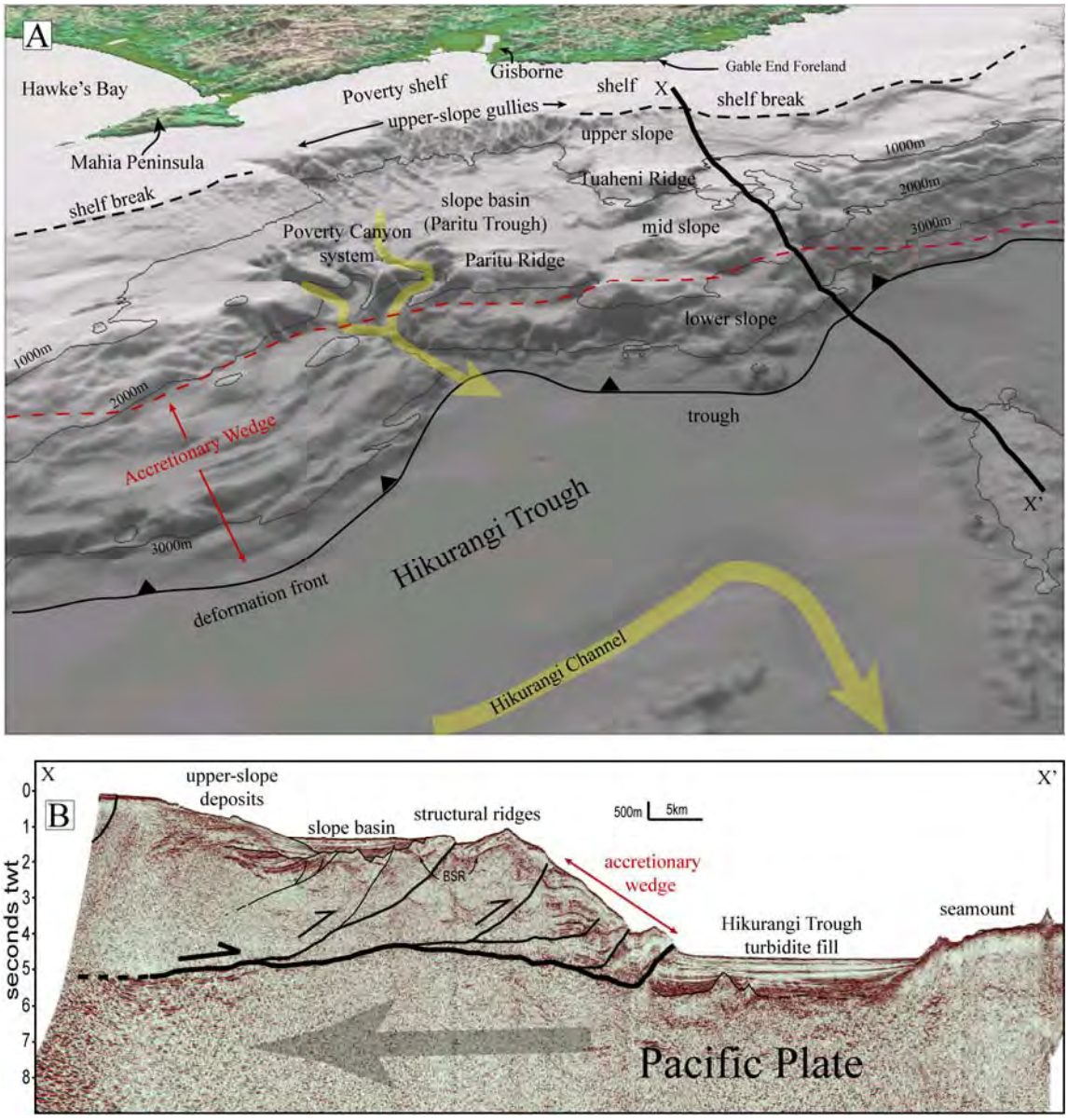

Figure 5.2: Regional morphology of the Hikurangi Margin at Poverty Bay. A) Shaded-relief oblique image based on a 100m DEM at 3 x vertical exaggeration. Geographic and physiographic features, and primary morphologic and geologic domains are labelled. B) MCS line 05CM-04 illustrating the relationship between the first-order structural and stratigraphic features of the margin. Profile is located in A.

5.1.1 Morphologic description

At the first-order geomorphic-scale the Poverty Bay sector of the Hikurangi Margin comprises the shelf, slope and trough domains characteristic of active subduction margins (Figure 5.2). Although the geometrical indentation of the Poverty re-entrant comprises a departure from the general form of the northern Hikurangi Margin, the primary features can be described in terms of these domains.

The Poverty shelf is 20–30 km wide and characterised by both smooth (mud) seafloor and several prominent and irregular (rock) reefs. The plan-view form of the shelf break is irregular along the length of Poverty re-entrant where canyon and gully heads incise into the upper slope. In contrast it is relatively smooth to the north and south of the re-entrant. The shelf break occurs at ~150 m water depth along the length of the re-entrant and between 150 and 200 m depth adjacent to the re-entrant.

The upper slope, from the shelf break to between 800 and 1200 m water depth, is typically steep in comparison to the mid slope. Either side of Poverty re-entrant the overall slope angles of the upper slope are approximately 3–5°, but steepen to 8–11° in the main re-entrant headwall.

The mid slope of the central and southern re-entrant is dominated by large gently sloping (~1°) basins at 1200–1500 m depth (e.g. Paritu Trough Figure 5.2). These basins are constrained at the downslope edge by several margin-parallel bathymetric ridges between the mid and lower slope (e.g. Paritu Ridge). Beyond Paritu Trough, to the north of the re-entrant, the mid slope location of Tuaheni Ridge forces basin development further up slope. In the northern part of the re-entrant, headwall-gully-systems exit to mid-slope basins. In the southern part of the re-entrant, gully systems and canyon heads feed into Poverty Canyon which is incised into the slope and passes between lower-slope ridges to reach the Hikurangi Trough (Figure 5.2). The lower slope is characterised by elongate margin-parallel basins and ridges that, in plan view, trend into the margin with a “v-shaped” geometry at the Poverty Canyon exit point.

5.1.2 Sedimentary system

The combination of high sediment input from the Waipaoa River and the complexity of shelf and slope bathymetry makes the Poverty Bay sedimentary system an interesting case study of source-to-sink sediment transfer. Currently the Waipaoa River system supplies some 15 $Mtyr^{-1}$ suspended sediment load to the Poverty Bay coast (Hicks et al., 2000). The

dispersal of modern sediment onto the outer shelf and slope has been studied using ^{210}PB activity to derive accumulation rates (Alexander et al., submitted). This study shows that 15% of this discharge is accumulating on the continental slope, with almost a third of this being trapped in slope-gullies and canyons. Of the total modern Waipaoa sediment discharge only 33-45% is estimated to accumulate on the Poverty shelf and slope system.

The modern day sedimentation rates are shown to be 2-3 times that of pre-European colonisation, reflecting land-use changes (Orpin et al., 2006). Since the last glacial maximum (LGM) ~18 km^3 sediment has accumulated in three shelf depocentres, two on the mid shelf and a smaller (~3 km^3) one on the outer shelf (Foster and Carter, 1997; Orpin, 2004; Orpin et al., 2006; Gerber et al., 2009). The highest post-glacial sedimentation rate occurs in the outer-shelf lobe (0.93 cm yr^{-1}), being almost twice the overall average of 0.5 cm yr^{-1}. On the slope, sediment accumulation rates for the Holocene have been estimated from 3 cores and vary from 0.13 cm yr^{-1} at the base of upper-slope gullies, to 0.09 cm yr^{-1} in two separate cores in mid-slope basins (Orpin et al., 2006). Despite this record of Holocene sediment deposition in mid-slope basins, it is apparent that some canyon heads are infilling and are not acting as through-going sediment conduits under present sea-level highstand conditions (Walsh et al., 2007).

Although the nature of the modern sediment-dispersal system and the Holocene to Recent sedimentation rates are relatively well known and understood there is a distinct lack of knowledge of the longer time-frame process of shelf- and slope-basin evolution. In other locations on the Hikurangi Margin the outer shelf/upper slope are underlain by lowstand systems tracts (Lewis, 1973; Lewis et al., 2004; Paquet et al., 2009). It is likely that upper-slope gully systems and canyons are cutting into a combination of these lowstand sequences and the underlying bedrock, as well as the outer edge of the modern highstand systems tract. To better understand slope gully formation it is necessary to get a fuller understanding of the stratigraphy and structure of the outer shelf and upper slope in the Poverty Bay study area.

5.2 Structure and stratigraphy of the shelf and upper slope

Prior to this study there has been relatively sparse mapping of continental-shelf structure from Mahia Peninsula north to East Cape (Field et al., 1997; Lewis et al., 1997; Lewis et al., 2004). This is primarily due to the previous lack of good-quality MCS data for the shelf region. Likewise the pre- last-glacial stratigraphy of the Poverty region has been little documented. What has been inferred has been limited to broad-scale age constraints on the

Cretaceous–Tertiary sequences (Field et al., 1997). Sequences underlying the outer shelf and upper slope are of primary interest to this study. These have been documented to the south in Hawke's Bay and include the lowstand wedge (LSW) of the last and previous glaciations on a foundation of Cretaceous–Miocene strata (e.g. Barnes et al., 2002; Barnes et al., 2009; Paquet et al., 2009).

Figure 5.3 shows the distribution of active structures on the Poverty Bay continental shelf mapped from MCS, boomer and high-resolution seismic data. The distribution of data used is presented in Figure 5.4. Detailed mapping of the shelf around Mahia Peninsula has shown that the primary shelf-structure extending north from outer Hawke's Bay is the Lachlan Fault; a seaward-vergent listric thrust fault (Barnes et al., 2002; Barnes and Nicol, 2004). The following section presents a structural interpretation of the Poverty Bay continental shelf and upper slope, and develops a stratigraphic model for the northern margin of the re-entrant. The purpose of this is to provide a framework for understanding the geomorphic evolution of the upper slope.

5.2.1 Regional stratigraphy

Within the framework of the wider Hikurangi Margin, the Poverty upper slope and continental shelf are underlain by the deforming backstop of pre-subduction-initiation (Cretaceous–Paleogene) material, overlain by Miocene basin sequences with Quaternary basins and cover sequences towards the surface (Lewis and Pettinga, 1993; Barnes et al., 2009). The only published interpretation of pre-LGM geology underlying the Poverty shelf is from Field et al. (1997) that shows the broad-scale distribution of Cretaceous, Paleogene, Miocene and post-Miocene rocks (Figure 5.5). This is in broad agreement with interpretations in Hawke's Bay, where stratigraphy can be tied from dated well sequences and rock-dredge samples into MCS profiles (Figure 5.6) (Barnes et al., 2002; Barnes and Nicol, 2004). An interpretation of upper-plate stratigraphy is possible based on these previous studies, and using unpublished dated rock-dredge sample.

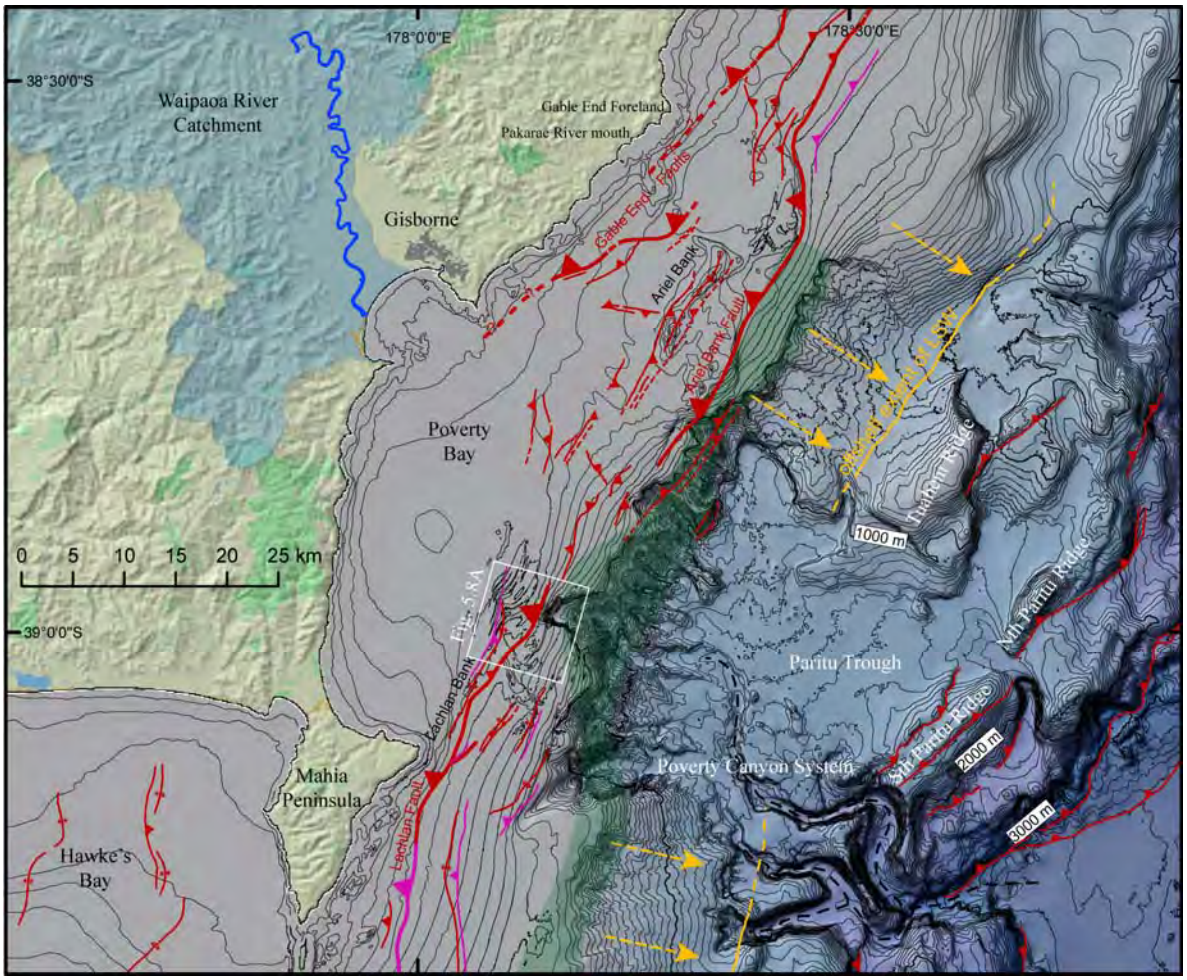

Figure 5.3: Structure of the Poverty Bay continental shelf and slope. Shelf structure to the east and west of Mahia Peninsula after Barnes et al. (2002) and Barnes and Nicol (2004); lower-slope structure partly after Barnes et al. (2009), and partly mapped during this study. All shelf structure shown to the north of Mahia Peninsula has been mapped as part of this study. Active structures shown are: active thrust faults (red with triangles showing dip direction); blind thrust faults (pink); and, anticlines (red with opposing arrows). A zone of inactive thrust fault tips is delineated underlying outer shelf/upper slope by a green transparency. Orange arrows show the outer extent of the lowstand wedge (LSW).

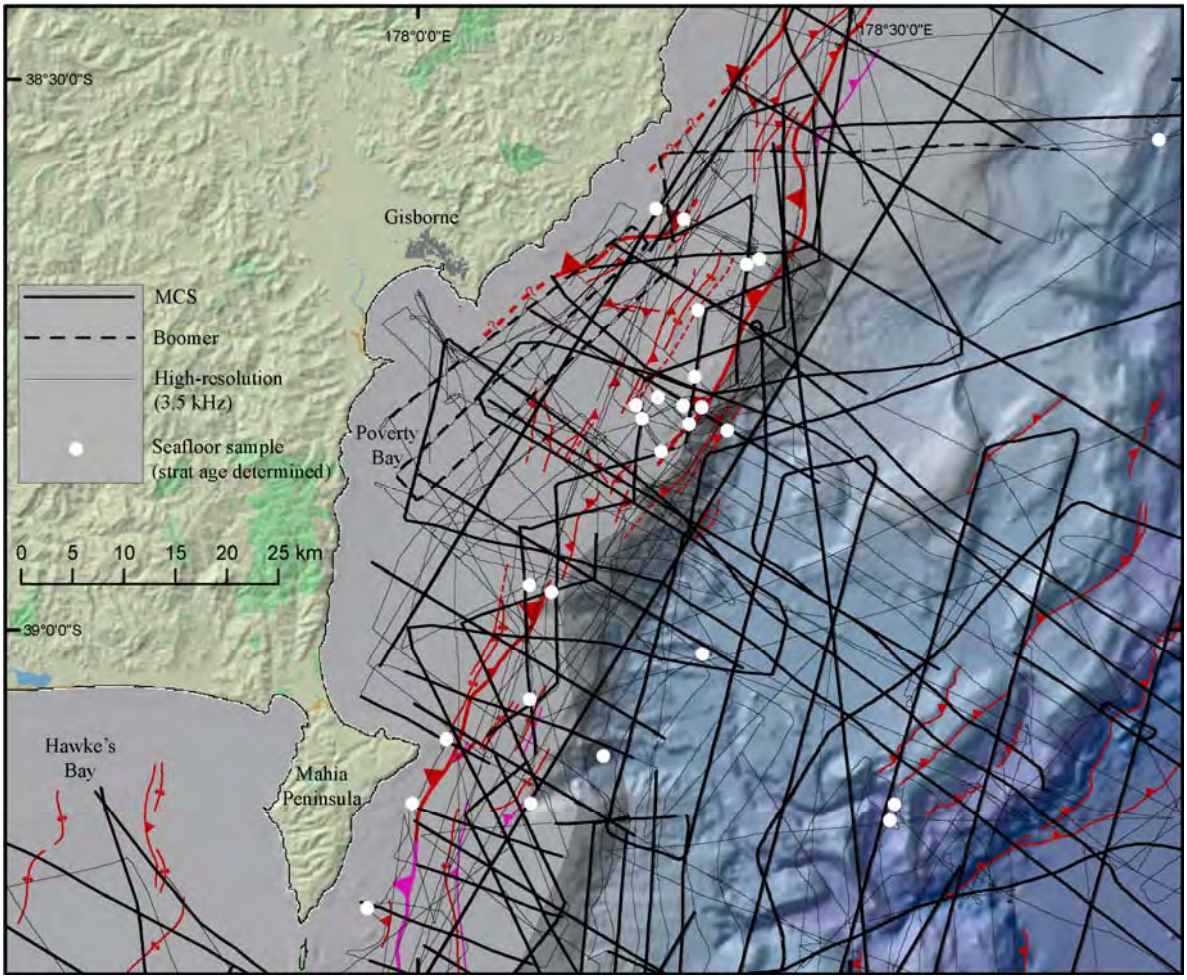

Figure 5.4: Data used to map the structure and identify stratigraphy beneath the Poverty Bay continental shelf and upper slope. Structure presented in Figure 5.3 is shown underlying the seismic navigation.

Upper-plate stratigraphy

The subducting Pacific Plate is generally clearly recognisable in deep-penetration seismic reflection profiles from comparably high-amplitude reflectivity below the plate-boundary decollement (e.g. Barnes et al., 2009). In the upper plate, pre-subduction Cretaceous and Paleogene sequences are characterised by discontinuous acoustic reflectivity, with large areas represented by weak reflectivity and opaque seismic character (Figure 5.7A and B). Cretaceous and Paleogene sequences typically occur below three seconds two way travel time (twt), but are exposed at the seafloor to the south-east of Mahia Peninsula as reefs such as Lachlan Ridge (Barnes et al., 2002). Miocene sequences are characterised by unconformity-bound packages of relatively continuous high-amplitude reflectivity, particularly in the upper section (Figure 5.5). Miocene rocks are directly overlain by Quaternary sequences, where they are not exposed at the seafloor (Barnes et al., 2002;

Paquet et al., 2009). The Quaternary sequences typically occur in basins bound by a diachronous, unconformable lower surface (Paquet et al., 2009), and have a distinctive seismic character represented by very-strong easily-traceable continuous acoustic reflectivity (Figure 5.7C). A direct tie of an early- to mid-Pleistocene sample into the shelf-basin sequence, using strike ridges exposed at the seafloor, confirms this as a Quaternary basin (Figure 5.8). Numerous dated samples confirm the age of the Miocene sequences from seafloor exposures (e.g. Figure 5.7). Details of dated dredge samples available for this study are presented in Table 5.1.

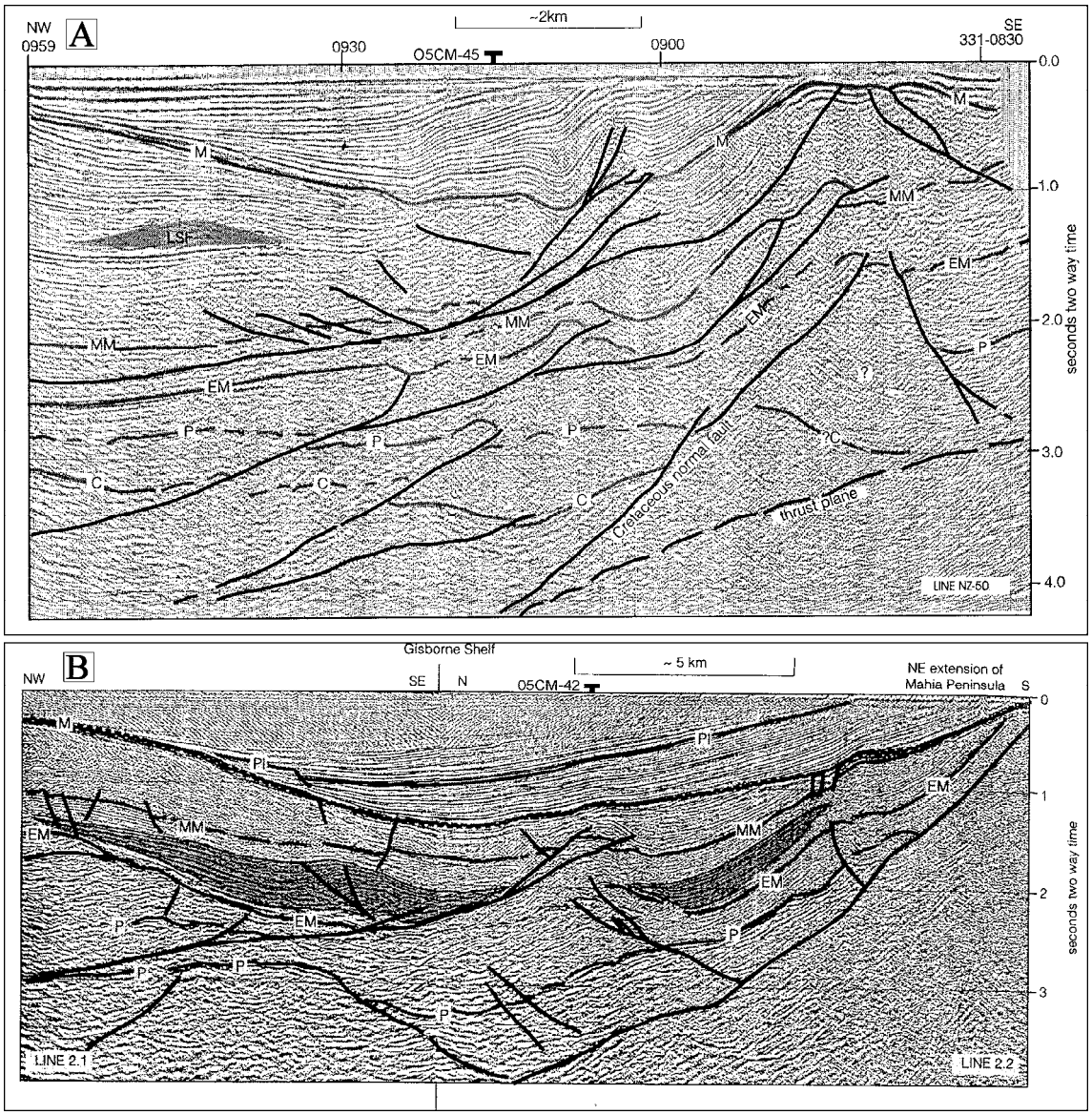

Figure 5.5: Published interpreted seismic lines in Poverty Bay (Field et al., 1997). A) NZ-50. B) BPSAT-2.1. The location of the lines is shown in Figures 5.13 and 5.14. Relevant abbreviations in interpreted sections are M top of Miocene, P top of Paleogene

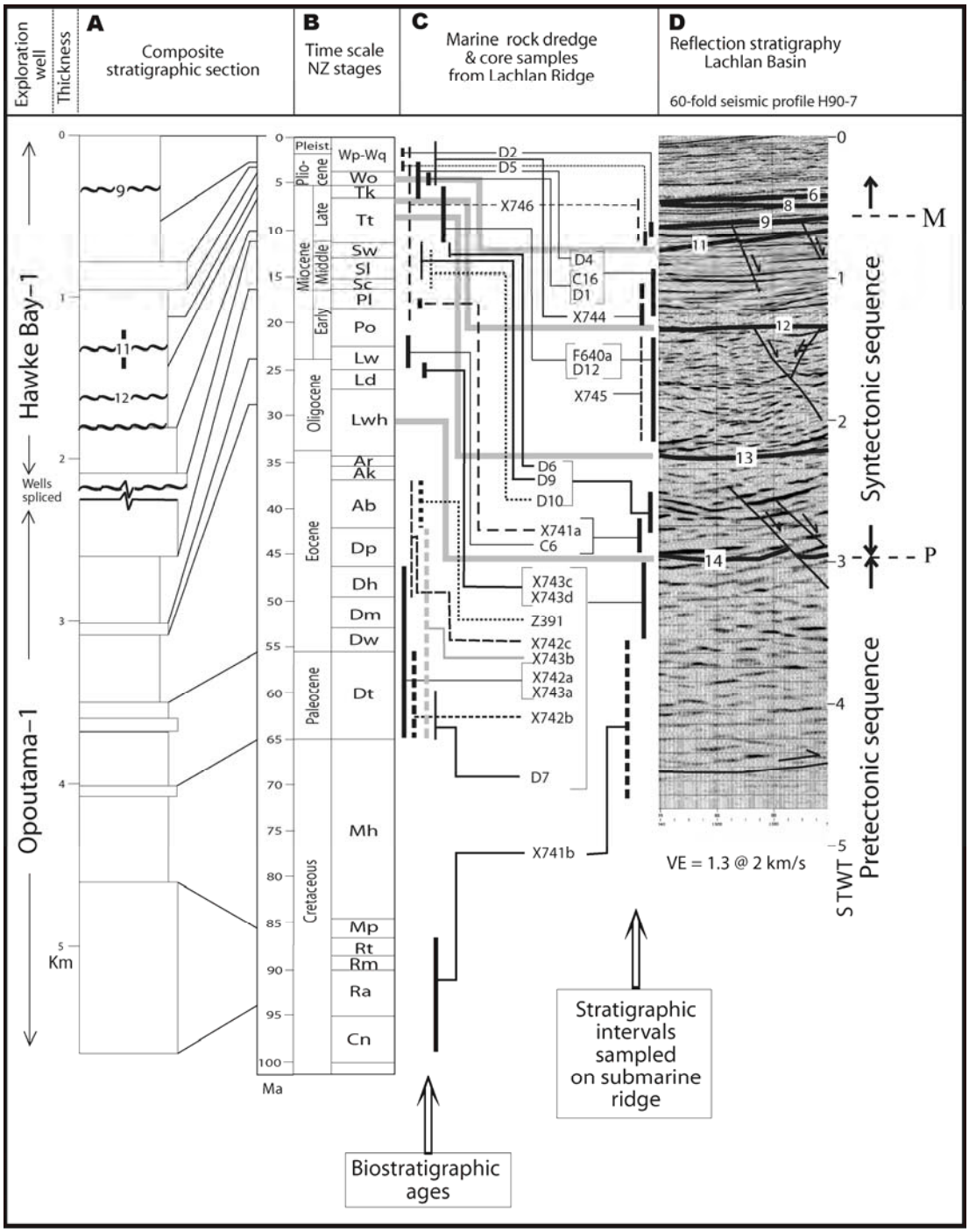

Figure 5.6: Compilation and interpretation of stratigraphic data in Hawke's Bay. After Barnes et al. (2002). A) Stratigraphic column from composite well sections. B) New Zealand time-scale stages. C) Marine rock-dredge and core samples for age constraint. Vertical bars to the left of the sample number indicate the biostratigraphic age ranges derived from analysis of nannoflora, foraminifera, and pollens. Vertical bars to the right of the number indicate the relative stratigraphic positions from which the samples were recovered. D) Seismic data from the central Lachlan Basin for seismic character. Bold gray lines left of reflections 11, 12, 13, and 14 are seismic well ties. Deep stratigraphic boundaries picked in this study - the top of the Miocene M, and top of the Paleogene P - are shown to the right of the figure in their position relative to the stratigraphy of Barnes et al. (2002).

Using the recognisable acoustic character of stratigraphic sequences in MCS data, and drawing on available dated seafloor samples (Figure 5.4), the stratigraphy underlying the Poverty Bay shelf has been interpreted in MCS profiles that are presented along with structural mapping in Figures 5.13 and 5.14. It is apparent that a significant period of the late Neogene is not represented here, as the Pleistocene–Recent shelf basin sits unconformably on the Miocene sequences below.

Table 5.1: Dated seafloor samples from the Poverty shelf and slope area

Stn	Gear	Biostrat Age	NZ Stage	Notes
V475	Dredge	E Miocene	UOt-lCl	
X715	Unknown	E-M Pleistocene	mWc	
X717	Dredge	E Miocene	mPl	Hard Pebbles, Mudstone
X718	Dredge	E Pleistocene	lWc	Firm gray shelly mud
X720	Cor. Grav	M Pleistocene	uWc-mWq	
X721	Cor. Grav	M Pleistocene	Wq	
X722	Dredge	E Miocene	mPl	muddy gravel, blocks mudstone
X723	Dredge	L Miocene - Pliocene	lTt-lWo	block mudstone, broken shells
X724	Dredge	E Pleistocene	uWn	Mudstone
X726	Dredge	M Pleistocene	uWc-mWq	shelly gravel, mudstone fragments
X727	Dredge	M Miocene	bSw-bTt	large well indurated mudstone boulders
X728	Unknown	M-L Miocene		
X729	Dredge	E-M Pleistocene	mWc	Hard mud with pebbles
X730	Dredge	M Miocene - E Pliocene	lSw-tWo	small rocks, muddy gravel
X732	Dredge	M Pleistocene	uWc-lWq	mud with traces of mudstone
X734	Dredge	E-M Pleistocene	lPo-tSl	soft mudsone & mud
X738	Dredge	E-M Miocene	mPl-lSl	mud shell hash
X739	Dredge	E-M Miocene	mPl-tSl	large rocks, concretionary blocks/tubes
X741	Dredge	E Miocene	lPl-mPl	mudstone, heavily bored
X742	Unknown	M-L Eocene	uAb-mAk	
X771	Dredge	E-M Miocene		Grey mudstone.
W703	Cor. pstn	M Miocene	uPl-lSl	mudstone at base of corer

Figure 5.7: Example of the seismic character of Paleogene to Quaternary stratigraphy in MCS data from the Poverty shelf area (following page). A) interpreted MCS profile 05CM-45 showing active structure (red), stratigraphic boundaries (blue), and location of dated seafloor dredge samples. The location of dated samples and the MCS profile are shown on Figures 5.13 & 5.14. B) Enlargement illustrating the seismic character of Miocene vs Paleogene stratigraphy. C) Enlargement illustrating the seismic character of the Quaternary sequences. Where horizons down-lap onto the diachronous unconformity defining the lower boundary of the basin these are indicated by pink arrows. Acoustic footwall cut-offs used to map structure are indicated by blue arrows. Note that the Miocene rocks exposed at the seafloor at the far right of the enlargement have a very strong and distinctive acoustic signature that is observed widely where such material is exposed on the shelf.

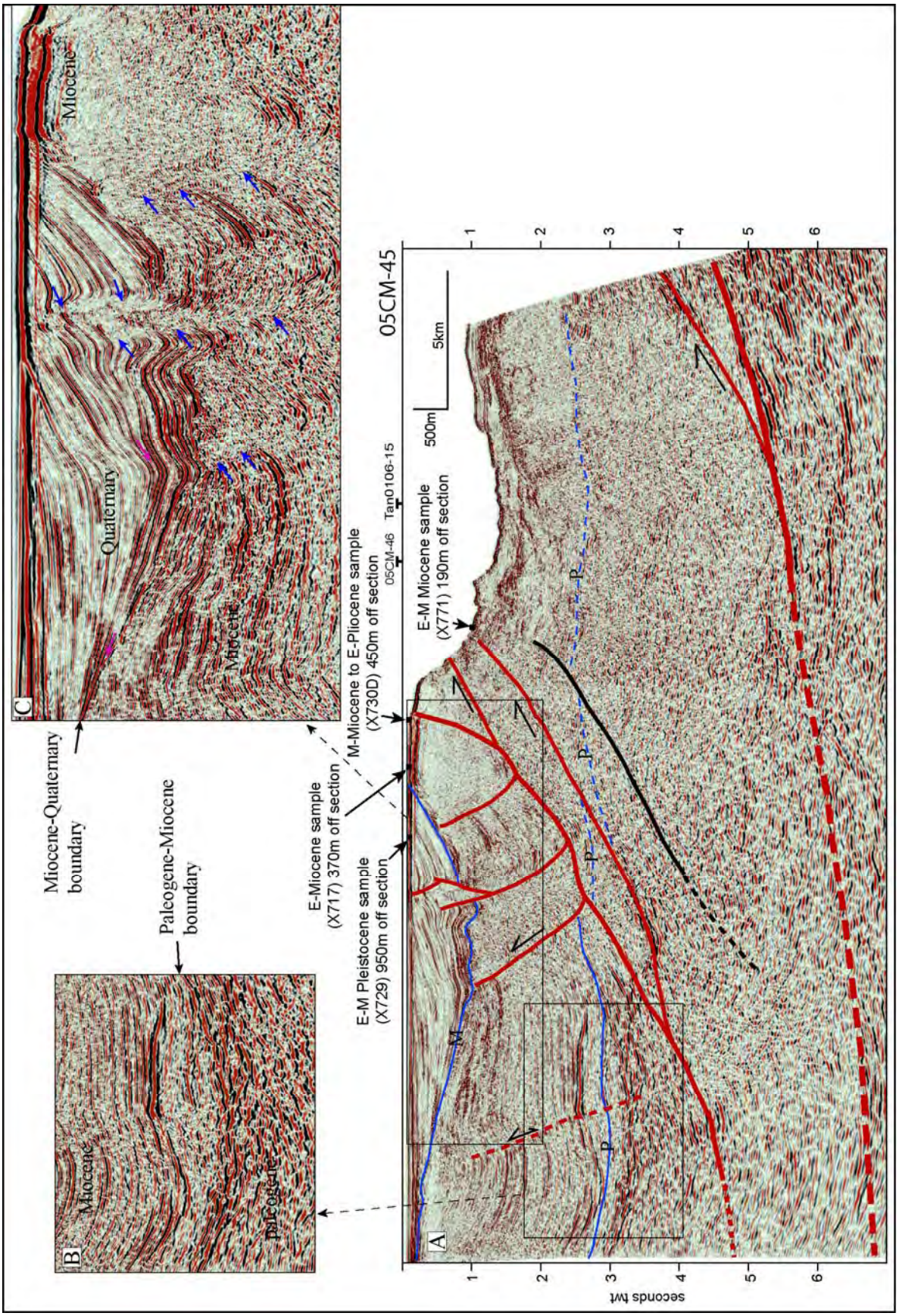

Figure 5.7 (caption on previous page)

5.2.2 Outer-shelf/upper-slope stratigraphy

Much of Poverty shelf is directly underlain by deforming Quaternary basins (e.g. Figure 5.8). In Hawke's Bay it has been established that basins with comparable character are at most early to mid Pleistocene in age (~1 Ma) (Paquet, 2007). While it has not been possible to clearly track dated reflectors north from Hawke's Bay, due to Lachlan Bank inhibiting preservation, the seismic character of the Poverty shelf basins suggests these are of similar age, and this is supported by projection of an early to mid Pleistocene sample into the lower part of the sequence (Figure 5.8). It is noted that the age analysis for the early to mid Pleistocene sample tied to MCS in Figure 5.8 included a second possible Miocene age. It is assumed that the material dated as Miocene was transported from another location and this interpretation is supported by: 1) an adjacent mid Pleistocene date; and 2) the distinctive morphological character of the exposed early to mid Miocene rocks compared to those interpreted as Pleistocene. While the majority of the Quaternary shelf-basin sequences are constrained at their outer extent by structural barriers/uplift (e.g. Figure 5.7), in places they extend off shelf onto the upper slope.

For the purpose of understanding the development of canyon and gully systems, landslide systems, and the evolution of the upper slope it is important to have some control on the age and nature of the upper part of the sequence. Paquet et al. (2009) were able to constrain the extent of the lower boundary of material deposited since the penultimate glacial lowstand (oxygen isotope stage (OIS) 6) at ~125–135 kyrs BP, defined as a reflector designated S1. Unfortunately, with the currently available MCS grid it is not possible to tie S1 between southern Hawke's Bay and Poverty Bay, primarily due to uplift and erosion of the surface and overlying sequence across Lachlan Fault. The approach taken here to constraining S1 through Poverty Bay is to independently interpret MCS profiles across the upper slope at Poverty Bay (Figure 5.9), compare them to profiles in southern Hawke's Bay (Paquet et al., 2009), and develop a sequence-stratigraphic model constraining the character and extent of post-OIS6 deposits.

Paquet et al. (2009) interpreted a sigmoidal sequence up to 0.5 seconds twt thick (~450m @ 1800ms twt) above S1, representing material deposited since the end of OIS6 (Figure 5.10A). Within this package more than seven parasequences occur, many of which show a down-lap relationship with the unit below.

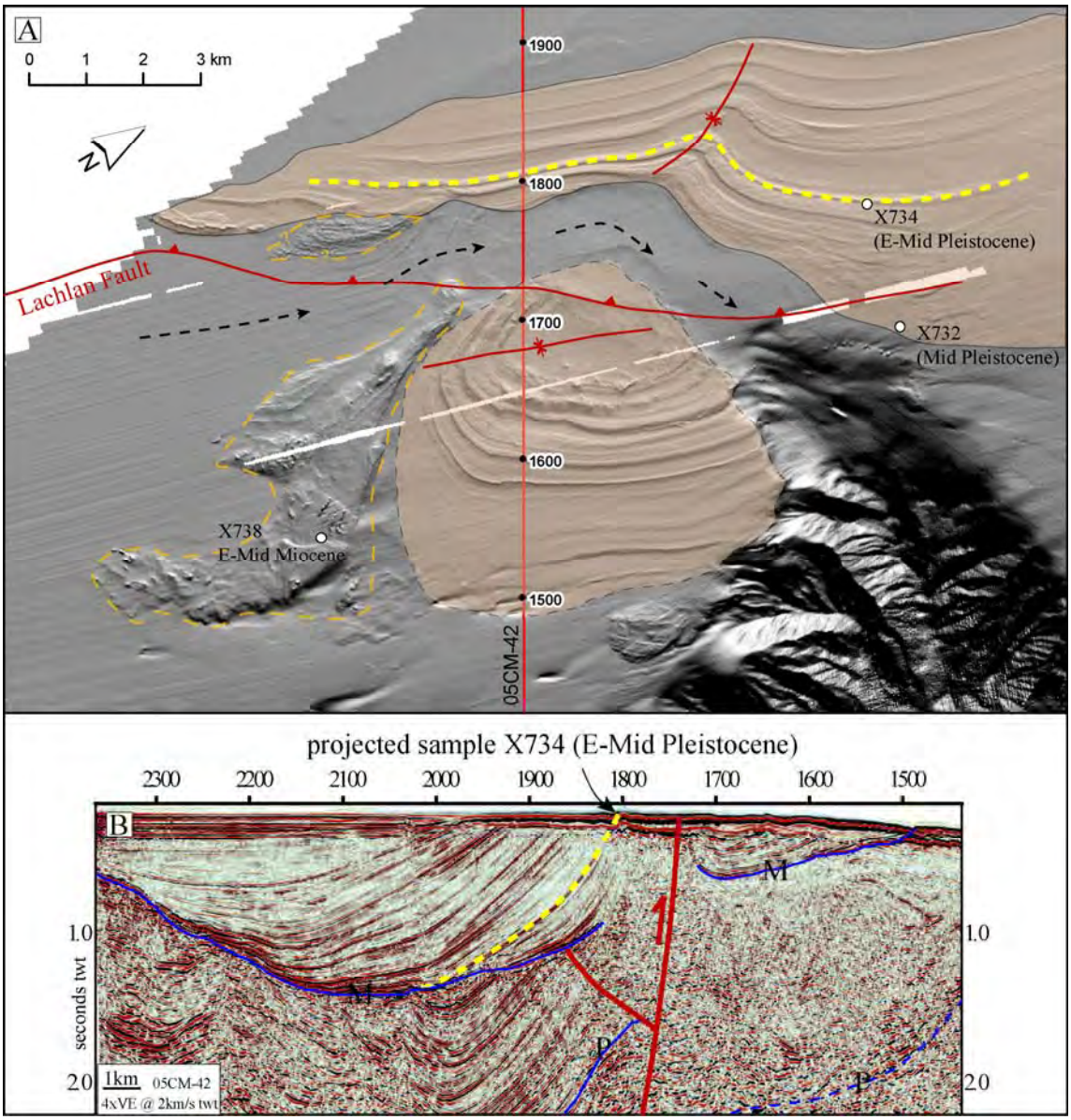

Figure 5.8: Tie of a seafloor sample into seismic stratigraphy using shelf multibeam data. A) Shelf multibeam image with strike ridges exposed at the seafloor and showing the local distribution of dated samples as well as active fault traces and the interpreted distribution of Pleistocene (brown transparency) vs Miocene (orange dashed lines) stratigraphy at the seafloor. An early to mid Pleistocene sample can be projected into the MCS profile. The extent of this figure is shown in Figure 5.3. B) MCS profile 05CM-42 tying the dated stratigraphic horizon to a reflector in the lower-basin sequence (bold yellow dashed line). Profile is located in Figures 5.13 and 5.14.

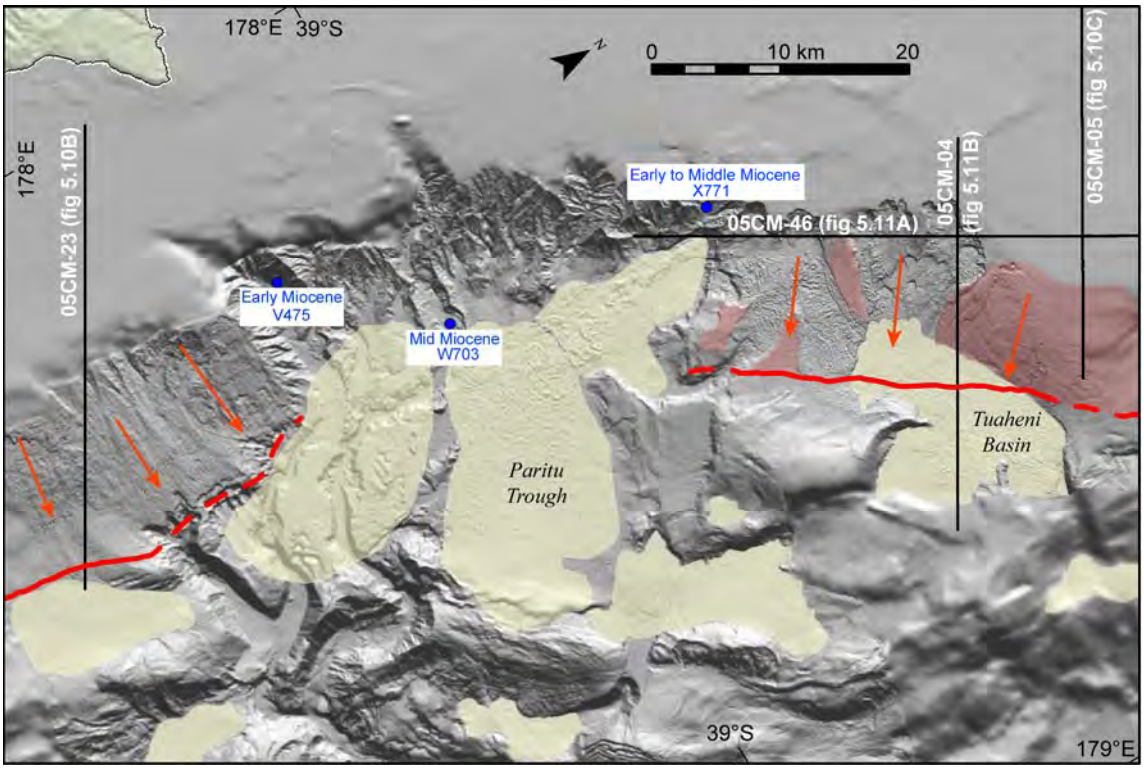

Figure 5.9: Location map for MCS profiles used in the interpretation of late Quaternary stratigraphy. Also shown is the extent of slope basins (yellow transparency), selected Miocene samples on the re-entrant upper slope (in blue), the seismically-resolved outer extent of the lowstand wedge (red lines and arrows), and interpreted relict surfaces of the lowstand wedge (red transparency).

Directly offshore of Mahia Peninsula there is a well preserved shelf-to-upper-slope sequence imaged in MCS (Figure 5.10B). As mentioned it is not possible to tie this stratigraphy to that of Paquet et al. (2009). In the upper part of the sequence, off-shelf prograding clinoforms with a sigmoidal geometry are preserved characteristic of deposition during progressively lowering sea level (Posamentier and Vail, 1988). The units top-lap with a high-amplitude reflector interpreted as the transgressive ravinement surface created by wave-base erosion during the landward migration of the shoreline between ~18–6 kyrs BP (Figure 5.10B inset). Above the transgressive ravinement, a thin shelf-parallel reflector likely represents the extent of post-glacial sediment across this part of the shelf. This part of the sequence is well imaged in high-resolution seismic data (e.g. Foster and Carter, 1997; Orpin et al., 2006; Gerber et al., 2009). The prograding units above S1 underlie the outer 5 km of the shelf and contain approximately five discrete sigmoidal packages bounded by high-amplitude acoustic reflectors. Approximately 5 km inward from the shelf break, and at ~100ms depth a gently-seaward-dipping high-amplitude acoustic reflector defines the upper

surface of another sequence of discrete sigmoidal packages. This high-amplitude reflector is interpreted as the penultimate transgressive ravinement (S1) based on the geometric and acoustic similarity to the modern-day system.

A number of facies relationships and geometric parameters support the interpretation of the last glacial-cycle package, when compared to the interpretation of Paquet at al. (2009):

1. A comparable number of “parasequences” are recognised within the post-S1 sedimentary body.
2. The thickness of the post-S1 ka sedimentary body is comparable beneath the outer shelf.

Below S1, in profiles 05CM-23 and 05CM-05 (Figure 5.10), more sigmoidal sedimentary packages are recognised that may record 100kyr glacial-cycle deposition (c.f. Figure 1.2). It is clear that this model may have significant error involved if the stratigraphic age interpretation is incorrect. It is possible that what are interpreted as parasequences are actually full 100 ka glacial cycles making the material significantly older. This does not however fit with the dated mid Pleistocene age of a low stratigraphic reflector in the shelf-basin sequence (Figure 5.8). If it is assumed, for argument sake, that the base of the Quaternary sequence in Figure 5.10B is at 1 Ma (~base of Pleistocene), we might expect something in the order of 10 full sea-level cycle sequences, which is reconcilable with observations. A landward migration of the shelf break, followed by a rapid seaward shift is well preserved in the progradational geometry (Figure 5.10B). At the inner end of the basin, sedimentary sequences are characterised by parallel, easily-traceable acoustic reflectors interpreted as representing sediments deposited in a shelf environment. Seaward of these, seismic character becomes significantly more disturbed and reflectors have steeper dips suggestive of slope deposition. Consequently the inflection point where an individual reflector changes character is interpreted as representing the location of the shelf break at the time of deposition. This overall sequence geometry implies a period of margin subsidence followed by uplift and/or increased sediment supply.

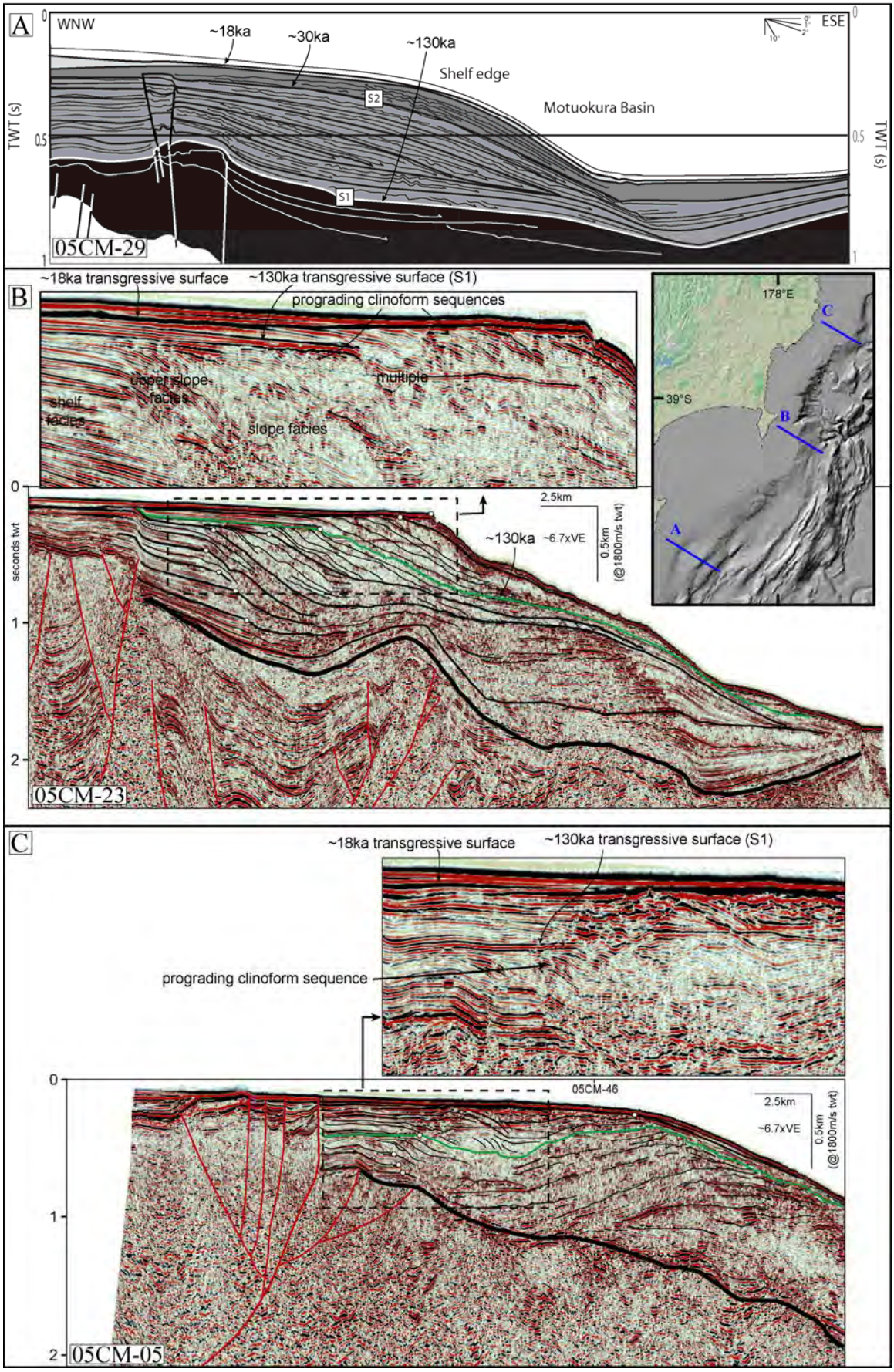

Figure 5.10 (caption on following page)

Figure 5.10: Stratigraphic interpretation of reflector S1 at the base of the MIS2-5 sedimentary sequence on three MCS reflection profiles (previous page). The location of the three profiles is shown on the inset map. A) Upper-slope sequence in Hawke's Bay, deposited since OIS6. Modified from Paquet at al. (2009) This MCS profile (05CM-29) is from the same survey as the profiles presented in B & C. Note that the vertical scale of this profile is different to B & C. B) Interpretation of MCS profile 05CM-23 defining the outer-shelf/upper-slope glacio-eustatically forced systems tracts to the south of the Poverty re-entrant. Inset shows an enlargement of the key part of the profile for defining the OIS6–2 sequence with main features labelled. White dots indicate paleo- shelf break locations. C) Interpretation of MCS profile 05CM-05 to define the location of S1 north of the Poverty re-entrant. Inset shows an (uninterpreted) enlargement of the key part of the profile. The heavy weight black line in B and C is the interpreted base of the glacio-eustatically forced systems tracts. The interpreted ~130 kyr reflector S1 is shown in green. White dots indicate paleo- shelf break locations.

It is unfortunately not possible to tie these sequences directly across the re-entrant to northern Poverty Bay. The stratigraphic model can, however, be applied to a sequence imaged in MCS at the northern end of the Poverty re-entrant (Figure 5.10C & 5.11). Profile 05CM-05 (Figure 5.10C) shows equivalent shelf-to-slope-depositional seismic character in the shelf-basin sequence, but in contrast there is folding of the sequence forcing strata to become landward dipping beneath the present shelf break. While this complicates the interpretation, a comparable landward- then seaward-stepping geometry is recognised suggesting a similar overall depositional history. Approximately 300 ms twt below the seafloor a comparable reflector to that observed in Figure 5.10B is interpreted as the penultimate ravinement surface, reflector S1. The relationship between this reflector and the top-lapping sigmoidal sedimentary packages below also strongly resembles that preserved to the south of the re-entrant, and in southern Hawke's Bay.

To summarise this interpretation:

- It is not possible to stratigraphically tie the base of the MIS2–5 sedimentary sequence (reflector S1) to the interpretation of Paquet at al. (2009) in Southern Hawke's Bay.
- There are a series of prograding parasequences underlying the last-post-glacial ravinement surface in southern Poverty Bay (Figure 5.10B).
- A very prominent reflector below this prograding sequence shows an equivalent relationship to an underlying series of prograding parasequences. This reflector is interpreted as the penultimate ravinement surface, reflector S1.

- Together the set of parasequences represent internal cycles within a 100kyr-type glacial cycle of deposition (mega-sequence), c.f. Paquet at al. (2009).
- The stack of up to 10 mega-sequences recognised in the upper 1 s twt thick section is reconcilable with a Pleistocene and younger age for the basin (Figure 5.8).
- To the north of the Poverty re-entrant a similar depositional geometry is recognised, allowing the location of the base of the MIS2–5 sedimentary sequence to be interpreted and tracked onto the upper slope as reflector S1 (Figure 5.10C).

S1 is assigned an age of 125–135 kyrs BP, but it is acknowledged that it could potentially be in the order of 100 kyrs older if this horizon represents the previous ravinement surface. The S1 surface can be interpreted beneath the upper slope, north of Poverty re-entrant (Figure 5.11A), and subsequently across the upper slope above Tuaheni Ridge (Figure 5.11B). The interpretation of the S1 reflector, within the sedimentary sequence provides a framework for the evolution of landslides on the upper slope and, combined with the structural framework, assists in an analysis of the evolution of the re-entrant headwall.

5.2.3 Shelf structure

Shelf structure has been mapped based on available MCS and high-resolution seismic data and bathymetry (Figures 5.3 & 5.4). Detailed interpretation of MCS profiles has enabled definition of structure based on footwall cut-off relationships in acoustic reflectivity and patterns of stratigraphic deformation (Figures 5.7 & 5.12). All structures that are mapped as active at the seafloor have been checked in high-resolution seismic to confirm post-glacial deformation. Structural mapping has primarily been limited to active structures, however an inactive thrust-fault stack has also been mapped underlying the outer shelf along the length of the Poverty re-entrant from the recognition of multiple buried thrust tips that do not deform the overlying sequence (Figure 5.12).

Figure 5.11: Stratigraphic tie of S1 from MCS profile 05CM-05 (Figure 5.10C) onto the upper continental slope (following page), in A) dip profile 05CM-46, and B) strike profile 05CM-04. Yellow transparent shade indicates landslide debris. The heavy-weight black line is the interpreted base of the glacio-eustatically forced systems tracts. The interpreted ~130 kyr reflector S1 is shown in green. The location of Figure 5.24 is indicated. Profiles are located in Figure 5.9.

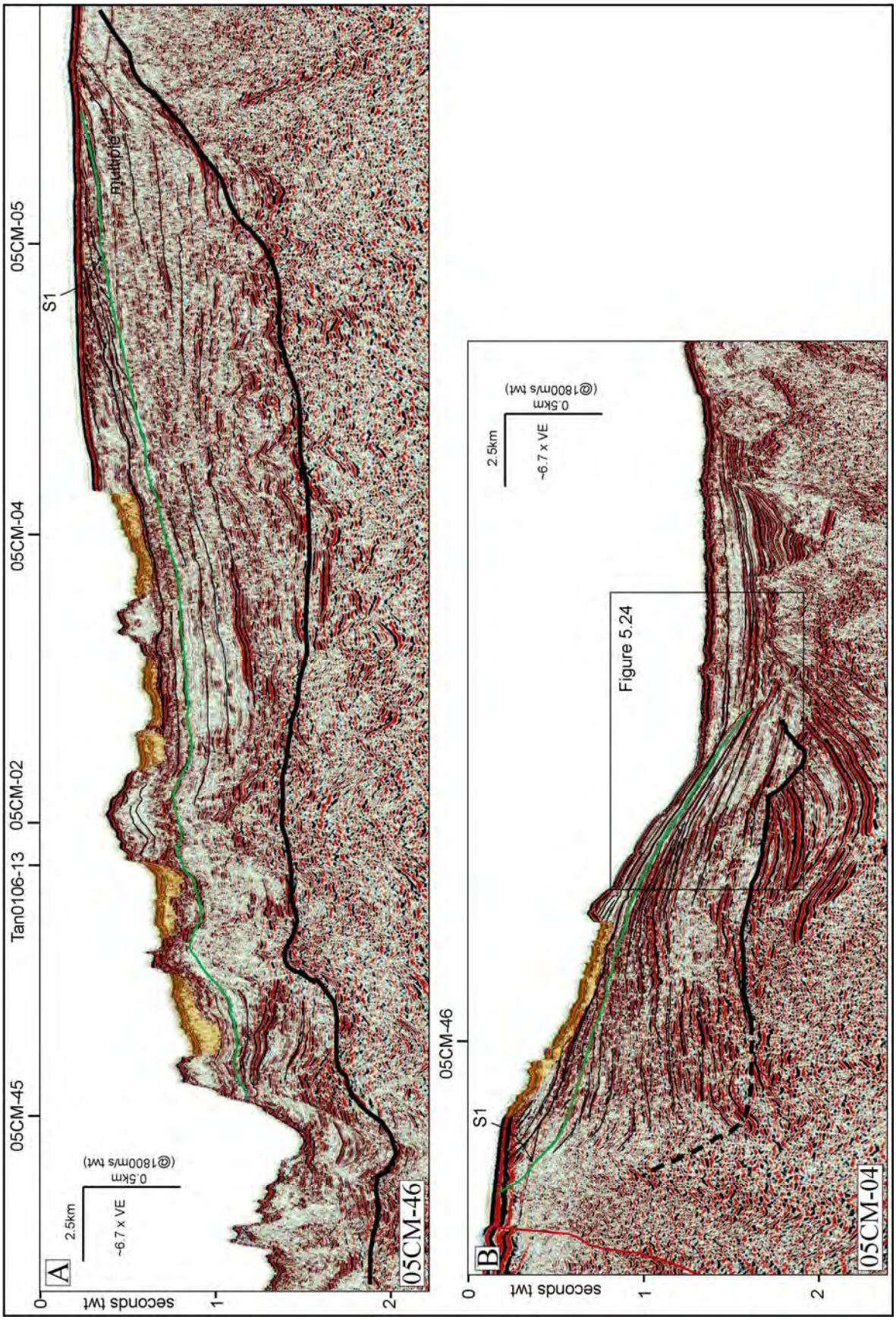

Figure 5.11 (caption on previous page)

The active structure of Poverty Bay is dominated by two major structures on the outer shelf; Lachlan Fault and Ariel Bank Fault, with a complex, discontinuous structural step-over between them (Figure 5.3, 5.13 & 5.14). Additionally, on the inner shelf to the north there is a zone of active structures that project to the seafloor, referred to here as the Gable End Faults. In the following sections the main structures are each described in detail, as this is the first time these faults have been presented.

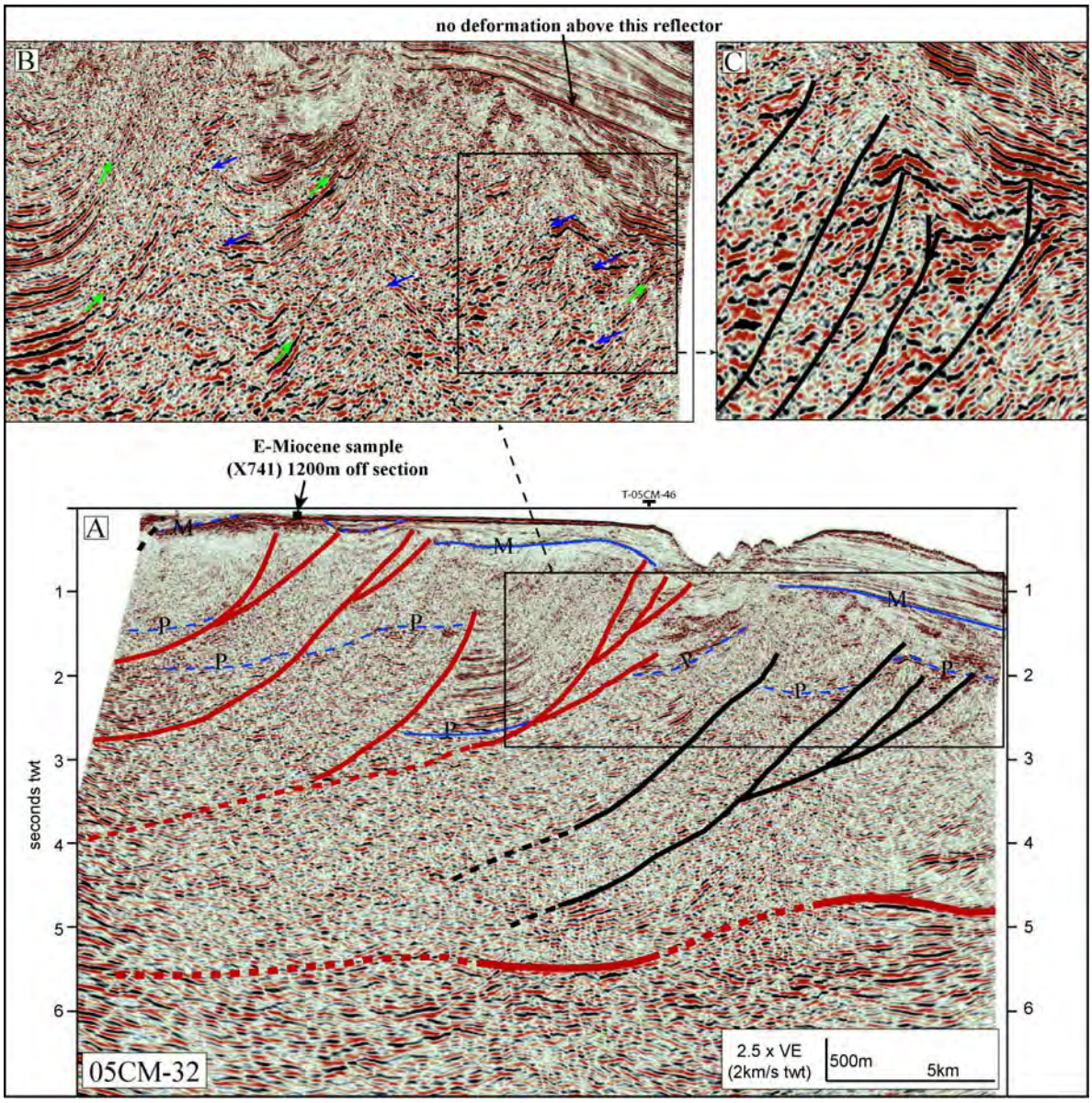

Figure 5.12: Example of mapping control for defining active and inactive structure in MCS reflection data. A) MCS profile 05CM-32 showing active (red) and inactive (black) structure and mapped stratigraphy. B) Uninterpreted enlargement illustrating foot-wall cut-offs (blue arrows) and hanging-wall deformation (green arrows). Note reflector at right that is undeformed despite structure mapped beneath it. C) Further enlargement of inactive thrust tips under undeformed cover-sequence. Profile is located in Figures 5.13 and 5.14.

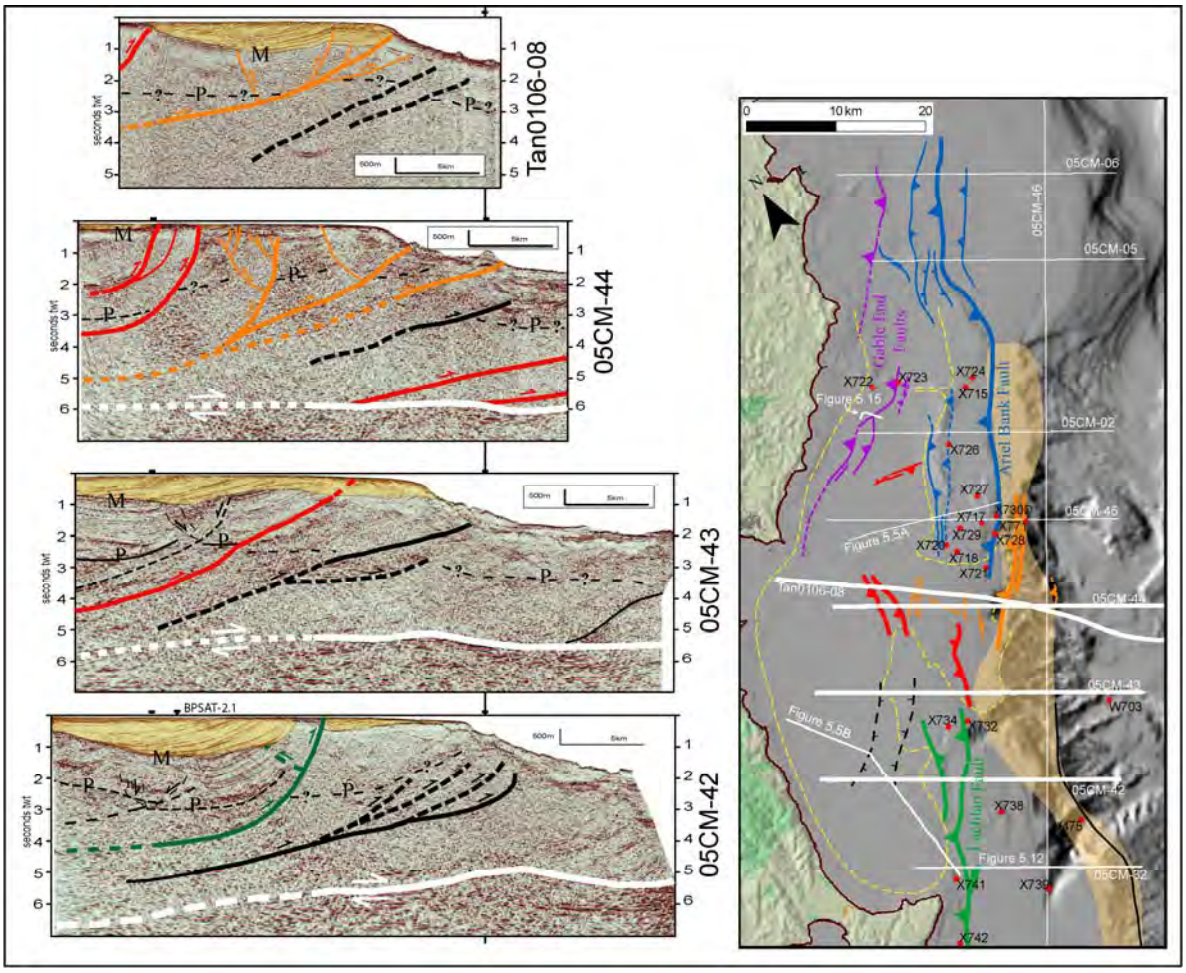

Figure 5.13: Interpreted MCS profiles along the southern Poverty shelf illustrating the major tectonic structures and stratigraphy. Green linework in the fault-trace map represents Lachlan Fault and associated structure. Blue linework represents the Ariel Bank Fault and associated structure. Purple line work represents the Gable End Faults. The major structures between Ariel Bank Fault and Lachlan Fault are shown in orange (related seismogenic faults) and red (undifferentiated faults). The zone of inactive thrust tips under the outer shelf/upper slope is indicated by the orange transparency. Dated samples are shown (red dots) with station numbers. Details of samples are presented in Table 5.1. For examples of how samples relate to MCS profiles refer to Figures 5.7, 5.8 & 5.12. The dashed yellow line is the extent of post-glacial sediment on the shelf, after Orpin (2004). The relationship between primary structures, splays and the plate boundary mega-thrust (white) is shown in the interpreted MCS profiles.

Lachlan Fault

Lachlan Fault is well expressed along the outer Hawke's Bay shelf in bathymetry (Lachlan Ridge and Lachlan Bank) and in MCS, and has been subject to detailed structural analysis (Barnes et al., 2002; Barnes and Nicol, 2004; Nicol et al., 2007). The fault has evolved through polyphase deformation involving the reactivation and inversion of inherited

extensional structure, and has a modern slip rate of 3.5–6.5 mm/yr. Lachlan Fault was previously mapped into three segments with an overall length of ~80 km, with the northern segment terminating at the northern end of Mahia Peninsula (Barnes et al., 2002). Remapping of the fault during this project extends the northern segment another ~20 km, beyond Mahia Peninsula and into Poverty Bay (Figure 5.13).

The main seaward-vergent listric structure has a back-thrust rooted onto it on the western side (Profile 05CM-42, Figures 5.13 & 5.8). The structure exposes Cretaceous rocks at the seafloor off Mahia Peninsula (Barnes et al., 2002), and Miocene sequences further north (Figure 5.8).

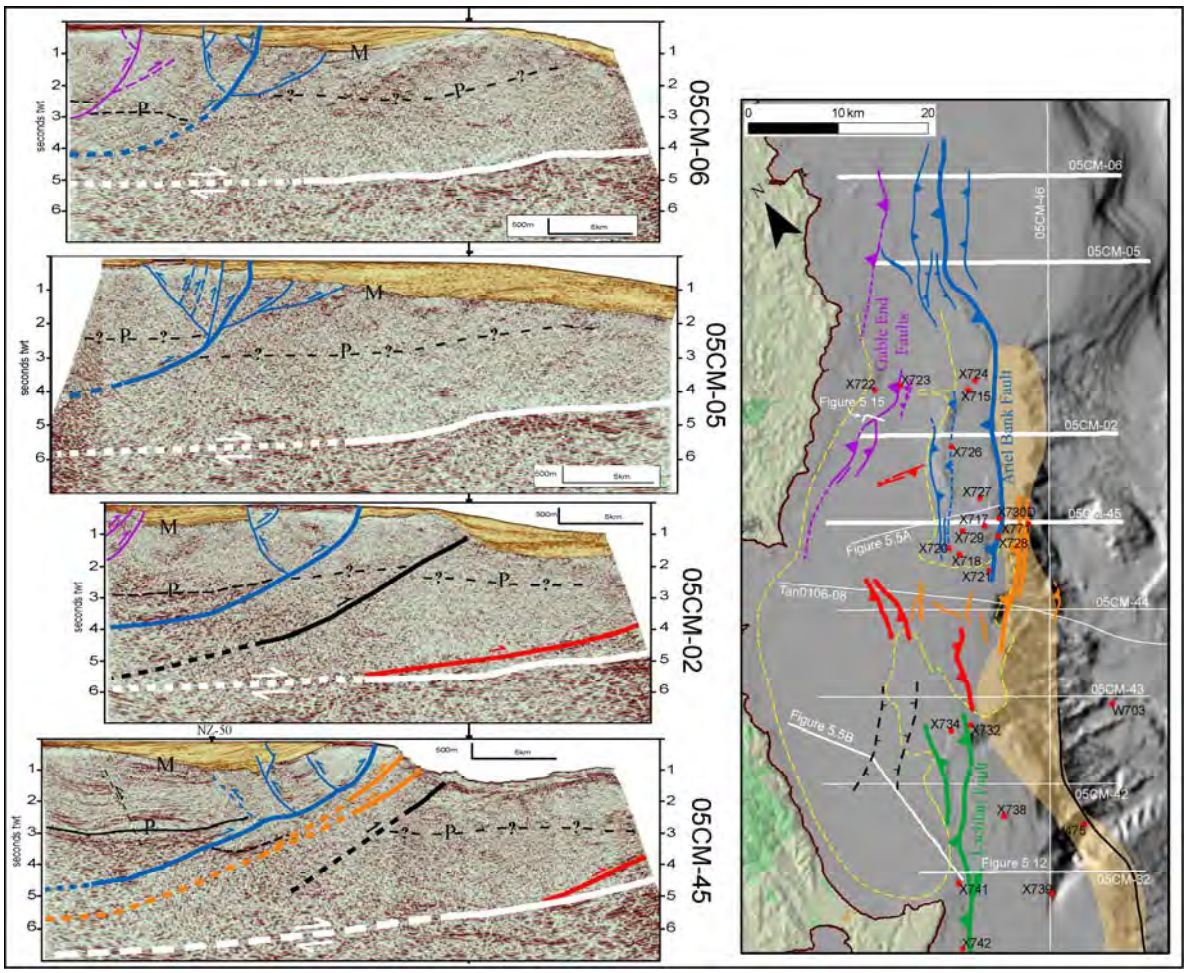

Figure 5.14: Interpreted MCS profiles along the northern Poverty shelf illustrating the broad-scale model of tectonic structure. Refer Figure 5.13 caption for details.

Step-over structures between the Lachlan and Ariel Bank faults

North along the shelf from Lachlan Fault there are several active structures that are short in extent (<10 km), but some of which have a significant expression in MCS (e.g. line 05CM-44 Figure 5.13). Together these structures represent a complex step-over zone between the Lachlan and Ariel Bank faults. MCS profile coverage (including that not presented here) confirms the segmentation between the green, red, orange and blue coded structures. It is possible that some of the step-over faults are more extensive than mapped, as seismic coverage is limited on the central inner shelf. What is clear in the seismic dataset we have is that there is a major discontinuity in structure here, which is readily apparent when lines 05CM-44 and Tan0106-08 are compared (Figure 5.13). These profiles are less than 1km apart but show distinctly different character. The 1 s twt thick Quaternary basin in Tan0106-08 is all but non-existent in 05CM-44 (the sequence has likely been exhumed by the complex active structure in 05CM-44). The outer splays of the thrust system shown in orange in Figure 5.13 represent the only active faults mapped on the upper slope. Their tips project close to the seabed and the outer fault tip is associated with an anticline.

Ariel Bank Fault

Ariel Bank has long been recognised as a structural feature (Katz, 1975), however resolution of the full character of the structure has been constrained by the poor quality of early-vintage seismic data. New data show that a seaward-vergent, listric outer-shelf thrust fault traverses approximately 60 km of the outer Poverty shelf, and is referred to here as the Ariel Bank Fault (Figures 5.3, 5.13 & 5.14). The Ariel Bank Fault is considered to be an analogous structure to the Lachlan Fault in Hawke's Bay, being a large outer-shelf structure with relatively similar expression in MCS reflection data. Multiple back thrusts and splay faults are recognised off the Ariel Bank Fault, one of which is driving uplift at Ariel Bank (Figure 5.14). North of Ariel Bank the continuous fault trace makes a ~5km landward step over some 10 km strike length. Where it realigns to the general margin strike there is another multiple hanging-wall thrust splay system with at least three splays rupturing to the seafloor and significantly deforming the Holocene sediment blanket in high-resolution seismic. Ariel Bank Fault has a slip rate of 3.9±0.5 mm/yr based on post- last-glacial deformation.

Gable End Faults

The Gable End Faults are the innermost structures recognised on the Poverty shelf. An inner-shelf structure has previously been inferred here to account for a segmented sequence of uplifted coastal marine terraces (Wilson et al., 2006), but has never been corroborated with direct geophysical evidence. The Gable End Faults are only partly imaged in MCS data (Figure 5.14, line 05CM-02), but are well imaged in high-resolution seismic; both boomer and 3.5 kHz data (e.g. Figure 5.15).

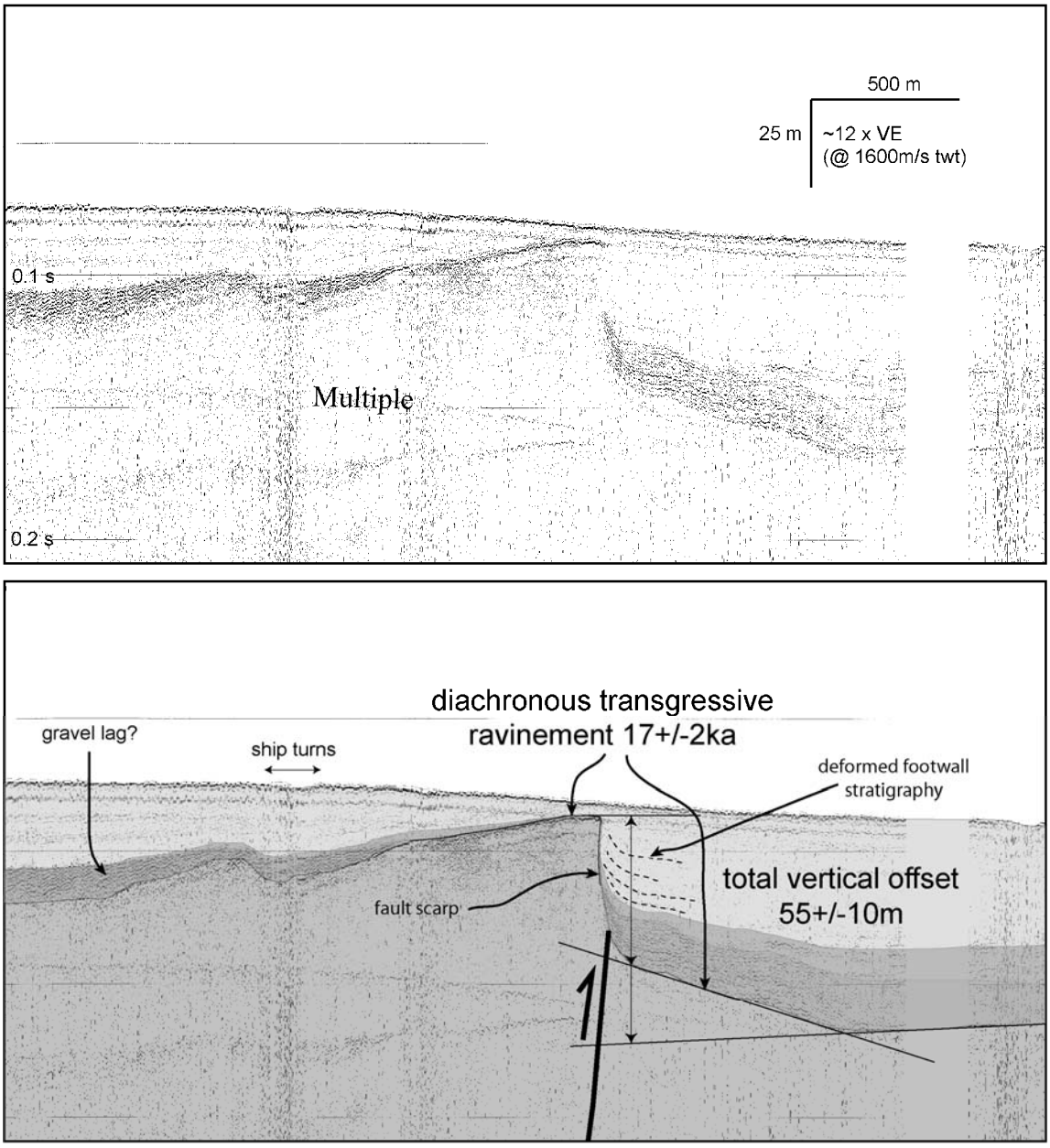

Figure 5.15 Boomer profile across a fault scarp in the Gable End Faults. Location shown in Figures 5.13/5.14. A) Uninterpreted boomer profile. B) Interpreted boomer profile showing subsurface features and details used to derive a vertical slip rate.

Displacement of the transgressive ravinement surface enables calculation of a Holocene slip rate of 3.3±1 mm/yr. This is in close agreement with the calculated uplift rate at the Pakarae River mouth of 3.2±0.8 mm/yr (Wilson et al., 2006) suggesting that coastal terraces are uplifting on the hanging-wall section of this structure. In addition to the structure that is clearly imaged in seismic, there is a prominent coastal-fringing reef that terminates 2.5–8 km off the coast. It is possible that the outer edge of this reef is coincident with a structure, and the inferred fault trace directly offshore of Gable End Foreland reflects this. A left-lateral fault step-over may occur around a reef of the Pakarae River mouth (Figure 5.3).

Outer-shelf/upper-slope inactive thrust stack

Barnes et al (2002) mapped an inactive thrust stack underlying the outer shelf off Hawke's Bay, projecting approximately half way up Mahia Peninsula. The faults are inferred to have been active during the Miocene, but ceased to be active as the Lachlan Fault accommodated shortening in this part of the upper plate. Translation on these thrust faults brought Paleogene rocks out of stratigraphic sequence with the younger Miocene to Recent rocks.

With the addition of the new MCS data it is possible to map this inactive thrust system north from the work of Barnes et al (2002), as far as the northern end of the Poverty re-entrant (Figures 5.13 & 5.14). The inactive thrust stack underlies the outer shelf and the upper-slope gully systems of the re-entrant, and it is apparent that erosion of the upper re-entrant slopes have exposed the older material uplifted during Miocene activity (Figure 5.7 & 5.9).

5.2.4 Earthquake potential of Poverty Bay structures

Structures mapped across Poverty Bay as part of this work have been incorporated into the latest iteration of the National Probabilistic Seismic Hazard Model as simplified principal earthquake sources (Figure 5.16) (Stirling et al., 2009). Based on this, a probabilistic study has been undertaken for the Poverty Bay area as part of the NSF Margins S2S project (Litchfield et al., 2009). A summary of the earthquake potential from these simplified fault sources is presented in Table 5.2, which has been developed from slip rates derived as part of this study. These data indicate that the canyons and slope gully systems are subjected to frequent strong ground shaking (Figure 5.16). As a contrast to the significant active offshore structures discussed here, active faults mapped onshore are shown in Figure 5.16 to illustrate their comparatively sparse and limited extent.

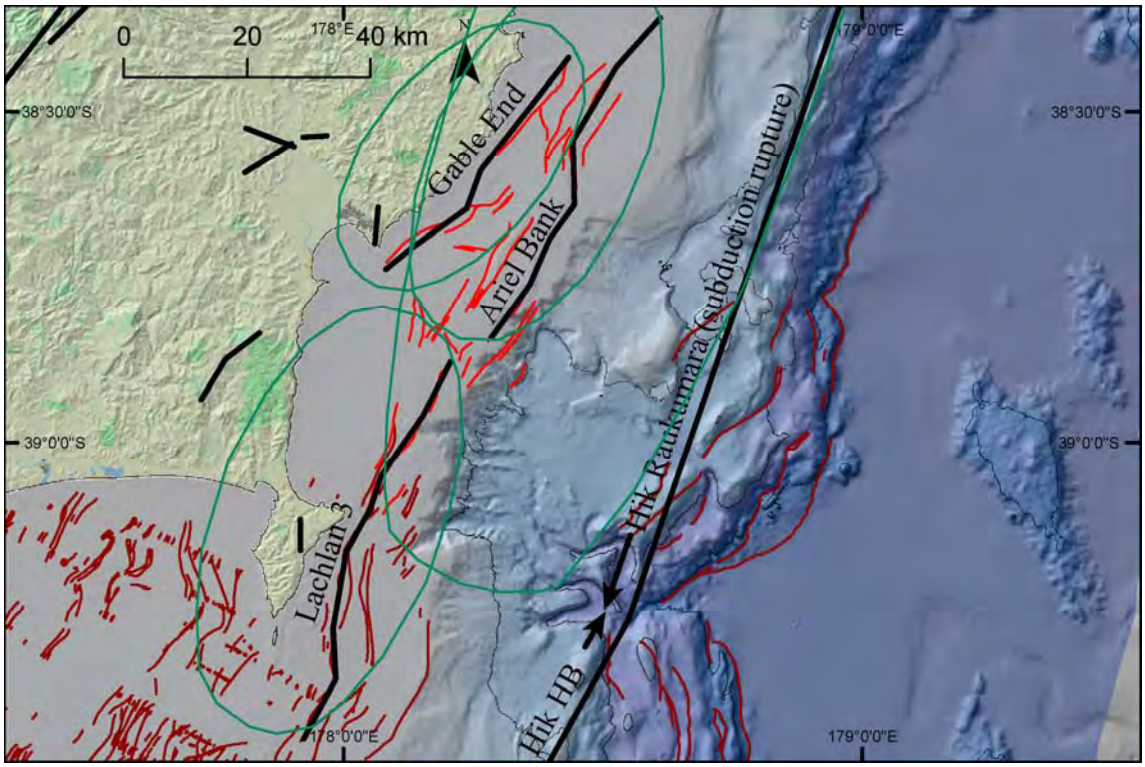

Figure 5.16: Major offshore structures simplified from detailed mapping to be included in the latest New Zealand National Probabilistic Seismic Hazard Model update (Stirling et al., 2009). Underlying red linework indicates structures mapped as part of this project. Brown linework indicates map work published elsewhere. Onshore structure to be included in the national model shown undifferentiated. Ellipses are mean MM9 isoseismals generated using preferred values for Mw and RI (Table 5.2), after Litchfield et al. (2009).

Table 5.2: Groundshaking potential of Poverty Bay structures as simplified for the NPSHM, Source Litchfield et al (2009). The location of simplified faults is shown in Figure 5.16. SR slip rate, Mw moment magnitude, RI return interval, MM Modified Mercalli intensity. [1]Fault mapped as part of this project. [2]vertical separation rate converted to dip-slip rate. [3]MMI-generation potential for the upper continental slope at Poverty Bay.

fault	SR[2]	Mw (pref)	RI (pref)	MM upper slope[3]
Ariel Bank[1]	6.1 ±2.7	7.3–7.6 (7.4)	323–1097 (626)	MM8-9 (RI ~630 yrs)
Gable End[1]	3.8 ±1.8	7.1–7.4 (7.2)	386–1502 (763)	MM7-8 (RI ~760 yrs)
Lachlan 3[1]	4.5 ±2.0	7.3–7.7 (7.5)	479–2114 (929)	MM8 (RI ~930 yrs)
Hik. Raukumara	8.3 ±2.8	8.1–8.3 (8.2)	not available	MM10 (RI ~970 yrs)

5.3 Morphometric analysis of bathymetric DEM's: Landslide styles in the Poverty re-entrant

In comparison to Cook Strait, where landslide scars occur widely on canyon walls but very little landslide debris is retained, the Poverty re-entrant provides an opportunity to analyse landslide systems from the perspective of the debris deposit. Two large mass-failure complexes occur on the upper slope; the Paritu Debris Avalanche (PDA), and the Tuaheni Landslide Complex (TLC) (Figure 5.17). In the following sections these landslide systems are analysed using a combination of shaded-relief interpretation and objective morphometric analysis. The eigenvalue analysis technique, developed for mapping terrestrial landslides in lidar data by McKean and Roering (2004), is applied to delineating deformation within the TLC in Section 5.3.1. This section comprises a manuscript in its entirety (Mountjoy et al., 2009b), and so may contain some repetition of the material contained within the rest of the chapter. In the subsequent section 5.3.2 the approach of Mountjoy et al. (2009b) is applied to the PDA to assist in developing a kinematic model for this landslide complex. The results of these analyses are then used in Section 5.3.4 to analyse post-failure dynamics of submarine landslide deposits, and integrated into the evolutionary model of the Poverty re-entrant in Sections 5.4 and 5.5.

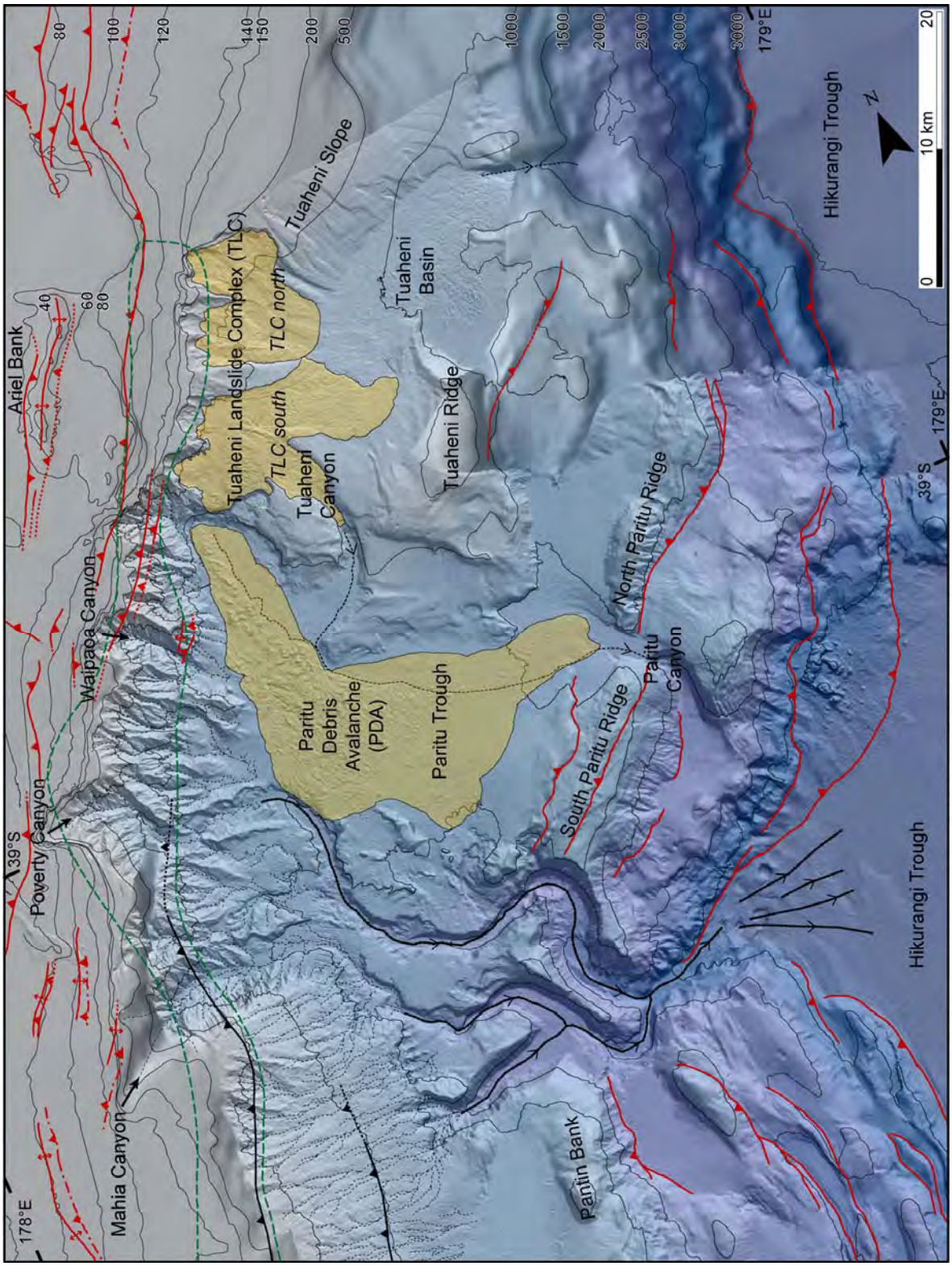

Figure 5.17: Poverty re-entrant structure and geomorphology. Map shows active faults (red), selected inactive faults (black) and zone of inactive faulting (green). Geomorphic features include: landslide deposits (yellow) and sediment flow paths. Several physiographic features are labelled. Mahia Canyon, Poverty canyon, Waipaoa Canyon, Tuaheni Canyon, Paritu Canyon, Tuaheni Basin and Tuaheni Slope are informal names used in this study.

5.3.1 Eigenvalue analysis as exemplified by the Tuaheni Landslide Complex (Mountjoy et al., 2009b)

This section comprises a manuscript presented in its published form.

Mountjoy, J.J., McKean, J. Barnes, P.B. and Pettinga, J.R. 2009: Terrestrial-style slow-moving earthflow kinematics in a submarine landslide complex. In press Marine Geology doi:10.1016/j.margeo.2009.09.007

ARTICLE IN PRESS
MARGO-04402; No of Pages 14
Marine Geology xxx (2009) xxx–xxx
Contents lists available at ScienceDirect
Marine Geology
journal homepage: www.elsevier.com/locate/margeo

Terrestrial-style slow-moving earthflow kinematics in a submarine landslide complex

Joshu J. Mountjoy [a,b,*], Jim McKean [c], Philip M. Barnes [a], Jarg R. Pettinga [b]

[a] National Institute of Water and Atmospheric Research Ltd, Private Bag 14901, Wellington, New Zealand
[b] Dept. of Geological Sciences, University of Canterbury, Private Bag 4800, Christchurch, New Zealand
[c] USDA Forest Service, 322 E. Front Street, Boise, ID 83702, United States

ARTICLE INFO

Article history:
Received 17 March 2009
Received in revised form 2 September 2009
Accepted 5 September 2009
Available online xxxx

Communicated by D.J.W. Piper

Keywords:
submarine earthflow
mass transport complex
morphometric analysis
landslide kinematics
EM300 multibeam
submarine geomorphology

ABSTRACT

Morphometric analysis of Simrad EM300 multibeam bathymetric DEMs reveals details of deformation patterns in a ~145 km^2 submarine landslide complex that are commonly associated with slow-moving earthflows in terrestrial settings. This mode of failure, where existing landslide debris is remobilised repeatedly along discrete shear boundaries and is progressively conveyed through the complex, has not previously been recognised in the submarine environment. The kinematics contrast with the more traditional models of submarine landslide complex development in which repeated catastrophic failures each mobilise new source material to form a composite stacked landslide deposit. In our study of the Tuaheni landslide complex on the Hikurangi Margin of New Zealand, remobilisation has formed boundary shear zones imaged at the seafloor surface in multibeam data, and at depth in multichannel seismic reflection data. A significant amount of internal deformation has occurred within the debris streams. Phases of deformation appear to be partitioned longitudinally as extensional and contractional zones rooted into a basal decollement, and laterally with strike–slip shears partitioning discrete debris streams. While slow-moving terrestrial earthflows are activated by fluctuating piezometric levels typically controlled by precipitation, different processes cause the equivalent mobility in a submarine earthflow. Elevated pore pressures in submarine earthflows are produced by processes such as earthquake-generated strong ground motion and/or gas/fluid release. Earthflow movement in submarine settings is prolonged by slow dissipation in pore pressure.

1. Introduction

Detailed characteristics of submarine landslide morphologies are ever more apparent with increasing resolution of multibeam bathymetry and 3D seismic imaging technologies (e.g. Greene et al., 2006; Gee et al., 2007; Micallef et al., 2007a). Failure modes of submarine landslides vary from translational and rotational movements of relatively intact slide masses, to fluidised flows which may involve a wide range of material from hard rock to underconsolidated sediment (e.g. Mulder and Cochonat, 1996; Hampton et al., 1996). Traditionally, the development of submarine landslide complexes is modelled as repeated failures mobilising new source material with each event, with the landslide debris either accumulating in the same depositional area where slope gradient decreases (Fig. 1A), or being repetitively flushed through a channelized system (e.g. Canals et al., 2004). In this representation, slopes fail catastrophically and slide material is only mobilised once. Ages of submarine landslides are generally determined using stratigraphic dating techniques (e.g. Evans et al., 2005), based on this conceptual model for the development of landslide complexes.

Terrestrial hillslopes also host a variety of catastrophic "event" style failures such as falls, slides and flows (Varnes, 1978; Cruden and Varnes, 1996) that involve the original mass instability of previously unfailed material. In addition, however, landslide complexes in areas of weak, clay-bearing rock can behave as slow, glacier-like debris streams that repeatedly remobilise the same material and are generally referred to as either earthflows (Hungr et al., 2001; Baum et al., 2003) or mudslides (Hutchinson, 1988; Picarelli et al., 2005; Glastonbury and Fell, 2008). The two terms refer to the same process (Hungr et al., 2001), and in this paper we will use the term earthflow or slow-earthflow.

Despite the identification of numerous slope failure modes that are common to subaerial and submarine settings, earthflow-type failures have not been documented on submarine slopes. We propose that earthflows do occur in the submarine environment and, that while they have very similar morphological characteristics to slow-moving terrestrial earthflows, they exhibit some important mechanical differences and are subject to different triggering mechanisms (Fig. 1C–F).

* Corresponding author. National Institute of Water and Atmospheric Research Ltd, Private Bag 14901, Wellington, New Zealand. Tel.: +64 4 3860336.
E-mail address: J.Mountjoy@niwa.co.nz (J.J. Mountjoy).

0025-3227/$ – see front matter © 2009 Elsevier B.V. All rights reserved.
doi:10.1016/j.margeo.2009.09.007

Please cite this article as: Mountjoy, J.J., et al., Terrestrial-style slow-moving earthflow kinematics in a submarine landslide complex, Marine Geology (2009), doi:10.1016/j.margeo.2009.09.007

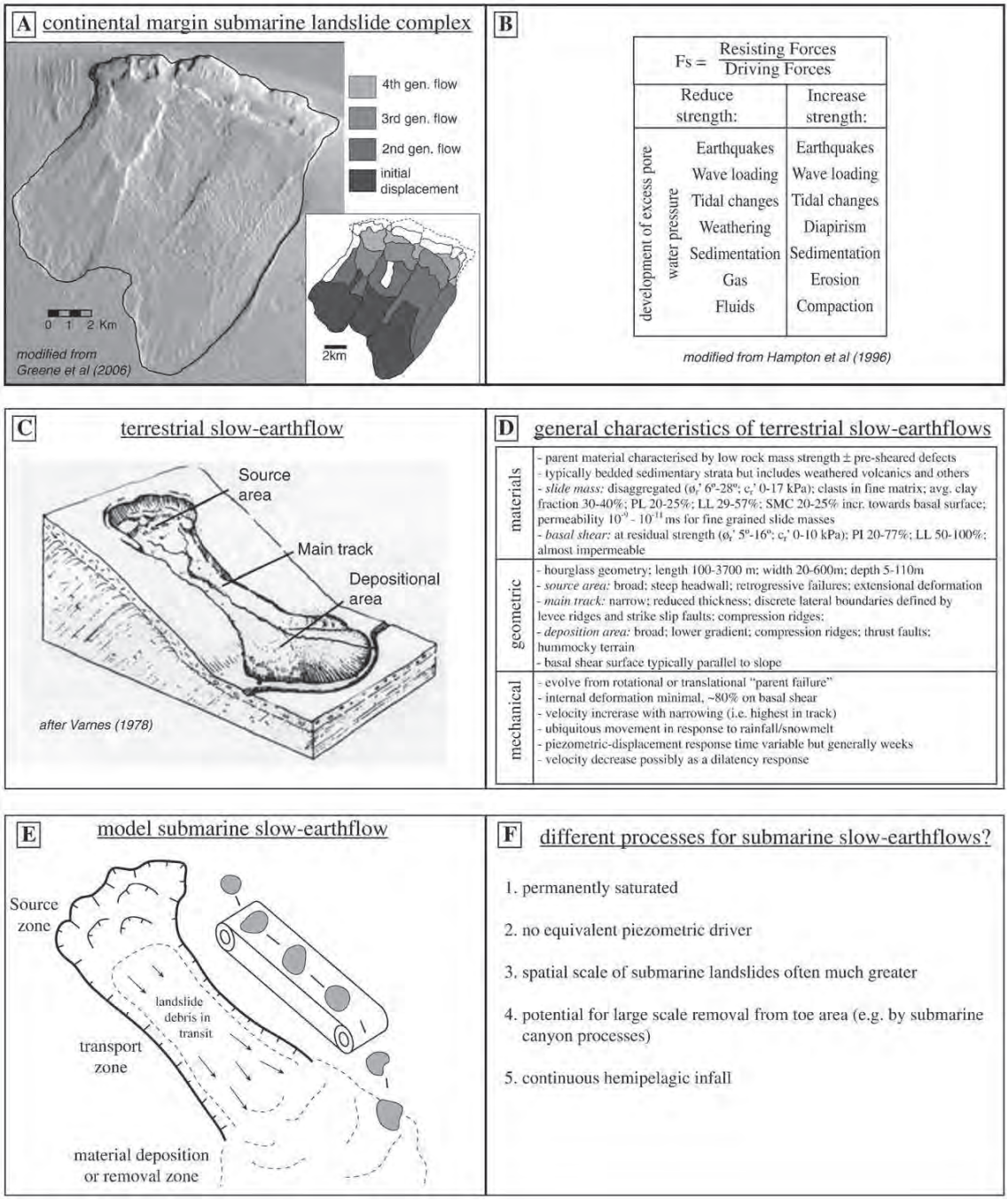

Fig. 1. A) The Goleta landslide. The landslide complex is formed by multiple discrete slope failure events (Greene et al., 2006). B) Controlling factors in the stability of a submarine slope in terms of a simple Factor of Safety (Fs) equation; and tabulated processes that increase and decrease slope strength. C) Schematic diagram of an active slow-moving terrestrial earthflow. D) Fundamental characteristics from a variety of case study earthflows (Hungr et al., 2001; Baum et al., 2003; Glastonbury and Fell, 2008). E) Generalised schematic model proposed for a submarine earthflow as a "conveyor belt" progressively transporting material from a source area to a depositional area. F) Contrasting factors for submarine vs terrestrial earthflows.

A newly mapped submarine landslide complex on the upper continental slope of the Hikurangi subduction margin of New Zealand, referred to here as the Tuaheni landslide complex, has morphological characteristics of a slow-moving earthflow. These features are revealed by Simrad EM300 multibeam bathymetric data and multichannel seismic reflection profiles, allowing detailed resolution of surface and subsurface character. In this paper we: 1) analyse the three dimensional geometry of this landslide complex; 2) consider the kinematic behaviour of the landslide; and, 3) present a conceptual model of repeated failure in a submarine earthflow complex.

Earthflows are persistently active landslides that move on seasonal to decadal and longer timescales. The main landslide body acts as a conveyor for material from the source area at the head of the slide and moves debris downslope though a transport zone or "track" to the

Please cite this article as: Mountjoy, J.J., et al., Terrestrial-style slow-moving earthflow kinematics in a submarine landslide complex, Marine Geology (2009), doi:10.1016/j.margeo.2009.09.007

depositional lobe and toe area (Fig. 1C and D). Mechanical movement of material through the transport zone is primarily (~80%) accomplished by displacement on lateral and basal shear surfaces/zones with a component of quasi-brittle deformation in the main landslide body (Fleming and Johnson, 1989; Hungr et al., 2001; Parise, 2003; Baum et al., 2003; McKean and Roering, 2004; Picarelli et al., 2005; Bertolini and Pizziolo, 2008). In the majority of subaerial slope failures, (re)activation of earthflows is predominantly triggered by elevated pore pressures accompanying a piezometric rise in the landslide body principally as a result of precipitation; but also in response to other mechanisms including earthquakes, snow melt and lateral groundwater inflow (Glastonbury and Fell, 2008; Bertolini and Pizziolo, 2008).

In contrast to the dominant role that precipitation plays in subaerial slope instability, no equivalent dominant trigger has been identified for submarine slope instability, with landslides initiating in response to a range of processes (e.g. Hampton et al., 1996; Locat and Lee, 2002) (Fig. 1B). While gravity is obviously a first-order effect on submarine slopes, it is typically other factors such as earthquake ground motion, gas expulsion and sediment loading that ultimately trigger slope failure, predominantly through the development of excess pore pressure.

Landslides can be distinguished from unfailed hillslopes by characteristic morphological features such as scarps and hummocky terrain (Cruden and Varnes, 1996), and in a more regional context by the scale of surface roughness of the landslide deposit (McKean and Roering, 2004; Glenn et al., 2006). Furthermore, the failure mode and mechanical behaviour of an individual landslide may be characterised by surface morphology reflecting behaviour of the landslide body at depth. For example, bedrock translational and rotational failures commonly have broad, steep head scarps and mid-slope benches reflecting the disruption of intact bedrock blocks within the slide mass (Cruden and Varnes, 1996). In contrast, earthflow morphology is characterised by: 1) deflation in the main landslide "track" (Picarelli et al., 2005); 2) lateral shear boundaries manifested as discrete shear zones or en-echelon cracks (Baum et al., 2003); and 3) extensional deformation features in the source area and compressional deformation features in the lower track and toe area (Glastonbury and Fell, 2008). Additionally, landslide features developed by multiple overlapping flow-like events (e.g. Fig. 1A) would be obliterated by repeated debris deformation in an earthflow. Given that submarine landslides are, as a matter of necessity primarily studied using remote sensing techniques, it is important to be able to investigate their kinematic behaviour from morphological characteristics.

2. Regional setting

The Tuaheni landslide complex (TLC) is located on the upper slope of the Hikurangi Margin, off the east coast of the North Island of New Zealand (Fig. 2A). Active subduction of the Pacific Plate under the Australian Plate occurs with an oblique convergence rate of ~46 mm/year (Beavan et al., 2002). Active eastward verging splay faults from the plate boundary mega-thrust project to the seafloor on the lower slope and across the continental shelf (Barker et al., 2009). On the mid- to upper slope, where this study is focused, there is a paucity of currently active structures, and the active fault most proximal to the landslide is the Ariel Bank Fault (Fig. 2B). To the south the Ariel Bank Fault steps over to the Lachlan Fault, which has a late Quaternary displacement rate of 3.0–6.5 mm/year (Barnes et al., 2002). Preliminary analysis shows that the rate of activity of both faults is similar. Probabilistic seismic hazard modelling of regional earthquake sources shows that peak ground accelerations (PGA) of the order of 0.3–0.4 g occur at a 475 year return time and, of the order of 0.5–0.6 g at a 1000 year return time (Stirling et al., 2002). Some moderately large magnitude historic earthquakes have occurred in the vicinity, the largest of which was the 1931 M7.8 Napier earthquake some 130 km to the southwest, and more recently in 2007 the M6.8 Gisborne earthquake with the epicentre within the study area, with a focal depth of ~44 km.

The TLC occurs within muddy sedimentary deposits that accumulated primarily during periods of eustatic sea level lowering (Fig. 2C) (c.f. Lewis et al., 2004; Paquet et al., 2009). These deposits extend offshelf onto the upper slope, and form a wedge shaped, gently dipping, parallel bedded sedimentary package (i.e. lowstand systems tract or lowstand wedge) that is well imaged in multichannel seismic data (Fig. 2C). 3.5 kHz seismic reflection data reveal a parallel stratified section in the upper ~50 m, in close agreement with a relatively undisturbed seafloor depositional surface, and characteristic of a Holocene hemipelagic succession (e.g. Carter and Manighetti, 2006) overlying the lowstand wedge. Geotechnical testing of similar sedimentary deposits on the upper slope to the south show that there is little variation between the character of underlying lowstand deposits and post-glacial sediment drape (Barnes et al., 1991). Results from Barnes et al. (1991) showed that average grainsize distribution is ~2% sand, ~53% silt and ~45% clay; with the clay fraction composed of smectite (24–47%), illite (23–34%) and chlorite (20–24%); and the Plasticity Index ranging from 34 to 50%. Residual strength from ring shear test on two samples found internal friction angles of 19.5–22.5°. These values are likely to be roughly applicable to the material within the TLC. No active fault or fold structure is mapped directly beneath the sedimentary wedge within which the Tuaheni landslide complex occurs, and the sequence does not appear to have experienced any post-depositional tectonic deformation.

3. Data and methodology

This study is primarily based on 30 kHz multibeam bathymetric data collected with a SIMRAD EM300 multibeam system mounted on the hull of New Zealand's National Institute of Water and Atmospheric Research (NIWA) ship *RV TANGAROA*. The system operates 135 $1\times2°$ beams at 30 kHz frequency. Shipboard navigation comprises a POS/MV system with differential GPS. Surveys were conducted in 2001 (Tan0106), 2006 (Tan0616) and 2008 (Tan0810). The relevant part of the multibeam data set spans water depths of 150–900 m and a grid size of 25 m is chosen to honor beam insonification and sounding density across these water depths. Data were processed to this resolution in Hydromap. High resolution data are augmented with a regional 100 m bathymetric grid built from a combination of 12 kHz SIMRAD EM12Dual multibeam data collected aboard *RV L'ATALANTE* in the early 1990s, and single beam echo sounder bathymetric data held in the NIWA database.

Two multichannel seismic reflection (MCS) datasets are presented in this study: 1) *RV TANGAROA* 2001 (TAN0106) 6 fold, 24-channel seismic profiles acquired with a GI gun source in 45/105 mode; and, 2) *MV PACIFIC TITAN* 2005 (CM05) up to 960-channel high fold 2D seismic reflection data recorded to 12 second TWT (Multiwave, 2005; Barker et al., 2009).

High resolution 3.5 kHz data are available from all *RV TANGAROA* multibeam cruises undertaken in the study area as well as additional data from NIWA archives.

3.1. Objective surface-feature delineation methodology

The surface roughness of landslide debris has been delineated using digital elevation models (DEMs) in terrestrial (McKean and Roering, 2004; Glenn et al., 2006), and submarine settings (Micallef et al., 2007a; Micallef et al., 2007b). McKean and Roering (2004) successfully applied 1-D, circular (2-D) and spherical (3-D) statistics to an airborne lidar-derived DEM, mapping both the location and extent of a terrestrial earthflow, as well as geomorphic detail on the landslide surface. The technique quantifies the degree and pattern of dispersion of unit vectors constructed normal to each grid cell in a DEM (Fig. 3A). Their spherical

Please cite this article as: Mountjoy, J.J., et al., Terrestrial-style slow-moving earthflow kinematics in a submarine landslide complex, Marine Geology (2009), doi:10.1016/j.margeo.2009.09.007

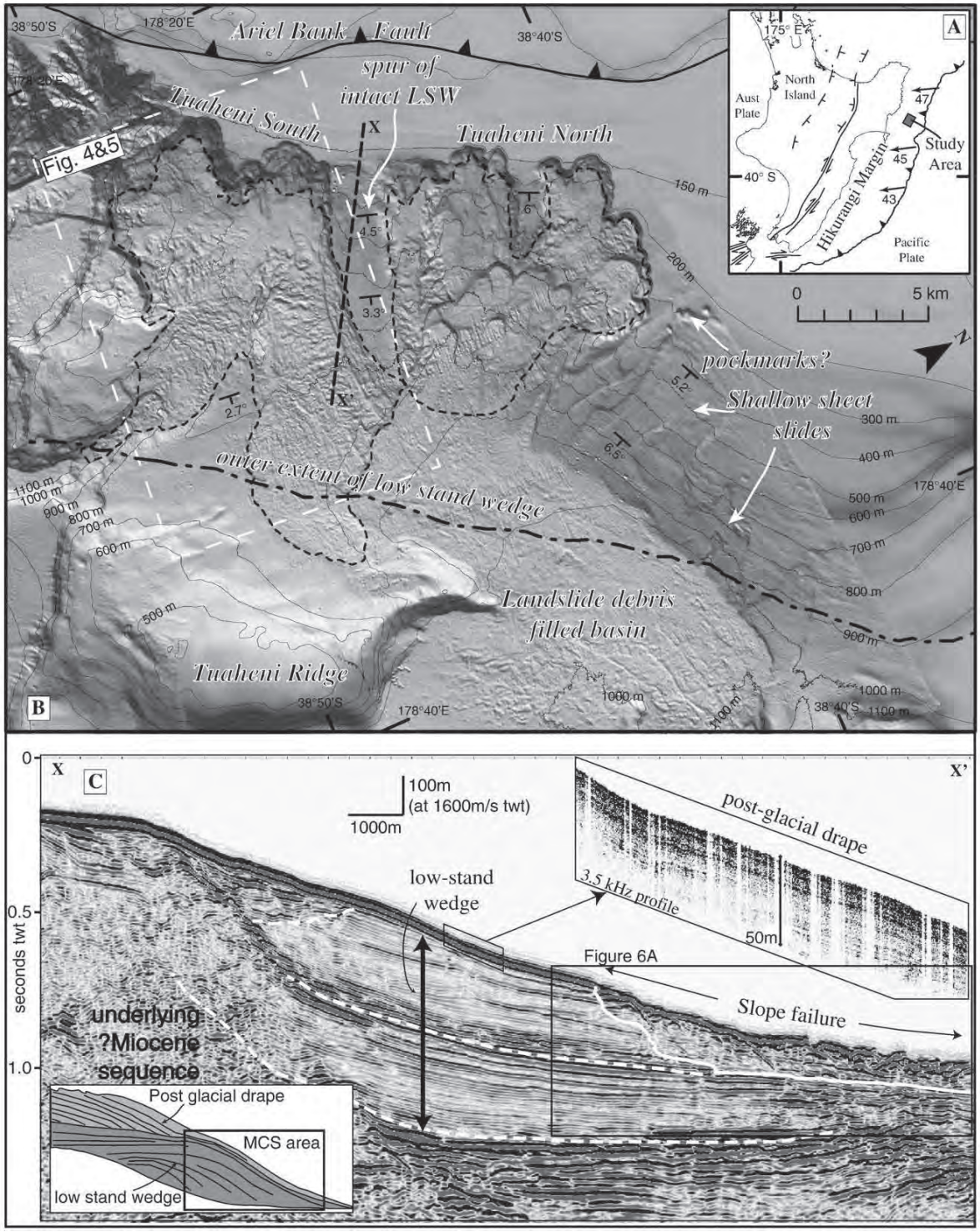

Fig. 2. A) Tectonic setting of New Zealand's North Island east coast showing the principal tectonic elements and plate convergence direction and rates (after Beavan et al., 2002). The study area is located within the grey box. B) Shaded relief map showing the Tuaheni landslide complex (TLC) on the upper continental slope. The two components of the TLC, Tuaheni South and Tuaheni North, are outlined in black dashed lines. The outer (off-shelf) extent of the lowstand wedge (LSW), as imaged in C, is shown by the black dash–dot line. C) Multichannel seismic profile X–X′ (located in 2B) illustrating the lowstand sedimentary deposit within which the TLC occurs. The white dashed lines indicate the base of, and a possible sequence boundary within, the sedimentary body. The solid white line defines the basal extent of landslide debris. The inset line drawing shows the simple lowstand systems tract model (after Posamentier and Vail, 1988). A 3.5 kHz seismic profile is presented to illustrate the undeformed nature of the hemipelagic accumulation on the upper sequence. The vertical data gaps are a result of acoustic bubble noise below the survey vessel.

Please cite this article as: Mountjoy, J.J., et al., Terrestrial-style slow-moving earthflow kinematics in a submarine landslide complex, Marine Geology (2009), doi:10.1016/j.margeo.2009.09.007

method was used in this study because it considers local changes in both slope and aspect of the ground surface, while the 1- and 2-D methods use only one or the other of these topographic attributes.

The spherical statistic is calculated from the ratios of normalized eigenvalues of the orientation matrix of the unit vectors in an area of a DEM. These ratios can describe not only the degree of variability in vector orientations, but also if there is pattern in the orientations. Here we restrict our analysis to the ratio of the first and second eigenvalues, which describe the degree of clustering of the vectors (see Fig. 3B, the ratio ln(S1/S2)). The spherical statistics analysis is made in a square window of DEM cells and then that local value of ln (S1/S2) is assigned to the central cell in the window. By moving the sampling window over a DEM as the calculation is repeated, the elevation matrix is remapped as the local topographic surface roughness. The roughness defined by ln(S1/S2) over some area of a DEM is a function of both the degree of local variability in slope and aspect and the distance over which the variation occurs. This spatial scaling can be evaluated by changing the size of the sampling window; an increase in sample window size gives a larger vector population across which clustering patterns are analysed. For a more detailed description of the technique the reader is referred to McKean and Roering (2004). In this study we refer to the methodology as the "spherical statistics" technique.

4. Results: the Tuaheni landslide complex

Much of the upper slope above Tuaheni Ridge exhibits significant bathymetric surface roughness at 10–100 m length scales and has a surface morphology indicative of mass movement. This area is referred to as the Tuaheni landslide complex (TLC) (Fig. 2B). Likewise in MCS data the mass movements cause highly chaotic reflectivity, characteristic of slope failure debris, in comparison to adjacent apparently unfailed material with well developed bedding (Fig. 2C). The ~145 km^2 landslide complex is divided into two domains; Tuaheni North and Tuaheni South, separated by a ~2 km wide spur of smooth unfailed seafloor (line X–X′ Fig. 2B). Sharply curved head scarps define individual component failures that initiate at the shelf-edge to upper-slope transition at ~150 m water depth. These arcuate failures collectively affect a ~20 km length of the upper slope. The individual scarp heights in the source area are variable, ranging from c. 300 m in the south and decreasing to c. 100 m in the north. Debris fans extend out from head scarp areas, and landslide toe areas occur in water depths of 750–900 m. Beyond the TLC to the southeast bathymetry shallows to less than 500 m on Tuaheni Ridge (Fig. 2B). Slopes adjacent to the TLC have gradients in the range of 2.5–6.5°, while the slope gradient on the surface of the landslide debris within the TLC is lower, with gradients of 1.5–4° in Tuaheni South and 3.5–4° in Tuaheni North.

Along slope to the south of the TLC, slopes are incised by gully systems; while to the east, the slope is generally smooth but does exhibit several subdued scarps up to 30 m high aligned down the slope (Fig. 2B). Circular "pockmarks" occur near the head of these scarps. At the toe of this slope, and to the north and northeast of Tuaheni Ridge there is a sedimentary basin with a >250 ms (~200 m at 1600 ms) thick sequence characterised by chaotic reflectivity in MCS data, and irregular surface roughness in bathymetry data (Fig. 2B).

The basal surface of the landslide debris in Tuaheni South is coincident with the well formed parallel stratification of the lowstand wedge sequence (Fig. 2C). The outer extent of the lowstand wedge was mapped from MCS profiles and underlies the entire TLC area, as well as the slope to the east. Observation in several MCS profiles shows that the relatively undisturbed surface of the lowstand wedge is sub-parallel to bedding (e.g. Fig. 2C main profile and 3.5 kHz inset), and it is apparent from this relationship that the dip of the lowstand wedge strata increases to the N/NE (Fig. 2B).

There are primary differences in the morphology of the Tuaheni North and Tuaheni South components of the TLC. The shelf break head scarp area of Tuaheni North has a complex "scalloped" morphology, with individual scallops between 700 m and 1800 m across. The heights of scarps are predominantly around 100 m, sloping at approximately 8–20°. Tuaheni North contains multiple arcuate scarps through the central part of the landslide debris area. In contrast to Tuaheni North, the surface character of the main debris body of Tuaheni South is totally composed of large areas of irregular, rough landslide debris and does not contain internal scarps similar to those in Tuaheni North. The shelf break area of Tuaheni South is characterised by larger scallops >2500 m wide, 300–350 m high sloping at 8–20°.

We focus on Tuaheni South for morphometric analysis of landslide surface roughness. The landslide debris in Tuaheni South does not exhibit the clear, first-order geomorphic features seen within Tuaheni North (e.g. arcuate scarps), but contains subtle features that require detailed interpretation afforded by roughness-based analysis (e.g. the spherical statistics technique).

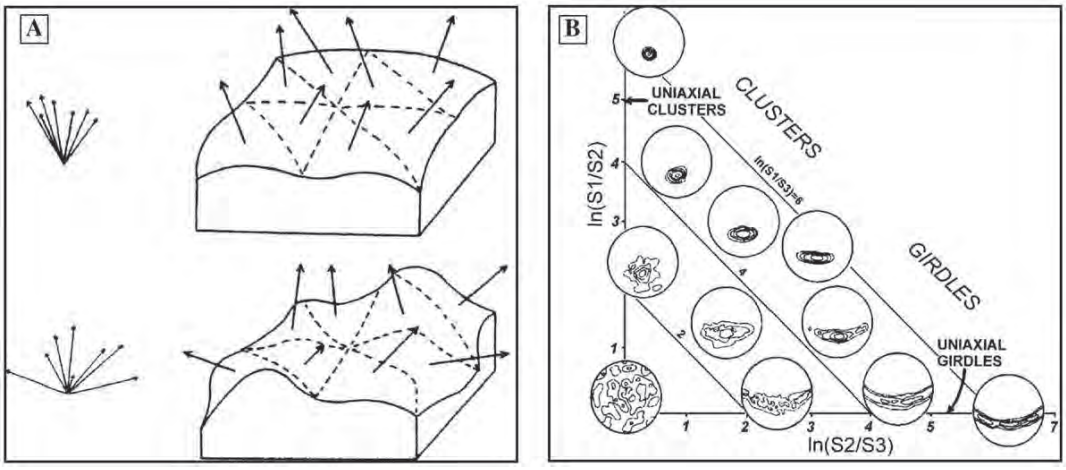

Fig. 3. The eigenvalue-based spherical statistics analysis technique. A) Unit direction vector orientation showing a smooth surface with minimal variations in orientation, and a rough surface with increased variations in orientation (modified from Hobson, 1972). B) Ratios of normalized eigenvalues for analysing vector orientations (modified from Woodcock, 1977).

Please cite this article as: Mountjoy, J.J., et al., Terrestrial-style slow-moving earthflow kinematics in a submarine landslide complex, Marine Geology (2009), doi:10.1016/j.margeo.2009.09.007

4.1. Tuaheni South landslide debris roughness characteristics

Tuaheni South contains a ~80 km^2 area of landslide debris. Debris thickness varies between 90 and 135 m (based on available MCS depth conversion assuming a velocity of 1600 m/s, e.g. Fig. 2C), yielding a total debris volume of 10 ± 0.1 km^3. The (re)activation and movement of a landslide deposit is typically accompanied by internal structural style deformation (compressional, shear and extensional faulting and associated folding) forming ridges and scarps that can be used to characterise landslide kinematics (Baum et al., 1998; Parise, 2003). The spherical statistics technique has been applied at different scales to map both local and regional scale patterns of deformation by adjusting the sampling window relative to the scale of the topography.

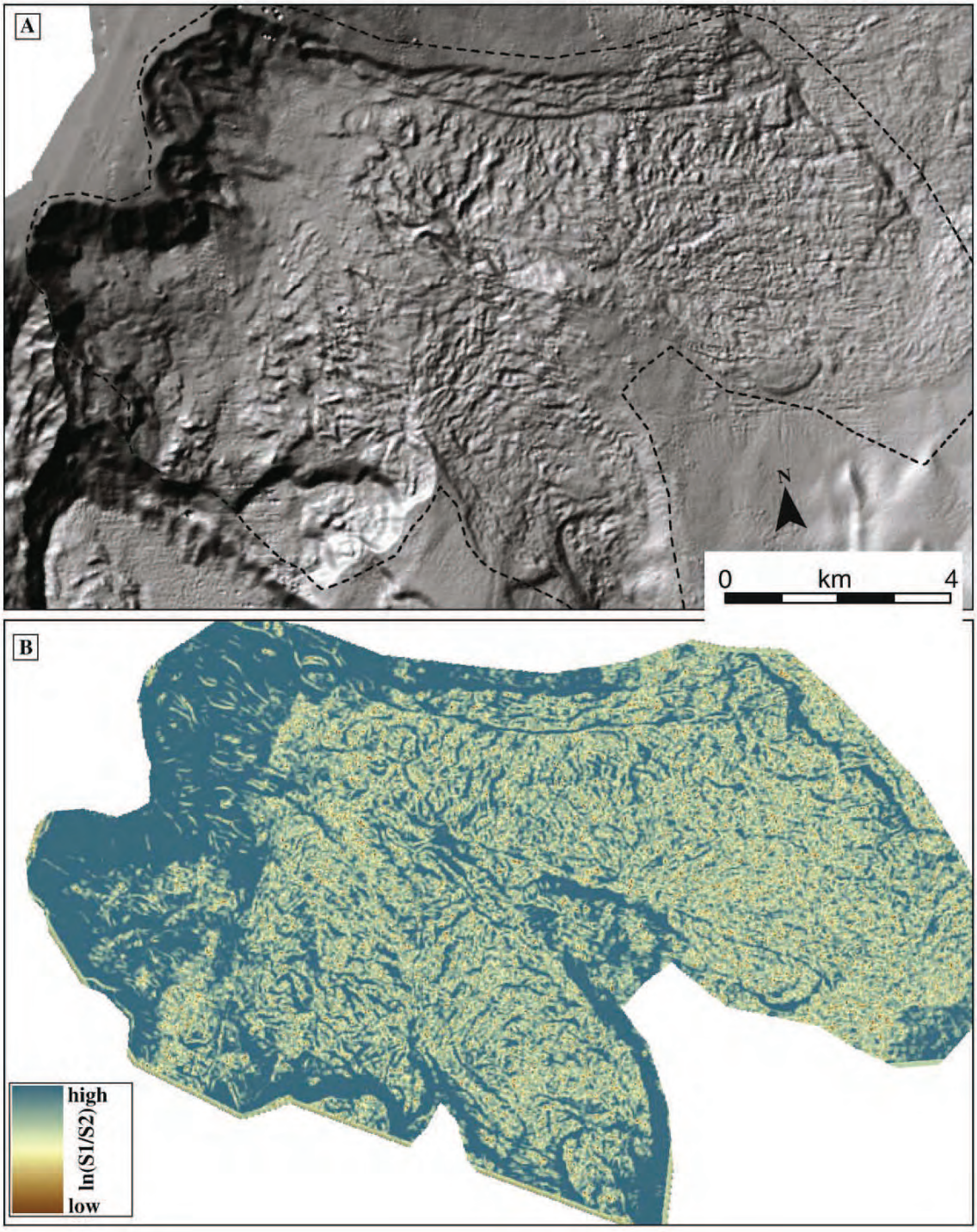

Fig. 4. Roughness characterisation of Tuaheni South (location in Fig. 2B). A). Shaded relief map of the 25 m DEM used for spherical statistics analysis. B) Spherical statistics analysis results (lnS1/lnS2) from 75×75 m roaming window for the Tuaheni South landslide complex.

Please cite this article as: Mountjoy, J.J., et al., Terrestrial-style slow-moving earthflow kinematics in a submarine landslide complex, Marine Geology (2009), doi:10.1016/j.margeo.2009.09.007

4.1.1. Local-scale spherical statistics analysis

Using the 25 m DEM from survey Tan0810, a 3×3 cell window is applied to Tuaheni South (Fig. 4A). At this 75×75 m scale, the spherical statistics technique isolates internal features within the debris, defining ridge crests as rough (dispersed vectors, low eigenvalues, light colours) and the sloping fronts of ridges and scarps as smooth (clustered vectors, high eigenvalues, dark colours). Minor areas of noise in the data do not significantly affect the analysis. The results of the spherical statistics analysis are incorporated in a GIS where a classified eigenvalue map is used to define roughness elements and assist with mapping surface features within the landslide area (Fig. 5).

Three separate areas of landslide debris are defined, delineated as debris bodies T1, T2 and T3. Debris bodies T2 and T3 have longitudinal scarps along their lateral boundaries, and MCS data show that these features persist at depth (Fig. 6A).

The most well formed example of these lateral scarps is on the northern margin of debris body T3 (Fig. 5), with a 6.5 km-long continuous scarp between 10 and 20 m high. MCS data show a clear reflector, coincident with the scarp base, projecting ~95 m below the seafloor at ~26° (geometrically derived true dip) (Fig. 6A). Along the length of the scarp, there is a change in strike from 107° to 089° as the debris stream widens from 1.8 to ~5.0 km at the toe of the failure (Fig. 5). Upslope or north of the main lateral shear, a less well defined scarp correlates to a reflector in MCS dipping at ~34°. Widespread failure scarps occur on across the northern-margin slope of the landslide. Other lateral scarps occur on the southern margin of debris body T3, and on both margins of debris body T2. Several linear scarp features occur within the T3 debris body toe area, aligned sub-parallel to the lateral scarps. We note a broad, diffuse reflector in MCS data, towards the base of the chaotic reflectivity (Fig. 6A).

4.1.2. Regional scale spherical statistics analysis

To map regional patterns of debris deformation, we make the assumption that larger scale (amplitude and wavelength) surface features are indicative of localised internal deformation within the landslide debris. Conceptually, if an area of a relatively smooth debris body deforms in either compression or extension then surface deformation features reflecting internal deformation (folds and/or extensional scarps, e.g. Fig. 6) would differentiate this area from the rest of the landslide debris body.

We have tested a range of increasing roaming window scales to determine which most efficiently distinguishes zones of larger scale surface features, and a 15×15 cell window (375×375 m) best maps larger regional features (Fig. 7). At the upper end of the landslide, the large slopes of the head scarp area are predominantly characterised by a high eigenvalue (orange). Across the three landslide debris bodies T1, T2 and T3 (Figs. 5 and 7B), areas of larger scale surface roughness are delineated as patchy areas of higher eigenvalues (green to orange colours, Fig. 7A).

5. Discussion

The landslide debris of Tuaheni South exhibits numerous features that provide information on kinematic behaviour. Interpretation of surface roughness analysis and MCS data (Figs. 5 and 6) defines numerous features that result from deformation of the debris body, including: 1) areas of compression defined by ridges reflecting compressional deformation correlated to reverse fault-style deformation; 2) areas of extension defined by concave downslope fissures, local sediment accumulation, and dislocated bathymetric features correlated to internal extensional deformation; 3) laterally bounding scarps that project to depth as well formed shear planes; 4) internal longitudinal shears within the toe area of debris body T3; and 5) a possible decollement zone or basal shear in the lower landslide debris. From these features we interpret the movement directions of the debris (the three identified debris bodies T1–T3 Fig. 5). Based on the prominent lateral scarps, and the deflation and lower slope angles of the landslide debris, there has been a large amount of material removed from the landslide scar (e.g. $\sim 2.3 \pm 0.5 \times 10^9 m^3$ for the debris body T3 area alone). The geomorphic interpretation can also be used to constrain the style of mass movement at this site.

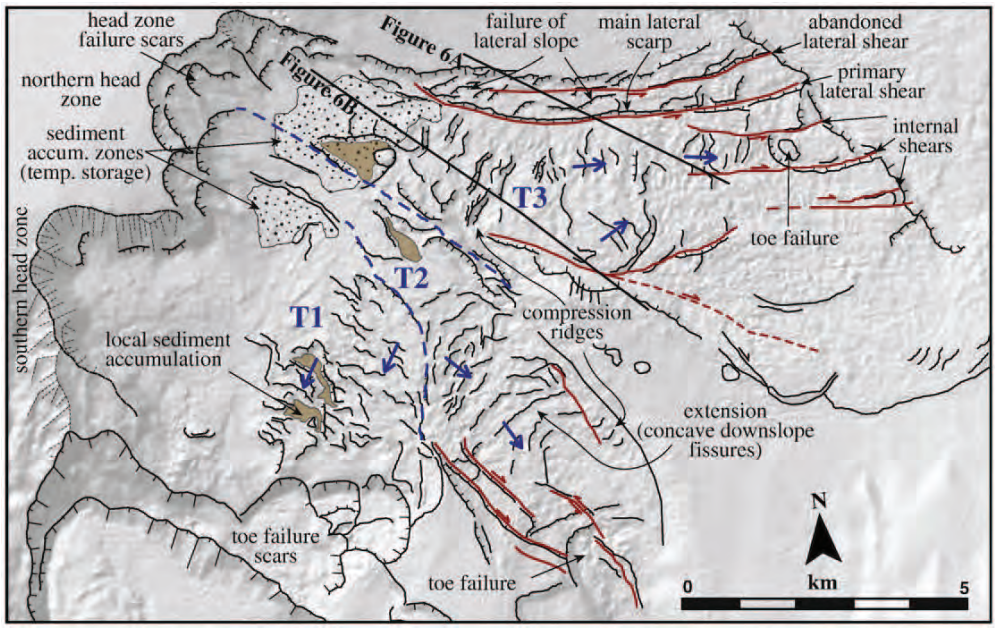

Fig. 5. Geomorphic interpretation of the Tuaheni South landslide complex based on interpretation of surface roughness patterns (see Fig. 4B) and shadowing in the shaded relief model (Fig. 4A). The boundaries of the three discrete earthflow debris bodies (T1–T3) are indicated by blue dashed lines and inferred directions of movement are shown by the blue arrows. Red linework delineates lateral shear zones. Black linework within the landslide bodies maps out internal deformation. (For interpretation of the references to colour in this figure legend, the reader is referred to the web version of this article.)

Please cite this article as: Mountjoy, J.J., et al., Terrestrial-style slow-moving earthflow kinematics in a submarine landslide complex, Marine Geology (2009), doi:10.1016/j.margeo.2009.09.007

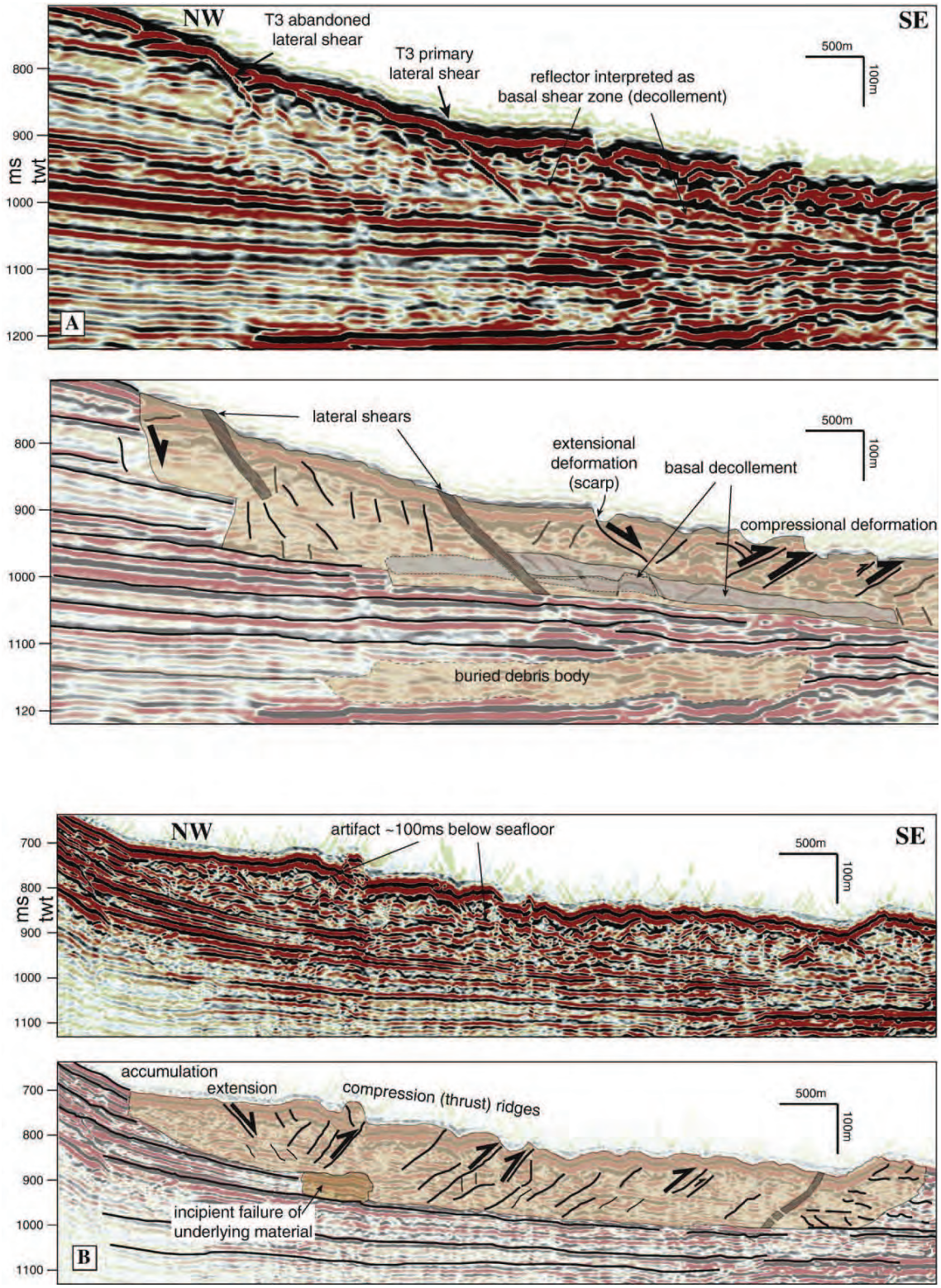

Fig. 6. Uninterpreted and interpreted MCS profiles illustrating subsurface landslide features including lateral shear zones and deformation structures. See Fig. 5 for profile locations. A) 05CM-02. B) Tan 0106-13. The annotated artefact is also clearly observed at ~100 ms below the seafloor in the same profile further to the southeast (not presented here). It is unclear what causes this artefact but, based on its continuation across multiple material types to the southeast, it is clearly not a horizon within the landslide debris.

Please cite this article as: Mountjoy, J.J., et al., Terrestrial-style slow-moving earthflow kinematics in a submarine landslide complex, Marine Geology (2009), doi:10.1016/j.margeo.2009.09.007

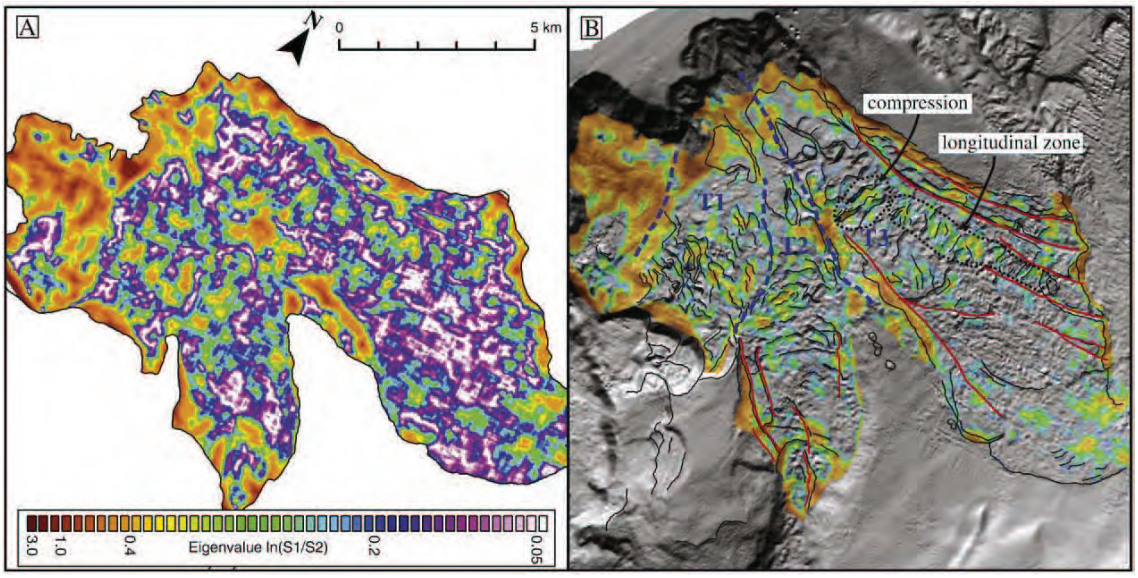

Fig. 7. A) Spherical statistics analysis of 25 m DEM for Tuaheni South using a 375 × 375 m roaming window. The analysis has been clipped to the Tuaheni South debris extent (Fig. 2B). B) Areas of eigenvalues below a cut-off value of 0.2 presented semi-transparent with the same colour classification as in A, over the geomorphic map (cf. Fig. 5). Black dotted lines delineate the approximate extent of areas referred to in text, and the general extents of debris bodies T1–T3 are shown. (For interpretation of the references to colour in this figure legend, the reader is referred to the web version of this article.)

5.1. Geomorphic constraints on landslide complex development

We propose several explanations for the mode of development of the Tuaheni South landslide complex: mode-1) landslides occur as single, catastrophic events and Tuaheni South is comprised of three discrete failures that produced debris bodies T1–T3, that have not deformed since emplacement; mode-2) Tuaheni South is a retrogressive landslide complex within which failures have occurred in sequence, upslope of an initial failure at the lower end of the landslide. This model implies a progressive younging of event age from the toe towards the head scarp; mode-3) several large failures have occurred and the debris bodies are composed of discrete, stacked (inter-fingered) landslide deposits; or mode-4) following some initial failure(s) that form a debris deposit on the slope, repeated slope failures and debris remobilisation has formed a conveyor-like debris-transport zone (earthflow). The kinematics of these different landslide modes will be reflected in the surface and subsurface morphology of the landslide complex. This morphology can be used to distinguish the model applicable to Tuaheni South.

Longitudinal internal shears occur within the toe area of debris body T3 (Fig. 5), and correlate to a longitudinal zone of large-scale surface roughness in the lower half of the landslide (Fig. 7). This deformation is interpreted as being the result of secondary failure of the landslide body, dismissing the single event emplacement model (mode-1). Additionally, as the subsequent deformation of the landslide deposit is longitudinal, a simple model of a sequence of stacked retrogressive failure bodies (mode-2) with no post-failure deformation is unlikely.

The geometry of surface features, and correlation to deformation at depth, indicates spatially distributed compression and extension across the Tuaheni South landslide debris. In debris body T3, compression occurs near the upper part of the landslide (Figs. 5 and 6B). In a single event failure (mode-1) the upper part of the landslide deposit would be expected to be dominated by extension. The local distribution of compression features indicates secondary reloading from upslope failure. Extension occurs through the lower part of debris body T2 (Fig. 5), interpreted as reflecting a reactivation of landslide debris from the bottom up.

Toe failure scars occur on all debris bodies (T1–T3) indicating secondary failure. Debris body T1 shows a movement direction that is perpendicular to the downslope direction of the large head scarp area above it ("southern head zone" in Fig. 5). This indicates that the most recent deformation in T1 is not related to failure from this southern head zone, but is likely to be as slow, retrogressive displacement of the debris as toe failures perturb the lower boundary stress condition. Whilst this generally fits with a retrogressive-type model (i.e. mode-2), surface morphology suggests slow creeping failure rather than discrete retrogressive failure events.

In addition to the well expressed lateral shears in T2 and T3, which could result from any of the failure modes 1–4 defined above, T3 contains an outer lateral shear on the northern boundary that is interpreted as an abandoned feature. This is both outside the continuous primary lateral shear and sits upslope of it. Volume calculations indicate that ~2 km^3 of material has been removed from the T3 scar area, and the abandoned lateral shear is interpreted as a remnant from earlier landslide activity instrumental in removing this material. The combination of this abandoned feature and the longitudinal movement band are interpreted as reflecting progressive inward stepping of deformation, supporting repeated longitudinal failure at the same site (mode-4).

Despite the extensive landslide deposit, and the multiple arcuate scarps in the head area suggesting numerous (small-scale) failure events, there is no indication in MCS data for internal partitioning of the landslide debris in Tuaheni South (i.e. there is a lack of internal coherent through going reflectors). If the debris bodies (e.g. T3) were composed of multiple, stacked landslide bodies (mode-3) then these would be likely to be distinguishable in MCS data.

The kinematic features outlined above are consistent with characteristic features of terrestrial earthflows and suggest repeated post-emplacement deformation and material transport within the TLC. This is concluded to be the mechanism for the conveyance of material introduced from the head zone, with the possibly addition of material scavenged from basal erosion, through the landslide transport zone to sediment basins beyond the toe of the landslide.

While we interpret Tuaheni South as a well established earthflow, Tuaheni North shows only localised areas exhibiting features

Please cite this article as: Mountjoy, J.J., et al., Terrestrial-style slow-moving earthflow kinematics in a submarine landslide complex, Marine Geology (2009), doi:10.1016/j.margeo.2009.09.007

indicating repeated movement. It is clear that the main landslide debris area of Tuaheni North is predominantly affected by comparatively small-scale discrete failures as evidenced by the numerous arcuate scarps in the debris area. There may be several reasons for the difference between the two areas, including: 1) the occurrence of a localised triggering mechanism enabling earthflow mechanics to occur in Tuaheni South (e.g. focused gas/fluid expulsion); 2) the buttressing effect of Tuaheni Ridge to the toe of Tuaheni South forcing the accumulation of landslide debris on the upper slope (note the clear division of the two TLC components by the ~2 km wide unfailed lowstand wedge surface coincident with the northern termination of Tuaheni Ridge, Fig. 2B); 3) the increase in stratigraphic dip to the N/NE affecting the force balance of slope materials (reflected by increased slope gradients to the north, Fig. 2B); 4) a progressive southward evolution of slope failure mode, i.e. the failures in Tuaheni North are a precursor to earthflow development; and 5) a lateral variation in geotechnical properties of the lowstand wedge material (e.g. grainsize, permeability). While further research is required to resolve the apparent contrast in behaviour between Tuaheni South and Tuaheni North; Tuaheni South provides an excellent case study upon which to base a model of submarine earthflow behaviour. In the remainder of this paper we develop a conceptual model for active submarine earthflows as a previously undocumented phenomena, and consider what might be the driving forces behind their mobility.

5.2. Submarine earthflow evolution

Active, or reactivated, subaerial earthflows/mudflows can originate from both large, "parent" landslides, and from local-scale slope failures that subsequently experience deformation from processes such as top-down loading and bottom-up relaxation (Parise, 2003; McKean and Roering, 2004; Borgatti et al., 2006; Comegna et al., 2007). Earthflow-style slope failure is strongly influenced by material properties (strength, grainsize, permeability), site/slope geometry and the nature of stress perturbations on the slope (Baum et al., 2003; Glastonbury and Fell, 2008).

5.2.1. Style of failure within Tuaheni South

Within Tuaheni South we interpret a combination of different earthflow initiation and reactivation processes. In the distal part of T3, failure debris has run up an opposing slope and interacted with existing slope sediments in a compressional manner (Fig. 8A and B), indicating a "parent failure" origin for this component of the landslide complex. Evidence for repeated failure in the T3 source area, as stratigraphically controlled translational block failures (Fig. 8C–E), supports a model of top-down reactivation for debris body T3. Comparison of the southern and northern head zones of Tuaheni South (Fig. 5) indicates that ongoing failures in these areas will deplete the lowstand wedge material (compare Fig. 8D and E), and material supply to the earthflow on the slope below will eventually decline. The occurrence of the two large head zones, interpreted to have formed through multiple small-scale slope failures, upslope of the landslide complex supports a model of top-down activation of earthflow deformation, at least in the early stages of landslide complex development.

Both of the T1 and T2 debris bodies contain concave downslope fissures and local sediment accumulation that indicate extension (Fig. 5). These landslide bodies both have kilometre-scale failures at the debris toe. This combination of extension through the debris body and lower boundary failure indicates earthflow development by lower boundary destabilisation and bottom-up propagation of displacement. In T1 it is apparent that the contribution of material from the southern head zone to the slope has declined, and deformation has propagated to the northeast through existing debris, likely in response to the stress change at the southern boundary.

Debris body T3 can be used as a case study to evaluate the top-down model of earthflow development and the conveyance of material through the landslide body.

5.2.2. Differential displacement within debris body T3

In debris body T3, the transfer of material from the source area (head scarp) to the toe appears to be dominated by multiple discrete, partitioned remobilisations, rather than by overall creeping movement. From the area of temporary accumulation below the head scarp, material is remobilised into the transport zone (Fig. 8F). Failures are of limited extent and cause compressional deformation within the earthflow body, as is evident in bathymetry and in MCS profiles (Fig. 8A and F). Deformation imaged in MCS data supports a model of failure occurring in sequence down the length of the earthflow body (Fig. 8G). Repeated movement of the landslide debris may cause basal erosion, as indicated by both deflation of the debris body and deformation (incipient failure) of the sequence at the slide base (Fig. 6B) Longitudinally distributed deformation within the transport zone is likely to be a response to perturbed stress states in adjacent material through static loading and the migration of excess pore pressure (c.f. Hutchinson and Bhandari, 1971; Comegna et al., 2007), as well as lower boundary stress relief following toe failure. Pore pressure migration may give rise to an effective pressure wave through the body of the earthflow, accompanied by a localised displacement pulse of the landslide debris.

Longitudinal shears dividing the toe of the earthflow indicates that movement is also partitioned laterally (Fig. 5). If material is being conveyed in "stick-slip" (i.e. punctuated movement) fashion, and inducing localised compressional and/or extensional deformation reflected in surface morphology, then it might be expected that areas currently under compressional stress will stand out as areas of larger scale surface roughness. It is likely that over time, as upslope stresses are relieved in the earthflow body, some "relaxation" will occur along the basal decollement and these larger scale surface features will dissipate. Regional scale spherical statistics analysis (Section 4.1.2) distinguishes different wavelength and amplitude scales of roughness within debris body T3 (Fig. 7). Analysis delineates: 1) a transverse area near the upper end of the transport zone where compression is occurring (cf. Fig. 8A and F); and 2) a discontinuous longitudinal strip down the length of the transport zone which passes between toe shears (Fig. 8A). This area is interpreted as the most recently (or currently) active zone in this earthflow.

5.3. Triggering submarine earthflow movement

Initial mass instability in both terrestrial and submarine hillslopes results from a combination of: 1) slow and sustained (conditioning) and 2) relatively rapid (triggering) processes. The stability of a slope gradually declines under the influence of the sustained processes until it is within a range in which other processes can trigger the ultimate failure (Fig. 9A). On land, the most common longer-term slope-conditioning processes which can both increase the shear stress and

Fig. 8. Conceptual model of the anatomy of a submarine earthflow, illustrated in multibeam bathymetric and multichannel seismic reflection data from Tuaheni South debris body T3. A) Geomorphic key map of the earthflow with selected eigenvalue >0.2 areas from Fig. 7 outlined in blue; B) 3.5 kHz profile across the toe of the interpreted parent failure. The vertical data gaps are a result of acoustic bubble noise below the survey vessel. C) Example of a landslide head zone failure. D and E) Conceptual and multibeam examples of the progressive excavation and eventual depletion of the lowstand wedge. F and G) Remobilisation of material in the accumulation zone and the upslope portion of the transport zone, and H) progressive deformation in the transport zone developing basal and lateral shear geometry, and illustrating the inward stepping movement and entrenchment of the earthflow body and the abandonment of previous lateral shear zones with progressive earthflow development. (For interpretation of the references to colour in this figure legend, the reader is referred to the web version of this article.)

Please cite this article as: Mountjoy, J.J., et al., Terrestrial-style slow-moving earthflow kinematics in a submarine landslide complex, Marine Geology (2009), doi:10.1016/j.margeo.2009.09.007

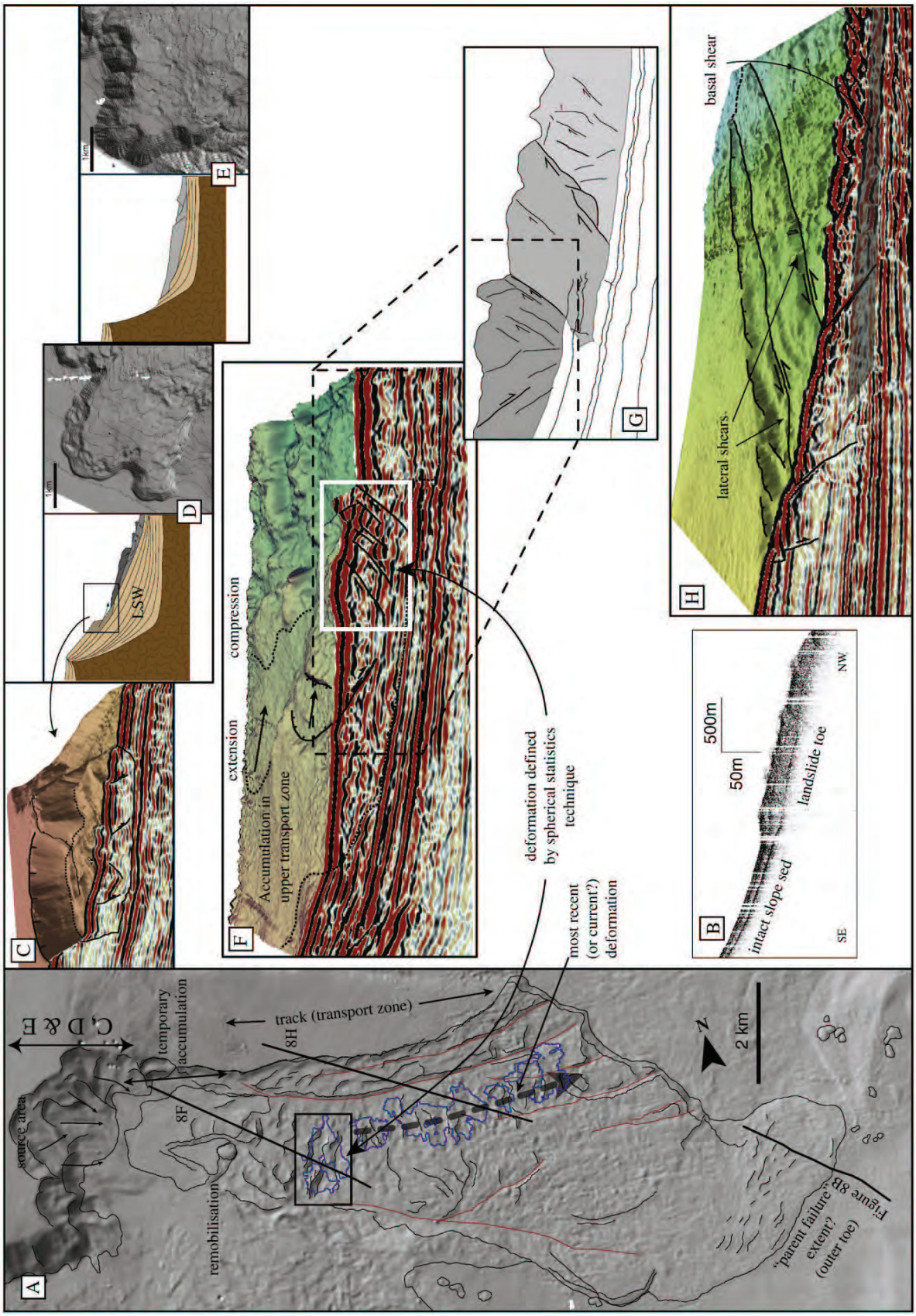

Please cite this article as: Mountjoy, J.J., et al., Terrestrial-style slow-moving earthflow kinematics in a submarine landslide complex, Marine Geology (2009), doi:10.1016/j.margeo.2009.09.007

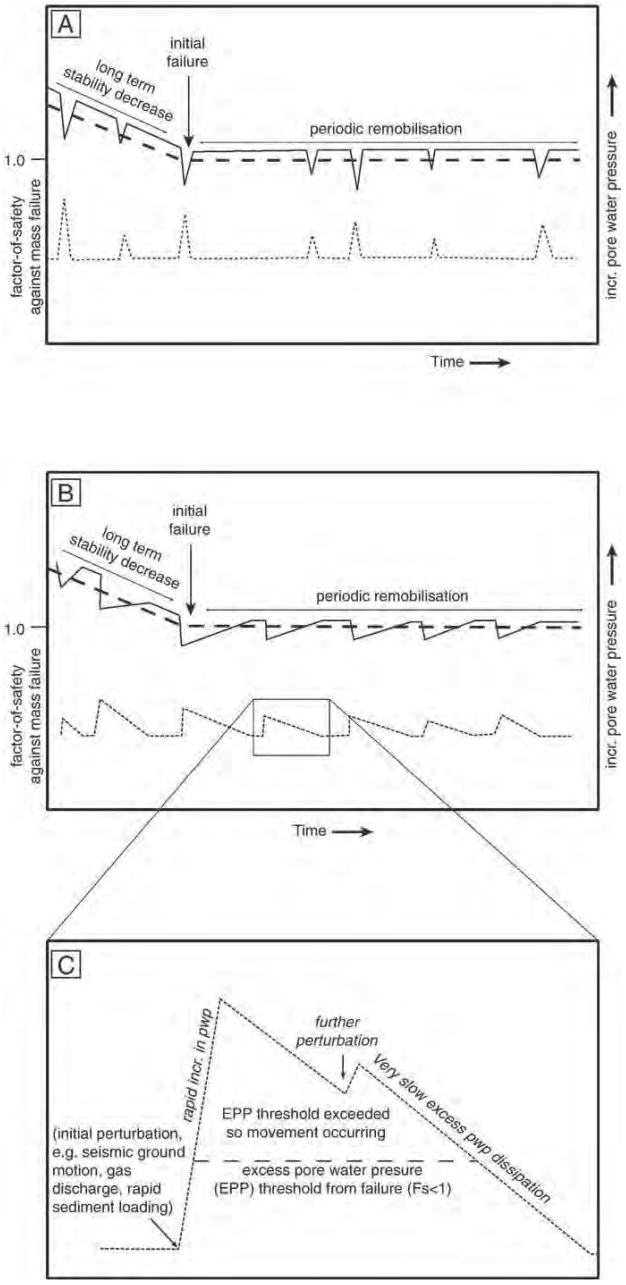

Fig. 9. Conceptual temporal trends of the Factors-of-Safety (Fs) of terrestrial (A) and submarine (B) slopes in response to a combination of long-term slope-weakening processes and final triggering mechanisms. (C) Detail of submarine pore water pressure during a period of slope instability. Dashed lines are the long-term trends of Fs and dotted lines are hypothetical pore pressure trends. Solid lines represent temporal patterns of stability resulting from the combination of long-term weakening of a slope and shorter-term fluctuations due primarily to pore pressure variations. For simplicity the gradual decrease in stability is shown as a linear decline, but in reality it is often more complex.

decrease the shear resistance in a slope include: 1) surcharge loading by material arriving from further upslope, 2) a slow increase in pore water pressure (e.g. associated with progressive surcharge loading), 3) removal of material supporting the toe of a slope (most often by stream erosion), and 4) rock or regolith strength degradation by a variety of physical and chemical processes (e.g. strength loss during earthquakes and other physical and chemical weathering).

In terms of rapid (triggering) processes in terrestrial slope instability, the ultimate trigger is predominantly rainfall. Likewise reactivations of earthflows are controlled by precipitation driven temporal fluctuations of pore water pressures, but also occur by other mechanisms such as snowmelt, earthquake loading and surcharge loading without time for dissipation of consequent elevated pore pressure (Malet et al., 2005; Iverson, 2005; Savage and Wasowski, 2006; Comegna et al., 2007; Calvello et al., 2008). In terrestrial hillslopes these elevated pore pressures often have durations of only hours to months (e.g. Iverson, 2005). Once initiated, terrestrial slides stop when the pore pressure drops below a critical level (shear strength recovers), the material travels onto a gentler slope, or the displaced mass is buttressed by downslope stable material. As noted previously, episodic remobilization of landslide debris is very common in terrestrial earthflows, and typically occurs whenever short-term pore water pressures rise above critical levels (Fig. 9A).

With respect to slope instability, the two most important contrasting differences between subaerial and submarine environments are 1) the effect of wetting and drying as a result of periodic rainfall (submarine slopes are permanently saturated); and 2) the difference in slope gradients (submarine slopes are generally significantly gentler). Despite these differences, most of the long-term processes that can "condition" a submarine slope and bring it to a state of near failure are similar to those for subaerial slopes. Likewise, the processes that ultimately trigger submarine landslides predominantly involve high pore pressures. However, submarine failures are removed from direct precipitation effects and instead high pore pressures are generated by processes such as seismic loading, rapid sedimentation and surcharge loading, and gas expulsion (Hampton et al., 1996) (Fig. 1).

The site for this study is potentially subject to all the triggering processes outlined above, as they are documented to occur elsewhere along the Hikurangi margin, including: high magnitude earthquakes (Reyners, 2000; Barnes et al., 2002); gas hydrates (Pecher et al., 2005); gas seeps (Kvenvolden and Pettinga, 1989; Pettinga, 2003; Klaucke et al., in press); and, high sedimentation rates (Orpin et al., 2006; Walsh et al., 2007). We note the presence of "pock mark" features on the slope immediately to the north east of the TLC (Fig. 2B) that may indicate shallow gas or fluid expulsion, and the close proximity of the TLC to earthquake sources such as the Ariel Bank Fault (Fig. 2A). The earthquake potential in this area means that earthquakes will certainly influence slope stability and are likely to play a role in earthflow mobility. The material within which the Tuaheni landslide complex occurs (c.f. Barnes et al., 1991, Section 2) is likely to fit within the range of material properties found for terrestrial earthflows (Fig. 1B), and is characterised as clay rich with a significant component of smectite. Geotechnical testing of comparable materials demonstrates rapid strength degradation under cyclic loading (Barnes et al., 1991). Local slope gradients are relatively steep for submarine slopes at 4–6°, while the landslide debris has a slightly lower gradient (e.g. 2° on debris body T3). Given that the landslides are failing along stratigraphic surfaces, and that surface slopes appear to mimic stratigraphy, this contrast reflects decreasing dips with depth in the lowstand wedge sequence. In comparison to subaerial earthflow debris-surface slope angles, which are typically 7.5–15° (Glastonbury and Fell, 2008), these slope gradients are low but fall within the same order of magnitude.

Perhaps the most significant difference in the mechanical behaviour of submarine vs terrestrial materials, is that elevated pore pressures may decline very slowly in submarine hillslopes relative to the rates in terrestrial settings (Leynaud et al., 2004; Strout and Tjelta, 2005; Sultan et al., 2008). This lower dissipation rate reflects factors including low permeability (fine grained) materials and permanently saturated sediments. As a consequence, submarine landslide debris tends to remain in a metastable condition for long periods of time during which there is an increased potential for remobilization (see

Please cite this article as: Mountjoy, J.J., et al., Terrestrial-style slow-moving earthflow kinematics in a submarine landslide complex, Marine Geology (2009), doi:10.1016/j.margeo.2009.09.007

the contrast in temporal pore pressure patterns in terrestrial, Fig. 9A, and submarine slopes, Fig. 9B and C).

One important implication of earthflow-type displacement on submarine slopes is that the low velocity of material movement means slide debris is less likely to transform to a fluidised flow (in comparison to rapid catastrophic failures) and remains in an unstable geometry on the slope. There is also an expected decrease in intrinsic material shear strength during initial failures that leaves the failed mass in a weakened condition (e.g. Skempton, 1985). Periodic reactivation of the earthflow debris leads to retrogressive failure of the head area, as the initial displaced debris moves away from the lower slope of the head scarp. Surcharging of the debris body by retrogressive head scarp failures can generate high pore pressures there with possible remobilization of the older metastable debris by undrained loading of the style discussed by Hutchinson and Bhandari (1971), Iverson (1986, 2005), Comegna et al. (2007) and Bertolini and Pizziolo (2008). While we do not attempt to isolate the specific triggering mechanism for earthflow mobilisation, earthquake ground shaking and gas release are considered the most likely candidates in this study area. Regardless of the specific triggering mechanism we conclude that the metastable condition of the landslide debris body due to sustained excess pore pressure is the critical factor that enables earthflows to develop on submarine slopes.

6. Summary

The field of submarine geomorphology is rapidly advancing, primarily as developments in seafloor imaging technology enable resolution, at unprecedented detail, of the topographic signature of processes affecting submarine slopes. It is no surprise that as we resolve these details, new features are revealed that do not fit traditional models of submarine slope processes. In this study, we have used quantitative morphometric techniques based on high resolution DEM's, combined with interpretation of multichannel seismic reflection data, to analyse patterns of deformation defining the kinematic behaviour of a submarine landslide complex.

This landslide exhibits characteristic features of a slow-moving terrestrial earthflow, contrasting with traditional models of submarine landslide complexes developing from repeated failures mobilising new source material with each event, with the material either accumulating in the same depositional area as slope gradient decreases, or being repetitively flushed through a channelized system. Earthflows are mass movement complexes where landslide debris is repeatedly remobilised along discrete bounding shear surfaces and transported at low velocities, in glacier-like, conveyor-belt style from a source zone in the landslide head area through the main landslide track to the toe where material is either deposited or removed by other processes (e.g. streams). Debris deformation by repeated reactivation of landslide debris bodies is reflected in surface roughness features.

An eigenvalue-based spherical statistics technique delineates a shear-bound elongate area of comparatively larger scale (wavelength and amplitude) surface topography within the Tuaheni landslide complex. This zone is interpreted as the most recently, and possibly the currently, active area of the landslide which is being repeatedly remobilised and is transporting material to the landslide toe. Adjacent shears in the toe area indicate that this is a spatially transient process that defines debris mobility in the lower part of the earthflow.

Movement is inferred to be fundamentally enabled by the ability for excess pore pressures to remain resident in submarine sediment bodies for extended periods of time. Earthflow-style instability is also promoted by the material properties of the extensive, well bedded, undeformed, gently dipping, fine-grained sedimentary sequence deposited on the upper slope. The driving forces that affect initial slope failures and periodic earthflow remobilisation on submarine slopes below the wave base include earthquakes, gas expulsion, and rapid sediment loading and the Tuaheni landslide complex occurs in an area that is subject to all of these processes. Given the subduction zone setting of the study site, and the numerous active faults mapped in the area, it is reasonable to assume that earthquakes have a significant role in the development of this landslide complex.

While further work is required to definitively show that the Tuaheni landslide complex is an active slow-moving earthflow, the surface and subsurface features observed are consistent with surface features developed in terrestrial earthflows that reflect their kinematic behaviour. The interpretation of submarine landslide complexes as active slow-moving earthflows has wide-ranging implications, including: landslide tsunami hazard analysis (e.g. the large volume of debris on the slope in comparison to the relatively small size of individual catastrophic head scarp failures); continental margin sediment transfer; submarine slope evolution; and design of submarine engineering works. We expect that this process will become widely recognised in other locations, and anticipate that a greater understanding of the driving mechanisms behind repeated remobilisation of submarine earthflow complexes will have a significant contribution to our understanding of submarine slope instability processes.

Acknowledgments

Special thanks to Geoffroy Lamarche for collecting the principle multibeam data set used in this study. The assistance of NIWA technicians Claire Castellazzi, Kevin Mackay, Arne Pallentin and Anne-Laure Verdier is greatly appreciated. Josh Roering assisted with coded spherical statistics routines. This research was partly supported by NZ FRST research contract C01X0702, and by NIWA capability funding. JJM received a Top Achiever Doctoral Scholarship from the New Zealand Tertiary Education Commission. An early draft benefitted from a review by Alan Orpin. The manuscript was much improved following reviews by David Mosher and an anonymous reviewer. Editor David Piper is thanked for his constructive feedback.

References

Barker, D.H.N., Sutherland, R., Henrys, S., Bannister, S., 2009. Geometry of the Hikurangi subduction thrust and upper plate, North Island, New Zealand. Geochemical Geophysical Geosystems 10.

Barnes, P.M., Ching Cheung, K., Smits, A.P., Almagor, G., Read, S.A.L., Barker, P.R., Froggatt, P.C., 1991. Geotechnical analysis of the Kidnappers Slide, upper continental slope, New Zealand. Marine Geotechnology 10, 159–188.

Barnes, P.M., Nicol, A., Harrison, T., 2002. Late Cenozoic evolution and earthquake potential of an active listric thrust complex above the Hikurangi subduction zone, New Zealand. Geological Society of America Bulletin 114 (11), 1379–1405.

Baum, R.L., Messerich, J., Fleming, R.W., 1998. Surface deformation as a guide to kinematics and three-dimensional shape of slow-moving, clay-rich landslides, Honolulu, Hawaii. Environmental and Engineering Geoscience 4 (3), 283–306.

Baum, R.L., Savage, W., Wasowski, J., 2003. Mechanics of earthflows. Proceedings of the International Conference FLOWS, Sorrento, Italy.

Beavan, J., Tregoning, P., Bevis, M., Kato, T., Meertens, C., 2002. Motion and rigidity of the Pacific Plate and implications for plate boundary deformation. Journal of Geophysical Research Solid Earth 107 (B10), 2261.

Bertolini, G., Pizziolo, M., 2008. Risk assessment strategies for the reactivation of earth flows in the Northern Apennines (Italy). Engineering Geology 102 (3–4), 178–192.

Borgatti, L., Corsini, A., Barbieri, M., Sartini, G., Truffelli, G., Caputo, G., Puglisi, C., 2006. Large reactivated landslides in weak rock masses: a case study from the Northern Apennines (Italy). Landslides 3 (2), 115–124.

Calvello, M., Cascini, L., Sorbino, G., 2008. A numerical procedure for predicting rainfall-induced movements of active landslides along pre-existing slip surfaces. International Journal for Numerical and Analytical Methods in Geomechanics 32 (4), 327–351.

Canals, M., Lastras, G., Urgeles, R., Casamor, J.L., Mienert, J., Cattaneo, A., De Batist, M., Haflidason, H., Imbo, Y., Laberg, J.S., 2004. Slope failure dynamics and impacts from seafloor and shallow sub-seafloor geophysical data: case studies from the COSTA project. Marine Geology 213 (1–4), 9–72.

Carter, L., Manighetti, B., 2006. Glacial/interglacial control of terrigenous and biogenic fluxes in the deep ocean off a high input, collisional margin: a 139 kyr-record from New Zealand. Marine Geology 226, 307–322.

Comegna, L., Picarelli, L., Urciuoli, G., 2007. The mechanics of mudslides as a cyclic undrained-drained process. Landslides 4 (3), 217–232.

Please cite this article as: Mountjoy, J.J., et al., Terrestrial-style slow-moving earthflow kinematics in a submarine landslide complex, Marine Geology (2009), doi:10.1016/j.margeo.2009.09.007

Cruden, D.M., Varnes, D.J., 1996. Landslide types and processes. In: Turner, A.K., Schuster, R.L. (Eds.), Landslides: Investigation and Mitigation. National Academy Press, Washington, D.C., p. 673.
Evans, D., Harrison, Z., Shannon, P.M., Laberg, J.S., Nielsen, T., Ayers, S., Holmes, R., Hoult, R.J., Lindberg, B., Haflidason, H., 2005. Palaeoslides and other mass failures of Pliocene to Pleistocene age along the Atlantic continental margin of NW Europe. Marine and Petroleum Geology 22 (9–10), 1131–1148.
Fleming, R.W., Johnson, A.M., 1989. Structures associated with strike–slip faults that bound landslide elements. Engineering Geology 27 (1–4), 39–114.
Gee, M.J.R., Uy, H.S., Warren, J., Morley, C.K., Lambiase, J.J., 2007. The Brunei slide: a giant submarine landslide on the North West Borneo Margin revealed by 3D seismic data. Marine Geology 246 (1), 9–23.
Glastonbury, J., Fell, R., 2008. Geotechnical characteristics of large slow, very slow, and extremely slow landslides. Canadian Geotechnical Journal 45 (7), 984–1005.
Glenn, N.F., Streutker, D.R., Chadwick, D.J., Thackray, G.D., Dorsch, S.J., 2006. Analysis of LiDAR-derived topographic information for characterizing and differentiating landslide morphology and activity. Geomorphology 73 (1–2), 131–148.
Greene, H.G., Murai, L.Y., Watts, P., Maher, N.A., Fisher, M.A., Paull, C.E., Eichhubl, P., 2006. Submarine landslides in the Santa Barbara Channel as potential tsunami sources. Natural Hazards and Earth System Science 6 (1), 63–88.
Hampton, M.A., Lee, H.J., Locat, J., 1996. Submarine landslides. Reviews of Geophysics 34, 33–59.
Hobson, R.D., 1972. Surface roughness in topography: a quantitative approach. Spatial Analysis in Geomorphology 221–245.
Hungr, O., Evans, S.G., Bovis, M.J., Hutchinson, J.N., 2001. A review of the classification of landslides of the flow type. Environmental and Engineering Geoscience 7 (3), 221–238.
Hutchinson, J.N., 1988. General report: morphological and geotechnical parameters of landslides in relation to geology and hydrogeology. landslides: Proc. 5th Symposium, Lausanne, vol. 1, pp. 3–35.
Hutchinson, J.N., Bhandari, R.K., 1971. Undrained loading, a fundamental mechanism of mudflows and other mass movements. Geotechnique 21 (4), 353–358.
Iverson, R.M., 1986. Unsteady, nonuniform landslide motion: 1 Theoretical dynamics and the steady datum state. Journal of Geology 94 (1), 1–15.
Iverson, R.M., 2005. Regulation of landslide motion by dilatancy and pore pressure feedback. Journal of Geophysical Research F: Earth Surface 110 (2).
Klaucke, I., Weinrebe, W., Petersen, C.J., Bowden, D., in press. Temporal variability of gas seeps offshore New Zealand: multi-frequency geoacoustic imaging of the Wairarapa area, Hikurangi margin. Marine Geology. doi:10.1016/j.margeo.2009.02.009.
Kvenvolden, K.A., Pettinga, J.R., 1989. Hydrocarbon gas seeps of the convergent Hikurangi Margin, North Island, New Zealand. Marine and Petroleum Geology 6, 2–8.
Lewis, K., Lallemand, S., Carter, L., 2004. Collapse in a Quaternary shelf basin off East Cape, New Zealand: evidence for passage of a subducted seamount inboard of the Ruatoria giant avalanche. New Zealand Journal of Geology and Geophysics 47, 415–429.
Leynaud, D., Mienert, J., Nadim, F., 2004. Slope stability assessment of the Helland Hansen area offshore the mid-Norwegian margin. Marine Geology 213 (1–4), 457–480.
Locat, J., Lee, H.J., 2002. Submarine landslides: advances and challenges. Canadian Geotechnical Journal 39 (1), 193–213.
Malet, J.P., van Asch, T.W.J., van Beek, R., Maquaire, O., 2005. Forecasting the behaviour of complex landslides with a spatially distributed hydrological model. Natural Hazards and Earth System Science 5 (1), 71–85.
McKean, J., Roering, J., 2004. Objective landslide detection and surface morphology mapping using high-resolution airborne laser altimetry. Geomorphology 57 (3–4), 331–351.
Micallef, A., Berndt, C., Masson, D.G., Stow, D.A.V., 2007a. A technique for the morphological characterization of submarine landscapes as exemplified by debris flows of the Storegga Slide. Journal of Geophysical Research F: Earth Surface 112 (2).
Micallef, A., Masson, D.G., Berndt, C., Stow, D.A.V., 2007b. Morphology and mechanics of submarine spreading: a case study from the Storegga Slide. Journal of Geophysical Research F: Earth Surface 112 (3).
Mulder, T., Cochonat, P., 1996. Classification of offshore mass movements. Journal of Sedimentary Research 66, 43–57.
Multiwave, 2005. 05CM 2D Seismic survey, offshore East Coast - North Island, New Zealand. Unpublished openfile petroleum report 3136. Ministry of Economic Development, Wellington.
Orpin, A.R., Alexander, C., Carter, L., Kuehl, S., Walsh, J.P., 2006. Temporal and spatial complexity in post-glacial sedimentation on the tectonically active, Poverty Bay continental margin of New Zealand. Continental Shelf Research 26 (17–18), 2205–2224.
Paquet, F., Proust, J.-N., Barnes, P.M., Pettinga, J.R., 2009. Inner-forearc sequence architecture in response to climatic and tectonic forcing since 150 Ka: Hawke's Bay, New Zealand. Journal of Sedimentary Research 79, 97–124.
Parise, M., 2003. Observation of surface features on an active landslide, and implications for understanding its history of movement. Natural Hazards and Earth System Science 3 (6), 569–580.
Pecher, I.A., Henrys, S.A., Ellis, S., Chiswell, S.M., Kukowski, N., 2005. Erosion of the seafloor at the top of the gas hydrate stability zone on the Hikurangi Margin, New Zealand. Geophysical Research Letters 32 (24), 1–4.
Pettinga, J.R., 2003. Mud volcano eruption within the emergent accretionary Hikurangi margin, southern Hawke's Bay, New Zealand. New Zealand Journal of Geology & Geophysics 46, 107–121.
Picarelli, L., Urciuoli, G., Ramondini, M., Comegna, L., 2005. Main features of mudslides in tectonised highly fissured clay shales. Landslides 2 (1), 15–30.
Posamentier, H.W., Vail, P.R., 1988. Eustatic controls on clastic deposition II — sequence and systems tract models. In: Wilgus, C.K., Posamentier, H., Ross, C.A., Kendall, C.G.S. (Eds.), Sea-level Changes: an Integrated Approach: Society of Economic Paleontologists and Mineralogists, Special Publication, pp. 125–154.
Reyners, M.E., 2000. Quantifying the hazard of large subduction thrust earthquakes in Hawke's Bay. Bulletin of the New Zealand National Society for Earthquake Engineering 33 (4), 477–483.
Savage, W., Wasowski, J., 2006. A plastic flow model for the Acquara–Vadoncello landslide in Senerchia, Southern Italy. Engineering Geology 83 (1–3), 4–21.
Skempton, A.W., 1985. Residual strength of clays in landslides, folded strata and the laboratory. Geotechnique 35 (1), 3–18.
Stirling, M.W., McVerry, G.H., Berryman, K.R., 2002. A new seismic hazard model for New Zealand. Bulletin. Seismological Society of America 92 (5), 1878–1903.
Strout, J.M., Tjelta, T.I., 2005. In situ pore pressures: what is their significance and how can they be reliably measured? Marine and Petroleum Geology 22 (1–2 SPEC. ISS), 275–285.
Sultan, N., Cattaneo, A., Sibuet, J.C., Schneider, J.L., 2008. Deep sea in situ excess pore pressure and sediment deformation off NW Sumatra and its relation with the December 26, 2004 Great Sumatra–Andaman Earthquake. International Journal of Earth Sciences 1–15.
Varnes, D.J., 1978. Landslide types and processes. In: Schuster, R.L., Krizek, R.J. (Eds.), Special Report 176: Landslides: Analysis and Control. Transportation Research Board, Washington DC, pp. 11–33.
Walsh, J.P., Alexander, C.R., Gerber, T., Orpin, A.R., Summers, B.W., 2007. The demise of a submarine canyon? Evidence for highstand infilling on the Waipaoa River continental margin, New Zealand. Geophysical Research Letters 34 (L20606).
Woodcock, N.H., 1977. Specification of fabric shapes using an eigenvalue method. Geological Society of America Bulletin 88, 1231–1236.

Please cite this article as: Mountjoy, J.J., et al., Terrestrial-style slow-moving earthflow kinematics in a submarine landslide complex, Marine Geology (2009), doi:10.1016/j.margeo.2009.09.007

5.3.2 The Paritu Debris Avalanche deposit: Product of repeated debris avalanches

The PDA had previously been recognised from echo-character and backscatter mapping as covering much of the Paritu Trough (Orpin, 2004). The extent of the Paritu Debris Avalanche (PDA) is now well defined in high-resolution (EM300) multibeam data (Bodger et al., 2006) (Figure 5.17) as well as at depth in MCS reflection profiles (e.g. Figure 5.20). The PDA provides an interesting contrast to the Tuaheni landslide Complex (TLC, discussed in Section 5.3.1) as it is: 1) much larger in extent; 2) comprises a large blocky deposit; and, 3) has a different surface character, interpreted as indicating catastrophic emplacement. In this section the techniques used by Mountjoy et al (2009b) are applied to the PDA deposit to evaluate the nature of emplacement.

The PDA covers ~250 km^2 of the Paritu Trough, sloping gently (~1°) to the south and south-east from water depths of ~1100 to ~1450 m. The landslide deposit itself is easily recognisable by its blocky and irregular surface roughness that is characteristic of submarine avalanche deposits (e.g. Lamarche et al., 2008) (Figure 5.17 & 5.18A). The scale of individual features within the blocky debris varies from close to 1000 m in the upper part of the deposit to less than 100 m in the lower part. An eigenvalue analysis run with a 50x50 m roaming window enhances the internal detail of the PDA debris deposit roughness (Figure 5.18B), and is used in combination with shaded-relief maps to develop a geomorphic interpretation of the deposit (Figure 5.19A).

From surface roughness and geometry the surficial PDA deposit can be divided into two main zones; an upper deposit characterised by an elongated zone of large-scale roughness, and a distal deposit characterised by “fan-like” zone of regular small-scale roughness. Between these zones is an area of large-scale roughness with smaller-scale roughness overprinted on top of it. It is apparent from the bathymetry that there has been some trimming of the lateral (north-eastern) edge of the landslide deposit (Figure 5.19A). Numerous smaller-scale failures are interpreted along the slopes to the north-east of the PDA deposit, from both source-area scars and debris deposits.

The PDA deposit is imaged in several MCS profiles (Figure 5.19C). While the orientation of these is not optimal for interpreting the internal anatomy of the landslide debris, as none are oriented along the deposit axis, the MCS reflection data still enable a comprehensive interpretation of the PDA as a polyphase event (Figure 5.20).

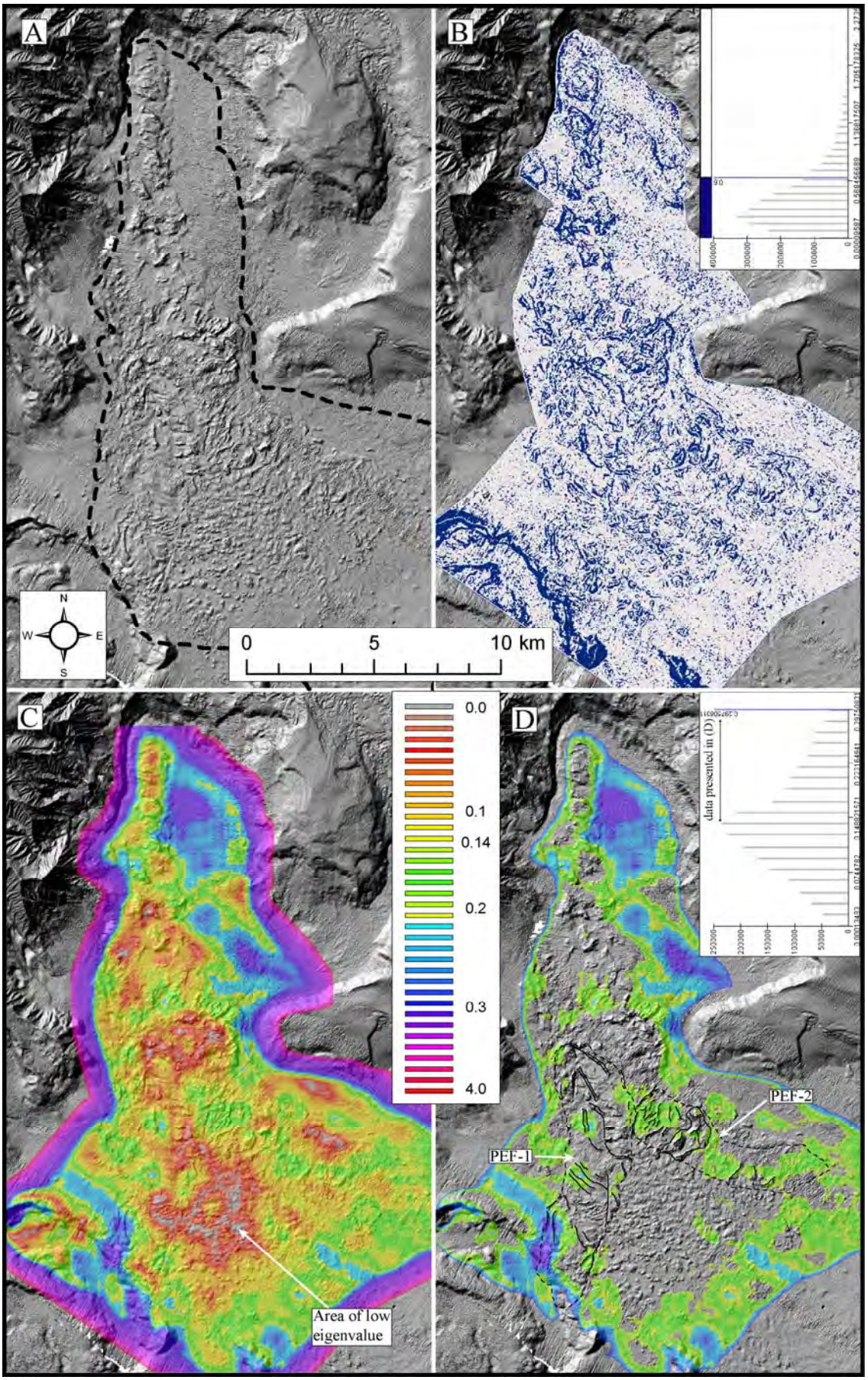

Figure 5.18 (caption on following page)

Figure 5.18: Paritu Debris Avalanche (previous page). A) Shaded-relief map at 3xVE showing the extent of debris related to the PDA (dashed black line). B) Eigenvalue analysis on a 50 x 50 m roaming window. The analysis has been split into two classes divided at 0.6. The inset histogram shows the distribution of values. The split value divides the peak from the tail of the histogram C) Eigenvalue analysis on a 1000 x 1000 m roaming window, with values classified in regular bin sizes of 0.01 up to 0.3, which accounts for the majority of relevant data (histogram inset right). D) Analysis from C showing only values between 0.14 and 0.3 (histogram inset). Map work shown is presented in full in Figure 5.19A.

5.3.2.1 Mass-transport deposit stratigraphy in Paritu Trough

In addition to the debris deposit related to that observed at the surface, deposits from previous mass-failure events occur at depth within the Paritu Trough sedimentary sequence, and are shown undifferentiated in grey in Figure 5.20. Between the PDA deposit and this "buried failure debris" a significant sequence (0.2 ms twt in the main basin) of undisturbed, parallel reflectors indicates a period of little or no large-scale mass-failure activity prior to the emplacement of the PDA deposit.

Anatomy of the PDA deposit

The anatomy of the PDA deposit has been interpreted based on all available MCS data. Only two lines are presented here (lines 05CM-44 and Tan0106-15 Figure 5.20) as these contribute the most to the interpretation. The remaining lines crossed the outer component of the deposit that is also imaged in these two profiles.

At the multi-kilometre-scale the "upper deposit" of the PDA is broadly characterised by large-scale blocky surface roughness (Figure 5.19A). MCS data show that the basal surface of the deposit is defined at the upper end by the boundary between chaotic reflectivity (landslide debris) and underlying coherent reflectivity (in-situ stratigraphy) (Figure 5.20A). Part way down the deposit a semi-continuous coherent reflector steps onto downslope debris, dividing the up-slope deposit from the down-slope one (inset Figure 5.20A enlargement). There is no indication of further internal partitioning within this upper debris body, and it is interpreted as the most recent event of the PDA, designated as F-1. The downslope end of the F-1 debris body is not clearly identifiable in bathymetry. A few compressional structures are interpreted in the distal part of F-1 (Figure 5.20A).

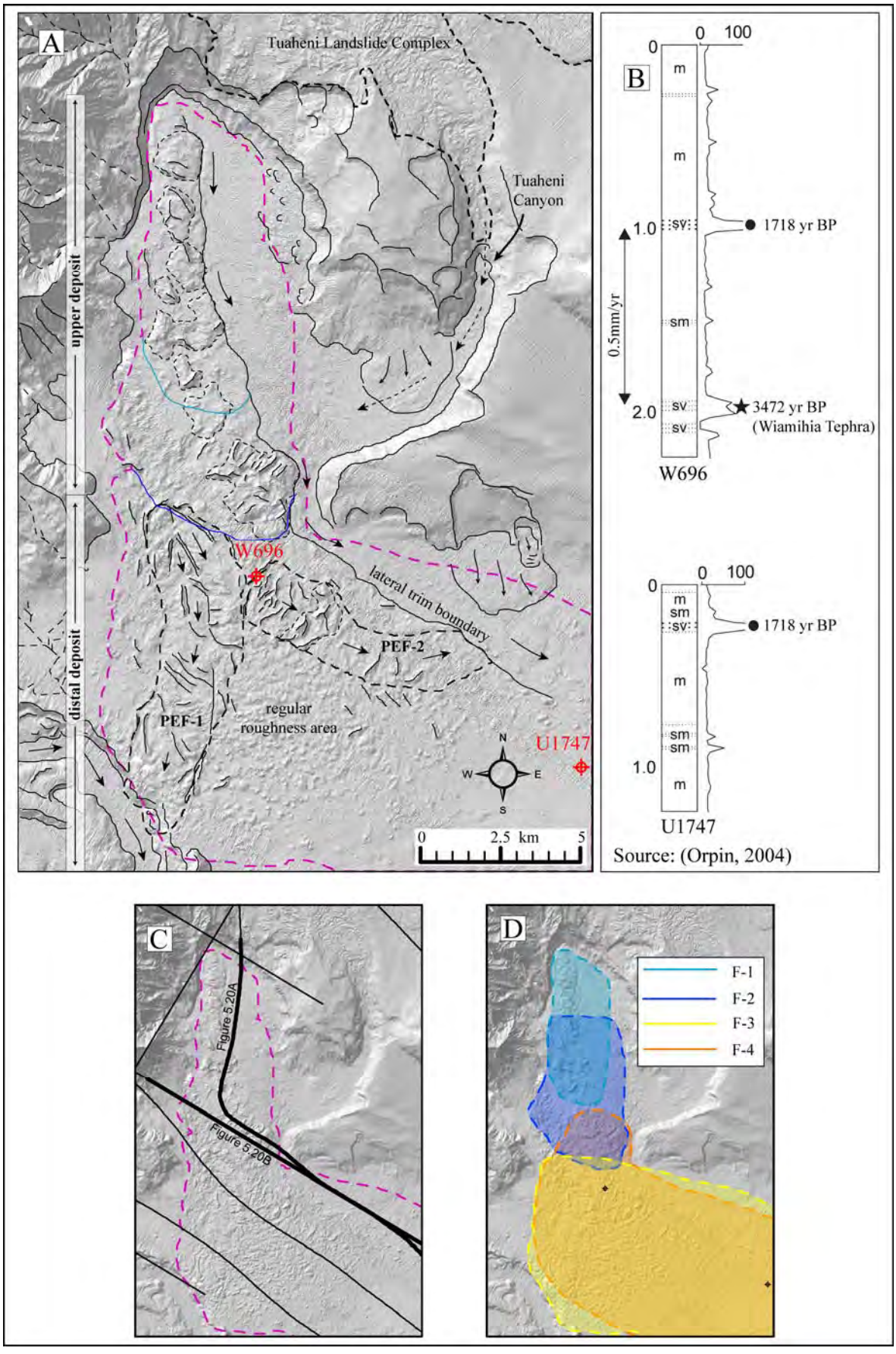

Figure 5.19 (caption on following page)

Figure 5.19: Geomorphic interpretation of the PDA (previous page). A) Geomorphic interpretation map of the PDA deposit and adjacent slopes overlain on a shaded-relief map at 3xVE. The extent of debris is indicated by a pink dashed line. B) Simplified core logs from the surface of the PDA deposit. Cores are located in A. C) MCS profile locations, with the two profiles presented in Figure 5.20 shown in bold. D) Interpreted debris bodies reflecting the polyphase emplacement of the landslide.

The debris body underlying and to the south of F1 is designated as F-2, and shows a significant amount of blocky surface roughness (Figure 5.19A), and internal compressional deformation (Figures 5.20A&B). The downslope limit of F-2 is primarily defined by the extent of blocky surface roughness in bathymetry, as the location of MCS profiles does not allow enable imaging of the lateral boundary between F-2 and debris in the distal part of the landslide. Within the debris mapped as F-2 in Figure 5.20 there is no indication of partitioning of the debris body.

The distal deposit of the PDA is better imaged in MCS, and is clearly separated into two chaotic debris bodies by a continuous, coherent reflector traced across the extent of the deposit (inset Figure 5.20B). The upper debris body (designated F-3) covers the majority of the Paritu Trough with the lower debris body (designated F-4) only exposed near the edges (Figure 5.19D). F-4 is interpreted as underlying F-2 (Figure 5.20) based on stratigraphic ties from additional MCS data not presented here (Figure 5.19C).

Thus, MCS data show that F-1 and F-4 are distinctively separate debris bodies. Whether F-2 and F-3 are distinctively separate debris bodies, or whether they were emplaced during the same event, cannot be definitively answered based on the available MCS data. To further interpret the components of the PDA deposit it is useful to determine the volume of both the landslide debris components distinguished in MCS data, and the source-area scars interpreted from bathymetric data. This will enable correlation between PDA deposit components and source areas that can be used to develop a sequential model for debris emplacement.

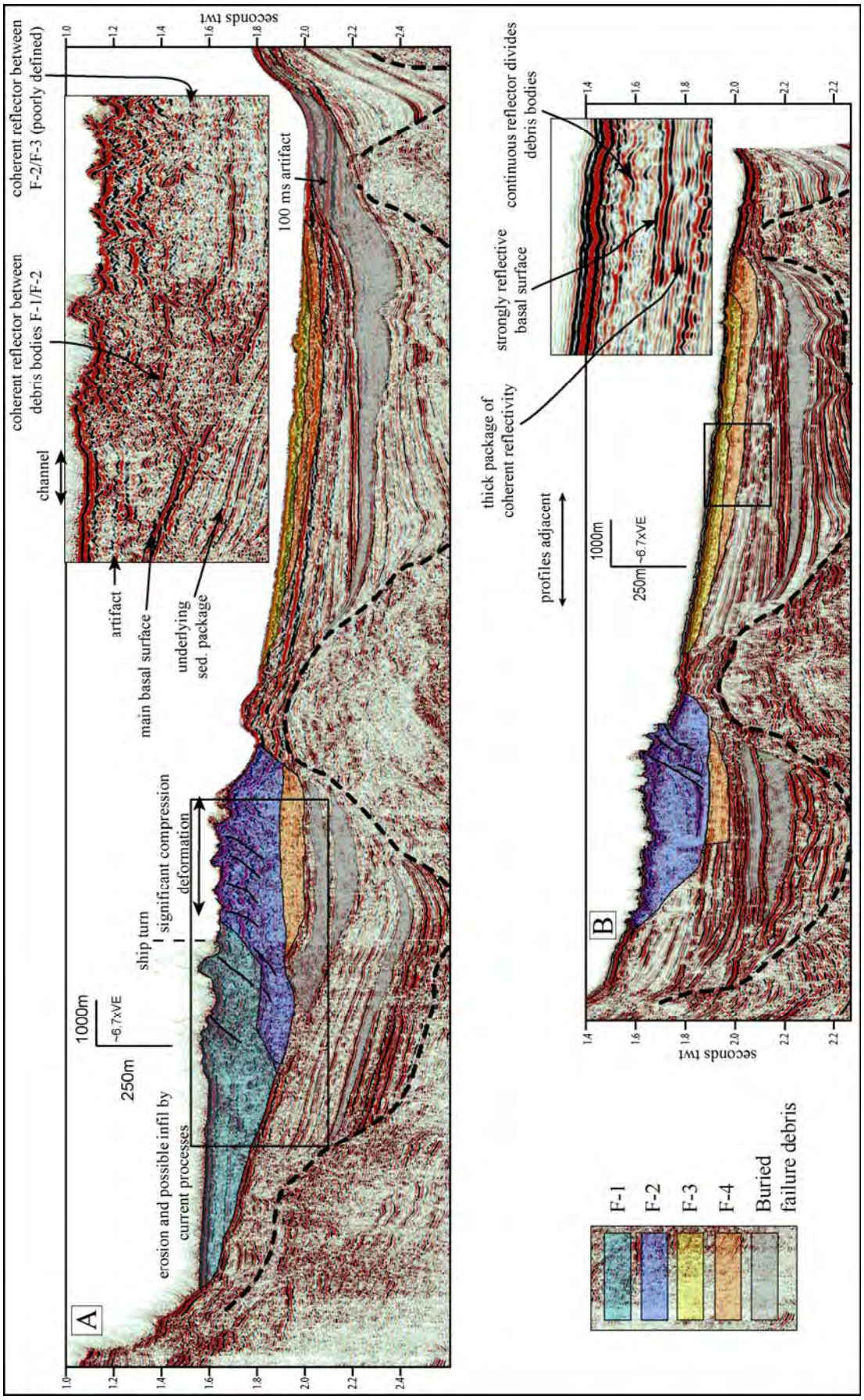

Figure 5.20 (caption on following page)

Figure 5.20: MCS profiles across the PDA deposit (previous page). Profiles are located in Figure 5.19C. The four debris bodies F-1 to F-4 have been mapped in the profiles and significant boundaries between these bodies are shown as uninterpreted enlargements. A) Profile Tan0106-15/16. B) Profile 05CM-44.

Volume calculation of the PDA debris deposit and inferred scar areas

Volume calculation for the PDA deposit and its components was achieved via a multistage process as follows:

1. Interpretation of the base of landslide debris in the available seismic grid (Figure 5.19C & 5.20)
2. Interpolation between these horizon picks in Seisvision® to create a continuous surface defining the base of the landslide debris
3. Export this surface to ArcGIS® (note the surface has z values in travel time)
4. Create a smoothed, average seafloor grid covering the extent of landslide debris converted from depth in metres to depth in travel time (using 1500 m/s as water-column velocity)
5. Subtract seafloor grid from debris-base grid to obtain debris thickness in travel time
6. Convert thickness to metres using a suitable material velocity (1800 m/s in this case)
7. Subtract thickness of debris from seafloor depth to obtain depth to base of debris as a grid layer.

The volumes derived using the constructed grid are shown in Table 5.3. Error budgets include uncertainty related to material velocity and the grid interpolation between MCS profiles.

Table 5.3: Volume calculations for the PDA

Item	volume (km^3)	Est. error (km^3)	comments
All PDA debris	33	5	
Debris F-1/F-2	10.6	1.5	Combined volume of F-1 and F-2
Total Source area	40.41	6	Refer Figure 5.21A
Source area F-1/F-2	8.7	1.3	Removed underlying F-3 material

The source area for the PDA is not immediately apparent. As debris emplacement is polyphase it is necessary to have either one large source scar or 2+ separate scars. There is no indication of an obvious single scar that might have produced the ~33 km^3 debris body so it is most likely that the material has multiple source areas. The area of the upper landslide debris has been reconstructed (Figure 5.21A), based on a projection of remnant surfaces of the lowstand wedge (e.g. Figure 5.9). With the existing PDA debris removed, a total volume of 40.41±6 km^3 is derived from this reconstruction (Table 5.3) indicating that this area is of sufficient size to be the composite source area of the PDA.

The most likely specific source areas will be related to the most recent failure, as this is expected to be the least degraded by post-failure surface erosion processes. At the upper end of the composite scar area a horseshoe-shaped slope, 150–250 m high with a gradient of 15–30°, surrounds the upper PDA debris. A reconstruction of the bathymetry of this upper area, using the top of the arcuate slope and stratigraphic orientation from MCS as geometrical control (seen at the upper end of the profile in Figure 5.20A), defines a volume of 8.7±1.3 km^3 (Table 5.3 and Figure 5.21B).

A short note on error budgets

The derived errors for calculations include as realistic variation in parameters as possible including ranges of inferred values for parameters, ranges of values for sediment velocities, measurement error, as well as accounting for error in lateral extrapolation from data. The errors have been calculated by taking the outer extremities considered reasonable for the relevant quantities to derive the upper and lower bound for the particular item; or alternatively a ± value if this is more appropriate. These have been derived to encompass as much of the expected variation of the values as possible, though it is acknowledged that,

given the large uncertainty associated with some measurements and data interpolation, it is possible that some errors have been overlooked.

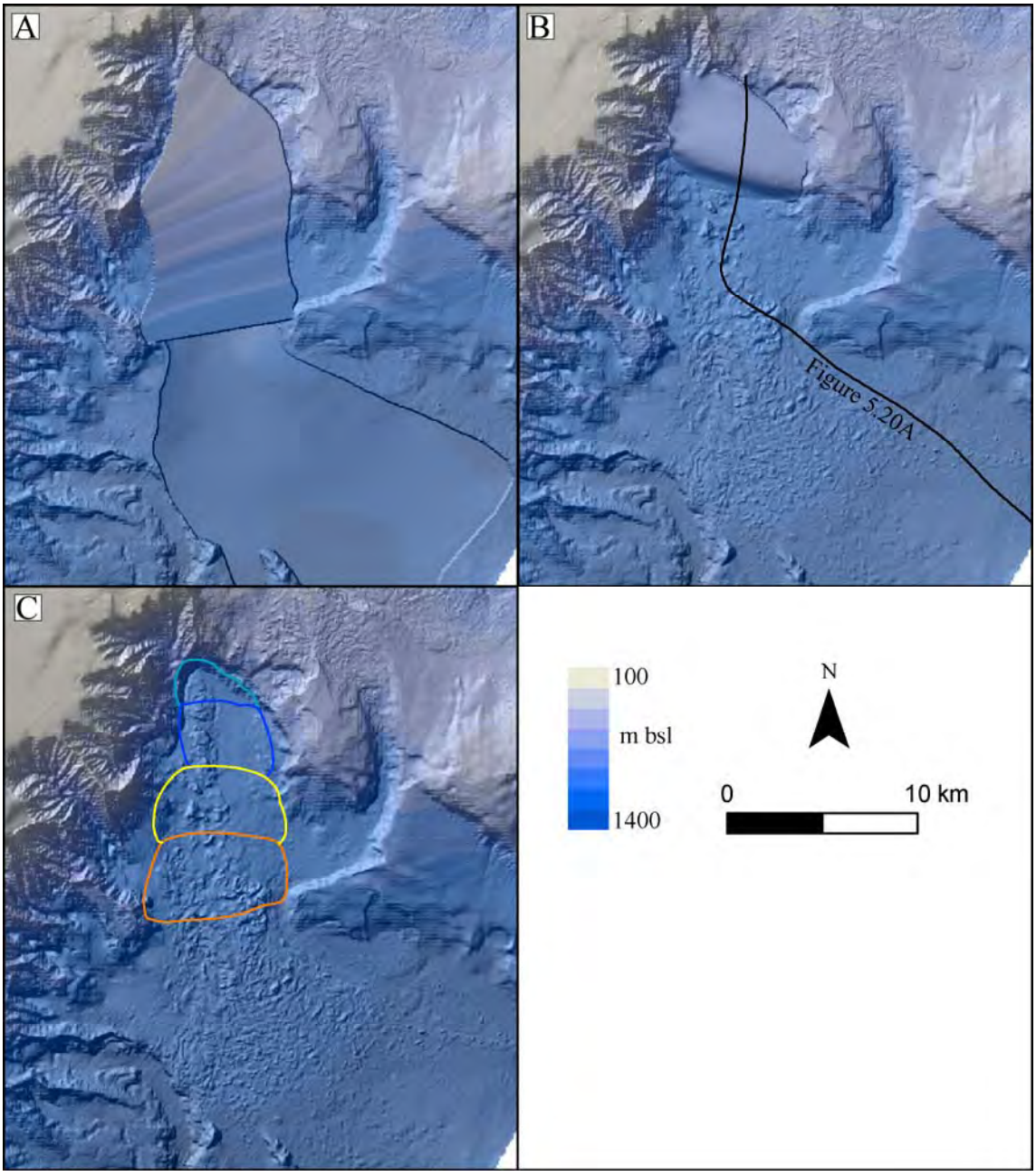

Figure 5.21: Bathymetric reconstruction in the PDA source area. The depth key, north arrow and scale shown apply to all panels. A) Reconstruction of entire upper PDA area, including removal of existing debris and construction of a drape surface based on remnants of the lowstand wedge (e.g. Figure 5.9). The derived volume difference between these two surfaces is presented in Table 5.3. B) Reconstruction of bathymetry for just the upper part of the scar. The derived volume difference between this surface and the basal surface of the debris is presented in Table 5.3. C) Inferred source areas for the four components of the polyphase PDA debris emplacement.

Interpretation of the landslide components in light of volume calculations

Volume calculations indicate that the well defined arcuate scar at the head of the PDA deposit is not sufficient to produce the entire PDA deposit, but matches well with the volume of the F-1 and F-2 debris (Table 5.3). This suggests that F-2 and F-3 are discrete debris bodies, and the PDA had evolved from four separate failure events. The volume of material required to completely rebuild the "embayment" surrounding the upper debris of the PDA (40.41±6 km^3) is more than the volume of the composite PDA deposit (33±5 km^3) but similar within the error budgets. Significant post-failure degradation of the composite landslide source scar makes it difficult to accurately define the pre-failure bathymetry; however the general match in the volumes indicates that the debris is likely to have been sourced from this area.

In terms of distinguishing the specific source area for each component of the PDA, the extent of the combined F-1/F-2 debris bodies is best constrained (Figure 5.21B). It is not, however, explicitly clear how the two failure sources are decomposed. It is reasonable to assume that an upslope portion of the F-1/F-2 source area relates solely to F-1 (Figure 5.21C). This is based on the interpretation that F-1 has run out over the tail of F-2, producing compressional structure in F-2 that is well imaged in MCS (Figure 5.20A). Figure 5.21C shows inferred source areas for the PDA, assuming a simple case of retrogressive failure.

5.3.3 Timing of emplacement of the PDA

Limited data is available to constrain the age of the PDA events. A core collected from the surface of F-3 contains the 3472 yr BP Waimihia Tephra (Figure 5.19B). The calculated accumulation rate from this core of 0.5 mm/yr (Orpin, 2004) suggests that the core base could be at approximately 4000 yrs BP, indicating that F-4 and F-3 were emplaced prior to this date. While there is no direct age control on Failures F-1 and F-2; adjacent geomorphic features provide some information on the relative occurrence of events. The western edge of the arcuate head scarp has a 200 m-high wall at the base of a well-formed shelf-indenting gully system (Figure 5.19A). The scarp truncates the lower gully system, removing the connection to the Paritu Trough. This scarp likely formed when the F-1 slide mass failed and, given its "fresh" appearance in comparison to other adjacent lower slope areas, it is likely that this has occurred significantly more recently than the F-3 failure. Consequently it is inferred that the PDA is a Holocene landslide complex, and furthermore that the most recent components (F-1 and F-2) are late Holocene features.

5.3.4 Post-emplacement deformation of landslide debris deposits: Implications for evolutionary studies of submarine mass-movement complexes

Submarine landslide deposits can be extensive, covering from tens to thousands of square kilometres, and can be complex debris bodies derived from multiple failure events. In polyphase landslide complexes the interaction of later-stage failures can have a significant impact on the morphology of the landslide complex. Consequently the surface morphology can be used as a tool to elucidate the history of a landslide complex. It is rare for submarine landslide deposits to be imaged in their entirety, resolving details of both surface roughness and the deposit at depth (i.e. the combination of full coverage with high-resolution bathymetric data and comprehensive coverage with high-quality seismic data). For this reason, studies defining the post-emplacement deformation of landslide deposits are rare. The two landslides documented here are imaged in both high-resolution bathymetry and MCS reflection data, and provide case study examples of end members resulting from different landslide modes.

Post-emplacement deformation of the PDA

It is apparent from surface morphology and morphometric analysis that there has been significant post-emplacement deformation within the PDA debris deposits. Within F-3 two distinctive failure streams are interpreted (Figure 5.19A). The most prominent of these in the south-western part of the landslide debris (PEF-1) shows distinctive landslide features including wedge-failure-geometry head scarps, lateral shears and compressional folds. PEF-2 is less well defined but shows a significant area of compressional deformation at the upper end, and transverse ridges down the length of the failure body. The PEF-2 failure was only interpreted following application of the eigenvalue technique. An expanded (1000x1000 m) roaming-window eigenvalue analysis was applied to the PDA debris using the methodology outlined in Mountjoy et al. (2009b) (Figures 5.18C&D). Within PEF-1 the technique picks up some areas of large-scale roughness related to compressional folds, but does not fully resolve the failure area. In PEF-2 however, the analysis reveals almost the entire failure body; which is not distinctively clear in shaded-relief maps. It is apparent that the post-emplacement remobilisation of F-3 debris has lead to the development of deformation features expressed at the seafloor. In comparison to the undisturbed F-3 debris, where regular, small-scale roughness is characterised by a large area of low eigenvalues, larger-scale roughness in PEF-2 is characterised by high eigenvalues (Figures 5.18C&D).

Significant compressional deformation at the frontal end of F-2 is revealed as both surface deformation (Figure 5.19A) and as structural-style deformation in MCS (Figure 5.20).

Post-emplacement deformation in a wider context

The post-emplacement deformation of both the PDA and TLC landslides is interesting as they are landslides of contrasting failure modes that have both experienced significant reactivation beyond their initial movement. This is an aspect of submarine landslide behaviour that has been poorly documented, and it is likely to be an important factor in the evolution of numerous landslide complexes. To date the main focus of submarine landslide studies in New Zealand's offshore environment has been failures at the extreme end of the size scale (e.g. Collot et al., 2001; Lewis et al., 2004; Lamarche et al., 2008). The failures documented within the Poverty re-entrant, while two orders of magnitude smaller than the Hikurangi Margin "mega-failures", are by no means small at 10+ km^3 and likely somewhere in the mid to upper size range of submarine landslides. The recognisable landslide deposits related to the TLC and PDA cover ~145 km^2 and ~250 km^2 respectively, yet each of these can be decomposed into multiple events. In the case of the PDA the landslide complex is interpreted to comprise four primary failure events with associated reactivation of the previously emplaced debris. The events are only distinguishable with the relatively comprehensive dataset of MCS and high-resolution multibeam available, and given a lesser dataset the landslide may not be interpreted as a poly-phase complex. In contrast the Tuaheni South landslides show no evidence indicating internal partitioning, which could easily lead to these being confidently interpreted as single, mass-failure events. To the contrary it is demonstrated that the TLC is an earthflow-style failure. This landslide transports material downslope by repeated introduction of material from the head of the landslide that is progressively conveyed through the main landslide body to the basin area beyond the landslide toe (Mountjoy et al., 2009b). The contrasting modes of post-emplacement deformation between the PDA and TLC are illustrated conceptually in Figure 5.22 with the sequence of events described in the figure caption.

The kinematic interpretation of the TLC shows the southern-most component (T1) moving towards the scar of the PDA (Mountjoy et al., 2009b - Figure 5). It is likely that this is a response to the most recent (F-1), or possibly penultimate (F-2), PDA event (Figure 5.21C). Furthermore, the source area of T1 is apparently depleted of LSW material potentially as a result of accelerated activity in the landslide, related to the influence of the PDA event. The effect is one of base-level modification; as the PDA failure occurs, the base level for the T1

is significantly lowered and the activity rate is likely to increase as toe failures occur and lateral stress relief is propagated up through the landslide body. It is apparent that this effect has modified the behaviour of T1 to the extent that it is encroaching into the T2 debris stream (Mountjoy et al., 2009b - Figure 5).

Observations of post-emplacement deformation of landslide complexes has implications for several aspects of both sedimentary process and landslide studies; including, tsunamigenesis, sediment transport rates, intra-slope sediment production and landslide-driven landscape evolution. It is clear that the earthflow style of submarine mass failure needs to be considered in the global context of landslide mapping and analysis and that post-emplacement deformation of landslide deposits can be an important aspect controlling their final morphology. These observations are principally the result of analysis of high-resolution multibeam datasets, illustrating the importance of such data in submarine landslide studies.

5.4 Rough quantification of sediment removal rates on the Tuaheni Slope

The disruption caused to the structural and sediment-transport systems of the Poverty sector of the Hikurangi Margin (likely as a result of repeated seamount impacts) has created dis-equilibrium of the “normal” subduction-margin geometry. Propagating lower to mid-slope structures have enabled sedimentary basins to form on the mid to upper slope that contain large debris deposits (Section 5.3). While not in themselves unusual, these basins are recording the products of apparently ongoing mass failures and may provide information on landslide rates and the temporally varying controls on mass-failure activity. Control on the distribution of material deposited on the upper slope during the last-glacial cycle (the Lowstand Wedge (LSW), Section 5.2.2) enables a first order, late Quaternary sediment budget to be developed for the upper slope. It is important to consider what the post-depositional form of the LSW may have been in order to obtain some idea of the amount of material deposited. This material volume can subsequently be balanced against that removed by mass-failure processes. It is interpreted that the ~20 km-length of Tuaheni Slope has been completely draped in a sedimentary wedge during the lowstand, and is now represented by minor remnants evident in seismic character and in seafloor morphology. It is possible to “virtually rebuild” this sediment body to consider the subsequent modifications that have occurred (Figure 5.23).

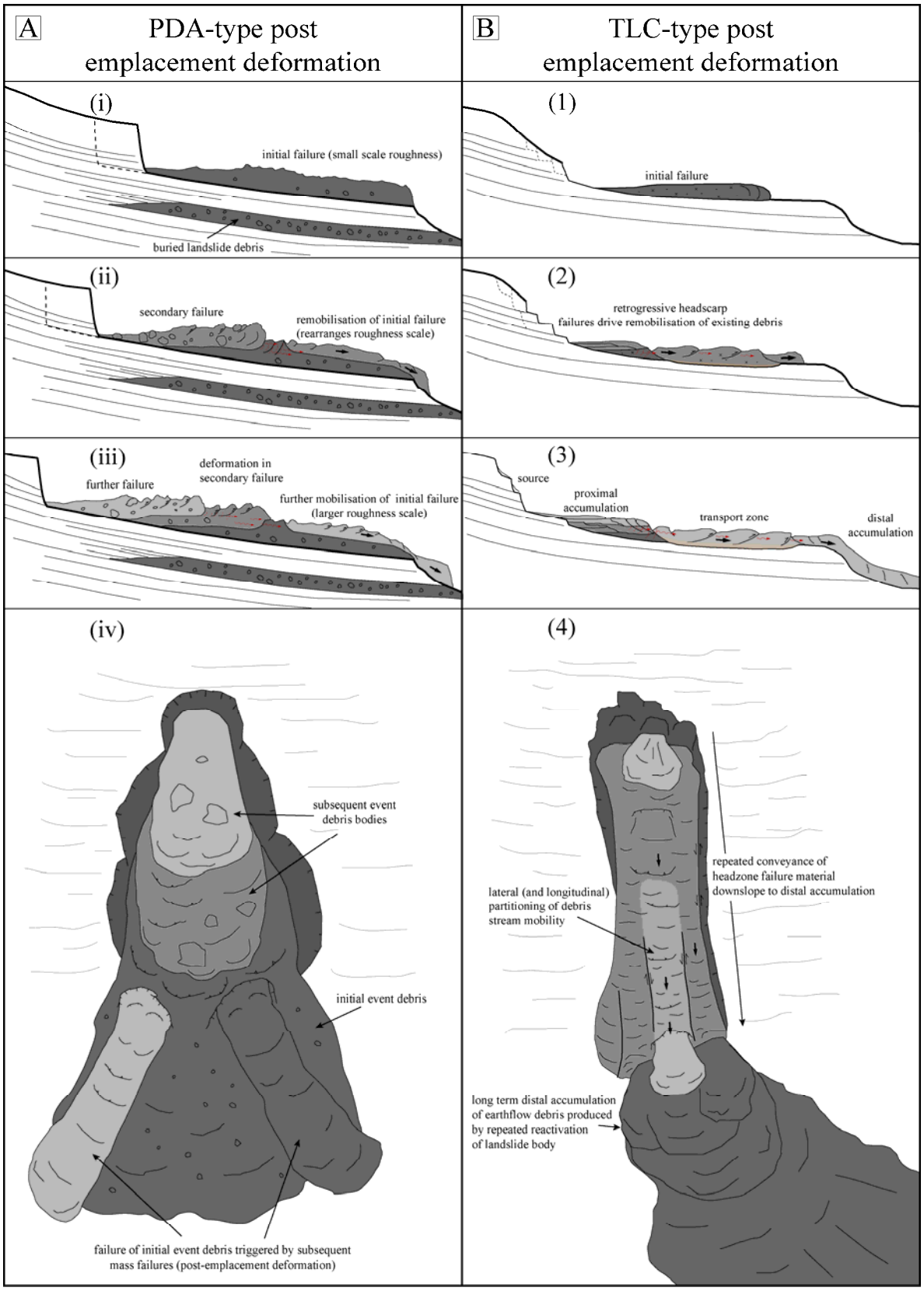

Figure 5.22 (caption on following page)

Figure 5.22: Conceptual model of two contrasting post-emplacement deformation scenarios (previous page). A) Model derived from analysis of the Paritu Debris Avalanche (PDA) (i) Initial failure emplaces a large debris body. Incipient failure block is shown dashed. (ii) Second failure partially overrides initial debris causing a bow-wave of compression and developing substantial excess pore-pressure (EPP). EPP triggers failure of a localised area of the distal part of the initial debris body. Incipient failure block is shown dashed. (iii) A third failure occurs, partially overriding the previous one and reactivating the distal failure from panel ii. Significant compressional deformation is reflected at the surface as compression ridges that introduce a larger-wavelength signature in eigenvalue analysis. iv) In plan view, the final geometry shows three overlapping debris bodies with post-emplacement deformation landslides developed in the initial, widespread landslide debris. B) Model derived from analysis of the Tuaheni Landslide Complex (TLC). (1) Initial slope failure occurs, at a smaller scale than PDA-type source failures. (2) Multiple small-scale head scarp regression failures occur. These statically load the upper end of the initial failure debris developing EPP, but are not of sufficient size to runout fully across previous debris. EPP, static loading and further dynamic loading by subsequent earthquakes trigger mobilisation of debris downslope, propagating motion downslope through the debris body. Slip occurs along a discrete basal surface and some basal erosion occurs. (3) Further head scarp failures occur and intermittent motion continues in the main debris stream. Compression within the debris stream develops compression folds at the surface. (4) In plan view this develops to an elongate geometry with well formed lateral shear boundaries. Movement partitioned longitudinally and laterally is reflected in surface deformation features.

To determine how much sediment has been deposited during the last glacial cycle it is possible to take a simple approach using the cross sectional area imaged in MCS (Mountjoy et al., 2009b - Figure 6A), and assume this to be a per-meter-of-shelf volume. Given the high likelihood for error in this calculation from e.g. variable deposit thickness, sparse MCS data coverage, incorrect seismic velocity assumption and simplified geometry among others, an error of plus and minus 50% is included. This produces a figure of $3 \pm 1.5 \times 10^6$ m^3/m-shelf length, and subsequently a total volume of 50 ± 25 km^3 for the 20 km length of the Tuaheni Slope.

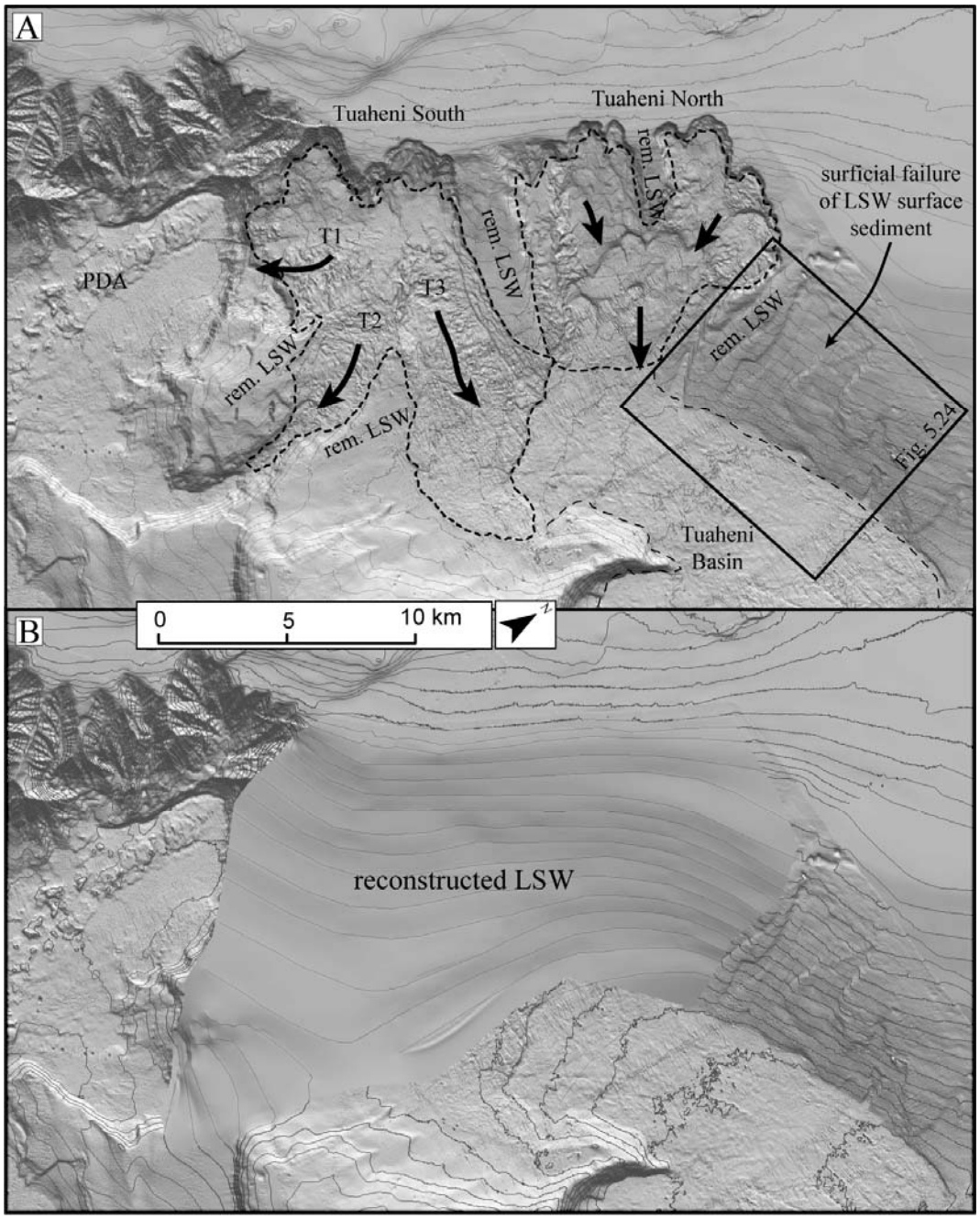

Figure 5.23: Reconstructed lowstand progradation surface assuming no syn-depositional slope deformation; i.e. landslides initiated post- LSW deposition. A) Present configuration with remnants of the progradational surface labelled as well as the direction of sediment movement in components of the Tuaheni Landslide Complex. B) Upper slope with the reconstructed LSW.

Material removal by the Tuaheni Landslide Complex

The surface of the Tuaheni Slope is dominated by the large Tuaheni Landslide Complex (TLC) which is wholly hosted within the LSW sediments (Mountjoy et al., 2009b). From the truncated reflectors at the slide-scar margins (Figure 5.11) it is apparent that these

landslides have eroded into a slope completely draped by a LSW. In the alternative situation, if landslides were occurring as the LSW was depositing we might expect to see reflectors draping into the slide scars, as well as areas of partially sediment-smothered landslide complex. Consequently, as this is not the case, it is inferred that activity in the TLC has initiated after accelerated lowstand deposition terminated, or post ~20ka sea-level rise. It is certainly likely that there was slope erosion occurring before 20ka in some form, and likely to be similar to the shallow "sheet erosion" observed immediately adjacent to Tuaheni North (Mountjoy et al., 2009b - Figure 2). This allows us to consider the volume of material removed, and to at least put an estimated time frame in place to derive an erosion rate.

The volume of material removed by the landslides is given in Table 5.4 and is an estimated total of ~20±4 km^3. If we assume that landslide activity initiated following sea-level rise, then a early Holocene initiation date (10ka) might be used, with a margin of error allowing for initiation once sea level rose to present-day levels at 6ka (Gibb, 1986) or during the marine transgression (i.e. ± 4 ka). This derives a rate of material removal of 2.1±1.8 x 10^6 m^3/yr. To test this model it is possible to deconstruct the stratigraphy of the Tuaheni Basin to look at balancing deposition in this basin with material eroded from the adjacent slopes.

Table 5.4: Material removal volumes based on reconstructed lowstand wedge surface (Figure 5.23). [1]Total debris accumulated in Tuaheni Basin with thickness derived from MCS reflection data (Figure 5.24). [2]Debris above the "blue" reflector, with thickness derived from MCS reflection data (Figure 5.24).

Item	Volume (km^3)	error (km^3)
Total material	20.872	4.174
Tuaheni North	8.452	1.69
Tuaheni South	9.939	1.988
Tuaheni South - T3 only	2.331	0.466
Tuaheni Basin[1]	25.669	4.174
Tuaheni Basin upper[2]	14.081	2.816

Accumulation in Tuaheni Basin

It is clear that part of the TLC (Tuaheni South-T1 & T2) is feeding material into the Paritu Trough, while part is feeding material into the "Tuaheni Basin" (Tuaheni South-T3 and Tuaheni North) (Figure 5.23). While material transferred to the Paritu Trough is incorporated with material from a variety of sources, the TLC is the primary source of material for the Tuaheni Basin. The Tuaheni Basin shows a 150–200m thick package of chaotic reflectivity interpreted as landslide debris (Figure 5.24B&C), with a total volume of 25.7±4.2 km^3 (Table 5.4). The calculated volume of material removed from the Tuaheni South-T3 and Tuaheni North component of the TLC is 10.8±2.2 km^3. Clearly this amount of material is beyond the production capacity of these landslides, even accounting for input from the small-scale sheet failures on the adjacent side walls. Additionally it is likely that a portion of material will have been siphoned off down the canyon at the lower end of the Tuaheni Basin. If the basin sequence is looked at in more detail it may be possible to gain further insight into material flux.

Within the Tuaheni Basin landslide debris there is a high-amplitude reflective package ~27 ms thick that is continuous across the basin and relatively undeformed. This is interpreted as a package of hemipelagic material (blue in Figure 5.24C) suggesting a period of quiescence in terms of landslide debris emplacement. The base of this horizon can be traced into the upper part of the lowstand wedge sequence. The horizon base, measured partway up Tuaheni Slope in an area of seafloor interpreted as not being affected by erosion, occurs at 56±6 m. Inferring an accumulation rate of 1±0.5 mm/yr, this horizon started accumulating at 56±45 kyr BP (Table 5.5). In the Tuaheni Basin the interpreted hemipelagic material has thickness of 47±5 m, equating to an age at the top of this package of 9±7 kyr BP. Using these accumulation rates the S1 reflector (Figure 5.10 & 5.11) would be 136±108 kyrs old, which falls within the expected age of 150-125 kyr BP. It is clear that these age constraints are crude and have a large margin of error. The values generally seem sensible, however, and provide the only available framework for Quaternary time-scale upper-slope sediment flux.

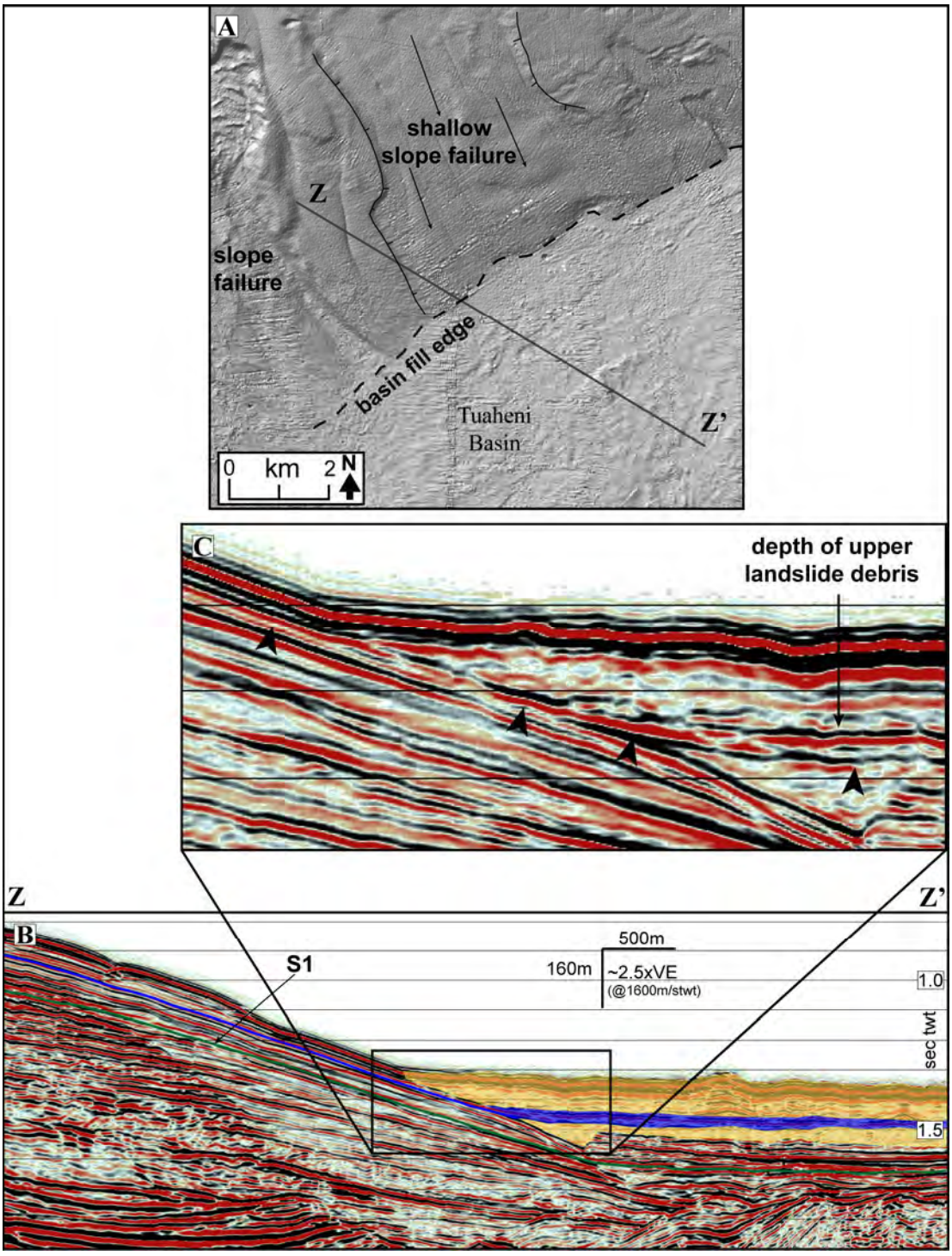

Figure 5.24: Sediment accumulation in Tuaheni Basin. Boundary between basin fill and the lowstand wedge surface. B) MCS profile across the lowstand wedge and basin fill, location is shown in A. The green reflector S1 has been tied from shelf stratigraphy. Basin fill is composed of two packages of chaotic reflectivity (yellow) divided by coherent reflectivity inferred to represent a period of hemipelagic sedimentation (blue). C) Enlargement of the MCS profile in B, without interpretation.

Table 5.5: Stratigraphic age constraints on landslide activity from Tuaheni Basin. Accumulation rates cover the range from measured post-glacial rates for the upper slope of 0.4–0.7 mm/yr (Barnes et al., 1991; Orpin, 2004) to modern rates around 1.7 mm/yr (Alexander et al., submitted).

item	best	lower bound	upper bound
Accumulation rate	1 m/yr	0.5 mm/yr	1.5 mm/yr
Age of "blue reflector"	56 kyr	33.6 kyr	123.2 kyr
Age at base of upper landslide debris	9 kyr	5.4 kyr	19.8 kyr
S1 age	136 kyr	81.6 kyr	299 kyr

The age constraints on sedimentation gained from Tuaheni Basin, while being crude provide a framework for the activity of the TLC. The entire 10.8±2.2 km^3 deficit of material from the Tuaheni South-T3 and Tuaheni North component of the TLC feeds into the Tuaheni Basin. The upper debris package has a volume of 14.1±2.8 km^3 (Table 5.4) which, within the margin of error and allowing for factors including material bulking and input from other slope sources is a reasonable match. Consequently it is inferred that the material removed from these landslides has accumulated in the upper part of the Tuaheni Basin.

Landslide-dominated sediment flux on Tuaheni Slope

Based on the documented constraints a model of sea-level highstand landslide activity is proposed (Figure 5.25). It is well established that large volumes of sediment accumulate on the upper slope during sea-level lowstand periods (Posamentier and Vail, 1988). During this time, while rapid sediment loading may negatively affect slope stability (i.e. excess pore-pressure generation), rapid sediment accumulation may also smother small-scale instabilities and provide lateral support to unstable slopes that limits them from developing into deep-seated instabilities. It is clearly apparent from the large body of relatively-undeformed sediment that syn-depositional slope deformations are limited in their extent if they occur. It is proposed that the majority of slope instability takes place during sea-level highstand periods, when sedimentation rates are lower.

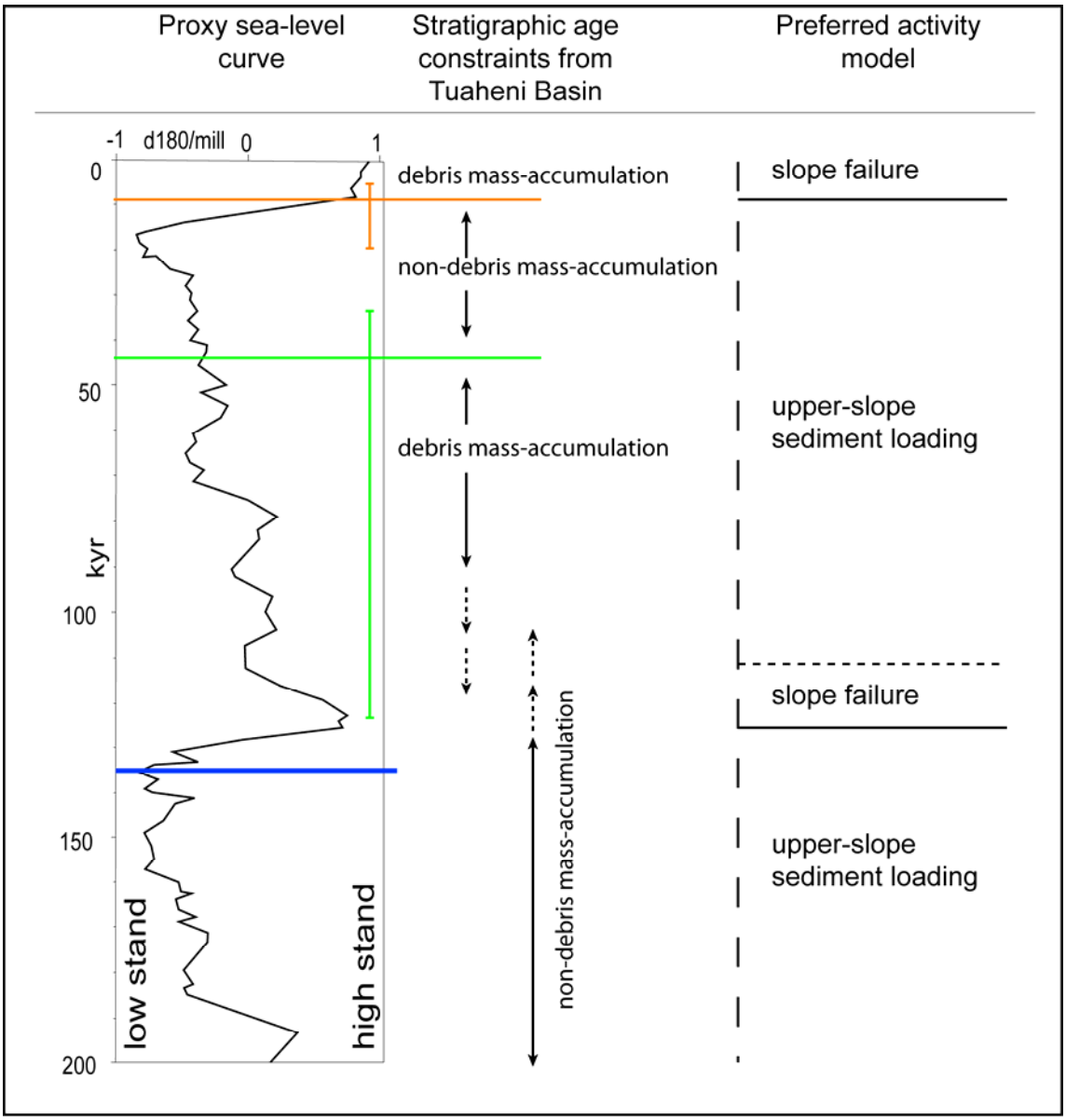

Figure 5.25: Conceptual model of landslide activity in the timeframe of the sea-level cycle. On the left is a sea-level curve (after Martinson et al. (1987)) with periods of debris accumulation shown with error bars (from table 5.5). The accumulation type is shown in the middle. The interpreted model of the dominant mechanism of sedimentation is shown to the right.

Using the interpreted sedimentary framework of the Tuaheni Slope LSW it is possible to determine a sediment removal rate by the TLC as an intra-slope sediment source. A sediment removal rate is calculated based on: 1) The initiation of deposition of the upper debris body in Tuaheni Basin; 2) The volume removed from the landslide; and 3) the length of the upper slope affected or alternatively, the area of slope affected. The derived rates are listed in Table 5.6.

Table 5.6: Rate of sediment removal by the TLC. [1]Rates of material removal by the combined activity of Tuaheni South-T3 and Tuaheni North components of the TLC. [2]Rates of material removal solely by Tuaheni South-T3.

item	best	lower bound	upper bound
Removal rate (m^3/km-slope length/year)[1]	75,000	26,000	158,000
Removal rate (m^3/km^2/year)[1]	6,700	3,000	18,000
Removal rate T3 (m^3/yr)[2]	350,000	140,000	630,000

5.5 Evolution model for the upper slope of the Poverty re-entrant

The Poverty re-entrant headwall is dominated by canyon heads and gully systems, while to the south and north the upper slope is characterised by preserved lowstand wedge sediments with associated surface erosion and landsliding (e.g. the TLC, Figure 5.17). While both the southern and northern domains are primarily depositional, the canyons and gully systems of the central domain are erosive features. These are considered to be primary sediment conduits during lowstand conditions (e.g. Orpin, 2004) but may receive little in the way of shelf-derived sediment input under the current highstand sea-level regime (e.g. Walsh et al., 2007). Despite their apparent top-down inactivity, mid-slope areas of gullies retain an angular and "youthful" form, suggestive of ongoing Holocene activity. It is interesting to consider two fundamental questions: 1) Are all the gully systems primarily active during sea-level lowstands; and 2) At what stage in the sea-level cycle do these features form.

While there is little quantitative landscape age-control data available to address these questions, the combination of available accumulation-rate data, and the knowledge of the tectonic structure and major landslides documented in this chapter enable the development of a model of upper-slope evolution that can, at the least, provide a framework for spatial and temporal formation of slope gullies.

5.5.1 Quantification of gully form

Quantification of the morphometric form of gully systems in the upper re-entrant headwall enables comparative analysis that might contribute to greater understanding of the evolution of these features. The gully systems have been mapped into "catchments" (Figure 5.26A), using the following steps:

1. Delineate channel networks using overland flow routines in ArcGIS® using the add-in tool TauDEM®.
2. Define the outlet points of contributing channel networks (catchments).
3. Delineate catchment extents manually, using hillshade, flow network and contour derivative layers. This was necessary as the automated catchment routine did not deal well with some of the "noise" within the flow network created by the composite grid from datasets of varied resolution.

The long profiles of principal channels in the main catchments encroaching on the shelf have been extracted. These have been plotted initiating from an arbitrary distance from the slope base, but along a line projected parallel to the shelf break (Figure 5.26A). The profiles then either follow channels across the infilled Tuaheni Trough (if these are clear) or are projected directly to the catchment outlet, and beyond to an arbitrary strike-projected line. Profiles are taken an equal distance across the upper slope and onto the shelf, and the data is plotted as distance-across-the-margin (i.e. not distance-along-channel-length) against elevation (Figure 5.26B). The area of the mapped catchments has also been extracted and plotted against the distance-along-slope from the catchment outlet (Figure 5.26C).

Interpretation of gully form

Data show a clear trend of decreasing catchment size towards the northern end of the re-entrant headwall (Figure 5.26C). Furthermore, there is some clustering in the distribution of these showing three populations of catchment sizes distributed along the headwall. In Figure 5.26B two areas of clustered gully long-profiles are observed, from both the northern end and from the centre of the headwall. The gully-catchment-size clustering, and the convergence in the amount of incision in the gully axis, indicates that these gully populations are of a similar age. The re-entrant headwall is therefore subdivided into three domains based on gully catchment morphometry; 1) mature gullies (Poverty Canyon heads); 2) intermediate gullies; and 3) immature gullies (Figure 5.26A).

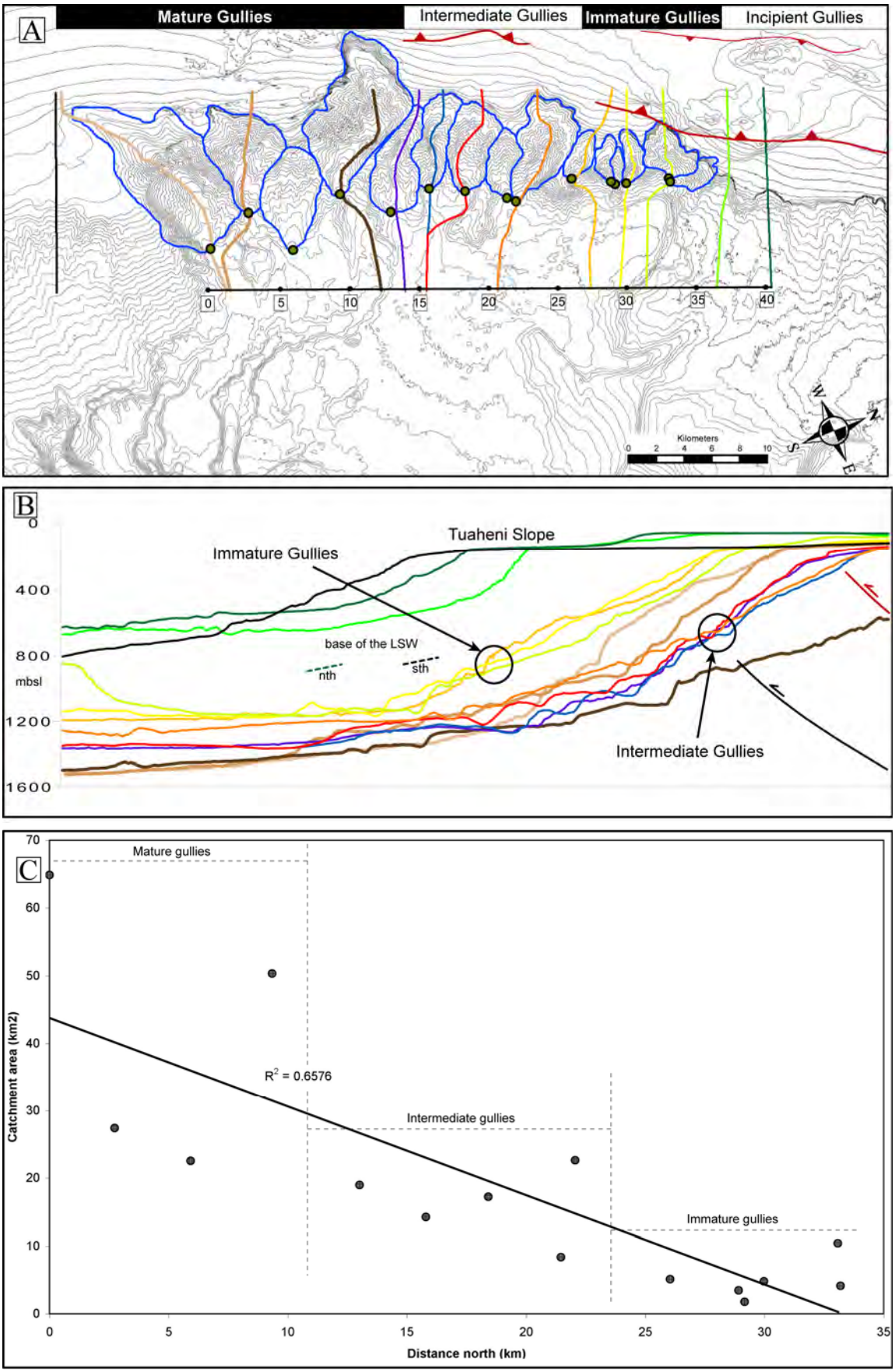

Figure 5.26: Quantification of the form of gullies on the upper Poverty re-entrant headwall. A) Gully "catchment" extent (blue) with outlet points (green dots) and axis

profile locations (multi-coloured). Gully profiles are projected to an arbitrary strike line, with distance in kilometres plotted along it relating to C. B) Long profiles of gully axes, at the locations indicated in A. Profiles are plotted as distance-across-the-margin vs water depth. General location of active vs inactive structure is shown. Also plotted is the depth of the base of the LSW, projected from MCs profiles to the north and south of the re-entrant. C) Plot of gully catchment size vs distance-along-strike of the margin. Data points have been grouped into three categories that relate to those in A.

It is logical that the main Poverty Canyon heads (mature gullies) are comparatively deeply incised, as these remain connected to cross-slope canyons/sediment conduits. While it has been demonstrated that they are not active as top-down sediment conduits under current conditions (Walsh et al., 2007), it is nonetheless likely that these canyon heads are primarily shaped as active shelf-to-trough sediment conduits during sea-level lowstands. The remaining intermediate and immature gullies, however, all exit to the Paritu Trough and are not linked to slope canyon systems. While the possibility that cross-slope canyons occurred at the base of some of these during the lowstand, it is unlikely that they were all canyon coupled. It may be that not all these features are sea-level lowstand features.

5.5.2 Qualitative model of re-entrant headwall evolution

The interpreted failure sequence of the PDA, both the source areas and stratigraphic relationships of the deposits, indicates a progressive northward-migration of the landslide source area. The conceptual model of the evolution of the upper slope of the re-entrant is as follows (domains refer to Figure 5.26A):

1. Start point: The Poverty Canyon system crosses the slope and heads into the shelf break (mature gully domain). The PDA has not failed.
2. Immediately to the north in the “intermediate gully domain”, possibly; 1) canyons also head into the shelf break to form gully systems on the upper slope; and/or 2) mass failure occurs destabilising the upper slope leading to gully development (NB buried landslide debris Figure 5.20).
3. Further to the north of this the incipient failure material for the PDA inhibits gully formation (cf. Figure 5.21A)
4. Failure of the PDA occurs; progressively undermining the upper slope at the northern end of the re-entrant headwall.
5. Following this lowering of the local slope base level, the erosive potential of grain flows increases and gullying initiates (immature gully domain).

6. Further north on the Tuaheni Slope the “incipient gully domain” will be able to achieve a similar incised gully form only once further large-scale mass failure has occurred, lowering the local base level through the removal of the Tuaheni “plateau”.

There is a progressive northward development of upper-slope gully systems and these are facilitated by the occurrence of large bedrock landslides. Deep gully erosion cannot take place until sediment cover-sequences have been removed by mass failure. While the canyons in the south of the re-entrant may have developed without the need for mass failures, the progressive northward evolution of upper-slope gully systems may only be enabled by the lowering of the base level for the slope by deep-seated landsliding. This suggests that bedrock landslides can play an important role in the development of submarine slope gully systems, a ubiquitous feature of active tectonic margins.

5.5.3 Role of structure in upper slope development

The structural framework developed earlier in this chapter provides some constraints on the development of the upper re-entrant headwall system. The distinct linearity of the headwall is inferred to result from the presence of the inactive thrust stack that is pervasive across the length of the upper slope, where the thrust tips have an aerial extent generally coincident with the gully systems (e.g. Figure 5.12 & 5.17). It is suggested that the older Miocene/Paleogene material exhumed by these structures (Figures 5.7 & 5.9) inhibits significant landward propagation of the canyons across the shelf. The two canyon heads at the southern end of the re-entrant do encroach into the shelf break and have apparently excavated beyond this barrier, and it is noted that the most incised (southern-most) canyon trends southward once on the shelf. Nonetheless, none of these canyons have developed into major shelf-indenting canyons and this is inferred to be a function of the margin-parallel structural configuration, meaning canyons would be required to incise through structures to cross the shelf.

The contrasting form of the upper slope either side of the re-entrant, i.e. contrast between pervasive deep-seated failures to the north and minor slope erosion to the south, may reflect the proximity of active structures. Strong ground motion is well documented to play a significant role in triggering slope-instability processes, and has been shown to be related to larger mass failures in canyon systems (Sultan et al., 2007). It is apparent from modelling of the return times of earthquake-generated ground shaking that the upper slope to the north of the re-entrant receives higher levels than those to the south (Figure 5.16), and this may

be reflected in the contrasting surface processes observed. That is, the presence of deep-seated failures to the north of the re-entrant in contrast to shallow surficial failure to the south directly reflects the distribution of high-magnitude earthquake-generated strong ground motion.

Other factors may also be relevant here, including the evolutionary history of the canyon (time since the re-entrant formed), river power in the terrestrial systems, and the occurrence of particular sedimentary processes. Given that there is a very limited library of dated bedrock material from the upper slope it is difficult to provide in-depth detail on the extent of lithological control on canyon incision. With a comprehensive sampling and dating survey in the future, it may be possible to attribute particular geomorphic form to underlying lithology.

5.6 Chapter summary

The combination of the morphostructural setting and extensive high-quality dataset of the Poverty shelf and upper slope provide a world-class opportunity to study the effects of structure, stratigraphy and mass-failure systems on the evolution of the shelf to upper slope transition.

1. As previous structural interpretations (Field et al., 1997; Lewis et al., 1997) were based on limited data it has been necessary to map the tectonic structure across the entire Poverty shelf to provide a framework for structural evolution of the upper slope. This extends the mapping of Barnes et al (2002) and Barnes and Nicol (2004) north from Mahia Peninsula to Gable End Foreland, filling a significant gap in knowledge of the Hikurangi Margin structure.
2. Additionally the broad-scale stratigraphy has been interpreted as part of this work.
3. The Quaternary glacial-cycle stratigraphy has been interpreted, based on knowledge gained from studies to the south in Hawke's Bay (Paquet et al., 2009) and a best interpretation of the late-Pleistocene stratigraphy in Poverty Bay. From this it has been possible to tie a reflector representing the base of the last-glacial cycle (~130 kyr) of sediment deposition, i.e. the last-lowstand wedge. This provides a framework for landslide activity on the upper slope.
4. The re-entrant contains large mass-failure deposits related to two distinct landslide complexes that are well imaged in the high-resolution bathymetry and MCS reflection profiles. This has been exploited by developing techniques of objective morphometric

mapping to defining the post-emplacement kinematic behaviour of the landslide debris that shows significant post-emplacement deformation within the landslide complexes.

5. In the TLC landslides are behaving as submarine earthflows, a previously undocumented phenomenon in the submarine environment (Mountjoy et al., 2009b); while the PDA is a large-volume polyphase landslide complex that has remobilised debris emplaced during initial events. The eigenvalue-based morphometric technique applied to the landslide debris enables delineation of areas of differential movement within the landslide complexes. A stratigraphic interpretation of landslide debris accumulation in the Tuaheni Basin supports a model of Holocene landslide activity. It is proposed that activity in the TLC initiated post- sea-level rise and furthermore that the earthflow continues to be active today.

6. The structural, stratigraphic, and mass-failure analysis provide a framework for a conceptual model for the progressive lateral evolution of the upper slope and the development of gully systems in the re-entrant headwall. While the Poverty re-entrant is a relatively unique feature on the Hikurangi Margin, slope gully systems are widespread on both the Hikurangi Margin and on active margins around the world. The insights gained here are likely to have implications for evolutionary studies in numerous other active margin locations.

Chapter 6: Relationship between landslides, structure and fluid expulsion on the Hikurangi Margin

The recent New Vents programme (Bialas et al., 2007) has bought together a wide range of disciplines and techniques focused on active fluid expulsion from the Hikurangi Margin subduction zone (Barnes et al., 2009; Crutchley et al., 2009; Jones et al., 2009; Law et al., 2009; Linke et al., 2009; Netzeband et al., 2009). Fluid expulsion has been proposed to play a role in the erosion of submarine slopes and the development of canyons (Orange et al., 1994; Orange et al., 1997), and the occurrence of gas hydrates is widely associated with slope failures and seafloor erosion (e.g. Paull et al., 1996; Pecher et al., 2005). The New Vents study provides an opportunity to assess multiple sites of documented fluid venting and interpreted gas-hydrate occurrence that are imaged with high-resolution bathymetry, enabling interpretation of seafloor-erosion processes.

As part of the New Vents programme, a framework for fluid vent areas has been developed characterizing the structural and morphological setting of five sites (Barnes et al., 2009). My contribution to this manuscript (eighth author) has been to map evidence of slope instability in the study sites based on multibeam data, in addition to research on the structure on the Wairarapa slope (Law et al., 2009; Mountjoy et al., 2009a). Evidence for mass failure is recognized across three of the sites, and in this short chapter the location of mass-failure scars at these sites is considered with respect to fluid-venting sites, structure and slope gradient. Figures reproduced here are modified from Barnes et al. (2009), and additionally the manuscript is included in its entirety as Appendix II.

6.1 Vent site bathymetry and the distribution of landslides

Of the five separate sites covered by Barnes et al. (2009) it has been possible to map landslide-related features in detail across three sites; namely Wairarapa, Uruti Ridge and Omakere Ridge (Figures 6.1–6.3). These sites are subsequently referred to as the Wairarapa, Uruti and Omakere sites, respectively. Landslide scars are recognised across all

three sites, though in the case of Uruti and Omakere the extent of mapping area is limited by the extent of higher-resolution bathymetric data. Bathymetry for these two sites includes lower-resolution Simrad 120 (12 kHz) multibeam data, limiting the interpretation of features below kilometer scales (for further details of data used in this study refer to Appendix II). Landslide scars have been mapped based on head and lateral scarps, and no examples can be documented where landslide debris-runout deposits are observed in bathymetry and can be matched to a specific source area.

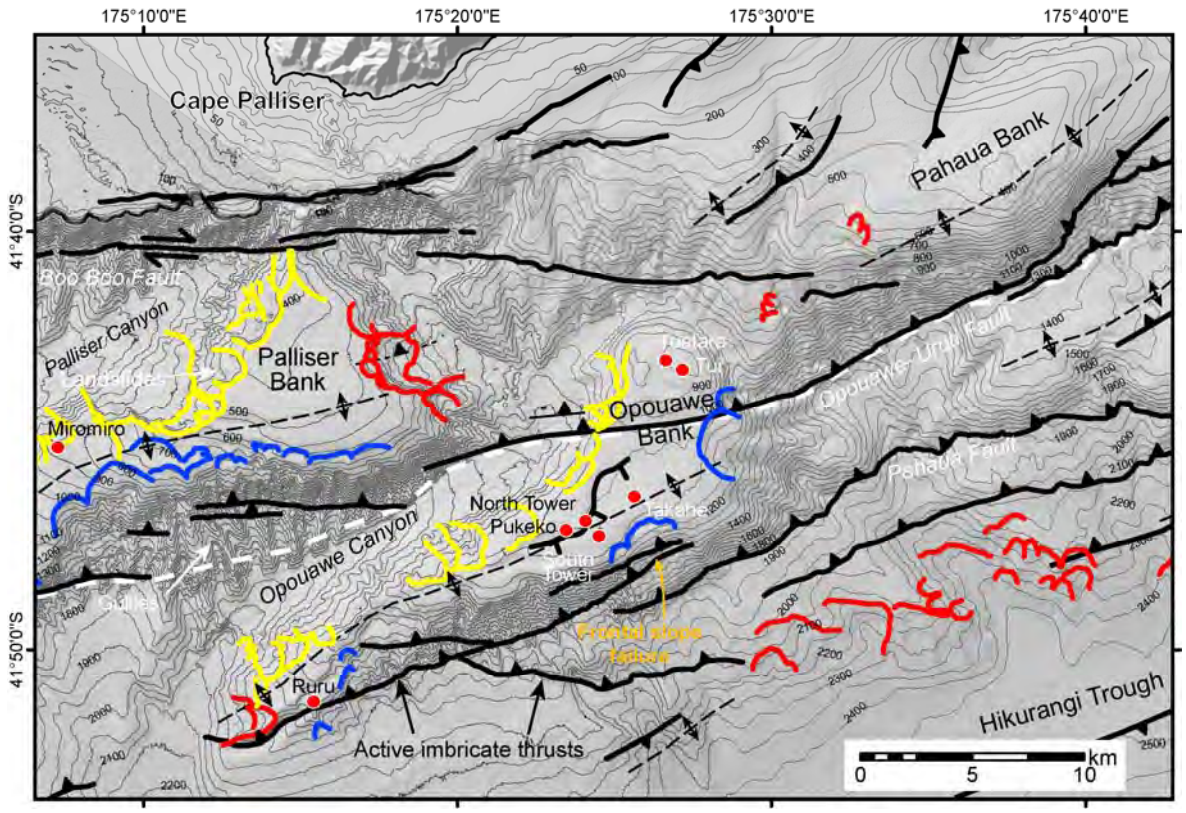

Figure 6.1: Wairarapa seep site showing: fault traces (black lines with teeth on up-thrown side), anticline axes (dashed black lines), accretionary wedge–deforming backstop boundary (white dashed line), and landslide scars (blue, yellow and red). Landslide scars are distinguished by their location on antiforms as: backlimb (yellow), forelimb (blue) and not attributed (red). Modified from Barnes et al. (2009).

6.1.1 Interpretation of landslide scar distribution

In the three mapped areas bathymetric relief is predominantly controlled by structure, and landslides primarily occur (as do vent sites) on thrust-fault-propagated anticline ridges. Mountjoy et al. (2009a) (Chapter 4) demonstrated that the seaward-vergent anticline ridges at the Wairarapa site (Palliser Bank and Opouawe Bank) are asymmetrically subject to differing slope-erosion processes, with stratigraphically-controlled mass failure on the

landward (back) limb, and gully incision on the seaward (fore) limb. The head area of seaward-limb gullies are also subject to mass-failure events in many instances (Figure 6.1). The distribution of landslides across the three sites has been colour coded to reflect their position on the frontal (SE facing flank) or trailing (NW facing flank) limbs of anticline ridges (Figures 6.1–6.3).

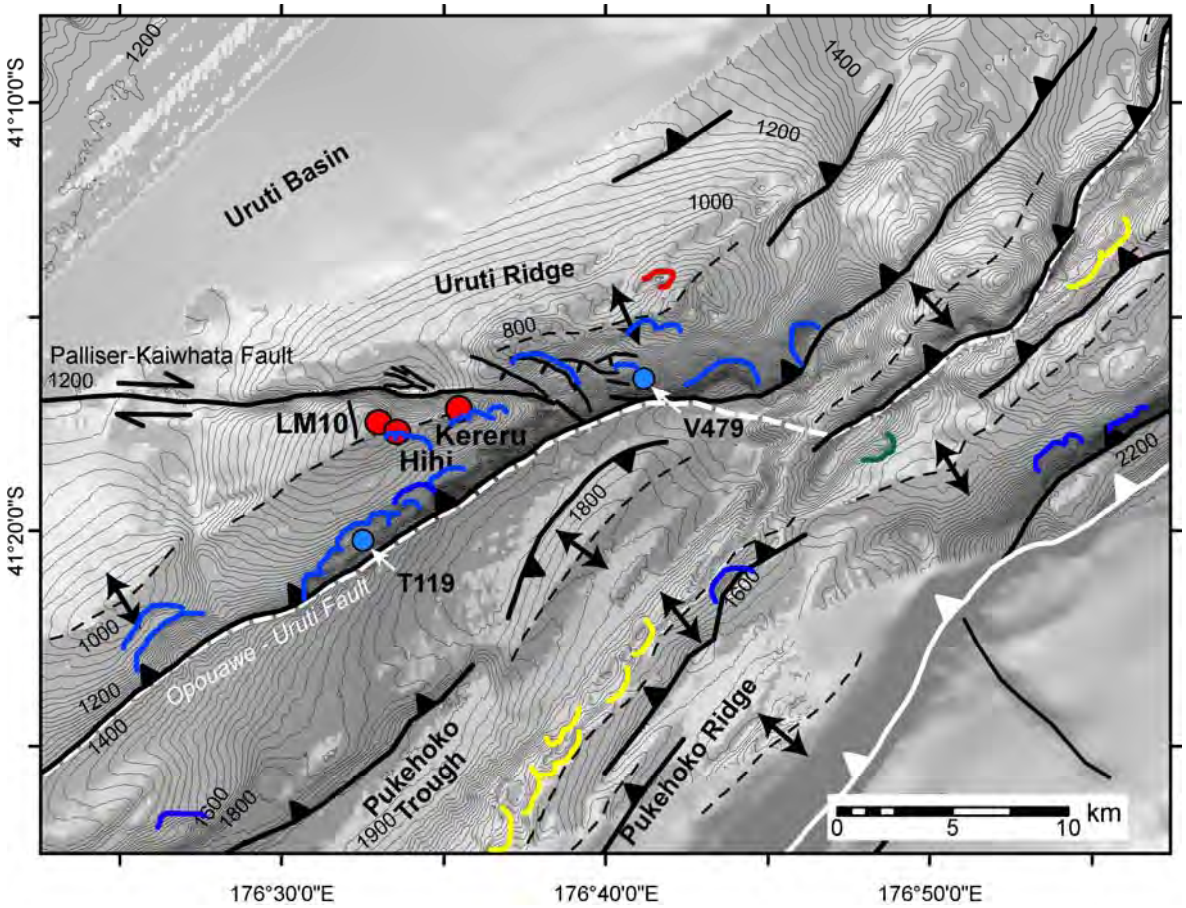

Figure 6.2: Uruti seep site showing: fault traces (black lines with teeth on upthrown side), anticline axes (dashed black lines), the deformation front (solid white line with teeth on upper plate), accretionary wedge–deforming backstop boundary (white dashed line), and landslide scars (blue, green and red). Landslide scars are distinguished by their location on antiforms as: backlimb (green), forelimb (blue) and not attributed (red). Modified from Barnes et al. (2009).

The stratigraphy of the three sites is broadly constrained (Barnes et al., 2009). At the Wairarapa site, Opouawe Bank straddles the boundary between the active accretionary wedge and deforming pre-subduction Cretaceous and Paleogene material, with the majority of the (south-western) ridge in the accretionary wedge. At Uruti Ridge, indurated early to mid Pliocene mudstone occurs between a foundation of pre-subduction Cretaceous and

Paleogene material and younger syn-tectonic cover sequences (Barnes et al., 1998a; Lewis et al., 1999). At Omakere Ridge, slope sediments directly overlie pre-subduction Cretaceous and Paleogene material.

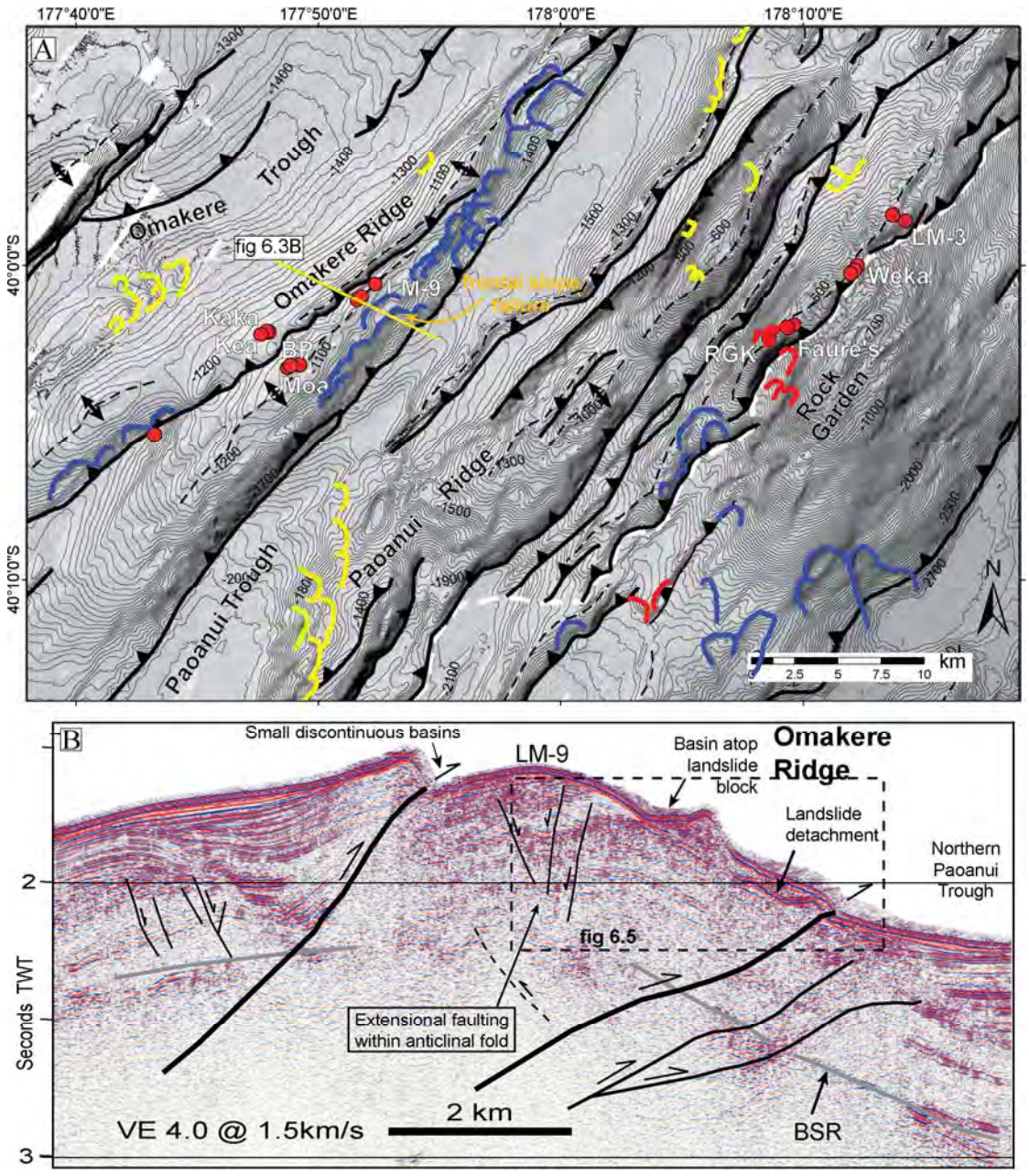

Figure 6.3: Omakere seep site. A) Showing, fault traces (black lines with teeth on upthrown side), anticline axes (dashed black lines), accretionary wedge–deforming backstop boundary (white dashed line), and landslide scars (blue, green and red). Landslide scars are distinguished by their location on antiforms as: backlimb (green), forelimb (blue) and not attributed (red). B) MCS reflection profile across Omakere Ridge illustrating the relationship between bathymetry-controlling structures and fluid-venting location LM-9. Location shown in A. Slope failure on the frontal limb is well imaged at depth and an enlarged interpretation of this area is presented in Figure 6.5. Modified from Barnes et al. (2009).

While across the Wairarapa site landslide scars cluster on the both flanks of thrust ridges, on the Uruti and Omakere sites landslide scarps predominantly populate frontal limbs of anticline ridges. Other less concentrated areas of landslide scars are also observed. The general distribution of landslide scars can be considered qualitatively in terms of three parameters: 1) the proximity of scars to vent sites; 2) the local slope gradient in the scar region; and 3) the proximity of scars to fault traces.

Fluid vent sites

All mapped fluid vent sites occur at or near ridge crests (N.B. one isolated inferred vent site in the Omakere site occurs off the ridge but has not been substantiated (Greinert et al., submitted)). Many of the vents have been identified by water column flares imaged with acoustic echo-sounder instruments (e.g. Jones et al., 2009; Law et al., 2009) and side-scan sonar images and as such the main vent sites are readily visible from surveys of the local regions. No vent sites have been identified on ridge flanks. Very few landslide scars occur in close proximity to vent sites as these predominantly occur at the crest or on the flanks of ridges in areas of greater slope gradient (Figure 6.4).

Bathymetric slope gradient

The spatial distribution of landslide-scar populations correlates well with slope oversteepening on thrust ridges (Figures 6.1-6.4). At the Wairarapa site the geometry and location of numerous landslides on trailing limbs are controlled by weak layers in the low-angle stratigraphy (Mountjoy et al., 2009a), whilst frontal-limb landslide populations are associated with incised gully systems in exposed, probably overconsolidated sequences in the older part of the accretionary wedge.

The highest concentrations of landslides at the Uruti and Omakere sites are on the frontal limbs of the Uruti Ridge (Figure 6.2) and Omakere Ridge (Figure 6.3), though these are not associated with gully systems. The frontal-limb slopes are generally steeper than trailing-limb slopes at these two sites, and it is apparent that this plays a role in the concentration of slope -failure scars. Slope-failure scars are not mapped across all steeply-sloping areas and in many case this is likely to reflect a lack of preservation of landslide features rather than a lack of slope failure in these locations. Trailing-limb-slope bedding-controlled landslides do not occur to the same extent as they do at the Wairarapa site, and this may reflect geomechanical properties of the stratigraphically-younger material forming Opouawe Bank. In summary, while isolated populations of landslide scars occur off thrust ridges (e.g. NW

corner of Figure 6.4C), the majority of scars occur on thrust-ridge flanks regardless of whether these host fluid vent sites.

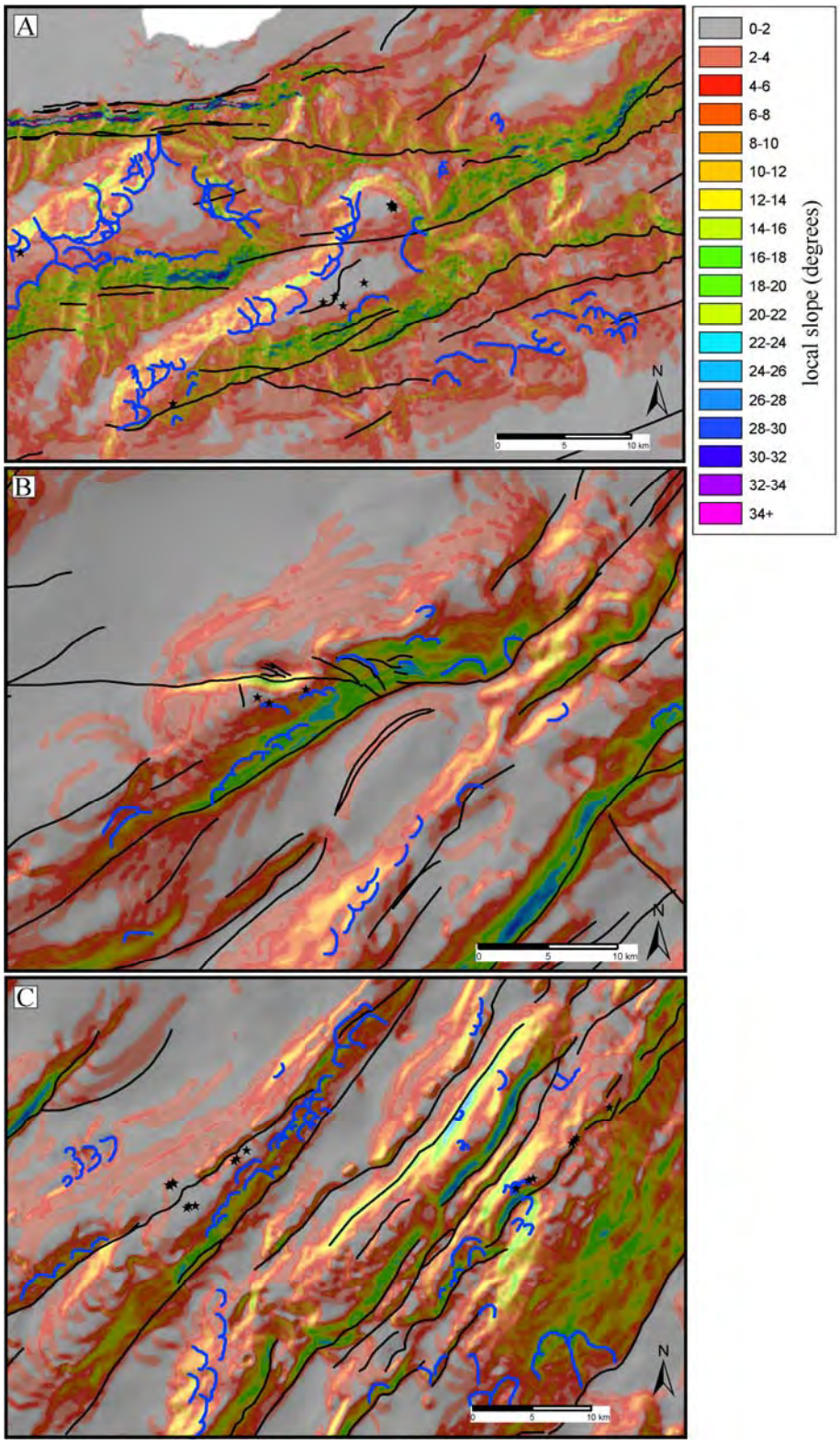

Figure 6.4: Slope-gradient maps of the three sites (following page). Landslide scars (blue), fault traces (black) and vent sites (stars) are plotted, for: A) Wairarapa; B) Uruti; and C) Omakere. Slope-gradient values are classified in 2 degree bins and are

the local slope derived from the adjacent upslope and downslope cells in ArcGIS®. The slope-gradient map and base shaded-relief map (slope-gradient map overlay has a 50% transparency) are derived from a 100 m DEM.

Fault traces

All three sites considered here have high concentrations of active-fault traces mapped across them. While it is not clear that there is a relationship between fault-trace location and landslide scarring, factors such as strong ground-motion focusing and rock-mass weakening in fault crush-zones are likely to be playing a role in slope destabilisation.

6.1.2 Deep-seated slope failures adjacent to vent sites

The majority of mapped landslides relate to evacuated scars. Additionally, two instances of deep-seated slope failures are interpreted where landslide failure-mass is retained in the scar area. These occur in direct proximity to fluid vent sites, on Opouawe Bank near Takahe/South Tower (Figure 6.1), and on Omakere Ridge near LM-9 (Figure 6.3). The proximity of these failures to vent sites raises the question of whether there may be a linkage between gas-hydrate occurrence and/or fluid venting and mass failure at these locations.

The structural model for the Opouawe Bank fluid vent sites developed in Section 4.2.1 infers that frontal collapse of the Opouawe bank is likely to be related to hanging-wall extension enabling fluid venting to occur. Mass failure is therefore a structural phenomenon rather than being fluid-seepage dependant. On Omakere Ridge the frontal collapse is poorly imaged in bathymetry (Figure 6.3A), but is well imaged in a MCS reflection profile (Figure 6.3B and 6.5). The Omakere Ridge failure is characterised by a displaced block with ponded sediment behind, disruption of acoustic stratigraphy, and strong acoustic-reflectivity defining a basal failure surface (Figure 6.5). All fluid seepage at this site is occurring at the anticline crest (i.e. LM-9 Figure 6.3A), and is interpreted as being released through a network of extensional faulting (Barnes et al., 2009) (Figure 6.3B and 6.5B). The bottom simulating reflector (BSR) occurs at over 0.5 seconds twt beneath the seafloor in Omakere Ridge, well below the basal depth of the landslide. This indicates that landslides are not related to instability of the gas hydrate stability zone.

Faure et al., (2006) document “slump scars” on the Rock Garden (Figure 6.3) and, noting that the depth of the scars coincides with the depth of BSR pinch-out, infer that “…gas hydrates are a significant, if not a controlling factor for [seepage and] seafloor instability along the Hikurangi Margin”. It is noted that the interpretation of gas hydrate influenced

failure of both Faure et al. (2006) and Crutchley et al. (2007) are at locations where the BSR pinches out at the seafloor. However, rather than being the norm for Hikurangi Margin cold fluid vent sites, the Rock Garden is the only site investigated during the New Vents program where the BSR does pinch out at the seafloor (Barnes et al., 2009), and in all other cases the BSR is located in the order of 0.5 seconds twt below the seafloor.

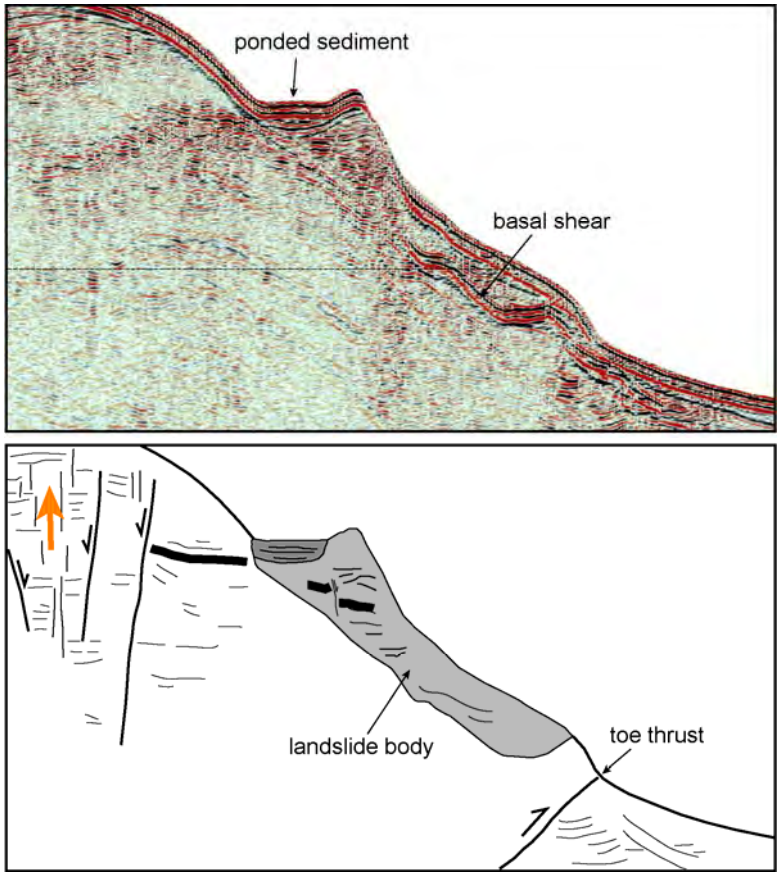

Figure 6.5: Uninterpreted and interpreted MCS reflection profile enlargement (from Figure 6.3), illustrating frontal-slope failure of Omakere Ridge.

6.2 Interpreted controls on mass failure in the vicinity of gas hydrates and fluid vent sites

It is apparent that all vent sites documented on the Hikurangi Margin occur on thrust-fault-propagated anticline ridges (Barnes et al., 2009). Likewise, the majority of landslide scars mapped during the New Vents study occur on structurally-controlled ridges (Figures 6.1–6.3). Propagating thrust faults and growing anticlines have several effects on the seafloor and the underlying rock material: 1) they generate positive bathymetry and steepen the seafloor slope-gradient; 2) repeated faulting weakens rock-material developing fault-damage zones, typically in regions of oversteepened slopes; 3) structural complexity may lead to dilation in the hanging wall and the development of structural permeability

(enabling fluid migration); and 4) fault rupture releases large amounts of energy in the form of strong ground motion.

Gas hydrate may affect slope stability in several ways: 1) Induce a strength increase due to hydrate (or ice) in pore spaces (e.g. Winters et al., 2007); 2) Induce a strength reduction via hydrate disassociation at the top of the hydrate occurrence zone, i.e. near the seafloor (e.g. Sultan et al., 2004b); and 3) Develop overpressure below the hydrate occurrence zone (Hornbach et al., 2004), leading to gas migration, excess pore-pressure generation and possibly material-strength reduction.

Large-scale disassociation of gas hydrate to free gas requires significant changes in pressure and/or temperature (Hornbach et al., 2004). Consequently, this is not a process that is likely to drive widespread slope instability over short time periods, but rather on a glacial–interglacial time frame (e.g. Paull et al., 1996). Given then the wide range of possible influences on submarine slope instability, and the wide distribution of submarine landslide scars irrespective of proximity to documented fluid vents and near-surface BSR's on the Hikurangi Margin, it seems unnecessary to invoke gas hydrate and fluid venting as major causes of slope instability.

The widespread instances of landslide scarring observed on the frontal slopes of structural ridges are likely to relate to both slope oversteepening and earthquake-generated strong ground motion, demonstrated to be dominant controls on submarine slope instability in active tectonic environments (Locat and Lee, 2002). It is certainly likely that gas-hydrate disassociation contributes to major slope instability at certain times during the sea-level cycle, however it is tentatively suggested that it is unlikely to have a significant influence during the current sea-level highstand period.

6.3 Chapter summary

This short chapter analyses the relationship between the spatial distribution of fluid vent sites, methane hydrate, and landslide scars mapped as part of the New Vents project (Barnes et al., 2009). While BSR's are present in seismic reflection data across much of the Hikurangi Margin, fluid vent sites ubiquitously occur at the crest of thrust-fault-propagated seafloor ridges. Evidence for slope failure is observed on all of the ridges that host fluid vent sites. However, landslide scars are ubiquitous features of thrust-fault-propagated ridges on the Hikurangi Margin regardless of whether fluid venting occurs. Landslide scars cluster on the seaward and landward facing sides of seafloor ridges at all sites, as well as

being distributed across adjacent slopes. The distribution of landslide scars is attributed to structurally-generated relief and the influence of earthquake-generated strong ground motion, and the role of fluid seepage, if any, is believed to be minor.

The spatial relationship between slope failure and the projection of the BSR to the seafloor has previously been used to infer that gas hydrates play a major role in slope instability on the Hikurangi Margin. This inference is not supported by the fact that there are few locations where the BSR projects to the seafloor, while there are numerous examples of submarine slope instability. The BSR typically occurs at ~0.5 seconds twt below the seafloor, far deeper than the majority of landslide basal surfaces. Oversteepened slopes on the Hikurangi Margin are either associated with, or occur within close proximity to, active tectonic structures. Slope oversteepening and seismically-induced dynamic loading are inferred to be the primary drivers of small- to medium-scale slope instability on the Hikurangi Margin.

Chapter 7: Synthesis and discussion

This thesis project is focused on the morphological and morphostructural development of canyon systems and slope domains on the tectonically active Hikurangi Margin of north-eastern New Zealand. The primary data sets used for analysis are high-resolution multibeam bathymetry data, multichannel and high-resolution seismic reflection profiles, and dated seafloor samples. The principal topic is the differentiation of the primary drivers that control the development of active margin canyon systems. This topic was identified as a research gap, not only for New Zealand's offshore environment but for much of the world's active tectonic margins. Special attention is given to the spatial and temporal relationships between active tectonic structures, to canyon and slope gully development, and to the bedrock mass failures that occur widely on active tectonic margins.

The present chapter synthesises the main findings of this study. In Section 7.1 these are summarised in terms of identified primary driver categories. In drawing together the key points of the project, this section implicitly includes the main conclusions. Reiterating these would be repetitive, so the remainder of the thesis concentrates on contextual discussion.

In Section 7.2 the implications of the study findings are discussed with reference to the development of canyon systems and slopes on active tectonic margins within the time frame of sea-level cyclicity. The resulting models are considered in the context of the Hikurangi Margin as well as generally in terms of global margins.

The development of high-resolution multibeam systems and the increasingly common acquisition of spatially continuous swath bathymetric data are enabling the advancement of the discipline of submarine geomorphology. While currently in its infancy, this discipline is likely to become widely practised in the coming decades. Section 7.3 considers the role of multibeam in analysing submarine geomorphology, specifically landslide systems, in terms of both what has been achieved in this project and what might be done in the future.

Finally, Section 7.4 outlines three possible future projects that could extend this study, using it as a framework and applying the techniques developed to other data sets.

7.1 Summary of findings related to the primary controls on canyon and slope development

This thesis draws on examples from the two study sites, Cook Strait and Poverty Bay, which contain the largest canyons on the southern and northern Hikurangi Margin respectively. While in both sites the large cross-slope canyons are deeply incised into the overriding Australian Plate, they occur in contrasting settings with contrasting slope morphology. The Cook Strait sector of the Hikurangi Margin is in the tectonic transition zone, characterised by both compressional and strike-slip faulting. Here the large (1800 km^2) multi-branched Cook Strait canyon system, which is deeply incised into the shelf, and other non-shelf-indenting canyons occur on the adjacent continental slope. The Poverty Bay site is on the northern margin where structure is purely compressional and dominated by margin-parallel thrust faults. Seamount subduction has formed the Poverty re-entrant, hosting the Poverty Canyon system; well-formed gully complexes on the upper slope; and large mass-failure deposits. The focus of the project has varied between the two sites. In Cook Strait the principal objective has been to understand controls on the development of large incised canyon systems crossing active margins. In Poverty Bay more attention has been given to smaller-scale processes including gully development and the role of large mass failures in upper-slope evolution. Consequently, the development of the large Poverty Canyon system is not a focus of this thesis but is considered in the context of canyon development on the wider Hikurangi Margin.

While Cook Strait and Poverty canyons are among the most prominent on the Hikurangi Margin, they occur within a large population of canyons across a range of scales (Figure 7.1). In addition to the specific examples of the two focus sites, the significant data set from the larger population of canyons is used to consider the controls on canyon development along the length of the obliquely convergent active margin.

7.1.1 Regional tectonic setting and structure

The active tectonic setting is the first-order control that differentiates canyons on active margins from those on passive margins. It defines macro-scale boundary conditions, both enabling and restricting cross-margin canyon development, and includes factors such as: plate convergence rate and obliquity; structural control on the gross margin morphology; and structural control on basin development and geological configuration.

Effects of regional tectonic setting on geomorphic processes

Major active margin canyons are fundamentally erosive features that are predominantly cut into bedrock material. They differ from, for example, submarine channel-fan systems, which are mainly hosted by unconsolidated sediment bodies originating in the same fan-channel processes. The gross morphology of active margin canyons can be related to the heterogeneity of the material into which they are incised, as defined by geological and tectonic boundary conditions. These controls provide a framework for the processes that erode/excavate canyons. As different processes may be efficient at the removal of different materials, spatially variable susceptibility to erosion can be a fundamental control on the extent of canyon incision.

The distribution of geological units on active tectonic margins is strongly controlled by structure. On convergent margins these are typically characterised by margin-parallel structurally controlled ridges and basins. Deep listric thrust structures may exhume older, typically more indurated rocks from greater crustal depths, providing a margin-parallel barrier to canyon incision. A transverse (strike-slip) component in convergent margins can lead to a divergence from this barrier-to-incision effect of compressional structure, as structures also develop oblique to the margin trend. Basin configuration may also reflect long-term geodynamic history, and the evolution of basin alignment may occur over a significant period of time.

Examples from this study

In addition to the two main canyons considered in this study, a number of other bedrock incised cross-margin canyons occur along the Hikurangi Margin. The majority of these are clustered to the southern end of the margin, between Kaikoura and Southern Wairarapa; while the Poverty Canyon system is the only shelf-to-trough sediment conduit that is incised deeply into the upper plate on the northern margin (Figure 7.1A).

The Hikurangi Margin has an inboard basement “backstop” of Mesozoic Torlesse greywacke that forms the axial ranges of the North Island, part of the east coast Wairarapa Ranges and much of the northern South Island. This is generally a relatively non-erodible material in comparison to more recent sedimentary units, and in the terrestrial setting exhibits few locations where breaks occur in the axial range (Cook Strait being the main one). Outboard of the basement backstop of the North Island, and defining the immediate backstop to the modern accretionary wedge of the subduction system, is the deforming

foundation of Cretaceous and Paleogene rocks. Between Wairarapa and East Cape the upper sequences of the Hikurangi Margin imbricated frontal wedge are dominated by margin-parallel slope-and-shelf basins, typically of Miocene to recent age. These basins are bound by bathymetric ridges on the slope and large seismogenic structures on the shelf, which commonly uplift older reef-forming sequences.

The skewed distribution of canyons on the margin can be related to structural setting, geology and the gross morphology of the margin. A series of cross-margin bathymetric profiles illustrate the lateral variability of the overall margin slope (Figure 7.1B). In the north the margin is steep (>5º in places) and relatively narrow (~50 km), reflecting high shortening rates and subduction erosion (Collot et al., 1996; Lewis et al., 1998; Wallace et al., 2004). The "yellow profile" illustrates the steep northern margin slope outside of the influence of the Poverty and Ruatoria re-entrants (Figure 7.1A&B). In the central margin, the low-taper accretionary wedge is characterised by a low angle (~1.5º) slope and wide margin (>100 km). In the south the margin narrows to ~30 km and steepens significantly. On the southern margin the shortening rate decreases to <20 mm/yr as much of the plate motion transfers into transverse structures (Figure 7.1A). The lateral variability of the margin morphology is well illustrated by the slope-gradient map presented in Figure 7.1C.

Figure 7.1: Structural morphology of the Hikurangi Margin (following page). A) Map of the margin showing the major deformation front thrust faults (heavy red); the uppermost slope or outermost shelf thrusts (lighter weight red); and the two main strike-slip faults on the southern margin. The continental slope has a blue transparency from the shelf edge to the deformation front illustrating the variable width of the margin. The dashed white line indicates the inboard extent of the modern accretionary wedge. Relative plate-convergence rates and direction shown in red. Blue text shows margin normal shortening rates after Wallace et al. (2004). The overall slope and width of the margin is shown at the location of the margin normal profiles presented in B. Figure modified from Barnes et al. (2009). B) Margin normal bathymetric profiles plotted at 10 x vertical exaggeration. Profiles are colour coded to match locations shown in A. C) Slope-gradient map for the entire offshore Hikurangi Margin based on a 100 m DEM along the continental slope, and a 250 m DEM elsewhere. Slope-gradient scale is classified in 2 degree bins.

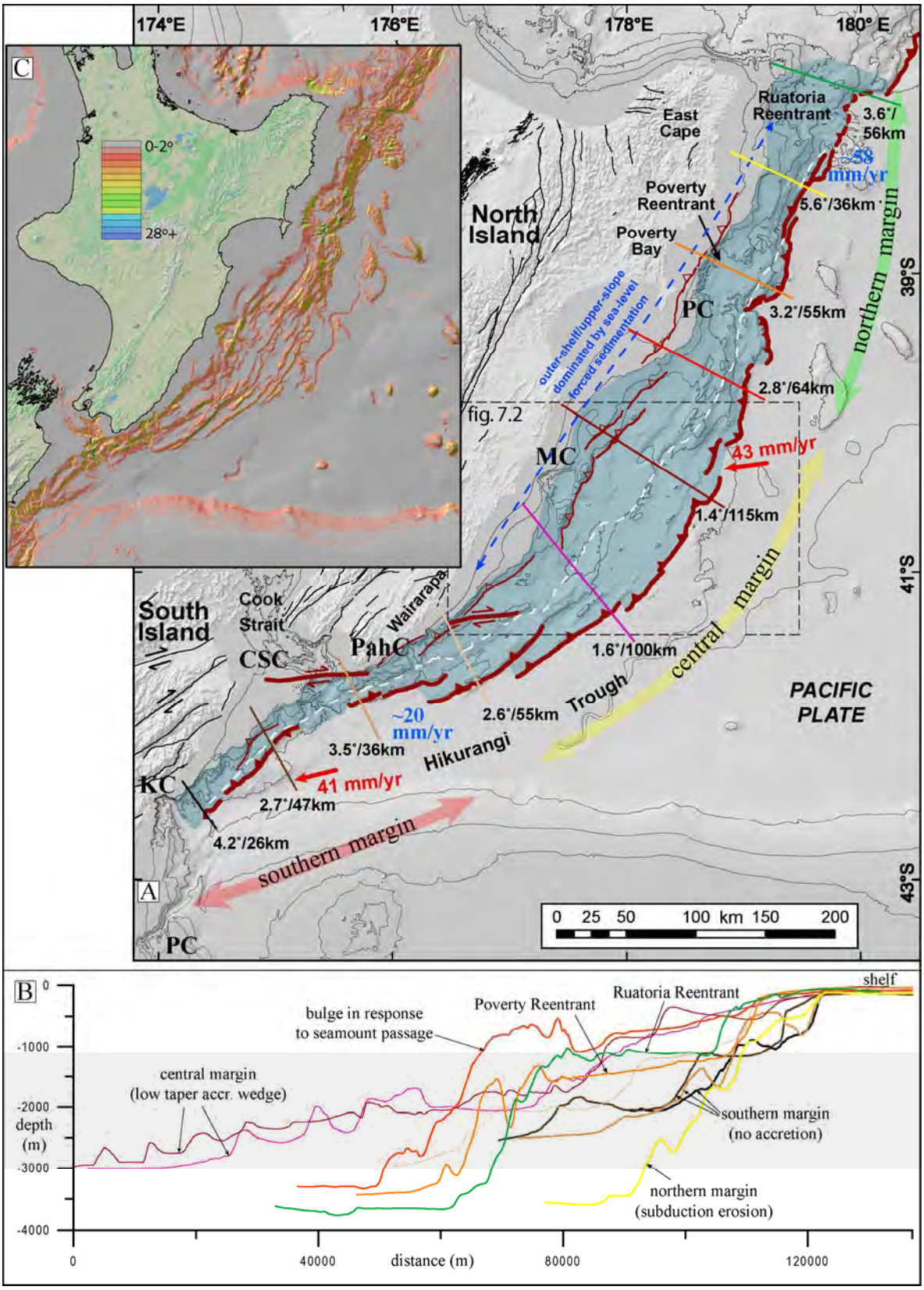

Figure 7.1 (caption on previous page)

On the northern margin the Poverty Canyon formed as a shelf-to-trough canyon system in a subsided re-entrant that formed as a result of seamount subduction (Lewis and Pettinga, 1993). On the outer Poverty Bay shelf a sequence of (now inactive) imbricated thrust faults has uplifted Cretaceous to Miocene rocks to the near surface. The upper-slope canyon heads of the Poverty re-entrant are incised into these rocks, and are inhibited from incising into and across the continental shelf by their presence, as well as by the continued uplift on other presently active shelf structures. Without the seamount impact-related subsidence in the Poverty re-entrant it is likely that no canyons would be present on the northern margin, due to the inhibiting effect of erosion-resistant material exhumed by margin-parallel structures.

To the south of the Rock Garden (Figure 7.2), where seamount subduction is forcing oversteepening (Barnes et al., 2009), the margin is characterised by an approximately 120 km length of low-angle accretionary wedge with well-expressed ridge-and-trough morphology. In the middle of this section of the margin Madden Canyon is deeply incised into the continental shelf to within 15 km of the coast. The large (>650 km^2) canyon head is constrained behind a large thrust-propagated ridge and has incised through this barrier to exit on the mid to upper slope. On the slope the canyon terminates at Porangahau Trough at least 80 km from the deformation front, the cross-slope passage of the canyon being baffled by 4–5 ridge-and-trough pairs (Figure 7.2).

From East Cape to south of Madden Canyon structures at the deformation front form an irregular but relatively continuous trace (Figure 7.1A). From Wairarapa south the trace of the deformation front makes a series of well-expressed landward steps defining the narrowing margin. From this point, strike-slip structures appear, aligned sub-parallel to the Pacific Plate plate-motion vector. These structures accommodate the increasingly oblique convergence of the plate boundary and transfer slip from the subduction zone into the strike-slip Alpine Fault zone of the South Island. From Pahaua Canyon the southern margin is dominated by incised cross-slope canyons.

At Cook Strait the margin-parallel ridge and basin pattern finishes. Three sedimentary basins underlie much of the extensive shelf area, and no margin-parallel thrust faults occur on the outer shelf (refer Mountjoy et al., 2009a - Figure 1). These basins have been related to the presence of Cook Strait between two mountainous islands of the New Zealand landmass (Lewis et al., 1994), and are believed to be fundamental to enabling the Cook Strait Canyon to develop as New Zealand’s only large shelf-indenting system. The Cook

Strait canyon system is incised across the shelf into these basin sequences, and the geometry of the upper multi-armed canyon system is defined by basin geometry. The absence of ongoing uplift on structures at the outer shelf region of Cook Strait is a significant differentiating factor that allows propagation of the canyon into the shelf zone. The width of the shelf at this location reflects the tectonic history.

South of Cook Strait the steep slope of the narrow margin hosts multiple incised canyon systems (Figure 7.1). It is inferred that the widespread occurrence of canyons here reflects the effect of lower shortening rates on margin geometry, transverse structures on the slope and shelf, and high levels of earthquake ground shaking.

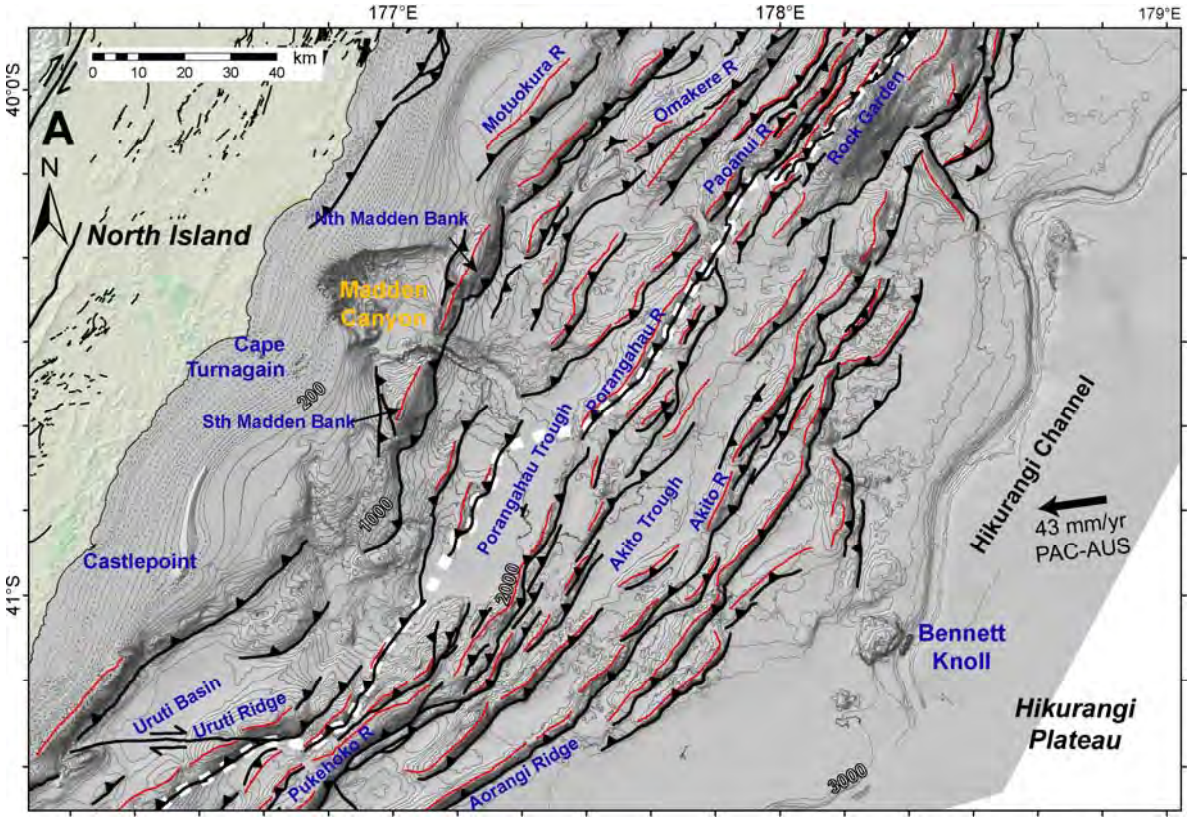

Figure 7.2: Morphostructure of central Hikurangi Margin. Tectonic and physiographic features of the low-taper accretionary wedge showing active thrusts (black) and ridge traces (red). Madden Canyon is incised into the outer shelf but terminates in Porangahau Trough on the mid-upper slope. Figure modified from Barnes et al. (2009).

At a high order, the distribution of slope-incised canyon systems on the Hikurangi Margin can be related to the regional tectonic and geologic setting. Steep narrow active margins

subject to oblique tectonic are apparently most susceptible to the development of large, deeply incised submarine canyons.

On the northern margin subduction erosion leads to margin oversteepening, which inhibits the development of slope relief and canyon systems. Canyons are able to develop in upper-plate subsidence areas (seamount re-entrants). On the central margin the low-taper accretionary wedge inhibits cross-margin canyon development through the formation of multiple margin-parallel ridge-and-trough pairs reflecting thrust-fault imbrication. On the southern margin strike-slip structures disrupt the margin-parallel fault geometry enabling shelf incision of canyons. The steep southern margin experiences significantly less shortening than the northern margin, allowing canyon systems time to evolve without the effect of subduction erosion.

The main factor that has enabled the largest Hikurangi Margin canyon system, Cook Strait Canyon, to become significantly shelf-indenting is the lack of margin-parallel contractional structure on the outer shelf, combined with the presence of erosion-susceptible basins underlying the shelf. This reflects the location of Cook Strait at the transition from subduction related compression to strike-slip faulting, a result of the geodynamic evolution of the Hikurangi Margin.

7.1.2 Tectonically influenced base level

The development and evolution of river-cut canyon systems in terrestrial fluvial catchments is strongly influenced by variation of stream base level, which exerts a fundamental control on the time-varying incision and aggradation of these systems (e.g. Whipple, 2004). Base level for fluvial systems is the lowest elevation to which they can flow, and the ultimate base level for terrestrial landscapes is sea level. Submarine geomorphic systems do not have such a clearly defined lower boundary, and little consideration has been given to base level in studies concerning the development of seafloor canyon systems and slopes.

It is widely recognised that the morphometric form of submarine channel networks is analogous to that of fluvial systems, with turbidity currents and grain-flow events playing much the same role as sediment-laden rivers and streams in terms of erosion of the landscape (Mitchell, 2005). Base-level control will similarly be exerted on submarine channel networks as the depth to which canyons can incise must be limited by a particular bathymetric benchmark.

Effect of base-level variation on geomorphic processes

Channels across areas of active tectonic uplift must compete with vertical deformation by bed erosion to maintain a theoretical equilibrium profile, or "grade", to their terminus. Natural processes are inherently temporally variable, and the response of a channel to combined regional and localised structural uplift will be episodic as well as both temporally and spatially variable. The base-level response of submarine channel networks may be present as axial channel steps or knickpoints, and avulsed and laterally entrenched channel reaches. Furthermore, as is being found in terrestrial systems, the up-channel propagation of a knickpoint may be accompanied by a direct response of increased erosional activity in channel coupled "hill-slopes" adjacent to the incising channel.

Examples from this study

In the Cook Strait canyon system several examples of canyon reach response to base level are observed.

Lower Cook Strait Canyon crosses the main upper-plate shortening zone of the southern Hikurangi Margin. Although the precise nature of cross-canyon structures is poorly constrained, due to the lack of high-quality MCS data, the canyon must be responding to vertical motion on these structures. Additionally, a component of regional tectonic uplift is likely to be occurring (e.g. regional uplift is recorded in coastal terraces and sequences). A "sub-catchment" to the middle reaches of lower Cook Strait Canyon exhibits a well-developed knickpoint in the lower channel, and comparable magnitude knickpoints occur in minor adjacent catchments. A knickpoint in the Cook Strait Canyon main channel is positioned immediately upstream of this sub-catchment. The step(s) in the main canyon stem are interpreted as transient down-cutting in response to combined regional and local uplift. Knickpoints in the sub-catchments are a secondary response to this main channel lowering, effectively lowering the local base level of tributary canyons.

Further down Cook Strait Canyon the channel has become entrenched by some 200 m, creating an abandoned "terrace" interpreted as a base-level response. As the canyon is forced to incise deeper to maintain grade, it either cuts a preferentially deeper channel in one location (an "inner gorge"), or migrates laterally and deepens at the same time, as in this case.

Numerous other areas in the Cook Strait canyon system exhibit axial channel steps and irregularities that may be a response to base-level control. The Poverty Canyon system also

shows several areas with channel knickpoints in isolated canyons, as well as multiple adjacent canyons. Although these have not been focussed on in this study, the Poverty Canyon system is likely to be responding in much the same way as Cook Strait Canyon, as it likewise crosses several tectonic structures driving vertical seafloor deformation.

Base-level control on submarine canyons is difficult to define explicitly. The regional base level for Hikurangi Margin continental slope canyon systems is the Hikurangi Trough. The majority of sediment exits the canyon to this basin, and slope gradients decrease to almost zero. A component of material delivered to the trough is transported north in the Hikurangi Channel, however the lower boundary remains the floor of the Hikurangi Trough.

7.1.3 Propagating tectonic structure

On active tectonic margins the majority of bathymetric relief is generated by, or influenced by, tectonic deformation at the seafloor. The propagation of tectonic structures, resulting in fold-related deformation and fault break-outs, controls a changing physical environment upon which surface-transport, erosional, depositional and oceanographic processes are over-printed. The interaction of the topography with surface processes is often considered in a static manner. However, given that canyons are likely to develop over 10^4–10^6 yr time frames, the role of propagating tectonic structures in canyon evolution is significant.

Effect of propagating tectonic structure on geomorphic processes

Sediment-flow paths on the continental slope route around relief where possible; consequently, tectonically-generated, time-varying, bathymetric relief has a role in the formation and location of submarine canyon systems. If present, canyons will divert around structurally generated relief and may pass between structures at fault segmentation zones. In some instances (e.g. where structure is continuous) this may not be possible and canyons must incise through structural relief. In this case the rate of vertical relief development must be offset by the channel-bed incision rate to enable canyons to maintain grade across a propagating structure.

Surface-rupturing earthquakes also have an effect on seafloor processes. In areas of limited relief (e.g. the continental shelf) repeated fault rupture leading to the development of surface relief may create a locus for preferential sediment routing, facilitating canyon inception. Fault rupture across an existing sediment conduit can effect the erosional behaviour of the channel and may initiate a period of channel entrenchment, for example in

the case of thrust-fault rupture with co-seismic fold development and fault breakout across the lower part of a channel incised into the (now uplifted) hanging wall.

Structural deformation can also have a significant impact on the rock mass adjacent to active faults, and this can be a controlling factor in large mass failures. Many mountain-range-scale collapses affecting subaerial landscapes can be attributed to a controlling structural influence (e.g. Agliardi et al., 2001; Ambrosi and Crosta, 2006), and similar processes act on submarine landscapes.

Examples from this study

The combination of detailed structural and geomorphic mapping from high-resolution bathymetry enables analysis of the role of propagating structures in geomorphic development. Examples of the role of propagating structures in canyon location and geometry, and the role of structurally influenced deep-seated slope failures on canyon development are provided below.

The Opouawe and Pahaua canyons on the Wairarapa slope show strongly linked relationships to structurally generated relief. Opouawe Canyon deflects around two thrust-fault-propagated anticlines, forcing the canyon to travel along the strike of the margin before exiting downslope to the Hikurangi Trough. In contrast, the Pahaua Canyon has been forced to incise through the northern end of Pahaua Bank, as there is no alternative/viable along-slope route. This has led not only to deep incision through the structural ridge but also to lateral excavation in the canyon-head area, upslope of the propagating structure. The sequence of events and processes that lead to a canyon incising into a propagating structural ridge are difficult to determine. Two scenarios are possible: 1) the canyon is antecedent to the propagating structure and is able to keep pace as relief develops; or 2) The propagating structure develops “blocking” relief inhibiting cross-slope transport processes. In the second scenario sediment accumulates upslope of the ridge to the point where overtopping occurs and the canyon begins to incise into relief, eventually achieving some “equilibrium profile”, which may or may not be maintained through competing uplift and incision. Episodes of infilling and excavation are evident in the head area of Pahaua Canyon, suggesting that at times the ridge does create a barrier to the downslope transport of material introduced into the canyon. Regardless of the initial setup conditions driving canyon incision through a propagating structure, it is apparent that on longer timescales canyon-head infilling and (re)incision is a temporally variable cyclic process.

Fault rupture across the lower reaches of smaller-scale canyon (gully) systems developed in the hanging wall of a major thrust fault is interpreted to have initiated a pulse of incision to migrate up antecedent drainage systems. Six adjacent small-scale canyon systems on the Wairarapa slope exhibit an incised lower-canyon reach with a significant (~300 m high) steep headwall at similar distances upslope of the thrust-fault trace. Upslope of the incised lower canyon reach, relict channel morphology indicates previous episodes of canyon development. In some channels the profile contains more than one step, possibly indicating ongoing response to multiple hanging-wall-uplift and fault-breakout events. Serial multibeam has demonstrated that material is actively being removed from these gully systems.

In comparison to Opouawe Canyon, the well-formed sinuosity of Cook Strait Canyon is difficult to relate to actively propagating structure. The lack of high-quality MCS data through this area limits mapping of active structural activity across the canyon. However, it is reasonable to infer that active structures on the continental slope are continuous across the lower canyon. The lower Cook Strait Canyon is deeply entrenched (>1000 m) and exhibits very well-formed meander loops. From the models developed from adjacent slope canyons it is logical to suggest that the form of these strong meander loops is shaped in response to deflection around propagating structures. Fluid flowing on a gently inclined slope will naturally develop a meandering sinuosity and likewise it might be suggested that the meanders in lower Cook Strait Canyon result from hydrodynamic processes. It is, however, considered unlikely that there was ever a continuous, smooth slope at this location for unconstrained fluidised flows to occur and develop such a meandering pattern. Any structurally generated relief on the slope will affect the path of downslope fluid flow, and therefore this is the more likely process defining canyon geometry.

The position and geometry of parts of the upper shelf-indenting component of the Cook Strait canyon system are affected by discrete structures. Wairarapa Canyon is incised into the footwall of the Wharekauhau thrust fault, suggesting that the propagation of this structure and subsidence in its footwall are likely to have played a role in the inception of the canyon at this location. The strike-slip BooBoo Fault crosses the Cook Strait canyon system where the three upper canyon arms merge. At this point the canyon makes a “dog-leg” turn before crossing the slope, interpreted as reflecting ~3 km of dextral offset on the BooBoo Fault.

Numerous large-scale canyon wall collapses have been mapped in the Cook Strait Canyon and adjacent canyons with mapped active-fault traces as bounding features. In Nicholson Canyon a large (~1 km^3) mass-failure scar occurs adjacent to the strike-slip Wairarapa Fault, which ruptured in 1855 generating a M8.2 earthquake. Multiple canyon-parallel extensional grabens occur here, and deep-seated dilatational deformation of the canyon wall is inferred to be related to movement on this structure. Other very large (~10 km^3) failures in the shelf-indenting canyon also have bounding structures likely to have played a role in deep-seated slope deformations. On the continental slope the frontal collapse of a thrust-propagated ridge is related to localised extension in a structural step-over. The canyon wall scale of slope collapses related to structural slope deformation indicates they are likely to be a significant process in canyon enlargement and slope evolution.

Propagating tectonic structures are a principal distinguishing feature of active margins and have a significant impact on canyon location, geometry and activity. Spatially and temporally variable seafloor relief development can be considered a high-order control on evolving active margin morphology and sediment-transport systems.

7.1.4 Sea-level cyclicity

Orbitally forced sea-level fluctuation has a significant impact on offshore sedimentary systems (e.g. Posamentier and Vail, 1988). During glacial periods sea level is lowered by up to ~120 m and the coastline shifts to the outer shelf in many locations, enabling some canyons to become directly coupled to the littoral zone and/or fluvial systems. Sea-level lowstand periods are recognised as times of significantly increased sediment supply to offshore areas (e.g. Carter and Manighetti, 2006).

For the majority of submarine canyons sea-level lowstand is the only time at which they receive direct input of coarse clastics (sand and gravel) from coastal sources. Some canyons remain “coast-coupled” during highstand (e.g. Kaikoura Canyon (Lewis and Barnes, 1999); Monterey Canyon (Greene et al., 2002)). It has been proposed that without a significant alternative sediment input mechanism canyons remain largely inactive during highstand periods (e.g. Baztan et al., 2005). Therefore, primary questions to consider are whether canyons on active tectonic margins are able to remain active during sea-level highstand periods, what drives that activity, and what form it takes. While it is generally difficult to quantify rates of erosion in submarine landscapes, comparative morphological character can provide a proxy for relative activity.

Effect of sea-level cyclicity on geomorphic processes

Canyons connected to littoral or direct fluvial input during lowstand periods are expected to receive coarse clastic material leading to top-down erosion of the channel bed. Conversely during highstand periods, in canyons not receiving direct sediment input, top-down erosion is unlikely. Canyons may become active by other mechanisms under highstand conditions.

In tectonically active regions the frequent occurrence of high-intensity ground-shaking events means that (bedrock) slope destabilisation within canyons is likely to continue irrespective of canyon-head sediment input. Canyons must continue to incise if they are to keep pace with uplift across actively propagating structures (discussed in Section 7.1.3), which appears to be the case with propagating base-level response in the Cook Strait canyon system (refer Section 7.1.2).

Sea-level cyclicity also plays a pivotal role in controlling where, how much and what type of sediment is deposited on the upper slope. This has a significant, if indirect, impact on canyon- and slope-shaping processes and is given detailed attention in Section 7.1.5.

Examples from this study

A model of contrasting lowstand vs highstand canyon activity is developed from a type example sub-catchment of the Cook Strait canyon system. This sub-catchment landscape has three components: 1) the upper reaches of the catchment have a smooth morphology interpreted as being draped with a blanket of fine-grained sediment; 2) the central catchment has a well-defined but partially smoothed gully morphology; and 3) the lower reach comprises a very steep and continuous canyon wall and gently sloping canyon floor. The central catchment is interpreted as a relict landscape from the last sea-level lowstand, at which time this canyon would have been coupled to either a littoral or fluvial sediment source. At this time the majority of the catchment would have exhibited this morphology as being coupled to the active axial channel. Following sea-level rise, direct sediment input is discontinued and the upper catchment receives diffuse sediment input from, e.g., sediment plumes. The catchment is now relict but activity is rejuvenated from the bottom up in response to base-level signals from the main Cook Strait Canyon (refer Section 7.1.2).

The processes of highstand infilling and bottom-up rejuvenation of canyon systems are apparent in numerous places in the Cook Strait and Poverty Bay study sites. The sedimentary throughput and activity of the main Cook Strait Canyon is poorly constrained, but the following observations suggest that this canyon experiences relatively regular top-

to-bottom sediment throughput under the current sea-level regime: 1) sediment cores from the canyon axis in three separate locations show multiple (if undated) graded units reconcilable with stacked sandy turbidites; and 2) landslide scarring is apparent across much of the canyon landscape, however very little debris can be observed on canyon floors.

The Cook Strait sector of the Hikurangi Margin lies within an area affected by high-recurrence, large-magnitude earthquakes, including a historical Mw8.2 event on a fault terminating in the Wairarapa/Nicholson canyons. Earthquakes are modelled to generate PGA levels of 0.5 g on a 475 yr return time (Stirling et al., 2002). Furthermore, a forthcoming revision of the national seismic hazard model to include new and revised offshore structure in the area (Mountjoy et al., 2009a; Pondard et al., in prep) results in an increase in the estimated magnitude of ground shaking at this return time (Stirling et al., 2009). It is difficult to reconcile a landscape that is affected by this level of strong ground motion (and widespread mass movement), and has a strongly immature, erosive morphology, with an inactive canyon system. Strong tidal flows in Cook Strait mobilise significant amounts of sediment and may provide persistent sediment input to Cook Strait Canyon, facilitating through-going sediment-transport activity under sea-level highstand.

7.1.5 Stratigraphic variability

Within sedimentary "bedrock" basin sequences inherent deposition-controlled anisotropy plays a critical role in defining the mode of sedimentary process that may subsequently erode that material.

Effect of stratigraphic variability on geomorphic processes

The geotechnical properties of bedding parallel "weak layers" within bedded sedimentary bodies are well documented to have a strong control on landslide geometry, failure mode and the general susceptibility of slopes to failure. Additionally, high-permeability bedding layers can influence slope stability. Direct characterisation of marine sedimentary sequences at depths likely to affect bedrock slope instability (commonly in the order of 100 m below sea level) is generally not possible. However, indirect characterisation of stratigraphic variability is possible based on: terrestrial analogies; comparative marine studies; sequence stratigraphic concepts; and the character of bedded sequences in MCS data. Other factors may also play a role in slope instability including: the effect of the distribution of sedimentary bodies on the type and magnitude of slope-erosion processes; and the effect of rock mass defects on mass-failure characteristics.

Examples from this study

It is possible to draw on both study sites for examples where stratigraphic variability is controlling the distribution and type of slope processes.

On the continental slope of the Cook Strait sector of the margin, landslides on the landward limb of seaward-verging anticlines are strongly stratigraphically controlled, failing on bedding-parallel surfaces that dip out of the slope at ~2 degrees. Strong acoustic reflectors in both MCS and 3.5 kHz seismic data are interpreted as tephra horizons within the stratigraphic sequence. It is possible that these are either: 1) chemically altered to smectite clays forming preferentially-weak surfaces upon which sliding occurs; or 2) of higher porosity, hosting fluids in which excess pore pressure can develop during earthquake events. In upper Cook Strait Canyon, large-scale (~10 km^3) canyon-wall collapses are also stratigraphically controlled and are likely to be similarly failing on preferentially-weak horizons and/or be controlled by horizons of relatively high permeability.

On the upper slope of the Poverty re-entrant, extensive bedded sedimentary sequences deposited during the sea-level lowstand (the lowstand wedge, LSW) host large, deep-seated mass-failure complexes. These are stratigraphically controlled and the mode of failure (as submarine earthflows) is interpreted to directly reflect both the vertical heterogeneity of geotechnical properties and the lateral homogeneity of continuity of the deposits. Towards the northern lateral boundary of the Tuahini Landslide Complex steepening stratigraphic dip may be reflected in a changing mode of failure, culminating in a transition from deep-seated failure to shallow sheet failure characteristic of other areas of lowstand wedge deposits. Deep-seated mass failures in the upper part of the Poverty re-entrant appear to be limited to those areas where LSW deposits occur.

7.1.6 Fluids and gas hydrates

Gas hydrate and cold-fluid venting are widely recognised features of subduction margins (e.g. Kvenvolden, 1993; Lewis and Marshall, 1996). Gas hydrates are interpreted to occur across much of the Hikurangi Margin from the widespread occurrence of BSRs in MCS data, and methane-rich fluid venting is documented in several locations including in the Cook Strait sector of the Hikurangi Margin (Barnes et al., 2009; Greinert et al., submitted).

Effect of fluids and gas hydrates on geomorphic processes

Fluid venting has been proposed as a primary driver for the upslope development of minor canyons/gully systems in thrust ridges through repeated slope failure initiated by seepage

forces (Orange et al., 1997). However, a review of terrestrial and extraterrestrial studies of seepage erosion by Lamb et al. (2006) concludes that while seepage erosion readily cuts valleys in unconsolidated sediments, it is unlikely to be the primary agent of valley incision into rock.

Gas hydrate disassociation may occur with changing pressure and temperature (e.g. during fluctuation sea levels) leading to excess pore pressures and mass failure (e.g. Nixon and Grozic, 2007; Owen et al., 2007). Gas hydrate is proposed to be a significant agent in the erosion of the seafloor in the Hikurangi Margin (Pecher et al., 2005).

Examples from this study

Opouawe Bank hosts 5 + methane vent sites, as well as exhibiting a strong BSR in MCS data. Well-formed gully development on the frontal slope of Opouawe Bank (and Palliser Bank) is of the type previously attributed to fluid-seepage erosion. Following analysis of the spatial relationship between gully morphology, BSR distribution and fluid vent site distribution, it is concluded that fluid seepage is unlikely to play a critical role in gully formation. Instead it is inferred that factors such as slope oversteepening, earthquake-generated strong ground motion and fault-zone weakening are likely to play a more significant role. No clear relationship is observed between mass failure and gas hydrate occurrence.

Analysis of landslide scar distribution across three well-documented Hikurangi Margin fluid-venting areas shows no conclusive relationship between landslide scarring and fluid vent site distribution. Conversely landslides occur across all thrust ridges imaged with high-resolution multibeam data and significant fluid vent sites are limited to some isolated ridges. Factors such as high levels of focused strong ground motion and tectonically forced bathymetric oversteepening are believed to be the controlling influences on landslides and gully systems eroding the flanks of thrust-fault-propagated ridges. The potential large-scale release of gas with fluctuating sea level may be a different mechanism to that considered here and is likely to play a significant role in slope destabilisation.

7.1.7 Bedrock landslides

Bedrock mass failures are a ubiquitous feature of active tectonic margins and occur across a wide spectrum of scales, from a few tens of cubic metres to thousands of cubic kilometre failures affecting the entire height of the continental slope. Many case studies exist relating bedrock landslides to hazards, hydrocarbon exploitation and engineering works (e.g.

Shanmugam, 1996; Kvalstad et al., 2005; Greene et al., 2006; ten Brink, 2009); but studies relating bedrock landslides to the geomorphic development of submarine canyons and slopes are few (Sultan et al., 2007). Middle-depth multibeam systems (e.g. Simrad EM300) now provide for large areal coverage of the seafloor enabling regional-scale assessments of the impact of landslides on canyon and slope geomorphology through detailed analysis of bedrock landslides at scales previously limited by data resolution.

Role of bedrock landslides in submarine geomorphic processes

Bedrock landslides have the potential to rapidly remove large volumes of material from the continental slope and introduce it to canyon channels and slope basins. The occurrence of large bedrock mass failures disturbs the rockmass, preconditioning it for further failure, and exposes underlying material to erosive processes. Bedrock mass failures can also affect adjacent slopes by both mass loading and support removal potentially leading to further destabilisation.

Examples from this study

Bedrock mass failures are widely recognised across the Hikurangi Margin. In both study areas these are shown to be playing an important role in canyon and slope development.

In the upper Cook Strait canyon system, ~55% of canyon walls are interpreted as affected by bedrock mass failure. This interpretation is primarily based on extrapolation of the morphology of mapped mass failures that affect the canyon wall in Cenozoic basin sequences, from canyon rim to canyon floor. These retain the majority of failure material in the landslide area and host numerous small-scale landslides that are progressively enlarging the canyon cross-sectional area. In Nicholson Canyon failure of probable Mesozoic basement rock has removed ~1 km^3 of material from the canyon wall, and extensional deformation at the canyon rim/shelf edge suggests that further failure is likely in the future. The regular occurrence of large-magnitude earthquakes in the Cook Strait area implies that (earthquake-triggered) bedrock landslides are a regularly occurring process over millennial and possibly even centennial timescales and, based on observations of their role in the enlargement of the upper canyon, are a primary contributor to canyon enlargement.

Gully systems on the frontal slopes of thrust-fault-propagated anticline ridges in the Cook Strait sector of the Hikurangi Margin contain widespread evidence of head-zone mass failure as well as more regional mass failure off frontal slopes. Immature ridges in the early stage of relief development also exhibit mass-failure scars. A model is proposed where

large-scale mass failure on structurally controlled propagating relief removes unconsolidated sediment and encourages gully formation. Smaller-scale failures play a role in individual gully development and gully spacing. Incision depth evolves as a function of relief development.

In the Poverty re-entrant, the occurrence of widespread mass failures on the upper slope can also be related to gully development. The upper re-entrant headwall is dominated by incised gullies of varying magnitudes. Large-scale mass-failure deposits occur in depositional basins downslope of these (PDA), and on a higher level plateau to the north (TLC). A northward migration of landslide activity is observed in both of these landslide complexes and is related to the progressive development of upper-slope gully systems. A population of similarly sized upper-slope gully systems is related to the scar area for the PDA, indicating that bedrock mass failure is a precursor to gully development. The TLC likewise shows a northward progression in landslide age, interpreted from relative morphological maturity. Where the landslide has fully excavated the LSW, fine-scale gully formation has been initiated. Gullies are not expected to be able to develop into mature systems until larger (PDA-style) failure occurs at the slope base. The development of this northern re-entrant headwall is inferred to have taken place approximately since sea level stabilised to its present level.

7.2 Conceptual framework for canyon initiation and evolution on active tectonic margins

The type and activity of geomorphic processes influencing canyon development and shaping submarine slopes on active tectonic margins shows significant variation between glacial and interglacial time periods (Figure 7.3). While some processes continue independent of the glacio-eustatic sea-level cycle, many are directly dependent on it. Independent processes include: tectonic uplift/subsidence, structural deformation, earthquakes, volcanism and weather events (though the magnitude and frequency of weather events may vary with an indirect relationship to sea-level stage due to other climatic controls). Dependent processes include: sediment supply, shoreline location (littoral zone), oceanographic currents, wave energy and possibly seabed gas release. From these simple lists it is apparent that the main processes occurring independently of the sea-level cycle are related to tectonics and so are specifically related to active tectonic margins. In the absence of tectonic processes, passive margins are strongly controlled by fluctuating sea level, climate and oceanography.

In Figures 7.4F&G the conceptual trend of tectonic activity, both the propagation of individual structures and the regional seismic moment release, are shown in terms of multi-sea-level cycle trends. An enlargement of these trends illustrates how these processes are occurring on shorter (10^3–10^4 yr) timescales (Figure 7.4E). Tectonic processes continue independently of the sea-level cycle and overprint its influence on slope and canyon processes on active margins.

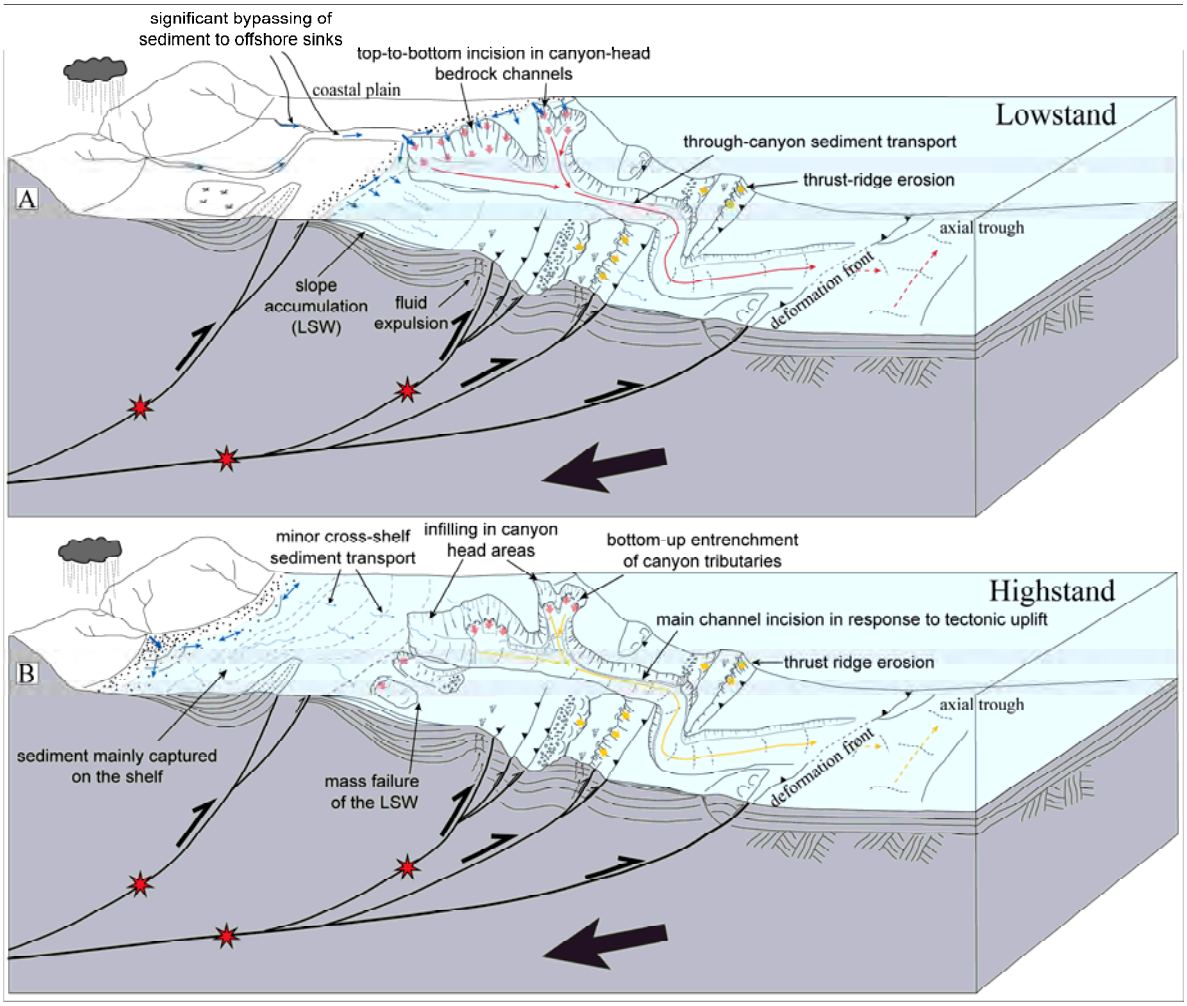

Figure 7.3: Submarine landscape response to contrasting sea-level stands on an active margin. A) Lowstand. B) Highstand. Arrow colours indicate activity levels. Red arrows: regularly active. Yellow arrows: intermittently active. Small red arrows indicate areas of active erosion. Thick blue arrows indicate significant proximal sediment dispersal. Thin blue arrows indicate paths of distal sediment dispersal mechanisms. Red stars illustrate seismic activity.

It is the forcing and exacerbation of local-scale processes by sea-level cyclicity that influences spatial and temporal variations in canyon development. It is possible to contrast lowstand and highstand sea levels for an active margin submarine slope-and-canyon system

in terms of both scenarios, and to consider the areas of the landscape affected by them at each sea-level stage, as well as independent of sea-level stage (Figure 7.3 & 7.4). In the following sections the geomorphic response of active margins to sea-level variation is discussed in the context of the findings of this study.

7.2.1 Canyon and slope activity on an active margin during lowstand

Classical models suggest that the majority of canyon activity takes place during sea-level lowstand. At this time the continental shelf is all but non-existent and major fluvial systems will cross the shelf and may be coupled to canyon and continental slope systems. In addition, coastal littoral processes occur near the outer-shelf/upper-slope transition. From studies of both terrestrial productivity and accumulation in ocean basins (Posamentier and Vail, 1988; Carter and Manighetti, 2006), lowstand periods are recognised as times of a dramatic increase in sediment yield. In active tectonic landscapes, the source of material is commonly relatively close to the sink on account of coastal orogenic development, and therefore a broad size distribution of material is able to reach the coast. In the lowstand environment there is a dichotomy between those areas of the continental slope system (canyons and gullies) that enable the "bypassing" of large quantities of sediment (typically the coarser fraction) and those areas that accumulate large volumes of (finer-grained) material (Figure 7.3). During the lowstand the contrast between these parts of the margin is likely to be higher than during the highstand, in response to both the increased sediment load and the proximity of shelf sediment-transport processes.

It is proposed that the following spatially and temporally distributed geomorphic processes and landscape responses dominate active margin slopes and canyons during sea-level lowstand.

Sediment-source canyon coupling

The most fundamental contrast between low- and highstand conditions is the coupling and decoupling of canyon systems to fluvial and littoral sediment sources as the coast migrates between the inner and outer shelf (Figure 7.3). Figure 7.4B illustrates the difference across the sea-level cycle between sediment delivery to the coast and that to submarine canyon systems, and shows the comparative amplification of sediment delivery to canyons. Regardless of sea level, the terrestrial production of sediment is highly variable, and it is delivered in pulses following large "landscape perturbation" events such as intensive weather episodes and large-magnitude earthquakes (e.g. Mw8+). The lack of shelf basins to

act as “sediment baffles” during sea-level lowstands means that these pulses of material will be delivered to canyon systems: 1) with comparatively minimal loss to intermediate storage areas (i.e. the continental shelf - Figure 7.3); and 2) rapidly following an event. Additionally, where large-magnitude earthquakes occur in sufficient proximity to a canyon, the submarine geomorphic system is likely to respond with significant intra-slope sediment production from strong ground motion triggered deep-seated and surficial mass failures.

The direct introduction of large volumes of sediment to canyon-head areas in active tectonic environments will lead to repeated gravity flow events that are likely to occur regularly, triggered by earthquake strong ground motion. These grain-flow events will be both erosive and depositional, depending on factors including volume, composition, source location and travel path. In large submarine canyons, such as the Cook Strait and Poverty Canyon systems, multiple sediment input points reflect the occurrence of multiple canyon heads. Consequently, most parts of the canyon will be active during sea-level lowstand via intermittent slope-channel coupling.

Figure 7.4: Conceptual cyclic activity of non-coupled canyon systems on active tectonic margins in terms of a generalised sea-level cycle and tectonic influences (following page). Small-term fluctuations in sea level are ignored and only the longer-term trend is considered. The vertical axis for all plots is in time relative to the sea-level curve timescale at left. A) Sea-level curve simplified from compilation of Caputo (2007) dashed in black with the general first-order trend (~100 kyr cycles) shown in red. B) Relative change in sediment supply at the coastline vs into submarine canyons. C) Incision in canyon-head areas in comparison to mid to lower parts of a canyon system. D) Enlargement of the curve in C illustrating the inferred trend on 10^2–10^3 yr timescales. Top: Incision of canyon-head area showing fluctuating magnitude of incision. Bottom: Incision and aggradation in the mid to lower canyon. E) Shorter term 10^2–10^3 yr tectonic activity for seismic moment release (top) and displacement on an individual structure (bottom). F) Displacement on individual faults over 10^5 yr timescales. G) Long-term regional seismic moment release, illustrating a constant trend over the 400 kyr timeframe shown.

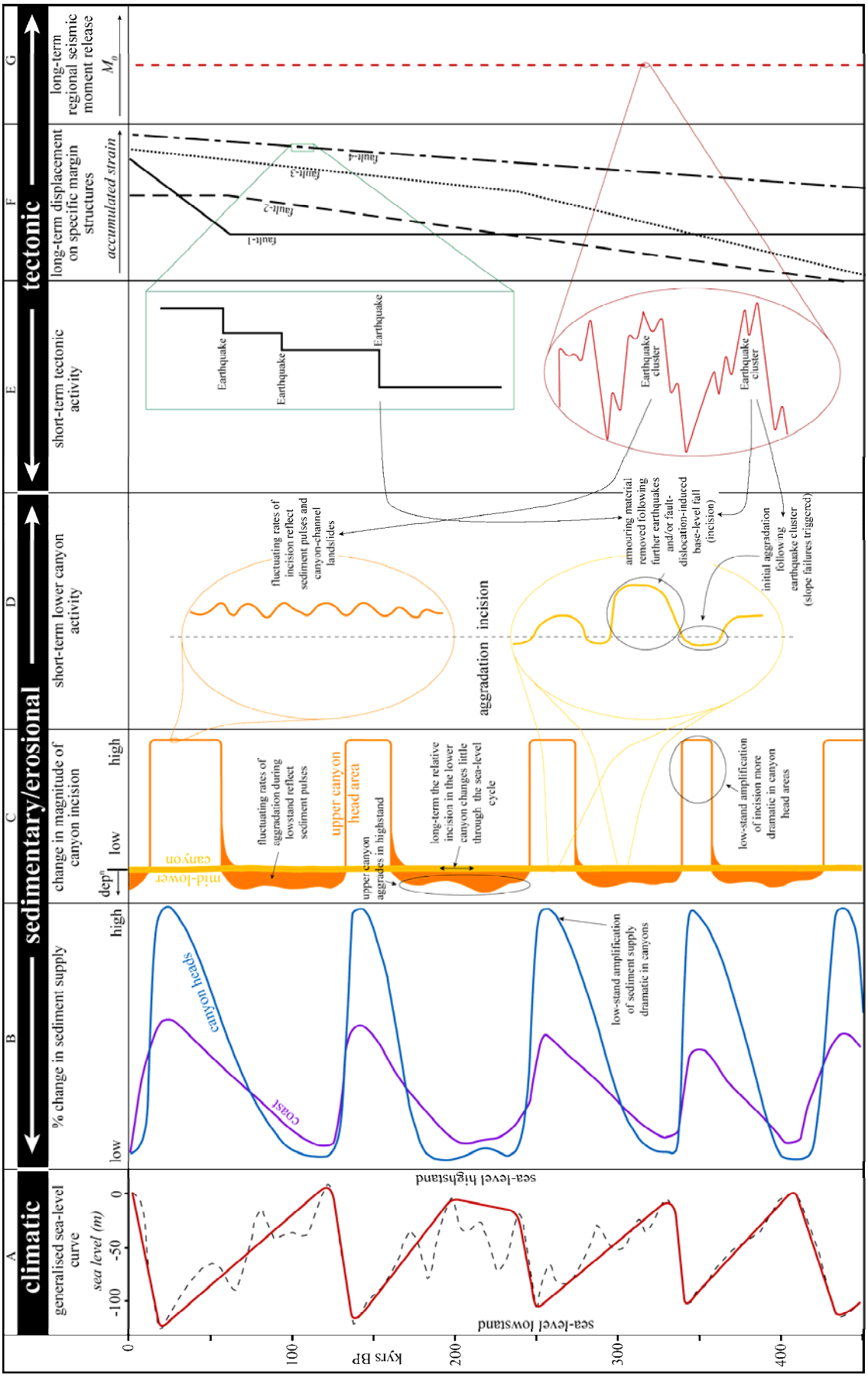

Figure 7.4 (caption on previous page)

Canyon-head areas where direct sediment-source coupling occurs will be subject to regular erosive scouring by sediment gravity flows. The initiation of incision will occur at a threshold level, when sea level lowers to the point where canyons can become coast-coupled (Figure 7.4C). At this point the relative change in the magnitude of incision will be significantly increased, as prior to this threshold being reached upper canyon areas are depositional zones. While canyons are coast coupled, canyon-head areas of these are expected to be dominated by incision (Figure 7.4D).

Transient aggradation and sediment removal

It has been proposed that, as the shore line progrades towards the shelf edge with lowering sea level, canyon infilling occurs because of increased sediment supply but without direct fluvial connection to canyon heads (e.g. Baztan et al., 2005). At maximum lowered sea level, for canyon heads that do become coupled to fluvial systems, re-excavation of accumulated material will occur but non-coupled canyons will continue to infill. On the Hikurangi Margin the morphology of canyon heads that encroach on the shelf break suggests that all of these receive sediment from shelf sources, either fluvial or littoral, and incise during sea-level lowstand.

In addition to the controlling effect of the sea-level cycle on sediment flux at relatively long time scales, large influxes of material will be introduced for a period of time following landscape perturbation events (Figure 7.3D). Thus, periods of aggradation and excavation in active margin canyon systems occur not just in response to the sea-level cycle but within shorter time frames as well. Excavation of sediment that transiently accumulates in canyons may occur by processes such as erosive hyperpycnal flows, and turbidity currents/debris flow transformations from mass failures.

In tandem with transient aggradation and sediment removal, parts of the canyon are subject to tectonic uplift/subsidence that can influence incision. As with terrestrial fluvial systems, areas of active uplift across submarine canyon channels may affect long-profile gradients, forcing channel erosion and incision to maintain grade and driving knickpoint incision through the system. With high sediment input to the system during sea-level lowstands, transient aggradation will armour channels and may limit lowstand amplification of bedrock incision in the mid to lower reaches of principal canyon channels (Figure 7.4C).

With the majority of canyon-system channel networks periodically active during sea-level lowstands, canyon slopes will likewise be active in response to toe erosion. Where axial

and lateral incision of canyon channels occurs, the submarine landscape will respond as lateral destabilisation leads to slope failure. This response is likely to propagate upslope in retrogressive fashion, with renewed destabilisation in response to further incision in principal channels.

Sediment accumulation on the upper slope

With the littoral zone near the shelf edge, sediment supply to the whole continental slope is enhanced. Where canyons are not siphoning off sediment to slope and deep-ocean basins, large volumes of sediment accumulate on the upper slope (Figure 7.3A). This part of the lowstand systems tract, or the "lowstand wedge" (LSW), is recognised on many types of margins including active margins. On the Hikurangi Margin, upper-slope LSW accumulation is identified in discrete stratigraphic units representing sea-level cycle deposition since the early Pleistocene (Lewis, 1973; Paquet et al., 2009, this study). In places the LSW is well preserved and shows little indication of substantial syn-depositional erosion or large-scale mass movement. From this study it is concluded that, where upper-slope deposition occurs during sea-level lowstand, sediment is largely preserved until sedimentation rates decrease with sea-level rise (i.e. the rate of sedimentation $\geq$ rate of removal by surficial failure).

Oceanographic variation

A direct oceanographic effect of changing shorelines is a variation in the tidal regime as significant embayments/inland seas are created or destroyed by fluctuating sea levels. The focusing and enhancement of tidal currents in specific areas of the continental shelf may have a significant effect on sediment distribution and seabed scour. Additionally, sea-level lowstand is accompanied by a major reconfiguration of ocean current regimes that can affect sediment dispersal.

Summary of lowstand landscape activity

As sea level lowers towards lowstand, it is accompanied by both a progression of the shoreline towards the outer shelf, and increased sediment supply to outer-shelf and slope areas. Tectonic processes continue independent of the sea-level cycle. The response of active tectonic margin submarine landscapes to sea-level lowstand periods can be summarised as follows:

- Where canyon and gully systems exist on the upper slope they will receive direct/increased sediment input from fluvial and/or littoral sources. Upper-slope

canyon heads are eroded by processes including gravity flows and hyperpycnal currents. Incision of bedrock channels in the upper parts of submarine canyon systems is likely to occur in the majority of cases during sea-level lowstand.

- Earthquakes continue to perturb the submarine landscape, mobilising slope and canyon fill material. Ongoing tectonic deformation of the seafloor drives base-level changes that propagate through the canyon/slope system and influence incision.
- Areas down-canyon of the upper bedrock channels are subject to transient aggradation as the system is overpowered by pulses of sediment. While this is subsequently removed by gravity-flow processes, sediment accumulation may temporarily armour bedrock channels and limit incision in the mid to lower canyon. Consequently the amplification of incision during sea-level lowstand may not be as dramatic in lower canyon areas as it is in upper-canyon/canyon-head areas.
- In areas of the upper slope where canyons do not occur, enhanced sediment supply leads to deposition and the development of distinctive lowstand systems tracts.

7.2.2 Canyon and slope activity on an active margin during highstand

With the initiation of sea-level rise and the progression to the highstand, the majority of canyon rims and canyon heads are "de-coupled" from the coastal system and lie at water depths of 100 m+. Consequently, direct sediment input into the majority of slope canyon systems is dramatically reduced (Figure 7.4B). This may not be the case if: 1) canyons are shelf-incised up to the coast and continue to be coupled to fluvial and/or littoral sediment-transport system (e.g. Paull et al., 2003); or 2) processes in shelf water depths are able to transport material to the canyon head, stimulating regular down-canyon sediment transport (e.g. Palanques et al., 2006). The number of canyons that remain sediment-source coupled are few, however. In general the spatial and temporal distribution and magnitude of geomorphic processes in submarine canyons and on the adjacent slopes contrasts with those occurring during sea-level lowstand.

Infilling of canyon heads

As sea level rises and the shore line retreats landward, offshore sediment supply begins to wane. In the early phase of the transgression remobilisation of shelf sediments by the migrating wave-abrasion zone is likely to result in continued supply via current-transport processes. It is apparent that the heads of upper-slope canyons that do not remain sediment source coupled become infilled and cease to be shelf-to-trough sediment conduits (Walsh et

al., 2007; Mountjoy et al., 2009a). This is shown in Figure 7.4C by the switch to deposition in the upper canyon incision trend. It is likely that a significant amount of this infilling takes place soon after the initiation of the marine transgression, although ongoing off-shelf sediment-transport processes continue to deposit minor amounts of sediment in upper canyon areas under highstand conditions (Alexander et al., submitted).

This top-down infilling does not, however, mean that submarine canyon systems on active tectonic margins cease to be active during periods of elevated sea level.

Bottom-up erosion of tributary canyon systems

On passive margins there are few mechanisms to drive highstand activity in the lower part of canyon systems if direct sediment input is not occurring at the top end. However, in active margin canyon systems the ongoing influence of tectonics provides a mechanism to maintain activity in perpetuity. Where canyons cross zones of active tectonic uplift they must respond with channel down-cutting to maintain grade across active structures. The period of the sea-level cycle during which canyons are coupled to sediment sources (maximum lowstand) is in the order of 10–20 kyrs. This leaves 80+ kyrs of the sea-level cycle when canyons are not receiving direct sediment input but the propagation of tectonic structures continues. Assuming a conservative 1 m/kyr vertical uplift rate across a thrust-propagated mid-slope anticline, this would create several tens of metres of uplift across canyon long profiles between sea-level lowstands. It would be difficult for canyon systems to recover from this profile disturbance if all the down-cutting needed to maintain grade from shelf to trough occurred during the comparatively brief lowstand period. It is apparent that major active margin canyons do generally achieve this grade, and it is likely that canyon axis incision occurs throughout the sea-level cycle.

Without the armouring effect of pulses of greatly increased sediment supply, any down-canyon sediment gravity flow may, at certain locations, be able to erode into bedrock substrate. Thus, while event recurrence may be lower during highstand periods, and canyon throughput intermittent, channel incision into bedrock is able to take place under highstand conditions (Figure 7.4C&D). The bottom-up propagation of tectonic knickpoints is a predicted mechanism by which bedrock incision of canyon axes occurs (e.g. Mitchell, 2006), as is well documented in fluvial catchments (e.g. Crosby and Whipple, 2006). Where a knickpoint propagates up-canyon past a tributary canyon, the tributary channel will correspondingly begin to incise in response to the perturbation of its local base level, i.e. the main canyon floor (Mountjoy et al., 2009a). This pulse of incision can then migrate

up tributary channels, driving bottom-up rejuvenation of the tributary slopes through slope-channel coupling. The propagation of these knickpoints is through a combination of head-wall mass failure and grain-flow diffusion. It is likely that the majority of activity takes place during or following large-magnitude earthquakes as these will trigger failure of canyon slopes, which may transform to erosive sediment gravity flows. The initial impact of earthquake swarms is likely to be channel aggradation following seismically triggered slope failures. Further earthquakes will trigger failures that re-excavate infill material enabling incision into the bedrock channel and up-canyon propagation of knickpoints (Figure 7.3B & 7.4D). The extent to which knickpoints can propagate may be limited by the decreasing catchment area, reflecting a decreasing potential for erosive sediment-flow generation, as is observed in terrestrial fluvial catchments (Crosby et al., 2007).

Remobilisation of lowstand sediment bodies by deep-seated mass failure

The large volumes of material that accumulate as the upper-slope lowstand wedge are significant potential sources for mass failure as they are typically bedded, normally consolidated to lightly over-consolidated, geomechanically weak and gently dipping sequences. Analysis as part of this study suggests that deep-seated mass failures that impart a lasting imprint on stratigraphic sequences develop within these sediment bodies once deposition decreases following sea-level rise. The remobilisation of this material provides a significant sediment source to the lower parts of canyon systems, in locations where slope failure areas are coupled to canyons via sediment pathways. Mass failure of the lowstand wedge is a recurrent process that, in some locations, repeatedly occurs at the same point of the sea-level cycle. Deep-seated bedrock failures may be precursors to upper-slope gully initiation, and therefore slope gully systems can evolve under highstand conditions.

Summary of highstand landscape activity

Sea-level rise is accompanied by landward migration of the coastline, and a corresponding reduction in both overall and direct sediment supply to offshore areas as the majority of canyons become de-coupled from direct sediment sources. Active tectonic margin submarine canyon systems and associated landscapes respond to this in several ways:

- Canyon heads become infilled where these are not coupled to direct sediment sources (i.e. fluvial/littoral).
- Ongoing seismic activity triggers mass-failure events across the canyon and slope system.

- Canyons respond to ongoing local tectonic uplift by incision and knickpoint propagation up principal canyon channels and into tributary canyons.
- Tributary canyons are rejuvenated from the bottom up in response to a lowered local base level (main canyon channel).
- Lowered sediment supply limits channel-bed armouring, and erosive sediment flows are able to incise into bedrock channels in lower canyon areas. This may occur at similar rates to during the sea-level lowstand.
- Redistribution of the lowstand wedge by deep-seated mass-movement processes provides a significant intra-slope sediment source.
- In summary: while the head areas of canyon systems become inactive and infilled under sea-level highstand conditions, areas of the lower reaches of canyons actively incise during this time because of the influence of tectonics.

7.2.3 Processes that continue independent of sea-level control

Some processes contributing to the geomorphic development of submarine canyon landscapes persist independently of the sea-level cycle, and are generally restricted to deep-water areas of active margins. Specifically, on the Cook Strait sector of the Hikurangi Margin it is apparent that thrust-fault-propagated ridges on the continental slope are eroding by mass failure and gully incision, and it is proposed that it is continuing irrespective of sea level.

Landsliding and gully erosion on structurally propagated relief

Compressional tectonic deformation leads to unstable slopes through oversteepening (thrust ridges) as well as being focus sites for earthquake-generated strong ground motion. Thrust ridges principally erode by bedrock slope failure and gully development. The expulsion of fluids via structural permeability may play a minor role in thrust-ridge slope instability. However landslides occur widely on thrust-ridge flanks where fluid venting has not been documented, suggesting that fluid expulsion is not the controlling factor in the erosion of ridge flanks. It is proposed that the development of gullies is enabled by slope failure in the early phase of ridge development, exposing underlying overconsolidated material that can be sculptured by sediment gravity flows. Ridges can develop more than a kilometre of relief, with overall slopes up to 20°, and local slopes up to 45° that are inherently unstable and enhance the erosional potential of sediment gravity flows. On the forelimb slopes of

thrust ridges, where the majority of landslide scarring occurs, multiple imbricate thrust-fault breakouts weaken the rock mass in fault-damage zones, and earthquake-generated strong ground motion is focused in the hanging wall. The erosive development of these ridges will continue independent of the sea-level cycle and continue to provide an intra-slope sediment source. The processes are of course interdependent with other aspects of submarine landscape activity that vary with the sea-level cycle, such as the temporal variation in the activity of canyons at the slope toe.

7.3 Quantitative morphometric analysis of multibeam datasets: identifying the signature of geomorphic processes

High-resolution multibeam datasets are revolutionising knowledge of the seafloor as they resolve the detail of surface features at tens-of-metres scale with continuous coverage of hundreds of square kilometres. This unprecedented view of the seafloor is opening the path for developing fields of research drawing on techniques that quantify the morphometrics of terrestrial landscapes. Many terrestrial landscape morphometric studies now rely on very high-resolution (~1 m) digital elevation models (DEMs) generated using lidar technology. Though the resolution of DEMs derived from middle-water-depth multibeam echosounder measurements is an order of magnitude coarser (~10 m at best), the data sets are in some ways comparable to terrestrial datasets as many processes shaping the submarine environment are correspondingly an order of magnitude larger. Very few studies have been published that use quantitative morphometrics to analyse multibeam datasets, and the methodologies are still in their infancy. However, with almost total reliance on remote sensing for submarine geomorphic studies, these will become increasingly important tools.

Quantitative morphometric analysis vs subjective interpretation

In this thesis a landslide case study has used modified techniques that were developed for analysing surface roughness characteristics in lidar data and delineating the location and extent of earthflows in terrestrial landscapes. Rather than being concerned with mapping where landslides are, in this study the technique has been used to delineate the location of internal deformation within an individual landslide body (Mountjoy et al., 2009b). The technique has been successful in that it has isolated important features in the debris surface roughness that were not apparent when the landslide was initially mapped using traditional geomorphic landscape interpretation techniques. Following the application of morphometric analysis it is apparent that the Tuahini Landslide Complex is behaving as an

active earthflow. This type of landslide has not been previously described in the submarine environment and the implications of its occurrence are significant.

Implications of active landslides in the submarine environment

Active landslides on terrestrial hillslopes are classified by Cruden and Varnes (1996) as "…those that are actively moving", whereas inactive landslides are "…those that last moved more than one cycle of seasons ago", and anything in between is considered dormant. The use of "seasons" in submarine landslide studies for the determination of activity is generally not relevant, as these have less impact on submarine slopes. Many examples of repeatedly active terrestrial landslides involve ongoing reactivation of previously failed landslide debris under the control of excess pore-water pressure (EPP) generation, predominantly a result of precipitation. If submarine landslides are behaving similarly, with EPP generated by processes such as earthquakes, static loading and gas release, they might be periodically active over the cyclic time frame of these processes. Therefore, a landslide activity vs inactivity definition needs to be developed specifically for submarine landslides. Developing such a schema is beyond the scope of this study, but any framework may need to account for triggering mechanisms for landslide movement, recurrence interval of that process and the lapsed time since previous events, and also consider the permeability of stratigraphic sequences and their susceptibility to EPP development. The occurrence of a class of dormant landslides on submarine slopes has important implications for engineering works, hazard assessments and sediment-transfer studies.

While the landslide interpreted as an earthflow as part of this study cannot be shown explicitly to be currently active, morphological features indicate that it is most likely to have developed through repeated failure over a sustained period of time, suggesting that it is at least dormant (possibly inter-seismically). The failure of landslides in this manner has several implications. The assessment of landslides as tsunamigenic is very dependent on their volume and runout velocity. By developing as an earthflow, a large-volume landslide complex can be constructed by numerous small-scale failures that runout at low velocities. Consequently the assumption of a single-event displacement and tsunami generation for a large-volume landslide deposit would be incorrect. Active landslides pose significant problems for seafloor engineering works, as they do for terrestrial engineering projects, e.g. the placement of telecommunication or power cables. In landscape-evolution and sediment-

transfer research studies active landslides erode landscapes and supply sediment on an ongoing basis, rather than at a point in space and time.

The interpretation of submarine earthflows raises a huge number of future research avenues that could be pursued to definitively show mobility, and to further understand the processes that drive the mobility of such landslides.

7.4 Future research directions

This study is in a field of research that is in its infancy. Submarine geomorphology focused on high-resolution multibeam is likely to become a major area of research in future years, and it is intended that aspects of this project will provide a foundation for further studies in this area. Additionally, it has become apparent that there is a significant amount of research to be done to better understand active tectonic margin submarine landscapes under highstand conditions. In this section three proposed directions for future studies are considered in terms of science questions, general methodologies and data requirements.

7.4.1 Application of quantitative morphometric analysis to gully formation

Closely spaced, linear, incised gully systems are ubiquitous features of steep slopes across submarine landscapes on active margins. Morphometric quantification could be applied to better understand aspects such as: gully system age; dominant formative processes; and level of activity under current conditions. The combination of quantitative morphometric analysis with other techniques such as sedimentological age constraint and seismic reflection data could provide a template for understanding these aspects across gully complex populations over large areas.

The fundamental research question that this science would contribute to is: “What is the distribution and activity of erosional processes shaping active margins, and what controls these processes?”

Numerous EM300 multibeam datasets collected on New Zealand’s offshore margins image slopes that are incised by gully systems. The environments in which these occur include: active margin slopes where significant sediment input occurs; active margin slopes where no significant sediment input occurs; and, passive-margin areas where no significant sediment input occurs. The approach of the study would be to make a comparison of the morphometric attributes of these sites through the application of previously developed

techniques (e.g. Micallef et al., 2007b; Morgan et al., 2008; Booth et al., 2009; Mountjoy et al., 2009b).

Type examples from each environment would require "ground truthing" to corroborate any interpretation of age, activity or lithological control. This aspect of the study may require further data to be collected. To gain control on the age or activity of specific gully systems, and to quantify the nature and magnitude of any accumulated hemipelagic material, data such as sedimentary cores and high-resolution seismic reflection profiling can be used. Accumulation of any significant thickness of hemipelagic material generally indicates inactivity of sediment gravity-flow processes as the material would be removed by any erosive events (depending on the periodicity of flows vs background sedimentation rates).

7.4.2 Activity of non-sediment-source-coupled canyons under sea-level highstand conditions

In many traditional models canyons that are not coupled to fluvial or littoral sediment sources during sea-level highstand have little or no sediment throughput. It has recently been shown that some non-coupled canyons are active under highstand conditions (e.g. Ogston et al., 2008; Palanques et al., 2008b), a discovery that has in part stemmed from the acquisition of high-resolution multibeam images of canyon floors (Puig et al., 2008). Of the numerous submarine canyon systems on the Hikurangi Margin, only one (Kaikoura Canyon) is sediment-source-coupled (Lewis and Barnes, 1999). Work on the morphology of Cook Strait Canyon during this study suggests that it also experiences erosive sediment gravity flows, and a possible sediment source is the high diurnal tidal current flow through Cook Strait.

The fundamental research question that this science would contribute to is: "What are the unique processes that enable non-shoreline-connected canyon systems to remain active as shelf-to-trough sediment conduits during highstand periods?"

A project focused on quantifying the activity of Cook Strait Canyon would benefit from a multi-phased approach.

1. A quantitative morphometric comparison of the canyon floor bedforms of Cook Strait and Kaikoura canyons. As Kaikoura Canyon is known to be presently active the character of the seabed should reflect this. In contrast, if Cook Strait Canyon is currently inactive, the ~18kyrs of inactivity since sea level rose may have a quantifiable geomorphic signature. Simrad EM300 derived 10 m DEMs exist for

both these canyons; however the signature of active down-canyon processes may be at an order of magnitude higher resolution than this (e.g. Paull et al., 2008).

2. A coring programme to define sediment gravity-flow stratigraphy down the canyon axis. Though coring is known to be difficult in the lower canyon due to the dense sand substrate (P. Barnes pers comm.), it has been possible to recover some cores in the past (Lewis and Pantin, 2002; Mountjoy et al., 2009a). As phase one of the project this would determine the frequency at which sediment gravity flows have occurred in post-glacial times.

3. NIWA has a three-dimensional hydrodynamic model set up that simulates the tidal regime in Cook Strait (Popinet, 2003). To assess the net transport of sediment into the Cook Strait Canyon head area, the model could be modified to include bed-stress parameters to analyse for surficial seafloor stability and sediment transport. This would likely benefit from additional "ground-truthing" surveys such as targeted coring in accumulation areas and/or repeated high-resolution shallow-water multibeam surveys (e.g. Simrad EM3000) to quantify bed-form migration.

7.4.3 Post-emplacement deformation of landslide debris: understanding geotechnical controls on submarine landslide remobilisation

High-resolution seafloor imaging of submarine landslide complexes provides insight into the emplacement and subsequent modification of landslide debris. The interpretation of the Tuahini Landslide Complex as a submarine earthflow raises significant questions about the activity of submarine landslides.

Major questions include:

- What processes enable submarine landslide debris to be repeatedly active?
- What determines if a landslide complex will develop into an earthflow?
- How does excess pore-water pressure transfer within landslide debris in response to static loading to enable longitudinally and laterally partitioned movement to occur?
- Do active/dormant submarine landslides have a quantifiable geomorphic signature?

This research has two primary aims that will allow these questions to be addressed:

Aim 1: To conclusively show that the earthflow is actively moving and has been active for a significant amount of time.

Aim 2: To test the sensitivity of the earthflow to environmental forcing using a numerical model.

To address Aim 1 it would be necessary to build on the morphologic interpretation of earthflow activity (Mountjoy et al., 2009b) and demonstrate displacement within the earthflow body. Existing bathymetry, seismic reflection and core data need to be augmented with targeted surveys, preferably collected on the back of other projects that are ongoing in the area. One or all of the following three methodologies could be used: 1) repeat existing high-resolution multibeam surveys over target areas; 2) repeat high-resolution single-beam echo-sounder lines over areas of likely activity; 3) collect a profile of marine cores down the earthflow body (these should show an increase in hemipelagic accumulation with greater distance rafted downslope if the earthflow is currently active).

To address Aim 2 a three-dimensional numerical model (e.g. finite element), using local geotechnical data (Barnes et al., 1991) and well-defined geometry, would be employed to test how partitioned movement has developed the earthflow features already characterised by surface and subsurface data. The isolation of an overriding control on the regular generation of spatially variable excess pore-water pressures will have significant implications for a wide range of submarine processes that shape continental margin slopes.

7.5 Closing statement

This chapter has: 1) summarised the main findings of this study within environmental frameworks; 2) developed a conceptual model of the activity of active margin canyon systems at differing sea-level stands; and 3) considered the possible future direction of research stemming from this doctoral study.

The findings of this doctoral study have implications for the large population of submarine canyons occurring on active margins globally whose initiation, evolution and activity is strongly influenced by tectonics.

Over the course of this project I have gained a great understanding of and appreciation for submarine landscape development and I foresee a positive and exciting future for the burgeoning field of submarine geomorphology. I hope and anticipate that this doctoral project will lay the groundwork for a long and productive research career focused around submarine surface processes and landforms.

Bibliography

Addington, L.D., Kuehl, S.A., McNinch, J.E., 2007. Contrasting modes of shelf sediment dispersal off a high-yield river: Waiapu River, New Zealand. Marine Geology, 243(1-4): 18-30.

Agliardi, F., Crosta, G., Zanchi, A., 2001. Structural constraints on deep-seated slope deformation kinematics. Engineering Geology, 59(1-2): 83-102.

Alexander, C.R., Walsh, J.P., Orpin, A.R., submitted. Modern Sediment Dispersal and Accumulation on the Waipaoa Outer Continental Margin. Marine Geology, Special Issue Waipaoa S2S.

Alloway, B.V., Lowe, D.J., Barrell, D., Newnham, R.M., Almond, P., Augustinus, P.C., Bertler, N., Carter, L., Litchfield, N., McGlone, M., Shulmeister, J., Vandergoes, M., Williams, P., N.Z.Intimate-members, 2007. Towards a climate event stratigraphy for New Zealand over the past 30 000 years (NZ-INTIMATE project). Journal of Quaternary Science, 22(1): 9-35.

Ambrosi, C., Crosta, G.B., 2006. Large sackung along major tectonic features in the Central Italian Alps. Engineering Geology, 83(1-3): 183-200.

Arron, E., Lewis, K.B., 1992. Mahia Bathymetry, 2nd Edition. New Zealand Oceanographic Institute Chart, Coastal Series, 1:200,000.

Barnes, P.M., 2005. The southern end of the Wairarapa Fault and surrounding structures in Cook Strait. In: J. Townend, R. Langridge and A. Jones (Editors), The 1855 Wairarapa Earthquake symposium, Wellington.

Barnes, P.M., Audru, J.-C., 1999a. Quaternary faulting in the offshore Flaxbourne and Wairarapa Basins, southern Cook Strait, New Zealand. New Zealand Journal of Geology and Geophysics, 42: 349-367.

Barnes, P.M., Audru, J.-C., 1999b. Recognition of active strike-slip faulting from high-resolution marine seismic reflection profiles: Eastern Marlborough fault system, New Zealand. Geological Society of America Bulletin, 111(4): 538-559.

Barnes, P.M., Ching Cheung, K., Smits, A.P., Almagor, G., Read, S.A.L., Barker, P.R., Froggatt, P.C., 1991. Geotechnical analysis of the Kidnappers Slide, upper continental slope, New Zealand. Marine Geotechnology, 10: 159-188.

Barnes, P.M., Lamarche, G., Bialas, J., Henrys, S., Pecher, I.A., Netzeband, G.L., Greinert, J., Mountjoy, J.J., Pedley, K., Crutchley, G., 2009. Tectonic and Geological Framework for Gas hydrates and Cold Seeps on the Hikurangi Subduction Margin, New Zealand. Marine Geology doi:10.1016/j.margeo.2009.03.012.

Barnes, P.M., Mercier de Lepinay, B., 1997. Rates and mechanics of rapid frontal accretion along the very obliquely convergent southern Hikurangi margin, New Zealand. Journal of Geophysical Research, 102(B11): 24931-24952.

Barnes, P.M., Mercier de Lepinay, B., Collot, J.-Y., Delteil, J., Audru, J.-C., 1998a. Strain partitioning in the transition area between oblique subduction and continental collision, Hikurangi Margin, New Zealand. Tectonics, 17(4): 534-557.

Barnes, P.M., Mercier de Lepinay, B., Collot, J.Y., Delteil, J., Audru, J.C., Team, a.G., 1998b. South Hikurangi GeodyNZ swath maps: Depths, Texture and Geological Interpretation, NIWA Chart, Miscellaneous Series No. 75.

Barnes, P.M., Nicol, A., 2004. Formation of an active thrust triangle zone associated with structural inversion in a subducting setting, eastern New Zealand. Tectonics, 23: TC1015.

Barnes, P.M., Nicol, A., Harrison, T., 2002. Late Cenozoic evolution and earthquake potential of an active listric thrust complex above the Hikurangi subduction zone, New Zealand. Geological Society of America Bulletin, 114(11): 1379-1405.

Barnes, P.M., Pondard, N., Lamarche, G., Mountjoy, J., Van Dissen, R., litchfield, N., 2008. Its Our Fault: Active faults and earthquake sources in Cook Strait. , NIWA Client Report WLG2008-56: 36p.

Barnes, P.M., Sutherland, R., Delteil, J., 2005. Strike-slip structure and sedimentary basins of the southern Alpine Fault, Fiordland, New Zealand. Geological Society of America Bulletin, 117(3/4): 411-435.

Baztan, J., Berne, S., Olivet, J.-L., Rabineau, M., Aslanian, D., Gaudin, M., Rehault, J.-P., Canals, M., 2005. Axial incision: The key to understand submarine canyon evolution (in the western Gulf of Lion). Marine and Petroleum Geology, 22(6-7): 805-826.

Berndt, C., Cattaneo, A., Szuman, M., Trincardi, F., Masson, D., 2006. Sedimentary structures offshore Ortona, Adriatic Sea - Deformation or sediment waves? Marine Geology, 234(1-4): 261-270.

Berryman, K.R., 2005. Review of tsunami hazard and risk in New Zealand, IGNS Client report 2005/104.

Bialas, J., Greinert, J., Linke, P., Pfannkuche, O., 2007. FS Sonne Fahrtericht / Cruise Report SO 191 – New Vents "Puaretanga Hou", Wellington-Napier-Auckland, 11.01-23.03.2007, IFM-GEOMAR Berichte aus dem Leibniz-Institut für Meereswissenschaften an der Christian-Albrechts-Universität zu Kiel.

Bodger, K.L., Pettinga, J.R., Barnes, P.M., 2006. Seafloor Structural Geomorphic Evolution in Response to Seamount Subduction, Poverty Bay Indentation, New Zealand, Eos Trans. AGU, 87(52), Fall Meet. Suppl., Abstract T21A-0392.

Booth, A.M., Roering, J.J., Perron, J.T., 2009. Automated landslide mapping using spectral analysis and high-resolution topographic data: Puget Sound lowlands, Washington, and Portland Hills, Oregon. Geomorphology, 109(3-4): 132-147.

Brackley, H.L., Blair, N.E., Trustrum, N.A., Carter, L., Leithhold, E.L., Canuel, E.A., Johnson, J., Tate, K.R., submitted. Dispersal and transformation of organic carbon across an episodic, high sediment discharge continental margin, Waipaoa sedimentary system, New Zealand. Marine Geology, Special Issue S2S.

Bucher, W.H., 1940a. Origin of the submarine valleys on the continental slopes of the North Atlantic. Nature, 146(3699): 407-408.

Bucher, W.H., 1940b. Submarine valleys and the related geologic problems of the North Atlantic. Geol. Soc. Am. Bull., 51: 489-512.

Bugge, T., Belderson, R.H., Kenyon, N.H., 1988. The Storegga Slide. Philosophical Transactions of the Royal Society of London, 325: 357 - 388.

Cacchione, D.A., Pratson, L.F., Ogston, A.S., 2002. The shaping of continental slopes by internal tides. Science, 296(5568): 724-727.

Canals, M., Puig, P., De Madron, X.D., Heussner, S., Palanques, A., Fabres, J., 2006. Flushing submarine canyons. Nature, 444(7117): 354-357.

Caputo, R., 2007. Sea-level curves: Perplexities of an end-user in morphotectonic applications. Global and Planetary Change, 57(3-4): 417-423.

Carlson, P.R., Karl, H.A., 1984. Discovery of two new large submarine canyons in the Bering Sea. Marine Geology, 56(1-4): 159-179.

Carter, L., 1992. Acoustical characterisation of seafloor sediments and its relationship to active sedimentary processes in Cook Strait, New Zealand. New Zealand Journal of Geology and Geophysics, 35: 289-300.

Carter, L., Garlick, R.D., Sutton, P., Chiswell, S., Oien, N.A., Stanton, B.R., 1998. Ocean Circulation New Zealand. NIWA Chart, Misc. Ser., 76.

Carter, L., Lewis, K.B., 1995. Variability of the modern sand cover on a tide and storm driven inner shelf, south Wellington, New Zealand. New Zealand Journal of Geology and Geophysics, 38: 451 - 470.

Carter, L., Manighetti, B., 2006. Glacial/interglacial control of terrigenous and biogenic fluxes in the deep ocean off a high input, collisional margin: A 139 kyr-record from New Zealand. Marine Geology, 226: 307-322.

Carter, L., Manighetti, B., Elliot, M., Trustrum, N., Gomez, B., 2002. Source, sea level and circulation effects on the sediment flux to the deep ocean over the past 15 ka off eastern New Zealand. Global and Planetary Change, 33: 339-355.

Carter, L., Neil, H.L., McCave, I.N., 2000. Glacial to interglacial changes in non-carbonate and carbonate accumulation in the SW Pacific Ocean, New Zealand. Palaeoceanography, Palaeoclimatology, Palaeoecology, 162: 333 - 356.

Carter, L., Wright, I.C., Collins, N., Mitchell, J.S., Win, G., 1991. Seafloor stability along the Cook Strait power cable corridor, 10th Australasian Conference on coastal and ocean Engineering, pp. 565 - 570.

Chiang, C.-S., Yu, H.-S., 2006. Morphotectonics and incision of the Kaoping submarine canyon, SW Taiwan orogenic wedge. Geomorphology, 80: 199 - 213.

Collot, J.-Y., Delteil, J., Herzer, R., Lewis, K.B., Wood, R., party, s., 1994. GeodyNZ-Sud Cruise Report, ORSTOM, Villefranche s/Mer, Noumea.

Collot, J.-Y., Delteil, J., Lewis, K.B., Davy, B., Lamarche, G., Audru, J.-C., Barnes, P., Chanier, F., Chaumillon, E., Lallemand, S.E., Mercier de Lepinay, B., Orpin, A., Pelletier, B., Sosson, M., Toussaint, B., Uruski, C., 1996. From oblique subduction to intra-continental transpression; structures of the southern Kermadec-Hikurangi margin from multibeam bathymetry, side-scan sonar and seismic reflection. Marine Geophysical Researches, 18(2-4): 357-381.

Collot, J.-Y., Lewis, K.B., Lamarche, G., Lallemand, S.E., 2001. The giant Ruatoria debris avalanche on the northern Hikurangi Margin, New Zealand: Result of oblique seamount subduction. Journal of Geophysical Research, 106(B9): 19,271 - 19,297.

Coulbourn, W.T., Campbell, J.F., Moberly, R., 1974. Hawaiian submarine terraces, canyons, and Quaternary history evaluated by seismic-reflection profiling. Marine Geology, 17(4): 215-234.

Crosby, B.T., Whipple, K.X., 2006. Knickpoint initiation and distribution within fluvial networks: 236 waterfalls in the Waipaoa River, North Island, New Zealand. Geomorphology, 82(1-2): 16-38.

Crosby, B.T., Whipple, K.X., Gasparini, N.M., Wobus, C.W., 2007. Formation of fluvial hanging valleys: Theory and simulation. Journal of Geophysical Research F: Earth Surface, 112(3).

Cruden, D.M., Varnes, D.J., 1996. Landslide types and processes. In: A.K. Turner and R.L. Schuster (Editors), Landslides: investigation and mitigation. National Academy Press, Washington, D.C., pp. 673.

Crundwell, M., Scott, G., Naish, T., Carter, L., 2008. Glacial-interglacial ocean climate variability from planktonic foraminifera during the Mid-Pleistocene transition in the temperate Southwest Pacific, ODP Site 1123. Palaeogeography, Palaeoclimatology, Palaeoecology, 260(1-2): 202-229.

Crutchley, G.J., Gorman, A.R., Fohrmann, M., 2007. Investigation of the role of gas hydrates in continental slope stability west of Fiordland, New Zealand. New Zealand Journal of Geology and Geophysics, 50(4): 357-364.

Crutchley, G.J., Pecher, I.A., Gorman, A.R., Henrys, S.A., Greinert, J., 2009. Seismic imaging of gas conduits beneath seafloor seep sites in a shallow marine gas hydrate province, Hikurangi Margin, New Zealand. Marine Geology, In Press, doi:10.1016/j.margeo.2009.03.007.

Daly, R.A., 1936. Origin of submarine "canyons", American Journal of Science, pp. 401-420.

Damuth, J.E., Flood, R.D., 1984 Morphology, sedimentation processes, and growth pattern the Amazon deep-sea fan. . Geo- Marine Letters, 3,: 109-117.

Dana, J.D., 1863. Manual of geology, treating of the principles of the science with special reference to American geological history. Philadelphia, 798 pp.

Davey, F.J., Hampton, M.A., Childs, J.R., Fisher, M.A., Lewis, K., Pettinga, J.R., 1986a. Structure of a growing accretionary prism, Hikurangi margin, New Zealand. Geology, 14(8): 663-666.

Davey, F.J., Lewis, K.B., Childs, J.R., Hampton, M.A., 1986b. Convergent margin off east coast of North Island, New Zealand, Parts I and II. In: R.E. Von Huene (Editor), Seismic images of modern convergent margin tectonic structure. AAPG Studies in Geol.Ammerican Association of Petroleum Geologist, pp. 49 - 53.

Dominguez, S., Lallemand, S.E., Malavieille, J., Von Huene, R., 1998. Upper plate deformation associated with seamount subduction. Tectonophysics, 293(3-4): 207-224.

Droz, L., Rigaut, F., Cochonat, P., Tofani, R., 1996. Morphology and recent evolution of the Zaire turbidite system (Gulf of Guinea). Geological Society of America Bulletin, 108: 253 - 269.

Exon, N., Hill, P., Mitchell, C., Post, A., 2005a. Nature and origin of the submarine Albany canyons off southwest Australia. Australian Journal of Earth Sciences, 52(1): 101-115.

Exon, N.F., Hill, P.J., Mitchell, C., Post, A., 2005b. Nature and origin of the submarine Albany canyons off southwest Australia. Australian Journal of Earth Sciences, 52(1): 101-115.

Farre, J.A., McGregor, B.A., Ryan, W.B.F., Robb, J.M., 1983. Breaching the shelfbreak: passage from youthful to mature phase in submarine canyon evolution. Society of Economic Paleontologists and Mineralogists, Special Publication, 33,: 25-39.

Faure, K., Greinert, J., Pecher, I.A., Graham, I.J., Massoth, G.J., De Ronde, C.E.J., Wright, I.C., Baker, E.T., Olson, E.J., 2006. Methane seepage and its relation to slumping and gas hydrate at the Hikurangi margin, New Zealand. New Zealand Journal of Geology and Geophysics, 49(4): 503-516.

Field, B.D., Uruski, C.I., others, 1997. Cretaceous - Cenozoic geology and petroleum systems of the East Coast region, New Zealand. Institute of Geological and Nuclear Sciences Monograph, 19. GNS, 301 pp.

Foster, G., Carter, L., 1997. Mud sedimentation on the continental shelf at an accretionary margin - Poverty Bay, New Zealand. New Zealand Journal of Geology and Geophysics, 40(2): 157-173.

Garett, C., Kunze, E., 2007. Internal tide generation in the deep ocean, Annual Review of Fluid Mechanics, pp. 57-87.

Garlick, R.D., Mitchell, J.S., 2002. Turnagain Bathymetry, 3rd edition. NIWA Chart, Coastal Series, 1:200.000.

Gaudin, M., Mulder, T., Cirac, P., Berne, S., Imbert, P., 2006. Past and present sedimentary activity in the Capbreton Canyon, southern Bay of Biscay. Geo-Marine Letters, 26(6): 331-345.

Gerber, T.P., Pratson, L.F., Kuehl, S., Walsh, J.P., Alexander, C.R., Palmer, A., 2009. The influence of sea level and tectonics on Late Pleistocene through Holocene sediment storage along the high-sediment supply Waipaoa continental shelf. Marine Geology, in press, doi: 10.1016/j.margeo.2009.10.002.

Gibb, J.G., 1986. A New Zealand regional Holocene eustatic sea-level curve and its application to determination of vertical tectonic movements. A contribution to IGCP-Project 200. Royal Society of New Zealand Bulletin, 24: 377-395.

Goring, D.G., Walters, R.A., 2002. Ocean-tide loading and Earth tides around New Zealand. New Zealand Journal of Marine and Freshwater Research, 36(2): 299-309.

Gorman, R.M., Bryan, K.R., Laing, A.K., 2003. Wave hindcast for the New Zealand region: Nearshore validation and coastal wave climate. New Zealand Journal of Marine and Freshwater Research, 37(3): 567-588.

Green, A.N., Goff, J.A., Uken, R., 2007. Geomorphological evidence for upslope canyon-forming processes on the northern KwaZulu-Natal shelf, SW Indian Ocean, South Africa. Geo-Marine Letters, 27(6): 399-409.

Greene, H.G., Clarke Jr, S.H., Kennedy, M.P., 1991. Tectonic evolution of submarine canyons along the California continental margin. In: R.H. Osbourne (Editor), From shoreline to abyss: contributions in marine geology in honor of Francis Parker Shepard. Soc. of Econ. Paleontologists and Mineralogists, pp. 231-248.

Greene, H.G., Maher, N.M., Paull, C.K., 2002. Physiography of the Monterey Bay National Marine Sanctuary and implications about continental margin development. Marine Geology, 181(1-3): 55-82.

Greene, H.G., Murai, L.Y., Watts, P., Maher, N.A., Fisher, M.A., Paull, C.E., Eichhubl, P., 2006. Submarine landslides in the Santa Barbara Channel as potential tsunami sources. Natural Hazards and Earth System Science, 6(1): 63-88.

Greinert, J., Lewis, K.B., Bialas, J., Pecher, I.A., Rowden, A., Linke, P., De Batist, M., Bowden, D.A., Suess, E., submitted. Methane seepage along the Hikurangi Margin, New Zealand: Review of studies in 2006 and 2007. Marine Geology, special issue.

Haflidason, H., Sejrup, H.P., Nygård, A., Mienert, J., Bryn, P., Lien, R., Forsberg, C.F., Berg, K., Masson, D., 2004. The Storegga Slide: Architecture, geometry and slide development. Marine Geology, 213(1-4): 201-234.

Hallet, B., Hunter, L., Bogen, J., 1996. Rates of erosion and sediment evacuation by glaciers: A review of field data and their implications. Global and Planetary Change, 12(1-4): 213-235.

Hampton, M.A., Lee, H.J., Locat, J., 1996. Submarine Landslides. Reviews of Geophysics, 34: 33 - 59.

Haq, B.U., 1991. Sequence stratigraphy, sea-level change, and significance for the deep sea. Special Publication International Association of Sedimentologists, 12: 3-39.

Henry, P., Lallemant, S., Nakamura, K.I., Tsunogai, U., Mazzotti, S., Kobayashi, K., 2002. Surface expression of fluid venting at the toe of the Nankai wedge and implications for flow paths. Marine Geology, 187(1-2): 119-143.

Henrys, S.A., Ellis, S., Uruski, C., 2003. Conductive heat flow variations from bottom-simulating reflectors on the Hikurangi margin, New Zealand. Geophysical Research Letters, 30(2): 37-1.

Herzer, R.H., 1979. Submarine slides and submarine canyons on the continental slope off Canterbury, New Zealand. New Zealand Journal of Geology and Geophysics, 22: 391-406.

Hicks, D.M., Gomez, B., Trustrum, N.A., 2000. Erosion thresholds and suspended sediment yields, Waipaoa River basin, New Zealand. Water Resources Research, 36(4): 1129-1142.

Hicks, D.M., Shankar, U., 2003. Sediment from New Zealand rivers, NIWA Chart, Miscellaneous Series No. 79.

Holbrook, W.S., Gorman, A.R., Hornbach, M., Hackwith, K.L., Nealon, J., Lizarralde, D., Pecher, I.A., 2002. Seismic detection of marine methane hydrate. Leading Edge (Tulsa, OK), 21(7): 686-689.

Hornbach, M.J., Saffer, D.M., Holbrook, W.S., 2004. Critically pressured free-gas reservoirs below gas-hydrate provinces. Nature, 427(6970): 142-144.

Huhnerbach, V., Masson, D.G., Bohrmann, G., Bull, J.M., Weinrebe, W., 2005. Deformation and submarine landsliding caused by seamount subduction beneath the Costa Rica continental margin - New insights from high-resolution sidescan sonar data, Geological Society Special Publication, pp. 195-205.

Hutton, E.W.H., Syvitski, J.P.M., 2004. Advances in the numerical modeling of sediment failure during the development of a continental margin. Marine Geology, 203(3-4): 367-380.

Huyghe, P., Foata, M., Deville, E., Mascale, G., Group, C.W., 2004. Channel profiles through the active front of the Barbados prism. Geology, 32(5): 429-432.

Imbrie, J., Imbrie, K.P., 1979. Ice Ages: Solving the mystery. MacMillan, New York, 224 pp.

Jones, A.T., Greinert, J., Bowden, D.A., Klaucke, I., Petersen, J., Netzeband, G., Weinrebe, W., 2009. Acoustic and visual characterisation of methane-rich seabed seeps at Omakere Ridge on the Hikurangi Margin, New Zealand. Marine Geology, In Press, doi:10.1016/j.margeo.2009.03.008.

Katz, H.R., 1975. Ariel Bank off Gisborne - an offshore Late Cenozoic structure, and the problem of acoustic basement on the east coast, North Island, New Zealand. N.Z. Jl Geol. Geophys., 18: 93-107.

Katz, H.R., 1981. Probable gas hydrate in continental slope east of the North Island, New Zealand. Journal of petroleum geology, 3: 315-324.

Klaucke, I., Weinrebe, W., Petersen, C.J., Bowden, D., 2009. Temporal variability of gas seeps offshore New Zealand: Multi-frequency geoacoustic imaging of the Wairarapa area, Hikurangi margin. Marine Geology, in press, doi:10.1016/j.margeo.2009.02.009.

Krastel, S., Schmincke, H.U., Jacobs, C.L., 2001. Formation of submarine canyons on the flanks of the Canary Islands. Geo-Marine Letters, 20(3): 160-167.

Kuehl, S., Alexander, C., Carter, L., Gerald, L., Gerber, T., Harris, C., McNinch, J., Orpin, A., Pratson, L., Syvitski, J., Walsh, J.P., 2006. Understanding sediment transfer from land to ocean. Eos, 87(29): 281-283.

Kukowski, N., Hampel, A., Hoth, S., Bialas, J., 2008. Morphotectonic and morphometric analysis of the Nazca plate and the adjacent offshore Peruvian continental slope - Implications for submarine landscape evolution. Marine Geology, 254(1-2): 107-120.

Kukowski, N., Schillhorn, T., Huhn, K., von Rad, U., Husen, S., Flueh, E.R., 2001. Morphotectonics and mechanics of the central Makran accretionary wedge off Pakistan. Marine Geology, 173(1-4): 1-19.

Kunze, E., Rosenfeld, L.K., Carter, G.S., Gregg, M.C., 2002. Internal waves in Monterey Submarine Canyon. Journal of Physical Oceanography, 32(6): 1890-1913.

Kvalstad, T.J., Nadim, F., Kaynia, A.M., Mokkelbost, K.H., Bryn, P., 2005. Soil conditions and slope stability in the Ormen Lange area. Marine and Petroleum Geology, 22(1-2 SPEC. ISS.): 299-310.

Kvenvolden, K.A., 1993. Gas hydrates-geological perspective and global change. Reviews of Geophysics, 31(2): 173-187.

Laberg, J.S., Guidard, S., Mienert, J., Vorren, T.O., Haflidason, H., Nyga?rd, A., 2007. Morphology and morphogenesis of a high-latitude canyon; the Andøya Canyon, Norwegian Sea. Marine Geology, 246(2-4): 68-85.

Lamarche, G., Joanne, C., Collot, J., 2008. Successive, large mass-transport deposits in the south Kermadec fore-arc basin, New Zealand: The Matakaoa Submarine Instability Complex. GEOCHEMISTRY GEOPHYSICS GEOSYSTEMS, 9(4).

Lamb, M.P., Howard, A.D., Johnson, J., Whipple, K.X., Dietrich, W.E., Perron, J.T., 2006. Can springs cut canyons into rock? Journal of Geophysical Research E: Planets, 111(7).

Lamb, M.P., Parsons, J.D., Mullenbach, B.L., Finlayson, D.P., Orange, D.L., Nittrouer, C.A., 2008. Evidence for superelevation, channel incision, and formation of cyclic steps by turbidity currents in Eel Canyon, California. Bulletin of the Geological Society of America, 120(3-4): 463-475.

Lastras, G., Arzola, R.G., Masson, D.G., Wynn, R.B., Huvenne, V.A.I., Huhnerbach, V., Canals, M., 2008. Geomorphology and sedimentary features in the Central Portuguese submarine canyons, Western Iberian margin. Geomorphology, 103(3): 310-329.

Lastras, G., Canals, M., Urgeles, R., Amblas, D., Ivanov, M., Droz, L., Dennielou, B., Fabrés, J., Schoolmeester, T., Akhmetzhanov, A., Orange, D., García-García, A., 2007. A walk down the Cap de Creus canyon, Northwestern Mediterranean Sea: Recent processes inferred from morphology and sediment bedforms. Marine Geology, 246(2-4): 176-192.

Laursen, J., Normark, W.R., 2002. Late Quaternary evolution of the San Antonio Submarine Canyon in the central Chile forearc (~ 33°S). Marine Geology, 188(3-4): 365-390.

Law, C.S., Nodder, S.D., Mountjoy, J.J., Marriner, A., Orpin, A., Pilditch, C.A., Franz, P., Thompson, K., 2009. Geological, hydrodynamic and biogeochemical characterisation of a New Zealand deep-water methane cold seep during a three year time-series study. Marine Geology doi:10.1016/j.margeo.2009.06.018.

Lee, H.J., 2005. Undersea landslides: Extent and significance in the Pacific Ocean, an update. Natural Hazards and Earth System Science, 5(6): 877-892.

Lee, H.J., Syvitski, J.P.M., Parker, G., Orange, D., Locat, J., Hutton, E.W.H., Imran, J., 2002. Distinguishing sediment waves from slope failure deposits: Field examples, including the 'humboldt slide', and modelling results. Marine Geology, 192(1-3): 79-104.

Lee, I.H., Lien, R.C., Liu, J.T., Chuang, W.s., 2009a. Turbulent mixing and internal tides in Gaoping (Kaoping) Submarine Canyon, Taiwan. Journal of Marine Systems, 76(4): 383-396.

Lee, I.H., Wang, Y.H., Liu, J.T., Chuang, W.S., Xu, J., 2009b. Internal tidal currents in the Gaoping (Kaoping) Submarine Canyon. Journal of Marine Systems, 76(4): 397-404.

Lewis, K., Collot, J.-Y., Lallemand, S., 1998. The dammed Hikurangi Trough: a channel-fed trench blocked by subducting seamounts and their wake avalanches (New Zealand-France GeodyNZ Project). Basin Research, 10(4): 441-468.

Lewis, K., Lallemand, S., Carter, L., 2004. Collapse in a Quaternary shelf basin off East Cape, New Zealand: evidence for passage of a subducted seamount inboard of the Ruatoria giant avalanche. New Zealand Journal of Geology and Geophysics, 47: 415-429.

Lewis, K.B., 1973. Sediments on the Continental shelf and slope between Napier and Castlepoint, New Zealand. N.Z. Jl mar. Freshwat. Res., 7,: 183-208.

Lewis, K.B., 1980. Quaternary sedimentation on the Hikurangi oblique- subduction and transform margin, New Zealand. In: P.F. Ballance and H.G. Reading (Editors), Sedimentation in oblique-slip mobile zones. International Association of Sedimentologists special publication, pp. 171-189.

Lewis, K.B., 1994. The 1500-km-long Hikurangi Channel: Trench-axis channel that escapes its trench, crosses a plateau, and feeds a fan drift. Geo-Marine Letters, 14: 19-28.

Lewis, K.B., Barnes, P.M., 1999. Kaikoura Canyon, New Zealand: active conduit from near-shore sediment zones to trench-axis channel. Marine Geology, 162(1): 39-69.

Lewis, K.B., Barnes, P.M., Collot, J.-Y., Mercier de Lépinay, B., Delteil, J., GeodyNZteam, 1999. Central Hikurangi GeodyNZ swath maps: depths texture and geological interpretation. NIWA Chart, Miscellaneous Series, 77.

Lewis, K.B., Carter, L., Davey, F.J., 1994. The opening of Cook Strait: Interglacial tidal scour and aligning basins at a subduction to transform plate edge. Marine Geology, 116(3-4): 293-312.

Lewis, K.B., Collot, J.-Y., Davy, B.W., Delteil, J., Lallemand, S.E., Uruski, C., GeodyNZ Team, 1997. North Hikurangi GeodyNZ swath maps: depths, texture and geological interpretation. NIWA, Wellington.

Lewis, K.B., Kohn, B.P., 1973. Ashes, turbidites, and rates of sedimentation on the continental slope off Hawkes Bay. New Zealand Journal of Geology and Geophysics, 16(3): 439-454.

Lewis, K.B., Marshall, B.A., 1996. Seep faunas and other indicators of methane-rich dewatering on New Zealand convergent margins. New Zealand Journal of Geology and Geophysics, 39: 181 - 200.

Lewis, K.B., Pantin, H.M., 2002. Channel-axis, overbank and drift sediment waves in the southern Hikurangi Trough, New Zealand. Marine Geology, 192(1-3): 123-151.

Lewis, K.B., Pettinga, J.R., 1993. The emerging, imbricate frontal wedge of the Hikurangi margin. In: P.F. Ballance (Editor), South Pacific sedimentary basin. Sedimentary Basins of the World, 2. Elsevier Sciences publishers, Amsterdam, pp. 225-250.

Leynaud, D., Sultan, N., Mienert, J., 2007. The role of sedimentation rate and permeability in the slope stability of the formerly glaciated Norwegian continental margin: The Storegga slide model. Landslides, 4(4): 297-309.

Linke, P., Sommer, S., Rovelli, L., McGinnis, D.F., 2009. Physical limitations of dissolved methane fluxes: The role of bottom-boundary layer processes. Marine Geology, In Press, doi:10.1016/j.margeo.2009.03.020.

Litchfield, N.J., Smith, W.D., Berryman, K.R., 2009. Return times for high levels of ground shaking ($\geq$ MM7) in the Waipaoa and Waitaki River catchments, GNS Science Report 2009/03. 94p.

Liu, C.S., Deffontaines, B., Lu, C.Y., Lallemand, S., 2004. Deformation patterns of an accretionary wedge in the transition zone from subduction to collision offshore southwestern Taiwan. Marine Geophysical Researches, 25(1-2): 123-137.

Locat, J., Lee, H., ten Brink, U., Twichell, D., Geist, E., Sansoucy, M., 2009. Geomorphology, stability and mobility of the Currituck slide. Marine Geology, 264(1-2): 28-40.

Locat, J., Lee, H.J., 2002. Submarine landslides: Advances and challenges. Canadian Geotechnical Journal, 39(1): 193-213.

Ma, Y., Wright, L.D., Friedrichs, C.T., 2008. Observations of sediment transport on the continental shelf off the mouth of the Waiapu River, New Zealand: Evidence for current-supported gravity flows. Continental Shelf Research, 28(4-5): 516-532.

Marden, M., Mazengarb, C., Palmer, A., Berryman, K., Rowan, D., 2008. Last glacial aggradation and postglacial sediment production from the non-glacial Waipaoa and Waimata catchments, Hikurangi Margin, North Island, New Zealand. Geomorphology, 99(1-4): 404-419.

Martinson, D.G., Pisias, N.G., Hays, J.D., Imbrie, J., Moore, T.C., Shackleton, N.J., 1987. Age dating and the orbital theory of the Ice Ages: Development of a high-resolution 0 to 300,000 year chronostratigraphy. Quarternary Research, 27: 1-29.

Masson, D.G., Harbitz, C.B., Wynn, R.B., Pedersen, G., LÃ¸vholt, F., 2006. Submarine landslides: Processes, triggers and hazard prediction. Philosophical Transactions of the Royal Society A: Mathematical, Physical and Engineering Sciences, 364(1845): 2009-2039.

Masson, D.G., Parson, L.M., Milsom, J., Nichols, G., Sikumbang, N., Dwiyanto, B., Kallagher, H., 1990. Subduction of seamounts at the Java Trench: a view with long-range sidescan sonar. Tectonophysics, 185: 51 - 65.

McAdoo, B.G., Capone, M.K., Minder, J., 2004. Seafloor geomorphology of convergent margins: Implications for Cascadia seismic hazard. Tectonics, 23(6).

McAdoo, B.G., Orange, D.L., Screaton, E., Lee, H., Kayen, R., 1997a. Slope basins, headless canyons, and submarine palaeoseismology of the Cascadia accretionary complex. Basin Research, 9(4): 313-324.

McAdoo, B.G., Orange, D.L., Silver, E.A., McIntosh, K., Abbott, L., Galewsky, J., Kahn, L., Protti, M., 1996. Seafloor structural observations, Costa Rica accretionary prism. Geophysical Research Letters, 23(8): 883-886.

McAdoo, B.G., Pratson, L., Orange, D.L., Anonymous, 1997b. Comparative landslide morphology, U.S. continental slope. Eos, Transactions, American Geophysical Union, 78(46, Suppl.): 687.

McAdoo, B.G., Watts, P., 2004. Tsunami hazard from submarine landslides on the Oregon continental slope. Marine Geology, 203(3-4): 235-245.

McKean, J., Roering, J., 2004. Objective landslide detection and surface morphology mapping using high-resolution airborne laser altimetry. Geomorphology, 57(3-4): 331-351.

Micallef, A., Berndt, C., Masson, D.G., Stow, D.A.V., 2007a. A technique for the morphological characterization of submarine landscapes as exemplified by debris flows of the Storegga Slide. Journal of Geophysical Research F: Earth Surface, 112(2).

Micallef, A., Berndt, C., Masson, D.G., Stow, D.A.V., 2008. Scale invariant characteristics of the Storegga Slide and implications for large-scale submarine mass movements. Marine Geology, 247(1-2): 46-60.

Micallef, A., Masson, D.G., Berndt, C., Stow, D.A.V., 2007b. Morphology and mechanics of submarine spreading: A case study from the Storegga Slide. Journal of Geophysical Research F: Earth Surface, 112(3).

Michels, K.H., Suckow, A., Breitzke, M., Kudrass, H.R., Kottke, B., 2003. Sediment transport in the shelf canyon "Swatch of No Ground" (Bay of Bengal). Deep-Sea Research Part II: Topical Studies in Oceanography, 50(5): 1003-1022.

Mitchell, J.S., 1988. Palliser Bathymetry. 2nd Edition. N.Z. Oceanographic Institute Chart, Coastal Series. 1:200 000.

Mitchell, J.S., Lewis, K.B., 1996. Cook Strait Bathymetry, 3rd edition. N.Z. Oceanographic Institute Chart, Coastal Series.

Mitchell, N.C., 2005. Interpreting long-profiles of canyons in the USA Atlantic continental slope. Marine Geology, 214(1-3): 75-99.

Mitchell, N.C., 2006. Morphologies of knickpoints in submarine canyons. Bulletin of the Geological Society of America, 118(5-6): 589-605.

Molnar, P., England, P., 1990. Late Cenozoic uplift of mountain ranges and global climate change: chicken or egg? Nature, 346,: 29-34.

Montgomery, D.R., 2002. Valley formation by fluvial and glacial erosion. Geology, 30(11): 1047-1050.

Moore, J.G., Normark, W.R., Holcomb, R.T., 1994. Giant Hawaiian landslides. Annual Review of Earth and Planetary Sciences, 22: 119-144.

Morgan, E.C., McAdoo, B.G., Baise, L.G., 2008. Quantifying geomorphology associated with large subduction zone earthquakes. Basin Research, 20(4): 531-542.

Morgenstern, N.R., 1967. Submarine slumping and the initiation of turbidity currents. In: A.F. Richards (Editor), Marine Geotechnique. University of Illinois Press, Urbana, pp. 189 - 220.

Mountjoy, J.J., Barnes, P.M., Pettinga, J.R., 2009a. Morphostructure and evolution of submarine canyons across an active margin: Cook Strait sector of the Hikurangi Margin, New Zealand. Marine Geology, 260(1-4): 45-68.

Mountjoy, J.J., McKean, J., Barnes, P.M., Pettinga, J.R., 2009b. Terrestrial-style slow-moving earthflow kinematics in a submarine landslide complex. Marine Geology doi:10.1016/j.margeo.2009.09.007.

Multiwave, 2005. 05CM 2D Seismic survey, offshore East Coast - North Island, New Zealand. Unpublished openfile petroleum report 3136. Ministry of Economic Developement, Wellington.

Mutti, E., Bernoulli, D., Lucchi, F.R., Tinterri, R., 2009. Turbidites and turbidity currents from alpine 'flysch' to the exploration of continental margins. Sedimentology, 56(1): 267-318.

Netzeband, G.L., Krabbenhoeft, A., Zillmer, M., Peterson, C.J., Papenberg, C., Bialas, J., 2009. The structures beneath submarine methane seeps: Seismic evidence from Opouawe Bank, Hikurangi Margin, New Zealand. Marine Geology, In press, doi:10.1016/j.margeo.2009.07.005.

Nicol, A., Mazengarb, C., Chanier, F., Rait, G., Uruski, C., Wallace, L., 2007. Tectonic evolution of the active Hikurangi subduction margin, New Zealand, since the Oligocene. Tectonics, 26(4).

Nixon, M.F., Grozic, J.L.H., 2007. Submarine slope failure due to gas hydrate dissociation: A preliminary quantification. Canadian Geotechnical Journal, 44(3): 314-325.

Noda, A., TuZino, T., Furukawa, R., Joshima, M., Uchida, J.I., 2008. Physiographical and sedimentological characteristics of submarine canyons developed upon an active forearc slope: The Kushiro Submarine Canyon, northern Japan. Bulletin of the Geological Society of America, 120(5-6): 750-767.

Ogston, A.S., Drexler, T.M., Puig, P., 2008. Sediment delivery, resuspension, and transport in two contrasting canyon environments in the southwest Gulf of Lions. Continental Shelf Research, 28(15): 2000-2016.

Okino, K., Kato, Y., 1995. Geomorphological study on a clastic accretionary prism: the Nankai Trough. Island Arc, 4(3): 182-198.

Orange, D.L., Anderson, R.S., Breen, N.A., 1994. Regular canyon spacing in the submarine environment the link between hydrology and geomorphology. GSA Today, 4(2): 29,36-39.

Orange, D.L., Breen, N.A., 1992. The effects of fluid escape on accretionary wedges 2. Seepage force, slope failure, headless submarine canyons, and vents. Journal of Geophysical Research, 97(B6): 9277-9295.

Orange, D.L., McAdoo, B.G., Moore, J.C., 1997. Headless submarine canyons and fluid flow on the toe of the Cascadia accretionary complex. Basin Research, 9: 303 - 312.

Orpin, A.R., 2004. Holocene sediment deposition on the Poverty-slope margin by the muddy Waipaoa River, East Coast New Zealand. Marine Geology, 209(1-4): 69-90.

Orpin, A.R., Alexander, C., Carter, L., Kuehl, S., Walsh, J.P., 2006. Temporal and spatial complexity in post-glacial sedimentation on the tectonically active, Poverty Bay continental margin of New Zealand. Continental Shelf Research, 26(17-18): 2205-2224.

Owen, M., Day, S., Maslin, M., 2007. Late Pleistocene submarine mass movements: occurrence and causes. Quaternary Science Reviews, 26(7-8): 958-978.

Palanques, A., Durrieu de Madron, X., Puig, P., Fabres, J., Guille?n, J., Calafat, A., Canals, M., Heussner, S., Bonnin, J., 2006. Suspended sediment fluxes and transport processes in the Gulf of Lions submarine canyons. The role of storms and dense water cascading. Marine Geology, 234(1-4): 43-61.

Palanques, A., El Khatab, M., Puig, P., Masque, P., Sa?nchez-Cabeza, J.A., Isla, E., 2005. Downward particle fluxes in the Guadiaro submarine canyon depositional system (north-western Alboran Sea), a river flood dominated system. Marine Geology, 220(1-4): 23-40.

Palanques, A., Guillen, J., Puig, P., Durrieu de Madron, X., 2008a. Storm-driven shelf-to-canyon suspended sediment transport at the southwestern Gulf of Lions. Continental Shelf Research, 28(15): 1947-1956.

Palanques, A., Puig, P., Latasa, M., Scharek, R., 2008b. Deep sediment transport induced by storms and dense shelf-water cascading in the northwestern Mediterranean basin. Deep-Sea Research Part I: Oceanographic Research Papers, 56(3): 425-434.

Paquet, F., 2007. Morphostructural evolution of active subduction margin basins: The example of the Hawke's Bay forearc basin, New Zealand, PhD Thesis, Universite De Rennes.

Paquet, F., Proust, J.-N., Barnes, P.M., Pettinga, J.R., 2009. Inner-forearc sequence architecture in response to climatic and tectonic forcing since 150 Ka: Hawke's Bay, New Zealand. Journal of Sedimentary Research, 79: 97-124.

Paull, C.K., Buelow, W.J., Ussler Iii, W., Borowski, W.S., 1996. Increased continental-margin slumping frequency during sea-level lowstands above gas hydrate-bearing sediments. Geology, 24(2): 143-146.

Paull, C.K., Caress, D.W., Ussler, W., Lundsten, E., Thomas, H., 2008. Axial Channel Morphology Fill and Movement Within Submarine Canyons off California. EOS Transactions AGU, 89(53): Fall Meeting Supplement; Abstract OS54A-01.

Paull, C.K., Ussler III, W., Greene, H.G., Barry, J., Keaten, R., 2005. Bioerosion by chemosynthetic biological communities on Holocene submarine slide scars. Geo-Marine Letters, 25(1): 11-19.

Paull, C.K., Ussler III, W., Greene, H.G., Keaten, R., Mitts, P., Barry, J., 2003. Caught in the act: The 20 December 2001 gravity flow event in Monterey Canyon. Geo-Marine Letters, 22(4): 227-232.

Pecher, I.A., Henrys, S.A., Ellis, S., Chiswell, S.M., Kukowski, N., 2005. Erosion of the seafloor at the top of the gas hydrate stability zone on the Hikurangi Margin, New Zealand. Geophysical Research Letters, 32(24): 1-4.

Pedley, K., Barnes, P.M., Pettinga, J.R., Lewis, K.B., 2009. Seafloor structural geomorphic evolution of the accretionary frontal wedge in response to seamount subduction, Poverty Indentation, New Zealand. Marine Geology, in press.

Pettinga, J.R., 1980. Geology and landslides of the eastern Te Aute district, Southern Hawke's Bay, New Zealand., Unpub. PhD Thesis, University of Auckland, 602p pp.

Pettinga, J.R., 1982. Upper Cenozoic structural history, coastal southern Hawke's Bay, New Zealand. New Zealand Journal of Geology and Geophysics, 25(2): 149-191.

Pillans, B., Chappell, J., Naish, T., 1998. A review of the Milankovitch climatic beat: template for Plio-Pleistocene sea-level changes and sequence stratigraphy. Sedimentary Geology, 122: 5 - 21.

Piper, D.J.W., Cochanat, P., Morrison, M.L., 1999. The sequence of events around the epicentre of the 1929 Grand Banks earthquake: initiation of debris flow and turbidity current inferred from sidescan sonar. Sedimentology, 46: 79 - 97.

Pondard, N., Barnes, P.M., Lamarche, G., in prep. Paleoearthquake records from seismic reflection profiles of active submarine faults, Cook Strait, New Zealand: Implications for earthquake rupture processes, fault interactions, and seismic hazard. For submittal to JGR.

Popinet, S., 2003. Gerris: A tree-based adaptive solver for the incompressible Euler equations in complex geometries. Journal of Computational Physics, 190(2): 572-600.

Posamentier, H.W., Erskine, R.D., Mitchum, R.M., 1991. Models for submarine fan deposition within a sequence stratigraphic frameworks. In: P. Weimer and M. Link (Editors), Seismic facies and sedimentary processes of submarine fans and turbidite systems. Springer-Verlag, pp. 197-222.

Posamentier, H.W., Jervey, M.T., Vail, P.R., 1988. Eustatic controls on clastic deposition I - conceptual framework. In: C.K. Wilgus et al. (Editors), Sea-level Changes: An Integrated Approach. Society of Economic Paleontologists & Mineralogists, Special Publication, pp. 109-124.

Posamentier, H.W., Vail, P.R., 1988. Eustatic controls on clastic deposotion II - sequence and systems tract models. In: C.K. Wilgus, H. Posamentier, C.A. Ross and C.G.S. Kendall (Editors), Sea-level changes: an integrated approach. Society of Economic Paleontologists & Mineralogists, Special Publication, pp. 125-154.

Pratson, L.F., Coakley, B.J., 1996. A model for the headward erosion of submarine canyons induced by downslope-eroding sediment flows. Geological Society of America Bulletin, 108(2): 225-234.

Pratson, L.F., Ryan, W.B.F., Mountain, G.S., Twichell, D.C., 1994. Submarine canyon initiation by downslope-eroding sediment flows; evidence in late Cenozoic strata on the New Jersey continental slope. Geological Society of America Bulletin, 106(3): 395-412.

Puig, P., Ogston, A.S., Mullenbach, B.L., Nittrouer, C.A., Parsons, J.D., Sternberg, R.W., 2004. Storm-induced sediment gravity flows at the head of the Eel submarine canyon, northern California margin. Journal of Geophysical Research C: Oceans, 109(3): C03019 1-10.

Puig, P., Ogston, A.S., Mullenbach, B.L., Nittrouer, C.A., Sternberg, R.W., 2003. Shelf-to-canyon sediment-transport processes on the Eel continental margin (northern California). Marine Geology, 193(1-2): 129-149.

Puig, P., Palanques, A., Orange, D.L., Lastras, G., Canals, M., 2008. Dense shelf water cascades and sedimentary furrow formation in the Cap de Creus Canyon, northwestern Mediterranean Sea. Continental Shelf Research, 28(15): 2017-2030.

Rahiman, T.I.H., Pettinga, J.R., 2006. The offshore morpho-structure and tsunami sources of the Viti Levu Seismic Zone, southeast Viti Levu, Fiji. Marine Geology, 232(3-4): 203-225.

Sansoucy, M., Locat, J., Lee, H.J., 2007. Geotechnical Considerations Of Submarine Canyon Formation: The Case Of Cap De Creus Canyon In: V. Lykousis, D.

Sakellariou and J. Locat (Editors), Submarine Mass Movements and Their Consequences. Springer, pp. 221-230.

Shanmugam, G., 1996. Slump and debris-flow dominated basin-floor fans in the North Sea: an evaluation of conceptual sequence-stratigraphical models based on conventional core data. Sequence stratigraphy in British geology: 145-175.

Shepard, F.P., 1932. Landslide modifications in submarine valleys. Am. Geophy. Union trans. 13th Ann. Mtg.: 226-230.

Shepard, F.P., 1981. Submarine canyons: multiple causes and long-time persistence. American Association of Petroleum Geologists Bulletin, 65: 1062-1077.

Smith, D.P., Kvitek, R., Iampietro, P.J., Wong, K., 2007. Twenty-nine months of geomorphic change in upper Monterey Canyon (2002-2005). Marine Geology, 236(1-2): 79-94.

Smith, D.P., Ruiz, G., Kvitek, R., Iampietro, P.J., 2005. Semiannual patterns of erosion and deposition in upper Monterey Canyon from serial multibeam bathymetry. Bulletin of the Geological Society of America, 117(9-10): 1123-1133.

Spencer, J.W., 1903. Submarine valleys off the American coasts and in the North Atlantic. Geol. Soc. Am. Bull., 14: 207-226.

Stephens, S.A., Gorman, R.M., 2006. Extreme wave predictions around New Zealand from hindcast data. New Zealand Journal of Marine and Freshwater Research, 40(3): 399-411.

Stirling, M.W., Litchfield, N., Gersenberger, M., Langridge, R., Berryman, K., Van Dissen, R., Villamor, P., Nicol, A., McVerry, G., Wilson, K., Barnes, P.M., Lamarche, G., Nodder, S., 2009. New national seismic hazard model for New Zealand. Seismological Research Letters (abstract), 80(2): 367.

Stirling, M.W., McVerry, G.H., Berryman, K.R., 2002. A new seismic hazard model for New Zealand. Bulletin of the Seismological Society of America, 92(5): 1878-1903.

Sultan, N., Cochonat, P., Canals, M., Cattaneo, A., Dennielou, B., Haflidason, H., Laberg, J.S., Long, D., Mienert, J., Trincardi, F., Urgeles, R., Vorren, T.O., Wilson, C., 2004a. Triggering mechanisms of slope instability processes and sediment failures on continental margins: A geotechnical approach. Marine Geology, 213(1-4): 291-321.

Sultan, N., Cochonat, P., Foucher, J.P., Mienert, J., 2004b. Effect of gas hydrates melting on seafloor slope instability. Marine Geology, 213(1-4): 379-401.

Sultan, N., Gaudin, M., Berne, S., Canals, M., Urgeles, R., Lafuerza, S., 2007. Analysis of slope failures in submarine canyon heads: An example from the Gulf of Lions. Journal of Geophysical Research F: Earth Surface, 112(1).

Talling, P.J., Amy, L.A., Wynn, R.B., 2007a. New insight into the evolution of large-volume turbidity currents: Comparison of turbidite shape and previous modelling results. Sedimentology, 54(4): 737-769.

Talling, P.J., Wynn, R.B., Masson, D.G., Frenz, M., Cronin, B.T., Schiebel, R., Akhmetzhanov, A.M., Dallmeier-Tiessen, S., Benetti, S., Weaver, P.P.E., Georgiopoulou, A., Zühlsdorff, C., Amy, L.A., 2007b. Onset of submarine debris flow deposition far from original giant landslide. Nature, 450(7169): 541-544.

ten Brink, U., 2009. Tsunami hazard along the U.S. Atlantic coast. Marine Geology, 264(1-2): 1-3.

Twichell, D.C., Roberts, D.G., 1982. Morphology, distribution, and development of submarine canyons on the United States Atlantic continental slope between Hudson and Baltimore Canyons. Geology, 10(8): 408-412.

Uruski, C.I., 1992. Sedimentary basins and structure of Cook Strait. 92/3, Institute of Geological and Nuclear Sciences, Lower Hutt, New Zealand.

Vail, P.R., Mitchum, R.M.J., Thompson, S.I., 1977. Seismic stratigraphy and global changes of sea level, part 4: global cycles of relative changes of sea level. In: C.W. Payton (Editor), Seismic stratigraphic applications to hydrocarbon exploration. American Association of Petroleum Geologists memoir, pp. 83-97.

Van Dissen, R., Berryman, K., King, A., Webb, T., Brackley, H., Barnes, P., Beavan, J., Benites, R., Barker, P., Carne, R., Cochran, U., Dellow, G., Fry, B., Hemphill-Haley, M., Francois-Holden, C., Lamarche, G., Langridge, R., Litchfield, N., Little, T., McVerry, G., Ninis, D., Palmer, N., Perrin, N., Pondard, N., Semmens, S., Stephenson, W., Robinson, R., Villamor, P., Wallace, L., Wilson, K., 2009. It's Our Fault: Better Defining the Earthquake Risk in Wellington - Results to Date & a Look to the Future, 2009 NZSEE Conference, Christchurch, New Zealand.

Varnes, D.J., 1978. Landslide types and processes. In: R.L. Schuster and R.J. Krizek (Editors), Special Report 176: Landslides: Analysis and Control. Transportation Research Board, Washington DC, pp. 11-33.

Veatch, A.C., Smith, P.A., 1939. Atlantic Submarine Valleys of the United States and the Congo Submarine Valley. Geol. Soc. of America special papers number 7, New York, 106 pp.

Vennell, R., 1994. Doppler current profiler measurements of tidal phase and amplitude in Cook Strait, New Zealand. Continental Shelf Research, 14(4): 353-364.

Walcott, R.I., 1978. Present tectonics and late Cenozoic evolution of New Zealand. The Geophysical Journal of the Royal Astronomical Society, 52(1): 137-164.

Wallace, L.M., Beavan, J., McCaffrey, R., Darby, D., 2004. Subduction zone coupling and tectonic block rotations in the North Island, New Zealand. Journal of Geophysical Research, 109(B12406).

Walsh, J.P., Alexander, C.R., Gerber, T., Orpin, A.R., Summers, B.W., 2007. The demise of a submarine canyon? Evidence for highstand infilling on the Waipaoa River continental margin, New Zealand. Geophysical Research Letters, 34(L20606).

Walsh, J.P., Corbett, D.R., Mallinson, D., Goni, M., Dail, M., Loewy, C., Marciniak, K., Ryan, K., Smith, C., Stevens, A., Summers, B., Test, T., 2006. Mississippi delta mudflow activity and 2005 gulf hurricanes. Eos, 87(44): 477-479.

Welbon, A.I.F., Brockbank, P.J., Brunsden, D., Olsen, T.S., 2007. Characterizing and producing from reservoirs in landslides: Challenges and opportunities, Geological Society Special Publication, pp. 49-74.

Whipple, K.X., 2004. Bedrock rivers and the geomorphology of active orogens, Annual Review of Earth and Planetary Sciences, pp. 151-185.

Wilson, K., Berryman, K., Litchfield, N., Little, T., 2006. A revision of mid-late Holocene marine terrace distribution and chronology at the Pakarae River mouth, North Island, New Zealand. New Zealand Journal of Geology and Geophysics, 49(4): 477-489.

Winters, W.J., Waite, W.F., Mason, D.H., Gilbert, L.Y., Pecher, I.A., 2007. Methane gas hydrate effect on sediment acoustic and strength properties. Journal of Petroleum Science and Engineering, 56(1-3): 127-135.

Wright, L.D., Friedrichs, C.T., Kim, S.C., Scully, M.E., 2001. Effects of ambient currents and waves on gravity-driven sediment transport on continental shelves. Marine Geology, 175(1-4): 25-45.

Xu, J.P., Wong, F.L., Kvitek, R., Smith, D.P., Paull, C.K., 2008. Sandwave migration in Monterey Submarine Canyon, Central California. Marine Geology, 248(3-4): 193-212.

Zhu, Y.M., Lu, X.X., Zhou, Y., 2008. Sediment flux sensitivity to climate change: A case study in the Longchuanjiang catchment of the upper Yangtze River, China. Global and Planetary Change, 60(3-4): 429-442.

Appendix I

Law, C.S., Nodder, S.D., Mountjoy, J.J., Marriner, A., Orpin, A., Pilditch, C.A., Franz, P. and Thompson, K., 2009. Geological, hydrodynamic and biogeochemical characterisation of a New Zealand deep-water methane cold seep during a three year time-series study. In press at Marine Geology doi:10.1016/j.margeo.2009.06.018.

Appendix I

ARTICLE IN PRESS
MARGO-04366; No of Pages 20
Marine Geology xxx (2009) xxx–xxx
Contents lists available at ScienceDirect
Marine Geology
journal homepage: www.elsevier.com/locate/margeo

Geological, hydrodynamic and biogeochemical variability of a New Zealand deep-water methane cold seep during an integrated three-year time-series study

C.S. Law [a,*,1], S.D. Nodder [a,1], J.J. Mountjoy [a,b], A. Marriner [a], A. Orpin [a], C.A. Pilditch [c], P. Franz [a], K. Thompson [d]

[a] National Institute of Water & Atmospheric Research (NIWA) Ltd, Private Bag 14-901, Kilbirnie, Wellington, New Zealand
[b] Department of Geology, University of Canterbury, Private Bag 4800, Christchurch, New Zealand
[c] Department of Biological Sciences, University of Waikato, Private Bag 3105, Hamilton, New Zealand
[d] NIWA Ltd, PO Box 11115, Hillcrest, Hamilton, New Zealand

ARTICLE INFO

Article history:
Received 24 November 2008
Received in revised form 3 June 2009
Accepted 26 June 2009
Available online xxxx

Communicated by G.J. de Lange

Keywords:
methane
hydrates
cold seeps
methane isotopes
methanotrophy
Hikurangi subduction Margin

ABSTRACT

Cold seeps are widely distributed on active and passive margins and display considerable temporal variability in terms of gas and fluid expulsion rates and volume, over scales of hours to days. To constrain this variability, two cold seeps, the North and South Tower, located at the Wairarapa Seep site on Opouawe Bank, Cook Strait, New Zealand, were monitored in an integrated geological and biogeochemical study during eight surveys between 2005 and 2008. To ensure sampling of the water column within the flare overlying the seeps the vessel was manoeuvred in response to the backscatter data from a hull-mounted 38 kHz single-beam echo-sounder. High methane concentrations (>100 nmol l^{-1}) were found within 400–450 m-high flares at both sites, and within an 825 m-high flare at a newly identified seep, southeast of Pahaua Bank. Elevated bottom water methane was also found over newly identified mud volcanoes on the Campbell Bank, Cook Strait. The locations of the seeps appear to be structurally controlled with active methane vents occurring on anticlinal ridges and associated with a 30 m-high normal fault scarp on Opouawe Bank. Fluid flow is facilitated by sedimentary layer permeability properties, structural focusing and dilational fracturing on the crest of a large anticlinal ridge, cored by a seaward-verging reverse fault. The South Tower cold seep did not significantly influence bulk sediment and water column particulates and nutrients, although high bacterial biomass, productivity and methane oxidation rates were associated with elevated methane in the flare. The seep flares exhibited depleted $\delta^{13}C$–CH_4 values (−63 to −70‰), characteristic of shallow biogenic gas sources. Incorporation of the $\delta^{13}C$–CH_4 and CH_4 concentration data in a mixing model, and comparison of the water residence time with methane oxidation rates, indicated that the primary fate of methane in the flare was dilution. The dissolved methane originating from the seeps was retained in the water column at depths >700 m, with minimal contribution to atmospheric emissions, as confirmed by surface methane mapping. Nevertheless, the South Tower seep was a significant source of methane with a column-integrated burden below 700 m of 5.6 mmol m^{-2}, and an estimated annual emission of $0.5–1 \times 10^6$ mol CH_4. The structural and tectonic setting of the Wairarapa Seep provides a useful analogue model for other convergent margin cold seeps on the Hikurangi Margin and elsewhere. This unique, three-year integrated study provided valuable insights into the linkage between geological structure and overlying water column biogeochemistry, and confirmed the value of this cold seep site for long-term monitoring.

1. Introduction

Global atmospheric methane concentrations have increased rapidly from pre-industrial levels of 700–740 ppbv but have stabilised over the last decade at ~1760 ppbv (Steele et al., 2002). The primary sources of atmospheric methane are human modification to the landscape via cultivation and natural emissions from swamp, peat, termites and, more recently, thawing permafrost environments (Prather et al., 1995; Walter et al., 2006). In the ocean, methane is produced primarily during organic matter decomposition in sediments by microbial methanogenesis (Canfield et al., 2005). In addition, methane is expelled from the sea-floor at hydrothermal and cold seep sites along active and passive continental margins (Kulm et al., 1986; Le Pichon et al., 1992; Kvenvolden, 1993; Judd, 2003). Collectively, marine sources of methane are relatively minor, contributing less than 2% of the total global methane budget (Prather et al., 1995). Nonetheless, methane hydrates in continental margin sediments, which are stable at water depths below ~500 m due to pressure and low-temperature dependency (Canfield et al., 2005), represent a huge reservoir of methane with global continental margin

* Corresponding author. Tel.: +64 4 3860300; fax: +64 4 3862153.
E-mail address: c.law@niwa.co.nz (C.S. Law).
[1] The first two authors contributed equally to this paper.

0025-3227/$ – see front matter © 2009 Elsevier B.V. All rights reserved.
doi:10.1016/j.margeo.2009.06.018

sediments containing ~2×10^{16} kg C methane (Kvenvolden, 1993). Hydrates are a potential energy resource (Kvenvolden, 1993) but also pose a possible threat if future warming of the ocean leads to large-scale methane release from the sediments into the water column and the atmosphere (Pecher et al., 2005; Kastner, 2001, Dickens, 2003).

Natural sources and sinks of methane are poorly constrained in New Zealand's large offshore Exclusive Economic Zone. Methane supersaturation in surface waters (relative to atmospheric methane) of up to 500% in the Cook Strait, central New Zealand (Law et al., unpublished data), indicates local methane production from microbial decomposition of organic matter in the water column and sediments, or riverine input. However, the presence of active cold seeps in the Cook Strait, as documented originally by Lewis and Marshall (1996), represents an alternative potential source of methane. Several other methane-rich seep sites were identified by Lewis and Marshall (1996). along the active Hikurangi Margin, E–SE of the North Island, where bottom-simulating reflectors (BSR) in geophysical profiles inferred the presence of methane hydrates (Katz, 1982; Henrys et al., 2003). Lewis and Marshall (1996) showed that many of the seep locations are related to faulting and folding processes and the lithological characteristics of the sub-surface geological units within the actively deforming accretionary wedge. Thus, it is apparent that structural patterns and sedimentary processes are likely to influence the chemical characteristics, the spatial extent and temporal variability of the cold seeps along the margin. Although these earlier studies did not identify active seep sites off the SE Wairarapa coast, sea-floor gas expulsion was subsequently identified in archived underwater photography and echo-sounder data in 1996 (L. Carter, pers. comm., NIWA unpublished data). Following initial investigations in 2005, this site was chosen as the location for an integrated time-series study of a cold seep. This site was informally named the Wairarapa Seep and is situated at a water depth of ~1050 m on Opouawe Bank, a transverse ridge at the southern end of the Hikurangi Margin (Fig. 1).

The subsequent time-series of geological and biogeochemical data is used in this paper to determine the influence of geological structures on the location and character of the seep fluids, and derive a local model for cold seep formation along the Hikurangi Margin from observations of the structural and tectonic setting. In addition, the study documents the temporal variability of methane emissions from the cold seep and its impact on water column and sediment geochemistry, with the fate of the seep methane determined including the contribution to the atmospheric methane pool. This time-series provides a unique reference for a cold-water seep for comparison with more recent studies of methane seeps on the Hikurangi Margin (Bialas et al., 2007; Greinert et al., 2007—this issue), and also for the assessment of future variations in methane emissions, both specifically at the Wairarapa seep and also on a more regional basis.

1.1. Regional setting

Cook Strait is a Z-shaped bathymetric depression that separates the North and the South islands of New Zealand (Fig. 1A,B) that is characterised by strong tidal currents and complex circulation (Heath, 1985; Harris, 1990). Geologically, the origin of Cook Strait is related to the progressive rotation of the several 2 to >3 km-deep sedimentary basins within the strait over the last 2 million years (Lewis et al., 1994), reflecting the ongoing development of the Hikurangi subduction Margin (e.g., Davey et al., 1986; Lewis and Pettinga, 1993; Barnes et al., 2009—this issue). Three main sedimentary basins that underlie the Cook Strait continental shelf and canyon system (Lewis et al., 1994), that have potential as petroleum source and reservoir rocks (Uruski, 1992). On the continental slope, margin-parallel ridges dominate inter-canyon bathymetry, and are best expressed along the SE Wairarapa coast and further north along the convergent Hikurangi Margin (Fig. 1A,B). These ridges strike approximately parallel to the subduction zone and are the southernmost expression of numerous anticlinal ridges that extend along the length of the offshore section of the accretionary prism of the subduction margin (see Barnes et al., 2009-this issue). The SE Wairarapa ridges (Opouawe, Palliser and Pahaua banks) are approximately ovoid in shape, ~15–30 km in length and 5–10 km in width and generally steeper on their eastern flanks (Mountjoy et al., 2009) (Fig. 2A). Ridges are separated by >1 km-deep canyon systems, including the Palliser, Opouawe and Pahaua canyons (Fig. 2A).

In this paper, we concentrate on two seep sites that lie in close proximity on the Opouawe Bank, the North Tower (41° 46.90'S 175° 24.09'E) and South Tower (41° 47.33'S 175° 24.42'E) (Fig. 2B). A third site at the previously undescribed Pahaua Seep site at 41° 41.83'S 175° 41.22'E, northeast of the Wairarapa Seep and southeast of Pahaua Bank (Mountjoy et al., 2009), was included for comparison. In addition, targeted sampling of recently identified mud volcano features on the outer Campbell Bank (Fig. 2C) was also conducted. A time-series of physical and biogeochemical data was collected from September 2005 during eight research voyages aboard the *RV Tangaroa* primarily at the South Tower (Table 1), including a 6-day voyage in September–October 2006 (TAN0612) and a three-day survey in September–October 2007 (TAN0711) that also targeted other locations in the Cook Strait and Wairarapa shelf region (Fig. 2A). Two other research initiatives followed subsequently in this region; the first, a NOAA–NIWA voyage in late 2006 (TAN0616, Baco et al., 2009—this issue), and the second, the SO-191 NewVents voyage on *RV Sonne* in early 2007 (Bialas et al., 2007; Greinert et al., 2009—this issue).

2. Methods

For all Methods, see online material.

3. Results

3.1. Geology, structure and morphology of the main Wairarapa Seep sites

The Opouawe Bank is one of several thrust fault-propagated, seaward-vergent, anticlinal ridges present along the length of the Hikurangi Margin (Davey et al., 1986; Lewis and Pettinga, 1993; Barnes et al., 1998; Mountjoy et al., 2009; Barnes et al., 2009-this issue) (Fig. 3A). Recently acquired MCS profiles and EM300 multi-beam data have enabled a reinterpretation of the structure in this area (Mountjoy et al., 2009). The controlling frontal thrust fault of Opouawe Bank is well-imaged in the upper one to two seconds two-way travel-time (TWT), and has been described previously by Barnes et al. (1998) as the Pahaua Fault (Fig. 3A). Fault-tip break-out lineaments, matched to sub-bottom MCS data, show a right-lateral, structural step-over of the Pahaua Fault at Opouawe Bank. Additionally, the Opouawe–Uruti Fault cuts through Opouawe Bank, isolating the north-eastern (shallowest) end of the ridge where a second main active seep area is located (Greinert et al., 2009—this issue). A ~30 m-high, S-shaped scarp on the crest of the Opouawe Bank, which is the location of the North Tower site, is interpreted to be a normal fault scarp that roots onto the Pahaua Fault. The exact relationship of these two faults cannot be confirmed with the existing data, however, since the reflectors on the SO-191 MCS reflection profile are obscured by the sea-floor multiple at this depth (Fig. 3B). A clearly defined bottom-simulating reflector (BSR) in the MCS profile indicates the base of the gas hydrate stability zone at approximately 0.5 s TWT. The BSR is disrupted beneath the seep sites on Opouawe Bank, and a network of near-surface faults and chimneys is interpreted to be facilitating fluid expulsion (Fig. 3C) (Netzeband et al., 2009—this issue). At the Pahaua Seep site (Fig. 2A), a MCS profile shows similar disturbance in sub-surface reflectivity to that seen on Opouawe Bank (Fig. 3D,E). This seep site also occurs in the hanging wall of an (unnamed) active, thrust fault-propagated anticline (Mountjoy et al., 2009). The continuity of the interpreted BSR at this location is disrupted, and additionally, in areas above this,

Please cite this article as: Law, C.S., et al., Geological, hydrodynamic and biogeochemical variability of a New Zealand deep-water methane cold seep during an integrated three-year time-series study, Mar. Geol. (2009), doi:10.1016/j.margeo.2009.06.018

Appendix I

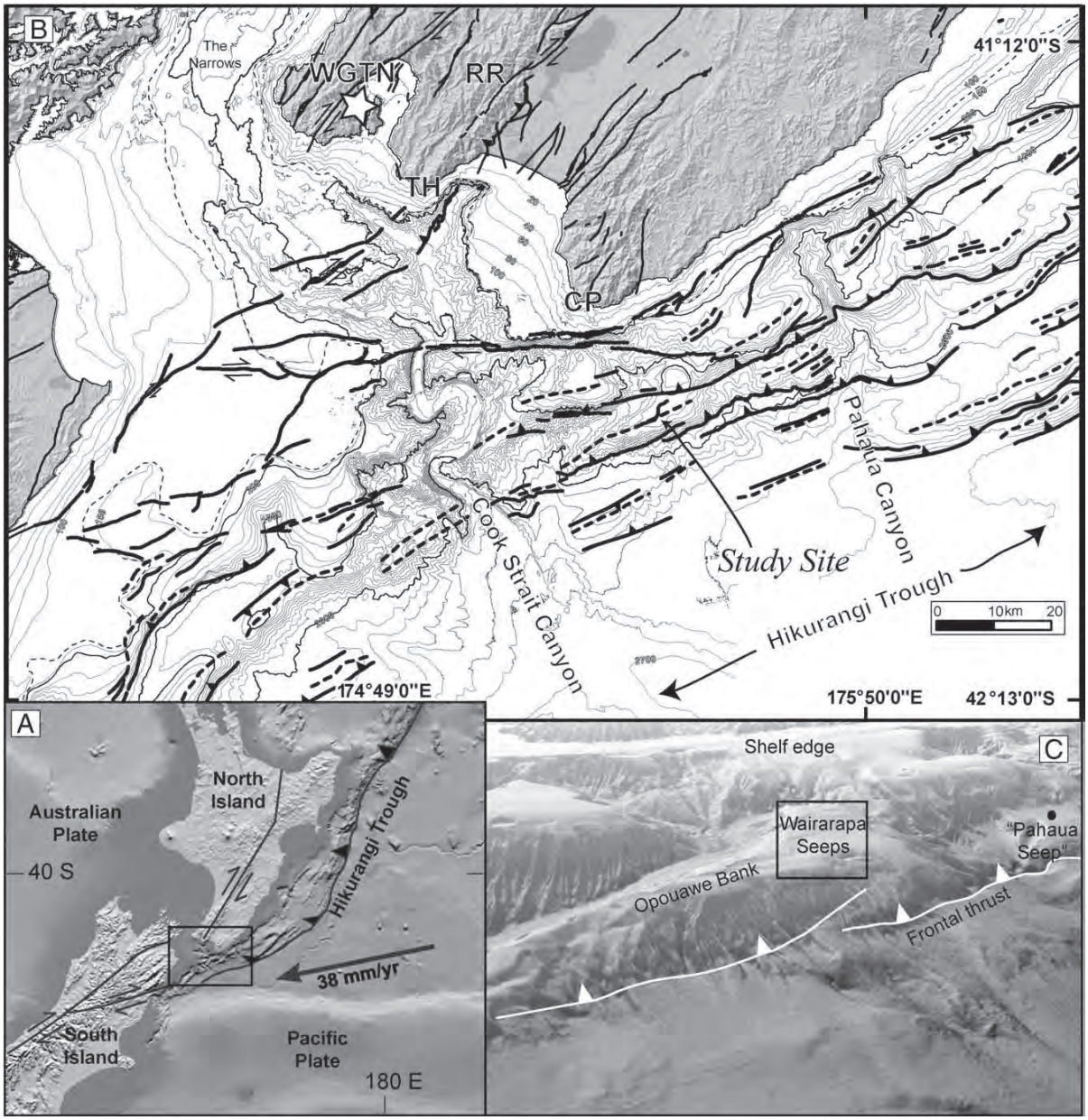

Fig. 1. (A) Plate margin setting with direction and magnitude of Nuvel-1A plate motion vector of the Pacific Plate, relative to the Australian Plate, at the Cook Strait study area, (B) Regional bathymetric map with principal structural elements (after Mountjoy et al., 2009). Solid lines delineate fault traces and dashed lines delineate fold axes. Abbreviations: WGTN denotes Wellington City, TH is Turakirae Head, CP is Cape Palliser, RR is Rimutaka Ranges, and (C) Oblique image of the study site showing Opouawe Bank with the location of the Wairarapa Seeps and the Pahaua Seep. Image derived from a Digital Terrain Model with 25 m resolution. Vertical exaggeration is 3×.

the horizontal reflectivity is masked. A bright spot occurs at the upper end of one of these masking zones (Fig. 3D,E).

New geomorphological interpretations suggest that the surficial slope morphology of the Opouawe Bank reflects the different processes shaping the NW and SE flanks. The ~200 m-high NW flank of the ridge is dominated by translational landslide scars identified by headscarps and sediment-mantled, low-angle failure surfaces (Fig. 3A). The lower boundary of this slope is the Opouawe Canyon, which is apparently subject to erosion by active sediment transport processes, based on the fresh appearance of scour features on the canyon floor. The ~800 m-high SE flank of the ridge is characterised by numerous, regularly spaced, sub-parallel and linear gullies, near where the South Tower site is located. The lower reaches of the gully systems are choked with sediment that is accumulating on the lower slope, while the heads of the gullies are commonly over-steepened, indicating active incision into the smooth-draped surface of the bank. There is also evidence for larger landslides occurring off the frontal slope, in terms of both scars and surface debris (Fig. 3A).

A near-surface sub-bottom seismic reflection dip profile across the North and South Tower sites shows that reflectors at the seeps are substantially different from the surrounding muddy sediment (Fig. 4). At the seep sites, strong discontinuous reflectors occur to a depth of 10–15 m below the sea-floor, and at the North Tower, sub-surface hyperbolic diffractions are evident in the profile. The quality of the seismic data across the South Tower is poor due to irregular ship speed during the surveying, but strong, discontinuous sub-surface reflectors

Please cite this article as: Law, C.S., et al., Geological, hydrodynamic and biogeochemical variability of a New Zealand deep-water methane cold seep during an integrated three-year time-series study, Mar. Geol. (2009), doi:10.1016/j.margeo.2009.06.018

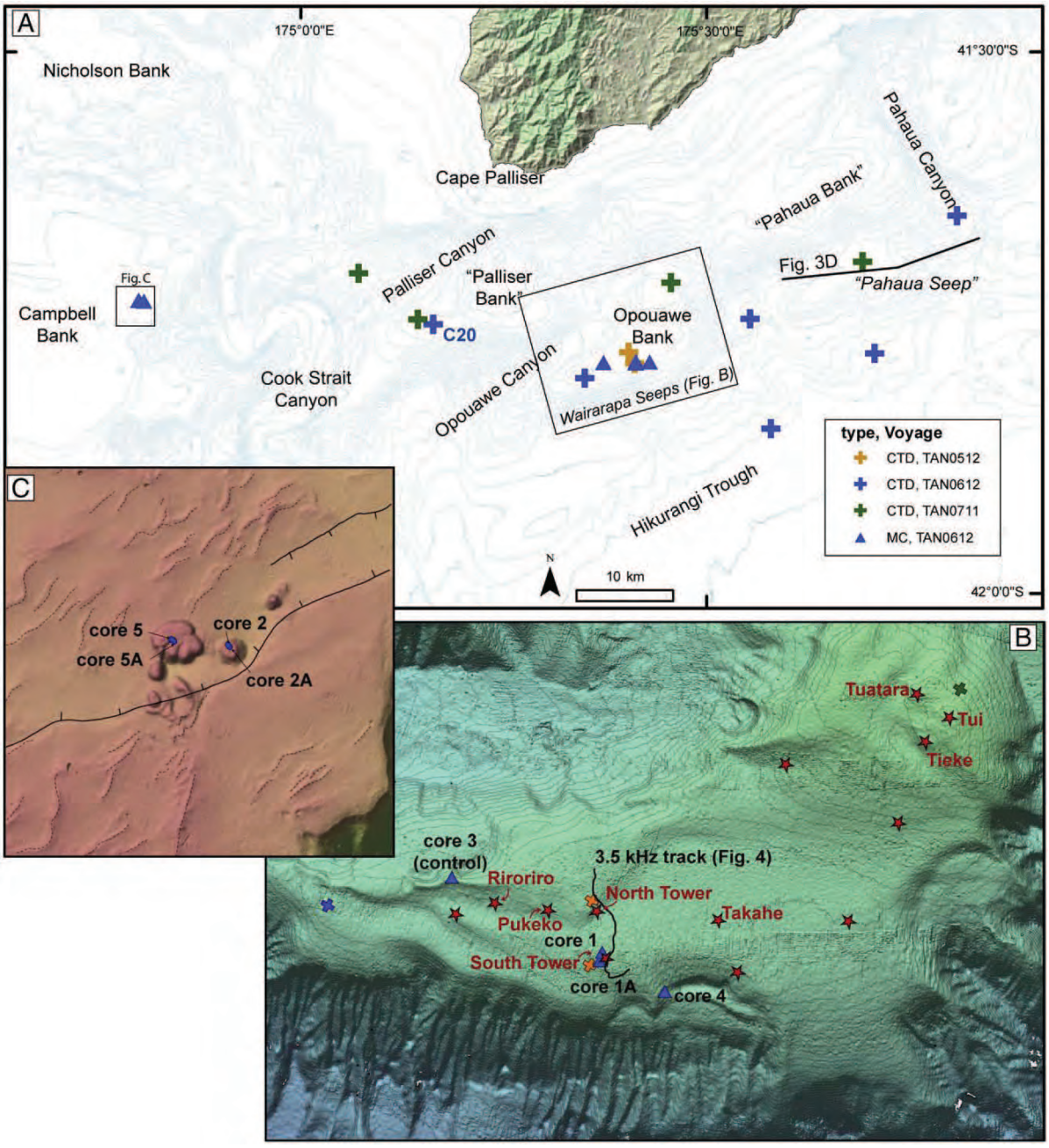

Fig. 2. (A) Location of stations and geophysical transect lines for all NIWA seep voyages since 2005 showing water column profile (CTD, crosses) and sediment sampling station locations (MC, blue triangles), overlain on regional bathymetric contours, (B) Opouawe Bank bathymetry in detail, showing positions of the North and South Towers (orange crosses), sediment coring sites (blue triangles), the track of the 3.5 kHz profile from TAN0616, as shown in Fig. 4, and other seep sites identified on SO-191 (red stars), as described in Bialas et al. (2007) and Greinert et al. (2009—this issue), and (C) Mud volcano sites on the Campbell Bank showing sampling positions of multi-cores and inferred faults overlain on high-resolution multi-beam bathymetry.

are still evident in the low quality record (Fig. 4). Here, segment up to 200 m in length at around 25–40 m below the surface display low frequency and prolonged echoes. Surficial material on the Opouawe Bank has the characteristic signature of accumulated hemipelagic sediment in the high-resolution 3.5 kHz profiles (Fig. 4). Away from the seep sites, the sea-floor reflector is sharp and underlain by 15–20 m-thick, diffuse to weakly laminated, sub-horizontal stratigraphic units. At 15–20 m sub-bottom depth, two sharp, parallel and continuous reflectors occur, separated by approximately 3–4 m. These reflectors are offset vertically by ~25 m across the North Tower seep site, and south of the South Tower, these paired reflectors are weak and diffuse.

The newly observed mud volcano on the outer edge of the Campbell Bank comprises several dome-like sea-floor features, adjacent to a normal fault scarp (Fig. 2C). The extensional structures adjacent to the mud volcano are inferred to provide the plumbing networks to allow fluidised mud to be expelled onto the sea-floor. Despite numerous examples from other offshore convergent margins

Please cite this article as: Law, C.S., et al., Geological, hydrodynamic and biogeochemical variability of a New Zealand deep-water methane cold seep during an integrated three-year time-series study, Mar. Geol. (2009), doi:10.1016/j.margeo.2009.06.018

Table 1
Sampling campaigns at the Wairarapa Seep sites (N = North Tower, S = South Tower). Methane samples that were poisoned using mercuric chloride and analysed later in the laboratory are indicated by *. Stored samples from TAN0702 were found to be contaminated and were not included in the interpretation.

Tangaroa voyage ID	Date	Seep	Sampling using ES60	Surface CH_4 mapping	$[CH_4]$ profile	$\delta^{13}C$–CH_4	Sediment coring	Geophysical surveying
TAN0504	Feb 2005			X				
TAN0512	Sept–Oct 2005	N&S	X	X	X	X		
TAN0608	July 2006	S	X	X	X	X		
TAN0612	Sept–Oct 2006	S	X	X	X	X	X	X
TAN0616	Oct–Nov 2006	N&S	X		X*		X	X
TAN0702	Jan–Feb 2007	S			X*			
TAN0711	Aug–Sept 2007	N&S	X	X	X	X	X	X
TAN0805	April–May 2008	S			X*	X		

(e.g., Barber et al., 1986; Reed et al., 1990; Olu et al., 1997; Judd and Hovland, 2007), to the best of our knowledge, this is the first identification of such features on the offshore Hikurangi Margin. Mud volcanoes have been observed onshore in the eastern North Island (e.g., Pettinga, 2003), and pock-marks in a harbour environment on the northern Hikurangi Margin (e.g., Nelson and Healy, 1984).

3.2. Hydrography

The Cook Strait is a physically dynamic area, characterised by strong tidal currents, augmented by enhanced mean flows driven by the constricted topography and meteorological wind forcing (Heath, 1985; Harris, 1990). The Wairarapa Seep site is influenced by different water masses and variable current flows, complicating determination of the fate of methane released from the seep. The general circulation field in this region is dominated by the interaction of large eddies to the east and south of the Wairarapa site and mixing of subtropical water from the northward-flowing Southland Current with the D'Urville Current flowing through the Cook Strait from the west. These merging current systems generate the Wairarapa Coastal Current (WCC), which lies inshore of the southward-flowing East Cape Current (Chiswell, 2000). This results in variability in the origin of surface waters above the seep site, as is apparent in a T–S plot (Fig. 5A,B), with the minimum salinity of ~34.9 indicative of a stronger influence of the Southland Current, and the maximum salinity of 35.1–35.3 reflecting the dominance of subtropical water from the D'Urville and East Cape currents (Chiswell and Roemmich, 1998). A transect of geostrophic current velocities across the Wairarapa Seep site in 1998 identified a northward-flowing tongue of WCC, with a speed of 0.1–0.2 m s^{-1} in the upper 200 m (Chiswell, 2000, reproduced in Fig. 5D). Waters deeper than 350 m are unaffected by the flow of the D'Urville Current through Cook Strait due to the shallow depth of the Terawhiti Sill in northern Cook Strait. However, Chiswell (2000) also identified secondary sub-surface flow towards the north to a depth of 600 m at 30 km offshore. Since the Wairarapa Seep site is ~20 km from the Wairarapa coast, the presence of this deeper sub-surface flow may obscure or suppress the influence of the seep in the upper water column. The bottom water at the seep site is Antarctic Intermediate water, which is characterised by a salinity minimum (Fig. 5B), and has not been recently ventilated. AAIW follows the surface circulation south along the east coast of the North Island, passing across the region of the seep before turning east and travelling along the northern flank of the Chatham Rise (S. Chiswell, pers. comm.).

Buoyancy frequency (N^2) profiles (Fig. 5C) show increased stability at the base of the surface mixed layer, with values on the order of 1–1.5×10^{-5} s^{-2}, and uniform low values of ~0.5×10^{-6} s^{-2} between 550 m and 750 m indicating that the water column in this depth range is reasonably well-mixed. However, stratification is apparent in bottom waters, with N^2 values of 1–1.5×10^{-5} s^{-2} that equal or exceed that at the base of the surface mixed layer. This stratification at 870–1000 m may suppress the vertical transport of dissolved methane. Although the rising bubbles will generate a vertical velocity, this does not appear to erode the bottom water stratification in contrast to the Haakon Mosby Mud Volcano, where uniform temperature and salinity up to 300 m above the sea-floor is attributed to bubble flare-induced mixing (Sauter et al., 2006).

Although current flow at depth is not well-documented in this region, an indication of the mean circulation was obtained using the NIWA Regional Ocean Model that incorporates regional bathymetry at 7 km resolution (Rickard et al., 2005) and has been validated for the surface flow in this area (Chiswell and Rickard, 2006). The model output indicated a net westward flow along the seabed in the Wairarapa Seep region (G. Rickard, pers. comm.), suggesting potential transport of methane from the seep flare across and into the southern Cook Strait. Currents at the South Tower site showed significant vertical gradients in the bottom 500 m over a 3-day period, with decreased speeds and greater variability in current direction near the sea floor (Fig. 6). A strong tidal signal is evident at 1048 m, (Fig. 6A–D), with temperature variation of 0.3 °C. Near-bottom currents were 2–15 cm s^{-1}, with progressive current vector analysis indicating transport to the southwest (Fig. 6G). Current speeds at 906 m averaged 0–10 cm s^{-1}, with brief periods of high flow (10–30 m s^{-1}) and progressive current vector analysis indicating water transport of ~10 km to the west (Fig. 6F). A more constant westerly flow of 5–15 cm s^{-1} was recorded at 700 m that would have transported water ~23 km into the Cook Strait over a 3-day period (Fig. 6E). The vertical gradient in current direction and speed, combined with the stratification between 700 and 850 m (Fig. 5C), would result in vertical and lateral smearing of the flare.

3.3. Flare sampling and characteristics

The South Tower was initially re-located in September 2005 (Table 1) at the approximate location of bubbles emanating from the sea-floor in 1996 (L. Carter, pers. comm., NIWA unpublished data). The North Tower was sampled subsequently in July 2006, followed by high-resolution measurements made at the South Tower during September 2006 (Table 1). The two flares were evident in the ES60 backscatter data, as hydroacoustic manifestations of bubbles on the echograms, at a seabed depth of 1040–1050 m separated by a distance of ~0.9 km (Fig. 7A). The flare at the South Tower, the larger of the two, rose to a water depth of 560 m (flare height of 490 m), whilst the North Tower flare reached a height of 422 m. The persistence of the flare to this height suggests that it is sustained by a layer of methane hydrate that reduces mass transfer and dissolution rate (McGinnis et al., 2006). The apices of the Wairarapa Seep flares were consistent with the top of the gas hydrate stability field of 570–645 m estimated for the Rock Garden region of the Hikurangi Margin (Pecher et al., 2005), which has a similar temperature–pressure relationship to the Opouawe Bank. Variability was observed in the geometry of the South Tower flare during the time-series, with the change in the direction and shape of the flare (Fig. 8) reflecting vertical variation in current flow and direction between 600 and 700 m (Fig. 6A, B). During the flare sampling in September 2006, the maximum bubble density centred on 41° 46.38'S, 175° 24.52'E showed significant

Please cite this article as: Law, C.S., et al., Geological, hydrodynamic and biogeochemical variability of a New Zealand deep-water methane cold seep during an integrated three-year time-series study, Mar. Geol. (2009), doi:10.1016/j.margeo.2009.06.018

Appendix I

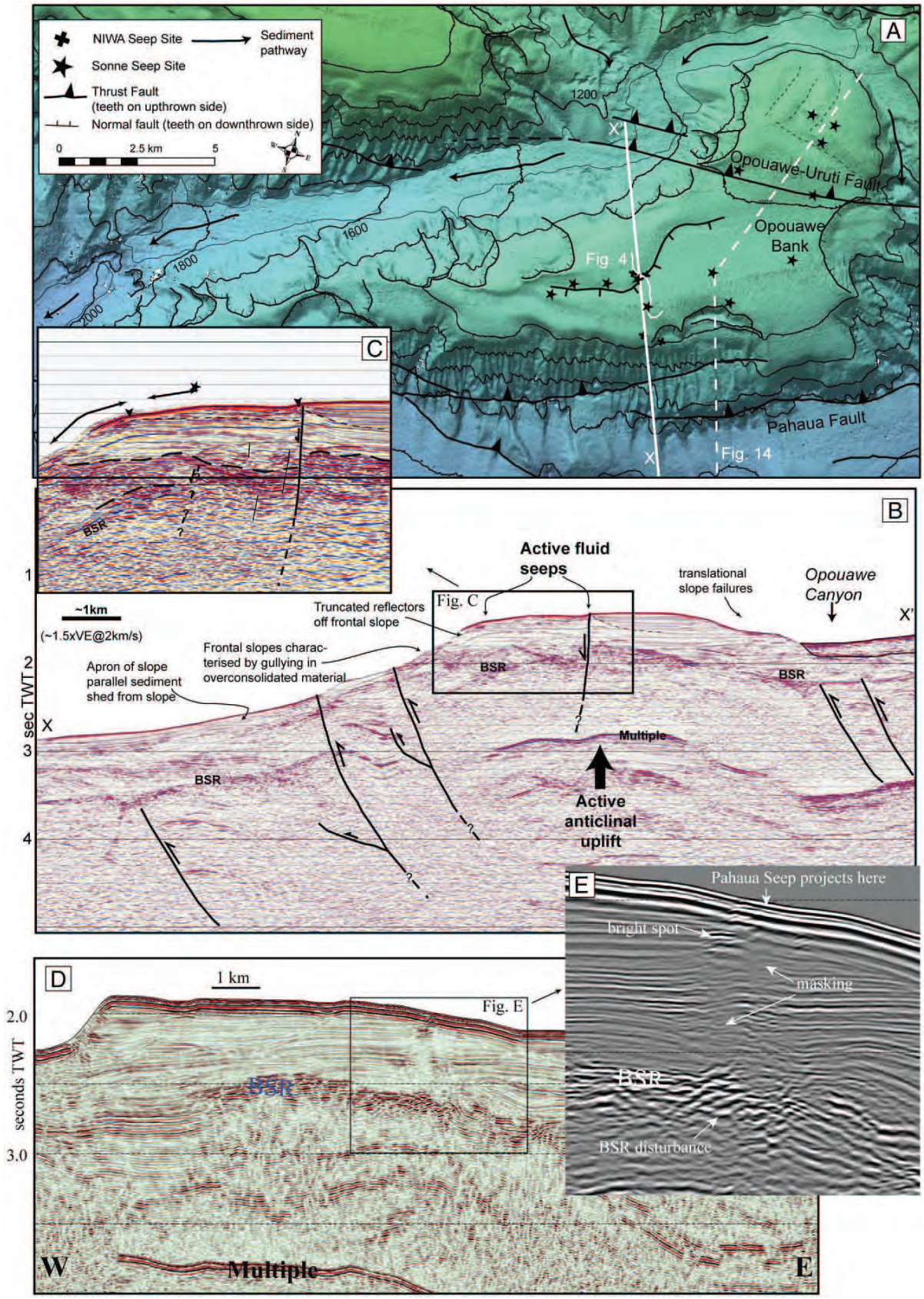

Please cite this article as: Law, C.S., et al., Geological, hydrodynamic and biogeochemical variability of a New Zealand deep-water methane cold seep during an integrated three-year time-series study, Mar. Geol. (2009), doi:10.1016/j.margeo.2009.06.018

Appendix I

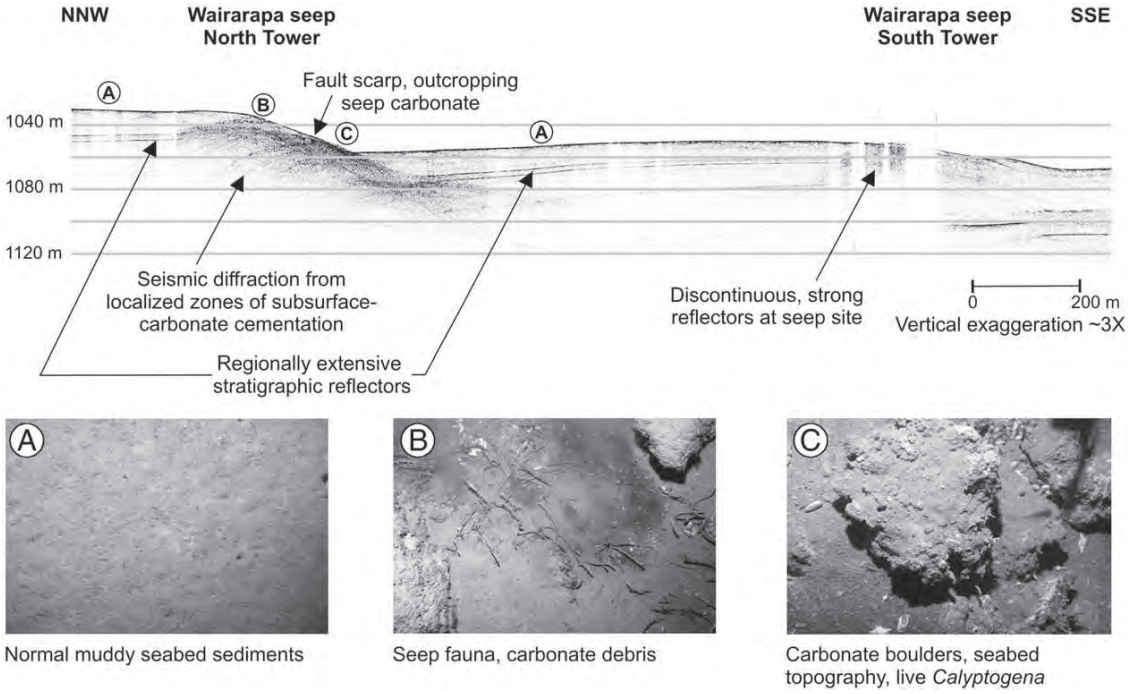

Fig. 4. A 3.5 kHz dip profile and DTIS camera images across the North and South Tower sites on Opouawe Bank showing that sub-surface seismic reflectors and sea-floor substrates at the seep sites are significantly different from the surrounding muddy sediment (photographic data from TAN0616; e.g., Baco et al., 2009—this issue). At the seep sites, strong discontinuous reflectors occur to a depth of 10–15 m below the sea-floor as a result of localised carbonate cementation. The location of the 3.5 kHz profile is shown on Fig. 2B and Fig. 4A.

variability in position and intensity, and one day later was offset by ~100 m to the southwest, indicating small-scale spatial variability. From the ES60 backscatter data in Fig. 7A, the NW–SE width of the South Tower flare at the seabed was 255 m, with a central band of elevated backscatter (Sv < −58 db) of 111 m wide. Although the sediment bubble release is intermittent (Linke et al., 2009—this issue), and enhanced backscatter will not correspond exactly with water containing elevated methane, the backscatter is used as a proxy for the calculation of residence time and total methane within the flare. On the assumption of a vertical flare originating from a sediment surface length of 111 m (as in Fig. 7B), with a lateral bottom current flow of 5–10 cm s^{-1}, the residence time of water and dissolved methane within the flare would be 18.5–37 min.

3.4. Dissolved methane

Water column profiling identified consistent trends in the presence of flares and elevated methane concentrations at the North and South Tower locations throughout the 3-year sampling period. Sampling within the flare was maintained by manoeuvring the vessel during CTD deployment relative to the real-time ES60 backscatter data. The distribution of bubbles and dissolved methane will deviate from each other as the bubbles rise and equilibrate with the surrounding water (Heeschen et al., 2005). Consequently, methane concentrations were always highest near the sea-floor (Fig. 9A,B), with an observed maximum of 312 nmol l^{-1} at the South Tower, consistent with methane concentrations exceeding 300 nmol l^{-1} at the Tui seep site on the north-eastern Opouawe Bank (Faure et al., 2009—this issue). The North Tower maximum concentration was lower (68 nmol l^{-1}), although the apparent difference in methane concentration between sites (Fig. 9A,B) may simply reflect the effectiveness of the sampling strategy relative to the non-continuous release of the bubbles. Alternatively, it may reflect actual differences between the two sites such as the 30–40 m difference in seabed elevation, or the degree of carbonate outcropping (Klaucke et al., 2009—this issue) and the distribution of infaunal groups (Sommer et al., 2009—this issue).

Throughout the time-series, methane generally decreased from the seabed to 750 m depth, although the profile obtained during October 2006 shows relatively high uniform CH_4 concentration of 80 nmol l^{-1} up to 800 m. Methane saturation was close to expected equilibrium with local air at 650–700 m at the South Tower, although supersaturation up to 10 nmol l^{-1} was apparent between 400 m and 500 m depths in some profiles (Fig. 9B). The absence of a vertical methane gradient suggests that horizontal transport may account for this low-level supersaturation at shallower depths. Methane saturation did not exceed 200% above 200 m indicating that, at least locally, seep-derived methane was not transported into the surface layer and did not contribute to the local air-sea emission of methane.

The Pahaua Seep flare rose 825 m from a sea-floor depth of 1475 m to ~650 m, and possibly higher as the head of the flare was obscured by a deep-scattering layer (Fig. 10A). The maintenance of the flare over such a vertical distance again indicates that the bubbles were sustained by a layer of methane hydrate (Sauter et al., 2006) with a

Fig. 3. (A) Morphostructure of Opouawe Bank with observed cold seeps in this study (black crosses) and SO-191 (stars, Bialis et al, 2007; Greinert et al, this issue) depicted, with the locations of the 3.5 kHz dip profile (Fig. 4), and the topography used to generate the section in Fig. 14 also included. (B) Seismic reflection profile SOL-9 (white X–X' on (A)) illustrating the thrust faults controlling bank uplift and extensional faulting that are likely the primary pathways for methane venting at the Wairarapa Seep site. The Digital Terrain Model (A) is shown at 5× vertical exaggeration (VE), while the seismic profile (B) is shown at ~1.5× vertical exaggeration at 2 km s^{-1} TWT. (C) Detail of seismic profile showing the vent sites (indicated by arrow heads, South Tower to left and North Tower to right). The inferred gas clathrate layer is also shown (as defined by the BSR and bright reflectors with dashed lined above). Arrowed lines above the profile indicate the extent of stratigraphic layers that crop out at the slope sea-floor. (D) MCS strike line adjacent to the Pahaua Seep site (location Fig. 2A) showing a diffuse BSR with significant disturbance of overlying reflectivity, including masking and a "bright spot" near the surface directly beneath the location of the projected Pahaua Seep (inset E).

Please cite this article as: Law, C.S., et al., Geological, hydrodynamic and biogeochemical variability of a New Zealand deep-water methane cold seep during an integrated three-year time-series study, Mar. Geol. (2009), doi:10.1016/j.margeo.2009.06.018

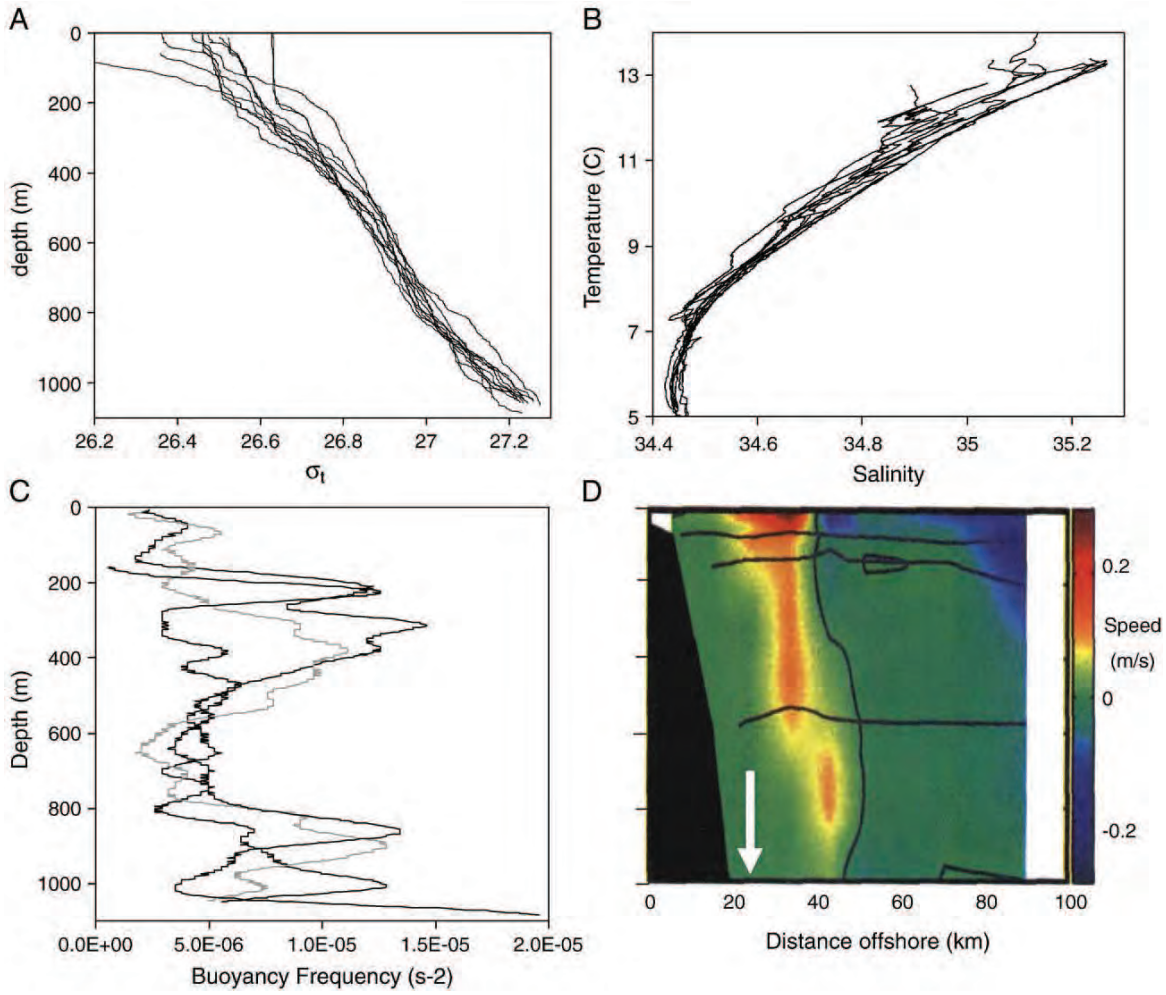

Fig. 5. Hydrographic properties at the Wairarapa Seep North and South Tower sites. (A) Potential density, σ_t. Note that σt decreased to 25.91 at the surface at the South Tower during July 2006, (B) temperature-salinity plots (C) buoyancy frequency, N^2 and (D) geostrophic section southwards from the Wairarapa coast (from Chiswell, 2000), with the approximate location of the Wairarapa Seep South Tower indicated by the white arrow. The northward-flowing current is shown as positive, with superimposed contours of σ_t at 26.55 and 26.9. Fig. 5d is reproduced with permission from the New Zealand Journal of Marine and Freshwater Research. (For interpretation of the references to colour in this figure legend, the reader is referred to the web version of this article.)

large proportion of the flare within the stability zone of pure methane hydrate. The Pahaua Seep exhibited a similar vertical methane distribution to the Wairarapa seeps, with a maximum CH_4 concentration of 268 nmol l^{-1} in bottom waters, declining to background levels of ~2 nmol l^{-1} at 800 m (Fig. 10B).

The dissolved methane originating from the North and South Tower seeps is restricted to the isopycnals σ_t 27–27.3, and is distinct from that of the Pahaua Seep with the latter on deeper isopycnals (σ_t 27.35–27.5). Elevated methane was also detected on this isopycnal range at sites northeast and southwest of the Pahaua Seep (see Fig. 11), suggesting along-shelf isopycnal transport of methane in both directions. Elevated methane (51.4 nmol l^{-1}) was present on the 27–27.3 σ_t isopycnals in bottom water at a site 5.4 km southwest of the Wairarapa Seep on the Opouawe Bank. This may reflect the lateral transport of methane from the North and South Towers, as supported by the southwesterly flow of bottom water recorded by the current meters (Fig. 6G). Elevated methane was also apparent at lower concentrations on the 27–27.3 σ_t isopycnal at sites southeast of the Wairarapa Seep and further up Cook Strait (Fig. 11). However, the methane on this isopycnal range may also originate from, or be contributed to, by other seep sites on the Opouawe Bank (Greinert et al., 2009—this issue; Faure et al., 2009—this issue).

3.5. Atmospheric methane

Atmospheric methane mixing ratios of 1720.6 ± 15.6, 1731.8 ± 15.5 and 1775.6 ± 17.7 ppbv were recorded during the TAN0504, TAN0508 and TAN0711 voyages (see Table 1), consistent with the annual range of 1720–1770 ppbv during 2005–2007 from the NIWA Baring Head atmospheric station, 45 km northwest of the seep site (41° 24.6'S, 174° 52.2'E) (A. Gomez, pers. comm.). The mean surface methane saturation in the 0.5° × 1° area surrounding the seep location was 132.4 ± 28.1% (range 98.8–210%). A regional gradient in the surface methane saturation was apparent, with elevated values in the northwest further up Cook Strait declining to atmospheric equilibrium levels to the east in the offshore waters (Fig. 12A). However, there was no evidence of a methane maximum in the surface waters in the immediate vicinity of the Wairarapa Seep, confirming that the seeps do not contribute to air–sea methane emissions locally. Instead, an inverse relationship between methane saturation and surface salinity

Please cite this article as: Law, C.S., et al., Geological, hydrodynamic and biogeochemical variability of a New Zealand deep-water methane cold seep during an integrated three-year time-series study, Mar. Geol. (2009), doi:10.1016/j.margeo.2009.06.018

Appendix I

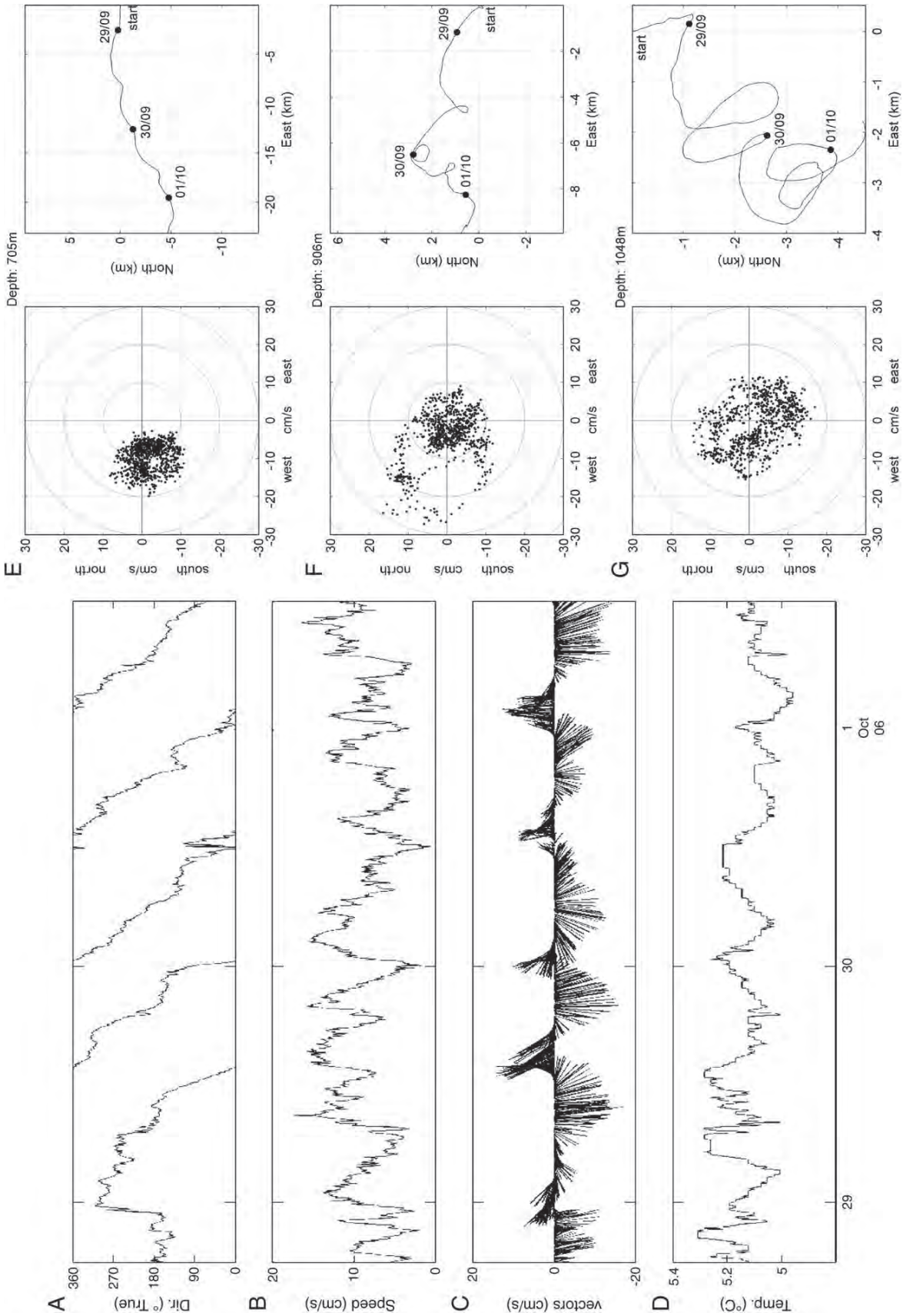

Fig. 6. Temporal variation over 3-days at the South Tower in (A) current direction, (B) current speed, (C) current vector and (D) water temperature at 1048 m water depth, with current velocity versus direction (left panel) and progressive current vectors (right panel) at (E) 705 m, (F) 906 m and (G) 1048 m water depths.

Please cite this article as: Law, C.S., et al., Geological, hydrodynamic and biogeochemical variability of a New Zealand deep-water methane cold seep during an integrated three-year time-series study, Mar. Geol. (2009), doi:10.1016/j.margeo.2009.06.018

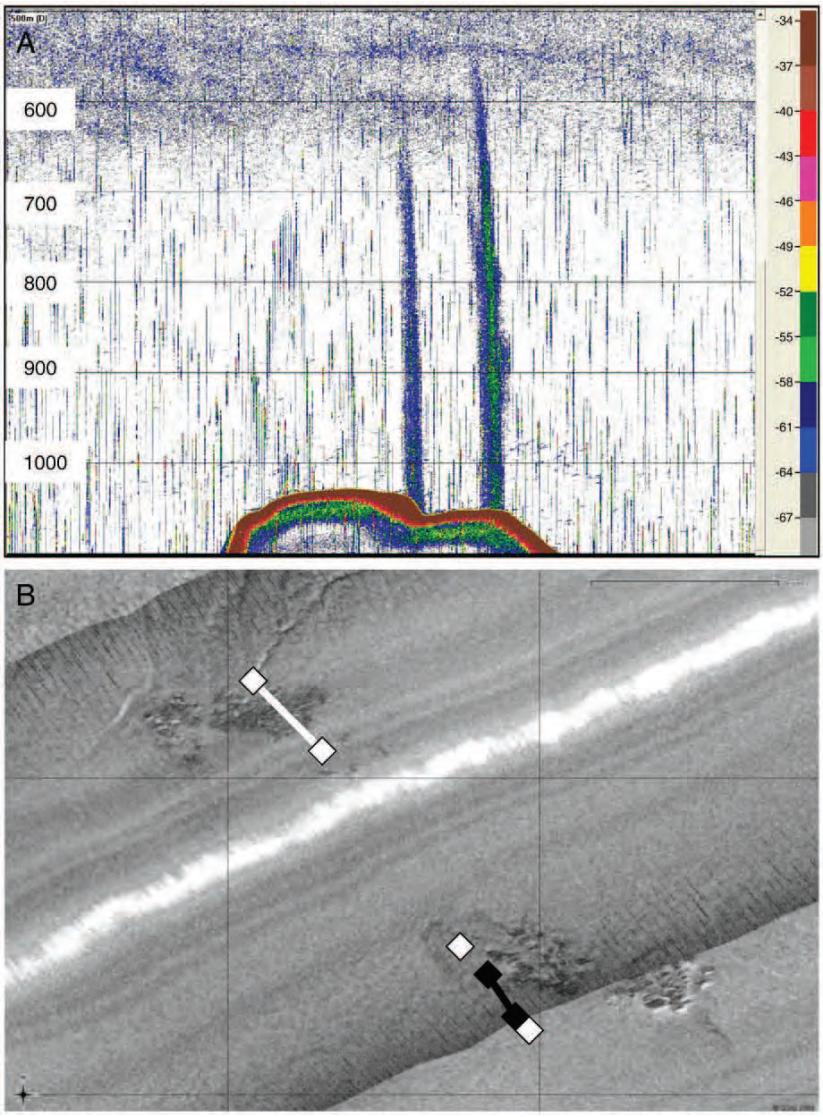

Fig. 7. (A) ES60 echogram of backscatter data during a transect across the Opouawe Bank showing bubble flares of the North Tower (left) and South Tower (right) on 2 October 2006 (TAN0612). (B) Side-scan sonograph across Opouawe Bank showing sea-floor chemoherms associated with the North (top left) and South Tower (bottom right) (Klaucke et al., 2009—this issue). The sea-floor locations of the bubble flares in the transect shown in (A) are indicated, with the white diamonds showing the full width of the bubble flare at both sites, and the black diamonds and line depicting the central flare region of the South Tower within the high backscatter region (< −58 dB).

(Fig. 12b) indicates that the observed surface methane saturation arises from an alternative source associated with riverine input and/or water masses in the Cook Strait (Law et al., unpubl. data).

3.6. Methane isotopes

Isotopic analysis of the dissolved methane was used to discriminate between methane sources, with samples from the seep site compared to surface and deep-water samples from the surrounding sites. The deep samples from the North and South Tower containing the highest methane concentrations, exhibited the most depleted $\delta^{13}C$–CH_4 values (Fig. 9C), ranging from −63 to −70‰, characteristic of methane derived from microbial fermentation and consistent with reported values from other methane seeps (Damm and Budéus, 2003; Heeschen et al., 2005; Faure et al., 2009—this issue). Between the sea-floor and 800 m depth, $\delta^{13}C$–CH_4 increased as CH_4 concentrations decreased to background levels. Three samples between 800 m and 950 m depths at the South Tower were undersaturated with $\delta^{13}C$–CH_4 values of −41 to −42 ‰. These were associated with low salinity AAIW, and likely reflect the "background" state in which methanotrophy has concentrated the ^{13}C signal as the lighter ^{12}C–CH_4 is preferentially oxidised. This indicates that bottom water currents ameliorate methane accumulation rapidly in the immediate vicinity of the seep, but also suggests that the Lagrangian flare sampling strategy was not always completely effective. Surface methane in southern Cook Strait exhibited variable $\delta^{13}C$–CH_4 values from −45 to −55‰, consistent with the atmospheric methane value of −47‰ (Quay et al., 1999), and values of −48.06 ± 1.6‰ recorded in the surface mixed layer east of New Zealand (39° 21.6'S, 178° 31.8'E). That $\delta^{13}C$–CH_4 values are depleted to −55‰ in surface Cook Strait waters suggests a biogenic contribution although this is unlikely to be due to the absence of vertical transport of seep methane to depths of above 700 m, as discussed in Sections 3.3 and 3.4.

Please cite this article as: Law, C.S., et al., Geological, hydrodynamic and biogeochemical variability of a New Zealand deep-water methane cold seep during an integrated three-year time-series study, Mar. Geol. (2009), doi:10.1016/j.margeo.2009.06.018

Appendix I

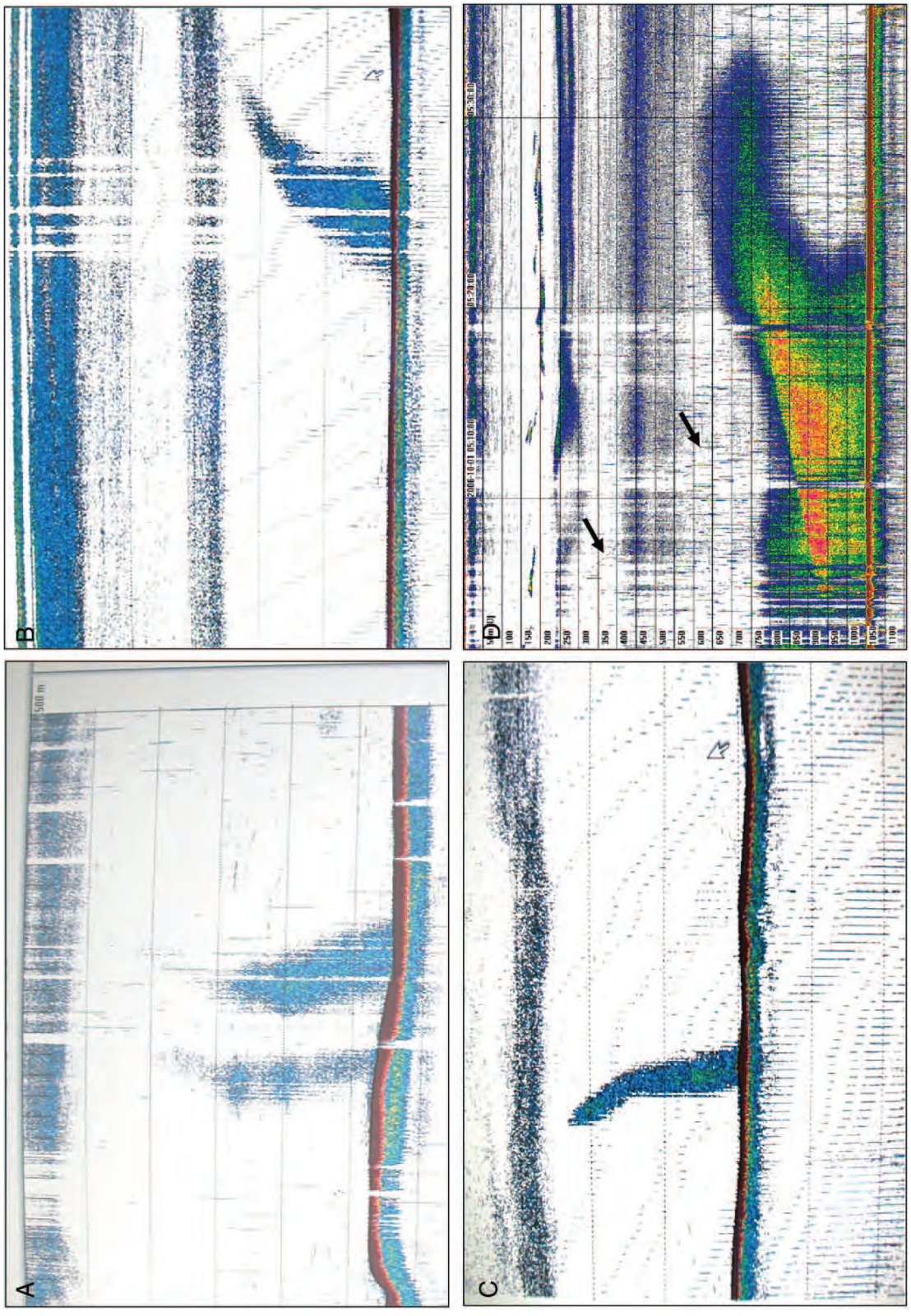

Fig. 8. ES60 echograms of the South Tower flare from (A) 27 September 2005, (B) and (C) 2 October 2005 showing the influence of water current on flare structure, and (D) high-resolution water-column sampling on 1 October 2006, with the descent of the CTD indicated by the arrow.

Please cite this article as: Law, C.S., et al., Geological, hydrodynamic and biogeochemical variability of a New Zealand deep-water methane cold seep during an integrated three-year time-series study, Mar. Geol. (2009), doi:10.1016/j.margeo.2009.06.018

Appendix I

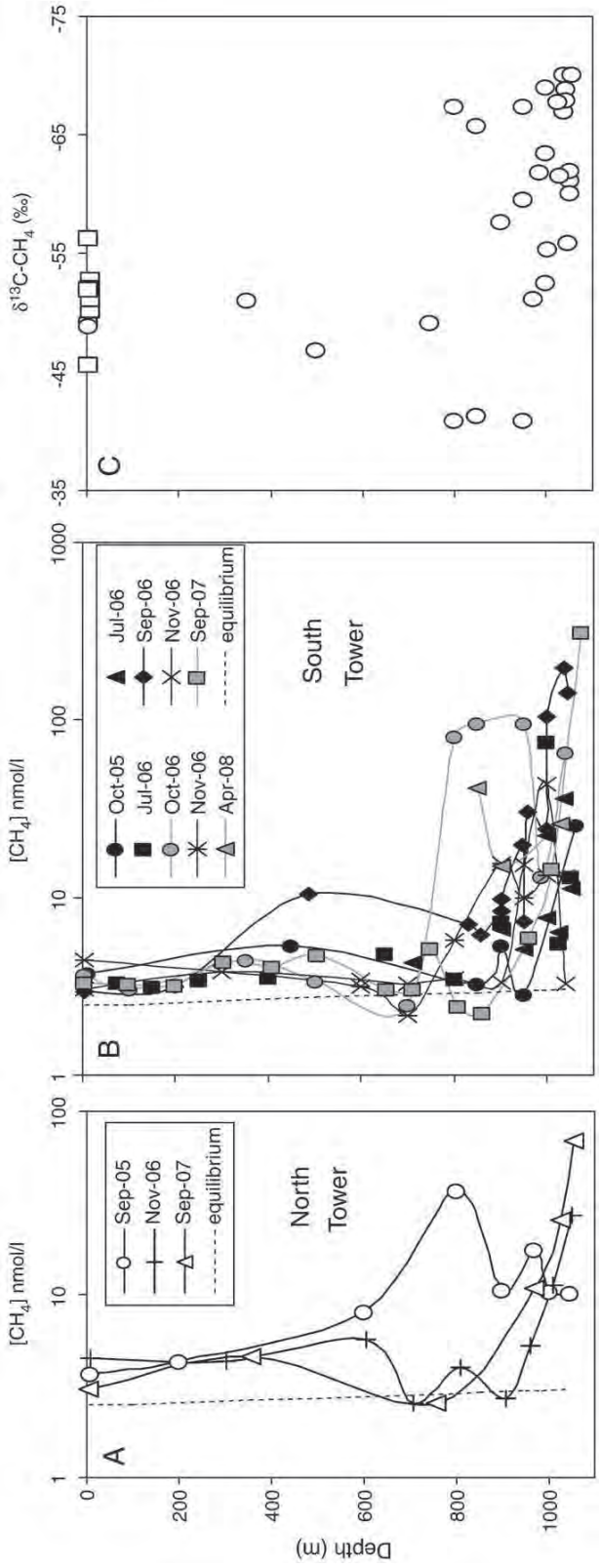

Fig. 9. Log plot of dissolved methane concentration at (A) the North Tower, (B) the South Tower and (C) $\delta^{13}C$–CH_4 depth profile from both sites (open circles) with surface water samples from the southern Cook Strait (open boxes). The dashed line in A and B represents the equilibrium methane concentration based upon an atmospheric methane of 1730 ppbv.

Please cite this article as: Law, C.S., et al., Geological, hydrodynamic and biogeochemical variability of a New Zealand deep-water methane cold seep during an integrated three-year time-series study, Mar. Geol. (2009), doi:10.1016/j.margeo.2009.06.018

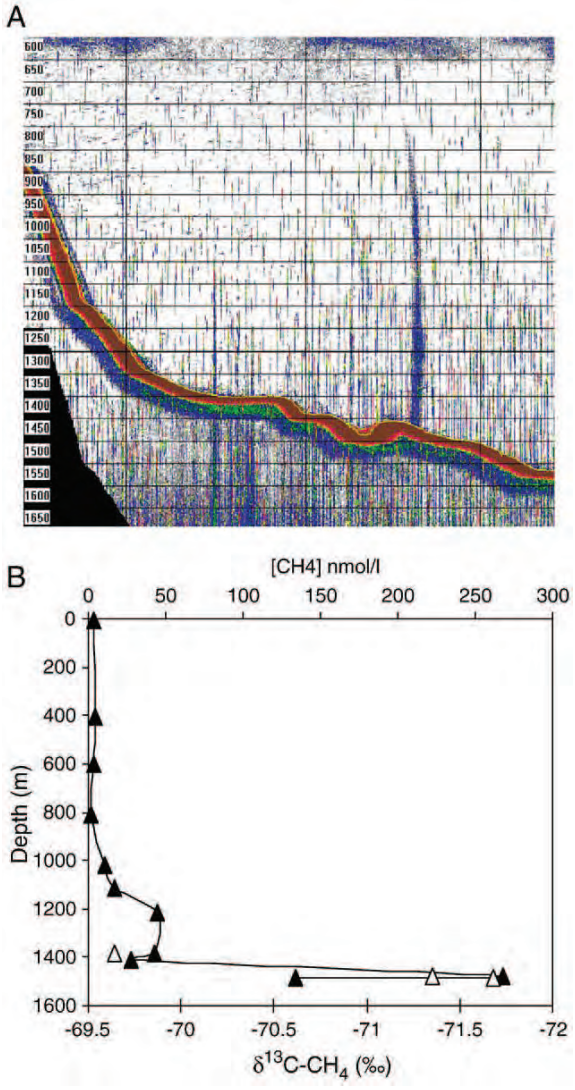

Fig. 10. The Pahaua Seep site (A) ES60 echogram (1 October 2006) showing a prominent water column flare at the newly discovered vent site, (B) methane concentrations ([CH_4], black triangles) and $\delta^{13}C$–CH_4 (white triangles) at the Pahaua Seep. (For interpretation of the references to colour in this figure legend, the reader is referred to the web version of this article.)

3.7. Methane oxidation

Methane oxidation rates in deep waters (850–1042 m) at the South Tower were 6.2–8.3 nmol l^{-1} d^{-1} in samples with an initial CH_4 concentration of 62–142 nmol l^{-1}. These rates are moderately high compared with that reported from other cold seep sites (Valentine et al., 2001), but consistent with the rates recorded in hydrothermal flares on the Juan de Fuca Ridge (De Angelis et al., 1993). The resulting turnover rates were 4.7–8.3% per day, exceeding reported turnover rates of <1% per day at the Haakon Mosby Mud Volcano (Sauter et al., 2006) and 0.1–4.1% at the Hydrate Ridge (Heeschen et al., 2005). A lower methane oxidation rate of 1.78 nmol l^{-1} d^{-1} and daily turnover of ~1% were obtained from control samples of the bottom water during sediment core incubations (see Section 3.9). Water column methane oxidation rates are generally too low to be measured robustly by concentration changes, and the recorded control rate from the sediment incubations was insignificant based upon the precision of 2.5% for our methane measurements. It may be speculated that the elevated oxidation recorded in the South Tower flare reflects the vertical transport of methanotrophs from the sea-floor entrained within the rising flare, whereas this process may have been excluded from the control water in the sediment incubations. Although methane oxidation is reported to be first-order with respect to CH_4 concentrations, no relationship was observed with CH_4 concentrations in the incubations. It should be noted that these oxidation rates represent "potential instantaneous" rates rather than in situ rates, as bottle incubations exclude the influence of dilution, which would rapidly reduce CH_4 concentrations and decrease oxidation rate proportionally (De Angelis et al., 1993, Valentine et al., 2001).

3.8. Water column biogeochemistry

Nutrient profiles from the seep site within the flares at the South Tower showed no significant differences in nutrient concentrations to neighbouring non-flare site profiles (data not shown, available on request). Furthermore, there were no discernible differences in the chemical composition of the suspended particulate organic matter (Table 2) and the dissolved carbonate chemistry (pH, DIC and alkalinity, K. Currie, pers. comm.) between the flares and the surrounding Cook Strait waters, with only slightly elevated particulate nitrogen in the deep flare waters at the South Tower (Table 2). Although methane oxidation in the seep flare may represent a source of particulate organic carbon (see Section 3.5), this is likely obscured by the generally high productivity of the region (e.g., Bradford et al., 1986). $\delta^{15}N_{POM}$ values increased with depth at many of the Cook Strait sites, with surface values (5 m) of 3–4‰ increasing to 5–6‰ at mid-water and near-bottom depths (Table 2). For $\delta^{13}C_{POM}$, near-surface values were generally between −22 and −24‰, decreasing to −27 to −29‰ at depth.

Water column profiles were obtained for total bacteria numbers and bacterial production rates during TAN0612 (Table 1). Total bacterial biomass exhibited significant variability in surface waters between stations, with a maximum (1.2×10^6 cells ml^{-1}) at the South Tower, declining to 7×10^4 cell ml^{-1} sub-surface (Fig. 13A). However, bacterial numbers were high (0.8×10^6 cells ml^{-1}) in bottom waters (>1000 m) at the South Tower coincident with CH_4 concentrations of >100 nmol l^{-1} (see Fig. 9B), indicating a common source for methane and bacteria. These samples contained an order of magnitude higher bacterial biomass than bottom water samples at other sites, and equal or greater bacterial biomass than in the surface waters. Conversely, a bacterial biomass maximum was absent from the deep waters at the South Tower three days later, when CH_4 concentrations were lower at <65 nmol l^{-1} (Fig. 13A). Bacterial production rates showed a similar profile to bacterial abundance, with maxima in surface waters at the C20 and South Tower sites of 1.6 and 1.34 μg C l^{-1} d^{-1}, respectively, and minima of 0.002 μg C l^{-1} d^{-1} in the mid-water column (Fig. 13B). However, there was no increase in bacterial production associated with the elevated CH_4 concentration and bacterial biomass in the flare on 28 September 2006, although bacterial productivity was elevated (0.06 μg C l^{-1} d^{-1}) below 900 m on 1 October 2006 relative to the other sites (Fig. 13B).

3.9. Sediment biogeochemistry

In general, sediments from the Wairarapa Seep (cores #1, 1A and #4) were similar in composition to those found at the control site (core #3, Fig. 2B), being dominated by low-carbonate (4–7%) silty muds (Table 3) (cf. Lewis and Mitchell, 1980). In contrast, samples from the Campbell Bank mud volcano (Fig. 2C) were a combination of low-carbonate (7–12%) sandy silts (40–65% mud) (core #5) and carbonate-enriched (20–50%) silty sands with a mud content of 30–50% (core #2). Total organic matter content in the surface sediments at the seep sites were no different from those at the control site (5–6%), but higher than at the mud volcano sites (2–4%). %POC in surficial sediments varied across the sample sites from ~0.5% at the mud volcano to 1–1.5% at the South Tower and control sites (Table 4). Some

Please cite this article as: Law, C.S., et al., Geological, hydrodynamic and biogeochemical variability of a New Zealand deep-water methane cold seep during an integrated three-year time-series study, Mar. Geol. (2009), doi:10.1016/j.margeo.2009.06.018

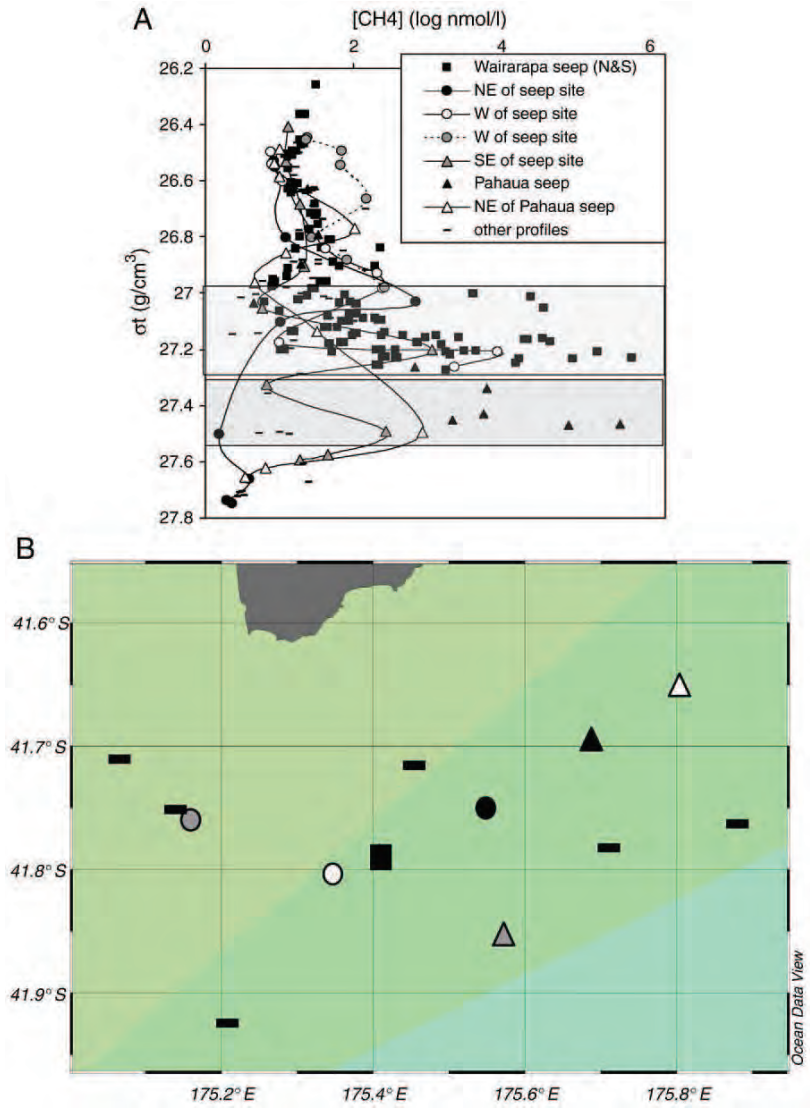

Fig. 11. (A) Log methane concentration ([CH_4]) plotted against potential density (σ_t), with symbols indicating site (refer to legend) and position on map (B). The upper light shaded area in (A) represents the density range of the CH_4 concentration maxima at the North and South Tower sites, and the lower dark grey box represents the density range of the CH_4 concentration maximum at the Pahaua Seep.

organic enrichment was apparent at the South Tower below the 0–1 cm surface layer with %POC and %PON higher by 0.2–0.5% and 0.04–0.08% ($n=2$), respectively, than at the control site (Table 4). Molar C:N ratios also did not vary significantly across sites, ranging from 8.7–9.4, with a high value of 12.5 measured at ~10 cm-depth in core #5 (Campbell Bank mud volcano). Carbon stable isotope ratios were similar at all sediment sample depths, varying from −21.8 to −23.5‰, except for a value of −16.8‰ from 10 cm-depth in core #5 at the mud volcano. There was no evidence of methanogenesis in $\delta^{13}C_{POCsediment}$ values, with all ratios characteristic of marine POC. Similar trends were observed in δ^{15}°N in near-surface sediments (Table 4). There was a slight enrichment (~1‰) at the South Tower and mud volcano sites in $\delta^{15}N_{PONsediment}$ compared to the control site, especially at and below 5 cm sediment depth.

Two sets of core samples were used for sediment core incubations at the South Tower, reflecting the small-scale heterogeneity expected at cold seep sites (e.g., Levin, 2005; Klaucke et al., 2009—this issue). Visually, the first set of two cores (Core 1A) comprised 2–3 cm-thick, brown silty mud, overlying grey clayey mud with noticeable H_2S content, in contrast to the second set of two cores (Core 1) that were apparently oxic throughout, consisting of brownish silty mud. The four cores collected from the control site were similar to the first South Tower set, with brown silty mud overlying stiff grey clay, although with no detectable H_2S smell. Biogeochemical rate measurements at the seep and control sites indicate that overall average rates of oxygen consumption ($n=4$) in the sediments were elevated at the seep, compared to the control site (e.g., 121.14 ± 28.63 μmol O_2 m^{-2} h^{-1} cf. 78.48 ± 17.19). The highest sediment oxygen consumption (SOC) rates were observed in the sediment cores characterised by a more anoxic appearance (mean 138 μmol O_2 m^{-2} h^{-1}, $n=2$), compared with 105 (79–130) μmol O_2 m^{-2} h^{-1} in the sediments with oxic characteristics. Overall, CH_4 concentrations decreased over the course of the sediment core incubations more rapidly at the South Tower with rates of 624.82 ± 414.46 nmol m^{-2} h^{-1}, compared to 59.38 ± 15.92 nmol m^{-2} h^{-1} at the control site, indicating active methanotrophy at the former site. Unlike oxygen consumption, methane consumption in the oxic seep cores was higher than in the anoxic cores (e.g., 975 nmol m^{-2} h^{-1}, cf. 285 nmol m^{-2} h^{-1}).

Please cite this article as: Law, C.S., et al., Geological, hydrodynamic and biogeochemical variability of a New Zealand deep-water methane cold seep during an integrated three-year time-series study, Mar. Geol. (2009), doi:10.1016/j.margeo.2009.06.018

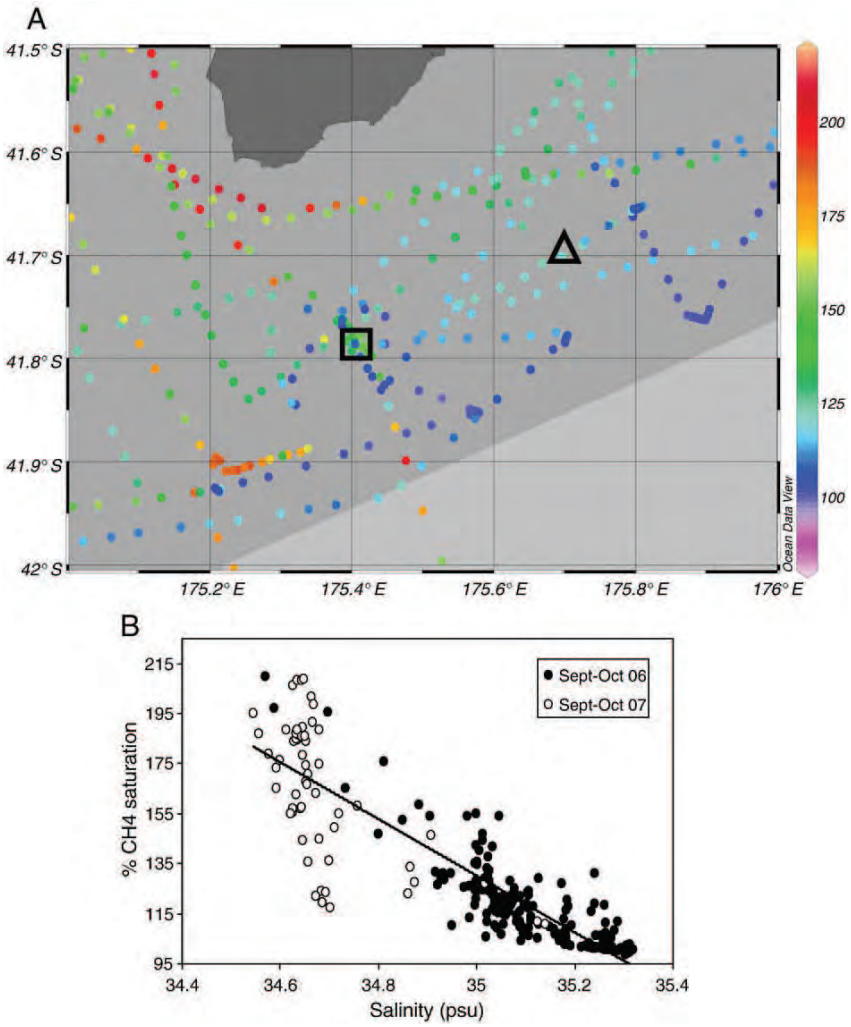

Fig. 12. (A) Surface % CH_4 saturation with the Wairarapa Seep (square) and Pahaua (triangle) locations indicated, and (B) % CH_4 saturation versus salinity for two voyages (TAN0612 and TAN0711).

4. Discussion

4.1. Physical characteristics of shallow sediments at the Wairarapa Seep site

From observations made with camera and geophysical systems, it is apparent that the zones associated with active methane seepage at the Wairarapa Seep sites are restricted spatially (e.g., Netzeband et al., 2009—this issue; Klaucke et al., 2009—this issue). In the present study, side-scan sonograms at the North Tower show the dense bubble flare coincident with the area of highest backscatter intensity that corresponds to carbonate chemoherms, whereas at the South Tower the flare is more diffuse and is offset to the southwest of the sea-floor carbonates (Fig. 7B). The apparent offset between the water column flare and the sea-floor carbonate formation at the South Tower may be driven partially by cementation processes whereby gas and fluid

Table 2
Percent C and N and the isotopic composition of water column particulate organic matter (average ± 1 standard deviation) collected in Cook Strait during TAN0612, specifically at the Wairarapa Seep and other locations.

Location	%PN	$\delta^{15}N$ (‰)	%POC	$\delta^{13}C$ (‰)
Wairarapa Seep — surface	4.90	4.45	30.46	−22.06
Wairarapa Seep — plume (850–1040 m)	0.41 ± 0.15	5.21 ± 1.10	3.86 ± 0.92	−27.31 ± 0.87
Pahaua Seep — plume (1000 m)	0.75	5.71	8.84	−27.65
Uruti Ridge — deep (1070 m)	0.67	3.41	4.50	−25.85
Mud volcano — surface (5 m)	2.28	3.77	11.32	−23.37
Mud volcano — deep (90–120 m)	1.65 ± 0.15	5.14 ± 0.19	11.40 ± 2.72	−23.82 ± 1.30
Cook Strait — surface (5 m)	3.04 ± 1.55	3.02 ± 1.38	15.82 ± 7.66	−23.40 ± 1.13
Cook Strait — deep (690–1110 m)	0.36 ± 0.10	4.67 ± 0.98	3.36 ± 1.23	−27.31 ± 1.96
Off Clarence River (NE South Island) — surface (5 m)	4.77	2.45	24.57	−22.93
Off Clarence River (NE South Island) — deep (160 m)	1.31	5.38	8.58	−24.29

Sample size (n) = 1–9.

Please cite this article as: Law, C.S., et al., Geological, hydrodynamic and biogeochemical variability of a New Zealand deep-water methane cold seep during an integrated three-year time-series study, Mar. Geol. (2009), doi:10.1016/j.margeo.2009.06.018

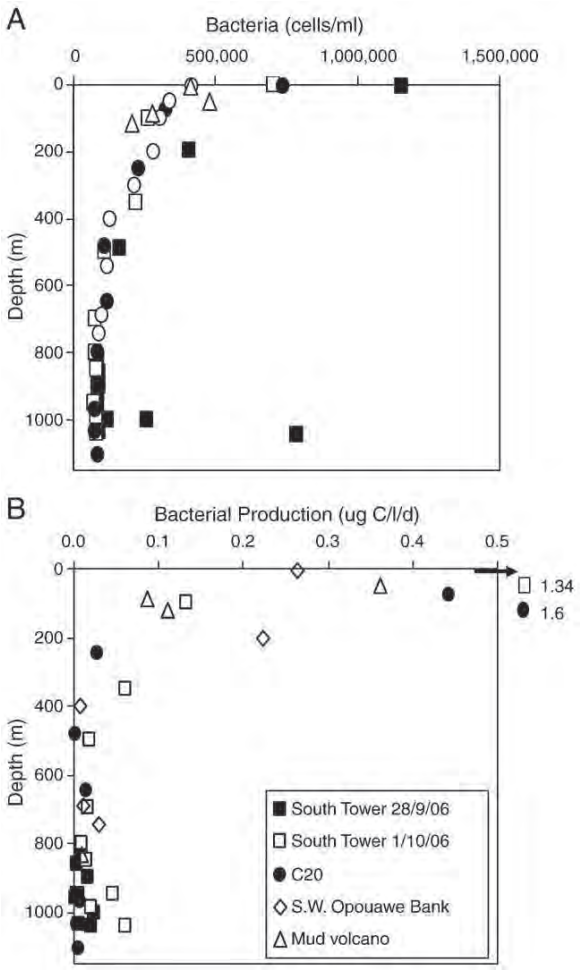

Fig. 13. (A) Water column profiles of bacterial abundance (cells ml^{-1}), and (B) bacterial production rates (μg C l^{-1} d^{-1}) at the South Tower and other sites (see Fig. 2). Surface values of 1.6 and 1.34 μg C l^{-1} d^{-1} for the C20 site and South Tower 1/10/06 are not shown.

expulsion at the sea-floor is forced laterally by the complete sealing of previous vent locations by active carbonate chemoherm formation, described by Naudts et al. (this issue) as a "self-sealing" effect.

The high-resolution sub-bottom echo-sounder data (Fig. 4) indicate consistently high-amplitude, near-surface reflectors, inferred to correspond to localised carbonate cementation, both at the sea-floor and extending to ~10 m below the surface. In nearly all cases, the first occurrence of seep fauna observed on the sea-floor occurs within tens of metres after a change in the sub-surface seismic stratigraphy (Fig. 4), consistent with the findings of Klaucke et al. (2009—this issue). The surrounding soft sediments are also variable with localised patches of black sulphide-rich material (Fig. 4) that are populated by abundant ampharetid polychaetes (Sommer et al., 2009—this issue). While seep sediments from the other environments, such as the Gulf of Mexico, have high concentrations of POC relative to the ambient margin sediments (e.g., Arvidson et al., 2004), bulk sedimentary parameters were not substantially different between the Wairarapa Seep and the control sites (Tables 3 and 4). These similarities may reflect the proximity and influence of other seeps subsequently identified less than 1 nautical mile away from the control site (Rironiro Seep, Greinert et al., 2009—this issue), although given the localised nature of seeps and the small-scale heterogeneity of sediments in the vicinity, this cannot be confirmed with certainty. The sediment

Table 3
General sediment characteristics (grain-size, moisture content, $CaCO_3$, total organic matter (TOM)) for cores collected in Cook Strait during TAN0612 at the Wairarapa Seep (cores #1 and 4), a control site (core #3) and the mud volcano on the Campbell Bank (cores #2 and 5).

Location — core #	Depth (cm)	% Coarse sand (>500 μm)	% Medium–fine sand (500–63 μm)	% Mud (<63 μm)	% Water	% CaCO3	% TOM
Wairarapa Seep							
Core #1	0–1	0.00	1.92	98.08	65.64	4.75	4.43
	9.5–10	0.17	1.87	97.96	45.60	6.00	4.47
Wairarapa Seep							
Core #4	0–1	0.27	2.69	97.04	61.44	5.20	6.27
	9.5–10	0.13	2.27	97.59	45.99	6.30	4.04
Control							
Core #3	0–1	0.38	4.38	95.25	57.13	5.70	5.12
	9–9.5	0.00	0.37	99.63	40.83	6.10	3.63
Mud volcano							
Core #2	0–1	53.38	16.82	29.80	35.63	50.65	2.67
	9.5–10	35.77	18.08	46.15	26.16	43.10	1.74
Mud volcano							
Core #5	0–1	6.29	42.03	51.70	41.71	8.00	2.48
	9–10	4.74	36.06	59.21	25.97	13.80	2.79

Sample size = 1–2.

characrteristics from Cook Strait are not, however, particularly different from the gas hydrate provinces on other convergent margins (see Table 1 in Kastner, 2001). There is also an absence of a distinctive "methanogenesis"-type isotopic signature in the Wairarapa Seep sediment organic matter (Table 4), supporting the contention that the origin of the methane at the Wairarapa Seep site is primarily from shallow biogenic gas sources, as found on other convergent margins (e.g., Kvenvolden and Barnard, 1983).

4.2. An integrated model for fluid venting at the Wairapapa Seep

It is well established that the geometry of geological structures influence the spatial location and character of seeps observed globally (e.g., Kulm et al., 1986; Le Pichon et al., 1992). The integrated approach, as presented here, also provides a framework to interpret the spatial and temporal variability at seep sites and the impact on fluid chemistry. In a New Zealand context, Barnes et al. (2009—this issue)

Table 4
Percent C and N and the isotopic composition of organic matter in sediment cores collected in Cook Strait during TAN0612 at the Wairarapa Seep (cores #1 and 4), a control site (core #3) and the mud volcano on the Campbell Bank (cores #2 and 5, the latter with average ± 1 standard deviation, $n = 3$).

Location — Core #	Depth (cm)	% PN	$\delta^{15}N$ (‰)	% POC	$\delta^{13}C$ (‰)	Molar C:N
Wairarapa Seep						
Core #1[a]	0–1	0.15	6.30	1.12	−22.46	8.99
	9.5–10	0.13	5.99	1.06	−22.27	9.17
Wairarapa Seep						
Core #4	0–1	0.14	5.65	1.05	−22.84	8.85
Control						
Core #3	0–1	0.12	5.61	0.96	−22.26	9.00
Mud volcano						
Core #2	0–1	0.09	6.79	ND	ND	ND
Mud volcano						
Core #5	0–1	0.07 ± 0.00	5.62 ± 0.13	0.50 ± 0.04	−23.28 ± 0.24	8.94 ± 0.14

[a] Samples from cores with well-developed surface oxic layer (see Section 3.9).

Please cite this article as: Law, C.S., et al., Geological, hydrodynamic and biogeochemical variability of a New Zealand deep-water methane cold seep during an integrated three-year time-series study, Mar. Geol. (2009), doi:10.1016/j.margeo.2009.06.018

propose a general model for fluid expulsion on the Hikurangi Margin noting that all vent sites occur near ridge crests in the hanging wall of thrust-propagated anticlines, and that vents are associated with BSR disturbance. Additionally, several sites are subject to extensional faulting (e.g. Netzeband et al., 2009—this issue). At Opouawe Bank, conduits for active methane venting are likely to be a combination of extensional faulting, stratigraphic pathways and fracture networks, but the common factor appears to be the extensional fracture networks requiring some hanging wall dilation. Fig. 14 shows an interpretive cross-section through Opouawe Bank, based on the actual bathymetry and aligned to intersect both of the general seep site areas and a region of frontal slope-failure.

At the southern Opouawe Bank seep sites, the extension in the hanging wall that allows dilation and fracturing to occur is inferred to be related to the step-over in the ridge-bounding frontal thrust. At the thrust step-over point, differential movement on these structures is clearly inducing compressional deformation of the rock between the overlapping fault planes, but could conversely induce extension in the hanging wall. The occurrence of a large mass failure in the frontal slope at this location supports a model of localised extension, and the step-over related extension is also inferred to be the mechanism controlling the development of the normal fault at the ridge crest. The observation of gas hydrate at shallow sediment depths (~2 m) at the Takahe seep site (Schwalenberg et al., 2009—this issue) suggests that gas hydrates may also have played a role in destabilising the slope sediments at Opouawe Bank, and contributed to the deep-seated mass failure as documented at other locations such as Blake Ridge (Dillon et al., 2001).

The northern Opouawe Bank seep sites (e.g., Tui, Tuatara, Tieke; Greinert et al., 2009—this issue) occur on the hanging wall of the Opouawe–Uruti Fault, and this part of the ridge has a 'dome-like' geometry. It is apparent that canyon erosion has isolated this dome feature (Fig. 3A), and the removal of lateral support may have destabilised the still uplifting dome, leading to structural/gravitational-induced relaxation and dilation. Bathymetric lineaments on the dome may reflect gravitational/structural collapse, although there is no clear support for localised dislocation associated with these lineaments in MCS profiles, other than the fracture networks at depth (Fig. 3A) (cf. Barnes et al. (2009—this issue) at the Rock Garden seep site). Alternatively, the lineaments could be caused by chemoherm formation (J. Greinert, pers. comm.).

At the Pahaua Seep site, significant disturbance to and masking of sub-surface acoustic reflectivity may indicate sustained venting at this location. The disrupted reflectivity might be interpreted as due to polygonal fault development, indicating hanging wall dilation at this site. Additionally, the presence of a "bright spot" suggests the occurrence of free gas and/or gas hydrate (cf. Holbrook et al., 2002). While observations are limited, the existing data indicate that the Pahaua Seep is a significant site of methane release at the sea floor, as evidenced by the well-imaged flare (Fig. 10A).

4.3. Sediment oxygen consumption and methane oxidation

Nutrient and dissolved carbon species and particulate carbon and nitrogen isotopes measured in the water column away from and within the Wairarapa Seep flares were not significantly different (Tables 2 and 4, nutrient and dissolved carbon data not included). Therefore, there does not appear to be any long-term effect of the methane release on ambient water column biogeochemical processes. Similarly, at the mud volcano site on the Campbell Bank, bulk biogeochemical characteristics, including isotopes, were not affected markedly by elevated levels of methane in near-bottom waters. Although no flare was apparent in the region of the mud volcano (Fig. 2C), the elevated methane concentrations and reported presence of seep-associated molluscan fauna (*Maorithyas* sp., Site 5, Lewis and Marshall, 1996) in fossiliferous concretions on the outer shelf off Cape Campbell, ~30 km to the southeast of the mud volcano site, suggest that active venting of methane-rich fluids occurs in the vicinity.

The SOC rates recorded at the South Tower seep were consistent with *in situ* rates at sites along the Hikurangi Margin (~3–6 mmol m^{-2} d^{-1}, Sommer et al., 2009—this issue), and also at similar depths on the Chatham Rise (Nodder et al., 2007). The rates from our study, however, are an order of magnitude lower than the *in situ* rates obtained in seep sediments of high biological activity (Sommer et al., 2009—this issue), indicating that the present study did not sample explicit "seep"-related sediments. Small-scale sediment variability was apparent in the two sets of "seep" cores from the South Tower site, as evidenced by the visual differences, and contrasting oxygen consumption rates. It is expected that shipboard SOC measurements in our study would be higher than the *in situ* measurements, due to experimental artefacts (e.g., Nodder et al., 2007). Since the SOC rates at the control site were lower than any from the South Tower, the obtained rates can still be

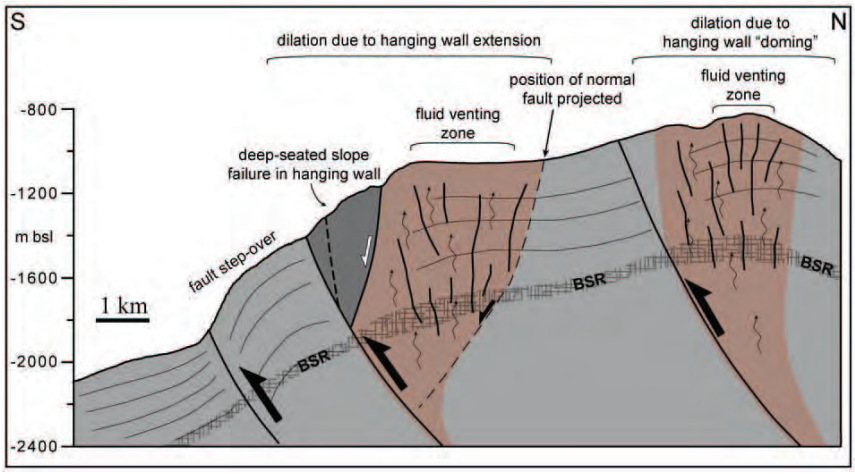

Fig. 14. Schematic profile across Opouawe Bank, derived from actual topography (for location of profile see Fig. 3A). The interpretive profile provides a model for the relationship between the two major thrust faults and the development of polygonal faulting and fluid conduits at this vent site. The brown zones show the general fluid migration area, containing polygonal fault/fracture development and a diffuse BSR. The frontal gravitational collapse is shown shaded grey and is inferred to be related to the fault step-over, as is the ridge crest normal fault (projected) upon which the North Tower vent site is located. (For interpretation of the references to colour in this figure legend, the reader is referred to the web version of this article.)

Please cite this article as: Law, C.S., et al., Geological, hydrodynamic and biogeochemical variability of a New Zealand deep-water methane cold seep during an integrated three-year time-series study, Mar. Geol. (2009), doi:10.1016/j.margeo.2009.06.018

regarded as representative of these seep locations, albeit at the lower end of activity. The low methane consumption in the South Tower sediments indicates that microbial oxidation is unlikely to significantly alter total methane emissions from the Wairarapa Seep. The *in vivo* methane consumption rates (0.015 ± 0.010 mmol m^{-2} d^{-1}) were an order of magnitude less than those reported by Sommer et al. (2009—this issue) from *in situ* measurements. However the exclusion of the underlying methane supply in the shipboard incubated cores (compared with the *in situ* incubations) does confirm the presence of an active methanotrophic community in the surface sediments at the seep site. Preliminary data suggest that unique anaerobic methanotrophs are associated with the South Tower flare and perhaps the sediments, and may play an important role in the oxidation of methane (Maas et al., submitted).

4.4. Fate of seep methane in the water column

The fate of methane in the water column is determined primarily by hydrodynamic factors. Diffusion results in the rapid transfer of a significant proportion of methane from the gas phase into the dissolved phase in bottom water (McGinnis et al., 2006, Suess et al., 1999; Sauter et al., 2006). Stratification in the bottom waters (Fig. 5C) will suppress the vertical exchange of the dissolved methane, but have minimal influence on bubble rise. The rising bubbles could potentially erode structure and stratification, although there is little evidence if this in the σ_t and N^2 profiles (Fig. 5A,C). Dissolved methane in the immediate vicinity of the flare would be subject to some degree of vertical transport associated with the bubbles, but lateral currents would lead to dissociation of the two. As a result, both dissolved methane and bubbles will broaden and smear laterally with distance above the seabed due to the influences of the vertical rise and shear, but the dissolved methane will be considerably more constrained to bottom waters, consistent with the CH_4 concentration profiles (Fig. 9A,B). Sauter et al. (2006) report that the rising bubbles at the Haakon Mosby Mud Volcano "push" a methane plume ahead vertically to shallower depths; however, there is no evidence of this at the Wairarapa Seep sites. Although moderate methane supersaturation (~4–10 nmol l^{-1}) was apparent in the upper water column, this more likely originates from lateral supply from shallow seeps or sediments. Regardless, stratification at the base of the surface mixed layer (Fig. 5C) presents a barrier to vertical methane transport, and so despite expulsion of significant volumes of methane, the impact of the Wairarapa Seep on air–sea methane emissions is minimal.

The methane concentration and isotopic data can be combined to provide insight into the local fate of seep methane in the water column. A simple two end-member mixing model was fitted to the data using a maximum CH_4 concentration of 197 nmol l^{-1} and corresponding $\delta^{13}C$–CH_4 of −70.1 ‰ for the flare end-member, and two "background" end-members to encompass the variability of methane in the bottom waters (see Fig. 15 legend for details). The seep end-member probably provides an under-estimate of the actual seep methane values, as it will have experienced some dilution. The CH_4 concentration minima at the South Tower (Fig. 9B) are below the equilibrium saturation value and exhibit elevated ^{13}C–CH_4 reflecting previous oxidation in deep waters; conversely, the other "background" end-member is supersaturated with respect to atmospheric methane indicative of a local methane source. Nevertheless, most of the variability in the observed values at σ_t>27.2 is captured by the use of two background end-members (Fig. 15). Methane oxidation would result in enrichment of ^{13}C, of which there is little evidence, and so dilution appears to the primary fate for methane in the flare. The apparent elevated $\delta^{13}C$–CH_4 values on lighter isopycnals (σ_t 27.0–27.2, Fig. 15) could be interpreted as evidence of oxidation, but alternatively reflects that the initial end-member CH_4 concentration on this isopycnal is lower due to the decreasing bubble-water methane concentration gradient as the flare enters this isopycnal. This is supported by a two end-member mixing line for σ_t of 27.0–27.2, fitted using a CH_4 concentration maximum of 95 nmol l^{-1} and corresponding $\delta^{13}C$–CH_4 of −67.4‰, which shows good agreement with the observed values on this isopycnal range (Fig. 15).

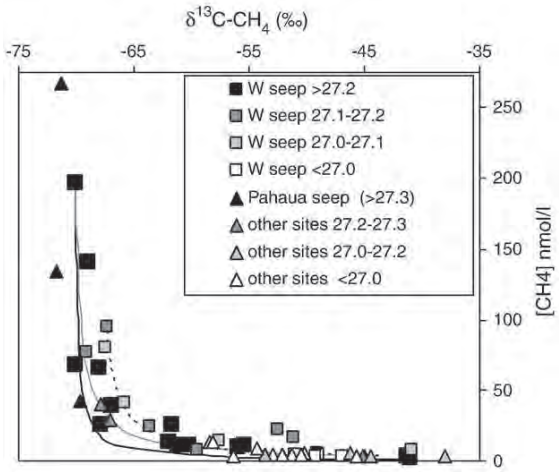

Fig. 15. Methane concentration ([CH_4]) plotted against $\delta^{13}C$–CH_4 for the Wairarapa and Pahaua sites, and surrounding locations, with the density ranges indicated in the legend. Two end-member mixing lines were used for σ_t>27.2, the first (black line) being "background" values at the CH_4 concentration minimum on the σ_t>27.0 isopycnal at the Wairarapa seep (CH_4 concentration is 1.01 nmol l^1, $\delta^{13}C$–CH_4 is −41.04‰) and the second (grey line) using the mean CH_4 concentration minimum (3.73 nmol l^{-1}, $\delta^{13}C$–CH_4 is −43.77‰) at σ_t>27.0 from surrounding stations. The dashed line indicates a two end-member mixing line for σ_t of 27.0–27.2, using a seep flare end-member of CH_4 concentration of 95 nmol l^{-1} and $\delta^{13}C$–CH_4 of −67.4‰.

That dilution is the primary fate of seep methane is not surprising since the adaptive flare sampling strategy would minimise the time for methane oxidation. Methanotrophy is a relatively slow process with reported rates on the order of days–months at other seep sites (Valentine et al., 2001; De Angelis et al., 1993). Although the measured water column oxidation rates were relatively high at the South Tower, <0.3% of methane would be oxidised during the residence time of water in the flare (18.5–37 min), supporting the contention that the immediate fate of the seep methane i dilution and advection. However, methane oxidation would undoubtedly be important in terms of the ultimate fate of the seep methane. Unique methanotroph phylotypes have been isolated and identified from the South Tower flare, although their presence was highly variable both spatially and temporally (Maas et al., submitted). Since methane consumption was observed in the sediment core incubations, consistent with reports of aerobic methane oxidation in surface sediments at other cold seep sites (Inagaki et al., 2004), the surface sediment represents a potential source of methanotrophs to the water column. The bubble release may provide a mechanism for the vertical transport of material including bacteria in the flare, consistent with the order of magnitude higher bacterial biomass at >900 m in the South Tower flare (Fig. 13), and other observations from hydrothermal flares and cold seep flares in the Black Sea (De Angelis et al., 1993, Schubert et al., 2006). Variability in bubble emission at the sea-floor, and/or tidal variations in the magnitude and direction of the bottom water currents (e.g., Linke et al., 2009—this issue; Naudts et al., 2009-this issue) may determine the degree of sediment suspension and vertical particle transport, and hence the presence of methanotrophs and methane oxidation in the flare. This may explain why the water column methane oxidation rates are higher than reported in other seep flares (Valentine et al., 2001; De Angelis et al., 1993). Consequently, the flare functions as a seeding mechanism for methane-oxidising bacteria to the surrounding bottom waters and sediment, so influencing the local fate as well as the supply of methane.

Please cite this article as: Law, C.S., et al., Geological, hydrodynamic and biogeochemical variability of a New Zealand deep-water methane cold seep during an integrated three-year time-series study, Mar. Geol. (2009), doi:10.1016/j.margeo.2009.06.018

4.5. Methane emissions at the South Tower

The majority of time-series studies on methane cold seeps to date have identified significant variability in bubble flare emissions (Leifer et al., 2004, Heeschen et al., 2005, Greinert et al., 2006, Greinert, 2008). Conversely, the present study indicates continuous emission at the South Tower seep, with relative uniformity in flare location and associated methane supersaturation over three years, and hence a relatively constant methane source. The column-integrated methane burden in the South Tower flare (700 m–1050 m) was estimated by summing the average excess dissolved methane (following subtraction of the CH_4 saturation value) for each 50 m depth interval (Fig. 9B). The resulting methane burden of 5.6 mmol m^{-2} is consistent with estimates from other methane hydrate regions (Valentine et al., 2001). A first-order estimate of the total methane inventory of the South Tower was obtained by applying the methane column burden to the high backscatter region (< −58 dB, Fig. 7) of the flare with a sea-floor footprint of 111 m × ~50 m. Assuming that the elevated backscatter data is a valid proxy for CH_4 concentration, and that the average CH_4 concentration for each depth is horizontally uniform across the flare, then the methane inventory for the South Tower would be 34.5 mol CH_4. Assuming steady state, with the lateral advective "clearing" of the flare being the primary sink for methane, then the residence time of the central flare of 18.5–37 min indicates an emission rate of 1340–2680 mol CH_4 d^{-1} for the South Tower. Estimates from other regions, including 2.3×10^6 mol d^{-1} (North Sea Tommeliten field, Hovland et al., 1993), and 8.6×10^6 mol d^{-1} (hydrate-bearing section of the Cascadia margin, Heeschen et al., 2005), are considerably greater as they represent whole field estimates as opposed to an individual flare. Similarly, the total annual emission of $0.5–1 \times 10^6$ mol CH_4 for the South Tower is smaller than the total emissions from the Costa Rica mud volcanoes (20×10^6 mol per annum), but consistent with individual annual volcano emissions of $10^2–10^4$ mol (Mau et al., 2006). Of course, the total regional methane source will be significantly greater since the South Tower is just one of a number of cold seeps on the Opouawe Bank, and the wider Hikurangi Margin (Bialas et al., 2007; Faure et al., 2009—this issue; Greinert et al., 2009—this issue), and consequently, a comprehensive regional identification of cold seeps and their associated methane inventories is required for this New Zealand accretionary margin.

5. Conclusions

- The Wairarapa Seep site is a locus of significant methane efflux into the water column of the south-eastern Cook Strait;
- Methane emissions and bubble flare activity remained relatively constant over a three-year period, with total annual emissions consistent with that reported for other individual seeps;
- Methane-rich cold seeps in Cook Strait have negligible impact on ambient water column nutrient, particulate and sediment biogeochemistry, but are a potential source of bacteria, including methanotrophs, to the water column;
- Dissolved methane of seep origin is advected laterally and primarily retained in deeper water, and so the impact on atmospheric methane is minimal;
- The Wairarapa Seep site provides a useful analogue for other mid-slope cold seeps known to occur on the convergent Hikurangi Margin and elsewhere; and
- The recognition of multiple areas of structurally controlled venting at the Wairarapa Seep site indicates that this is a valuable site for further long-term monitoring to improve the understanding of the occurrence, release and methane gas efflux from the sea-floor on accretionary margins. Furthermore, given its proximity to the coast and accessibility, it is an excellent location for determining New Zealand's gas hydrate resources and offshore methane inventories.

Acknowledgements

Thanks to the *RV Tangaroa* officers and crew (especially given the manoeuvring required to sample the flares) and shipboard assistance from Matt Walkington (CTD), Peter Gerring (CTD and sediment sampling), Craig Stewart & Brett Grant (moorings deployment, recovery and current data analysis, CTD operation), Stu Pickmere (nutrient analyses) and Kim Currie (carbonate chemistry). Acknowledgement also to Sarah Bury and Julie Brown (C and N stable isotope analyses), Dominic Ferretti ($^{13}C–CH_4$ isotope analyses), Lisa Northcote (sediment analyses), Gavin Macaulay and Stephane Gauthier (ES60 data), Els Mass and Ashley Rowden (gas sample collection), Peter Hill (electronics support) and Graham Rickard, Steve Chiswell, Craig Stevens and Murray Smith (physical oceanography). Thanks to Lionel Carter for the initial seep site location, Jorg Bialas, Gesa Netzeband and Phil Barnes for permission to use SO-191 seismic profiles, Ingo Klaucke and David Bowden for the side-scan sonar image, Amy Baco and Ashley Rowden for geophysical and camera data from TAN0616, and David Weller for $\delta^{13}C–CH_4$ sample collection from 178°E. We acknowledge Jens Greinert for facilitating the collaborative research highlighted in this special issue, and thank him and the other journal reviewers for comments. Funding for this study was provided by the New Zealand Foundation of Research, Science and Technology research programmes C01X0501, C01X0702 and C01X0703.

Appendix A. Supplementary data

Supplementary data associated with this article can be found, in the online version, at doi:10.1016/j.margeo.2009.06.018.

References

Arvidson, R.S., Morse, J.W., Joye, S.B., 2004. The sulfur biogeochemistry of chemosynthetic cold seep communities, Gulf of Mexico, USA. Mar. Chem. 87, 97–119.

Baco, A.R., Rowden, A.A., Levin, L.A., Smith, C.R., Bowden, D., and the RENEWZ I cruise scientific party, 2009-this issue. Initial characterization of cold seep faunal communities on the New Zealand margin. Mar. Geol. doi:10.1016/j.margeo.2009.06.015.

Barber, A.J., Tjokosapoetro, S., Charlton, T.R., 1986. Mud volcanoes, shale diapers, wrench faults and melanges in accretionary complexes, eastern Indonesia. AAPG Bull. 70, 1729–1741.

Barnes, P.M., Mercier de Lépinay, B., Collot, J.E., Delteil, J., Audru, J.-C., 1998. Strain partitioning in the transition area between oblique subduction and continental collision, Hikurangi Margin, New Zealand. Tectonics 17, 534–557.

Barnes, P.M., Lamarche, G., Bialas, J., Henrys, S., Pecher, I., Netzeband, G.L., Greinert, J., Mountjoy, J.J., Pedley, K., Crutchley, G., 2009-this issue. Tectonic and geological framework for gas hydrates and cold seeps on the Hikurangi subduction Margin, New Zealand. Mar. Geol. doi:10.1016/j.margeo.2009.03.012.

Bialas, J., Greinert, J., Linke, P., Pfannkuche, O., 2007. FS Sonne Fahrtericht / Cruise Report SO 191 — New Vents "Puaretanga Hou", Wellington-Napier-Auckland, 11.01-23.03.2007. IFM-GEOMAR Berichte aus dem Leibniz-Institut für Meereswissenschaften an der Christian-Albrechts-Universität zu Kiel (9 April 2007), 139 pp + appendices.

Bradford, J.M., Lapennas, P.P., Murtagh, R.A., Chang, F.H., Wilkinson, V., 1986. Factors controlling summer phytoplankton production in greater Cook Strait, New Zealand. N.Z. J. Mar. Freshw. Res. 20, 253–279.

Canfield, D.E., Kristensen, E., Thamdrup, B., 2005. Chapter 10 — the methane cycle. Aquatic Geomicrobiology. Adv. Mar. Biol. 48, 383–418.

Chiswell, S.M., 2000. The Wairarapa Coastal Current. N.Z. J. Mar. Freshw. Res. 34, 303–315.

Chiswell, S.M., Rickard, G.J., 2006. Comparison of model and observational ocean circulation climatologies for the New Zealand region. J. Geophys. Res. 111, C10011. doi:10.1029/2006JC003489.

Chiswell, S.M., Roemmich, D., 1998. The East Cape Current and two eddies: a mechanism for larval retention? N.Z. J. Mar. Freshw. Res. 32, 385–397.

Damm, E., Budéus, G., 2003. Fate of vent-derived methane in seawater above the Håkon Mosby mud volcano (Norwegian Sea). Mar. Chem. 82, 1–11.

De Angelis, M.A., Lilley, M.D., Olson, E.J., Baross, J.A., 1993. Methane oxidation in deep-sea hydrothermal flares of the Endeavour Segment of the Juan de Fuca Ridge. Deep-Sea Res. I 40, 1169–1186.

Davey, F.J., Hampton, M., Childs, J., Fisher, M.A., Lewis, K.B., Pettinga, J.R., 1986. Structure of a growing accretionary prism, Hikurangi Margin, New Zealand. Geology 14, 663–666.

Dickens, G.R., 2003. Rethinking the global carbon cycle with a large, dynamic and microbially mediated gas hydrate capacitor. Earth Planet. Sci. Lett. 213, 169–183.

Dillon, W.P., Nealon, J.W., Taylor, M.H., Lee, M.W., Drury, R.M., Anton, C.H., 2001. Sea-floor collapse and methane venting associated with gas hydrate on the Blake Ridge — causes

Appendix I

and implications for sea-floor stability and methane release. In: Paull, C.K, Dillon, W.P. (Eds.), Natural Gas Hydrates: Occurrence, Distribution, and Detection, vol. 124. AGU Monogr., pp. 211–233.
Faure, K., Greinert, J., Schneider von Deimling, J., McGinnis, D.F., Kipfer, R., Linke, P., 2009. Methane seepage along the Hikurangi Margin of New Zealand: geochemical and physical evidence from the water column, sea surface and atmosphere. Mar. Geol., this issue.
Greinert, J., 2008. Monitoring temporal variability of bubble release at seeps: the hydroacoustic swath system GasQuant. J. Geophys. Res. 113, C7 Art No. C07048 , Jul 30 2008.
Greinert, J., Artemov, Y, Egorov, V, De Batist, M, McGinnis, D., 2006. 1300-m-high rising bubbles from mud volcanoes at 2080 m in the Black Sea: hydroacoustic characteristics and temporal variability. Earth Planet. Sci. Lett. 244 (1–2), 1–15.
Greinert, J., Lewis, K., Suess, E, Pecher, I., Rowden, A., de Batis, M., Bialas, J., 2009. Methane seepage along the Hikurangi Margin, New Zealand: overview of methane seepage and gas hydrate-related studies until March 2007. Mar. Geol., this issue.
Harris, T.F.W., 1990. Greater Cook Strait — Form and Flow. Department of Scientific and Industrial Research, Marine & Freshwater, Wellington, New Zealand. 212 pp.
Heath, R.A., 1985. A review of the physical oceanography of the seas around New Zealand — 1982. N.Z. J. Mar. Freshw. Res. 19, 79–124.
Heeschen, K.U., Collier, R.W., de Angelis, M.A., Suess, E., Rehder, G., Linke, P., Klinkhammer, G.P., 2005. Methane sources, distributions and fluxes from cold water vent sites at Hydrate Ridge, Cascadia Margin. Global Biogeochem. Cycles 19, GB2016. doi:10.1029/2004GB002266.
Henrys, S.A., Ellis, S., Uruski, C., 2003. Conductive heat flow variations from bottom simulating reflectors on the Hikurangi Margin, New Zealand. Geophys. Res. Lett. 30. doi:10.1029/2002GLO15772.
Holbrook, W.S., Gorman, A.R., Hornbach, M., Hackwith, K.L., Nealon, J., Lizarralde, D., Pecher, I.A., 2002. Seismic detection of marine methane hydrate. Lead. Edge (Tulsa, OKla.) 21 (7), 686–689.
Hovland, M.A., Judd, A.G., Burke, R.A.J., 1993. The global flux of methane from shallow submarine sediments. Chemosphere 26, 559–578.
Inagaki, F., Tsunogai, U., Suzuki, M., Kosaka, A., Machiyama, H., Takai, K., Nunoura, T., Nealson, K.H., Horikoshi, K., 2004. Characterization of C1-mtabolizing prokaryotic communities in methane seep habitats at the Kuroshima Knoll, southern Ryukyu arc, by analyzing pmoA, mmoX, mxaF, mcrA, and 16S rRNA Genes. Appl. Environ. Microbiol. 70, 7445–7554.
Judd, A.G., 2003. The global importance and context of methane escape from the seabed. Geo-Mar. Lett. 23, 147–154.
Judd, A.G., Hovland, M., 2007. Seabed Fluid Flow: The Impact of Geology, Biology and the Marine Environment. Cambridge University Press. 475 pp.
Kastner, M., 2001. Gas hydrates in convergent margins: formation, occurrence, geochemistry, and global significance. In: Paull, C.K, Dillon, W.P. (Eds.), Natural Gas Hydrates: Occurrence, Distribution, and Detection, vol. 124. AGU Monogr, pp. 67–86.
Katz, H.R., 1982. Evidence of gas hydrates beneath the continental slope, East Coast, North Island, New Zealand. N.Z. J. Geol. Geophys. 25, 193–199.
Klaucke, I., Weinrebe, W., Petersen, C.J., Bowden, D., 2009-this issue. Temporal variability of gas seeps offshore New Zealand: multi-frequency geoacoustic imaging of the Wairarapa area, Hikurangi Margin. Mar. Geol. doi:10.1016/j.margeo.2009.02.009.
Kulm, L.D., Suess, E., Moore, J.C., et al., 1986. Oregon subduction zone: venting, fauna, and carbonates. Science 231, 561–566.
Kvenvolden, K.A., Barnard, L.A., 1983. Hydrates of natural gas in continental margins. In: Watkins, J.S., Drake, C.L. (Eds.), Studies in Continental Marine Geology, vol. 34. AAPG Memoir, pp. 631–640.
Kvenvolden, K.A., 1993. Gas hydrates — geological perspectives and global change. Rev. Geophys. 31, 173–187.
Leifer, I., Boles, J., Clark, J.F., Luyendyk, B.P., 2004. The dynamic nature of marine hydrocarbon seepage. Environ. Geol. 46 (8), 1038–1052.
Le Pichon, X., Kobayashi and Kaiko-Nankai Scientific Crew, 1992. Fluid venting activity within the eastern Nankai Trough accretionary wedge: a summary of the 1989 Kaiko-Nankai results. Earth Planet. Sci. Lett. 109, 303–318.
Levin, L.A., 2005. Ecology of cold seep sediments: interactions of fauna with flow, chemistry and microbes. Oceanogr. Mar. Biol. Ann. Rev. 43, 1–46.
Lewis, K.B., Marshall, B.A., 1996. Seep faunas and other indicators of methane-rich dewatering on New Zealand convergent margins. N.Z. J. Geol. Geophys. 39, 181–200.
Lewis, K.B., Mitchell, J.S., 1980. Cook Strait Sediments, NZOI (now NIWA) Coastal Chart Series, 1:200 000, originally published by Department of Scientific and Industrial Research, Marine & Freshwater, Wellington, New Zealand.
Lewis, K.B., Pettinga, J.R., 1993. The emerging, imbricate frontal wedge of the Hikurangi Margin. In: Ballance, P.F. (Ed.), Basins of the Southwest Pacific, Sedimentary Basins of the World, vol. 3, pp. 225–250.
Lewis, K.B, Carter, L., Davey, F.J., 1994. The opening of Cook Strait: interglacial tidal scour and aligning basins at a subduction to transform plate edge. Mar. Geol. 116, 293–312.
Linke, P., Sommer, S., Rovelli, L., McGinnis, D.F., 2009-this issue. Physical limitations of dissolved methane fluxes: the role of bottom-boundary layer processes. Mar. Geol. doi:10.1016/j.margeo.2009.03.020.
Maas, E. W., Hirayama, H., Law, C S. submitted. Diversity of the particulate methane monooxygenase at a New Zealand seep site". Environmental Microbiology Reports.
Mau, S., Sahling, H., Rehder, G., Suess, E., Linke, P., Soeding, E., 2006. Estimates of methane output from mud extrusions at the erosive convergent margin off Costa Rica. Mar. Geol. 225, 129–144.
McGinnis, D.F., Greinert, J., Artemov, Y., Beaubein, S.E., Wűest, A., 2006. Fate of rising bubbles in stratified waters: how much methane reaches the atmosphere? J. Geophys. Res. 111, C09007. doi:10.1029/2005JC003183 2006.
Mountjoy, J.J., Barnes, P.B., Pettinga, J.R., 2009. Morphostructure and evolution of submarine canyons across an active margin: Cook Strait sector of the Hikurangi Margin, New Zealand. Mar. Geol. 260, 45–68.
Naudts, L., Greinert, J., Poort, J., Belza, J., Vangampelaere, E., Boone, D., Linke, P., Henriet, J.-P., and De Batist, M. Active venting sites on the gas-hydrate-bearing Hikurangi Margin, Off New Zealand: diffusive versus bubble-released methane. Marine Geology, this issue.
Nelson, C.S., Healy, T.R., 1984. Pockmark-like structures on the Poverty Bay seabed — possible evidence for submarine mud volcanism Note N.Z. J. Geol. Geophys. 27, 225–230.
Netzeband, G.L., Krabbenhoeft, A., Zillmer, M., Petersen, C.J., Papenberg, C., Bialas, J., 2009. Seeps and their structure underneath — seismic evidence from the Wairarapa area. Mar. Geol. (this issue).
Nodder, S.D., Duineveld, G.C.A., Pilditch, C.A., Sutton, P.J., Probert, P.K., Lavaleye, M.S.S., Witbaard, R., Chang, F.H., Hall, J.A., Richardson, K.M., 2007. Focusing of phytodetritus deposition beneath a deep-ocean front, Chatham Rise, New Zealand. Limnol. Oceanogr. 52, 299–314.
Olu, K., Lance, S., Sibuet, M., Henry, P., Fiala-Medioni, A., Dinet, A., 1997. Cold seep communities as indicators of fluid expulsion patterns through mud volcanoes seaward of the Barbados accretionary prism. Deep-Sea Res. I 44, 811–841.
Pecher, I., Ellis, S., Henrys, S.A., Chiswell, S.M., Kukowski, N., 2005. Erosion of the sea-floor at the top of the gas hydrate stability zone on the Hikurangi Margin, New Zealand. Geophys. Res. Lett. 32, L24603. doi:10.1029/2005GL024687.
Pettinga, J.R., 2003. Mud volcano eruption within the emergent accretionary Hikurangi Margin, southern Hawke's Bay, New Zealand. N.Z J. Geol. Geophys. 46, 107–121.
Prather, M.J., Derwent, R., Ehhalt, D., Fraser, P., Sanheuza, E., Zhou, X., 1995. Other trace gases and atmospheric chemistry. In: Houghton, J.T., Meira-Filho, L.G., Bruce, J.P., Lee, H., Callander, B.A., Haites, E.F., Harris, N., Mashell, K. (Eds.), Climate Change (1994). Cambridge University Press, UK, pp. 73–126.
Quay, P.D., Stutsmann, J., Wilbur, D., Snover, A., Dlugokencky, E., Brown, T., 1999. The isotopic composition of atmospheric methane. Glob. Biogeochem. Cycles 13, 445–461.
Reed, D.L., Silver, E.A., Tagudin, J.E., Shipley, T.H., Vrolijk, P., 1990. Relations between mud volcanoes, thrust deformation, slope sedimentation, and gas hydrate, offshore north Panama. Mar. Pet. Geol. 7, 44–54.
Rickard, G.J., Hadfield, M.G., Roberts, M.J., 2005. Development of a regional ocean model for New Zealand. N.Z. J. Mar. Freshw. Res. 39, 1171–1191.
Sauter, E.J., Muyakshin, S.I., Charlou, J.-L., Schlüter Boetius, A., Jerosch, K., Damm, E., Foucher, J.-P., Klages, M., 2006. Methane discharge from a deep-sea submarine mud volcano into the upper water column by gas hydrate-coated methane bubbles. Earth Planet. Sci. Lett. 243, 354–365.
Schubert, C.J., Durisch-Kaiser, E., Holzner, C.P., Klauser, L., Wehrli, B., Schmale, O., Greinert, J., McGinnis, D.F., De Batist, M., Kipfer, R., 2006. Methanotrophic microbial communities associated with bubble flares above gas seeps in the Black Sea. Geochem. Geophys. Geosyst. 7, Q04002. doi:10.1029/205GC001049.
Schwalenberg, K., Haeckel, M., Poort, J., Jegen, M., 2009-this issue. Evaluation of gas hydrate deposits in an active seep area using Marine Controlled Source Electromagnetics: results from the Wairarapa area, New Zealand. Mar. Geol. doi:10.1016/j.margeo.2009.07.006.
Sommer S., Linke P., Pfannkuche O., Niemann H., Treude T., 2009-this issue. Benthic respiration in a novel seep habitat dominated by dense beds of ampharetid polychaetes at the Hikurangi Margin (New Zealand). Mar. Geol. doi:10.1016/j.margeo.2009.06.003.
Steele, L. P., Krummel, P. B., Langenfelds, R. L., 2002. Atmospheric CH_4 concentrations from sites in the CSIRO Atmospheric Research GASLAB air sampling network (October 2002 version). In: Trends: A Compendium of Data on Global Change. Carbon Dioxide Information Analysis Center, Oak Ridge National Laboratory, US Department of Energy, Oak Ridge, Tennessee, USA.
Suess, E., Torres, M.E., Bohrmann, G., Collier, R.W., Greinert, J., Linke, P., Rehder, G., Trehu, A., Wallmann, K., Winckler, G., Zuleger, E., 1999. Gas hydrate destabilization: enhanced dewatering, benthic material turnover and large methane flares at the Cascadia convergent margin. Earth Planet. Sci. Lett. 170, 1–15.
Uruski, C.I., 1992. Sedimentary basins and structure of Cook Strait. Institute of Geological & Nuclear Sciences Report 92/3. 18 pp.
Valentine, D.L., Blanton, D.C., Reeburgh, W.S., Kastner, M., 2001. Water column methane oxidation adjacent to an area of active hydrate dissociation, Eel River Basin. Geochim. Cosmochim. Acta 65, 2633–2640.
Walter, K.M., Zimov, S.A., Chanton, J.P., Verbyla, D., Chapin III, F.S., 2006. Methane bubbling from Siberian thaw lakes as a positive feedback to climate warming. Nature 443, 71–75. doi:10.1038/nature05040.

Please cite this article as: Law, C.S., et al., Geological, hydrodynamic and biogeochemical variability of a New Zealand deep-water methane cold seep during an integrated three-year time-series study, Mar. Geol. (2009), doi:10.1016/j.margeo.2009.06.018

Appendix II

Barnes, P.M., Lamarche, G., Bialas, J., Henrys, S., Pecher, I.A., Netzeband, G.L., Greinert, J., Mountjoy, J.J., Pedley, K. and Crutchley, G., 2009. Tectonic and Geological Framework for Gas hydrates and Cold Seeps on the Hikurangi Subduction Margin, New Zealand. In press at Marine Geology doi:10.1016/j.margeo.2009.03.012.

Appendix II

ARTICLE IN PRESS
MARGO-04326; No of Pages 23
Marine Geology xxx (2009) xxx–xxx
Contents lists available at ScienceDirect
Marine Geology
journal homepage: www.elsevier.com/locate/margeo

Tectonic and geological framework for gas hydrates and cold seeps on the Hikurangi subduction margin, New Zealand

Philip M. Barnes [a,*], Geoffroy Lamarche [a], Joerg Bialas [b], Stuart Henrys [c], Ingo Pecher [d], Gesa L. Netzeband [b], Jens Greinert [e,1], Joshu J. Mountjoy [a,f], Katherine Pedley [f], Gareth Crutchley [g]

[a] National Institute of Water & Atmospheric Research, P.O. Box 14901, Kilbirnie, Wellington 6041, New Zealand
[b] Leibniz Institute of Marine Sciences, IFM-GEOMAR, Wischhofstr. 1-3, 24148, Kiel, Germany
[c] GNS Science, P.O. Box 30368, Lower Hutt, New Zealand
[d] Institute of Petroleum Engineering, Heriot-Watt University, Edinburgh, EH3 9HP, Scotland, UK
[e] Renard Centre of Marine Geology, University of Gent, Belgium
[f] Department of Geological Sciences, University of Canterbury, Private Bag 4800, Christchurch, New Zealand
[g] Department of Geology, University of Otago, P.O. Box 56, Dunedin 9054, New Zealand

ARTICLE INFO

Article history:
Received 2 July 2008
Received in revised form 18 February 2009
Accepted 8 March 2009
Available online xxxx

Keywords:
Hikurangi
subduction
interplate décollement
thrust wedge
thrust faults
accretion
subducting seamounts
anticline
turbidites
gas hydrates
fluid seeps

ABSTRACT

The imbricated frontal wedge of the central Hikurangi subduction margin is characteristic of wide (ca. 150 km), poorly drained and over pressured, low taper (~4°) thrust systems associated with a relatively smooth subducting plate, a thick trench sedimentary sequence (~3–4 km), weak basal décollement, and moderate convergence rate (~40 mm/yr). New seismic reflection and multibeam bathymetric data are used to interpret the regional tectonic structures, and to establish the geological framework for gas hydrates and fluid seeps. We discuss the stratigraphy of the subducting and accreting sequences, characterize stratigraphically the location of the interplate décollement, and describe the deformation of the upper plate thrust wedge together with its cover sequence of Miocene to Recent shelf and slope basin sediments. We identify approximately the contact between an inner foundation of deforming Late Cretaceous and Paleogene rocks, in which widespread out-of-sequence thrusting occurs, and a 65–70 km-wide outer wedge of late Cenozoic accreted turbidites. Although part of a seamount ridge is presently subducting beneath the deformation front at the widest part of the margin, the morphology of the accretionary wedge indicates that frontal accretion there has been largely uninhibited for at least 1–2 Myr. This differs from the offshore Hawkes Bay sector of the margin to the north where a substantial seamount with up to 3 km of relief has been subducted beneath the lower margin, resulting in uplift and complex deformation of the lower slope, and a narrow (10–20 km) active frontal wedge.

Five areas with multiple fluid seep sites, referred to informally as Wairarapa, Uruti Ridge, Omakere Ridge, Rock Garden, and Builders Pencil, typically lie in 700–1200 m water depth on the crests of thrust-faulted, anticlinal ridges along the mid-slope. Uruti Ridge sites also lie in close proximity to the eastern end of a major strike-slip fault. Rock Garden sites lie directly above a subducting seamount. Structural permeability is inferred to be important at all levels of the thrust system. There is a clear relationship between the seeps and major seaward-vergent thrust faults, near the outer edge of the deforming Cretaceous and Paleogene inner foundation rocks. This indicates that thrust faults are primary fluid conduits and that poor permeability of the Cretaceous and Paleogene inner foundation focuses fluid flow to its outer edge. The sources of fluids expelling at active seep sites along the middle slope may include the inner parts of the thrust wedge and subducting sediments below the décollement. Within anticlinal ridges beneath the active seep sites there is a conspicuous break in the bottom simulating reflector (BSR), and commonly a seismically-resolvable shallow fault network through which fluids and gas percolate to the seafloor. No active fluid venting has yet been recognized over the frontal accretionary wedge, but the presence of a widespread BSR, an extensive protothrust zone (>200 km by 20 km) in the Hikurangi Trough, and two unconfirmed sites of possible previous fluid expulsion, suggest that the frontal wedge could be actively dewatering. There are presently no constraints on the relative fluid flux between the frontal wedge and the active mid-slope fluid seeps.

* Corresponding author. Tel.: +64 4 386 0372; fax: +64 4 386 2153.
E-mail address: p.barnes@niwa.co.nz (P.M. Barnes).
[1] Present address: Royal Netherlands Institute for Sea Research, P.O. Box 59, 1790 AB, Den Burg (Texel), The Netherlands.

0025-3227/$ – see front matter © 2009 Elsevier B.V. All rights reserved.
doi:10.1016/j.margeo.2009.03.012

1. Introduction

Gas hydrates and cold seeps are characteristics of many active continental margins. They reflect the migration of fluids and gas towards the seabed as a result of tectonic deformation, compaction, porosity reduction, and dewatering of the sedimentary sequence (Kvenvolden, 1993). Seafloor sites of methane rich fluid expulsion may be characterized by the presence of chemosynthetic biological communities, development of carbonate hard grounds, pockmark depressions, mud volcanism, and/or hydroacoustic flares (e.g., Kulm and Suess, 1990; Henry et al., 1990; Trehu et al., 1999; Faure et al., 2006). In subduction margins, particularly those dominated by accretion, high fluid pressures are thought to play an important mechanical role in maintaining thrust wedges (Moore and Byrne, 1987; Bryne and Fisher, 1990, Moore and Vrolijk, 1992; Bangs et al., 1999, 2004; Saffer and Bekins, 2002), and in the seismogenic cycle by producing fluctuations in frictional strength of faults (Sibson, 1992; Dixon and Moore, 2007 and papers therein). Fault zones are commonly interpreted as important conduits for the upward flow of fluid (e.g., Moore et al., 1990, 1995).

The 25 Myr old Hikurangi Margin of north eastern New Zealand epitomizes subduction systems and their tectonic complexity and variability. Lying at the southern end of the Tonga–Kermadec–Hikurangi subduction zone, the margin has formed in response to the westward subduction of the thick and bathymetrically elevated oceanic Hikurangi Plateau (Pacific Plate) beneath the Australian Plate at about 40–50 mm/yr (Fig. 1). The structural trench, referred to as the Hikurangi Trough, is shallow (c. 3000 m) compared to the deep Kermadec trench (>9000 m), and the plate interface dips at a gentle angle of about 3° for at least 100 km beneath the margin, before steepening beneath the North Island (Davey et al., 1986a; Henrys et al., 2006; Barker et al., 2009). The margin exhibits complex tectonic structure and stratigraphic evolution (e.g., Lewis and Pettinga, 1993; Collot et al., 1996; Field et al., 1997; Barnes et al., 2002; Barnes and Nicol, 2004; Henrys et al., 2006; Nicol et al., 2007). The northern margin off Raukumara Peninsula is characterized by non-accretion and tectonic erosion associated with seamount impact scars (Lewis et al., 1997, 1998, 2004; Collot et al., 2001), whereas the central margin off the Wairarapa coast is a classical imbricated thrust wedge dominated by accretion (Davey et al., 1986b; Lewis and Pettinga, 1993; Collot et al., 1996; Barnes and Mercier de Lépinay, 1997; Lewis et al., 1999). The relatively narrow southern end of the margin lies in the transition from oblique subduction to continental strike-slip deformation (Barnes et al., 1998a; Barnes and Audru, 1999; Holt and Haines, 1995) and is incised by Cook Strait Canyon (Mountjoy et al., 2009).

To a first order, Townend (1997a) estimated that an enormous volume of 24 m^3 of fluid per meter of strike length is added to the Hikurangi Margin by frontal accretion per year. Of that, >80% was inferred to be released by subsequent compaction and tectonic deformation, together with an additional 3 m^3 per meter of strike length per annum released by smectite dehydration at depths of 5–10 km. There is ample evidence of fluid flow within the margin. This includes the many oil, gas and mud expulsion sites observed on land (Field et al., 1997), widespread cold vent seep sites and associated chemosynthetic faunas offshore (Lewis and Marshall, 1996; Faure et al., 2006; Greinert et al., 2009-this issue), the occurrence of direct hydrocarbon indicators in industry seismic reflection data (Frederik, 2004), and a widespread bottom simulating reflection (BSR), interpreted as marking the base of the gas hydrate stability zone (Katz, 1981; Henrys et al., 2003; Pecher et al., 2004, 2005; Henrys et al., in press). Studies of exposed rocks in the forearc basin indicate that fluid seepage has occurred on the margin for at least 22 Myr (Campbell et al., 2008). The BSR has been modelled to reveal low values (44 ± 10 mW m^{-2}) of heat flow (Townend, 1997b; Henrys et al., 2003; Netzeband et al., 2009-this issue). Elevated pore pressures have been commonly encountered in exploration wells (Davies et al., 2000; Darby et al., 2000), and assumed to be widespread within the accretionary wedge (Barnes and Mercier de Lépinay, 1997).

Since 2001, multichannel seismic reflection and high-resolution multibeam bathymetric data have been acquired from the Hikurangi Margin by research institutes, oil companies, and the New Zealand Government as part of hydrocarbon exploration and research initiatives. The improved understanding of tectonic structure that can be gained from these data, combined with the widespread occurrence of gas hydrates and cold seeps makes this margin an excellent example to study the relationship between thrust tectonics and fluid flow. This paper presents a revision and synthesis of the tectonic morphology, fault structure, and composition of the imbricated thrust wedge between Mahia Peninsula and Cook Strait (Fig. 1). We then establish the tectonic and geological framework for each of five study areas with submarine seep sites, and we interpret these sites within the context of regional structural processes. Finally we discuss the role of the deformation structures as fluid conduits.

2. Data used in this study

The continental shelf of the Hikurangi Margin is relatively well covered with multichannel seismic reflection (MCS) data, from which detailed accounts of active tectonics (e.g., Barnes et al., 2002; Barnes and Nicol, 2004; Lewis et al., 2004), sequence stratigraphy (Paquet, 2008; Paquet et al., 2009), and exploration geology (e.g., Field et al., 1997; Uruski et al., 2004) have been published. The continental slope however, is less well surveyed. Previous regional interpretations of the tectonic structure were based largely on *RV L'ATALANTE* SIMRAD EM12Dual multibeam bathymetry and Hawaii MR1 sidescan sonar images, supported by the SP LEE MCS profile, *RV L'ATALANTE* and pre-1980s oil company low-fold MCS data (Fig. 1D), and widespread single channel seismic data (not shown in Fig. 1D) (Davey et al., 1986a,b; Lewis and Pettinga, 1993; Collot et al., 1996; Barnes and Mercier de Lépinay, 1997, Lewis et al., 1997, 1999; Barnes et al., 1998a,b).

MCS data acquired since 2001, and available for this study, includes (Fig. 1D) (1) the GECO RESOLUTION NIGHT high-fold profile off Hawkes Bay (Pecher et al., 2004, 2005; Henrys et al., 2006), (2) the large grid of *MV MULTIWAVE* high-fold MCS data (CM05) from the upper margin off Hawkes Bay and East Coast (Multiwave, 2005; Nicol et al., 2007), (3) low-fold MCS data acquired off Hawkes Bay and Mahia Peninsula on several surveys by *RV TANGAROA* (CR3044, TAN0106, TAN0313, TAN0412) (Barnes et al., 2002; Paquet et al.,

Fig. 1. A. Overview of the Pacific–Australia plate boundary in the New Zealand region, showing the Kermadec–Hikurangi subduction zone. B. Morphology and major active faults of the Hikurangi Subduction margin. Bold thrust is the principal deformation front. Isopachs in the Hikurangi Trough indicate approximate thickness (km) of trench-fill turbidites (Lewis et al., 1998). Bold black numbers along the deformation front are modelled convergence rates (mm/yr) between the Hikurangi Margin and the Pacific Plate (Wallace et al., 2004). Plate motion vectors are from Beavan et al. (2002). The bold dashed white line along the middle slope separates the late Cenozoic frontal accretionary wedge beneath lower continental slope from a deforming foundation of pre-subduction, Cretaceous and Paleogene passive margin rocks and overlying Miocene to Recent slope basins beneath the middle to upper margin. The bold black line in the Hikurangi Trough is the meandering Hikurangi Channel. Labels Wairarapa, Uruti Ridge, Porangahau Ridge, Omakere Ridge, Rock Garden, and Builders Pencil are seep sites discussed in this paper and elsewhere in this issue. LR, Lachlan Ridge; RR, Ritchie Ridge. C. Schematic section across the Hikurangi subduction zone, axial ranges of North Island, and back arc volcanic rift. Shading with wavy line pattern is Mesozoic Torlesse basement rocks. Smooth grey shade is deforming Cretaceous and Paleogene pre-subduction sequences with Miocene to Recent slope basins, and white is accreted trench-fill turbidites. D. Distribution of regional multichannel seismic reflection coverage across the Hikurangi Margin. Notable surveys include GECO RESOLUTION 2001 NIGHT high-fold profile, grey line off Hawkes Bay; *RV TANGAROA* low-fold data, purple lines off Hawkes Bay and Mahia; *MV MULTIWAVE* 2005 high-fold CM05 profiles, black lines (profile labeled 1 is CM05#1); *RV SONNE* SO191 2007 regional low-fold profiles, red lines; *RV SP LEE* 1983 high-fold profile, dark blue line across central margin; *RV L'ATALANTE* 1993 "GeodyNZ" low-fold profiles, gold lines. (For interpretation of the references to colour in this figure legend, the reader is referred to the web version of this article.)

Please cite this article as: Barnes, P.M., et al., Tectonic and geological framework for gas hydrates and cold seeps on the Hikurangi subduction margin, New Zealand, Mar. Geol. (2009), doi:10.1016/j.margeo.2009.03.012

2009), and (4) regional low-fold MCS profiles acquired by *RV SONNE* SO191 in 2007 from the central part of the margin.

On the *RV SONNE* SO191 survey in 2007, we acquired a total of 710 km of regional seismic reflection data (red lines in Fig. 1D). An array of five SODERA G-guns with total capacity of 2080 in.^{3} (32 l) was used as the seismic source on lines 1 to 6, and a 250/105 in.^{3} (5.5 l) GI gun on lines 8 to 10. The data were received on a 32 channel digital GEOMETRICS GeoEel hydrophone array. Standard processing included trace editing,

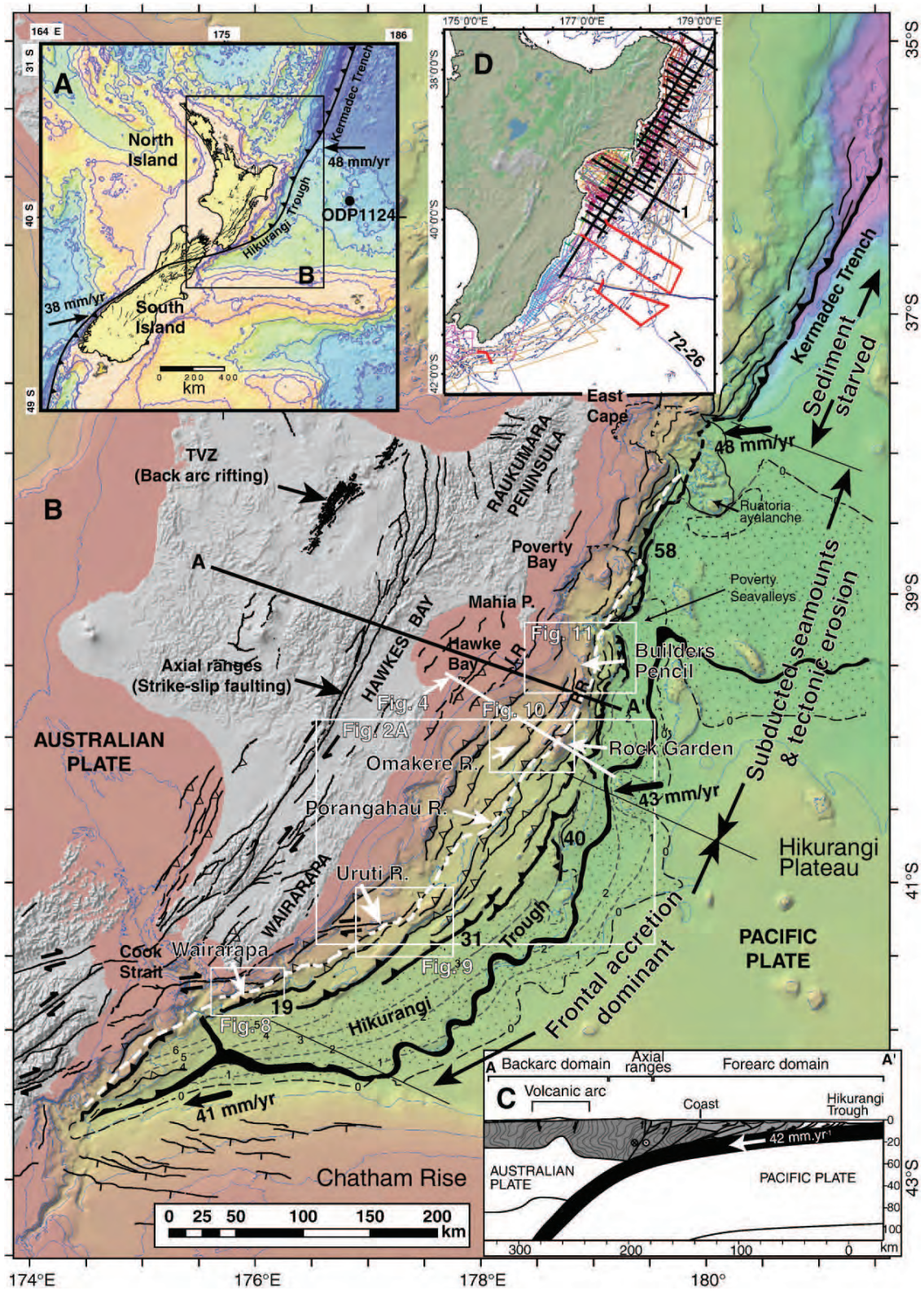

Please cite this article as: Barnes, P.M., et al., Tectonic and geological framework for gas hydrates and cold seeps on the Hikurangi subduction margin, New Zealand, Mar. Geol. (2009), doi:10.1016/j.margeo.2009.03.012

Appendix II

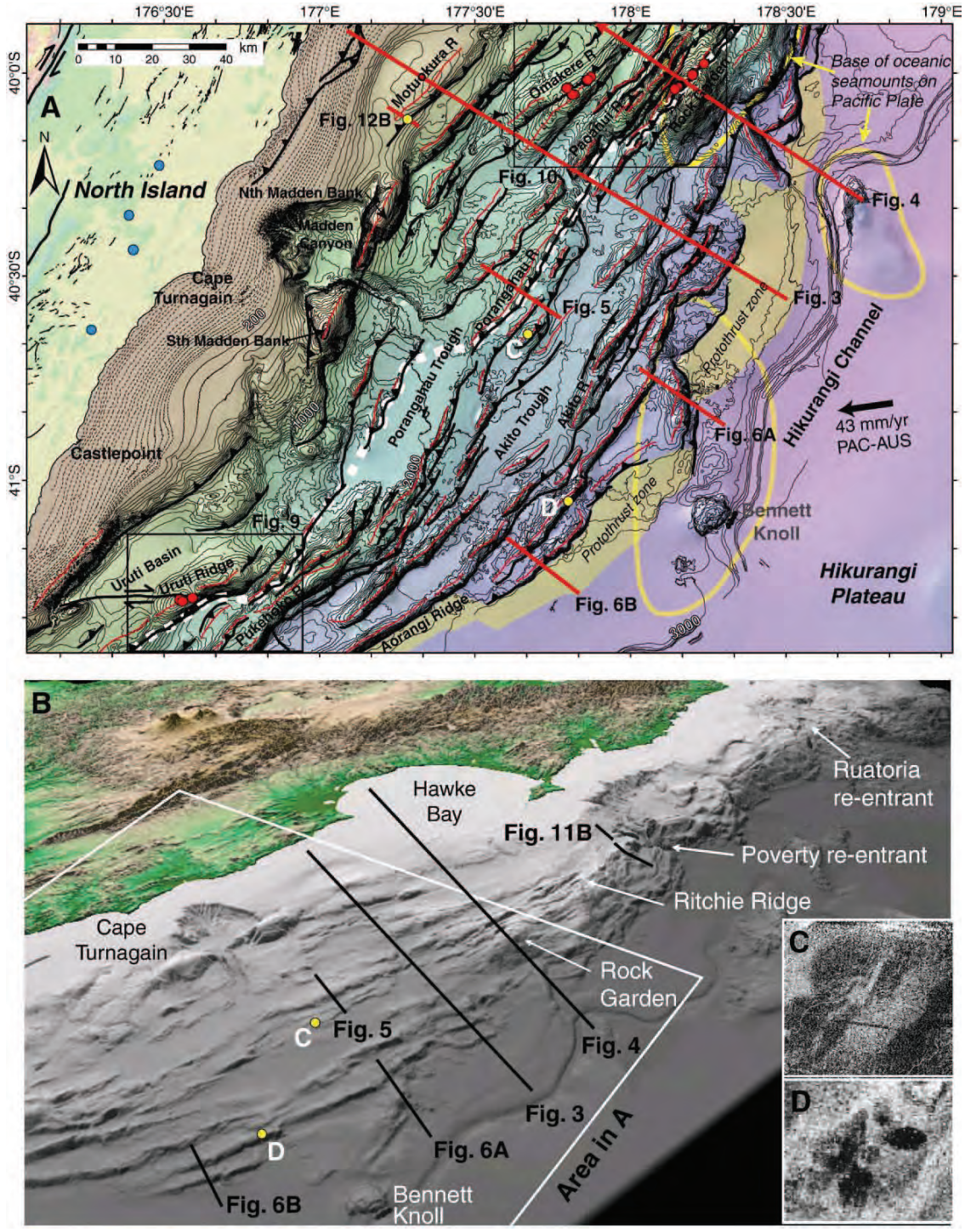

Fig. 2. A. Bathymetry and major tectonic structures of the central section of the Hikurangi Margin, interpreted as part of this study, and modified significantly from Lewis et al. (1999). Red lines are crests of thrust-faulted bathymetric ridges, and represent a close proxy to the axial traces of anticlines imaged in seismic sections. Bathymetric labels are in metres. The protothrust zone is shaded mustard yellow. Onshore active faults are courtesy of the GNS Science active faults database. The bold dashed white line along the middle slope separates the late Cenozoic frontal accretionary wedge beneath lower continental slope from a deforming foundation of pre-subduction, Cretaceous and Paleogene passive margin rocks and overlying Miocene to Recent slope basins beneath the middle to upper margin. Plate motion vector is from Beavan et al. (2002). Bold yellow ellipses are the bases of oceanic seamounts on the subducting Pacific Plate. Note the northern of these underlies Rock Garden, whereas the southern partially underlies the present deformation front. Blue bold dots are active seep sites on land. Red dots are seep sites discussed in this issue. Yellow dots are other sites of suspected fluid expulsion from seismic reflection and MR1 deep-tow sidescan sonar data. B. Oblique view of hillshaded bathymetry derived from 100 m grid data. C. MR1 sidescan image of suspected fluid expulsion site surrounded by possible radiating mud flows. D. MR1 sidescan image of suspected mud volcano (Barnes and Mercier de Lépinay, 1997). (For interpretation of the references to colour in this figure legend, the reader is referred to the web version of this article.)

Please cite this article as: Barnes, P.M., et al., Tectonic and geological framework for gas hydrates and cold seeps on the Hikurangi subduction margin, New Zealand, Mar. Geol. (2009), doi:10.1016/j.margeo.2009.03.012

correction for spherical divergence energy loss, frequency domain filtering, CDP gather at 12.5 m, Normal Move-Out correction following velocity picking using semblance plots, nominal 4 fold CDP stack, and finite difference time migration. In addition to the regional seismic lines, we acquired about 415 km of high-resolution MCS data from the Wairarapa, Uruti Ridge, Omakere Ridge and Builders Pencil seep sites (Fig. 1B) using a 250/105 in.^{3} GI gun source and SIG 4-channel towed streamer (e.g., Netzeband et al., 2009-this issue).

Greinert et al. (2009-this issue) outlined new multibeam bathymetry data available to this study, including 30 kHz SIMRAD EM300 data acquired on *RV TANGAROA* surveys TAN0616 and TAN0607, and 12 kHz SIMRAD EM120 data acquired on *RV SONNE* SO191. In addition to these data, and archived SIMRAD EM12Dual L'ATALANTE data, we have also used SIMRAD EM300 multibeam data collected over the southern Wairarapa region on *RV TANGAROA* surveys TAN0215, TAN0309, and TAN0510 (Mountjoy et al., 2009), and over the Poverty Seavalleys off Mahia Peninsula on TAN0106. These data have been processed to variable grids of 10 m to 30 m resolution. The Hawaii MR1 sidescan sonar data previously presented by Barnes and Mercier de Lépinay (1997) and Lewis et al. (1998) have been reinterpreted in light of the new multibeam bathymetric and seismic reflection data. In discussion of bathymetric features, we refer to Mitchell (1988), Arron and Lewis (1992), and Garlick and Mitchell (2002).

3. Tectonic and stratigraphic architecture of the Hikurangi Margin

3.1. Composition of the imbricated frontal wedge

The Hikurangi Margin comprises a thrust imbricated frontal wedge up to 150 km in width (Lewis and Pettinga, 1993). It is built against a Mesozoic basement backstop of Torlesse terrane greywackes. These latter rocks developed on the active margin of Gondwana supercontinent, and are now exposed in the axial ranges of North Island, Raukumara Peninsula, and the coastal hills of southern Wairarapa (Fig. 1). The imbricated frontal wedge extends eastwards across the coastal ranges and offshore margin, where it has a ridge and basin morphology (Fig. 2). The wedge comprises three major components, all of which are deforming together as one sedimentary body. These include (1) an inner foundation of Late Cretaceous and Paleogene, pre-subduction rocks (Figs. 3 and 4); (2) an outer wedge of late Cenozoic accreted trench-fill turbidites; and (3) a deforming cover sequence of Miocene to Recent shelf and slope basin sediments, which are up to several kilometers thick beneath the upper margin and generally thin seawards over the frontal accretionary wedge. The deforming cover sequences of the upper margin are partially exposed in uplifted forearc basins on land, and at structural ridges offshore, and exhibit sequence architectures that are strongly influenced by sea-level cycles and active tectonics (e.g., Lewis, 1973; Barnes et al., 2002; Paquet, 2008; Paquet et al., 2009). The cover sequences include terrestrial, nearshore marine, shelf, and slope sediments.

The inner, Late Cretaceous and Paleogene foundation was deposited prior to initiation of Hikurangi subduction, and subsequently became highly imbricated as a result of poly-phase deformation following the onset of subduction some 25 Myr ago (Ballance, 1976; Rait et al., 1991; Lewis and Pettinga, 1993; Field et al., 1997; Barnes et al., 2002; Barnes and Nicol, 2004, Henrys et al., 2006; Nicol et al., 2007). Whilst substantial deformation of these rocks occurred in the Miocene, active thrust faulting and folding continues across the inner margin to present day. These rocks produce highly disrupted seismic reflections, with footwall and hanging wall cutoffs typical of thrust tectonic geometries (e.g., Figs. 3 and 4). The rocks outcrop widely along the coast where they exhibit complex mesoscopic deformation fabrics (Pettinga, 1982), have been encountered in a drill hole in Hawke Bay, and dredged from structural highs both within and offshore of Hawke Bay (Lewis and Pettinga, 1993; Lewis and Marshall, 1996; Barnes et al., 2002). In the middle slope region these rocks are typically characterized by variable amplitude, relatively discontinuous, and complex seismic reflections, compared to the accreted turbidites beneath the lower slope (Figs. 5 and 6).

The outer wedge of accreted late Cenozoic turbidites is thrust beneath the front of the inner foundation (Figs. 3–5). This frontal wedge is highly imbricated and produces characteristic seismic reflections correlated with the Hikurangi Trough sequence, which is described in Section 3.3. We have identified the contact between these two components of the imbricated frontal wedge to within c. 10 km in widely spaced (~35 km) seismic profiles along the margin, and have revised its position in Figs. 1 and 2A relative to previous interpretations (Lewis and Pettinga, 1993; Lewis et al., 1997, 1999; Barnes and Mercier de Lépinay, 1997; Barnes et al., 1998a,b).

3.2. Lateral variations in structural and morphological development of the margin

The overall morphology of the Hikurangi Margin varies significantly along strike as a result of variations in the thickness of trench-fill sediment, efficiency of frontal accretion, smoothness/roughness of the Pacific Plate, and obliquity and rate of convergence (Lewis and Pettinga, 1993). Because the trough and its axial channel are supplied with turbiditic sediment largely from submarine canyons in the south (Lewis et al., 1998; Lewis and Barnes, 1999; Mountjoy et al., 2009), the thickness of the turbidites decreases northwards from more than 5 km near Cook Strait to about 1 km off the Raukumara Peninsula (Fig. 1B). Whereas trench-fill sediment thickness decreases northwards, the rate of convergence between the forearc and the subducting Pacific Plate increases northwards by three times, from about 20 mm/yr off southern Wairarapa to nearly 60 mm/yr off the Raukumara Peninsula (Wallace et al., 2004) (Fig. 1B). These variations coincide with relatively low relief on the southern part of the subducting Hikurangi Plateau, compared to the seamount studded northern region, where basement relief commonly exceeds several kilometers (e.g., Figs. 1 and 4) (Wood and Davy, 1994; Davy and Wood, 1994; Lewis et al., 1998; Davy et al., 2008).

Along the northern half of the margin, the combination of relatively thin trench-fill sediment (~1 km), high convergence rate, and rough topography of the subducting plate promotes non-accretion, localized tectonic erosion, and deformation processes within the frontal wedge that reflect the progressive passage of basement asperities beneath the margin (Collot et al., 1996, 2001; Lewis et al., 1997, 1998, 2004; Pecher et al., 2005). The lower margin between the bathymetric bank referred to informally as Rock Garden and the southern Kermadec Trench, is typically about 50–60 km in width, has a relatively steep gradient (>10°), and is characterized by large seamount impact scars, particularly at Poverty Seavalleys and East Cape (Figs. 1 and 2B).

The NIGHT seismic reflection profile off Hawke Bay (Fig. 4) is reasonably representative of the northern half of the margin. It shows a clear interplate thrust décollement extending to 6–8 s TWT (ca. 12–15 km) beneath the coastal region, numerous upper plate thrusts, and a seamount subducted beneath the outer margin bank referred to informally as Rock Garden (Fig. 2) (Pecher et al., 2004, 2005; Henrys et al., 2006). The upper margin structures are correlated to and mapped with an extensive set of high-quality industry and research seismic sections, and they include reactivated thrusts, inversion structures, and thrust triangle zones (Barnes et al., 2002; Barnes and Nicol, 2004). Depth conversion using wide-angle velocity control indicates that the subducted seamount beneath the lower margin has about 3 km of basement relief (Fig. 4 inset). The plate boundary décollement and the overriding ridge above the seamount have been uplifted (Fig. 7), and upper plate thrust faulting is now focused beneath the northern Paoanui Ridge, along the landward side of the elevation (Fig. 2A). Inactive thrusts imaged beneath the steep seaward flank of the ridge have been abandoned in the wake of the seamount,

Please cite this article as: Barnes, P.M., et al., Tectonic and geological framework for gas hydrates and cold seeps on the Hikurangi subduction margin, New Zealand, Mar. Geol. (2009), doi:10.1016/j.margeo.2009.03.012

Please cite this article as: Barnes, P.M., et al., Tectonic and geological framework for gas hydrates and cold seeps on the Hikurangi subduction margin, New Zealand, Mar. Geol. (2009), doi:10.1016/j.margeo.2009.03.012

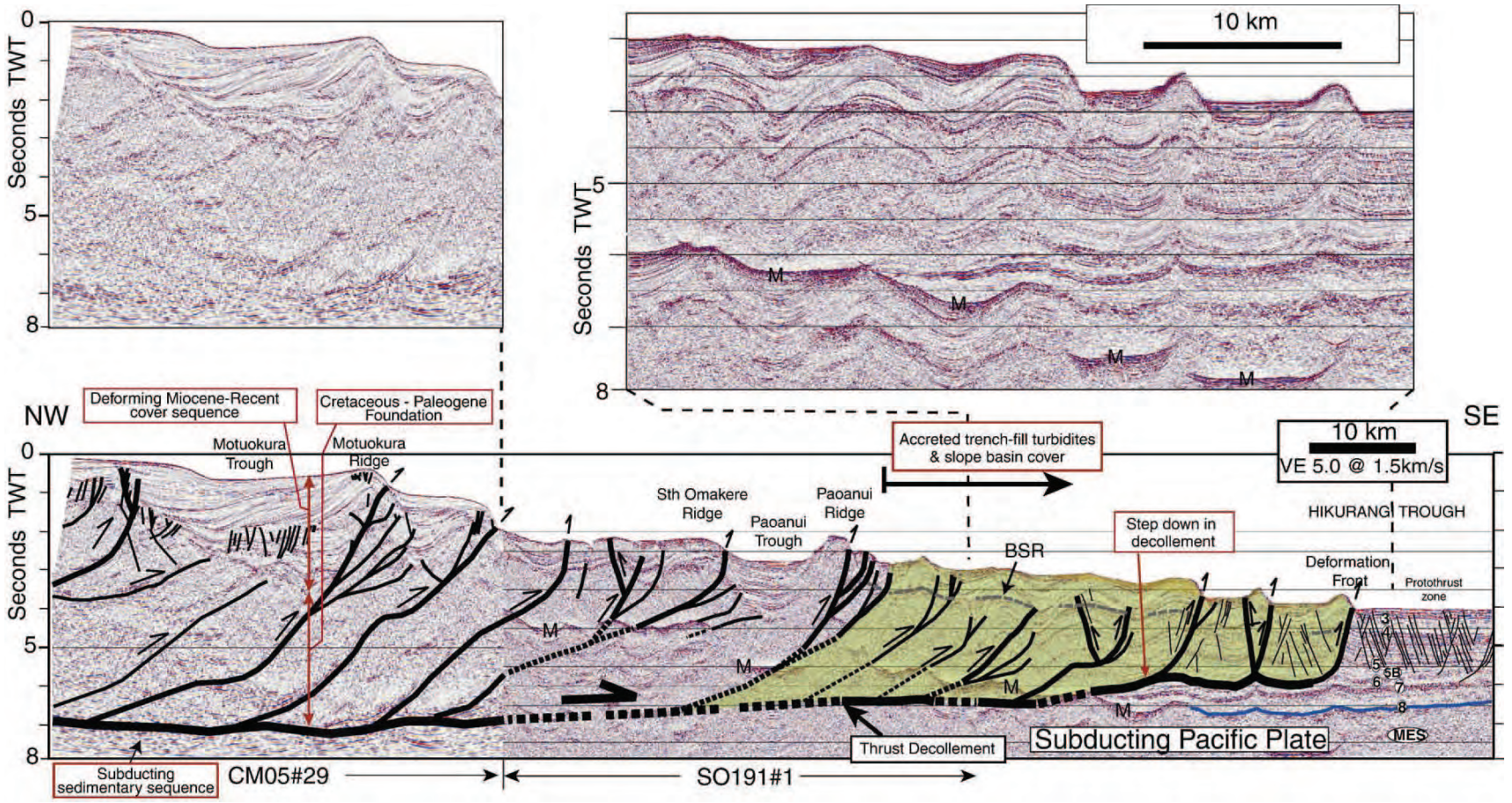

Fig. 3. Uninterpreted and interpreted multichannel seismic section across the central Hikurangi Margin. The seismic data are two spliced sections, including high-fold seismic data across the continental shelf (CM05#29) and low-fold data across the slope and trough (SO191#1). Profile locations are shown in Fig. 2. Note that structures illustrated are reproductions of interpretations originally made in detail on large sections with low (2.5×) vertical exaggeration. This transect is representative of the more classical accretionary structure and processes dominating the margin south of Rock Garden. M is the first seafloor multiple. Numbered reflections in the trench sequence are from Barnes and Mercier de Lépinay (1997) and this study (see Fig. 6B). The dotted lines in the lower centre of the low-fold profile are hypothetical extensions of the faults beneath the multiple.

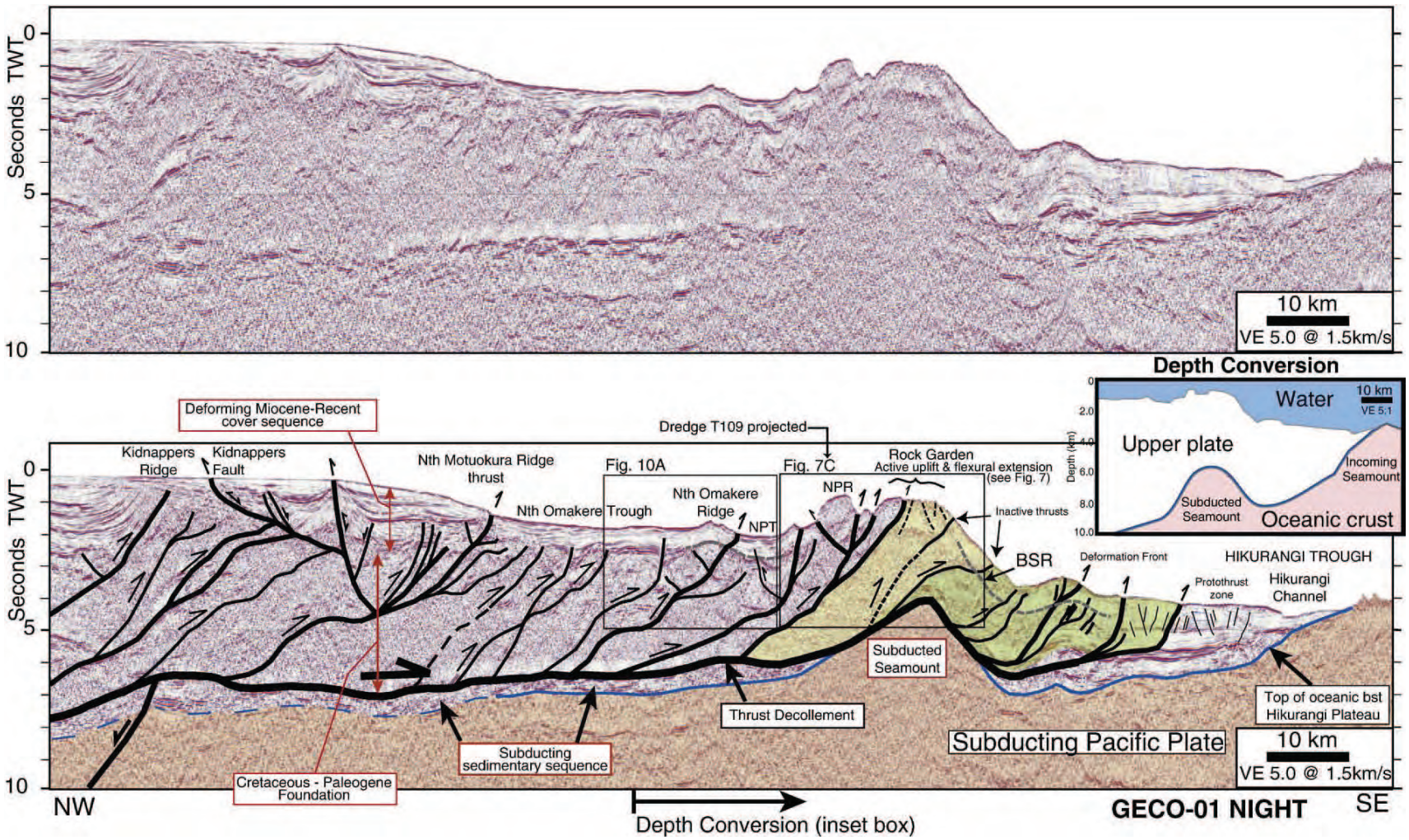

Fig. 4. Uninterpreted and interpreted high-fold NIGHT multichannel seismic section acquired by GNS Science on *MV GECO RESOLUTION* across the Hawke Bay margin, Rock Garden, and a subducting seamount. This section is representative of the structure and processes dominating the northern Hikurangi Margin between Rock Garden and East Cape. Upper margin structures are correlated to and mapped with an extensive set of high-quality industry and research seismic sections (Barnes et al., 2002; Barnes and Nicol, 2004). Bold faults are considered to be active. NPT, northern Paoanui Trough; NPR, northern Paoanui Ridge. The green shading is the extent of the accreted trench-fill section (yellow shading indicates region of compositional uncertainty at the rear of the wedge). The inset shows the plate interface in the frontal half of the section depth converted using velocities derived from wide-angle reflection data. (For interpretation of the references to colour in this figure legend, the reader is referred to the web version of this article.)

whereas active frontal thrust faulting has since re-established in the Hikurangi Trough sequence to the east. A similar tectonic history is recorded on profile CM05#1 across Ritchie Ridge 30 km to the north (Fig. 1B and D) (e.g., see Fig. 8 of Nicol et al., 2007).

As a result of seamount subduction beneath the Rock Garden, numerous cross-cutting faults are developed on the seafloor over the crest of the bank (Fig. 7A and B) (Pecher et al., 2005; Faure et al., 2006). These structures produce bathymetric scarps typically a few tens of meters in height on the eroded crest of the bank, and they exhibit a landward diverging radial pattern. They appear to be superimposed over a major NE–SW striking thrust scarp, which may or may not be currently active. The observed fault array is analogous to those produced in laboratory sandbox experiments of deformation above subducting asperities (e.g., Dominguez et al., 1998; Lewis et al., 2004) and observed elsewhere in other natural examples (e.g., Huhnerbach et al., 2005). Major collapse of the margin in the wake of the seamount, at the scale evidenced further north at Poverty Seavalleys and at Ruatoria Avalanche (e.g., Lewis et al., 1998; Collot et al., 2001), has not occurred yet indicating that it is a later deformation stage that will occur when the seamount passes further landward (e.g., Von Huene and Lallemand, 1990) or perhaps that some seamounts previously subducted further north had different geometry and/or substantially greater relief.

Compared to the northern margin, the tectonic accretion that dominates the central margin off southern Hawkes Bay and Wairarapa has been facilitated by thicker trench-fill sediment (~3–4 km), relatively smooth and sediment-covered subducting plate, and slower (by ~20 mm/yr) rate of convergence (Fig. 1) (Davey et al., 1986a; Lewis and Pettinga, 1993; Barnes and Mercier de Lépinay, 1997; Lewis et al., 1999; Wallace et al., 2004). East of Cape Turnagain, where the deformation front lies up to 130 km offshore, the frontal accretionary wedge reaches 65–70 km in width (Figs. 2 and 3). The transition between the inner foundation of imbricated passive margin rocks and accreted trench-fill turbidites (e.g., Fig. 5) is interpreted to lie seaward of Uruti, Porangahau and Paoanui ridges (Fig. 2A). Although a series of apparent right steps in this transition potentially mirrors the shape of the deformation front, the overall structure and morphology of the wedge indicates that its growth has not been significantly perturbed by relief on the subducting plate for at least 1–2 Myr. The exception to this is where the northern end of Bennett Knoll seamount ridge, which is about 80 km in length and has relief of several kilometers, is presently subducting beneath the deformation front east of Akito Ridge (Figs. 2 and 6A).

The repetitive ridge and basin morphology across the central margin reflects up to 10 major seaward-vergent thrust faults between the shelf and Hikurangi Trough. The longer thrust systems reach up to 120 km in length (Figs. 1 and 2). On the whole, the crests of successive ridges become progressively deeper seaward. Individual ridges typically have up to about 1 km of bathymetric relief, and an asymmetric profile, with a relatively gentle landward (back) limb and steeper seaward (fore) limb. Thrust faults generally steepen upward in the sedimentary section from dips of <20° in the lower part of the wedge to as much as 40–50° in the upper 1 km or so near the deformation front. Barnes and Mercier de Lépinay (1997) identified the fault growth sequence on the back limbs of the thrust ridges within the frontal 30 km of the wedge (e.g., Fig. 6) and estimated the horizontal shortening of the turbidite sequence there to be of the order of 6 km. They interpreted that 80% of this shortening occurred within 0.4 ± 0.1 Myr, at an average rate of 12 ± 3 mm/yr. They also inferred that the deformation front had advanced seaward by as much as 50 km since about 0.5 Ma, an observation consistent with the recent results of Nicol et al. (2007).

3.3. The Hikurangi Trough and the subducting Hikurangi Plateau sequence

The Hikurangi Trough sedimentary sequence and the top of the subducting Hikurangi Plateau is imaged well in our new seismic sections (Figs. 3 and 6B). We correlated the seismic stratigraphy in the trough, imaged on the *RV SONNE* profiles at about 41°S (Fig. 6B), with

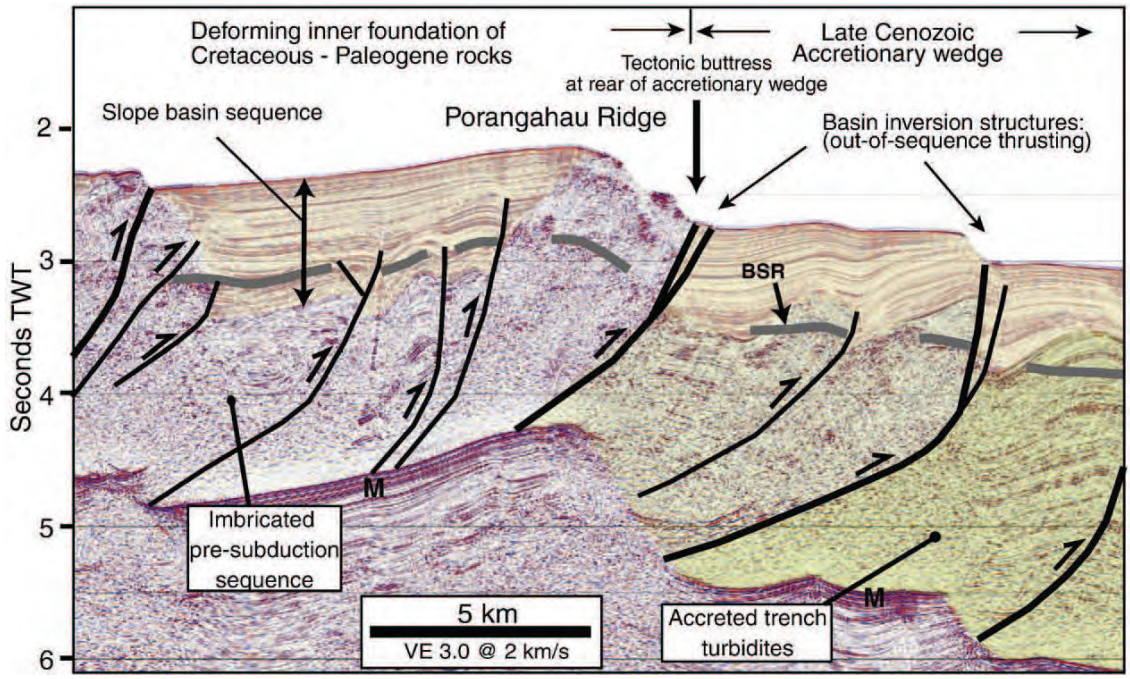

Fig. 5. Part of multichannel seismic section SO191#3 illustrating the contact between the outer edge of the imbricated Cretaceous–Paleogene foundation rocks and the landward part of the late Cenozoic accretionary wedge (bold dashed white line in Figs. 1 and 2A). All seep sites documented in this study lie above or relatively near this contact. The contact is imaged as a boundary marking a significant change in seismic reflectivity, somewhat transitional where indicated by the intermediate shading. The reflectivity changes from relatively coherent accreted trench-fill turbidite reflections to an acoustically chaotic foundation of complexly deformed pre-subduction stratigraphy landward. These units are variably covered by deforming slope basins, and there is a discontinuous BSR. Profile location is shown in Fig. 2.

Please cite this article as: Barnes, P.M., et al., Tectonic and geological framework for gas hydrates and cold seeps on the Hikurangi subduction margin, New Zealand, Mar. Geol. (2009), doi:10.1016/j.margeo.2009.03.012

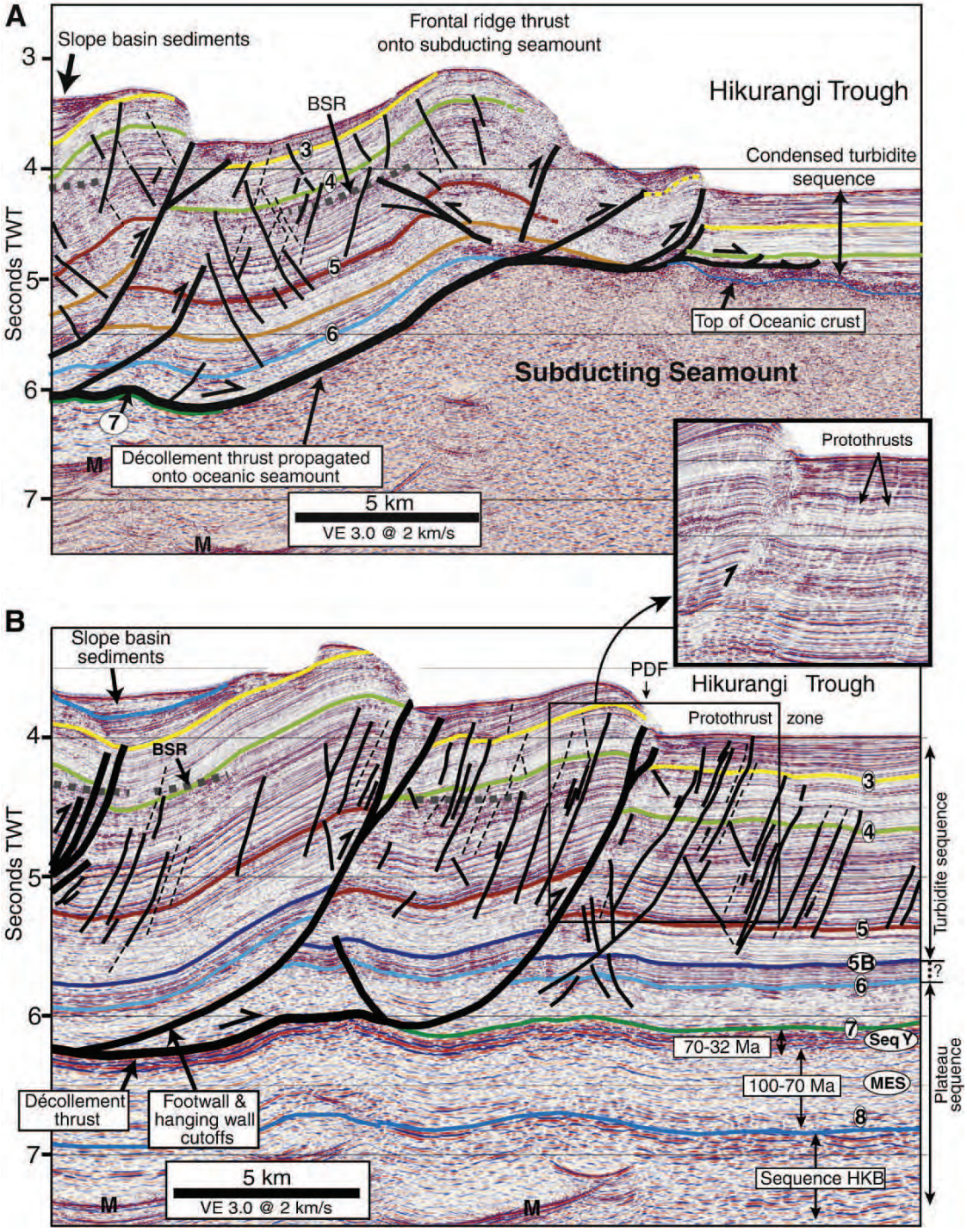

Fig. 6. Multichannel seismic sections illustrating examples of active tectonic structures across the central Hikurangi Margin deformation front. A. Part of SO191#3 showing incipient subduction of the Bennett Knoll seamount complex, causing increased uplift of the frontal ridge. B. Part of SO191#6 across classic frontal accretionary thrusts. The inset illustrates protothrusts. PDF, principal deformation front. Trench-fill stratigraphy in both sections, included numbered reflections, is from Barnes and Mercier de Lépinay (1997) and this study. Profile locations are shown in Fig. 2.

archived *RV L'ATALANTE* profiles (Barnes and Mercier de Lépinay, 1997) and with Mobil oil company profile 72–26 (Fig. 1D). The later profile extends southeast of the axial turbidite system and onto the Hikurangi Plateau north of the Chatham Rise, where a widespread seismic stratigraphy has been established by Davy et al. (2008). Davy et al. (2008) considered seismic velocities, tied reflections to ODP 1124 (Fig. 1A) and to rock dredge samples, and compared sections with dated sequences on the Manihiki Plateau, which is thought to have rifted from the Hikurangi Plateau in the Cretaceous. Although line 72–26 cannot be tied directly to profiles located further east presented by

Please cite this article as: Barnes, P.M., et al., Tectonic and geological framework for gas hydrates and cold seeps on the Hikurangi subduction margin, New Zealand, Mar. Geol. (2009), doi:10.1016/j.margeo.2009.03.012

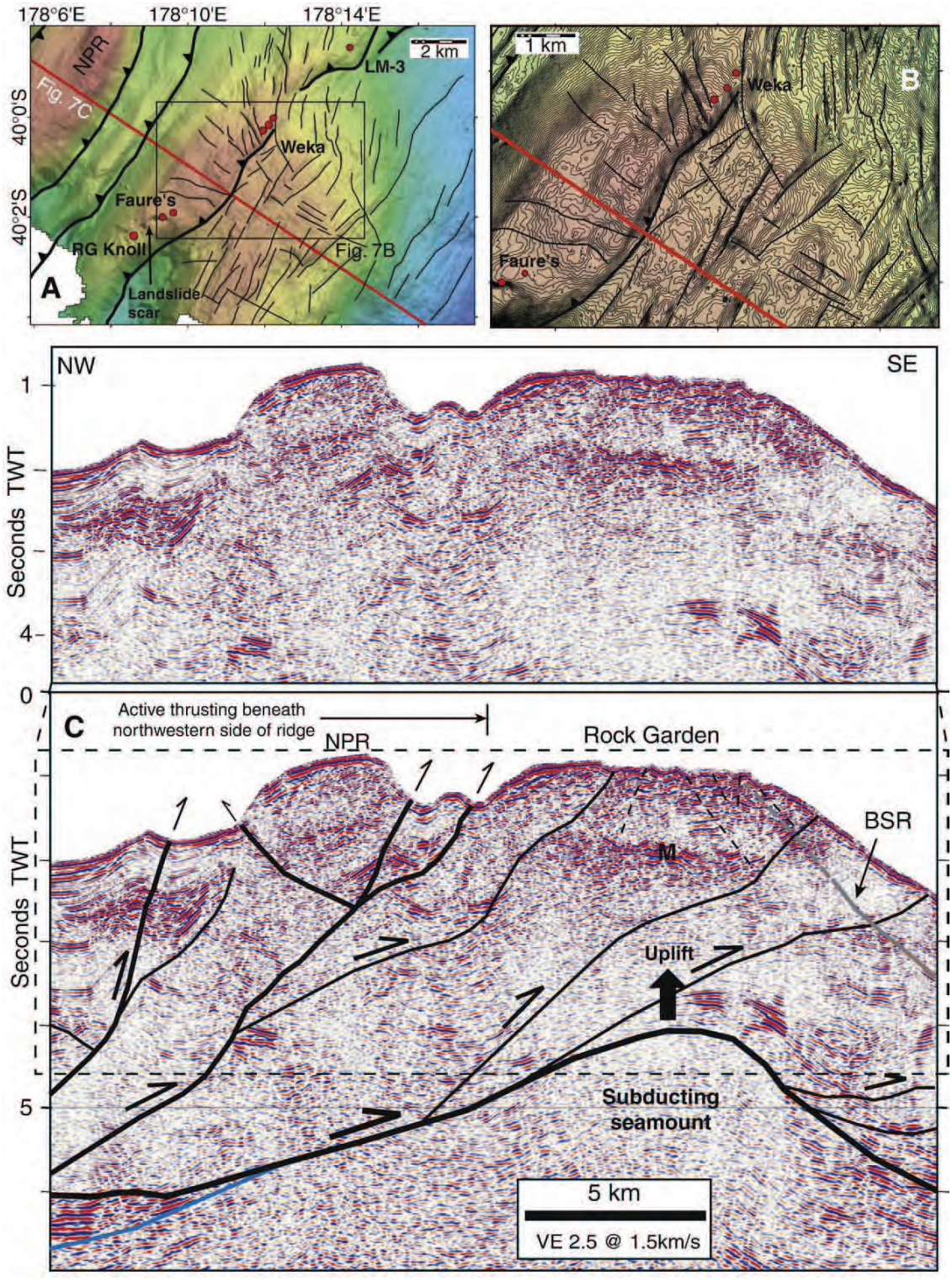

Fig. 7. A. Bathymetric and structural map of Rock Garden developed from 25 m binned, *RV TANGAROA* SIMRAD EM300 multibeam data. Location of A is shown in Fig. 10. B. Detail of bathymetric contours at 5 m interval. Location of B is shown in A. NPR, northern Paoanui Ridge. Red dots are seep sites. C. Uninterpreted and interpreted part of high-fold NIGHT multichannel seismic section, revealing active thrusts beneath the western side of the ridge and a subducting seamount driving uplift and extension of the Rock Garden. M is the first seafloor multiple. (For interpretation of the references to colour in this figure legend, the reader is referred to the web version of this article.)

Please cite this article as: Barnes, P.M., et al., Tectonic and geological framework for gas hydrates and cold seeps on the Hikurangi subduction margin, New Zealand, Mar. Geol. (2009), doi:10.1016/j.margeo.2009.03.012

Davy et al. (2008) (e.g., profile HKDC1), we recognize the same seismic stratigraphy of the plateau sequence in line 72–26, based on very similar reflection characteristics and two way travel time (TWT) depths. Our correlations between the Hikurangi Trough and the Hikurangi Plateau sequences identified by Davy et al. (2008) provide the first insights into the nature of the sedimentary sequence within which the interplate thrust is developed (see Section 3.4).

Our correlations indicate that in the central Hikurangi Trough reflection 8 (Fig. 6B) is approximately equivalent to the top of unit HKB of Davy et al. (2008). This unit has been interpreted as Early Cretaceous (>100 Ma) volcaniclastic sediments and/or limestone/chert with relatively low seismic velocities (~2.4–3.5 km/s) compared to the underlying basaltic basement rocks (>4 km/s) (not imaged in Fig. 6B). Reflection 8 is overlain by a c. 0.5 s TWT thick sequence (~575–650 m, assuming 2.3–2.6 km/s interval velocities) of weaker reflectivity. This sequence correlates with unit MES of Davy et al. (2008), inferred to represent Cretaceous (100–70 Ma) clastic sedimentary rocks. These rocks are overlain by a uniformly thick (0.15 s TWT, c. 170–250 m) sequence of widely traceable, high-amplitude reflections beneath reflector 7. This interval is the Hikurangi Plateau sequence Y of Wood and Davy (1994), identified by Davy et al. (2008) as Late Cretaceous–Early Oligocene (70–32 Ma) nannofossil chalks with alternating mudstones. Above this interval, the upper part of the Hikurangi Plateau sequence, which reaches 1.4 s TWT thickness east of the Hikurangi Trough, includes the 0.3 s TWT thick, weakly reflective interval between reflectors 6 and 7 (Fig. 6B). This interval is inferred to correlate with nannofossil chalks interbedded with tephras and clays at ODP 1124 (Fig. 1A). The upper plateau sequence may also include the interval of high-amplitude reflections between reflectors 5B and 6. Reflector 5B is locally a strong erosion surface, above which are easterly onlapping, coherent reflections from trench turbidites (Figs. 3 and 6) associated with local paleo-channels and channel levee sediment waves (see also Lewis et al., 1998). Although not directly dated, reflectors 3, 4 and 5 (Fig. 6) were inferred by Barnes and Mercier de Lépinay (1997) to be of the order of 0.8 Ma, 2.0 Ma, and 5.0 Ma, respectively.

3.4. Décollement position and protothrust zone

The refined seismic stratigraphy of the Hikurangi Trough sequence and clear imaging of the frontal deformation structures in the *RV SONNE* SO191 profiles enables improved identification of the interplate thrust where it is propagating into the trench sediments (Fig. 6B). The interplate thrust is recognized as the major décollement, above which the accreted sequence is shortening by distributed thrust faulting and folding, and below which undeformed sediments are being subducted. Near the front of the wedge, the stratigraphic position of the décollement is tightly constrained to within a couple of wavelets of the seismic data, by recognition of the down-dip extent of the accretionary thrusts from observations of inclined hanging wall reflections, and foot wall reflection cutoffs (e.g., Fig. 6B).

In the centre of the margin west of Bennett Knoll the décollement coincides with reflector 7 for at least 30 km down dip (Fig. 6B). This position, within the pelagic sediments (nannofossil chalks, tephras, mudstone, clays) of the Hikurangi Plateau sequence, is some 400–450 m stratigraphically below what are clearly turbidites. Immediately below the décollement are unfaulted high-amplitude reflections correlated with Late Cretaceous–Early Oligocene (70–32 Ma) nannofossil chalks and alternating mudstones. Immediately above it is the thrusted sequence inferred to be Cenozoic (probably Miocene) alternating chalk, tephras and clays. In comparison, on profile SO191#1 (Fig. 3), about 100 km to the northeast, the frontal 15 km of the décollement is developed at a stratigraphic position about 0.3–0.4 s TWT (~300–400 m) higher in the plateau sequence. There, it lies just below reflection 5B before stepping down to reflector 7 beneath the third major thrust landward of the deformation front and continuing at that stratigraphic position landwards for at least 15 km down dip. Off the southern Wairarapa coast about 150 km to the southwest of Bennett Knoll, the décollement imaged in archived seismic data is less well constrained, but appears to be developing at the deformation front at a stratigraphic position close to reflector 6 (Barnes and Mercier de Lépinay, 1997). Thus, we recognize in the *RV SONNE* seismic sections that the décollement coincides primarily with reflection 7 in the Hikurangi Plateau pelagic sequence, but that over lateral distances of 100–150 km, its stratigraphic position varies by up to 300–400 m within up to 15 km of the deformation front.

The new seismic profiles combined with archived data also provide new insights into the distribution of a conspicuous protothrust zone in the Hikurangi Trough (Figs. 3 and 6B). Protothrusts were previously recognized mainly west of Bennett Knoll seamount, where they have been interpreted as fluid conduits in an incipient zone of compression between the incoming seamount and the deformation front (e.g., Davey et al., 1986a,b; Lewis and Pettinga, 1993; Barnes and Mercier de Lépinay, 1997; Lewis et al., 1998). It is now clear that the protothrust zone is developed in the turbidite sequence of the Pacific Plate for over 200 km along the central margin (Fig. 2A), and formed not in response to local seamount collision, but primarily to deformation and dewatering associated with forward propagation of the décollement into the trench sequence. The zone is developed up to 20 km seaward of the frontal ridge, in the stratigraphic sequence above the reflector at which the primary thrust décollement is developed further landward (Figs. 3 and 6B). Protothrusts are also clearly imaged in the hanging wall sequence of the frontal two or three major structures in the accretionary wedge, and appear to have been transferred to the wedge (i.e., captured by the Australian Plate) as the décollement and principal deformation front have propagated seawards. The protothrusts are characterized by weak reflectivity (Fig. 6B inset), and dips of the order of $40 \pm 5°$, which is similar to the dip typical of the shallow part of the frontal thrust. The protothrusts imaged in the seismic data have fault spacing typically of several hundred meters to 1 km, with displacements typically of up to a few tens of meters. Although conjugate faults are present (Fig. 6B inset), the dominant vergence is seaward (i.e., northwest dipping faults) west and south of Bennett Knoll, and landward (south east dipping) north of Bennett Knoll (Fig. 3). Similar structures in the Nankai Trough (e.g., Moore et al., 1990) have been interpreted as evolving arrays of brittle–ductile shears that undergo rotation as a result of larger scale ductile flow (Karig and Lundberg, 1990).

4. Tectonic and stratigraphic framework of known seep sites

Elsewhere in this issue, other papers present detailed studies of gas hydrates, geophysically imaged gas plumbing systems, heat flow, fluid seepage, seabed substrate and biological fauna at sites referred to as Wairarapa, Uruti Ridge, Porangahau Ridge, Omakere Ridge, Rock Garden, and Builders Pencil (Fig. 1) (Greinert et al., 2009-this issue; and other papers herein). In the following sections of this paper we outline the distribution of these sites with respect to the major fault structures, tectonic morphology, and stratigraphy.

4.1. Wairarapa sites

The Wairarapa sites lie in the narrowest part of the Hikurangi Margin, some 15–25 km south east of Cape Palliser (Fig. 8). Three major subparallel fault systems dominate the tectonic structure of this part of the margin. From north to south, these include the strike-slip Boo Boo Fault, which extends from the north eastern shelf of South Island into the upper slope area 4–10 km north of the seep sites, and the Opouawe–Uruti and Pahaua thrust faults which underlie the mid-slope bathymetric banks on which the seeps are developed (Barnes and Mercier de Lépinay, 1997; Barnes et al., 1998a; Mountjoy et al., 2009). The region is incised by submarine canyons including Opouawe

Please cite this article as: Barnes, P.M., et al., Tectonic and geological framework for gas hydrates and cold seeps on the Hikurangi subduction margin, New Zealand, Mar. Geol. (2009), doi:10.1016/j.margeo.2009.03.012

and Palliser canyons, and is heavily scarred by active submarine landslide systems.

Five seep sites, namely Takahe, North Tower, South Tower, Pukeko and Ruru, lie on Opouawe Bank, typically in about 1000–1100 m water depth. Seismic data show that these sites have developed on the hanging wall of the Pahaua Fault (Fig. 8B), which is characterized by several imbricates that break out as segmented traces on the steep southern forelimb of the bank. These imbricate traces are clearly expressed in the high-resolution EM300 multibeam data, as obvious inflections in the slope gradient, cutting across ridge and gully systems. The other three sites, including Tuatara and Tui on the upper Opouawe Bank, and Miromiro on the western edge of Palliser Bank, lie on the hanging wall sequence of the Opouawe–Uruti Fault in about 850–900 m water depth. This fault similarly breaks out on the seabed as several discontinuous traces on the gullied forelimb of Palliser and Pahaua banks, but its tip is covered by landslide debris in Opouawe Canyon (Fig. 8B), and is blind at about 0.5 s TWT depth beneath the upper Opouawe Bank on seismic profile P036 (see Fig. 4 of Netzeband et al., 2009-this issue).

Regional seismic reflection profiles show that the sedimentary sequence seaward of the Pahaua Fault is trench turbidites (Barnes and Mercier de Lépinay, 1997; Barnes et al., 1998a; Lewis et al., 1998). Although the available seismic data illustrated in Fig. 8B are not of the same quality as in Figs. 3–7, we infer that the Cretaceous and

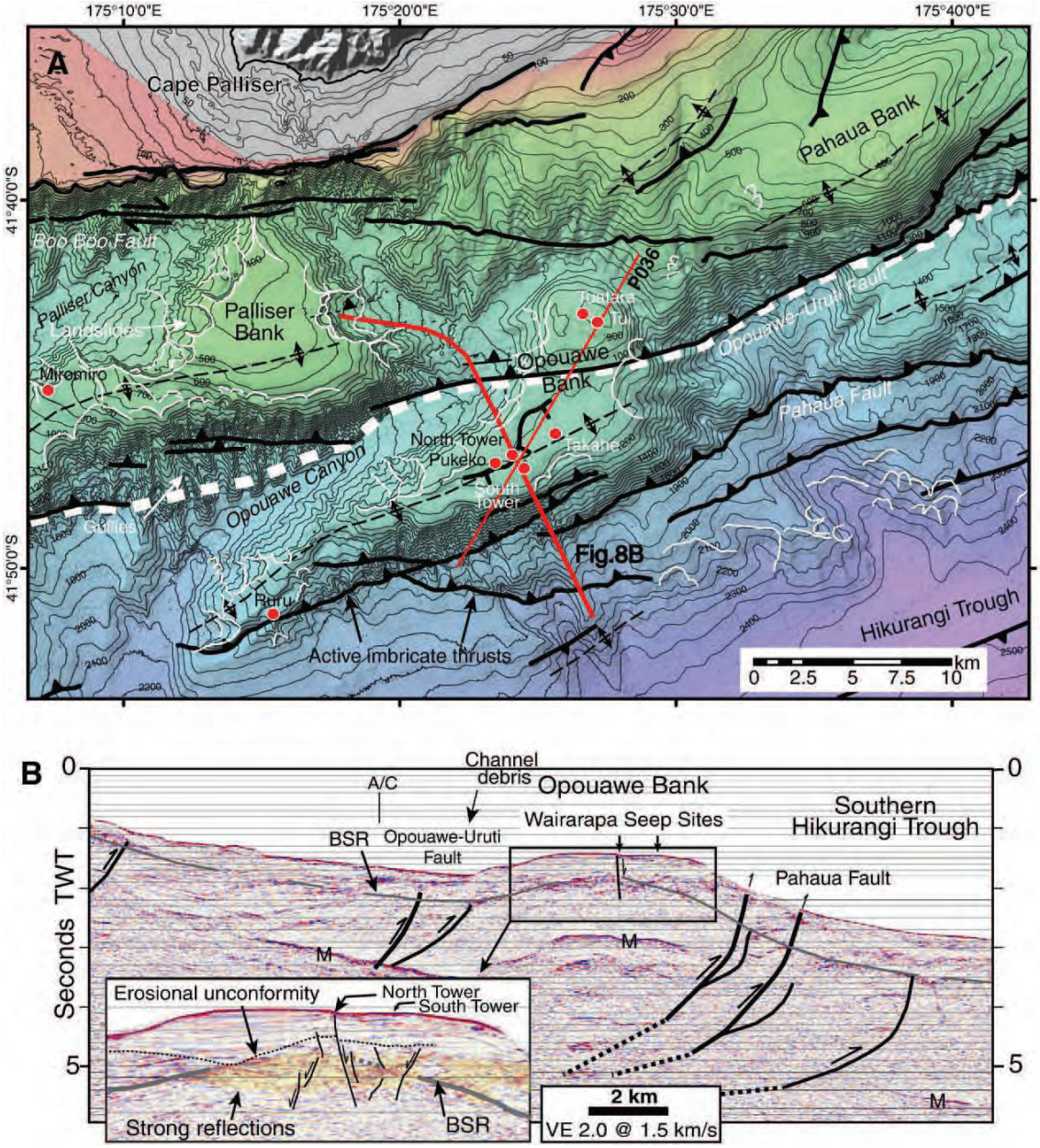

Fig. 8. A. Major tectonic and geomorphic features associated with the Wairarapa seep sites. Bathymetry is 25 m binned, *RV TANGAROA* SIMRAD EM300 multibeam data, with 50 m contour interval. Red dots with white labels are seep sites. The fine white lines indicate major landslide scars. The bold white dashed line is inferred to be the rear of the late Cenozoic accretionary wedge. Pahaua Bank is an informal name used by Mountjoy et al. (2009). Map location is shown in Fig. 1. B. Multichannel seismic section SO191#9/10 revealing structures beneath Opouawe Bank. Yellow shading on seismic zoom indicates packages of high-amplitude reflections beneath seeps.

Please cite this article as: Barnes, P.M., et al., Tectonic and geological framework for gas hydrates and cold seeps on the Hikurangi subduction margin, New Zealand, Mar. Geol. (2009), doi:10.1016/j.margeo.2009.03.012

Paleogene inner foundation rocks underlie Palliser and Pahaua banks, and the upper part of Opouawe Bank, based on correlation of major thrust faults along the margin (Fig. 8A). This foundation was previously considered to extend further seaward beneath the lower part of Opouawe Bank (Barnes and Mercier de Lépinay, 1997). Beneath Opouawe Bank, the upper 0.5 s TWT (c. 440 m) sequence appears to be part of the slope sediment cover, in which there is at least one erosional unconformity (Fig. 8B). Below a packet of strong reflections, the stratigraphy is not clear, but is inferred to include accreted trench turbidites. Therefore the interpreted boundary is tentatively moved to the Opouawe–Uruti Fault.

The seismic data show that a strong and continuous BSR underlies the flanks of Opouawe Bank (Fig. 8B). The BSR shallows from about 0.7 s TWT below the seafloor south of the bank to about 0.35 s TWT (c. 300 m) beneath the crest, and appears to become disrupted in a stratigraphic interval characterized by strong discontinuous reflectors, shallow normal faults, and gas chimneys (Netzeband et al., 2009-this issue). The largest normal fault displaces the seabed at North Tower seep site. Netzeband et al. (2009-this issue) interpreted the strong reflections as evidence of free gas, and the steep faults to penetrate the base of the gas hydrate stability zone. The seep sites are characterized by anomalous resistivities indicative of large amounts of gas or gas hydrate beneath them (Schwalenberg et al., 2009-this issue), hydroacoustic flares (Greinert et al., 2009-this issue), and carbonate mounds and seep faunas (Klaucke et al., 2009-this issue; Naudts et al., 2009-this issue).

4.2. Uruti Ridge sites

Uruti Ridge lies on the middle slope off the Wairarapa coast, where the offshore part of the imbricate wedge is about 90 km wide (Figs. 1 and 2A). The ridge is an anticlinal structural high with bathymetric relief of about 1000 m. A seismic profile presented by Barnes et al. (1998a, their Fig. 5C) reveals the ridge is underlain by the northern part of the Opouawe–Uruti thrust, which breaks out at the toe of the steep, landslide scarred forelimb flank (Fig. 9A). The ridge is dissected by an E–W striking, strike-slip fault, considered by Barnes et al. (1998a) as the northern part of the Palliser–Kaiwhata Fault (Figs. 2 and 9). The latter structure is steeply dipping, and is associated with a small pull-apart basin developed at a releasing bend in the centre of the ridge. There are a number of extensional splay faults on the steep forelimb of the ridge, where the fault intersects the Opouawe–Uruti thrust (Fig. 9B and C). Based on EM300 multibeam bathymetry data, the crest of the ridge, and both its flanks, appear to be dextrally displaced by perhaps 1.0–1.5 km. It is not clear from the data whether the northern end of the Palliser–Kaiwhata Fault penetrates deep into the imbricate wedge, or is confined to the hanging wall of the Opouawe–Uruti thrust.

Dated samples T119 and V479 dredged from the steep forelimb of the ridge (Fig. 9A and B) indicate that the sequence in the hanging wall of the Opouawe–Uruti thrust includes indurated mudstone of Early to middle Pliocene age (see Electronic Data Supplement and Fig. 5 profile C of Barnes et al., 1998a). Above these strata, younger sediments of the Uruti Basin sequence thin towards the ridge crest, having been deposited contemporaneously with uplift of the ridge. Below them, the foundation of the ridge is thought to consist of pre-subduction, passive margin Cretaceous and Paleogene rocks (Lewis et al., 1999).

Three seep sites, including LM-10, Hihi, and Kereru are located at small mounds on the anticlinal crest of the ridge in about 800 m water depth (Fig. 9A). These sites lie about 700–1100 m south of the Palliser–Kaiwhata fault. Projecting sample T119 onto profile P041 (Fig. 9B) indicates that strata on the ridge crest in the vicinity of the seep sites are likely to be of Pliocene age. A BSR is imaged beneath the ridge, rising slightly to ~0.28 s TWT depth beneath the seep sites. The seep sites themselves are characterized by strong backscatter in sidescan sonar images, prolonged echos in 2–10 kHz Chirp profiles, and acoustic flares in the water column (Greinert et al., 2009-this issue).

4.3. Omakere Ridge sites

Omakere Ridge is one of the many slope parallel thrust-faulted anticlinal ridges that characterize the wider part of the Hikurangi Margin off southern Hawkes Bay (Figs. 1 and 2A). The ridge lies in about 1100 m water depth, and has about 500 m of bathymetric relief (Fig. 10B). Its morphology is heavily scarred by landslides, which are particularly common on the steep forelimb flank. The variable subsurface structure of the ridge is illustrated in three seismic reflection profiles from the southern (Fig. 3), central (Fig. 10C) and northern (Figs. 4 and 10A) areas of the ridge. The main active trace of the Omakere Ridge thrust breaks out at the seabed at the toe of the steep seaward flank. The profiles reveal that inactive imbricate thrusts lie below this structure, their tips now buried by sediments in Paoanui Trough. A second active imbricate thrust branches upwards through the hanging wall sequence of the main fault. This structure breaks out at the seabed along the crest of the ridge, where a scarp about 100 m high is associated with a series of discontinuous basins. Based on the change in seismic characteristics of the thrust wedge across Paoanui and Porangahau ridges further seawards (Figs. 2A, 3 and 5), and a Late Cretaceous rock sample dredged from the western flank of Ritchie Ridge (Figs. 1 and 2B) (see also sample T109 projected onto Fig. 4) (Lewis and Marshall, 1996), the thrust wedge beneath Omakere Ridge is interpreted to comprise imbricated Cretaceous and Paleogene rocks lying landward of the accreted trench-fill turbidites (Fig. 3). These rocks are covered by about 0.8 s TWT (700–800 m) of slope sediments that have been folded in the hanging wall of the lower thrust faults.

Several seep sites are recognized on the crest of the ridge, typically in about 1100–1500 m water depth (Jones et al., 2009-this issue; Greinert et al., 2009-this issue). These include LM-9 and Bear's Paw (we are not sure if Moa is a seep site, it might be an inactive one) on the hanging wall of the main Omakere Ridge thrust, as well as Kaka, Kea and Kakapo lying above the upper imbricate thrust (Fig. 10B). They are characterized by methane rich fluid seepage, acoustic flares, authigenic carbonate forming meter high chemoherm structures, and seep fauna (Jones et al., 2009-this issue). At LM-9 a BSR is visible under the seaward flank of the ridge (Fig. 10C), but not directly beneath the crest. In the latter area reflections are disturbed by a shallow extensional fault array and by apparent gas masking. North of the seep sites, the BSR is particularly strong beneath the ridge crest on GECO RESOLUTION NIGHT profile (Fig. 10A).

4.4. Rock Garden sites

The surface of Rock Garden lies in about 600–800 m water depth. The anomalous bathymetric elevation and complex tectonic history of this area and Ritchie Ridge further to the north (Figs. 10B and 11), relative to structural ridges in a comparable position in the outer margin south of Rock Garden, reflects the enhanced uplift and deformation of these features above positive relief on the subducted Pacific Plate (Fig. 4) (refer to Section 3.2 above). Based on the seismic reflection characteristics beneath the ridge (Fig. 7), and rock samples of Late Cretaceous age from the southwestern part of Ritchie Ridge some 30 km to the north (Lewis and Marshall, 1996, sample T109), it is likely that at least the western crest and flank of Rock Garden is cored by the Cretaceous and Paleogene rocks (Fig. 4). The outer flank of Rock Garden is interpreted here to be cored by accreted turbidites, however the surface and subsurface stratigraphy over the outer crest remains uncertain. The flanks of Rock Garden, particularly in the south, are characterized by numerous landslide scars (Fig. 10B) (Faure et al., 2006).

The plateau-like crest of Rock Garden is eroded, and strongly reflective (Fig. 7) (Lewis and Marshall, 1996). Beneath the surface is a discontinuous BSR and packages of high-amplitude reflections that have been interpreted by Pecher (2002), Pecher et al. (2004) and Crutchley et al. (2009-this issue) as gas migration pathways. The BSR is generally strong beneath the seaward flank, and locally pinches out at the edges of the plateau. Pecher et al. (2005) suggested that the erosion of the ridge crest is linked

Please cite this article as: Barnes, P.M., et al., Tectonic and geological framework for gas hydrates and cold seeps on the Hikurangi subduction margin, New Zealand, Mar. Geol. (2009), doi:10.1016/j.margeo.2009.03.012

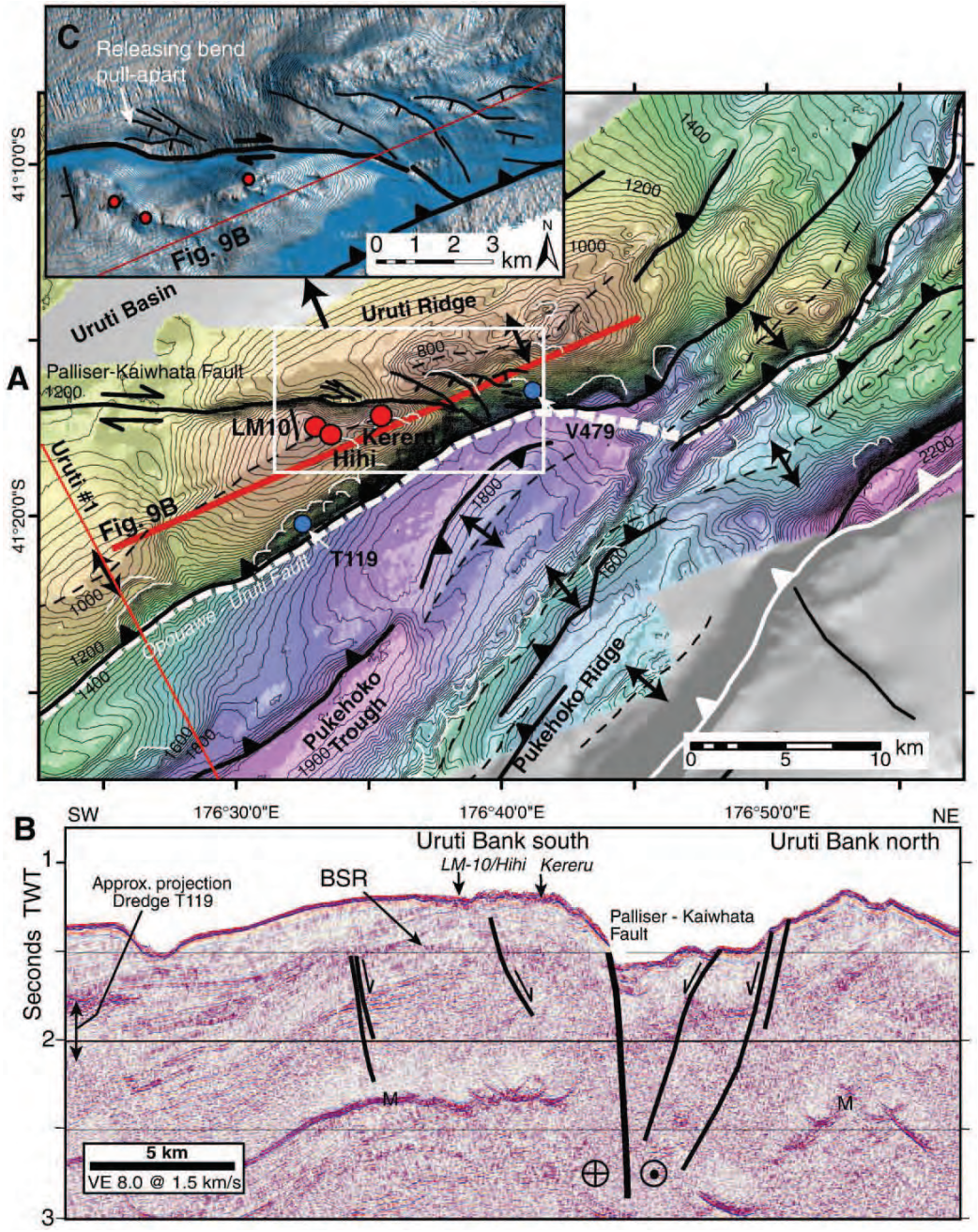

Fig. 9. Major tectonic and bathymetric features associated with the Uruti Ridge seep sites. A. Regional map with stretched colour DTM on 150 m grid multibeam bathymetry data acquired on *RV TANGAROA* and *SONNE*, and 20 m contour interval. Grey area is a background hillshade from archived SIMRAD EM12 Dual multibeam data acquired by *RV L'ATALANTE*. The profile labeled Uruti#1 is illustrated in Fig. 5C of Barnes et al. (1998a). The bold dashed white line is inferred to be the back of the late Cenozoic accretionary wedge. See Figs. 1 and 2 for location of map. Red dots are seep sites. B. High-resolution multichannel seismic section SO191#P041 illustrating structure of the eastern end of the Palliser–Kaiwhata Fault. M is the first seafloor multiple. Note the major seaward-vergent thrust fault beneath the ridge is not imaged in this profile. C. Zoom map of structure and bathymetry based on a 25 m grid hillshade with 5× vertical exaggeration from *RV TANGAROA* SIMRAD EM300 data.

primarily to temperature-controlled fluctuations in the stability of gas hydrate. Recent modelling by Ellis et al. (2009-this issue), indicates erosion of the ridge top likely relates to interactions between tectonic uplift caused by seamount subduction, and the stability of shallow gas hydrates.

Seep sites have been recognized in four areas on Rock Garden (Figs. 7A and 10B) (Lewis and Marshall, 1996; Faure et al., 2006; Greinert et al., 2009-this issue; Crutchley et al., 2009-this issue). These sites, including LM-3, Weka, Faure's Site, and Rock Garden Knoll, are associated with seep faunas, methane-derived carbonates and acoustic water column flares that have been proven to be caused by methane bubbles (Faure et al., 2009-this issue; Naudts et al., 2009-this issue). All sites lie on the hanging wall, and within 1.2 km of the surface trace of a major NE–SW striking, seaward-vergent thrust fault that has displaced the top of the bank. In addition, Faure's Sites are associated with the headwall scarp of a large, deep seated landslide on the southern flank of the bank (Fig. 7A and B) (Faure et al., 2006).

Please cite this article as: Barnes, P.M., et al., Tectonic and geological framework for gas hydrates and cold seeps on the Hikurangi subduction margin, New Zealand, Mar. Geol. (2009), doi:10.1016/j.margeo.2009.03.012

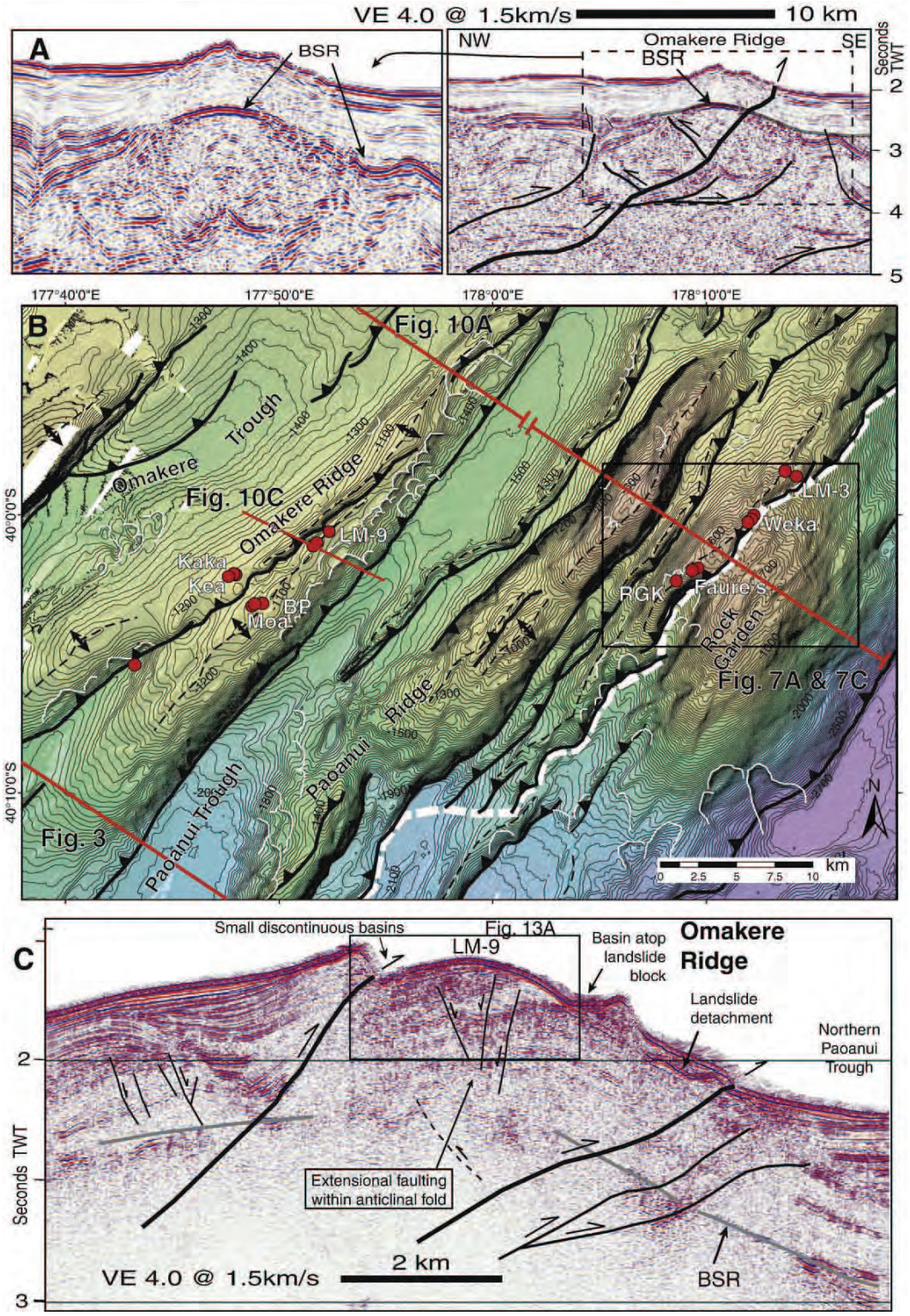

Fig. 10. Major tectonic and bathymetric features associated with the Omakere Ridge and Rock Garden seep sites. A. Uninterpreted zoom and interpreted high-fold NIGHT seismic data across Omakere Ridge. B. Structure map with 30 m grid multibeam bathymetry data acquired on *RV TANGAROA* and *SONNE*, and 20 m contour interval. Red dots are seep sites (Abbreviation RGK is Rock Garden Knoll). The bold dashed white line is inferred to be the back of the late Cenozoic accretionary wedge. See Figs. 1 and 2A for map location. C. High-resolution multichannel seismic section SO191#P054 indicating major structures beneath LM-9.

Please cite this article as: Barnes, P.M., et al., Tectonic and geological framework for gas hydrates and cold seeps on the Hikurangi subduction margin, New Zealand, Mar. Geol. (2009), doi:10.1016/j.margeo.2009.03.012

4.5. Builders Pencil (Ritchie Ridge) sites

The Builders Pencil and LM-1 seep sites lie on the landward flank of Ritchie Ridge, which is located in the middle slope region about 50 km southeast of Mahia Peninsula (Figs. 1 and 11) (Lewis and Marshall, 1996; Greinert et al., 2009-this issue). On the ridge crest are Ritchie, Calyptogena, and Pantin banks, rising to about 300 m, 850 m, and 1050 m, respectively. The ridge is underlain by an anticline above an active thrust fault. This fault is the first major active upper plate structure east of the Lachlan Fault, which lies beneath the inner shelf >30 km to the west (Fig. 11A) (Barnes et al., 2002). The fault ramps off the plate interface and splays upwards into 2–3 imbricates which break out at the seabed across the seaward flank of the ridge (Fig. 11B). Inactive backthrusts are observed off the upper imbricate.

The spliced seismic profiles in Fig. 11B illustrate that the Ritchie Ridge thrust transports previously imbricated Cretaceous and Paleogene foundation rocks, and their overlying slope basin sequence, over

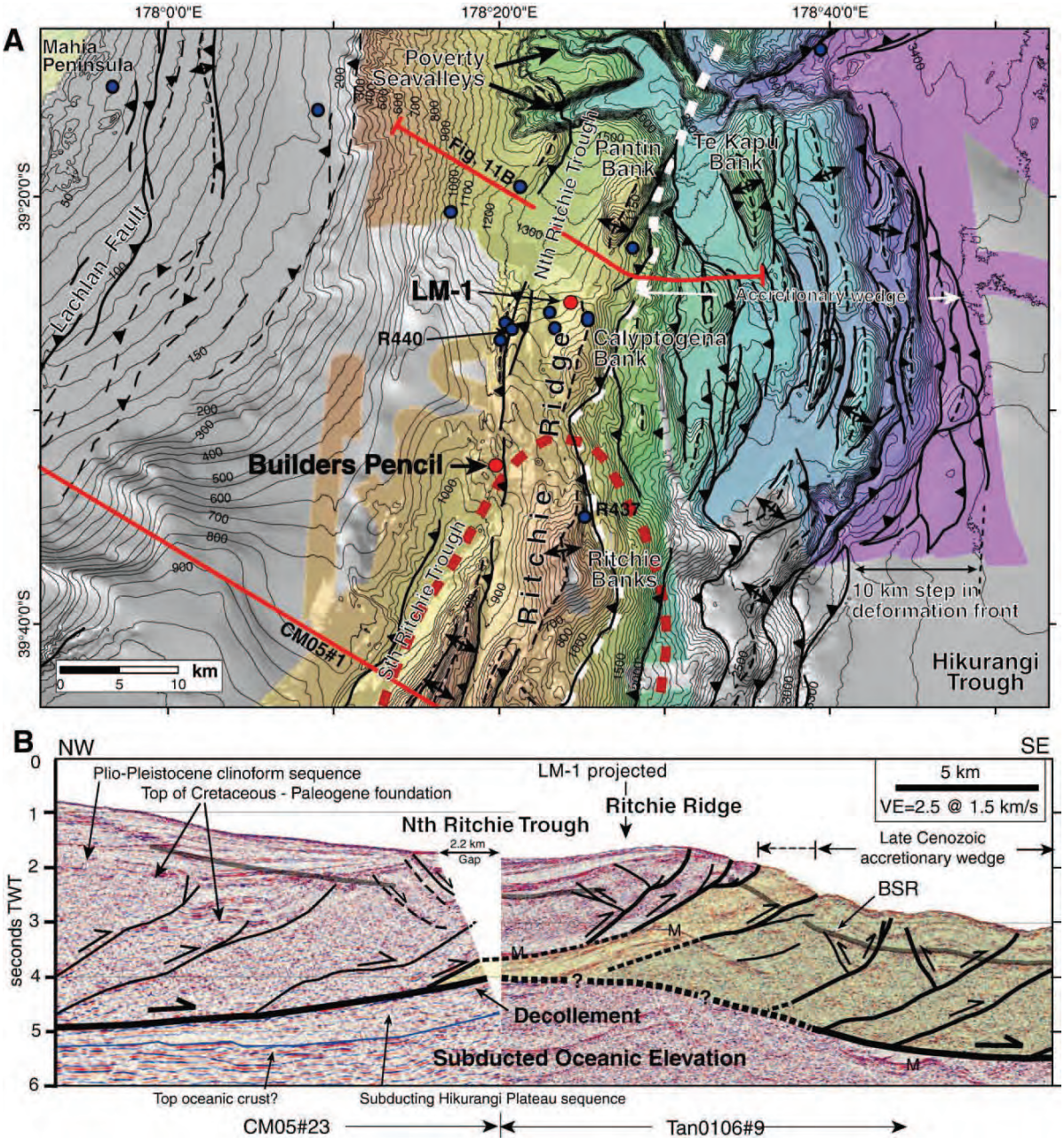

Fig. 11. Major tectonic and bathymetric features associated with the Builders Pencil and LM-1 seep sites off Mahia Peninsula. A. Regional map has stretched colour DTM on 25 m binned, *RV TANGAROA* SIMRAD EM300 multibeam data and 30 m grid *RV SONNE* EM120 multibeam. Contour interval is 50 m. Grey area is a background hillshade from archived SIMRAD EM12 Dual multibeam data acquired by *RV L'ATALANTE*, and coastal echosoundings. See Fig. 1 for map location. The bold dashed white line is inferred to be the back of the late Cenozoic accretionary wedge. The bold dashed red line is the inferred extent of high relief on the subducting Pacific Plate (see southern part of this feature beneath the Rock Garden in Fig. 2A, where it is highlighted in yellow). Red dots are seep sites. Blue dots are dredge sites from NIWA's database. B. Spliced multichannel seismic section including high-fold CM05#23 and low-fold Tan0106#9 data, revealing major structures beneath Ritchie Ridge. The green shading is the extent of the accreted trench-fill turbidites (yellow shading indicates region of compositional uncertainty at the rear of the frontal wedge).

Please cite this article as: Barnes, P.M., et al., Tectonic and geological framework for gas hydrates and cold seeps on the Hikurangi subduction margin, New Zealand, Mar. Geol. (2009), doi:10.1016/j.margeo.2009.03.012

accreted trench turbidites beneath the seaward flank of the ridge. The accreted trench sequence is highly imbricated and covered by thin slope basin sediments. The older foundation rocks landward have been dredged from the seafloor near the coast west of the Lachlan Fault (Barnes et al., 2002), and at Ritchie Banks, where hard massive siltstone of possible mid Eocene–E. Miocene age has been recovered at station R437 (Fig. 11) (A. Edwards, pers. comm, 1991). Middle Miocene strata overlying these rocks were recovered from a structural high on the western edge of Ritchie Ridge (station R440) about 5 km west of LM-1 (Lewis and Marshall, 1996). The upper part of the cover sequence west of Ritchie Ridge is part of a classical Plio-Pleistocene shelf–slope clinoform succession that is well developed off eastern Mahia Peninsula. This sequence thins onto the back of Ritchie Ridge and is being actively uplifted and folded.

The Builders Pencil and LM-1 sites lie in about 850–1200 m water depth, are characterized by widespread relict seep faunas, and appear to be presently inactive (Lewis and Marshall, 1996; Greinert et al., 2009-this issue). Greinert et al. (2009-this issue) demonstrate that the seafloor surrounding the sites is characterized by tilted, highly eroded and exposed bedrock sequences. Considering the seismic stratigraphy and structure outlined above, we infer this sequence on the backlimb of the ridge is Miocene and/or Pliocene age.

5. Discussion

5.1. Comparison of seep site settings

The five areas of seeps described above represent a variety of different local geological settings within the imbricate thrust wedge, but they also have some important similarities. All sites lie on the crests of seaward-vergent, thrust-faulted ridges, none lie in slope basins between thrust ridges. The locations therefore differ from some relict early Miocene seeps documented in uplifted forearc basins on land (Campbell et al., 2008). The Uruti Ridge sites are unusual in that they also lie in close proximity to the eastern end of a major strike-slip fault. Rock Garden sites differ from others to the south in that they occur directly above a substantial seamount that is currently being subducted. Greinert et al. (2009-this issue) demonstrate that the Wairarapa, Uruti Ridge, Omakere Ridge and Rock Garden seeps are currently active, whereas Builders Pencil appears to be relict of a very active earlier phase.

Another important similarity between all confirmed seep sites is that they lie approximately along the middle slope, commonly in about 700–1200 m water depth, near the outer edge of the deforming Cretaceous and Paleogene foundation rocks (Figs. 1 and 12A) (Lewis and Marshall, 1996). The Uruti Ridge, Rock Garden, and Builders Pencil sites all occur on ridges directly above the outer edge of the Cretaceous and Paleogene foundation (Figs. 2A, 4, 9–11). The southern Wairarapa sites, Omakere Ridge, and the southern Porangahau Ridge investigated by Pecher et al. (2009-this issue), lie within one ridge either side of this buttress (Figs. 1–3 and 8). These seep locations collectively indicate that the imbricated Cretaceous and Paleogene foundation rocks play an important role in focusing present fluid flow and seepage along the middle part of the margin (see discussion in Section 5.3).

The shallow seismic stratigraphy of the different seep areas appears to vary greatly, but has not been accurately dated at the specific seep sites. Consideration of regional seismic reflection characteristics and sparse seafloor samples leads us to infer that the Wairarapa and Omakere Ridge seeps are located on late Pleistocene slope sediments. At Uruti Ridge they are developed on probable Pliocene strata which are exposed at the crest and seaward flank of the ridge. The Builders Pencil substrate appears to be Miocene and/or Pliocene strata, which overlie older rocks exposed on the seaward flank of Ritchie Ridge. The Rock Garden seeps, located on the western side of Rock Garden, may lie on a substrate of exposed Cretaceous and Paleogene rocks, or on an eroded cover sequence of Miocene–Pliocene age.

5.2. New insights into the structure of the Hikurangi Margin

Whilst to a first order, the major tectonic and stratigraphic attributes of the central Hikurangi Margin were established previously (Davey et al., 1986a,b; Lewis and Pettinga, 1993; Collot et al., 1996; Barnes and Mercier de Lépinay, 1997; Lewis et al., 1997, 1999; Field et al., 1997; Barnes et al., 1998a,b; Henrys et al., 2006; Nicol et al., 2007), we make five significant contributions in this study. These are (1) improved mapping of the major structures within the margin based on wider seismic reflection coverage, including high-fold deep penetration datasets, and higher resolution multibeam bathymetry data (e.g., Fig. 2); (2) improved definition of the subducting seamounts at Rock Garden (Figs. 4, 7, and 10B) and Bennett Knoll (Fig. 6A), and better understanding of the tectonic responses of the margin to seamount subduction; (3) improved geophysical clarity and revised mapping of the contact between the imbricated Cretaceous–Paleogene inner foundation rocks and the late Cenozoic frontal wedge of accreted trench-fill turbidites (e.g., Figs. 2A and 5); (4) improved seismic stratigraphy of the subducting and accreting sedimentary sequences in the Hikurangi Trough, and clearer identification of the interplate décollement within the pelagic sequence (e.g., Fig. 6B); and (5) improved seismic imaging and wider mapping of the protothrust zone (Figs. 2A and 6B).

At up to 150 km in width, the imbricated frontal wedge of the central Hikurangi Margin is considered to be a wide subduction margin (c.f., von Huene and Scholl, 1991). Its tectonic structure, morphology, and inferred hydrogeological system, summarized in Fig. 12A, are characteristic of wide, low taper thrust wedges associated with relatively smooth subducting plate, thick trench-fill sedimentary sequence, and moderate convergence rate. The low taper (~4°) of the wedge, with average surface slope of about 1°, is low by comparison with many subduction systems (Davis et al., 1983; Lallemand et al., 1994). This taper is typical of poorly drained, low permeability thrust wedges (Saffer and Bekins, 2002) with substantial fluids channeled along a weak basal décollement (Moore et al., 1995; Bangs et al., 1999, 2004; Brown et al., 2003; Lamb, 2006; Morgan et al., 2007; Saffer, 2007). It is also consistent with high fluid pressures approaching lithostatic overburden encountered in exploration wells from the upper Hikurangi Margin (Davies et al., 2000; Darby et al., 2000), and interpreted in the frontal parts of similar thrust systems (e.g., Maltman et al., 1993; Tobin et al., 1994; Moore and Saffer, 2001; Saffer, 2003, 2007).

One of the possible effects of rapid frontal accretion is to lower the taper of a thrust wedge. This may produce a mechanical response, whereby out-of-sequence thrusting behind the propagating deformation front leads to thickening of the rear and middle parts of the wedge in order to maintain a critical taper (e.g., Davis et al., 1983; Lallemand et al., 1994). Out of sequence thrusts are active across the upper and middle parts of the central Hikurangi Margin. These include reactivated Miocene thrust systems such as Motuokura Ridge (Figs. 3 and 12B), Lachlan Ridge (Fig. 1B) (Barnes et al., 2002), and Kidnappers Ridge (Barnes and Nicol, 2004), and reactivated thrusts presently inverting mid-slope basins (e.g., Fig. 5) (Davey et al., 1986a; Lewis and Pettinga, 1993; Barnes and Mercier de Lépinay, 1997). Similar out-of-sequence thrusting has been recognized at a number of other subduction margins (Moore et al., 2007).

The classical accretionary wedge of the central Hikurangi Margin contrasts strongly with the narrower and steeper northern margin, the latter of which is representative of subduction systems characterized by relatively thin (~1 km) trench-fill sequence, high relief (~1–3 km) on the subducting plate, relatively rapid convergence rate (~45–58 mm/yr), and non-accretion and/or frontal tectonic erosion processes (Von Huene and Lallemand, 1990; von Huene and Scholl,

Please cite this article as: Barnes, P.M., et al., Tectonic and geological framework for gas hydrates and cold seeps on the Hikurangi subduction margin, New Zealand, Mar. Geol. (2009), doi:10.1016/j.margeo.2009.03.012

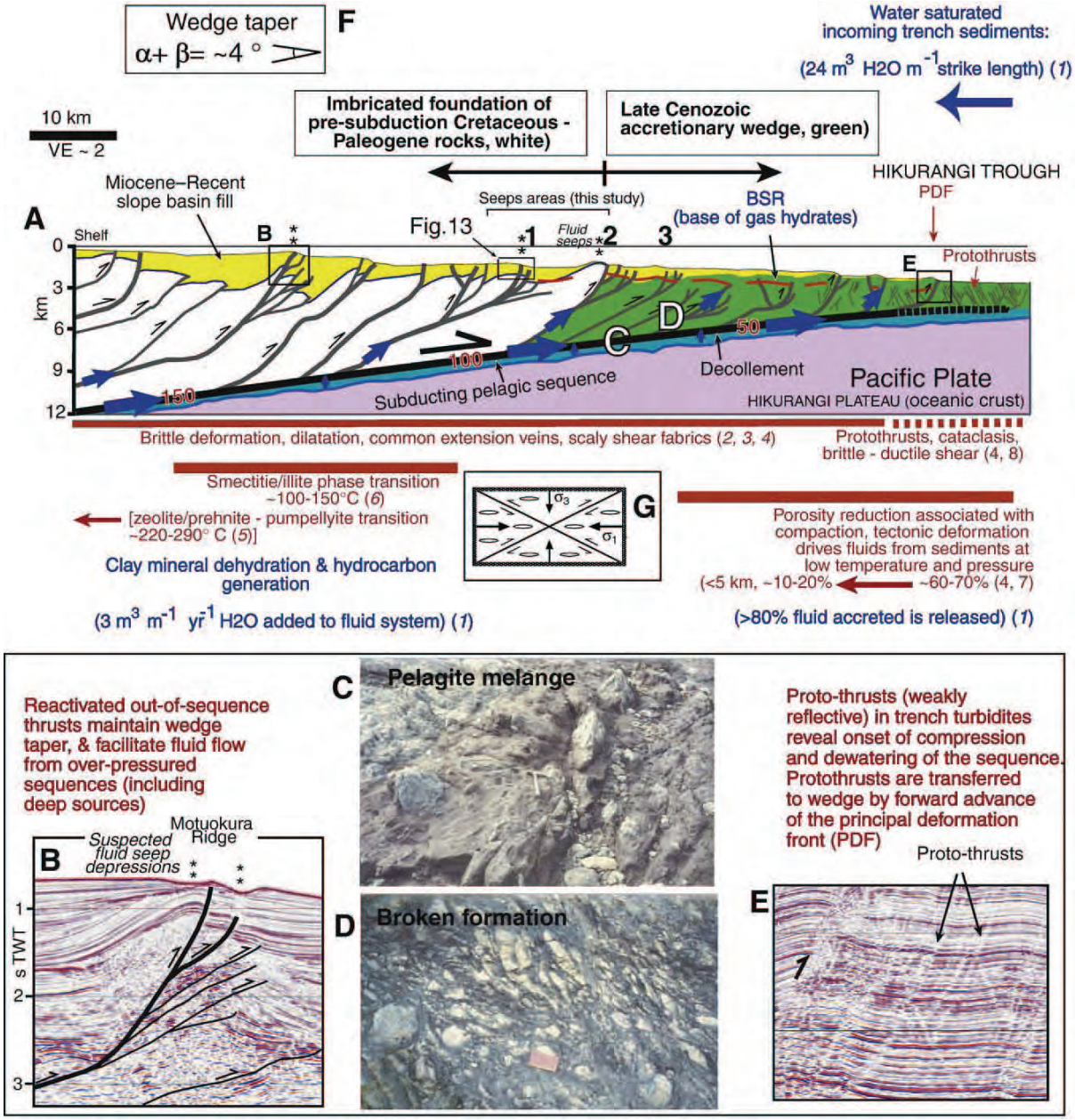

Fig. 12. Summary of tectonic, stratigraphic, and hydrogeological aspects of the Hikurangi Margin imbricate thrust wedge. A. Cross-section of the offshore margin 35 km south of Rock Garden, at ~2× vertical exaggeration, based in Fig. 3. Depth to plate interface is based in Fig. 4 inset, and data from Davey et al. (1986a), Henrys et al. (2006), and Nicol et al. (2007). Bold numbers above the cross-section refer to the indicative locations of the seep sites discussed in this paper, whereby: (1) includes Omakere Ridge (Figs. 2 and 10); (2) includes Palliser Bank and upper Opouawe Bank (Wairarapa sites, Figs. 1 and 8), Uruti Ridge (Figs. 2 and 9), Rock Garden (Figs. 2, 4 and 10), and Builders Pencil (Ritchie Ridge) (Figs. 1 and 11); and (3) includes lower Opouawe Bank (Fig. 8). Porangahau Ridge, studied by Pecher et al. (2009-this issue), is also represented by location 3. Text in blue (1) concerns the fluid budget, with estimates from Townend (1997a). Bold blue arrows illustrate primary fluid flow along décollement and thrust splay faults. Bold red numbers along the décollement are estimates of temperature in °C at the interplate thrust (McCaffrey et al., 2008). Selected references for deformation fabrics and mineral phase changes include: 2, Bryne and Fisher (1990); 3, Maltman et al. (1993); 4, Morgan et al. (2007); 5, Ernst (1990); 6, Vrolijk (1990); 7, Moore (1989); 8, Morgan and Karig (1995). B. High-fold multichannel seismic section CM05#30 illustrating thrust imbricates beneath suspected seeps sites on the southern Motuokura Ridge. The profile is projected 11 km onto cross-section A, whilst its actual location is shown in Fig. 2A. C and D illustrate what is interpreted to be analogous field examples of low *P–T* accretionary deformation fabrics from 100 Myr old subduction complex exposed in south eastern Wairarapa (Barnes and Korsch, 1991). C, tectonic mélange with pelagite matrix and "exotic" oceanic floaters; D, broken formation developed in turbidites. E. Zoom of seismic section SO191#6 (Fig. 6B) illustrating protothrusts at the deformation front. F. Thrust wedge taper where α and β are the surface slope and décollement dip, respectively. G. Schematic of thrusts and dilatational fractures developing in relation to maximum and minimum axes of principal compression (e.g., Sibson, 1992). (For interpretation of the references to colour in this figure legend, the reader is referred to the web version of this article.)

1991). The transition between these two present segments of the margin can now be located with greater confidence at the southern end of Rock Garden (Figs. 1B and 2B). The substantial relief (~3 km) associated with the seamount subducted beneath Rock Garden can be inferred to extend at least as far north as Ritchie Banks, based on its similarly high bathymetric elevation, and lies west of a 10 km-wide right step in the line of the deformation front at about 39 35′S (Fig. 11A).

Please cite this article as: Barnes, P.M., et al., Tectonic and geological framework for gas hydrates and cold seeps on the Hikurangi subduction margin, New Zealand, Mar. Geol. (2009), doi:10.1016/j.margeo.2009.03.012

5.3. The role of faulting in fluid migration and expulsion

Subduction systems associated with thick trench sequences have dynamic fluid systems because accreting and subducting sediments dewater in response to compaction and contractional deformation (e.g., Fig. 12A) (Moore, 1989; Moore and Vrolijk, 1992; Morgan et al., 2007). Water saturated trench sediments entering accretionary wedges undergo a change of stress regime, from one where the gravitational load dominates in the trench sequence as it approaches the deformation front, to one where the principal compressive stress approaches horizontal within the accretionary wedge (e.g., Davis et al., 1983). The latter produces structural permeability which facilitates lateral fluid flow (Fig. 12G) (Sibson and Roland, 2003; Saffer, 2007). Fluid flow in thrust fault zones has been reported widely from field observations (e.g., Sibson, 1992), as well as from geophysical and borehole evidence from subduction margins (e.g., Moore et al., 1986; LePichon et al., 1990; Taira et al., 1992; Tobin et al., 1994; Moore et al., 1995; 2004., Bangs et al., 1999, 2004). Field studies of ancient accretionary rocks (e.g., Moore and Wheeler, 1978; Cowan, 1982) and Ocean Drilling Project cores (e.g., Maltman et al., 1993; Morgan and Karig, 1995) show that a turbidite sequence entering an accretionary wedge undergoes substantial (c. 30–40%) porosity reduction and consolidation associated with deformation under low confining pressure and temperature, but high strain rates. Within the frontal part of the wedge, localized ductile flow, cataclasis, kink band development, and brittle faulting typically produces stratal disruption fabrics from previously coherent sequences, at up to kilometer scale (e.g., Fig. 12D) (e.g., Moore, 1989; Karig and Lundberg, 1990; Barnes and Korsch, 1991; Moore and Vrolijk, 1992; Maltman et al., 1993; Morgan and Karig, 1995; Morgan et al., 2007). Complex vein arrays in disrupted sequences referred to as broken formation, indicate that brittle faulting and fractures facilitate fluid flow by creating structural permeability (Moore and Byrne, 1987). Mesoscale broken formation is inferred to exist in the frontal wedge of the Hikurangi Margin, particularly in proximity to the major seismically imaged thrust faults (Lewis and Marshall, 1996; Barnes and Mercier de Lépinay, 1997). Such deformation fabrics, together with steep bedding dips and shallow gas, may contribute to loss of seismic reflection character commonly observed in the vicinity of the major faults (e.g., Fig. 12B and E) (Crutchley et al., 2009-this issue; Pecher et al., 2009-this issue).

The décollement beneath the frontal wedge of the central Hikurangi Margin is inferred to be located within the pelagic sediments (nannofossil chalks, tephras, mudstone, clays) of the Hikurangi Plateau sequence (Fig. 6B). Based on ocean drilling of other margins (Maltman et al., 1993; Morgan et al., 2007), and field examples of ancient analogues (Barnes and Korsch, 1991), the décollement deformation zone may be tens of meters in thickness, and have an internal structure resembling the Cretaceous mélange illustrated in Fig. 12C. The low pressure and temperature (zeolite facies) analogue field example in Fig. 12C is characterized by a pervasively sheared matrix of pelagite mudstone containing sheared blocks of greywacke from the upper plate, together with basalt and chert blocks from the oceanic lower plate.

To date, acoustic flares indicative of active fluid/gas venting have not been identified beneath the lower continental slope of the Hikurangi Margin (Lewis and Marshall, 1996; Greinert et al., 2009-this issue). Three lines of evidence, however, indicate that the frontal wedge is dewatering seaward of where the active seep sites are located. Firstly the presence of a gas hydrate BSR extending across the frontal wedge essentially to the deformation front indicates rising gas-charged fluids (Figs. 3, 4, 6, 8B, 11B) (Lewis and Marshall, 1996; Henrys et al., 2003). Secondly, there is an extraordinarily large (200 km length by 20 km width) protothrust zone beyond the principal deformation front in the Hikurangi Trough (Figs. 2A, 6B, 12A and E). Such incipient thrusts, and/or mega-kink bands characterized by relatively weak reflectivity, are commonly interpreted as dewatering conduits above the tip of the interplate thrust where it is propagating into the trench sequence (e.g., Moore et al., 1986, 1995; Platt, 1990; Morgan and Karig, 1995; Barnes and Mercier de Lépinay, 1997). Thirdly, two unconfirmed sites of suspected former fluid seepage are inferred on lower slope thrust ridges, from Hawaii MR1 sidescan sonar images (Fig. 2). One site (Fig. 2D) is a possible mud volcano (Barnes and Mercier de Lépinay, 1997), the other appears to be an edifice surrounded by radiating mud flow deposits (Fig. 2C). Whilst it is apparent that the frontal wedge is dewatering, its relative volumetric contribution to the total fluid release estimated from the margin is very poorly constrained (Townend, 1997a).

There is a clear relationship between the mid-slope line of confirmed fluid seep sites and major thrust faults near the outer edge of the Cretaceous and Paleogene foundation rocks (Figs. 1 and 12A) (Lewis and Marshall, 1996). Only one submarine site of suspected (i.e., unconfirmed) fluid seepage is recognized well inboard (~50 km) of this mid-slope buttress, on Motuokura Ridge (Figs. 2A, 12A and B). The major thrust faults beneath the active seeps are seaward-vergent and inferred to be primary fluid conduits (Fig. 13). The source of the fluids tapped by these faults must therefore be largely landward of the seep sites. These source rocks potentially include the Cretaceous and Paleogene sequences, the innermost (landward) part of the late Cenozoic frontal accretionary wedge, and sediments subducted and possibly underplated at depths of >9 km beneath the inner foundation or basement backstop of the margin (Barker et al., 2009). Estimates of temperatures at the Hikurangi interplate thrust indicate that offshore deformation and fluid expulsion is occurring at <150 °C (Fig. 12A) (McCaffrey et al., 2008). The fluids that supply onland seeps and overpressured stratigraphic intervals encountered in exploration wells near the coast are generally considered to have been sourced from the imbricated Cretaceous and Paleogene foundation rocks at depths of <5–6 km (Ridd, 1970, Kvenvolden and Pettinga, 1989; Lewis and Marshall 1996; Field et al., 1997; Davies et al., 2000; Darby et al., 2000; Pettinga, 2003; Uruski et al., 2004).

We consider that the apparent concentration of active submarine fluid seeps above the outer edge of the Cretaceous–Paleogene foundation, reflects the overall poor permeability of this unit, and the migration of fluids being channeled eastwards along the interplate décollement and on major low-angle thrust splay faults towards its outer edge (Fig. 12A) (cf. Lewis and Marshall, 1996). The low permeability of the Cretaceous–Paleogene foundation is consistent with (1) fluid pressures approaching lithostatic overburden encountered in east coast exploration wells, which have been shown to relate to low permeability mudstones with high smectite contents in the Cretaceous–Paleogene sequence (Darby et al., 2000; Darby, 2002), and (2) presence of former low-angle detachments associated with listric faulting in the upper margin, which have been inferred to be rooted in weak mudstone-rich stratigraphic intervals within the sequence (Barnes and Nicol, 2004).

Any fluids sourced from subducted sediments beneath the inner margin must firstly enter the décollement zone, and later the thrust wedge. Fluid flow into the décollement could potentially be achieved by progressive downward migration of the décollement deformation into the top of the subducting sequence, and/or by increased fluid pressure gradient resulting from temporarily increased permeability in décollement rocks by dilatation of scaly shear fabric during and after décollement rupture (e.g., Moore, 1989; Saffer, 2007). Fluid flow within the décollement may be episodic, associated with fluid pressure cycling produced by fault valve action (Sibson, 1992; Sibson and Roland, 2003). Fluid migration into the upper plate wedge will be enhanced at sites where splay thrusts ramp upward from the décollement.

All of the active fluid seeps recognized on the Hikurangi Margin lie on anticlines developed in the hanging wall of thrust faults (Figs. 12A and 13). Although thrust tips commonly break out at the seabed on the relatively steep forelimb (seaward) side of anticlinal ridges, the seeps are generally on the top of the ridges. Beneath each active seep site, there is a conspicuous break in the BSR, and common occurrence of high-amplitude reflections inferred to result from gas-charged stratigraphic

Please cite this article as: Barnes, P.M., et al., Tectonic and geological framework for gas hydrates and cold seeps on the Hikurangi subduction margin, New Zealand, Mar. Geol. (2009), doi:10.1016/j.margeo.2009.03.012

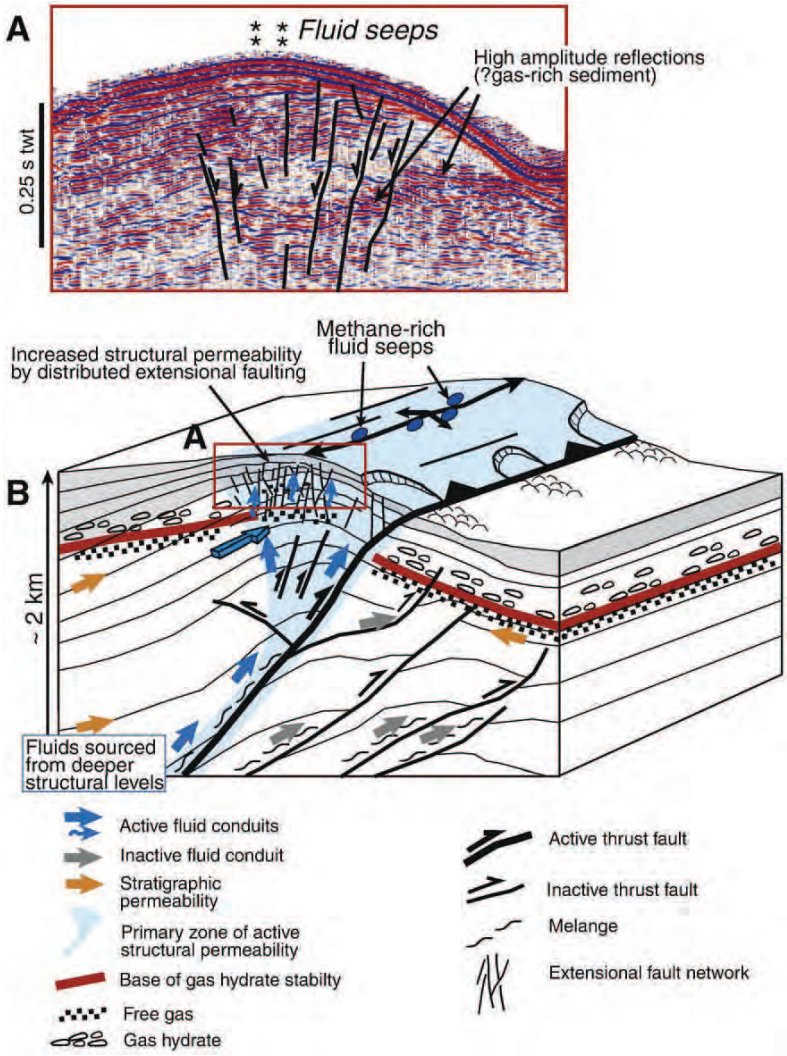

Fig. 13. Illustration of structural and stratigraphic permeability beneath active seep sites on Hikurangi Margin thrust ridges. A. Zoom of seismic section SO191#P054 across seep LM9 on Omakere Ridge (Fig. 10C), illustrating distributed extensional fault network in the shallow core of the anticline above an active thrust fault and beneath the seeps. B. Schematic 3D view of a typical Hikurangi Margin seep site illustrating various relationships.

horizons (Fig. 13). The existence of the fluid seeps and the disrupted BSR indicate that gas hydrates are not a barrier to fluid flow at these sites (e.g., Nimblett and Ruppel, 2003). Seismic sections reveal arrays of distributed shallow faults within the anticlines (see also Pecher et al., 2009-this issue). These shallow faults are commonly normal such as at Omakere Ridge (Fig. 13A) and Wairarapa sites (Netzeband et al., 2009-this issue), but also include backthrusts such as at LM-3, Rock Garden (Crutchley et al., 2009-this issue). Similar extensional fault arrays have been documented in the upper parts of growth folds beneath the NW Borneo margin (Gee et al., 2007). The normal faults, and probable subseismic fractures, in the anticlines may be a response to flexural extension, and/or hydrofracturing related to excessive pore pressures. Fluids rising along the major thrust faults appear to be siphoned off the faults directly into the shallow fault/fracture networks, and to percolate to the seabed on ridge crests (Pecher et al., 2004, 2009-this issue; Netzeband et al., 2009-this issue; Crutchley et al., 2009-this issue). What has sometimes been referred to as diffusive upward fluid flow related to increased stratigraphic permeability beneath ridges (e.g., Taira et al., 1992) may in fact be distributed fluid flow facilitated principally by fault and fracture permeability. Dipping, permeable stratigraphic layers within the hanging wall and footwall sequences of thrust faults are likely to be secondary fluid conduits that also focus fluid flow towards ridge crests (e.g., Langseth and Moore, 1990; Moore et al., 1990; Lewis and Marshall, 1996; Pecher et al., 2004).

6. Conclusions

1. New seismic reflection and multibeam datasets shed new insights into the tectonic structure, stratigraphy, and morphology of the imbricated frontal wedge of the Hikurangi Margin, and enable us to establish the geological framework for each of five areas in which seep sites are investigated and documented elsewhere in this issue. The imbricated wedge, which is up to 150 km in width, includes an inner foundation of deforming Late Cretaceous and Paleogene rocks, an outer wedge of late Cenozoic accreted trench-fill turbidites, and a deforming cover sequence of Miocene to Recent shelf and slope basin sediments. The contact between the inner foundation and the accretionary wedge has been recognized and located to within c. 10 km. The contact is interpreted to be a significant feature with respect to the hydrogeology of the margin, as it appears to control the location of presently active fluid seeps. The frontal accretionary wedge has a maximum width of c. 65–

Please cite this article as: Barnes, P.M., et al., Tectonic and geological framework for gas hydrates and cold seeps on the Hikurangi subduction margin, New Zealand, Mar. Geol. (2009), doi:10.1016/j.margeo.2009.03.012

70 km in the central margin, excluding a 20 km-wide protothrust zone.

2. The tectonic structure and morphology of the central part of the Hikurangi Margin is characteristic of wide, low taper thrust wedges associated with a relatively smooth subducting plate, a thick trench-fill sedimentary sequence, and moderate convergence rate. On the whole, the low taper (~4°) is consistent with the interpretation that the wedge is poorly drained, has low permeability, a weak basal décollement, and high fluid pressures. The protothrust zone in the Hikurangi Trough seaward of the principal deformation front extends along the margin for over 200 km. Its origin is related to incipient deformation and dewatering processes above the propagating décollement. Although part of the Bennett Knoll seamount ridge is presently subducting beneath the deformation front, the morphology of the accretionary wedge indicates that frontal accretion in the centre of the margin has been largely uninhibited for at least 1–2 Myr. Active out-of-sequence thrusting distributed widely across the margin behind the deformation front maintains the wedge taper.
3. Correlation of the seismic stratigraphy of the central Hikurangi Trough with published stratigraphy of the Hikurangi Plateau sedimentary sequence (Davy et al., 2008) constrains the ages and stratigraphy of the Mesozoic and Cenozoic sequence subducting beneath the interplate décollement. This sequence is inferred to include Cretaceous volcaniclastics, pelagic and clastic sedimentary rocks, and Late Cretaceous–Early Oligocene (70–32 Ma) nannofossil chalks with alternating clays. The décollement is developed within the Hikurangi Plateau sequence up to 400–450 m below what are clearly trench turbidites. Its stratigraphic position for at least 30 km down dip coincides primarily with reflection 7, but over lateral distances of 100–150 km, its stratigraphic position varies by up to 300–400 m within 15 km of the deformation front.
4. Offshore of Hawke Bay a substantial seamount with about 3 km of relief has been subducted beneath the lower margin, resulting in uplift and complex superposed deformation of Rock Garden and southern Ritchie Ridge, and a dramatically reduced active frontal wedge. The southern end of Ritchie Ridge therefore marks the transition from the classical accretionary system along the central margin to the narrower and steeper northern margin characterized by high-relief subducting plate, relatively thinner trench-fill sequence, relatively faster convergence rate, and predominantly non-accretion and/or frontal tectonic erosion processes.
5. The five areas of confirmed seep sites documented elsewhere in this issue, referred to as Wairarapa, Uruti Ridge, Omakere Ridge, Rock Garden, and Builders Pencil, typically lie in about 700–1200 m water depth on the crests of thrust-faulted anticlinal ridges along the mid-slope. The Uruti Ridge sites are unusual in that they also lie in close proximity to the eastern end of a strike-slip fault, whereas Rock Garden sites occur directly above a substantial seamount that is currently subducting. The seeps sites are associated with a variety of substrate stratigraphy. There is a clear relationship between the seeps and major seaward-vergent thrust faults near the outer edge of the deforming Cretaceous and Paleogene inner foundation rocks, indicating that thrust faults are primary fluid conduits and that the Cretaceous and Paleogene inner foundation rocks play a role in focusing fluid flow. The source rocks for the fluids expelling at the seeps potentially include the Cretaceous and Paleogene sequences, the innermost (landward) part of the frontal accretionary wedge, and sediments subducted and possibly underplated at depths of >9 km beneath the inner foundation or basement backstop of the margin. We interpret that the Cretaceous and Paleogene inner foundation is, on the whole, relatively impermeable and focuses fluid migration to its outer edge via major low-angle thrust faults and the interplate décollement.
6. Beneath each area of active seep sites there is a conspicuous break in the BSR, and commonly a seismically-resolvable fault-fracture network and gas-charged horizons within the shallow part of the anticlines. Structural permeability is interpreted to be crucial, within the décollement, the major thrust splay faults, and within shallow anticlinal fault networks which siphon fluids from thrust faults and allow vertical percolation to the seafloor on ridge crests. Stratigraphic permeability within dipping sequences is likely to be secondarily important.
7. No active fluid venting has yet been recognized over the frontal accretionary wedge, but the presence of a widespread BSR, extensive protothrust zone, and two unconfirmed sites of possible previous fluid expulsion, indicates that the frontal wedge is actively dewatering. There are presently no constraints however on the relative fluid flux between the frontal wedge and the active mid-slope fluid seeps.

Acknowledgments

We thank the crew and officers of *RV SONNE* cruise SO191, and the multiple *RV TANGAROA* voyages that contributed data to this study. The New Zealand Ministry for Economic Development provided us access to the CM05 seismic dataset. PB and GL were funded by NZ FRST research contracts CO1X0203 and CO1X0702. SH was funded by NZ FRST contract CO5X0302. The 'New Vents' project including the cruise SO191 was funded by the German Ministry of Education and Research (BMBF). JM was partly funded by a Tertiary Education Top Achiever Award. GC was funded through the Royal Society of New Zealand Marsden Grant contract GNS0403. The distribution of active faults on land was provided by GNS Science. We thank John Mitchell, Steve Wilcox and Peter Gerring for assistance with data acquisition, Claire Castellazzi for processing and display of seismic data, and Rob Funnell for discussion of heat flow. The *RV TANGAROA* seismic and EM300 multibeam dataset used here from the southern Poverty Bay margin were acquired for a related study by Keith Lewis. We appreciate constructive reviews of the manuscript by Andy Nicol and Chris Goldfinger.

References

Arron, E.S., Lewis, K.B., 1992. Mahia, 2nd Edition, N. Z. Oceanographic Institute Chart, Coastal Series, 1:200 000. Department of Scientific and Industrial Research, Wellington, New Zealand.

Ballance, P.F., 1976. Evolution of the Upper Cenozoic magmatic arc and plate boundary in northern New Zealand. Earth Planet. Sci. Lett. 28, 356–370.

Bangs, N.L., Shipley, T.H., Moore, J.C., Moore, G.F., 1999. Fluid accumulation and channeling along the northern Barbados décollement thrust. J. Geophys. Res. 104, 20,399–20,414.

Bangs, N.L., Shipley, T.H., Gulick, S., Moore, G., Kuomoto, S., Nakamura, Y., 2004. Evolution of the Nankai Trough décollement from the trench into the seismogenic zone: inferences from three-dimensional seismic reflection imaging. Geology 32, 273–276.

Barker, D.H.N., Sutherland, R., Henrys, S., Bannister, S., 2009. Geometry of the Hikurangi subduction thrust and upper plate, North Island, New Zealand. Geochem. Geophys. Geosyst. 10, Q02007. doi:10.1029/2008GC002153.

Barnes, P.M., Audru, J.-C., 1999. Quaternary faulting in the offshore Flaxbourne and southern Wairarapa basins, southern Cook Strait, New Zealand. N. Z. J. Geol. Geophys. 42, 349–367.

Barnes, P.M., Korsch, R.J., 1991. Melange and related structures in Torlesse accretionary wedge, Wairarapa, New Zealand. N. Z. J. Geol. Geophys. 34, 517–532.

Barnes, P.M., Mercier de Lépinay, B., 1997. Rates and mechanics of rapid frontal accretion along the very obliquely convergent southern Hikurangi margin, New Zealand. J. Geophys. Res. 102, 24 931–24 952.

Barnes, P.M., Nicol, A., 2004. Formation of an active thrust triangle zone associated with structural inversion in subducting setting, eastern New Zealand. Tectonics 23 (1), TC1015.

Barnes, P.M., Mercier de Lépinay, B., Collot, J.-Y., Delteil, J., Audru, J.-C., 1998a. Strain partitioning in the transition area between oblique subduction and continental collision, Hikurangi margin, New Zealand. Tectonics 17, 534–557.

Barnes, P.M., Mercier de Lépinay, B., Collot, J.-Y., Delteil, J., Audru, J.-C., and GeodyNZ team, 1998b. South Hikurangi GeodyNZ swath maps: depths, texture and geological interpretation. 1:500,000., N.Z. Oceanogr. Inst. Chart, Miscellaneous Series 75. National Institute of Water and Atmospheric Research, Wellington.

Appendix II

Barnes, P.M., Nicol, A., Harrison, T., 2002. Late Cenozoic evolution and earthquake potential of an active listric thrust complex above the Hikurangi subduction zone, New Zealand. Geol. Soc. Am. Bull. 114, 1379–1405.

Beavan, J., Tregoning, P., Bevis, M., Kato, T., Meertens, C., 2002. Motion and rigidity of the Pacific Plate and implications for plate boundary deformation. J. Geophys. Res. 107, 2261 (ETG 19).

Brown, K.M., Kopf, A., Underwood, M.B., Weinberger, J.L., 2003. Compositional and fluid pressure controls on the state of stress on the Nankai subduction thrust: a weak plate boundary. Earth Planet. Sci. Lett. 214, 589–603.

Bryne, T., Fisher, D., 1990. Evidence for a weak and overpressured décollement beneath sediment-dominated accretionary prisms. J. Geophys. Res. 95, 9081–9097.

Campbell, K.A., Francis, D.A., Collins, M., Gregory, M.R., Nelson, C.S., Greinert, J., Aharon, P., 2008. ?Hyrdocarbon seep-carbonates of a Miocene forearc (East Coast Basin), North Island, New Zealand. Sediment. Geol. 204, 83–105.

Collot, J.-Y., Delteil, J., Lewis, K.B., Davy, B., Lamarche, G., Audru, J.-C., Barnes, P.M., Chanier, F., Chaumillon, E., Lallemand, S., Mercier de Lépinay, B., Orpin, A.R., Pelletier, B., Sosson, M., Toussaint, B., Uruski, C., 1996. From oblique subduction to intra-continental transpression: structures of the southern Kermadec–Hikurangi margin from multibeam bathymetry, side-scan sonar and seismic reflection. Mar. Geophys. Res. 18, 357–381.

Collot, J.-Y., Lewis, K.B., Lamarche, G., Lallemand, S., 2001. The giant Ruatoria debris avalanche on the northern Hikurangi margin, New Zealand; results of oblique seamount subduction. J. Geophys. Res. 106, 19271–19297.

Cowan, D.S., 1982. Structural stles in Mesozoic and Cenozoic mélanges in the Western Cordellia of North America. Geol. Soc. Am. Bull. 96, 451–462.

Crutchley, G.J., Pecher, I.A., Gorman, A.R., Henrys, S.A., Greinert, J., 2009-this issue. Seismic imaging of gas conduits beneath seafloor seep sites in a shallow marine gas hydrate province, Hikurangi Margin, New Zealand. Mar. Geol. doi:10.1016/j.margeo.2009.03.007

Darby, D., 2002. Seal properties, overpressure and stress in the Taranaki and East Coast Basins, New Zealand. New Zealand Petroleum Conference Proceedings. Ministry of Commerce, Wellington.

Darby, D., Funnell, R., Uruski, C., Field, B., 2000. Patterns of fluid flow in the East Coast Basin. New Zealand Petroleum Conference Proceedings. Ministry of Commerce, Wellington.

Davy, B., Wood, R., 1994. Gravity and magnetic modelling of the Hikurangi Plateau. Mar. Geol. 118, 139–151.

Davy, B.R., Hoernle, K., Werner, R., 2008. The Hikurangi Plateau — crustal structure, rifted formation and Gondwana subduction history. Geochem. Geophys. Geosyst. 9, Q07004. doi:10.1029/2007GC001855.

Davey, F.J., Lewis, K.B., Childs, J., Hampton, M., 1986a. Convergent margin off the east coast of North Island, New Zealand, Parts I and II. In: von Huene, R.E. (Ed.), Seismic Images of Modern Convergent Margin Structure. Am. Assoc. Pet. Geol. Stud. Geol., vol. 26, pp. 49–53.

Davey, F.J., Hampton, M., Childs, J., Fisher, M.A., Lewis, K.B., Pettinga, J.R., 1986b. Structure of a growing accretionary prism, Hikurangi margin, New Zealand. Geology 14, 663–666.

Davies, E.J., Frederick, J.B., Leask, W.L., Williams, T.J., 2000. East Coast drilling results. New Zealand Petroleum Conference Proceedings. Ministry of Commerce, Wellington.

Davis, D., Suppe, J., Dahlen, F.A., 1983. Mechanics of fold and thrust belts and accretionary wedges. J. Geophys. Res. 88, 1153–1172.

Dixon, T.H., Moore, J.C., 2007. The seismogenic zone of subduction thrust faults: introduction. In: Dixon, T.H., Moore, J.C. (Eds.), The Seismogenic Zone of Subduction Thrust Faults. Columbia University Press, New York, pp. 2–14.

Dominguez, S., Lallemand, S.E., Malavieille, J., von Huene, R., 1998. Upper plate deformation associated with seamount subduction. Tectonophysics 293, 207–224.

Ellis, S., Pecher, I., Kukowski, N., Xu, W., Henrys, S., Greinert, J., 2009-this issue. Testing proposed mechanisms for seafloor weakening at the top of gas hydrate stability, Rock Garden, New Zealand. Mar. Geol.

Ernst, W.G., 1990. Thermobarometric and fluid expulsion history of subduction zones. J. Geophys. Res. 95, 9047–9053.

Faure, K., Greinert, J., Pecher, I.A., Graham, I.J., Massoth, G.J., Ronde, C.E.J.D., Wright, I.C., Baker, E.T., Olson, E.J., 2006. Methane seepage and its relation to slumping and gas hydrate at the Hikurangi Margin, New Zealand. N. Z. J. Geol. Geophys. 49, 503–516.

Faure, K., Greinert, J., Schneider v.D., J., McGinnis, D.F., Kipfer, R., Linke, P., 2009-this issue. Free and dissolved methane in the water column and the sea surface: Geochemical and hydroacoustic evidence of bubble transport. Mar. Geol.

Field, B.D., Uruski, C.I., et al., 1997. Cretaceous–Cenozoic Geology and Petroleum Systems of the East Coast Region, New Zealand. Institute of Geological & Nuclear Sciences Monograph, vol. 19. Institute of Geological & Nuclear Sciences Ltd, Lower Hutt, New Zealand. 301 pp.

Frederik, J.B., 2004. East Coast hydrocarbon potential — Tawatawa prospect, offshore Wairarapa shelf. New Zealand Petroleum Conference Proceedings. Ministry of Commerce, Wellington.

Garlick, R., Mitchell, J.S., 2002. Turnagain Bathymetry, 3rd Edition. NIWA Chart, Coastal Series, 1:200 000. National Institute of Water and Atmospheric Research Ltd, Wellington, New Zealand.

Gee, M.J.R., Uy, H.S., Warren, J., Morley, C.K., Lambaise, J.J., 2007. The Brunei slide: a giant submarine landslide on the North West Borneo Margin revealed by 3D seismic data. Mar. Geol. 246, 9–23.

Greinert, J., Lewis, K., Bialas, J., Pecher, I., Rowden, A., Linke, P., De Batist, M., Bowden, D., Suess, E., 2009-this issue. Methane seepage along the Hikurangi Margin, New Zealand: review of studies in 2006 and 2007. Mar. Geol.

Haeckel, M., Sommer, S., Linke, P.: this volume. Porewater geochemistry and methane fluxes of cold seeps at the Hikurangi Margin, offshore New Zealand. Mar. Geol.

Henry, P., Le Pichon, X., Lallemant, S., Foucher, J.-P., Westbrook, G., Hobart, M., 1990. Mud volcano field seaward of the Barbados accretionary complex: a deep-towed side-scan sonar survey. J. Geophys. Res. 95, 8917–8930.

Henrys, S.A., Ellis, S., Uruski, C., 2003. Conductive heat flow variations from bottom simulating reflectors on the Hikurangi margin, New Zealand. Geophys. Res. Lett. 30. doi:10.1029/2002GL015772.

Henrys, S., Reyners, M., Pecher, I., Bannister, S., Nishimura, Y., Maslen, G., 2006. Kinking of the subducting slab by escalator normal faulting beneath the North Island of New Zealand. Geology 34, 777–780.

Henrys, S.A., Woodward, D., Pecher, I.A., in press. Variation of bottom-simulating reflector (BSR) strength in a high-flux methane province, Hikurangi margin, New Zealand. Am. Assoc. Pet. Geol. Memoirs.

Holt, W.E., Haines, A.J., 1995. The kinematics of northern South Island, New Zealand, determined from geological strain rates. J. Geophys. Res. 100, 17991–18010.

Huhnerbach, V., Masson, D.G., Bohrmann, G., Bull, J.M., Weinrebe, W., 2005. Deformation and submarine landsliding caused by seamount subduction beneath the Costa Rica continental margin — new insights from high-resolution sidescan sonar data. In: Hodgson, D.M., Flint, S.S. (Eds.), Submarine Slope Systems: Processes and Products. Geol. Soc. Lond. Spec. publ., vol. 244, pp. 195–205.

Jones, A.T., Greinert, J., Bowden, D., Klaucke, I., Petersen, J., Netzeband, G., Weinrebe, W., 2009-this issue. Acoustic and visual characterisation of methane-rich seabed seeps at Omakere Ridge on the Hikurangi Margin, New Zealand. Mar. Geol. doi:10.1016/j.margeo.2009.03.008

Karig, D.E., Lundberg, N., 1990. Deformation bands from the toe of the Nankai accretionary prism. J. Geophys. Res. 95, 9099–9109.

Katz, H.R., 1981. Probable gas hydrate in continental slope east of the North Island, New Zealand. J. Pet. Geol. 3, 315–324.

Klaucke, I., Weinrebe, W., Petersen, C.J., Bowden, D., 2009-this issue. Temporal variability of gas seeps offshore New Zealand: multi-frequency geoacoustic imaging of the Wairarapa area, Hikurangi margin. Mar. Geol. doi:10.1016/j.margeo.2009.02.009

Kvenvolden, K.A., 1993. Gas hydrates — geological perspective and global change. Rev. Geophys. Space Phys. 31, 173–187.

Kvenvolden, K.A., Pettinga, R., 1989. Hydrocarbon gas seeps of the convergent Hikurangi margin, North Island, New Zealand. Mar. Pet. Geol. 6, 2–8.

Kulm, L.D., Suess, E., 1990. Relationship between carbonate deposits and fluid venting: Oregon accretionary prism. J. Geophys. Res. 95, 8899–8916.

Lallemand, S., Schnurle, P., Malavieille, J., 1994. Coulomb theory applied to accretionary and nonaccretionary wedges: possible causes for tectonic erosion and/or frontal accretion. J. Geophys. Res. 99, 12033–12055.

Lamb, S., 2006. Shear stresses on megathrusts: implications for mountain-building behind subduction zones. J. Geophys. Res. 111, B07401. doi:10.1029/2005JB003916.

Langseth, M.G., Moore, J.C., 1990. Introduction to special section on the role of fluids in sediment accretion, deformation, diagenesis, and metamorphism in subduction zones. J. Geophys. Res. 95, 8737–8742.

LePichon, X., Henry, P., Lallement, S., 1990. Water flow in the Barbados accretionary complex. J. Geophys. Res. 95, 8945–8968.

Lewis, K.B., 1973. Erosion and deposition on a tilting continental shelf during Quaternary oscillations of sea level. N. Z. J. Geol. Geophys. 16, 281–301.

Lewis, K.B., Barnes, P.M., 1999. Kaikoura Canyon, New Zealand; active conduit from near-shore sediment zones to a trench-axis channel. Mar. Geol. 162, 39–69.

Lewis, K.B., Marshall, B.A., 1996. Seep faunas and other indictors of methane-rich dewatering on the New Zealand convergent margins. N. Z. J. Geol. Geophys. 39, 181–200.

Lewis, K.B., Pettinga, J.R., 1993. The emerging, imbricate frontal wedge of the Hikurangi margin. In: Balance, P.F. (Ed.), South Pacific Sedimentary Basins. Sedimentary Basins of the World 2, Basins of the Southwest Pacific. Elsevier, Amsterdam, pp. 225–250.

Lewis, K.B., Collot, J.-Y., Davy, B.W., Delteil, L., Lallemand, S.E., Uruski, C.I. and GeodyNZ team, 1997. North Hikurangi GeodyNZ swath maps: depth, texture and geological interpretation. NIWA chart miscellaneous series vol. 72. National Institute of Water & Atmospheric Research, Wellington.

Lewis, K.B., Collot, J.-Y., Lallemand, S.E., 1998. The dammed Hikurangi Trough: a channel-fed trench blocked by subducting seamounts and their wake avalanches (New Zealand–France GeodyNZ Project). Bas. Res. 10, 441–468.

Lewis, K.B., Barnes, P.M., Collot, J.-Y., Mercier de Lépinay, B., Delteil, J., and GeodyNZ team, 1999. Central Hikurangi GeodyNZ swath maps: depth, texture and geological interpretation. NIWA chart miscellaneous series 77. National Institute of Water & Atmospheric Research, Wellington.

Lewis, K.B., Lallemand, S., Carter, L., 2004. Collapse in a Quaternary shelf basin off East Cape, New Zealand: evidence for the passage of a subducted seamount inboard of the Ruatoria giant avalanche. N. Z. J. Geol. Geophys. 47, 415–429.

Maltman, A.J., Byrne, T., Karig, D.E., Lallemant, S., 1993. Deformation at the toe of an active accretionary prism: synopsis of results from ODP Leg 131, Nankai, SW Japan. J. Struct. Geol. 15, 949–964.

McCaffrey, R., Wallace, L.M., Beavan, J., 2008. Slow slip events, temperature, and interseismic coupling at the Hikurangi subduction zone, New Zealand. Nat. Geosci. 1, 316–320.

Mitchell, J.S., 1988. Palliser Bathymetry 2nd Edition, N. Z. Oceanographic Institute Chart, Coastal Series, 1:200 000. Department of Scientific and Industrial Research, Wellington, New Zealand.

Moore, J.C., 1989. Tectonics and hydrogeology of accretionary prisms: role of the decollement zone. J. Struct. Geol. 11, 95–106.

Moore, J.C., Byrne, T., 1987. Thickening of fault zones: a mechanism of melange formation in accretionary sediments. Geology 15, 1040–1043.

Moore, J.C., Saffer, D., 2001. Updip limit of the seismogenic zone beneath the accretionary prism of southwest Japan; an effect of diagenetic to low-grade metamorphic processes and increasing effective stress. Geology 29, 183–186.

Moore, J.C., Vrolijk, P., 1992. Fluids in accretionary prisms. Rev. Geophys. 30, 113–135.

Please cite this article as: Barnes, P.M., et al., Tectonic and geological framework for gas hydrates and cold seeps on the Hikurangi subduction margin, New Zealand, Mar. Geol. (2009), doi:10.1016/j.margeo.2009.03.012

Appendix II

Moore, J.C., Wheeler, R.W., 1978. Structural fabric of a mélange, Kodiac Isalnds, Alaska. Am. J. Sci. 278, 739–765.

Moore, J.C., Roeske, S., Lundberg, N., Schoonmaker, J., Cowan, D.S., Gonzales, E., Lucas, S.E., 1986. Scaly fabrics from Deep Sea Drilling Project cores from forearcs. In: Moore, J.C. (Ed.), Structural Fabrics in Deep Sea Drilling Project Cores. Mem. Geol. Soc. Am., vol. 166, pp. 55–74.

Moore, G.F., Shipley, T.H., Stoffa, P.L., Karig, D.E., Taira, A., Kuramoto, S., Tokuyama, H., Suyehiro, K., 1990. Structure of the Nankai Trough accretionary zone from multichannel seismic reflection data. J. Geophys. Res. 95, 8753–8765.

Moore, J.C., Moore, G.F., Cochrane, G.R., Tobin, H.J., 1995. Negative-polarity seismic reflections along faults of the Oregon accretionary prism: indicators of over-pressuring. J. Geophys. Res. 100, 12895–12906.

Moore, G.F., Bangs, G.F., Taira, A., Kuramoto, S., Pangborn, E., Tobin, H.J., 2007. Science 318, 1128–1131.

Morgan, J.K., Karig, D.E., 1995. Decollement processes at the Nankai accretionary margin, southeast Japan: propagation, deformation, and dewatering. J. Geophys. Res. 100, 15221–15231.

Morgan, J.K., Sunderland, E.B., Ask, M.V.S., 2007. Deformation and mechanical strength of sediments at the Nankai subduction zone: implications for prism evolution and décollement initiation and propagation. In: Dixon, T.H., Moore, J.C. (Eds.), The Seismogenic Zone of Subduction Thrust Faults. Columbia University Press, New York, pp. 210–247.

Mountjoy, J., Barnes, P., Pettinga, J., 2009. Morphostructure of submarine canyons on an active margin: Cook Strait Canyon system, New Zealand. Mar. Geol. 260, 45–68. doi:10.1016/j.margeo.2009.01.006.

Multiwave, 2005. 05CM 2D Seismic Survey, Offshore East Coast — North Island. New Zealand unpublished openfile petroleum report 3136. Ministry of Economic Development, Wellington.

Naudts, L., Greinert, J., Poort, J., Belza, J., Vangampelaere, E., Boone, D., Linke, P., Henriet, J.-P., De Batist, M., 2009-this issue. Active venting sites on the gas-hydrate-bearing Hikurangi Margin, Off New Zealand: diffusive versus bubble-released methane. Mar. Geol.

Netzeband, G.L., Krabbenhoeft, A., Zillmer, M., Petersen, C.J., Papenberg, C., Bialas, J., 2009-this issue. The structures beneath submarine methane seeps: Seismic evidence from Opouawe Bank, Hikurangi Margin, New Zealand. Mar. Geol.

Nicol, A., Mazengarb, C., Chanier, F., Rait, G., Uruski, C., Wallace, L., 2007. Tectonic evolution of the Hikurangi subduction margin, New Zealand, since Oligocene. Tectonics 26. doi:10.1029/2006TC002090.

Nimblett, J., Ruppel, C., 2003. Permeability evolution during the formation of gas hydrates in marine sediments. J. Geophys. Res. 108. doi:10.1029/2001JB001650.

Paquet, F. 2008. Morphostructural evolution of active subduction margins: the example of the Hawke bay Forearc Basin, New Zealand. PhD Thesis, Universite de Rennes 1, Rennes, France and University of Canterbury, Christchurch, New Zealand, 253 pp.

Paquet, F., Proust, J.-N., Barnes, P.M., Pettinga, J., 2009. Inner forearc sequence architecture in response to climate and tectonic forcing since 150 Ka: Hawke's Bay, New Zealand. J. Sediment. Res. 79, 97–124. doi:10.2110/jsr.2009.019.

Pecher, I.A., 2002. Gas hydrates on the brink. Nature (News and views) 420, 622–623.

Pecher, I.A., Henrys, S.A., Zhu, H., 2004. Seismic images of gas conduits beneath vents and gas hydrates on Ritchie Ridge, Hikurangi Margin, New Zealand. N. Z. J. Geol. Geophys. 47, 275–279.

Pecher, I.A., Henrys, S.A., Ellis, S., Chiswell, S.M., Kukowski, N., 2005. Erosion of the seafloor at the top of the gas hydrate stability zone on the Hikurangi Margin, New Zealand. Geophys. Res. Lett. 32, L24603.

Pecher, I.A., Henrys, S.A., Wood, W.T., Kukowski, N., Crutchley, G.J., Fohrmann, M., Kilner, J., Senger, K., Gorman, A.R., Coffin, R.B., Greinert, J., Faure, K., 2009-this issue. Focused fluid flow on the Hikurangi Margin, New Zealand - evidence from possible local upwarping of the base of gas hydrate stability. Mar. Geol.

Pettinga, J.R., 1982. Upper Cenozoic structural history, coastal southern Hawke's Bay, New Zealand. N. Z. J. Geol. Geophys. 25, 149–191.

Pettinga, J.R., 2003. Mud volcano eruption within the emergent accretionary Hikurangi margin, southern Hawke's Bay, New Zealand. N. Z. J. Geol. Geophys. 46, 107–121.

Platt, J., 1990. Thrust mechanics in highly overpressured accretionary wedges. J. Geophys. Res. 95, 9025–9034.

Ridd, M.F., 1970. Mud volcanoes in New Zealand. Am. Assoc. Pet. Geol. Bull. 54, 601–616.

Rait, G., Chanier, F., Waters, D.W., 1991. Landward- and seaward-directed thrusting accompanying the onset of subduction beneath New Zealand. Geology 19, 230–233.

Saffer, D.M., 2003. Pore pressure development and progressive dewatering in under-thrust sediments at the Costa Rican subduction margin: comparison with northern Barbados and Nankai. J. Geophys. Res. 108, 2261. doi:10.1029/2002JB001787.

Saffer, D.M., 2007. Pore pressure within underthrust sediment in subduction zones. In: Dixon, T.H., Moore, J.C. (Eds.), The Seismogenic Zone of Subduction Thrust Faults. Columbia University Press, New York, pp. 148–170.

Saffer, D.M., Bekins, B.A., 2002. Hydrologic controls on the mechanics and morphology of accretionary wedges and thrust belts. Geology 30, 271–274.

Schwalenberg, K., Wood, W., Pecher, I., Hamden, L., Henrys, S., Jegen, M., Coffin, R.B., 2009-this issue. Preliminary interpretation of CSEM, heatflow, seismic, and geochemical data for gas hydrate distribution across the Porangahau Ridge, New Zealand. Mar. Geol.

Sibson, R.H., 1992. Fault-valve behaviour and the hydrostatic–lithostatic fluid pressure interface. Earth Sci. Rev. 32, 141–144.

Sibson, R.H., Roland, J., 2003. Stress, fluid pressure and structural permeability in seismogenic crust, North Island, New Zealand. Geophys. J. Int. 154, 584–594.

Taira, A., Hill, I., Firth, J., Berner, U., Bruckmann, W., Bryne, T., Chabernaud, T., Fisher, A., Foucher, J.-P., Gamo, T., Gieskes, J., Hyndman, R., Karig, D., Kastner, M., Kaot, Y., Lallemant, S., Lu, R., Maltman, A., Moore, G., Moran, K., Olaffson, G., Owens, W., Pickering, K., Siena, F., Taylor, E., Underwood, M., Wilkinson, C., Yamano, M., Zhang, J., 1992. Sediment deformation and hydrogeology of the Nankai Trough accretionary prism: synthesis of shipboard results of ODP Leg 131. Earth Planet. Sci. Lett. 109, 431–450.

Townend, J., 1997a. Subducting a sponge: minimum estimates of the fluid budget of the Hikurangi margin accretionary prism. Geol. Soc. N.Z. Newslett. 112, 14–16.

Townend, J., 1997b. Estimates of conductive heat flow through bottom-simulating reflectors on the Hikurangi and southwest Fiordland continental margins, New Zealand. Mar. Geol. 141, 209–220.

Tobin, H.J., Moore, J.C., Moore, G.F., 1994. Fluid pressure in the frontal thrust of the Oregon accretionary prism: experimental constraints. Geology 22, 979–982.

Trehu, A.M., Torres, M.E., Moore, G.F., Suess, E., Bohrmann, G., 1999. Temporal and spatial evolution of a gas hydrate-bearing accretionary ridge on the Oregon continental margin. Geology 27, 939–942.

Uruski, C., Field, B., Sykes, R., Funnell, R., Darby, D., 2004. Is the offshore East Coast Basin an accessible source of gas? New Zealand Petroleum Conference Proceedings. Ministry of Commerce, Wellington.

Von Huene, R., Lallemand, S., 1990. Tectonic erosion along the Japan and Peru convergent margins. Geol. Soc. Am. Bull. 102, 704–720.

von Huene, R., Scholl, D.W., 1991. Observations at convergent margins concerning sediment subduction, subduction erosion, and the growth of continental crust. Rev. Geophys. 29, 279–316.

Vrolijk, P., 1990. On the mechanical role of smectite in subduction zones. Geology 18, 703–707.

Wallace, L.M., Beavan, J., McCaffrey, R., Darby, D., 2004. Subduction zone coupling and tectonic block rotation in the North Island, New Zealand. J. Geophys. Res. 109. doi:10.1029/2004JB003241.

Wood, R., Davy, B., 1994. The Hikurangi Plateau. Mar. Geol. 118, 153–173.

Please cite this article as: Barnes, P.M., et al., Tectonic and geological framework for gas hydrates and cold seeps on the Hikurangi subduction margin, New Zealand, Mar. Geol. (2009), doi:10.1016/j.margeo.2009.03.012